NANYANG TECHNOLOGICAL UNIVERSITY

Punching Shear Strength of High Strength Concrete and Steel Fibre Reinforced Concrete Slabs

KHATTHANAM CHANTHABOUALA

SCHOOL OF CIVIL AND ENVIRONMENTAL ENGINEERING

2017

Punching Shear Strength of High Strength Concrete and Steel Fibre Reinforced Concrete Slabs

KHATTHANAM CHANTHABOUALA

School of Civil and Environmental Engineering

A thesis submitted to the Nanyang Technological University in partial fulfillment of the requirement for the degree of Doctor of Philosophy

2017

Acknowledgements

Most importantly, I would like to express my special appreciation and thanks to my supervisor, Associate Professor, **Dr Susanto Teng**, who has been an inspirational teacher and a motivational mentor for me. I am grateful for his entrustment in me, his patient guidance, encouragement and kind supports throughout the period of my research. His advice and sharing have been invaluable for my research as well as my knowledge development. All these will continue to influence my future career and personal life positively.

I am thankful to Professor, **Dr Tan Kang Hai**, who has been helpful, especially during the period of completing this thesis. His valuable comments on my research works are appreciated. I gratefully thank Professor, **Dr Claudia P. Ostertag**, from University of California, Berkeley, especially for her in-depth and insightful comments on the discussions of steel fibre reinforced concrete slabs.

I would like to thank my current and former research groupmates: **Darren L.**, **Felicia**, **Jimmy C.**, and **Dr Liu Y.** for their generous help with experimental and technical works. I thank **Dr Soerya W.** and **Hidayat R.** for sharing their research experiences and research materials with me when I first joined the research team.

This research work is part of NRF-CRP research program "Underwater Infrastructure and Underwater City of Future". I gratefully acknowledge grants from **National Research Foundation of Singapore (NRF)**.

My sincere appreciations go to the **School of Civil and Environmental Engineering**, **Nanyang Technological University** for the scholarship and the best research facilities and resources. I also appreciate the assistances from the **CEE Laboratory technicians** during the long-hour experiment sessions.

I thank my beloved friends for their cheerful supports during both happy and difficult time, they know who they are.

My final thanks go to my family: my dear parents, my brother, and my sister, I could not have imagined being where I am now if I have not been receiving the unconditional love, supports and cares from them.

I dedicate this thesis to my mother and father.

Abstract

This thesis presents new in-depth discussions and design methods for high strength concrete (HSC) and steel fibre reinforced concrete (SFRC) slabs that are subjected to punching shear. Experimental programmes of 22 full-scale slabs are presented to accompany the discussions and the new design methods proposed in this thesis. All of the 22 slab specimens were constructed with high strength concrete. Some of the advantages of using high strength concrete compared to normal strength concrete include an increase in cracking load of the slab and a reduction in deflection at service load level due to higher tensile strength and higher elastic modulus of high strength concrete.

This research focuses on the investigation of the influences of two main structural parameters on the punching shear strength of a slab. The two parameters concerning this research are (1) the effect of low flexural reinforcement ratios, and (2) the influence of a new type of fibres - the double hooked end fibre. Recently, several researchers have addressed and investigated the influences of these parameters; however, more research are still needed. Therefore, the following paragraphs provide a brief summary of this thesis that includes both experimental and analytical works.

First, punching shear tests of 12 high-strength concrete slabs ($f'_c > 95$ MPa) with various flexural reinforcement ratios and column aspect ratios are presented. The dimensions of the specimens are 2.2 × 2.2 × 0.15 m and 2.7 × 2.2 × 0.15 m. The resulting slab data represent a complete set of slab specimens having low to high reinforcement ratios. The purpose of the tests is to investigate if Code equations (ACI 318, Eurocode 2) for punching shear overestimate the actual punching shear strengths of slabs that are provided with low amount of flexural reinforcement or low reinforcement ratio. Other influencing factors, such as column rectangularity ratio, concrete strength, and size (thickness) effect are also addressed. The author's new experimental results will be combined with 355 existing published data and together they will be used to evaluate the accuracy and safety of the ACI 318-14 and Eurocode 2 methods for punching shear, as well as some methods proposed by other researchers.

Second, punching shear tests of 10 steel fibre reinforced concrete (SFRC) slabs tested under punching shear loads are presented. The dimensions of the specimens are 2.2 × 2.2 × 0.15 m. The influence of high strength concrete ($f'_c \geq 80$ MPa) and a new type of steel fibre (the double hooked end fibre) were investigated. The fibre contents were varied from zero to 1.2% volume fraction for each set of the reinforcement ratio ρ. The reinforcement ratio ρ was varied from ρ = 0.9% to ρ = 1.4%. Key attributes, such as: ultimate state and serviceability performances, of these high strength SFRC slabs are discussed. The experimental results highlight that high strength SFRC enhances the slab performance in many aspects. As the fibre volume V_f was increased from 0% to 1.2% or to an equivalent fibre dosage of 93.6 kg/m^3, the flexural stiffness of the slabs increased while both the deflections and crack widths reduced. At the ultimate state, the punching shear strength increased by up to 156% compared to non-fibrous concrete slabs, which is significantly higher than the increment introduced by conventional single hooked-end fibres; the ductility and energy absorption capacity of the slabs were also significantly improved. Comparisons of design methods with the experimental results show that the TR34 method by the Concrete Society performs very well while the yield line theory overestimates the strengths of the slabs. The Model Code 2010 method is unconservative.

Finally, some relevant design recommendations are given. New design methods are proposed, they will be shown to be very reliable and accurate for calculating the punching shear strength of both reinforced concrete and steel fibre reinforced concrete slabs.

Keywords: punching shear; flexural failure; shear failure; building codes; high strength concrete; concrete slabs; reinforcement ratio; column aspect ratio; size effect; design method; reinforced concrete; double hooked-end fibre; SFRC; failure mode; slab; Code; Eurocode 2; ACI 318

Table of Contents

Acknowledgements i

Abstract ii

List of Tables xi

List of Figures xii

Notations xvii

1 **Chapter 1** ••••••••• 1

INTRODUCTION 1

1.1 Background of the research 3

1.1.1 High strength reinforced concrete slabs and effect of low reinforcement ratios 3

1.1.2 Steel fibre reinforced concrete slabs and influences of double hooked steel fibres 6

1.2 Objectives and scope of the research 8

1.2.1 Main objectives 8

1.2.2 Scope of work 9

1.3 Research significance 9

1.4 Thesis organisation 10

2 **Chapter 2** ••••••••• 12

LITERATURE REVIEW 12

2.1 Introduction 12

2.2 Brief history of beamless slab systems and the research 13

2.2.1 Reinforced concrete slabs 13

2.2.2 Fibre reinforced concrete slabs 15

2.3 Influences of structural parameters on punching shear 16

2.3.1 Influence of concrete strength 16

2.3.2 Influence of flexural reinforcement 18

2.3.3 Influence of column rectangularity 20

2.3.4 Influence of size effect 21

2.3.5 Influence of span-to-depth ratio 23
2.3.6 Influence of column width-to-depth ratio 24
2.3.7 Influence of fibre reinforced concrete 25
2.4 Types of punching shear models 27
2.4.1 Models based on Flexural Capacity 27
2.4.2 Models based on Plasticity Theory 27
2.4.3 Models based on The Kinnunen and Nylander approach 28
2.4.4 Models based on fracture mechanics and concrete tensile stresses 29
2.4.5 Models based on Strut-and-tie Models 29
2.4.6 Critical Shear Crack Theory Model 30
2.4.7 Tangential Strain Theory Model 30
2.4.8 Empirical and Semi-Empirical Models 31
2.5 Review of key literature 32
2.5.1 Past research works on reinforced concrete slabs 32
2.5.2 Past research works on fibre reinforced concrete slabs 36
2.5.2.1 Design Methods based on residual tensile strength approach 36
2.5.2.2 Methods based on fibre parameters approach 39
2.6 Summary 50
3 **Chapter 3** • • • • • • • • • 51
REVIEW OF DESIGN CODE PROVISIONS, GUIDELINES, AND ANALYSIS METHODS 51
3.1 Introduction 51
3.2 Code provisions for punching shear 53
3.2.1 ACI 318-14 (2014) 53
3.2.2 Eurocode 2 (2004) 55
3.3 Non-code design guidelines for punching shear 56
3.3.1 ACI 544.6R-15 (2015) 56
3.3.2 TR 34 by Concrete Society (2015) 58
3.3.3 Model Code 2010 59
3.4 Analysis methods 61
3.4.1 Direct design method 61
3.4.2 Equivalent frame method 63

3.4.3 Yield line theory (limit analysis) 64
3.4.3.1 Background and limitations 64
3.4.3.2 Calculation of the ultimate load using yield line analysis 66
3.4.3.3 Ultimate moment capacity of RC and FRC slabs 69

3.5 Summary 71

4 **Chapter 4** • • • • • • • • • 72
EXPERIMENTAL PROGRAMME 72

4.1 Introduction 72
4.1.1 Objectives of high strength concrete (HSC) slab tests 73
4.1.2 Objectives of Steel fibre reinforced concrete (SFRC) slab tests 74

4.2 Specimen Details and Material Properties 75
4.2.1 Details of 12 HSC Slabs 75
4.2.2 Details of 10 SFRC Slabs 78
4.2.3 Material properties 79
4.2.3.1 Steel fibre properties 79
4.2.3.2 Reinforcing steel properties 79
4.2.3.3 Concrete properties 81

4.3 Specimen Preparations and Test Setup 84
4.3.1 Castings of specimens 84
4.3.2 Test setup 85

4.4 Instrumentation 87
4.4.1 Steel strain gauges 87
4.4.2 Transducers (LVDTs) 88
4.4.3 Test and post-test procedure 89

4.5 Summary 91

5 **Chapter 5** • • • • • • • • • 92
HSC SPECIMENS – RESULTS AND DISCUSSIONS 92

5.1 Introduction 92

5.2 Experimental results 92
5.2.1 Failure loads and failure modes 92
5.2.2 Crack Patterns and Characteristics 93

5.2.2.1 Crack patterns 93
5.2.2.2 Crack characteristics 96
5.2.3 Deflections 97
5.2.4 Strains in flexural reinforcements 99
5.3 Discussions 102
5.3.1 Comparisons of design equations with test results 102
5.3.1.1 Performance of ACI 318-14: 103
5.3.1.2 Performance of Eurocode 2: 103
5.3.1.3 Performance of yield line theory: 104
5.3.2 Influence of the reinforcement ratio 105
5.3.3 Influence of the column rectangularity 106
5.3.4 Influences of the high strength concrete 107
5.4 Summary 109
6 **Chapter 6** • • • • • • • • • 110
SFRC SPECIMENS – RESULTS AND DISCUSSIONS 110
6.1 Introduction 110
6.2 Experimental results 110
6.2.1 Crack patterns and Characteristics 110
6.2.1.1 Crack patterns and propagations 110
6.2.1.2 Shear crack inclinations 112
6.2.2 Ultimate failure loads and failure modes 113
6.2.2.1 Ultimate failure loads 113
6.2.2.2 Failure modes 114
6.2.3 Load-Deflection curves 115
6.2.4 Energy absorptions 116
6.2.5 Strains in flexural reinforcements 117
6.3 Discussions 119
6.3.1 Influence of SFRC using double hooked fibres 119
6.3.1.1 On crack and serviceability behaviours 119
6.3.1.2 On ultimate failure load and comparison with other slabs using single hooked-end fibres 119
6.3.1.3 On post-punching behaviour 121
6.3.1.4 On ductility and energy absorption 121

6.3.2 Comparisons of design methods with test results 122
6.3.2.1 Performance of yield line theory: 122
6.3.2.2 Performance of TR34: 123
6.3.2.3 Performance of Model Code 2010: 123
6.3.2.4 Summary of comparisons 124
6.4 Summary 125
7 **Chapter 7** • • • • • • • • • 126
PROPOSED SHEAR DESIGN METHOD FOR REINFORCED CONCRETE SLABS 126
7.1 Introduction 126
7.2 Derivation of the proposed equation 126
7.2.1 Factor for low reinforcement ratio, k_{RR} 126
7.2.2 Factors for size effect and column rectangularity ratio 130
7.2.3 The Proposed Equation 132
7.3 Comparison with experimental results 133
7.3.1 Comparison with author's 12 new HSC slab specimens 133
7.3.2 Comparison with Slab Database of 367 specimens 136
7.3.2.1 Influence of reinforcement ratio 137
7.3.2.2 Influence of effective depth 138
7.3.2.3 Influence of compressive strength of concrete 138
7.3.2.4 Other parameters, failure modes, and summary 139
7.4 Summary 144
8 **Chapter 8** • • • • • • • • • 145
PROPOSED SHEAR DESIGN METHOD FOR STEEL FIBRE REINFORCED CONCRETE SLABS 145
8.1 Introduction 145
8.2 Proposed Standard FRC method 147
8.2.1 Main assumptions and limitations 147
8.2.2 Derivation 148
8.2.3 Summary 155
8.3 Proposed General method 156

8.3.1 Fibre orientation factor 157
8.3.2 Effective fibre length factor 157
8.3.3 Fibre-matrix bond strength 157
8.3.4 Ultimate punching shear strength formula 158
8.3.5 Summary 163
8.4 Comparison with experimental results 164
8.4.1 Comparison of design methods with author's 10 new SFRC slabs 165
8.4.2 Validation of the proposed standard FRC method with other data 167
8.4.3 Comparison of design methods with existing data from Database 169
8.4.3.1 Influence of fibre volume fractions 170
8.4.3.2 Influence of reinforcement ratios 171
8.4.3.3 Influence of fibre types 172
8.4.3.4 Concrete strength, failure modes, and summary 173
8.5 Summary 178
9 **Chapter 9** • • • • • • • • • 179
GENERAL CONCLUSIONS 179
9.1 Conclusions 179
9.2 Final remarks and contributions 182
9.3 Suggestions for future works 183
References 184

Appendix A
EXPERIMENTAL PHOTOGRAPHS
A.1 Specimen preparation photos A-1
A.2 Post-test photographs A-5
A.3 Time-lapse photograph during testing A-11

Appendix B
EXPERIMENTAL DATA
B.1 Crack-width measurements B-1
B.2 Strain gauge data for 12 HSC slab specimens B-3
B.3 Strain gauge data for 10 SFRC slab specimens B-25
B.4 LVDT (Deflection) data for 12 HSC slab specimens B-46
B.5 LVDT (Deflection) data for 10 SFRC slab specimens B-55

Appendix C
ANALAYSIS AND DERIVATIONS
C.1 Design procedure for ACI direct design method C-1
C.2 Derivations of flexural strength (Shear load) V_{flex} using Yield line analysis C-3

Appendix D
MS-EXCEL SUB-ROUTINE FOR DESIGN METHODS AND ANALYSIS D1-D14

Appendix E
SLAB DATABASE
E.1 Property and analysis results of 367 RC slab specimens E-1
E.2 Property and analysis results of 148 SFRC slab specimens E-16

List of Tables

CHAPTER 4

Table 4. 1 – Properties of 12 HSC slab specimens 76

Table 4. 2 – Properties of 10 SFRC slabs 78

Table 4. 3 – Properties of steel reinforcement 80

Table 4. 4 – Concrete mix design for HSC slab specimens 80

Table 4. 5 – Mechanical properties of concrete specimens 82

CHAPTER 5

Table 5. 1 – Failure loads and failure mode of the 12 specimens 93

Table 5. 2 – Comparisons of code equations with experimental results 102

Table 5. 3 – Comparisons of current test results with data from Teng et al. (2004 108

CHAPTER 6

Table 6. 1 – Experimental results of SFRC specimens 114

Table 6. 2 – Comparisons of design methods with experimental results 124

CHAPTER 7

Table 7. 1 – Comparison of design methods with current test results of 12 HSC slabs 135

Table 7. 2 – Comparison of experimental and calculated failure load by all methods 143

CHAPTER 8

Table 8. 1 – Values of bond factor for different types of steel fibres 164

Table 8. 2 – Comparison of design methods with the SFRC slab specimens 166

Table 8. 3 – Comparison of design methods with results of 16 slabs that have their residual flexural tensile strength available 168

Table 8. 4 – Comparison of experimental and calculated failure load by all methods 176

List of Figures

CHAPTER 1

Fig.1. 1 – Two-way slab floor system: (a) Flat slab with drop-down panels and column capitals, (b) Flat plate 2

Fig.1. 2 – Typical load-deflection curves for slabs with various reinforcement ratios (ρ). 4

Fig.1. 3 – Double hooked-end steel fibres in single and bundle forms (Bekaert). 8

CHAPTER 2

Fig.2. 1 – Turner "mushroom" slab system [source: Gasparini (2002)] 14

Fig.2. 2 – (a) Size effect law, (b) Effect of size in the author 'database 22

Fig.2. 3 – Relationship between normalised shear strength and span-depth ratio (taken from Lovrovich and Mclean 1990) 23

Fig.2. 4 – Relationship between normalised shear strength and column-to-depth ratio. note the data is from Vanderbilt (1971). 24

Fig.2. 5 – Different steel fibre types (Soroushian and Bayasi 1991) 26

Fig.2. 6 – RILEM's flexural strength model (taken from RILEM (2003)) 38

Fig.2. 7 – (a) Stress distribution at the middle section of the notched beam without consideration of crack openings; (b) Idealised stress distribution at the middle section of the notched beam for various depths of crack openings. (taken from RILEM (2003)) 38

Fig.2. 8 – Compression zone and fibre shear resistance contributions along failure surface (Theodorakopoulos and Swamy 1999) 41

Fig.2. 9 – (a) Bond strength of the fibre-matrix interface for various types and shapes of steel fibres [taken from Lim, Paramasivam, and Lee (1987)]; (b) Composite element under uniaxial stress [taken from Lim, Paramasivam, and Lee (1987)] 43

Fig.2. 10 – Shear component due to the presence of fibres in SFRC beam [taken from Foster (2008)] 47

CHAPTER 3

Fig.3. 1 – (a) Value of β for nonrectangular columns; (b) Critical sections of circular column and rectangular columns 55

Fig.3. 2 – Typical basic control perimeters. note by and bz are the lengths of the long side and the short side of the critical perimeter, respectively (taken from Eurocode 2 (2004)) 56

Fig.3. 3 – (a) Idealised strain-softening frc models for: (left) tension; and (right) compression). (b) A simply supported round slab and its corresponding circular fan yield line pattern. (taken from ACI 544.6r-15) 57

Fig.3. 4 – Example of the load-cmod response curves (EN 14651 2008) 58

Fig.3. 5 – Constitutive laws of fibre reinforced concrete 60

Fig.3. 6 – Flat plate floor plan showing column strips and middle strips in both directions 62

Fig.3. 7 – Definition of equivalent frame (ACI 318-14) 64

Fig.3. 8 – Examples of yield line patterns (Mcgregor and Wright 2005) 65

Fig.3. 9 – (a) Yield line pattern a ductile slab loaded around the edges; (b) Yield line pattern for a simply supported ductile slab; (c) Circular fan yield line pattern 68

Fig.3. 10 – Design assumptions for analysis of singly reinforced concrete beams containing steel fibres (Henager and Doherty, 1976) 71

CHAPTER 4

Fig.4. 1 – Idealised test specimen in flat plate structure 73

Fig.4. 2 – Flexural reinforcement ratios for a typical column strip of a slab in a flat plate building with various column spans and applied loading 74

Fig.4. 3 – General dimensions and loading positions of the hsc slab specimens. note the SFRC slabs have the same dimensions as S11 series slabs 77

Fig.4. 4 – Top reinforcement details of the HSC slab specimens. note F09 series and F14 series slabs have the same details as S11-090 and S11-139, respectively 77

Fig.4. 5 – **(**a) Double hooked-end steel fibre and its geometric properties. (b) Single (normal) hooked-end steel fibre 79

Fig.4. 6 – Stress-strain curves of steel bar specimens 80

Fig.4. 7 – Photograph from the notched beam test according to EN 14651:2007 82
Fig.4. 8 – Flexural tensile stress - cmod curves of (a) The current SFRC specimens for V_f = 0.3%, 0.6%, 0.9% and 1.2%; (b) The SFRC specimen (using single hooked fibres) obtained from Teng et al. (2015) 833
Fig.4. 9 – (a) Photographs taken during casting of SFRC slab specimens; (b) Photographs of some shrinkage cracks in SFRC slab specimens. 85
Fig.4. 10 – (a) Schematic drawings of test setup details; (b) Photographs of the in-progress sequences of test setup of a slab specimen. note Fig. 4.10(b) is placed in the next page. 86
Fig.4. 11 – (a) Typical locations of steel strain gauges in the tension reinforcements; (b) Typical positions of LVDTs 88
Fig.4. 12 – Photographs of test setup showing testing equipment and instruments 89

CHAPTER 5

Fig.5. 1 – Photographs of ultimate crack patterns for S11 series slabs. 94
Fig.5. 2 – Photographs of ultimate crack patterns for S13 series slabs. 95
Fig.5. 3 – Photographs of ultimate crack patterns for S15 series slabs. 95
Fig.5. 4 – Development cracks om specimen S11-028 (flexural mode) 97
Fig.5. 5 – Development cracks om specimen S11-028 (punching shear mode) 97
Fig.5. 6 – Load-deflection curves of the 12 slabs (a) S11 series, (b) S13 series, (c) S15 series. 98
Fig.5. 7 – Development of strains in the reinforcements of specimen (a) S11-028, (b) S11-050, (b) S11-090, and (d) S11-139 100
Fig.5. 8 – Steel strains in several reinforcing bars near the columns at failure loads for (a) S11 series slabs, (b) S13 series slabs, (c) S15 series slabs. 101
Fig.5. 9 – Strain developments in reinforcements within the lines of column face and outside lines of columns faces of the slabs (a) S13-143, and (b) S15-143 101
Fig.5. 10 – Performance of ACI 318 equation with respect to column aspect ratio ($\beta = C_1/C_2$) 107

CHAPTER 6

Fig.6. 1 – Ultimate cracks patterns of the F09 series specimens 111

Fig.6. 2 – Ultimate cracks patterns of the F14 series specimens 112

Fig.6. 3 – Punching shear cracks of (a) Specimen F09-00, (b) Specimen F09-12 113

Fig.6. 4 – Load deflection curves of F09 series slabs, (a) Full curves, (b) Early load stage 116

Fig.6. 5 – Load deflection curves of F14 series slabs, (a) Full curves, (b) Early load stage 116

Fig.6. 6 – Engery absorption of the 10 slab specimens 117

Fig.6. 7 – Strain profiles of F09 series slabs, (a) Strain locations at 50 mm from a line of column face, (b)) Strain locations at 170 mm from a line of column face 118

Fig.6. 8 – Strain profiles of F14 series slabs, (a) Strain locations at 50 mm from a line of column face, (b)) Strain locations at 170 mm from a line of column face 119

Fig.6. 9 – Relationship between the normalized punching shear stress at failure with fibre volume fraction V_f. 121

CHAPTER 7

Fig.7. 1 – Idealized yield line pattern representing transition from punching failure mode to flexural failure mode. 129

Fig.7. 2 – Relationship between V_{exp} and ρ for slabs with low reinforcement ratios. 130

Fig.7. 3 – Performance of the proposed column rectangularity factor K_{cr}. 132

Fig.7. 4– Failure load predictions of 367 test data by ACI 318-14 in term of (a) Reinforcement ratio ρ; (b) Effective depth d; (c) Concrete strength f'_c 140

Fig.7. 5 – Failure load predictions of 367 test data by Eurocode 2 in term of (a) Reinforcement ratio ρ; (b) Effective depth d; (c) Concrete strength f'_c 140

Fig.7. 6 – Failure load predictions of 367 test data by CSCT in term of (a) Reinforcement ratio ρ; (b) Effective depth d; (c) Concrete strength f'_c 141

Fig.7. 7 – Failure load predictions of 367 test data by Peiris-Ghali's method in term of (a) Reinforcement ratio ρ; (b) Effective depth d; (c) Concrete strength f'c 141

Fig.7. 8 – Failure load predictions of 367 test data by proposed standard method in terms of (a) Reinforcement ratio ρ; (b) Effective depth d; (c) Concrete strength f'_c 142

CHAPTER 8

Fig.8. 1 – (a) Force diagram in the punching shear model of a fibre reinforced concrete slab; (b) Schematic model showing the crack-width opening increases linearly. 149

Fig.8. 2 – Stress (linear) distribution along the plane of inclined shear cracks for (a) Case 1: post-crack strain-softening behaviour; (b) Case 2: post-crack strain-hardening behaviour. 149

Fig.8. 3 – Schematic model of the notched beam (EN 14651,2007) 153

Fig.8. 4 – Idealised stress distribution at the middle section of the notched beam for (a) CMOD = 0.5 mm; (b) CMOD = 3.5 mm. [modified from Fig. 2.7 (RILEM (2003))] 153

Fig.8. 5 – Relationship between vexp and ρ for SFRC slabs with low reinforcement ratios 160

Fig.8. 6 – Failure load predictions of 148 test data by the Narayanan and Darwish method in term of (a) Fibre volume fraction V_f; (b) Reinforcement ratio ρ 174

Fig.8. 7 – Failure load predictions of 148 test data by the Shaaban and Gesund method in term of (a) Fibre volume fraction vf; (b) Reinforcement ratio ρ 174

Fig.8. 8 – Failure load predictions of 148 test data by the Hagashiyama et al 174

Fig.8. 9 – Failure load predictions of 148 test data by the CSCT+VEM method in term of (a) Fibre volume fraction Vf; (b) Feinforcement ratio ρ 175

Fig.8. 10 – Failure load predictions of 148 test data by the proposed (standard) general method in term of (a) Fibre volume fractionVf; (b) Reinforcement ratio ρ 175

Fig.8. 11 – Performances with respect to concrete strength of (a) The Narayanan and Darwish method; (b) The Shaaban and Gesund method; (c) The Hagashiyama et al. method; (d) The CSCT+VEM method; and (e) The proposed (standard) general method. 177

Notations

Greek symbols

α = average shear crack angle [in Eq. (8.16)]

α_o = geometric coefficient for the strength of a slab calculated using yield line analysis ($V_{flex} = \alpha_o m$)

α_s = ACI 318's coefficient that accounts for the interior, edge and corner columns

β = ratio of long to short sides of the column

β_c = proposed ratio of the depth of compression zone to effective depth

ψ = rotation of a slab

ρ = average reinforcement ratio

ρ_x = reinforcement ratio $100A_s/(L \times d)$ in the x-direction

ρ_y = reinforcement ratio $100A_s/(L \times d)$ in the y-direction

ρ_{fs} = limiting reinforcement ratio

σ_{cu1} = tensile strength at the tip of the inclined shear crack

σ_{cu2} = tensile strength at the opening of the inclined shear crack

σ_{f1} = equivalent tensile stress ($= 0.45 f_{r1}$)

σ_{f2} = equivalent tensile stress ($= 0.37 f_{r4}$)

τ_{fb} = basic bond strength of fibre-matrix interface (= 5.5 N/mm^2)

Alphabetic symbols

A_f = equivalent projection of the failure cone surface

A_s = Total cross-sectional area of flexural reinforcement within a slab length L

b_o = critical perimeter (used in ACI 318, CSCT, Peiris-Ghali, and authors' proposed Method)

b_1 = length of the longer side of critical perimeter b_o

b_2 = length of the shorter side of critical perimeter b_o

c_1 = length of the longer side of the column

c_2 = length of the shorter side of the column

D_f = fibre diameter

d = average effective depth

d_g = maximum aggregate size (used in CSCT)

d_{go} = reference aggregate size (= 16 mm)

E_s = elastic modulus of concrete

E_s = elastic modulus of steel reinforcement

f_c' = cylinder compressive strength of concrete

$f_{r1}, f_{r2}, f_{r3}, f_{r4}$ = residual tensile strength corresponding with CMOD = 0, 1.5, 2.5, 3.5, respectively

f_y = yield strength of flexural reinforcement

h = slab thickness

k = Eurocode 2's size effect factor

k_{CR} = column rectangularity factor (used in authors' proposed method)

k_{RR} = low reinforcement ratio factor (used in authors' proposed method)

k_{SZ} = size effect factor (used in the authors' proposed method)

k_E = stiffness factor for bi-axial compression in the compression zone

L_1 = length of the longer edge of the slab

L_2 = length of the shorter edge of the slab

L_f = fibre length

m_u = ultimate moment capacity per unit width

n_{fo} = fibre orientation factor (=0.41)

n_{fl} = fibre effective length factor

n_{fb} = fibre-matrix bond factor

n_S = reduction factor for the proposed FRC method (= 0.41)

r = radius of a slab, taken as $0.2L$ where L is column-to-column span

r_s = radius of a slab used in CSCT, take as $0.22L$ where L is column-to-column span

u = critical perimeter used in Eurocode 2 method

V = Shear load of a slab

v_c, V_c = punching shear strength of a RC slab (N/mm^2, N)

V_{calc} = calculated strength of a slab

V_{exp} = failure load (experimental) of a slab

V_f = fibre volume fraction

V_{flex} = shear force that will cause flexural failure of the slab calculated using yield line analysis

V_{Rd} = punching shear strength (defined by Eurocode 2 and CSCT)

v_f, V_{Rf} = shear strength component due to the presence of fibres (N/mm^2, N)

v_u, V_u = ultimate punching shear strength of an SFRC slab (N/mm^2, N)

z_c = depth of the compression zone

Acronyms

ACI = American Concrete Institute

CMOD = crack mouth opening displacement as defined in EN 14651 (2007)

COV = coefficient of variation

CSCT = critical shear crack theory

VEM = variable engagement model

EC2 = Eurocode 2

FRC = fibre reinforced concrete

HSC = high strength concrete

LVDT = linear variable differential transformers

NSC = normal strength cocnrete

RC = reinforced concrete

SFRC = steel fibre reinforced concrete

TR 34 = Technical Report 34

1

INTRODUCTION

Flat slabs and flat plates are two common forms of beamless floor systems. A flat slab, as shown in Fig. 1.1(a), is a concrete slab supported directly on columns and walls with the presence of drop-down panels and (with or without) column capitals. On the other hand, a flat plate is a slab with a constant thickness throughout the entire floor as shown in Fig. 1.1(b). Flat slabs are used when the structure has large span (i.e. greater than 6 m) and is required to carry heavy floor loads. A drop-down panel (a thicker slab section) in a flat slab is intended to resist shear force that exceeds the punching shear capacity of a flat plate. Essentially, both flat slabs and flat plates have the same design considerations. This research concerns the punching shear design of flat plates which is directly applicable to flat slabs.

A flat plate floor system is an economical choice for buildings such as condominiums, apartments, hotels and multi-storey offices where spans are relatively small (i.e. less than or equal to 6 m). Flat plates can improve construction productivity and save costs because they require much simpler formworks, simpler detailing of reinforcements, and faster construction time. A flat plate structure allows the floor-to-floor height to be shorter while maintaining the required ceiling height; thus, the building height, weight, and overall cost can be reduced substantially. A flat plate system can also accommodate demands of modern architecture very well, the system allows designers the flexibility in designing irregular floor plans where walls and columns are often seen flush together in non-uniform layouts.

Punching shear failure is one of the critical failure modes that can happen in a flat plate floor system. Punching shear failure is known to occur abruptly with little warnings. Progressive collapse of a flat-plate structure can be triggered by punching shear failure, several tragically collasped buildings that were primilary caused by punching shear failure have been reported, such as the 2000 Commonwealth

Avenue building in 1971(King and Delatte 2004), Skyline Plaza Complex in 1973(Perkins 2009), Harbour Cay Condominium in 1981(Kukorlo 2009), and Sampoong Department Store in 1995(NEMA 2004). There might be more events of structural failures due to punching shear failure that are not documented in this thesis.

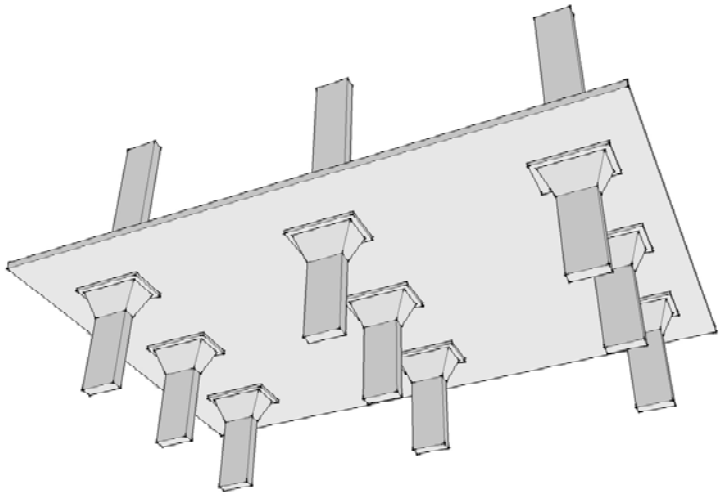

(a)

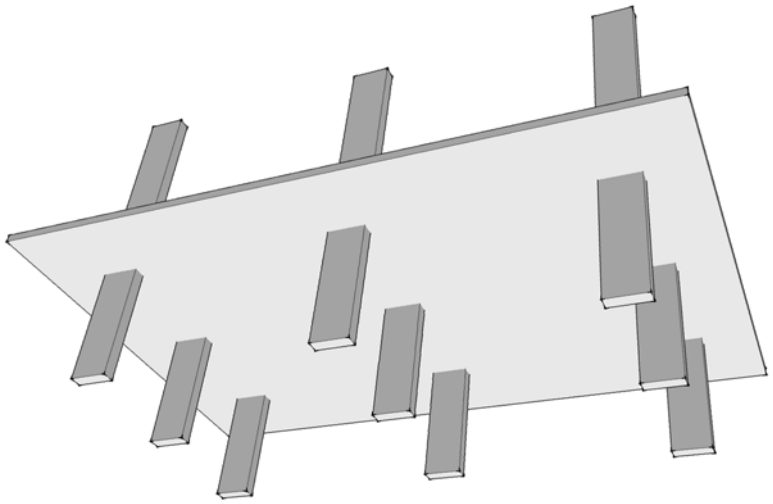

(b)

Fig.1. 1 – Two-way slab floor system: (a) flat slab with drop-down panels and column capitals, (b) flat plate

1.1 Background of the research

This research emphasises on punching shear strength of *high strength reinforced* and *steel fibre reinforced concrete* slabs. The overview and background of the research are described as follows.

1.1.1 High strength reinforced concrete slabs and effect of low reinforcement ratios

Some of the important design parameters that influence the punching shear strength of concrete slabs include geometrical properties of the slabs, concrete strength, amount of flexural reinforcement, column rectangularity (aspect) ratio, as well as size (thickness) effect. Influences of various structural parameters will be discussed in Section 2.3 of this thesis.

One parameter that has not been sufficiently investigated in the past is the influence of flexural reinforcement ratio ρ (=A_s/bd), especially low flexural reinforcement ratio. Consider four cases of slabs with very low, low, medium, and high flexural reinforcement ratios; their load-deflection curves are shown in Fig. 1.2.

Case 1: If the reinforcement ratio ρ is very low (ρ smaller than 0.3%), typical failure will be flexure with widespread yielding of almost all of the flexural reinforcement. Shown in Fig. 1.2, further loading beyond the peak load will only lead to an increase in deflection until final failure occurs. In this case, the final failure would still look like a punching failure with a punching shear perimeter that is very close to the column. The maximum load that can be carried by this slab is not more than the peak load that causes yielding of the flexural reinforcement.

Case 2: If the reinforcement ratio is in the low range (ρ about 0.3% to 0.6%), the slab will fail in flexure first before punching shear failure. Many of the flexural reinforcing bars, especially those near the column will yield. The peak load in the load-deflection curve will be higher than Case 1 and the curve will remain flat for a short segment, indicating flexural yielding, before it drops suddenly in the end in the form of punching failure. The slab is less ductile compared to Case 1.

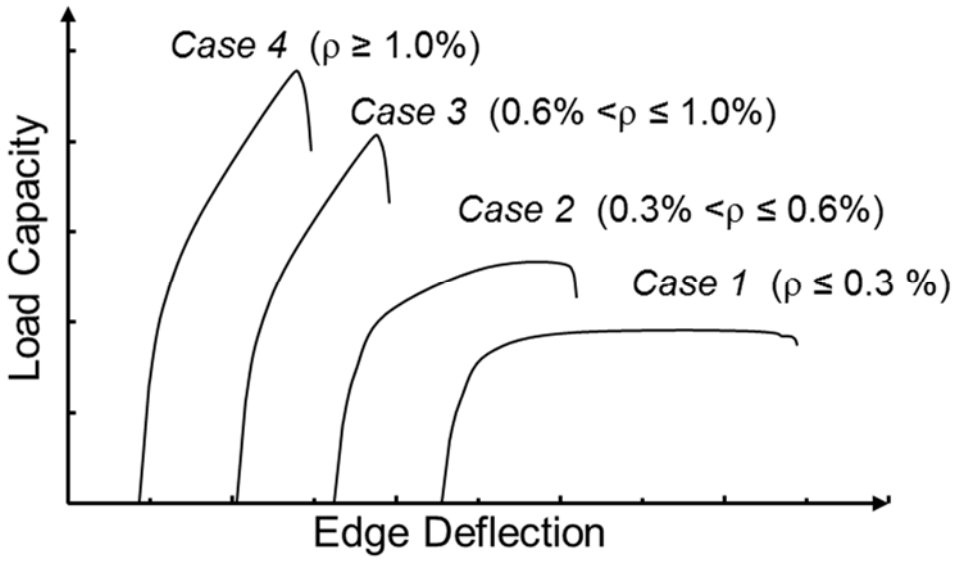

Note: the load-deflection curves shown in the chart are obtained and modified from the author's experimental results which are presented in Chapter 5.

Fig.1. 2 – Typical load-deflection curves for slabs with various reinforcement ratios (ρ).

Case 3: If the reinforcement ratio is in the medium range (ρ about 0.6% to 1%), the failure mode of a slab is most likely to be punching with only a few of the flexural reinforcements reaching yield. As can be seen in Fig. 1.2, the load-deflection curve of the slab is essentially a bilinear curve until it reaches the peak and then it drops suddenly, indicating a brittle shear failure. Due to the increase of the amount of reinforcement, the peak load is also higher than Cases 1 and 2.

Case 4: If the reinforcement ratio is in the high range (ρ about 1% or higher), the slab will fail in pure punching mode, and none or very few of the flexural reinforcements will yield and those bars are limited to locations next to the column. The peak load is higher than the other cases and the failure is brittle.

So far, Cases 3 and 4 have been considered as the typical case for reinforced concrete slabs. Building codes, such the ACI 318-14 (2014), has punching shear formulas that turn out to be applicable mainly to Cases 3 and 4 (medium to high reinforcement ratio ρ). However, Cases 1 and 2 are also common in practice, especially in lightly loaded flat plates for residential or office buildings. A typical procedure used in design practice to ensure safety of the overall slab is to make sure that the flexural strength of the slab is lower than its punching shear strength. The

Code equations can be modified so that they become safely applied to all cases. Recently, Guandalini, Burdet, and Muttoni (2009), Peiris and Ghali (2011), and Widianto, Bayrak, and Jirsa (2009) attempted to address this issue by testing some lightly reinforced concrete slabs or by suggesting a practical step for design. However, more data and analysis are needed to investigate this effect further.

The use of rectangular or elongated columns is very common nowadays, especially in high-rise residential buildings. In these buildings, elongated column sections are employed to ensure that the columns are flush with the walls. It is known that under a uniform loading the distribution of stresses around the four sides of a square column are more uniform compared to those around the four sides of a rectangular column. The middle portions of the longer sides of a rectangular column are stressed less, indicating that they are less effective in carrying punching load. This means that the length of the critical perimeter b_o around a rectangular column is not entirely effective. This issue will also be addressed in this paper.

This study aims to develop a new method for calculating the shear strength of concrete slabs under punching loads that is applicable to all four cases above. Therefore, the current punching shear tests of 12 high strength concrete slabs with varying flexural reinforcement ratios and varying column aspect (rectangularity) ratio will be used together with other existing data to discuss the influence of reinforcement ratios and to derive a new design method.

Note that the concrete specimens used in the test programme had compressive strength f'_c that ranged between 95 to 115 MPa. Some of the advantages of using high strength concrete compared to normal strength concrete include an increase in cracking load of the slab and a reduction in the deflection at service load level due to higher tensile strength and higher elastic modulus of high strength concrete.

1.1.2 Steel fibre reinforced concrete slabs and influences of double hooked steel fibres

The use of SFRC can effectively solve critical design issues concerning the ultimate performance (i.e. punching shear strength) and serviceability (i.e. deflections and cracks). Some of the advantages of SFRC over the conventional reinforced concrete (RC) slabs (ACI 544.3R-08, 2008; ACI 544.4R, 1988 (Reapproved 2009); ACI 544.6R-15, 2015; The Concrete Society, 2015; Chandler and Neal, 1988; Henager, 1977; Victor Li, 2002; Mobasher and Destree, 2010) are: (1) Faster construction times and lower labour costs due to the time saved from detailing works of reinforcement (in actual projects, SFRC has already been used to partially or entirely replace the conventional steel bars for both flexural and shear reinforcements). (2) lower risks of durability problems because SFRC can prevent and control cracks. (3) better strength, ductility, and energy absorption due to the post-crack behaviours of SFRC.

Although SFRC has been widely used in practices in the past decades, the development of standard design procedures is still insufficient. Major building codes such as ACI 318-14 (2014) and Eurocode 2 (2004) have yet to implement any design provisions for SFRC structures. Nevertheless, there are available code-like design guidelines and recommendations for design and analysis of SFRC slabs such as the ACI 544.6R (2015), the Technical Report 34 (TR 34) by the UK's Concrete Society (2015), and the Model Code 2010 (fib bulletin 65-66, 2012).

The main functions of fibres are to bridge and resist crack openings through pull-out mechanism (Romualdi and Mandel, 1964; Swamy and Mangat, 1974; Blunt and Ostertag, 2009). This post-crack characteristic of SFRC allows the presence of tensile stresses and concrete tensile strains along the crack openings, which are omitted in the analysis of conventional RC elements. Therefore, theoretically, the post-crack tensile strength of SFRC enhances the ultimate strength of a concrete section, be it shear strength or flexural strength. Observations from past experiments (Swamy and Ali, 1982; Narayanan and Darwish, 1987; Shaaban and Gesund, 1994; Theodorakopoulos and Swamy, 1993; Alexander and Simmonds, 1992; Harajli et al. 1995; Higashiyama et al. 2011; Gouveia et al. 2014) show that the

addition of single hooked end steel fibres can increase th punching shear strength of by 40- 65% compared to a non-fibrous slab, depending on the types and volume fraction of fibres. Analytically, it has been known (RILEM, 2003) that the increase in shear and flexural strengths due to the inclusion of steel fibres scales with the concrete residual tensile strengths, where these residual tensile strengths can be obtained from the notched beam test EN 14651 (2007). Both of the ultimate punching shear and flexural strengths can also be reasonably correlated with several parameters such as fibre volume fraction, fibre shapes, fibre aspect ratio (a ratio of fibre length to diameter), and others. Therefore, these parameters, such as: fibre volume fraction V_f and fibre aspect ratio (D_f/L_f), have become basic variables in most of existing design methods for SFRC structural elements. Several researchers (Maya et al., 2012; Theodorakopoulos and Swamy, 2003) also attempted to develop analytical models for predicting the punching shear strength of SFRC slabs based on experimental observations. Therefore, to ensure reliable and safe design procedures, wider ranges of practical SFRC slab data are still needed for verifying the existing methods, as well as for supporting the on-going development of new approaches.

This thesis presents the punching shear tests of 10 high strength SFRC slabs with varying flexural reinforcement ratios and varying fibre volume up to 1.2%. The author investigated a new type of steel fibres (the double hooked-end steel fibre (BEKAERT) shown in Fig. 1.3. The concrete specimens used in the test program had concrete strengths f'_c that ranged between 80 to 100 MPa. The experimental results are then used to verify the applicability of the yield line theory (Johansen, 1962), the Model Code 2010 method (fib bulletin 65-66, 2012), the TR 34 method (The Concrete Society, 2015) as well as other design methods.

Therefore, this research will show that the use of double hooked-end fibres can improve the overall structural performances of HSC slabs. New design approaches that can accurately predict the punching shear strength of SFRC slabs will be developed based on experimental and theoretical basis.

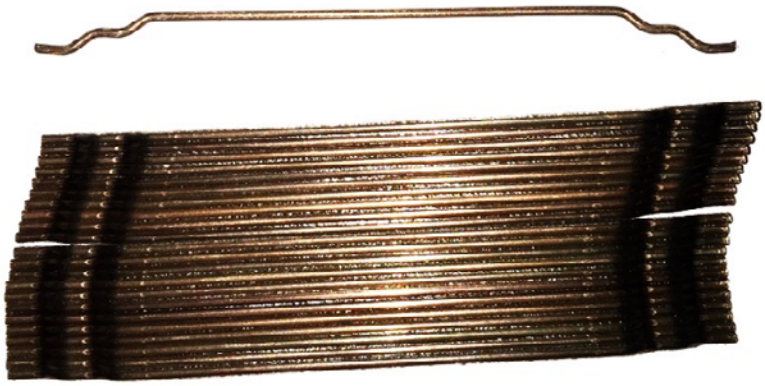

Fig.1. 3 – Double hooked-end steel fibres in single and bundle forms (BEKAERT).

1.2 Objectives and scope of the research

1.2.1 Main objectives

- To investigate the influence of flexural reinforcement ratios on the punching shear strength of slabs, especially when the reinforcement ratio is low.
- To investigate and further confirm the effects of the column rectangularity on the punching shear strength of slabs.
- To provide additional test data for validating the author's proposed design method, and for verifying the applicability of existing design codes such as ACI 318, Eurocode 2 and as well as other available design methods.
- To investigate the influence of SFRC and double-hooked end steel fibres on the structural performances of HSC slabs such as cracking behaviours, failure behaviours and the emphasis is on the punching shear strength.
- To provide a new set of SFRC slab data for validating the author's proposed methods, and for evaluating the existing standard guidelines such as Model Code 2010, TR 34, and also other available design methods.
- To develop and propose a new and reliable design method for a reinforced concrete slab, in which the effect of low reinforcement ratio can be considered.

- To develop and propose a new method for calculating punching shear strength of a steel fibre reinforced concrete slab that is applicable for various types of fibres and especially for the new type of fibre, the double-hooked fibres.
- Based on the test results, to recommend design considerations for both HSC and SFRC slabs subjected to concentric punching loads.

1.2.2 Scope of work

Current research work is limited to punching shear strength and behaviours of *interior* RC and SFRC slabs without shear (transverse) reinforcement that are subjected to concentric punching loads. In these two sets of experimental programmes, 22 slab specimens were tested to failure by gravity loads through the applied forces from hydraulic jacks to simulate interior slab-column connections. The static tests of interior slab-column connections can provide fundamental information towards the understanding and development of different structural mechanisms under specific influences of parameters.

The effects of size, shear reinforcement, unbalanced moment transfer, prestressing force, cyclic loading, edge, and corner slab-column connections are outside the scope of current work. Punching shear test of fibre reinforced concrete slabs without flexural reinforcements is outside the scope of this research. Numerical works such the finite element model and analysis are excluded in this thesis.

1.3 Research significance

Twelve high strength concrete slabs with various flexural reinforcement ratios and column aspect ratios were tested under punching shear. These new experimental data together with existing data from the literature were then used to verify the accuracy of existing methods for designing against punching shear, such as those of the ACI Code, Eurocode 2, and several researchers. It is found that most of those methods including the ACI method can be unconservative for slabs with low flexural reinforcement ratios.

Experimental data of new SFRC slabs are also presented. A new type of high-performance steel fibres, i.e. double hooked-end steel fibres, was used and investigated. The results are discussed in details and used to verify the applicability of the yield line theory, the Model Code 2010(fib bulletin 65-66, 2012) method, the UK's Concrete Society TR 34 (2015) method and also other design methods proposed by various researchers.

The author believes that this study provides an important set of data and new discussions for on-going development of SFRC as well as HSC slabs. New design methods are proposed in this work, and it is found to be reliable and accurate for calculating the punching shear strength of both reinforced concrete and steel fibre reinforced concrete slabs.

1.4 Thesis organisation

The thesis has nine chapters with several appendices as described below.

Chapter 2 covers the review of current knowledge, past and present research of punching shear in reinforced concrete and steel fibre reinforced concrete slabs. Specific review of the literature that are relevant to the current works is also presented in this chapter. **Chapter 3** presents the review of design codes, code-like design guidelines and as well as some design and analysis methods for flat plates that will be evaluated and verified with the current results and other published data.

Chapter 4 provides the details of the experimental programmes such as the design, detailing and casting process of the slab specimens, the test-set up, the instrumentation, the test and post-test procedure. Test results of material properties (concrete and steel reinforcements) are reported in this chapter. **Chapter** 5 presents the results and discussions of the 12 HSC slab specimens. Influences of reinforcement ratios and column rectangularity are highlighted. Performances of Code methods are compared with the results. **Chapter 6** presents the results and discussions of the 10 SFRC slabs. Influences of steel fibre reinforced concrete using double hooked fibres are discussed. Performances of relevant design methods as well as the yield line theory are compared with the results.

Chapter 7 presents the development of a new proposed punching shear strength equation for reinforced concrete slabs. The proposed method is validated

with current test results and compared with other design methods. **Chapter 8** has a similar framework as Chapter 7, and new approaches for calculating punching shear strength for slab with fibres are presented.

Chapter 9 summarises all the key conclusions of this thesis. Final remarks and contributions of the current works are highlighted, suggestions for future works are provided. Photographs from experiments, complete test data, derivations of equations, excel VBA codes, and Database of 515 slab data from the current works and collected from the literature are provided in **Appendices.**

2

LITERATURE REVIEW

2.1 Introduction

This chapter presents a summary of past research developments on punching shear in both reinforced concrete and fibre reinforced concrete slabs. History of early applications and research of beamless two-way slab floor systems are briefly reviewed in Section 2.2.

In Section 2.3, past studies and general knowledge on the influences of various parameters on the shear strength of slabs are covered. Some relevant existing data are also analysed to accompany the discussions. This section highlights some important research areas that have influenced the development of design code provisions. The section also presents some essential problems regarding punching shear design which have been partially addressed but further research is still needed, essentially they are the main subjects of this study. Thus, potential contributions of the author's current study are emphasised and laid out.

In Section 2.4, existing punching shear models are generalised into different types that represent distinguished design principles and theories. A more focused review of past research works that are directly relevant to the author's current study is presented in Section 2.5. This literature review is limited to the research on punching shear in RC and FRC slabs without transverse shear reinforcement. The research group led by the author's supervisor (Teng et al., 2004; Lee, 2004; Geng, 2004; Teng and Tan, 2005; Anggadjaja and Teng, 2008; Widjaja, 2008, Himawan and Teng, 2014) have previously investigated several structural parameters (using normal strength concrete) such as the presences of opening, pre-tensioning, column rectangularity, and various types of shear reinforcements. Different types of column-slab connections (interior column, edge column and corner columns) under cyclic and eccentric loadings were also tested.

2.2 Brief history of beamless slab systems and the research

2.2.1 Reinforced concrete slabs

Investigations of beamless two-way slabs supported on columns directly have their histories traced back to the early 20th Century. According to the review by Sozen and Siess (1963), Section 13.2 of the textbook by McGregor and Wight (2005, 4th edition), and Gasparini (2002), one of the first flat slab structures was built in a period of 1906 in Minneapolis, Minnesota, USA. The name of the building is Lindeke-Warner Building. The structure of the building was designed by a renowned American structural engineer, Claude Allen Porter (C.A.P) Turner, who had a patent in 1908 for "Mushroom flat-slab system (the Turner system). The Turner's Mushroom flat-slab system has unique column-slab connection and reinforcement detailing as shown in Fig. 2.1, the term "Mushroom" somewhat represents the bulk-out shape of the column dimension near the slab connection.

There was no standard practice or design guideline for the analysis and design of the beamless floor system at the time; the Turner flat slabs were design based on the then-underdeveloped plate analysis theory. Only from 1914, Nichols (1914) initiated the simple static analysis of two-way slab which becomes the current ACI direct design method (discussed in Chapter 3). Ingerslev (1923) first introduced the (limit) analysis method of concrete slabs, called "yield line theory", and Johansen (1962) extended the theory into the more advanced form (discussed in Chapter 3). In 1961, Corley, Sozen and Siess (1961) proposed a more versatile analysis technique for flat slab system, called equivalent frame method (also discussed in Chapter 3). Only until the early 1970s to 1980s, building Codes started to include provisions for analysis and design of flat slabs explicitly.

Research on punching shear in concrete slabs started as early as 1913 by Tabolt (1913) who investigated the punching shear in concrete footings of walls and columns. In 1933, Graff (1933), in Germany, tested slabs under punching loads. In 1956, Elstner and Hognestad (1956) conducted comprehensive test programme to investigate the punching shear strength of reinforced concrete slabs, in which 39

slabs were tested. Since then, punching shear in concrete slabs has gained considerable research attentions and been on-going research topics.

Research on punching shear before the year 1985 were comprehensively summarised in the technical report (CEB-Bulletin 168 1985) by Regan and Braestrup (1985). Similarly, the report Fib-bulletin 12 (2001) presented in-depth discussions on the development of punching shear models up to the year 2001 including databank of concrete slab tested under punching loads. There currently are more than 500 slab data (Both full and small scale) available in the literature comprising of slabs with and without shear reinforcements, openings, prestressing reinforced steels and various steel fibre reinforced concrete (SFRC). The report Fib-bulletin 57 (2010) summarised some research on the shear and punching shear in reinforced concrete (RC) and fibre reinforced concrete (FRC) elements, which influenced the development of Model Code 2010 (2012), especially for the FRC design guidelines sections.

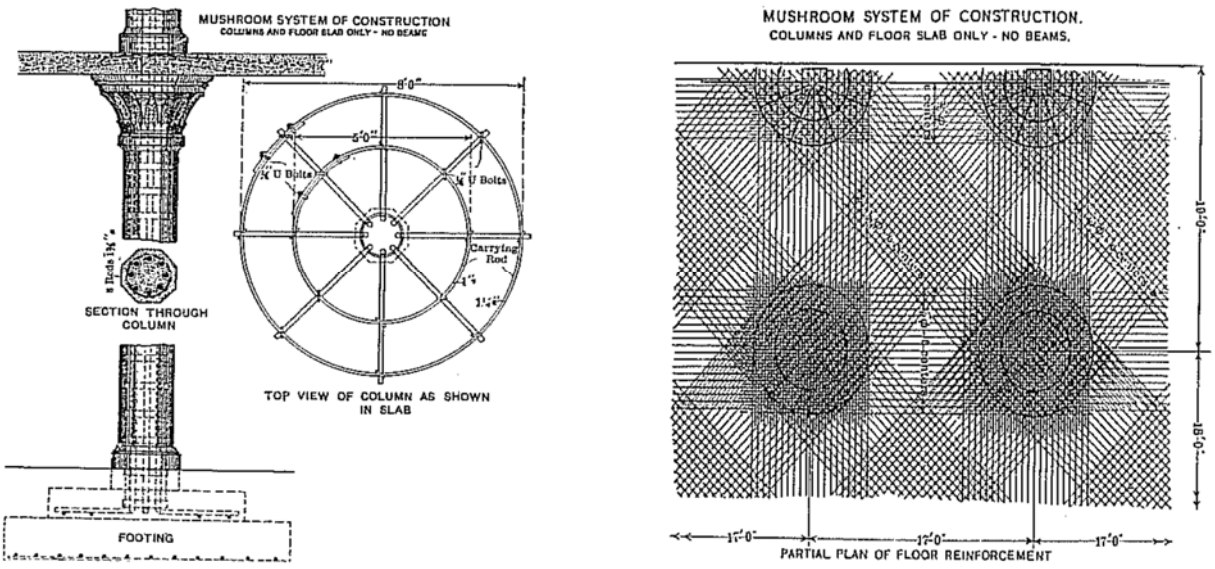

Fig.2. 1 – Turner "Mushroom" slab system [Source: Gasparini (2002)]

2.2.2 Fibre reinforced concrete slabs

First modern applications of fibre reinforced concrete (FRC) may probably start in the early 1960s (Li 2000, ACI 544.6R 2015). However, only after the 1980s, the uses of FRC become more common especially in the slabs-on-ground (ground supported slabs) for heavy industrial buildings such as warehouses, factories, etc. The design of FRC structures at that time was purely based on engineering judgement and structural tests. In 1992, one of the first comprehensive guidelines (Technical Report 34) for design and construction of FRC ground supported slabs were developed in the UK by the Concrete Society (2015). Around the early 2000s, the applications of FRC had been extended to the suspended floor slabs supported on vertical elements such as columns, columns, walls. According to ACI 544.6R (2015), by 2004, there were already more than 10 actual buildings in European countries that used steel fibre reinforced concrete (SFRC) for the floor slabs. Destree and Mandl (2008) reported that there were more than 40 realised projects that used SFRC flat plate or flat slab systems by 2008.

Research on punching shear in SFRC slabs probably started in the late 1970s and the early 1980s. Test data on SFRC slabs are much fewer than the counterpart RC slabs. According to the author's collected database, there are less than 150 (published) verifiable interior SFRC slabs data. The collected 138 SFRC slab specimens in the author's Database are given in Table E.2 in Appendix E, the data was collected from the experiments conducted by Swamy and Ali (1982), Narayanan & Darwish (1987), Alexander & Simmonds (1992), Theodorakopoulos and Swamy (1993), Shaaban and Gesund (1994), Harajli et al. (1994), McHarg et al. (2000), Ozden et al. (2006), De Hahai and Holanda (2008), Cheng and Parra-Montesinos (2010), Higashiyama et al. (2011), Nguyen-Minh et al. (2012), and Gouveia et al (2014).

2.3 Influences of structural parameters on punching shear

2.3.1 Influence of concrete strength

Compressive concrete strength f'_c has been the basic parameter used to calculate many mechanical properties of concrete member including the shear strength. Other mechanical properties of concrete such as tensile strength, flexural strength (Modulus of rupture), and also modulus of elasticity have all been known to be proportional to the concrete strength f'_c. There is no theoretical rule for the relationship between concrete strength f'_c and shear strength v_c. However, in general, the relationship is known to be either

$$v_c \propto \sqrt{f'_c} \qquad \text{or} \qquad v_c \propto \sqrt[3]{f'_c}$$

By and large, it can be related that models or methods that use $\sqrt{f'_c}$ for calculating the shear strength or the punching shear strength are those that do not consider the influence of flexural reinforcement in the shear strength equation directly. Some of these methods are the ACI Code equations, Model Code 2010, modified compression field theory (MCFT) (Vecchio and Collins 1986, Collins et al. 2005), critical shear crack theory (CSCT) by Muttoni (2008), and several others methods.

Thus, methods that use $\sqrt[3]{f'_c}$ in shear strength equations are generally those that consider the influence of both reinforcement ratios and concrete strength all together, i.e. $v_c \propto (\rho f'_c)^{1/3}$. Former and current Codes of European countries such as the old British Code, the current Eurocode 2, and as well as Japanese Code use this relationship in their equations for calculating the shear strength. Other existing design methods as proposed by Gardner (1990), Marzouk and Hussein (1991), Regan el al. (1993), and Teng et al. (2004) also adopted this relationship.

Effect of high strength concrete:

Research on the effect of high strength concrete on the punching shear strength started around the early 1990s. Marzouk and Hussein (1991), Tomaszewicz (1993), Hallgren (1996), and Ozden et al. (2006) investigated the punching shear strength of HSC slabs with concrete strength f'_c more than 60 MPa. Observations from past experiments showed that high strength concrete (HSC) improve service load level of a slab and as well as the punching shear strength. The flexural stiffness prior to major flexural cracking is enhanced, but their post-crack stiffness deteriorates more significantly. With the effect of high strength concrete, the increment in the punching shear strength is more pronounced when there are more reinforcements in a slab. The inclination of the punching shear crack for the HSC slab without shear reinforcement were reported to vary between 30° to 40°.

According to the author's current database (367 relevant data in Table E.1 Appendix E), there are about less than 40 existing slab data having concrete strength greater than or equal to 70 MPa that is about 10% of the whole data (Details of the slabs can be obtained in Appendix).

In short, Code formulas such ACI 318-14, Eurocode 2 are generally conservative for predicting the strength of these HSC slabs, and note that ACI Code limits the concrete strength to 10,000 psi or 70 MPa for calculating the shear strength of a reinforced concrete member. Also, note that all of existing HSC slabs have high reinforcement ratios. So, if the results of the author's current slabs are included in the comparisons, it will be shown that the Code methods can become unconservative, especially for the HSC slabs that are lightly reinforced. This highlights some influences from the effect of low reinforcement ratios, which will be discussed briefly next in Section 2.3.2.

2.3.2 Influence of flexural reinforcement

Since early tests of slabs that had the flexural reinforcement ratio as the main variable, it has been known that the punching shear strength of a slab increases as the flexural (tension) reinforcement ratio increases. Bottom (compressive) reinforcement has negligible effects on the punching shear strength (Elstner and Hognestad 1956). Many Codes except ACI Code consider the influence of flexural (tension) reinforcement on their punching shear strength equation.

The influence of flexural reinforcement is usually described by using the reinforcement ratio raised to certain values of exponents. Dilger et al. (2005) studied the series of tests by Richardt (1948) and showed that the influence of flexural reinforcement ratio on the punching shear strength, based on trend of data, can be described using the following relationships

$$v_c \propto (\rho)^{1/3} \quad \text{or} \quad v_c \propto (\rho)^{1/4}$$

Code methods such as the Eurocode 2, JSCE (Japanese Code) methods and other design methods proposed by various researchers such as Regan and Braestrup (1985), Gardner (1990) and Teng et al. (2004) use $v_c \propto (\rho)^{1/3}$.

Moe (1961) studied the effect of concentrating flexural reinforcement near the column, it was shown that there is no any significant effect on the punching shear capacity of a slab, however the stiffness can be improved. The conclusions are in agreement with the observations by Elstner and Hognestad (1956), Vanderbilt (1972), Regan (1986) and Hawkins, Criswell et al. (1974). Similarly, McHarg et al. (2000) tested series of slabs with concentrated reinforcements around columns; the test results showed that the punching shear strength, post-cracking stiffness, and distribution of flexural steel strains are better as compared to the slabs with uniformly distributed flexural reinforcement.

Stein, Ghali, and Dilger (2007) tested several slabs under punching shear loads, the test results revealed that the flexural reinforcements within sections of 1.5*d* to *3d* away from the column faces reached the yield strains at failure. Similar observations were also reported by Tian et al. (2008) and Lee (2004).

Effect of low reinforcement ratios:

As already addressed in the background of the current research in Section 1.1, one of the parameters that has not been sufficiently investigated in the past is the influence of flexural reinforcement ratio ρ (=A_s/bd), especially the low reinforcement ratio. It has been known that when a floor slab is provided with a low flexural reinforcement ratio (ρ about 0.8% or less), the slab may not be able to attain its punching shear capacity as calculated using the ACI Code equations for punching shear. That is because it may have failed at a lower load due to widespread yielding of the flexural reinforcement. Essentially that is a flexural failure under punching shear load. Further increase in loading beyond the peak load will only increase slab rotation or deflection before it reaches the final failure in what looks like a punching failure; albeit, a ductile punching failure. So far, the ACI 318 equations for punching shear have not been sufficiently verified for cases of slabs with low reinforcement ratios where flexural failure under punching load may occur ahead of the normal punching shear failure.

One typical way to treat this lightly reinforced slab case in practice is to calculate the punching strength of the slab using the punching shear equations and compare it with the failure load (ultimate shear force) that causes flexural failure of the slab as calculated using the yield line theory. The lower of these two failure loads will be the punching shear capacity of the slab.

Another way is to modify the code equations themselves so that they can be safely applied to all cases of low reinforcement ratios without checking for the flexural failure mode. Recently, a number of researchers, such as Stein, Ghali, Dilger (2007); Guandalini, Burdet, and Muttoni (2009); Widianto, Bayrak, and Jirsa (2009); Peiris and Ghali (2012) and Ospina and Hawkins (2013) attempted to address this issue by testing some lightly reinforced concrete slabs or by suggesting a practical step for design. However, more data and analysis are still needed to look into this issue further. More in-depth discussions, analysis and comparisons of slabs with low reinforcement ratios are presented in Chapter 7, where a new design method is proposed to take into account this effect.

2.3.3 Influence of column rectangularity

Previously, researchers such as Rosenthal (1959), Moe (1961), Hawkins et al. (1971), Oliveira et al. (2004) and Teng et al. (2004) have investigated the effect of column rectangularity on the punching shear strength of slabs. Past experimental results revealed that punching shear stress of the slabs reduced with the increase in the column aspect ratio or long-to-short column width ratio.

Hawkins et al. (1971) proposed the reduction factor for the stress reduction due to effect of column rectangularity to be proportional to the column aspect ratio β (= c_1/c_2), or $v_c \propto 1/\beta$. The reduction factor is taken to be effective for the ratio β greater than or equals to 2.0. Note that the nominal stress values became the basis for the ACI Code equation.

Regan (1981) also made same conclusions about the effect of column rectangularity on the punching shear strength of the slabs that led to the recommendation of reduction factor, $k_{sc}=1.15[(\pi c_1 c_2)/(c_1+c_2)^2]^{0.5}$.

Teng et al. (2004) also proposed a reduction factor to account for the reduction in punching shear stress due to the effect of column rectangularity, the factor is a function of the length of the critical shear perimeter instead (details of the proposed method by Teng et al. (2004) are discussed separately in Section 2.5.1). Anggadjaja and Teng (2008) conducted punching shear tests on edge-column slabs with varying column rectangularity. The test observations showed that stiffness of the slabs in the weak column direction are lower than the stiffness in the strong column direction. The punching of slabs tended to occur first in the strong column direction due to higher shear stresses that concentrated around the shorter side of the column which was also in agreement with Tan and Teng (2001), Teng, Cheong et al.(2004).

Not many design methods including the Eurocode 2 method consider the influence of the column rectangularity. Analysis and comparisons of the author's current slabs in Chapter 7 highlights that Eurocode 2 tend to be unconservative for the slabs with high column aspect ratios (i.e. β = 5.0).

2.3.4 Influence of size effect

Size effect in reinforced concrete member has gained research attentions since the 1950s and they are still on-going research problems. Compared to beam data, there are much fewer slab data with large sizes which make it more challenging to completely understand the size effect on slabs. According to the current interior-column slab database (given in Appendix E), there are less than 10 available data that have the effective depth greater than 300 mm (Graf 1938, Kinnunen et al. 1980, Li 2000, Guandalini et al. 2009). Among these 10 slab data, the thickest slab is by Kinnunen et al. (1980), which has the effective depth of 670 mm (h = 730 mm).

Past studies have shown that the punching shear strength of a slab decreases as the effective depth increases (Regan 1986, Bažant and Cao 1987, Walraven 1994, Bažant and Yu et al. 2007).

Bažant (1984) described the size effect in concrete slab by the fracture mechanics which depends on the length and area of the crack band. He stated that a strength criterion governs the shear strength of small brittle structures, whereas an energy criterion or the size effect law (linear/nonlinear elastic fracture mechanics) is more suitable for much larger structures as demonstrated in Fig. 2.2(a). However, the energy criterion, or the linear fracture mechanics (shown in Fig. 2.2(a)) tends to overestimate the strength of RC members with considerably large sizes. Hence, the non-linear fracture mechanics, shown in Fig. 2.2(a), was proposed to represent the gradual transition from the failure criterion of limit analysis to the linear fracture mechanics. The general form of Bazant's size effect factor k is expressed as

$$k = 1/(1+d/d_o)^{1/2}$$

where d is the effective depth and d_o is an empirical parameter depending on concrete strength and aggregate size; in typical cases, the value of d_o can be approximated as 300 mm. Bazant's size effect factor is plotted in Fig. 2.2(b) together with the normalised strength of slab data from the author's database in the y-axis and the corresponding effective depth is plotted in the x-axis.

Walraven (1994) proposed a similar form of size factor ($\propto A(1+d/B)^{1/2}$) where A and B are the constants. Essentially, by a power law, a size effect factor can be taken to be in between a proportion of $(1/d)^{1/4}$ to $(1/d)^{1/2}$. Note that ACI Code does

not consider the influence of size effect in its shear equations. Eurocode 2 equations use the power 1/2, or ($k = 1 + \sqrt{(d/200)} \leq 2$). Model Code 2010's size effect factor is proportional to ($1/d$). Bazant and Yu et al. (2007) has evaluated performances of various design methods regarding size effect considerations.

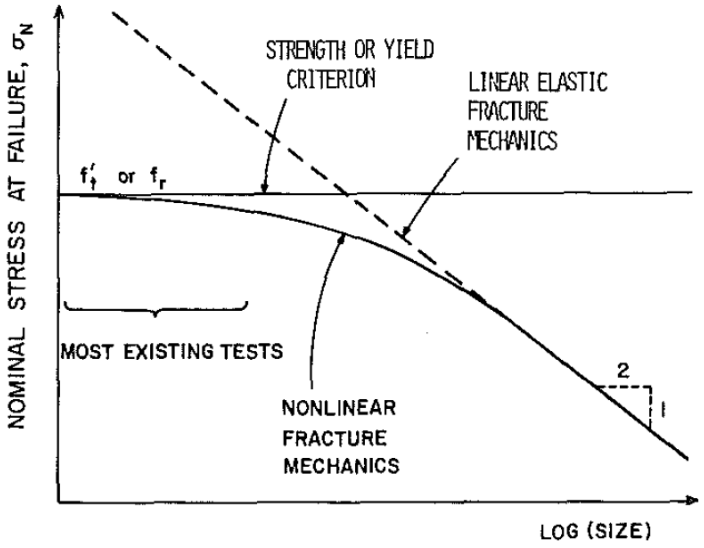

(a) (taken from Bažant and Cao 1987)

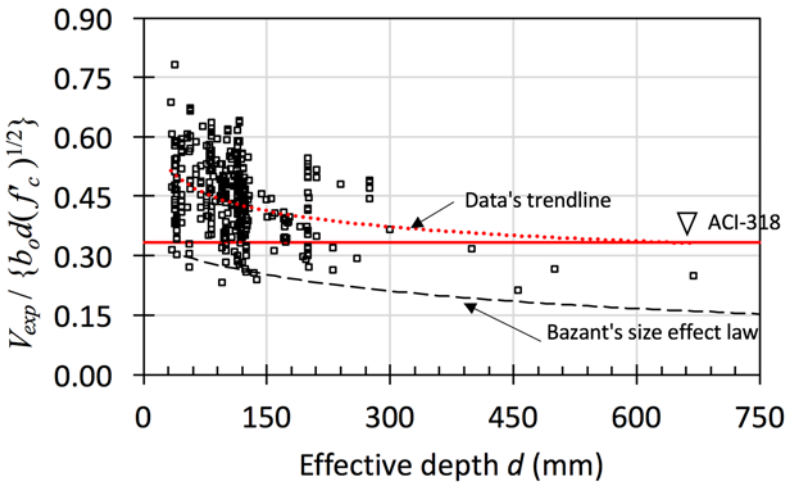

(b)

Fig.2. 2 – (a) Size effect law, (b) Effect of size in the author 'database

2.3.5 Influence of span-to-depth ratio

Influence of the span-to-depth ratio on the punching shear strength of a slab was investigated by Lovrovich and McLean (1990) who tested a series of 10, in which five of them were with shear reinforcement. In the experiment, the slab thickness was kept constant, and the shear span-to-depth ratio was varied from 2.0 to 12.0. The test results were plot in Fig. 2.3 showing the effect of span-to-depth ratio on the punching shear strength. It can be seen from Fig. 2.3 that the punching shear strengths of both slabs with and without shear reinforcements are high for the span-to-depth ratio of lower than 4. Lovrovich and McLean (1990) explained that the reason for an increase in the shear strength could probably be due to the formation of compression struts (tied-arch mechanism) from the loading point to the support, as also observed in deep beams. It can be seen also that, as the span-to-depth ratio increases beyond 6, the punching shear strength of the slabs become more or less stable. Other researchers such as Gardner (1990) and Marzouk and Hussein (1991) also tested a series of concrete slabs varying the span-to-depth ratio from about 4 to 9; their test results also showed that there were slight reductions in shear strength with an increase in the span-depth ratio. However, the effect is not so significant..

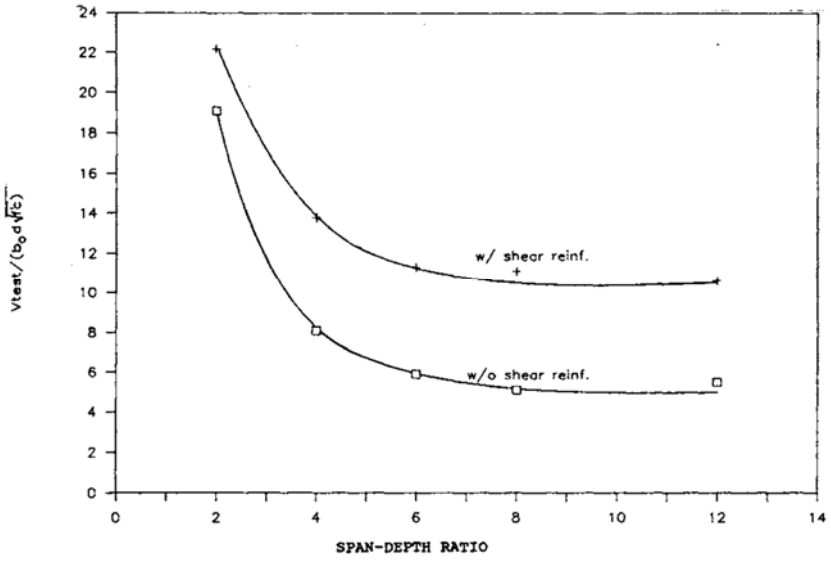

Fig.2. 3 – Relationship between normalised shear strength and span-depth ratio (taken from Lovrovich and McLean 1990)

2.3.6 Influence of column width-to-slab depth ratio

Vanderbilt (1972) investigated the influence of column width-to-slab depth ratio (c/d) on the punching shear strength of slabs. The ratio c/d was varied from 2 to 8 as shown in Fig. 2.4. Slabs with square columns and circular columns were also compared. The Vanderbilt (1972) showed that the punching shear strength of a slab tends to decrease as the column width-to-slab depth ratio increases. The strength of the slabs supported on circular columns were generally higher than those on square columns throughout the ratio c/d from 2 to 8. The influence of reinforcement ratio ρ can also be seen in Fig. 2.4, in which the heavier reinforced slabs (ρ =2%) failed at higher loads compared to the slabs with ρ = 1%.

Note that one of the three punching shear equations of ACI 318 [Eq. (3.1c)] was indeed influenced by the test of Vanderbilt, in which the effect of column width-to-depth ratio is considered in term of the ratio of the critical perimeter to the effect depth b_o/d instead of c/d. The ACI method does not consider the influence of reinforcement ratio. Details of the ACI 318-14 method for punching shear design is given in Section 3.2.1.

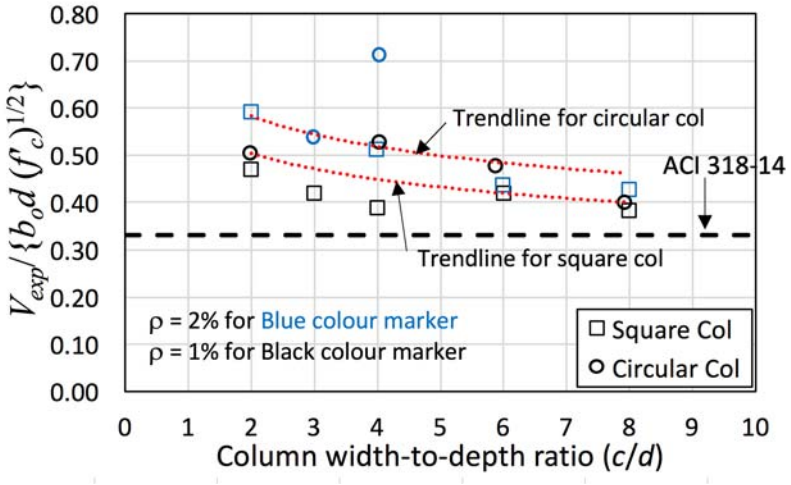

Fig.2. 4 – Relationship between normalised shear strength and column-to-slab depth ratio. Note the data is from Vanderbilt (1971).

2.3.7 Influence of fibre reinforced concrete

The main functions of fibres are to bridge and resist the crack openings through the fibre pull-out mechanism. This post-crack characteristic of SFRC allows the presence of tensile stress and concrete tensile strains along the crack openings, which are omitted in the analysis of conventional RC elements. Therefore, theoretically, the post-crack tensile strength of SFRC enhance the ultimate strengths of a concrete section, be it shear strength or flexural strength. Observations from past experiments [Swamy and Ali (1982), Narayanan and Darwish (1987), Alexander & Simmonds (1992), Theodorakopoulos and Swamy (1993), Shaaban and Gesund (1994)] have shown that the additional strength and ductility due to the inclusion of SFRC are proportional to the residual tensile strengths. The residual tensile strengths can be obtained directly from the flexural beam test EN 14651, which can also be correlated to various fibre parameters such as fibre volume fraction (fibre content), fibre shapes (straight, crimped, paddle-ended, hooked-end, etc.), and fibre aspect ratio (more specific review of the literature are presented in Section 2.5.2).

Past experiments have shown that the ultimate punching shear strengths of SFRC slabs can range from 40-65% higher than the strengths of non-fibrous slabs, for fibre volume V_f of greater than about 1.0%, depending on the fibre type [Swamy and Ali, (1982); Narayanan & Darwish, (1987); Alexander and Simmonds, (1992); Theodorakopoulos and Swamy, (1993); Shaaban and Gesund, (1994); Harajli et al., (1994); McHarg et al., (2000); Ozden et al., (2006), De Hahai and Holanda, (2008); Cheng and Parra-Montesinos (2010); Higashiyama et al., (2011); Nguyen-Minh et al., (2012); and Gouveia et al., (2014)].

On the influences of conventional hooked end fibres, McHarg et al. (2000) conducted punching shear tests of SFRC slabs using single hooked-end steel fibres; the results showed that the additions of steel fibre [V_f = 0.5%, L_f = 30 mm, L_f/D_f = 60] to non-fibrous slabs can increase the punching shear strength by 26% to 38%, increase in the ductility and post-crack stiffness of the specimens were also observed. The experimental results from Cheng and Parra-Montesinos (2010) revealed that the punching shear strength of a medium reinforced non-fibrous slab ($\rho \approx 0.6\%$) increases up to 40% with an addition of single hooked end fibre of 1.5%

fibre volume (with L_f = 30 mm, L_f/D_f = 80). The similar properties (L_f = 30 mm, L_f/D_f = 80) of hooked end fibres were investigated by Gouveia et al. (2014) who showed that the punching shear strength of a non-fibrous slab (with ρ = 1%) increases by 65% when the fibre volume V_f increases to 1.0%.

Test results obtained from the punching shear tests on lightweight aggregate SFRC slabs conducted by Theodorakopoulos and Swamy (1993) showed that an addition of steel fibres reduces the inclination of punching crack with an average inclination varying from 22° to 28°. An addition of steel fibres were shown to change a brittle mode of falure to a more ductile one (i.e from punching to flexure), depending on different variables. The test results also highlighted that slabs containing longer steel fibre lengths L_f have better structural performance (ultimate loads and service loads) compared to those with shorter steel fibre lengths.

Swamy and Mangat (1974), Soroushian and Bayasi (1991), and many other researchers have investigated influences of fibre types and parameters on the mechanical properties of fresh and hardened fibrous concrete. Several types of steel fibres can be categorised as shown in Fig. 2.5. In general, higher fibre aspect ratio L_f/D_f improves structural performances of RC members but reduces the workability of fresh concrete mix. Additions of steel fibres have little effects on the compressive concrete strength. Among the fibres shown in Fig. 2.5, the single hooked end fibres perform the best. Published research works on influences of the double hooked end fibres on the punching shear strength of an SFRC slab are still unavailable.

Experimental results obtained from the current research will show that the double hooked end fibres perform even better than the single hooked end fibres.

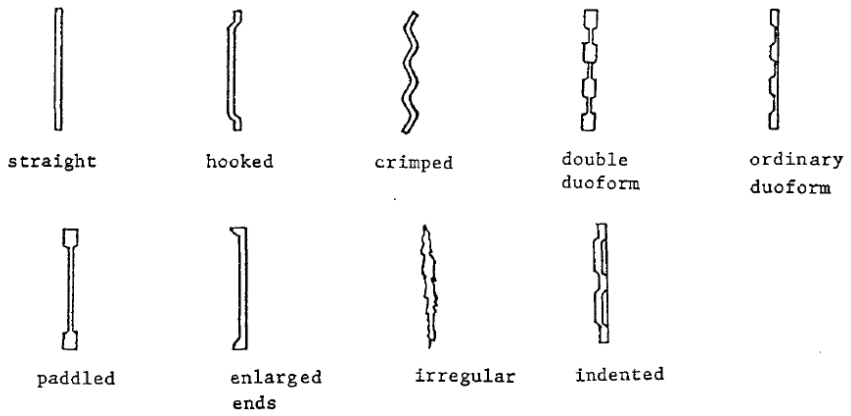

Fig.2. 5 – Different steel fibre types (Soroushian and Bayasi 1991)

2.4 Types of punching shear models

The models for punching of slabs have been developed using various approaches such as mechanical approaches, empirical and semi-empirical approaches. The main aims of researchers were to get accurate predictions of ultimate punching capacity. Hence, different assumptions inevitably had to be made for different model which many of the models have been subjected to criticisms. For any mechanical model, it is necessary to satisfy the general criteria such as equilibrium, compatibility, postulated constitutive law, material strengths and failure criteria of the element. Subsections shown below are the brief descriptions of different types of the punching shear models that have been proposed since the 1960s and brief history of respective models would be described subsequently.

2.4.1 Models based on Flexural Capacity

Many researchers (Moe 1961, Yitzhaki 1966, Gesund 1971, Rankin and Long 1987) have incorporated the flexural strengths of slabs into the derivation of punching strength of slabs, because observations of many punching tests indicated that the difference between the punching shear loads and the loads causing flexural failure was somehow insignificant and ambiguous. Thus, their proposed punching formulas contained or derived from the flexural capacity or the ultimate load V_{flex} that causes yielding of the reinforcements.

2.4.2 Models based on Plasticity Theory

A plastic solution is essentially the upper bound values for punching shear strength, this approach was initiated by Bræstrup et al. (1976). Main assumptions are: the deformation is concentrated in a rotationally symmetric surface; and the concrete body is punched out perpendicular to the slab while the remaining slab parts remain undeformed or rigid. The solution is derived from the energy conservation equation when the rate of work done by external loads is set equal to the rate of internal work by the failure. Marti and Thürlimann (1977) also developed a simplified upper bound solution for punching load of a slab. However, flexural reinforcements have no contributions to the solutions of the punching shear strength.

There are also the lower bound solutions that were discussed by Braestrup (CEB-Bulletin 168 1985), the theory states that the stresses at any point should satisfy the equilibrium equations as well as the boundary conditions. In addition, they should correspond to a yield line along the optimal failure surface and do not violate the yield condition. Pralong (1982) proposed an alternative lower bound approach involving the concrete tensile strength.

Bortolotti (1990) was also among the researchers who developed plastic theory for punching of slabs. He applied the plasticity theory to calculate the punching load by utilising a modified Coulomb yield criterion to become his proposed failure criterion for concrete. The failure mechanism for slabs indicates that a concrete slab is constrained in a ring shape and punched out by a circular plate which is subjected to uniform vertical displacement rate field. He introduced a procedure to consider the strain softening of concrete. Then, an upper bound solution is found by applying the virtual work equation. In order to solve the lowest upper bound solution from complex equations, the advanced mathematic technique, known as the variational calculus (or Euler equation), was employed together with specified boundary conditions. The theoretical model would be valid only if the slabs have enough rigidity and have no boundary displacements and rotations.

2.4.3 Models based on The Kinnunen and Nylander approach

Kinnunen and Nylander (1960) first introduced this mechanical model which can to give a good prediction of the punching shear strength of a slab and is capable of describing the flow of forces in slabs as well. The model consists of a central truncated cone surrounded by tangential shear cracks and rigid slab segments, which are separated by radial cracks. The failure criteria of the model are determined by the limitations of the inclined radial compressive stress and tangential compressive strain at the shear crack (semi-empirical). Hence, the predicted punching shear load of a slab is obtained by satisfying the failure criterion and forces equilibrium in a truncated segment. Other researchers such as Broms (1990), Shehata (1990) and particularly Hallgren (1996) have adopted this approach

and further improved the theoretical part of the model i.e. a simple fracture mechanical model was incorporated to construct the modified failure criterion.

2.4.4 Models based on fracture mechanics and concrete tensile stresses

Bažant and Cao (1987) are among the researchers who applied fracture mechanics in the development of a mechanic model to predict punching shear strength of slabs. They opposed the idea of punching shear failure of slabs without transverse steel as being plastic - but being brittle instead which makes the size-effect law (Bažant 1984) for blunt failures more applicable. Tests showed that the nominal stress at ultimate loads decreases with the increase of slabs sizes which lead to the development of design formula that takes account of size-effect. At punching shear failure, Bažant and Cao (1987) suggested that behaviour of a thinner slab is somewhat closer to the plasticity model than a thicker slab, the behaviour of the thicker slab is more relevant to linear elastic fracture mechanics.

The model by Georgopoulos (1989) has the concrete tensile strength and the mechanical reinforcement ratio as the main parameters. He proposed the inclination of shear crack angle to be a function of mechanical reinforcement ratio, the punching load is a function of tensile strength which is assumed to be distributed, as third order polynomial function, in the surface of punching crack. Note that the original papers were written in German script, the description of the model was comprehensively summarised in the technical report, fib bulletin 12 (2001).

2.4.5 Models based on Strut-and-tie Models

Strut-and-Tie Models are useful analytical tools for the design of a non-flexural member or of a member that have discontinuity regions (D-regions) such as deep beams, corbels and shear walls. ACI 318-14 (2014) includes provisions on design with strut-and-ties method, Eurocode 2 (2004) has also fully recognised strut-and-tie analysis as a part of the code (Chapter 6 of Eurocode 2-2004, 6.5).

Researchers such as Alexander and Simmonds (1992, 1992a), Tiller (1995), Marzouk, Risk, and Tiller (2010) and Rizk, Marzouk, Tiller (2012) used the strut-

and-tie approach to develop force mechanisms and formulas for calculating the punching shear strength of a slab.

2.4.6 Critical Shear Crack Theory Model

Muttoni and Schwartz (1991) first introduced an analytical model or a theory called Critical Shear Crack Theory (CSCT) to predict punching shear strength of RC slabs without transverse reinforcements (or shear reinforcements) by incorporating the rotation of slabs (moment-curvature relationships) under applied loads, flexural cracking pattern and shear-carrying mechanisms to construct the model's failure mechanism. The punching shear strength is determined by the equilibrium equations in a slab sector, i.e. the equilibrium of moments created by external load and accumulation of internal moments at various curvatures. The model was then simplified to become a shear formula in the Swiss design code (SIA 2003) and Model Code 10 (fib bulletin 65 2012). According to the CSCT (Muttoni 2008), the rotation capacity of a slab member has a significant influence on its punching shear strength, a slab with a lower amount of flexural reinforcement would have lower nominal punching shear strength and possess higher curvature at failure, compared to a heavier reinforced slab. The CSCT has gained significant recognition in structural concrete research. The application of the theory has also been extended to slabs with transverse shear reinforcement, post-tensioning slabs, and as well as fibre reinforced concrete slabs (Muttoni and Ruiz 2010). Details of CSCT will be reviewed in details later in Section 2.5.1.

2.4.7 Tangential Strain Theory Model

Recently, Brom (2016) proposed a new theory for predicting the punching shear strength of a reinforce concrete slab, it is "a mechanical model for the punching failure at interior columns of at slabs without shear reinforcement is presented. It is based on fundamental structural mechanics and the stress-strain relation of compressed concrete. The shear force is assumed to be transferred to the column by an inclined circumferential compression strut that squeezes the concrete within the column perimeter, and when the compression stress in this area approaches the yield level, an increasing part of the squeezing pressure is anchored back to the

surrounding concrete. Ultimately, the compression zone outside the column is assumed to collapse due to the generation of radial tension strain." Brom (2016)

2.4.8 Empirical and Semi-Empirical Models

The empirical models are usually developed using statistical tools such as linear/non-linear, single/multiple regression analysis of experimental data. Parameters that influence the punching shear strength such as concrete compressive strength, flexural reinforcement ratios, and others are included in the mathematical expression of the regression analysis. Regarding the aspect of general criteria — particularly equilibrium, the empirical models certainly have inevitable limitations and cannot be used to describe punching shear failure behaviours. Nevertheless, empirical models are generally preferred for code equations due to their simple expressions which are indeed necessary for problems like punching shear design. Punching shear is undeniably a complex design issue, hence, even many the rigorous mechanical models do contain empirical forms or substances in a certain way, such as the simplifications of constitutive laws, failure criteria, and the postulation of geometric parameters like failure surface are forms of empiricism.

2.5 Review of key literature

The following subsections cover review of specific design methods, past research, and experimental works that are relevant to the author's current study. Some of them will be the main references to construct the author's proposed new design methods for both reinforced concrete and steel fibre reinforced concrete slabs in Chapter 7 and Chapter 8, respectively. Also, they will be evaluated and compared with the current experimental results and also with the existing 355 RC slab data and 138 SFRC slab data that will be presented in Chapter 7 and Chapter 8.

2.5.1 Past research works on reinforced concrete slabs

Method by Teng et al. (2004)

Teng et al. (2004) investigated the effects of slab openings and column rectangularity in normal strength reinforced concrete slabs. Punching shear tests of 20 slabs having high reinforcement ratios ($\rho > 1.0\%$) with openings were conducted. Their works led to a proposed modification to the critical perimeter that takes into account of holes with effects of column rectangularity. They also proposed a design equation for the punching shear strength V_c as shown below.

$$V_c = 0.6k_{CR}(100\rho f_c^{'})^{1/3} b_o d \quad \text{(in SI units: MPa, mm)}$$

$$= 16.6k_{CR}(100\rho f_c^{'})^{1/3} b_o d \quad \text{(in U.S. units: psi, in.)} \qquad (2.1)$$

$$\text{where } k_{CR} = (b_2/b_1)^{1/4} \leq 1.0 \qquad (2.2)$$

where b_1 and b_2 are the longer and shorter sides of the critical shear perimeter, respectively. The use of b_1 and b_2 in the column rectangularity factor, k_{CR}, rather than c_1 and c_2 is to take into consideration the thickness of the slab in influencing the distribution of stresses around the column. The critical shear perimeter b_o has square corners for both square and circular columns and is located at a distance $d/2$ away from column faces. For a circular column, an equivalent square column of the same area can be used for b_o calculations. The equation was verified by Teng et al. (2004) with 223 slab data having a broad range of relevant parameters. However, the applicability of the equation for slabs with very low reinforcement ratios and very thick slabs has not been verified thoroughly.

Critical Shear Crack Theory

Muttoni (2008) introduced the Critical Shear Crack Theory (CSCT) for calculating the punching shear strength of slabs without shear reinforcement. The method assumes that the punching shear strength V_{Rd} of a slab depends on the rotation ψ of the slab at failure, as well as crack width and aggregate interlock along the critical shear crack. The CSCT also considers that the rotation ψ of the slab depends on the applied punching shear force V and a few other parameters. Failure is reached when the applied punching shear force V is equal to the punching shear strength of the slab V_{Rd}.

The method requires an iterative solution to two equations: (1) the relationship between the punching shear strength V_{Rd} and rotation ψ, and (2) the relationship between the rotation ψ and applied shear force V. Eqs. (2.3) and (2.4) show these two equations.

$$V_{Rd} = \frac{0.75}{1+15\dfrac{\psi d}{d_{go}+d_g}}\sqrt{f_c'}\,b_o d \quad \text{(in SI units: MPa, mm)}$$

$$= \frac{9}{1+15\dfrac{\psi d}{d_{go}+d_g}}\sqrt{f_c'}\,b_o d \quad \text{(in U.S. units: psi, in.))} \tag{2.3}$$

$$\psi = 1.5\frac{r_s}{d}\frac{f_y}{E_s}\left(\frac{V}{V_{flex}}\right)^{1.5} \tag{2.4}$$

where r_s is the radius of the slab (= half of a slab length or $0.22L$ where L is column-to-column span). V_{flex} is the shear force that will cause flexural failure of the slab. b_o is calculated at a distance $d/2$ away from column edges with round corners. d_{go} is set to be 16 mm and d_g is the maximum aggregate size. Muttoni[6] states that the size effect in CSCT is a function of r_s or slab span rather than the effective depth d.

The CSCT method can become complex as it requires an iterative procedure to solve for V_{Rd}. In addition, every slab geometry, reinforcement ratio, and loading condition would lead to different yield line pattern, requiring yield line analysis in order to obtain V_{flex}. Consequently, for general design purpose, V_{flex} can be approximated (Muttoni 2008, Guandalini, Burdet, and Muttoni 2009) and taken as

$$V_{flex} = 8m_R \tag{2.5}$$

where according to the CSCT (Muttoni 2008), the moment capacity per unit width m_u (using the European method) is calculated by the following equation.

$$m_R = \rho f_y d^2 (1 - 0.5 \frac{f_y \rho}{f_c'}) \tag{2.6}$$

Note that the yield line theory and the moment capacity of reinforced concrete and fibre reinforced concrete slabs are described separately in Section 3.4 of this thesis.

Guandalini, Burdet, and Muttoni (2009) conducted a punching shear test of 11 reinforced concrete slabs supported on square columns to investigate the effect of low reinforcement ratio. The reinforcement ratio was varied at the values of 0.22 to 0.28%, 0.33%, 0.75%, and 1.5%. The effects of sizes and aggregate sizes were also investigated, in which the thickness of the slab was varied at 125 mm, 250 mm, and 500 mm. Two sizes of aggregate were used which are 4 mm and 16 mm. The details of the 11 specimens (PG series) are given in Appendix E of this thesis.

The results from the test by Guandalini, Burdet, and Muttoni (2009) were compared with design codes and the critical shear crack theory. It was shown that the ACI 318 method can overestimate the punching shear strength for thick slabs and lower reinforcement ratios. The test results were also used to confirm the applicability of the CSCT for slabs with and without significant plastic deformations in the flexural reinforcement (that is, with low or large reinforcement ratios).

Method by Peiris and Ghali (2011)

Peiris and Ghali (2011) proposed a straightforward method to improve the ACI Code method by introducing a reduction factor, ρ/ρ_{fs}, to make it safer for slabs with low flexural reinforcement ratios. ρ_{fs} is the limiting reinforcement ratio. If the provided reinforcement ρ is reduced to below ρ_{fs}, the slab is assumed to fail in flexural mode instead of the usual punching mode.

For slabs with provided reinforcement $\rho > \rho_{fs}$, the punching shear strength of the slab V_c is determined by the usual ACI equations (given in Section 3.2.1 of this thesis). If the provided ρ in the slab is reduced below ρ_{fs}, the punching shear strength V_c becomes equal to V_{flex}, that is, the shear force that causes the slab to fail in flexural mode.

For slabs with $\rho < \rho_{fs}$, Peiris and Ghali (2011) assume that V_{flex} to be a linear function of ρ. So, the failure load for slabs with $\rho < \rho_{fs}$ is then equal to $(\rho/\rho_{fs})V_c$.

The key lies in the term ρ_{fs}. The V_{flex} can be calculated by using the yield line theory. For some simple cases, V_{flex} can be approximated by $8m$ as discussed earlier for the CSCT method in Eq. 2.5, where m is moment capacity per unit width (ACI 318). By setting $V_{flex} = V_{c(ACI)}$, the ρ becomes ρ_{fs}, and the ρ_{fs} can be obtained. Thus,

$$8m = 4\sqrt{f_c'}\,b_o d \text{ , where } m = 0.95\, f_y\, d^2\, \rho \tag{2.7}$$

Then, solving for ρ or ρ_{fs},

$$\rho_{fs} = \frac{4\sqrt{f_c'}\,b_o d}{8 \times 0.95 f_y d^2} \text{ (U.S. Units)} \tag{2.8}$$

2.5.2 Past research works on fibre reinforced concrete slabs

In general, there are two distinguished approaches for calculating the shear strength of FRC members such as:

(1) An approach that calculates the shear strength by using the residual tensile strengths obtained from the bending test (notched beam test, EN 14651 (2007)) which is subsequently discussed in Section 2.5.2.1

(2) An approach that approximates the shear strength to be a function of semi-empirical and empirical fibre parameters, such as fibre geometry, fibre content, and various reduction factors. Methods that use this approach are reviewed in Section 2.5.2.2.

2.5.2.1 Design Methods based on residual tensile strength approach

RILEM TC 162-TDF (2003)

RILEM (2003) recommended design methods for both ultimate flexural strength and shear strength of FRC beams. The ultimate bending moment can be determined based on the stress-strain relationship of a cracked FRC beam section as shown in Fig. 2.6. The tensile stresses of the section (σ_1, σ_2 and σ_3) are proportional to residual tensile stresses as obtained from notched beam tests EN 14651 (2007). The equations are shown in Fig. 2.6. A simple equation for an increase in shear strength due to the presence of fibres was proposed to be

$$v_f = 0.12 f_{r4} \tag{2.9}$$

where f_{r4} is the residual flexural tensile strength corresponding with CMOD = 3.5 mm (crack mouth opening displacement). The residual flexural tensile strengths f_{r1} and f_{r4} (obtained experimentally according to the standard EN 14651:2007) are calculated considering a linear elastic stress distribution in the notched section of the notched beam.

Note that tensile stresses σ_2 and σ_3 shown in Fig. 2.6 are derived from the residual flexural tensile strength as explained below. However, in reality, the tensile stress distribution is different along the cracked section. To calculate a more realistic stress in the cracked part of the section, the RILEM (2003) made the

following assumptions in Figs. 2.7(a) and 2.7(b): tensile stress σ_f in the cracked part of the steel fibre concrete section is constant. The stresses σ_2 and σ_3 are the equivalent stresses of the residual stresses f_{r1} and f_{r4} at CMOD = 0.5 mm and CMOD = 3.5mm, respectively. The crack height is taken to be $0.66h_{sp}$ and $0.90h_{sp}$ for the loading stage corresponding with f_{r1} and f_{r4}, respectively (see Fig. 2.7), where h_{sp} is the depth of the notched beam at the notch location (mid-span) minus off the notch depth (150 mm – 25 mm = 125 mm). Equate the bending moments corresponding to the sections shown in Fig. 2.7(a) and 2.7(b) [or take $M_1 = M_2$], the equivalent stresses can then be expressed as:

$$\sigma_{f,2} = 0.45 f_{r1}(k_h) \tag{2.10}$$

$$\sigma_{f,3} = 0.37 f_{r4}(k_h) \tag{2.11}$$

where $\sigma_{f,2}$ and $\sigma_{f,3}$ are to be reduced by a size factor k_h that ranges from 1.0 to 0.40, which is taken to be:

$$k_h = 1.0 - \frac{0.6(h - 125)}{475} \qquad (h \text{ is in mm}) \tag{2.12}$$

Note also that the RILEM's model is the basis of the punching shear strength equation as provided by the design guidelines TR 34 by the Concrete Society (2003, 2015). Another method that uses a similar approach to calculate the punching shear strength of an FRC slab is the method by Model Code 2010 (2012). The details of TR 34 and Model Code 2010 are presented in Section 3.3.2 of this thesis.

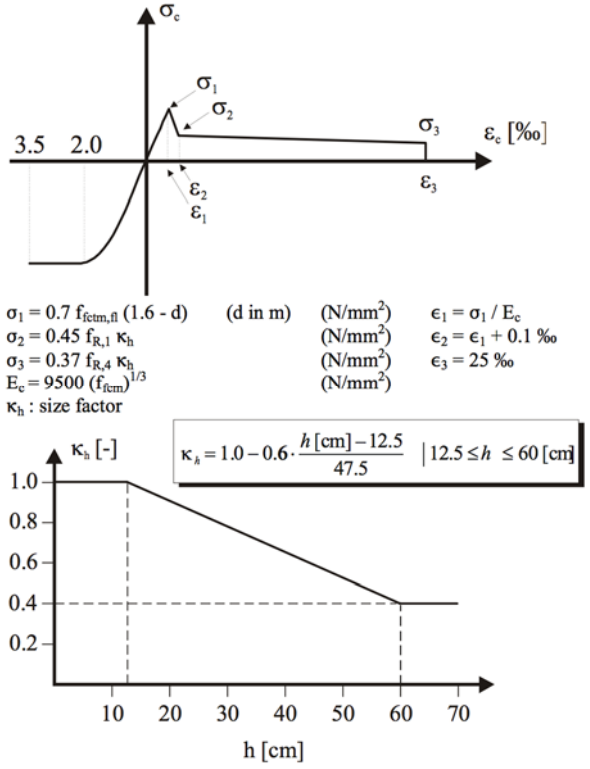

Fig.2. 6 – RILEM's flexural strength model (Taken from RILEM (2003))

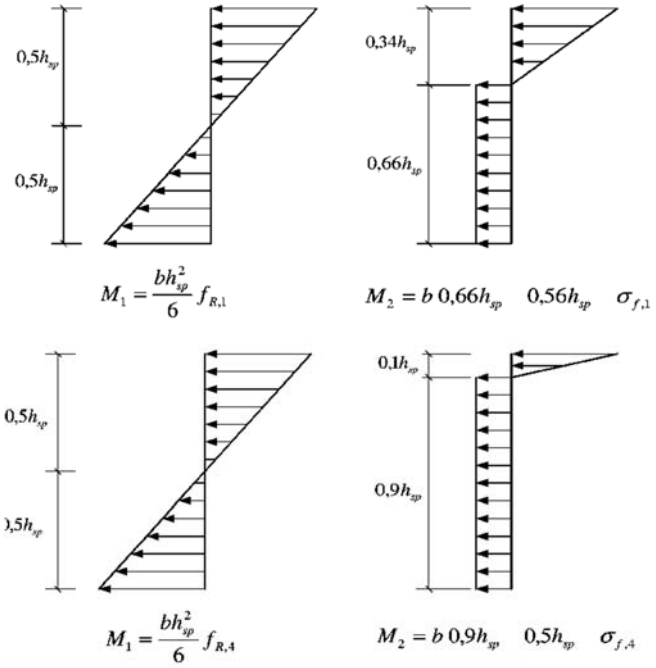

(a) (b)

Fig.2. 7 – (a) Stress distribution at the middle section of the notched beam without consideration of crack openings; (b) idealised stress distribution at the middle section of the notched beam for various depths of crack openings. (Taken from RILEM (2003))

2.5.2.2 Methods based on fibre parameters approach

Method by Swamy et al. (1974)

Swamy and Mangat (1974) proposed a theory for predicting the flexural tensile strength of steel fibre reinforced concrete under uniaxial load. The theory was developed based on the following considerations. The behaviour and mode of failure of the composite depend on the relative stiffness of the matrix and the fibre, the strain compatibility of the matrix and fibre, as well as the fibre geometry and the fibre-matrix interfacial bond strength.

Two failure mechanisms were considered in the theory which are (1) failure by the simultaneous yielding of both fibre and concrete matrix, and (2) failure by the bond failure of the fibre-matrix interface (fibre pull-out failure). The first mechanism (the yielding of fibre) occur when the fibre length L_f is greater than the theoretical critical length of fibre L_c ($L_f > L_c$). This critical length L_c is the minimum development length that allows the yield strength of the fibre to be attained. It can be determined using the equilibrium consideration as given below

$$L_c = \sigma_{fu} D_f / 2\tau_u \tag{2.13}$$

where σ_{fu} is the yield strength or the ultimate strength of the fibre, D_f is the fibre diameter and τ_u is the ultimate interfacial bond stress.

By Hooke's law of mixtures, a general form of the tensile strength of an FRC composite can be expressed as series of the product of stresses and volume fractions as follows

$$\sigma_c = \sigma_m V_m + \sigma_f V_f \tag{2.14}$$

where σ_c, σ_m, and σ_f represent stresses in the composite, matrix and fibre, respectively. V_m and V_f are the volume fraction of matrix and fibre, respectively. Only 41% of fibre volume fraction is considered be effective in contributing to the tensile stress and this value can be called the orientation factor (n_o = 0.41). σ_f is a function of an average bond stress that can be expressed as $\sigma_f = 2\tau L_f/D_f$. At failure, the bond strength τ reaches ultimate τ_u that is taken to be 4.15 N/mm^2, the value of 4.15 N/mm^2 was obtained from regression analysis of pull-out test data.

The theory above led to the development of an analytical model to determine the punching shear strength of an FRC slab proposed by Theodorakopoulos and Swamy (1999). The model of Theodorakopoulos and Swamy (1999) assumes that the punching shear resistance of an FRC slab occurs over the compression depth *X* as shown in Fig. 2.8. Essentially, the ultimate shear strength is contributed by two constituents such as (1) the concrete tensile stress v_{cc} orthogonal to the inclined crack surface and (2) the shear stress v_{FF} along the inclined crack surface (Fig. 2.8). The ultimate punching shear strength of the model is as follows.

$$V_u = v_c b_o X \cot\alpha + 4\sigma_{cu}(c + X\cot\alpha) \tag{2.15}$$

where

$$X = \frac{2X_s X_f}{X_S + X_f} \tag{2.16}$$

where v_c is the concrete limiting shear stress taken to be equal to concrete tensile strength at failure ($v_c = f_{ct} = 0.27(f_{cu})^{2/3}$); f_{cu} is the cube strength of concrete, critical perimeter b_o is calculated at 1.5d away from column face ($b_o = 4c+12d$); c is the column width; X is the fictitious combined neutral axis; X_s is the neutral axis depth of shear critical section, take as 0.25d; X_f is the neutral axis depth of flexural critical section that is an equilibrium function of the flexural reinforcements and state of tensile stresses in the reinforcement (iterative analysis is needed). The punching crack inclination is assumed to be 30°.

The shear contribution due to the presence of fibres v_{FF} is taken to be the ultimate tensile strength σ_{cu} of the FRC (or $v_{FF} = \sigma_{cu}$). With the introduction of fibre orientation factor n_o and the length efficiency factor n_l [by Law (1971)], the equation of ultimate tensile strength σ_{cu} was simply represented by

$$\sigma_{cu} = n_o n_l \sigma_{fu} V_f \tag{2.17}$$

where,

n_o = 0.41(fibre orientation factor)

$$n_l = \begin{cases} L_f/2L_c & \text{For } L_f \le L_c \\ 1 - L_f/2L_c & \text{For } L_f > L_c \end{cases} \tag{2.18}$$

The critical length L_c in Eq. (2.13) was adjusted with the bond efficiency factor n_b, and the concrete type (normal weight or light weight) factor for bond strength n_c. The equivalent critical strength L_c is

$$L_c = \frac{\sigma_{fu} D_f}{2(n_b n_c \tau)} \tag{2.19}$$

where the term ($n_b n_c$) is to adjust the average bond strength τ to become the ultimate bond strength τ_u of each type of fibre. The average bond strength τ is taken to be 4.15 N/mm^2. n_b is empirically assigned and different for different type of fibre and fibre geometry. The factor n_b is lowest for the plain types of fibres and highest for the deformed types such as the crimped and paddle types. n_c is taken as 1.0 for normal weight concrete and 0.85 for light weight concrete.

A complex iterative process is required for this model because the (fictitious) compression depth X depends on other parameters such as the amount of (tension and bottom) reinforcements, yield strength and strain of the reinforcements, concrete strength. The calculation procedure of the model is detailed in a paper by Theodorakopoulos and Swamy (1999), and a more simplified procedure was presented in a paper by Theodorakopoulos and Swamy (2003).

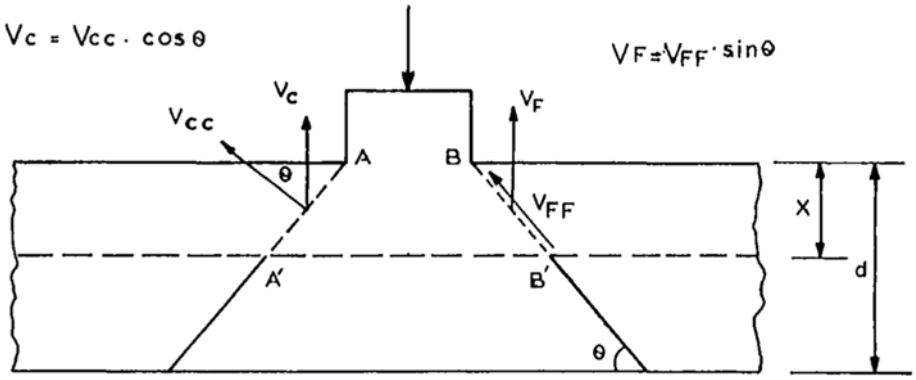

Fig.2. 8 – Compression zone and fibre shear resistance contributions along failure surface (Theodorakopoulos and Swamy 1999)

Method by Lim, Paramasivam, and Lee (1987)

Lim, Paramasivam and Lee (1987) proposed an equation for the ultimate tensile strength of an FRC member that has the similar principle as the theory proposed by Swamy et al. (1974) (discussed earlier). A general form of the ultimate tensile strength of an FRC composite is the same as Swamy et al.'s Eq. (15), that is

$$\sigma_c = \sigma_m V_m + \sigma_f V_f \tag{2.20a}$$

The behaviours of FRC composites under tension and bending stresses were studied through series of beam bending tests and pull-out tests which led to an equation for the ultimate tensile strength σ_{cu} as shown below.

$$\sigma_{cu} = n_l n_0' V_f L_f \frac{\tau_u}{2r} \tag{2.20b}$$

where

$n'_o = 0.405 \approx 0.41$ (fibre orientation factor)

$$n_l = \begin{cases} 0.5 & \text{For } L_f \leq L_c \\ 1 - L_c/2L_f & \text{For } L_f > L_c \end{cases} \tag{2.21}$$

V_f is the fibre volume fraction; L_f is the fibre length; r is the ratio of the fibre cross-section area to its perimeter (or $r \approx ¼D_f$). n_l is the fibre length efficiency factor. L_c is the critical length of fibre and taken to be the same as Eq. (14) or $L_c = 0.5\sigma_{fu}(D_f/\tau_u)$. The bond strength of the fibre-matrix interface τ_u can be obtained experimentally from the fibre pull-out test; some results of the fibre pull-out tests are shown in Fig. 2.9(a). A more accurate value of the orientation factor n'_0 can be obtained mathematically by computing the mean value of a probability function over the domain, which is taken to be a function of the fibre orientation or the fibre angles (θ and ρ) illustrated in Fig. 2.9(b). The equation of is n'_0 given by

$$n'_o = \frac{\int_0^{\bar{\rho}} \int_0^{\bar{\theta}} \cos\theta \cos\rho \, d\theta d\rho}{\int_0^{\bar{\rho}} d\theta d\rho} = \frac{\sin\bar{\theta} \sin\bar{\rho}}{\bar{\theta}\bar{\rho}} \tag{2.22}$$

where

$$\bar{\theta} = \sin^{-1}\left(\frac{h}{L_f}\right) \leq \frac{\pi}{2}; \qquad \bar{\rho} = \sin^{-1}\left(\frac{b}{L_f}\right) \leq \frac{\pi}{2}$$

Note that n'_o is equal to 0.405 when the fibre length L_f is smaller than the thickness h and the width b of the FRC member ($L_f < h$ *and* $L_f < b$). Therefore, the value of $n'_o = 0.405 \approx 0.41$ should be applicable for most cases in design.

This review is to show that the ultimate tensile strength of an FRC composite can be somewhat determined empirically. This ultimate tensile strength has been utilised in various punching shear models for FRC slabs as shown previously; more methods will be discussed subsequently.

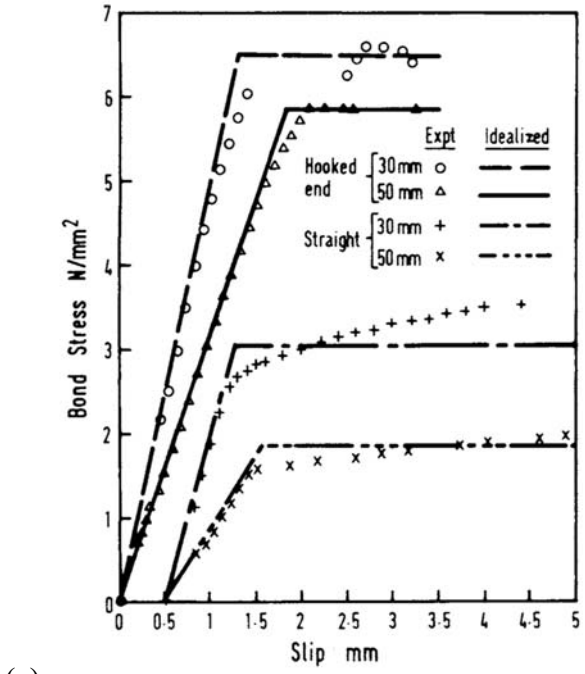

(a)

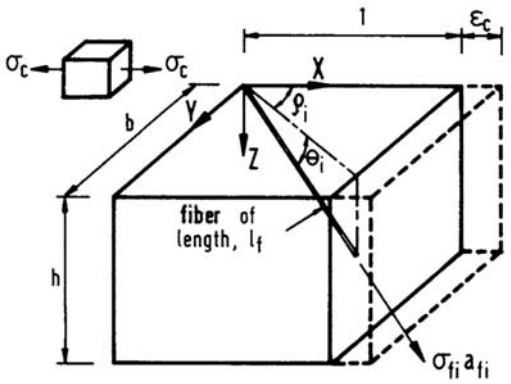

(b)

Fig.2. 9 – (a) Bond strength of the fibre-matrix interface for various types and shapes of steel fibres [taken from Lim, Paramasivam, and Lee (1987)]; (b) Composite element under uniaxial stress [taken from Lim, Paramasivam, and Lee (1987)]

Method by Narayanan and Darwish (1987)

Narayanan and Darwish (1987) proposed a shear design method for FRC members (beams and slabs). The method was empirically developed. They proposed that there are three factors that contribute to the ultimate shear strength such as: (1) the strength of the compressive zone at the end of the inclined cracks; (2) the pull-out forces on the fibres along the inclined cracks; and (3) the shear forces carried by dowel and membrane actions. The punching shear strength of an FRC slab is:

$$V_u = \xi\left(0.24 f_{spt} + 16\rho + v_f\right) b_{of} d \qquad \text{(in SI units)} \tag{2.23}$$

where

ξ is the factor to account for the shear span-to-depth ratio, the value is taken to be 1.40 for slabs

f_{spt} is the split tensile strength of the FRC composite, taken to be:

$$f_{spt} = \frac{f_{cu}}{20 - \sqrt{F}} + 0.7 + \sqrt{F} \tag{2.24}$$

f_{cu} is the concrete cube strength.

ρ is the flexural reinforcement ratio (= A_s/bd).

b_{of} is the reduced critical perimeter, taken to be $b_{of} = b_o(1\text{-}0.55F)$; b_o is the critical perimeter calculated at $1.5h$ away from the column faces with round corners.

Shear strength v_f due to the presence of fibres is a function of the fibre-matrix bond strength and other fibre parameters such as the fibre type, the fibre volume fractions V_f, and the fibre aspect ratio (L_f/D_f). From the formulation of the v_f shown below, it can be seen that the shear strength v_f is basically a simpler form of the ultimate tensile strength σ_{cu} of a FRC given by Swamy et al. and Lim et al. (discussed earlier). The shear strength due FRC v_f is given by

$$v_f = 0.41\tau F \tag{2.25}$$

and,

$$F = \left(\frac{L_f}{D_f}\right) V_f n_f \tag{2.26}$$

where τ is taken to be 4.15 N/mm^2, it is the basic bond strength defined as the average fibre-matrix interfacial bond stress that is also the same value as originally proposed by Swamy and Mangat (1976) and also used in the model by Theodorakopoulos and Swamy (1999, 2003). F is a parameter called "Fibre factor" (Eq. 2.26) which was intended to adjust the average basic bond strength (4.15 N/mm^2) when different types, contents and geometries of fibres are used. n_f is the bond factor that depends on the shapes of fibres, it is taken to be 0.5 for round fibres, 0.75 for crimped fibres, and 1.0 for douform fibres. The hooked end fibres were not considered at the time.

Note that in this method by Narayanan and Darwish (1987), an addition of fibres influences the size of critical shear perimeter, where the basic critical perimeter b_o is reduced by a factor (1-0.55F). This factor is empirically derived based on the observations from the punching shear tests of 12 slabs by Narayanan and Darwish (1987), in which the fibre volume fraction was varied at 0%, 0.25%, 0.75%, 1.00% and 1.25%. The type of fibre used was the crimped steel fibres with aspect ratio of 100. Their conclusions are: as the fibre volume fraction increases, the punching shear strength of a slab increases, and the position of the critical shear perimeter around the loaded area is reduced.

Method by Shaaban and Gesund (1994)

Shaaban and Gesund (1994) conducted an experimental study of steel fibres reinforced concrete (SFRC) slabs, the corrugated type of steel fibre was used and the volume fraction of fibre was varied from 0.6% to 2.0%. A simple empirical expression to predict the punching shear strength of a SFRC slab based on the ACI Code punching shear equation was then proposed as follows.

$$V_u = 0.05\left(0.3W_f + 6.8\sqrt{f_c'}\right)b_o d \tag{2.27}$$

where W_f is the percent of fibres by weight of concrete, taken as $W_f = 7859V_f/w_c$, and w_c is the unit weight of plain concrete, the critical perimeter b_o is calculated at $0.5d$ away from the column faces. Note that the term ($0.3W_f$+$6.8\sqrt{f'_c}$) is in psi units which is an approximate equation for the concrete tensile strength f_{ct} obtained from a linear regression analysis by Shaaban and Gesund (1993).

Variable Engagement Model (VEM) By Voo and Foster (2003)

Voo and Foster (2003) developed the Variable Engagement Model (VEM) to predict the ultimate tensile strength of a FRC composite subjected to uniaxial tension. In brief, the VEM defines a term called "the engagement length w_e", where w_e is a tangential equation ($w_e = \alpha \tan \theta$), θ is the random angle of fibre orientation in a FRC element, α is an empirical value depending on type of fibre. So, the basic criteria of the model and the use of this engagement length are: (1) when the crack

opening displacement or crack width w is smaller than w_e and bigger than the fibre embedment length L_a ($w < w_e$ and $w > L_a$), there is no pulling force developed in the fibre. (2) The pulling force is only developed when the crack opening displacement w is in between the engagement length w_e and the fibre embedment length L_a ($w_e \leq w < L_a$).

Technically speaking, the VEM are also based on the same principles as the theory for tensile strength of FRC composite discussed in previous sections. In here, the ultimate tensile strength of an FRC composite is denoted as f_{tf} ($= \sigma_{cu}$) and it is given in a form of

$$f_{tf} = K_f \alpha_f \rho_f \tau_b \tag{2.28}$$

where α_f is the fibre aspect ratio ($= L_f/D_f$), ρ_f is the same as V_f or the fibre volume fraction, and τ_b is defined as the bond stress between the fibres and the concrete matrix (same as τ_u, the ultimate bond strength of fibre matrix interface). Voo and Foster (2003) proposed the ultimate bond strength τ_b to be proportional to $\sqrt{f'_c}$ as shown by

$$\tau_b = k_b \sqrt{f_c'} \tag{2.29}$$

where k_b is a bond factor and taken as 0.8 for hooked-end fibres, 0.6 for crimped fibres, and 0.4 for straight steel fibres.

One of the main contributions of VEM is the term K_f, a global orientation factors, that has the same role as the orientation factors n_o and n'_o described earlier in σ_{cu} [Eq. (2.14) or Eq. (2.20)], but this factor K_f is not taken to be a constant value as proposed by Swamy et al. and Lim et al. (1987) (discussed above).

With respect to the derivation of the factor n'_o shown by Eq. (2.22), this factor K_f is also a mean value of the probability function over the domain of fibre orientation. The VEM's domain of fibre orientation is different to the one used by Lim et al. (1987); it is a function of the crack width w. Detailed derivation of K_f can be obtained in a paper by Voo and Foster (2003).

By assuming the failure of FRC composite is solely by the fibre-matrix interface bond failure or the fibre pull-out mechanism, the final from of K_f is:

$$K_f = \frac{1}{\pi} \tan^{-1}\left[\frac{w}{\alpha_l L_f}\right]\left(1 - \frac{2w}{L_f}\right)^2 \leq 0.5 - \frac{0.645}{\alpha_f^{0.45}} \tag{2.30}$$

where α_I is defined as the engagement parameter that is empirically taken to be proportional to the fibre aspect ratio ($\alpha_f = L_f/D_f$), that is $\alpha_I = 1/(3.5\alpha_f)$. w is the crack width, and there is no specific equation for w given in VEM.

Application of VEM for shear design of FRC beams

Foster (2010) proposed an application of VEM to be applied to the shear strength component contributed by FRC shown in Fig. 2.10, that is:

$$V_{Rd,f} = k_{fd}\, f_{tf}\, b_w\, z\cot\theta \tag{2.31}$$

where k_{fd} is a reduction factor due to the fibre dispersion, taken as $k_{fd} = 0.82$. b_w is the width of the beam section, z is the depth of between the centroids of compression and tension reinforcing bars. The ultimate tensile strength of FRC composite f_{tf} is given earlier in Eq. (2.28) which is essentially a function of the crack width w, and Foster (2008) proposed a simple equation for w, that is:

$$w = 0.2 + 1000\epsilon_x \geq 0.125 \text{ mm} \tag{2.32}$$

where the longitudinal strain ε_x is calculated at the mid-depth of the beam's section. Model Code 2010, Foster (2010), and Collins et al. (2008) have provided the equation for the longitudinal strain ε_x.

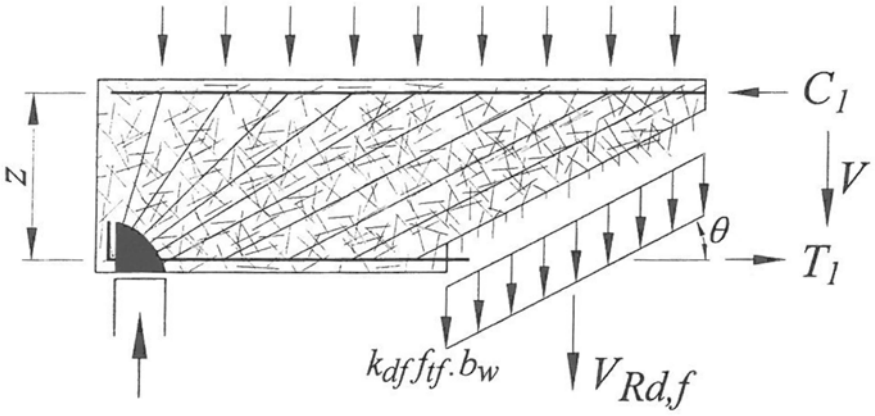

Fig.2. 10 – Shear component due to the presence of fibres in SFRC beam [taken from Foster (2008)]

Application of VEM for punching shear design of FRC slabs

Maya, Ruiz, Muttoni and Foster (2012) incorporated VEM with the critical shear crack theory (CSCT) [Muttoni (2008)] to predict the ultimate punching shear strength of an SFRC slab. As similar to other methods, the total punching shear strength of the method VEM+CSCT is also a summation of two components such as

$$V_u = V_c + V_{Rf}$$

where V_c is the shear strength contributed by non-fibrous concrete component determined by the CSCT method which was already discussed earlier by Eqs. (2.3) and (2.4) in Section 2.5.1. V_{Rf} is the shear contribution from FRC composite. The VEM's ultimate tensile strength f_{tf} [Eq. (2.28)]is assumed uniform across the inclined crack surfaces, therefore the equation of V_{Rf} was simply expressed as

$$V_{Rf} = f_{tf} A_p \tag{2.33}$$

where A_p is the horizontally projected area of the punching shear failure surface, the inclination of the failure surface can be taken as 45 °. The uniform tensile stress is calculated using the crack opening w at a control distance $d/3$ from the bottom face of the slab. Muttoni and Ruiz (2010) proposed the crack opening at this location to be a function of slab rotation ψ, that is

$$w = \psi d/6 \tag{2.34}$$

To calculate the ultimate punching shear strength, complex procedures and iterative analysis are needed. Note that the equation of the slab rotation itself is also a function of the variables such as the applied shear load V and the shear load V_{flex} by yield line analysis; where V_{flex} depends on the ultimate moment capacity that is also influenced by the fibre parameters. Therefore, all these make the CSCT+VEM method complex for practical application.

Method by Higashiyama et al. (2011)

Hagashiyama, Ota, and Mizukoshi (2011) investigate the influence of SFRC on the punching shear strength of a slab by conducting the punching shear test of 12 small-scale slabs (1.2 m × 1.2 m, 100 mm thick), hooked-end steel fibres were used. The fibre volume fraction was varied from about 0.6% to 1.0%. The design method by JSCE (Japan Society of Civil Engineers 2008) for predicting the punching shear strength of RC slab was modified to be applicable for SFRC slabs. The modification is based on the design method by Narayanan and Darwish (1987) as discussed previously. Hagashiyama, Ota, and Mizukoshi (2011) proposed punching shear strength V_u equation to be as follows.

$$V_u = \beta_d \beta_p \beta_r (f_{pcd} + v_f) u_p d \tag{2.35}$$

where

$$f_{pcd} = 0.2\sqrt{f_c'} \leq 1.2 \text{ N/mm}^2 \tag{2.36}$$

$$v_f = 0.41\tau F \tag{2.37}$$

$$\beta_d = \left(\frac{1000}{d}\right)^{1/4} \leq 1.5 \tag{2.38}$$

$$\beta_p = (100\rho)^{1/3} \leq 1.5 \tag{2.39}$$

$$\beta_r = 1 + \frac{1}{1 + 0.25u/d} \tag{2.40}$$

$$u_p = (u + \pi d)(1 - 0.32F) \tag{2.41}$$

$$F = \left(\frac{L_f}{D_f}\right) V_f n_f \tag{2.42}$$

where f_{pcd} is the shear strength due to the plain concrete, v_f is the shear strength increment due to the presence of fibres (same as Eq. (2.25)); τ is the average bond stress, taken as 4.15 N/mm^2; u_p is the critical perimeter calculated at 0.5d away from a column face with round corners with an empirical reduction factor (1- 0.32F) to account for the influence of FRC on the critical section (according to Narayanan and Darwish (1987)); u is the length of the column perimeter. F is the fibre factor which is calculated the same as the fibre factor given in Eq. (2.26) by Narayanan and Darwish (1987). β_d is the size effect factor; β_p is the factor to take into account the influence of reinforcement ratios; β_r is the reduction factor to account for the effect of column width-to-depth ratio.

Several researchers have also proposed design methods which are mainly based on the approach that uses fibre parameters to approximate the shear strength of an SFRC. Some these researchers are: Harajli et al. (1995), Choi et al. (2007), Nguyen-mind et al. (2012), and Gouveia et al. (2014). Their respective methods are not covered in detailed in this study.

2.6 Summary

This chapter summarises past studies and research on the punching shear strength of both reinforced concrete (RC) and fibre reinforced concrete (FRC) slabs. From the literature review above, a key summary is as follows:

Punching shear design is critical for both RC and FRC slabs. Design rules for RC flat slab system were initiated around the 1970s to 1980s. Since then, punching shear in concrete slabs has been on-going research topics. Research on FRC slabs are relatively new compared to conventional RC slabs.

Influences of several structural parameters on the punching shear strength were discussed in Section 2.3. The key parameters that the author investigates in this study are: (i) The flexural reinforcement (the effect of low reinforcement ratios), (ii) the concrete strength (the effect of high strength concrete), (iii) the column aspect ratio (the effect of column rectangularity), and (iv) the steel fibre reinforced concrete, particularly the influence of the double hooked end fibres. The review showed that further investigations on these parameters are still needed.

In Section 2.5, the author discussed details of past research and design methods that have addressed the influences of the key parameters on the punching shear strength as highlighted in the previous paragraph. The author will use some of the literature in Section 2.5 to compare, validate with test results and existing data; and they will also be the main references for the development and comparisons of the author's proposed design methods that will be presented later in Chapter 7 and Chapter 8.

3

REVIEW OF DESIGN CODE PROVISIONS, GUIDELINES, AND ANALYSIS METHODS

3.1 Introduction

This chapter covers some relevant Code provisions, design guidelines and also analysis methods for both reinforced concrete (RC) slabs and fibre reinforced concrete (FRC) slabs. ACI 318's and Eurocode 2's design provisions for punching shear in concrete slabs without shear (traverse) reinforcement are presented and reviewed. Singapore has recently (since 2012) adopted Eurocode 2 as the national code for design of concrete structures. The previous Singapore Code CP65-1 (1997) was essentially based on the old British code BS 8110-1 (1997). Other codes such as Australian Code (AS 3600-2001), New Zealand Code, NZS 3101-2006 (NZS 2006), Canadian (Code CSA-A23.3-04) treat shear design of concrete slabs the same way as ACI 318 does (American Code). Therefore, in this study, only ACI 318-14 and Eurocode 2 are considered, since the ACI Code and the Eurocodes have been widely adopted by many countries.

In this chapter, the author discusses code-like design guidelines that are particularly applicable to the design of FRC slabs. These design guidelines are from the ACI-544.6R report prepared by ACI Committee 544 (2015), the TR34 (Technical Report 34) by the Concrete Society (2015), and Model Code 2010 by fib committee 65-66 (2012).

The author briefly discusses some of the common analysis methods for calculating moments in two-way slabs such as the direct design method and the equivalent design method. A yield-line analysis for calculating the failure load of a ductile slab is also discussed. Equations of the shear (failure) loads corresponding to several yield line patterns that are relevant to the author's current research works are presented.

To design a slab, a typical design procedure listed below can be followed:

1. Select a trial thickness h of a slab to satisfy the requirements for the deflection control at service load conditions, which can be the minimum slab thickness as provided by ACI 318-14's Sect 8.3 or Eurocode 2's Sect 7.4. Note that the minimum thickness of a slab is influenced by the types of slab systems, the strength of the reinforcements (considered by ACI), reinforcement ratios (considered by EC 2). Essentially, the trial thickness can be approximated as $L_n/30$, where L_n is the clear span in the longer direction.
2. Select the analysis methods for calculating and distributing bending moments in the slab. The methods can be the computer finite element analysis (FEA) method, the direct design method (covered in Section 3.4.1 of this thesis), and equivalent frame method (covered in Section 3.4.2 of this thesis).
3. Obtain the distributed moments in critical regions where negative and positive bending moments are highest.
4. Determine the flexural reinforcements required for the moments obtained in step 3.
5. Check that the punching shear strength of a slab at the column-slab connection is not lower than the design load.

3.2 Code provisions for punching shear

3.2.1 ACI 318-14 (2014)

According to the American Concrete Institute ACI 318-14(2014), in Section 22.6.5.2 of the code, the punching shear strength V_c of slabs without shear reinforcement can be determined from the lowest of the following expressions:

$$V_c = 4\lambda\sqrt{f_c'}\,b_o d \quad \text{(U.S. units)}$$
$$= \frac{1}{3}\lambda\sqrt{f_c'}\,b_o d \quad \text{(SI units)} \qquad (3.1a)$$

$$V_c = \left(2 + \frac{4}{\beta}\right)\lambda\sqrt{f_c'}\,b_o d \quad \text{(U.S. units)}$$
$$= \frac{1}{12}\left(2 + \frac{4}{\beta}\right)\lambda\sqrt{f_c'}\,b_o d \quad \text{(SI units)} \qquad (3.1b)$$

$$V_c = \left(2 + \frac{\alpha_s d}{b_o}\right)\lambda\sqrt{f_c'}\,b_o d \quad \text{(U.S. units)}$$

$$= \frac{1}{12}\left(2 + \frac{\alpha_s d}{b_o}\right)\lambda\sqrt{f_c'}\,b_o d \quad \text{(SI units)} \qquad (3.1c)$$

Note: SI units: [MPa, mm]; U.S. units: [psi, in.]

where

β is the ratio of the lengths of the long and short sides of a rectangular column or loaded area is larger than 2.0; for the nonrectangular columns, β can be calculated as illustrated in Fig. 3.1(a).

α_s is taken to be 40, 30, 20 for interior, edge, and corner columns, respectively;

b_o is the length of the critical perimeter located at 0.5d away from the column face as illustrated in Fig. 3.1(b). For a circular column, the critical section can also be defined by assuming a square column of equivalent area.

λ is taken as 1.0 for the normal-weight concrete. It is the modification factor ranging from 0.75 to 1.0 for different types of concrete (i.e

normal-weight, lightweight concrete, etc.)

Discussions: The influences of flexural reinforcement and size effect are neglected in the ACI Code equations. ACI 318-14 does not limit the maximum concrete strength f'_c for general uses, but the value of $\sqrt{f'_c}$ used to calculate shear strength V_c is limited to 100 psi or 8.3 MPa. An increase in the shear strength due to fibre reinforced concrete (FRC) has not been considered in ACI Code.

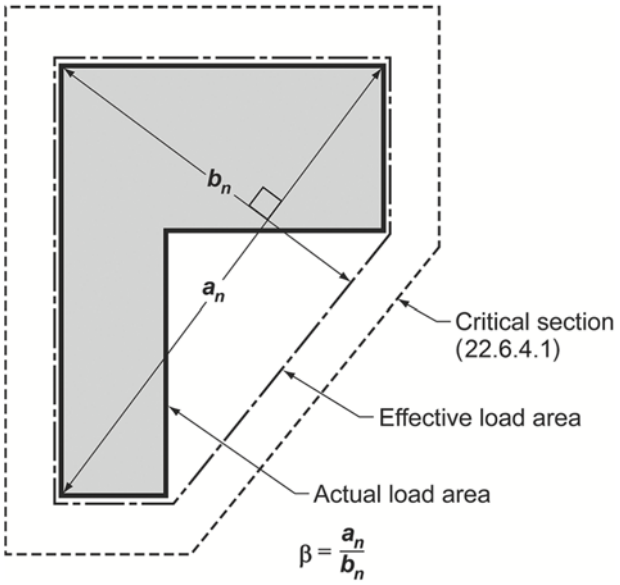

(a) Taken from ACI 318-14 (Fig. R22.6.5.2)

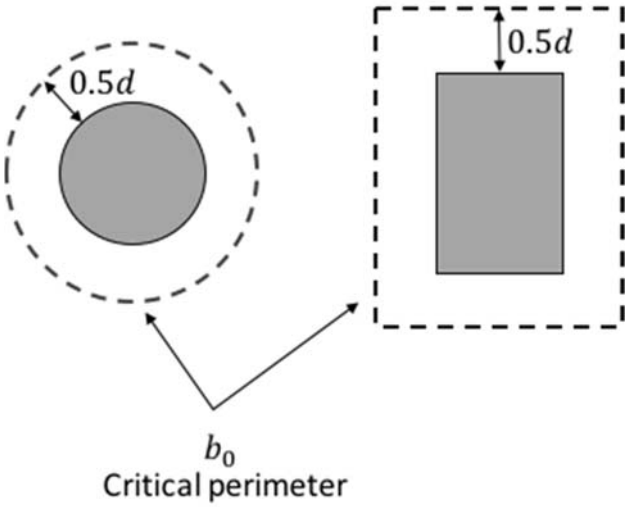

(b)

Fig.3. 1 – (a) Value of β for nonrectangular columns; (b) Critical sections of circular column and rectangular columns

3.2.2 Eurocode 2 (2004)

According to the Eurocode 2's Sect. 6.4, the punching shear resistance $V_{Rd,c}$ of a slab without shear reinforcement is given as follows.

$$V_{Rd,c} = 0.18k(100\rho f_c')^{1/3}u_1 d \geq v_{min}u_1 d \quad \text{(SI units)}$$
$$= 5k(100\rho f_c')^{1/3}u_1 d \geq v_{min}u_1 d \quad \text{(U.S. units)} \qquad (3.2)$$

Note: SI units: [MPa, mm]; U.S. units: [psi, in.]

where

k is the size effect coefficient, taken as $k = 1+\sqrt{(200/d)} \leq 2.0$ (in SI units);

$k = 1+\sqrt{(8/d)} \leq 2.0$ (in U.S. units).

ρ is the average flexural reinforcement ratio, or $\rho = \sqrt{(\rho_x \rho_y)}$

u_1 is the critical shear perimeter located at a distance $2d$ (2 times the effective depth) away from the column faces and it has around corners as shown in Fig. 3.2.

v_{min} is the minimum shear strength, taken as $v_{min} = 0.035k^{3/2}(f'_c)^{1/2}$ (in SI units); or $v_{min} = 0.42\ k^{3/2}(f'_c)^{1/2}$ (in U.S. units)

The EC2's basic shear strength $v_c = 0.18k(100\rho f'_c)^{1/3}$ is essentially the shear strength corresponding to the cross-sections at the end of an idealised shear-failure plane. The inclination of the failure plane is taken to be about 26.6°; hence, the critical shear perimeter u_1 is located at a distance $2d$ or about [cot (26.6°)×d] away from a column face. The EC2 equation does not specifically limit the compressive strength of concrete in the shear equation like the case of the ACI Code. However, in Eurocode 2 (2004) Section 3, the provision for concrete strength f'_c is provided up to 90 MPa.

Discussions: The EC2 equation neglects the effect of column rectangularity in symmetrically loaded slabs. However, for a case where an unbalanced moment is transmitted by uneven shear and by bending and torsion, the design load should be increased or the punching shear capacity should be reduced by a factor that is a

function of column aspect ratio. Eurocode 2 does not consider an influence of fibre reinforced concrete (FRC) on the shear strength of a concrete member.

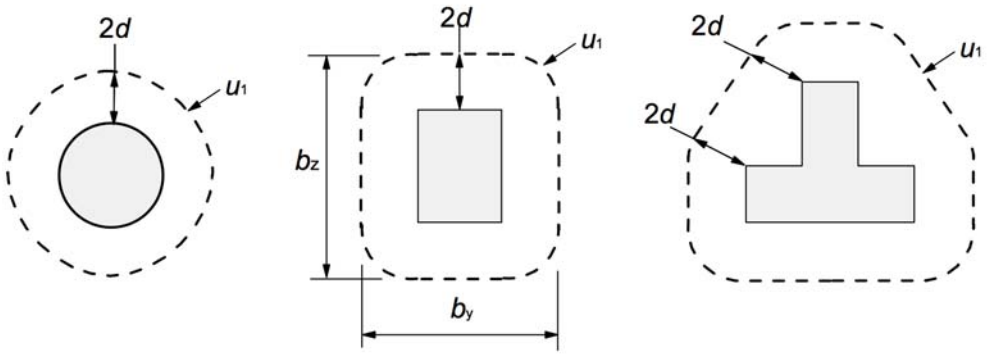

Fig.3. 2 – Typical basic control perimeters. Note by and bz are the lengths of the long side and the short side of the critical perimeter, respectively (taken from Eurocode 2 (2004))

3.3 Non-code design guidelines for punching shear

3.3.1 ACI 544.6R-15 (2015)

ACI Committee 544 (2015) provides design approaches for Steel FRC (SFRC) slabs in the report ACI 544.6R-15. In Section 6.3 of ACI 544.6R-15, it is interesting to point out that that the punching shear failure is considered as not critical in SFRC flat-plate slabs. In another word, ACI 544.6R only considers the flexural design of the SFRC slabs.

In ACI 544.6R, two approaches to evaluate the moment capacity of an SFRC slab have been proposed, such as: (1) the first approach is based on the post-cracking residual strength concept of FRC; (2) the second approach is based on the results obtained from round slab tests and applying yield-line analysis to determine the corresponding moment capacity.

First approach:

The moment capacity obtained using the first approach is rather straightforward and was developed based on the fibre concrete behaviour shown in Fig. 3.3. Some simplifications were made, and the ultimate moment capacity per unit width of a FRC section can be calculated by the following expression.

$$m_u = \frac{3\mu\omega}{\mu + \omega} m_{cr} \qquad \text{(SI units)} \qquad (3.3)$$

where parameters μ (≤ 1.0) and ω (≥ 1.0) represent a reduction in tensile stress and an increase in the compressive strength due to a presence of FRC, respectively. The moment at first crack m_{cr} is taken as $m_{cr} = \sigma_{cr}h^2/6$; σ_{cr} is tensile stress at first crack (or modulus of rupture) which ACI 318-14 provides this value to be approximated as $\sigma_{cr} = 7.5\sqrt{f'_c}$ (in U.S. units) or $\sigma_{cr} = 0.625\sqrt{f'_c}$ (in SI units).

Second approach:

In the second approach, the yield line analysis is applied to a round slab specimen that is simply supported around the edge and loaded at the centre shown in Fig. 3.3 (b). Therefore, take the yield line pattern to be circular fan and the loading area to be a concentric point load, the moment capacity can be given by

$$m_u = \frac{P_{max}}{2\pi} \tag{3.4}$$

where P_{max} is the failure load of a round FRC slab specimen. Note that yield line theory is reviewed and discussed later Section 3.4.3. ACI 544.4R (2009) also provided an empirical equation for calculating moment capacity of an FRC beam which will be discussed later in Section 3.4.3.3.

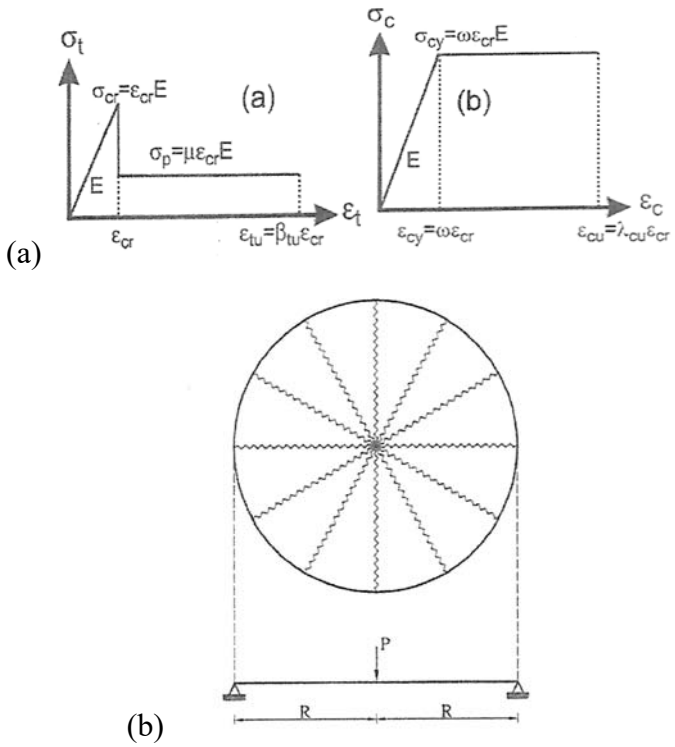

Fig.3. 3 – (a) Idealised strain-softening FRC models for: (left) tension; and (right) compression). (b) a simply supported round slab and its corresponding circular fan yield line pattern. (taken from ACI 544.6R-15)

3.3.2 TR 34 by Concrete Society (2015)

The Concrete Society (2015)'s TR 34 (Technical Report 34, edition 4) provides a design equation for calculating the punching shear strength of an FRC slab shown. The method is based on the Eurocode 2 equation and the recommendations by RILEM (2003). The punching shear strength comprises of two components such as the shear strengths contributed by the non-fibrous reinforced concrete v_c (EC2's equation, Eq. (3.2)) and by the FRC v_f. TR 34 recommends to use only 50% of the RILEM's shear strength v_f (= 0.5×0.12f_r). The method can be summarised as follows.

$$V_{Rd} = (v_c + v_f)ud \tag{3.5}$$

where

$$v_f = 0.5\times0.12f_r = 0.06f_r \tag{3.6}$$

$$f_r = (1/4)(f_{r1} + f_{r2} + f_{r3} + f_{r4}) \tag{3.7}$$

The shear strength v_c is given by the EC2 equation in Eq. (3.2), or $v_c = 0.18k(100\rho f'_c)^{1/3}$; the average residual flexural strength f_r is taken to be the average value of f_{r1} , f_{r2}, f_{r3} and f_{r4}, which are the residual flexural strengths corresponding with the CMOD (crack mount opening displacement) = 0.5, 1.5, 2.5, and 3.5, respectively. In which, $f_{rj} = (3F_j l)/(2bh^2_{sp})$, where F_j is the load at each CMOD; l, b, and h_{sp} are the dimensions of the beam specimen defined in EN 14651. Figure 3.4 shows an example of the load F - CMOD response curve of a notched FRC beam, taken from EN 14651 (2007).

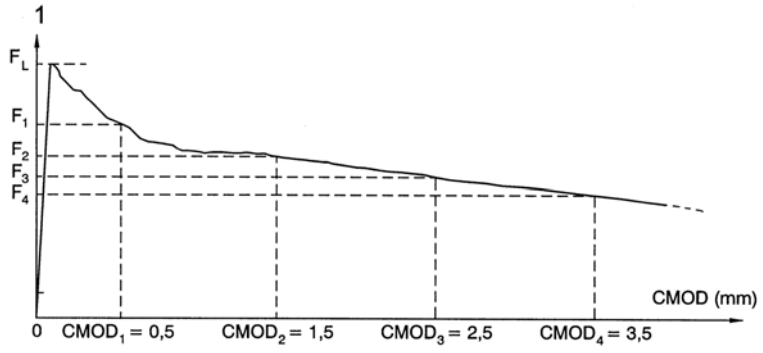

Fig.3. 4 – Example of the load-CMOD response curves (EN 14651 2008)

3.3.3 Model Code 2010

Similar to the TR34 as discussed above, the shear strength due to FRC v_f is linearly added up to the basic shear strength of non-fibrous reinforced concrete v_c to become the total punching shear strength V_{Rd} as shown by

$$V_{Rd} = (v_c + v_f) b_o d \tag{3.8}$$

where, v_c and v_f are subsequently described as follows:

The basic punching shear strength v_c here is based on the critical shear crack theory (CSCT) (Muttoni 2008) reviewed in Chapter 2, the punching shear strength v_c [Eq. (3.9)] is a function of $\sqrt{f'_c}$ and k_ψ; where k_ψ (= 1/[1.5+0.9$k_{dg}\psi d$]) is a factor accounting for the opening and the roughness of the cracks. The formulations of the shear strength are as follows.

$$v_c = k_\psi \sqrt{f'_c} = \frac{1}{1.5 + 0.9 k_{dg} \psi d} \sqrt{f'_c} \le 0.6 \sqrt{f'_c} \tag{3.9}$$

where

$$\psi = 1.5 \frac{r_s}{d} \frac{f_y}{E_s} \tag{3.10}$$

$$k_{dg} = \frac{32}{16 + d_a} \tag{3.11}$$

The slab rotation ψ is calculated using the simplest form of equations for approximating the rotation of a slab provided in Model Code 2010. Other robust forms of equations need an iterative analysis. The basic control perimeter b_o has round corners and it is calculated at $d/2$ away from the column faces. k_{dg} is the size effect factor that depends on the maximum aggregate size d_a. r_s is the radius of the slab (= half of a slab length or 0.22L) where L is column-to-column span. The maximum value of $\sqrt{f'_c}$ in Eq. (8) is limited to 8.0 MPa. In Eq. (8), d_a is taken to be zero for high strength concrete (f'_c > 70 MPa) and for lightweight concrete.

The shear strength contribution due to the presence of FRC v_f can be derived based on the simplified post-cracking constitutive laws in Sect 5.8 of the Model Code 2010. Model Code 2010 provides two equations for calculating v_f. The first equation shown in Eq. (3.12) is based on the constitutive law called "rigid-plastic model" in which the residual tensile stress is assumed a constant (= f_{r3}/3) at any

crack opening. The second equation shown in Eq. (3.13) is based on the "linear model" where the residual tensile stress is 0.45 f_{r1}at the tip crack opening and linearly proportional to the maximum crack opening w_u, with the w_u taken to be 1.5 mm in Eq. (10). The two equations of v_f are:

Frist method, from the rigid – plastic model [Fig. 3.5(a)]

$$v_f = f_r/3 \tag{3.12}$$

Second method, from the linear model [Fig. 3.5(b)]:

$$\begin{aligned} v_f &= 0.45f_{r1} - \frac{w_u}{2.5}(0.45f_{r1} - 0.5f_{r3} + 0.2f_{r1}) \\ &= 0.45f_{r1} - 0.6(0.65f_{r1} - 0.5f_{r3}) \end{aligned} \tag{3.13}$$

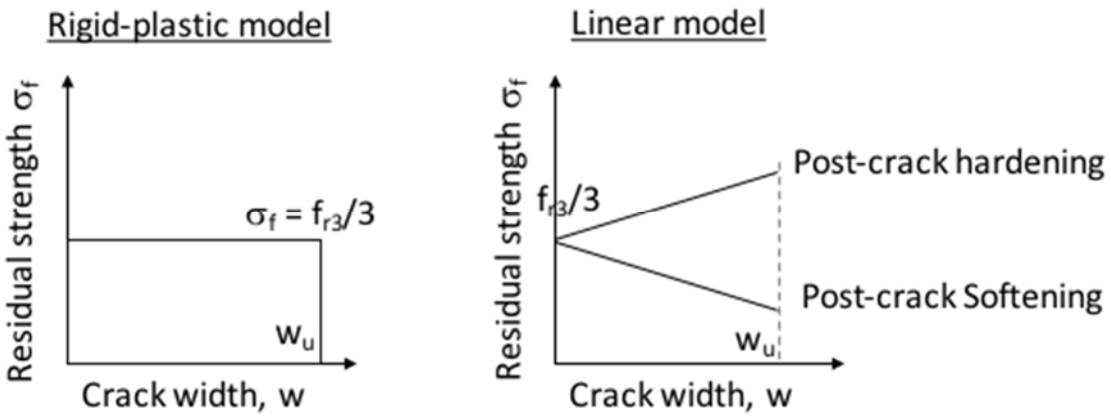

(a) (b)

Fig.3. 5 – Constitutive laws of fibre reinforced concrete

It can be seen that the second equation of v_f in Eq. (10) takes into account the post-crack hardening and also post-crack softening behaviours of the cracked FRC members. Since these post-crack behaviours were observed and will discussed in the chapter, the authors use v_f in Eq. (3.13) for the Model Code 2010's method for the subsequent analysis and comparison with the test results.

3.4 Analysis methods

3.4.1 Direct design method

The direct design method is an approximate analysis method to determine the distributing bending moments in uniformly loaded two-way slabs, which is applicable for both flat slabs system and beam-slabs system. ACI 318-14 Section 8.10 provides the provisions for this method. Two-way slabs can be designed using the direct design method if the following limitations are satisfied:

1. There should be at least three continuous spans in each direction.
2. Column-to-column span lengths should not differ by more than one-third the longer span
3. Panels (slab bay) should be rectangular, with the aspect ratio not to exceed 2 (the ratio of the longer to shorter sides of the panel, measured centre-to-centre of supports).
4. Column offset shall not exceed 10% of the span in the direction of offset from either axis between centrelines of successive columns.
5. All loads should be due to gravity only and uniformly distributed over an entire panel.
6. Unfactored live load shall not exceed two times the unfactored dead load.
7. For a panel with beams between supports on all sides. The relative stiffness requirement provided in ACI 318-14 Sect. 8.10.2.7 should be satisfied (details are not needed in this study).

Application of the direct design method is to determine the factored static moment M_o in each slab panel that is then distributed to critical design moments (negative moments, positive moments) in various regions of a slab structure. The regions of a slab structure are defined by longitudinal strips such as the column strips and the middle strips as illustrated in Fig. 3.6. Comprehensive design examples using the ACI direct design method are provided in a textbook by McGregor and Wight (2000 4th edition in SI units).

Note the procedure of the direct design method is summarised and provided in Appendix C.

Discussions: The direct design method is a simple approximate method to calculate the distributed moments in a two-way slab structure. In most cases, the method will give reliable and conservative analysis results. Thus, considering the complexity of analysis and calculation efforts, the direct design method is substantially more effective than other approximate methods such as the equivalent frame method (discussed in next section). It is an efficient design tool for determining the preliminary slab dimensions and flexural reinforcements. The preliminary design can then be counter-checked by more advanced analysis techniques such as the finite element method.

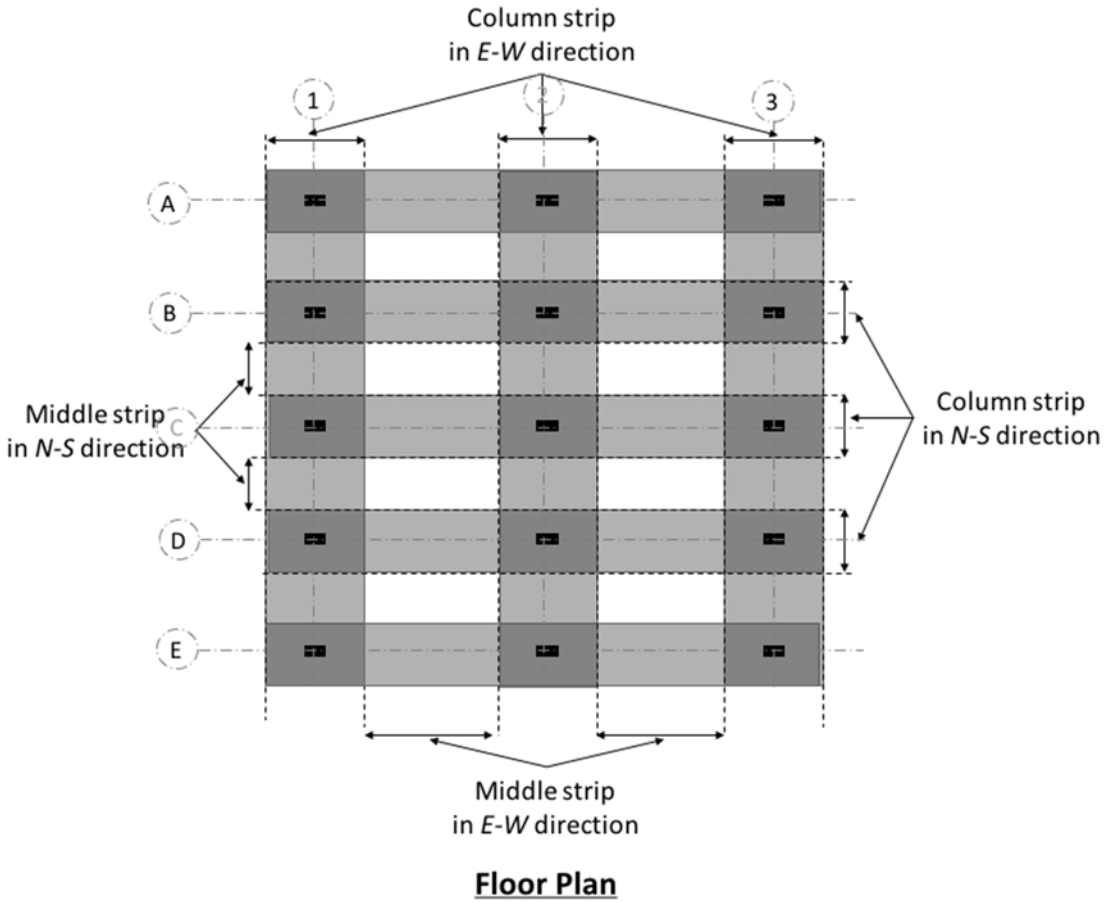

Fig.3. 6 – Flat plate floor plan showing column strips and middle strips in both directions

3.4.2 Equivalent frame method

The equivalent frame method is also an approximate method that is more complex and complete the direct design method. The equivalent frame method is based on past studies reported in Corley, Sozen, and Siess (1961), Corley and Jirsa (1970). The provisions for the equivalent frame method is provided in ACI 318-14 Section 8.11.

In the equivalent frame method, the design loads need not be restricted to uniformly distributed loads only; the lateral loads are permitted in the analysis, a slab structure having only two spans in both directions are eligible. Essentially, the method utilises the conventional two-dimensional frame analysis techniques to determine the distributions of moments and shears. According to ACI 318-14 Section 8.11, the width of each equivalent frame is bounded by the centrelines of the adjacent panels as shown in Fig. 3.7. The equivalent frame consists of three parts: (1) the horizontal slab strip, including any beams spanning in the direction of the frame; (2) the columns or other vertical supporting members, extending above and below the slab; and (3) the elements of the structure that provide moment transfer between the horizontal and vertical members.

Discussions: Although the equivalent frame method is more versatile than the direct design method, but the analysis requires considerable calculation efforts. The frame analysis is also highly repetitive and almost impractical to be done manually. Thus, computer programmes are necessary to aid the analysis. With constantly improving and affordable technologies, there have been a number of FEA (finite element analysis) software that can perform complex analyses of a whole structure with high accuracy, reliability, and time efficiency. Therefore, in current practice, the equivalent frame method may not be a preferred choice as before.

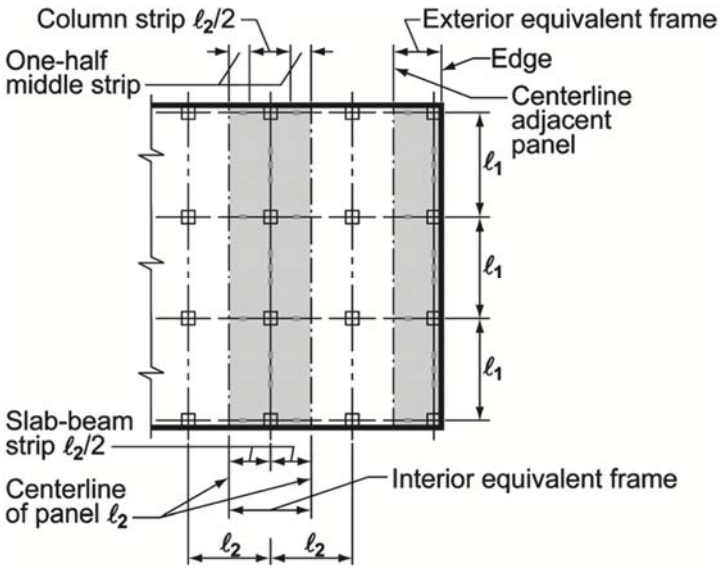

Fig.3. 7 – Definition of equivalent frame (ACI 318-14)

3.4.3 Yield line theory (limit analysis)

3.4.3.1 Background and limitations

Yield line theory is the method for the analysis of reinforced concrete slabs which was first introduced by Ingerslev (1923), and Johansen (1962) extended the theory into the more advanced form. The yield-line theory is an upper-bound approach for calculating the flexural strengths of ductile slabs, which means that the calculated load using the yield line analysis is either greater than or equal to the correct failure load. Park and Gamble (2000) have comprehensively detailed and discussed the basis of yield line theory and other aspects of reinforced concrete slabs in their book. From the review of past works on yield line theory, following summaries are made:

The ultimate load of a slab system is determined by postulating a collapse mechanism which has to be compatible with the loading and boundary conditions. A collapse mechanism is initiated by the plastic rotations of several slab segments bounded by the yield lines, in which concrete plastic hinges are assumed to occur along the assumed yield lines. Therefore, for the collapse mechanism to be completely developed, slab sections need to be sufficiently ductile to allow redistribution of moments, which permits the reinforcements across the yield lines

to yield. Note that the term "yield line" is indeed an idealised straight line of a band of flexural cracks across the yielded reinforcements.

One of the challenges in the yield line analysis is to identify the admissible yield line pattern of a slab that can represent the actual failure mechanism. If an incorrect pattern is used, the calculated ultimate load can be unsafe for design. However, most of the common yield line patterns in practice are generally known. To construct a possible yield line pattern of a slab, following basic rules can be applied.

(1) Yield lines must be straight lines which act as axes of rotation for the movements of the slab segments.
(2) The supports or the lines of supports of the slab must form axes of rotation.
(3) Deformation of each slab segments must be compatible, so a yield line must pass through the intersection of the axes of rotation of the adjacent slab segments.

Examples of yield line patterns with various support conditions are shown in Fig. 3.8.

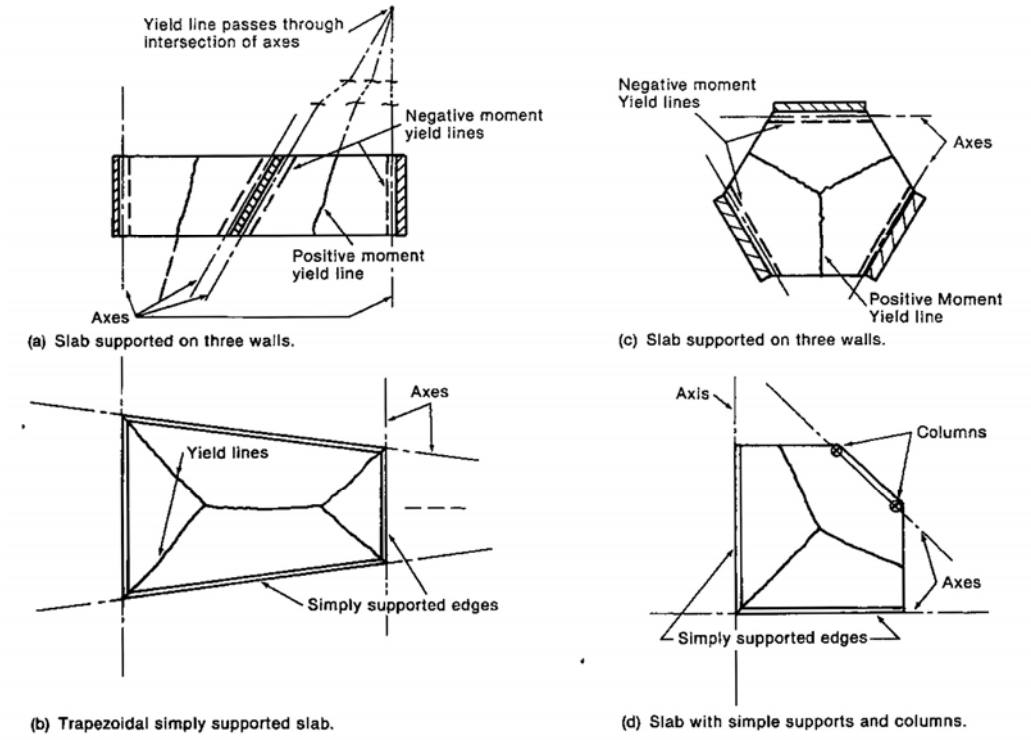

Fig.3. 8 – Examples of yield line patterns (McGregor and Wright 2005)

Limitations of yield line theory: Yield line theory is most applicable for the slabs with uniform arrangement of reinforcement in both directions (isotropic reinforcement). If the reinforcements are orthotropic (non-uniform arrangement in both directions) and non-orthogonal in the x and y directions, the analysis may lead to an inaccurate prediction of correct yield line patterns and ultimate loads. For this unusual case, a more complex yield line analysis method (analysis by the equilibrium method) may be used. Note that the equilibrium method is not covered in this thesis.

The theory requires a slab section to be ductile; however, it can be somewhat challenging to determine whether or not a given reinforcement ratio can satisfy the ductility requirement. This can lead to an issue when the shear (brittle) failure may occur before the calculated ultimate strength using yield line analysis is attained. Note that yield line theory cannot provide other design data such as the slab deflection and flexural stress at any state of non-ultimate loading (i.e. at service load state).

3.4.3.2 Calculation of the ultimate load using yield line analysis

To calculate the ultimate load of a slab using yield line analysis, two approaches can be used which are (1) the virtual work method; and (2) the equilibrium method. In this study, only the virtual work method is considered. At equilibrium, the principle of virtual work states that the external work U_E must be equal to the internal work U_I, that is

$$U_E = U_I$$

where the external work U_E is a summation of the products of all given applied forces to a rigid body and their corresponding virtual (arbitrary) displacements.

For cases of flat-plates supported on columns, the external force is the reaction acting on the column stub's centroid; at ultimate, this reaction becomes the ultimate load of the slab or the shear load that causes the reinforcements across the yield lines to yield. This load can be denoted as V_{flex}. Thus, take a virtual displacement δ parallel to the direction of the external force to be a unit displacement (δ = 1), note that this virtual displacement can be any arbitrary value

and it will be cancelled out eventually. Thus, the external work U_E can be expressed as:

$$U_E = V_{flex} \times \delta = V_{flex} \times 1.0$$

The internal work U_I is a summation of the (Vector) products of all the internal stresses induced by the external forces and the corresponding strains. For yield line theory, the internal work is the work done by the plastic rotation along each yield line, which is given by

$$U_I = \sum (m \times \theta \times l)$$

where m is the moment capacity per unit length along each yield line. θ is the rotational angle of each yield line, which is the ratio of the relative virtual displacement (proportional to δ) to the rotational length normal to the direction of the yield line. l is the length of each yeild line. Therefore, by applying the principle of virtual work ($U_E = U_I$), the ultimate load V_{flex} can then be obtained.

Some of the common yield lines patterns for slab specimens in punching shear tests are shown in Fig. 3.9. where, Fig. 3.9(a) is the yield line pattern for a lightly reinforced rectangular slab supported on the column and loaded around the edges; the pattern in Fig. 3.9(b) is for a lightly reinforced rectangular slab simply supported along the four edges and loaded through the column. Fig. 3.9(c) is the circular fan yield line pattern for a slab with medium to higher reinforcement ratios and for a slab containing fibre reinforce concrete which is also recommended by the ACI 544.6R (discussed earlier in Section 3.3.1).

In this current work, the equations of the ultimate load V_{flex} of the three yield line patterns as shown in Fig. 3.9 are presented below in Eqs. (3.14) to (3.16), respectively. The derivation of each equation can be obtained in Appendix C.

$$V_{flex} = m_u \left(\frac{4 + 2\left(\frac{c_2}{c_1} - 1\right)\frac{c_2}{L_2}}{\frac{\sqrt{2}}{2}\cos\frac{\pi}{8} - \frac{c_2}{L_2}} \right) \quad \text{(For Fig. 3.9(a))} \tag{3.14}$$

$$V_{flex} = m_u \left(\frac{4L_1}{L_2 - c_2} + \frac{4L_2}{L_1 - c_1} \right) \quad \text{(For Fig. 3.9(b))} \tag{3.15}$$

$$V_{flex} = m_u\left(\frac{2(c_1 + c_2)}{r} + 2\pi\right) \quad \text{(For Fig. 3.9(c))} \tag{3.16}$$

where c_1 and c_2, L_1 and L_2 are the dimensions of the column and the slab, respectively, as shown in Fig. 3.9. r is the radius of circular yield line or the distance from the column face to a point load, (for design purpose, r can be assumed to be $0.2L$, that is the distance from the column to the inflexion point in a flat plate floor). m_u is the ultimate moment capacity per unit length that can also consider the influence of FRC. The details of m_u are discussed immediately in the next section.

Note for some simple cases, where square columns and typical ranges of the column width to span length ratio are used; the ultimate load V_{flex} can be simply approximated (Park and Gamble 2000, Muttoni 2008) as $V_{flex} = 8m_u$.

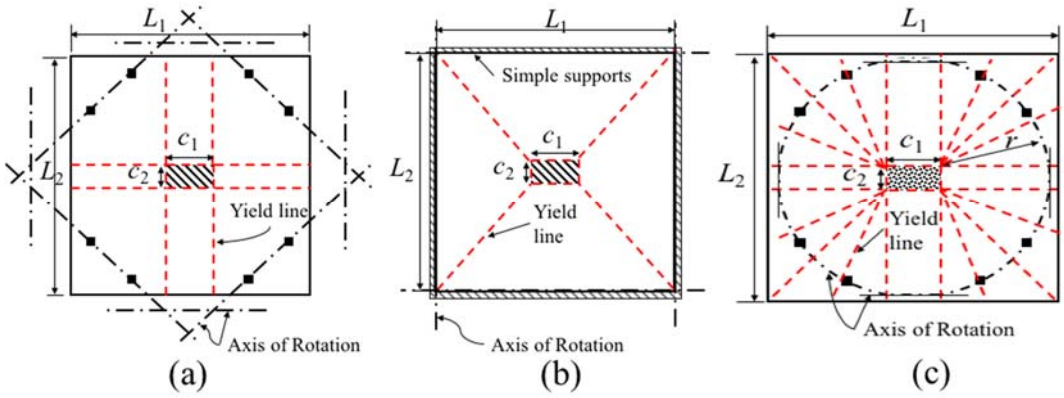

Fig.3. 9 – (a) yield line pattern a ductile slab loaded around the edges; (b) yield line pattern for a simply supported ductile slab; (c) circular fan yield line pattern

3.4.3.3 Ultimate moment capacity of RC and FRC slabs

Reinforced concrete (RC) slabs:

According to the ACI method for calculating the flexural strength of a singly reinforced slab or beam. For a non-fibrous concrete slab, the moment capacity per unit length m_u can be calculated as follows.

$$m_u = \rho d^2 f_y (1 - 0.59\frac{\rho f_y}{f'_c}) \qquad \text{(For RC member)} \qquad (3.17a)$$

where ρ is the average reinforcement ratio f_y is the yield strength of the reinforcement, f'_c is the (cylinder) compressive strength of the concrete; d is the average of the effective depths in both directions. For simple analysis purposes the term $(1 - 0.59\rho f_y/f'_c)$ in this moment capacity mu can be approximated as 0.95 without causing significant errors,. Thus,

$$m_u = 0.95\rho d^2 f_y \qquad (3.17b)$$

The influence of bottom (compressive) reinforcements on the moment capacity of a slab is considered insignificant; Park and Gamble (2000) have showed that design errors caused by the omission of bottom reinforcements are negligible.

Fibre reinforced concrete (FRC) slabs:

There is no standard design rule for calculating the moment capacity of SFRC member yet. The TR 34 method uses the classical beam bending approach to derive a standard equation for calculating ultimate moment capacity per unit width for an SFRC member, where tension controlled failure is assumed. The concrete tensile stress along crack openings is included in the analysis that leads the following equation.

$$\begin{aligned} m_u &= h^2(0.16\sigma_{r1} + 0.29\sigma_{r4}) + \rho d^2 f_y (1 - 0.048\frac{h}{d}) \\ &= h^2(0.072 f_{r1} + 0.107 f_{r2}) + \rho d^2 f_y (1 - 0.048\frac{h}{d}) \end{aligned} \qquad \text{(For FRC member)} \qquad (3.18)$$

where σ_{r1} (= $0.45f_{r1}$) and σ_{r4} (= $0.37f_{r4}$) are the equivalent tensile stresses [RILEM (2003)] at the neutral axis (tip of the crack opening) and the at the maximum crack opening at the tension face, respectively. Note m_u in Eq. (3.18) may not be accurate for calculating the moment capacity of an FRC slab with high reinforcement ratio

because the compression-controlled failure may govern. A more complex form of m_u is also provided in the TR34 (The Concrete Society, 2003) which requires an iterative analysis.

ACI Committee 544.4R (2009) provided a method for calculating moment capacity of a beam containing both conventional reinforcement and fibres. The method was developed by Henager and Doherty (1976) which based on the ACI method for the ultimate moment capacity of a singly-reinforced concrete beam, and the basic design assumptions of the method is shown in Fig. 3.10. The ultimate moment capacity M_u of a singly-reinforced FRC beam is expressed as follows:

$$M_u = A_s f_y \left(d - \frac{a}{2}\right) + \frac{1}{2}\sigma_t b(h-e)(h+e-a) \tag{3.19}$$

where

$$e = \left[\epsilon_{sf} + 0.003\right]c/0.003 \tag{3.20}$$

$$\sigma_t = 0.00772 F_{be}\, V_f \left(\frac{L_f}{D_f}\right) \tag{3.21}$$

a is the depth of rectangular stress block; h is the beam thickness; b is the width of the beam. A_s and f_y are the cross-sectional area and the yield strength of the reinforcement. e is the distance from extreme compression fibre to top of tensile stress block (Fig. 3.10); ϵ_{sf} is fibre strain (σ_f/E_s) based on the fibre stress developed at pull-out state, this stress is termed the dynamic bond stress and take as σ_f = 333 psi or 2.3 MPa. c is the distance from extreme compression fibre to neutral axis found by equating the internal tension and compression forces. σ_t [Eq. (3.21)] is the approximated tensile stress in the tension side of the neutral axis (See Fig. 3.10); L_f/D_f is the fibre aspect ratio (the fibre length-to-diameter ratio); V_f is the fibre volume fraction; F_{be} is the bond efficiency of the fibre 1.0 to 1.2 depending on fibre characteristics.

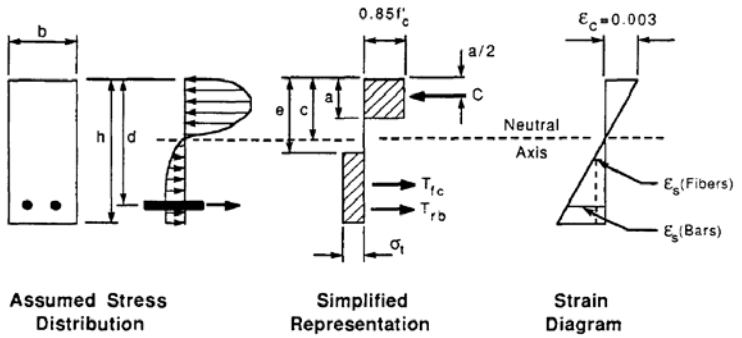

Fig.3. 10 – Design assumptions for analysis of singly reinforced concrete beams containing steel fibres (Henager and Doherty, 1976)

3.5 Summary

The author discussed the Code equations such as ACI 318-14 and Eurocode 2 (2004). ACI 318 has not considered the influences of reinforcement ratio and size effects in its shear equation. Eurocode 2 neglects the effect of column rectangularity in its shear equation. Both of the codes have not explicitly addressed the effect of low reinforcement ratio on the punching shear strength.

Other code-like design guidelines for SFRC slabs were discussed. These design guidelines are from the ACI-544.6R report prepared by ACI Committee 544, the TR34 (Technical Report 34) by the Concrete Society (2015), and Model Code 2010 by fib committee (2012). The ACI 544 method does not explicitly consider the punching shear failure to be critical for SFRC slabs. Both TR 34 and Model Code 2010 adopt the approach that uses the residual tensile strength obtained from the notched beam test (EN 14651:2007) to predict the punching shear strength of an SFRC slab.

The author also discussed some of the common analysis methods for calculating moments in two-way slabs such as the direct design method and the equivalent frame method. A yield-line analysis for calculating the failure load of a ductile slab and its limitations were discussed. Equations of the ultimate failure loads corresponding to several yield line patterns that are relevant to the author's current research works were presented. Equations for calculating the ultimate moment capacity of an SFRC slab were discussed and presented.

4

EXPERIMENTAL PROGRAMME

4.1 Introduction

In this experimental programme, 22 slab specimens were tested to failure under symmetric punching loads. The specimens were designed to model the negative bending moment region of an interior column as highlighted in the prototype floor plan Grid B-2 shown in Fig. 4.1. Note that the slab models can also be represented by other grids of interior columns in Fig. 4.1 such as Grid B- (3 to 6), C-2 and C-6. The dimensions of all specimens represent an actual model of the column zone of flat plates having column-to-column spans of about 5.0 to 6.0 m, that is the radii (half lengths) of the slabs are about 0.22 times the column-to-column spans. The compressive strengths of the concrete used in the specimens are high strength, i.e. $f'_c \geq 80$ MPa. Some of the advantages of using high strength concrete (HSC) compared to normal strength concrete (NSC) include an increase in cracking load of the slab and a reduction in deflection at service load level due to higher tensile strength and higher elastic modulus of higher strength concrete. In many cases of flat plate floors, higher concrete strength is chosen to eliminate or reduce service load cracking near the columns. As a result, the stiffness of the flat plate floor at service load level remains close to its uncracked value, which leads further to a reduction in long-term deflection. Higher concrete strength also leads to higher durability in adverse environments. In this study, there are two series of experimental programmes such as:

1. The punching shear tests of 12 high strength reinforced concrete (HSC) slabs varying reinforcement ratios and column aspect ratios.
2. The punching shear tests of 10 steel fibre reinforced concrete (SFRC) slabs varying steel fibre contents and reinforcement ratios.

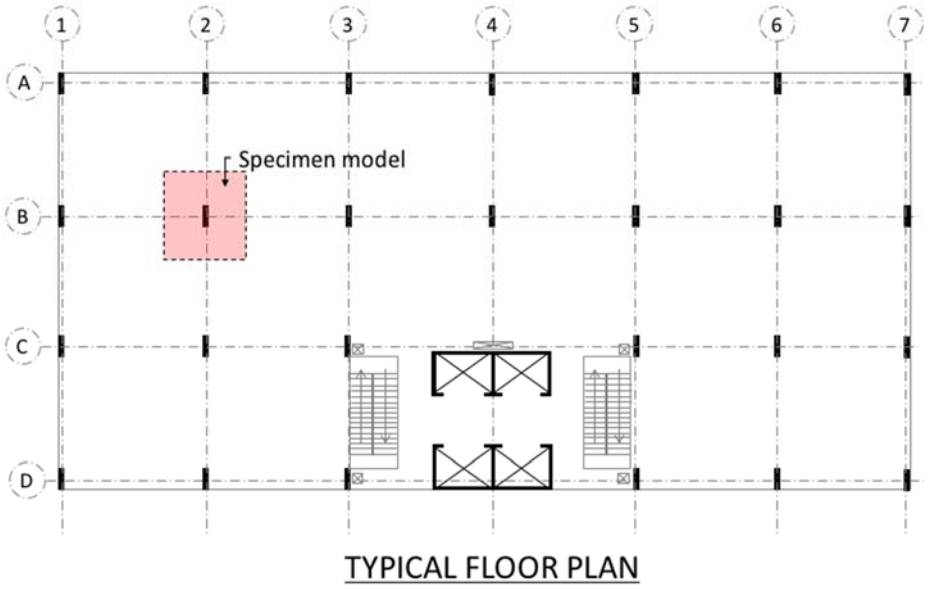

Fig.4. 1 – Idealised test specimen in flat plate structure

4.1.1 Objectives of high strength concrete (HSC) slab tests

Floor slabs with low reinforcement ratios is frequently encountered in the design of flat plate floors for lightly loaded buildings, such as low-rise apartments to high-rise condominium or office buildings. Figure 4.2 shows that the typical values of the required flexural reinforcement ratios ρ (=A_s/bd) in the column strips of the flat plate floors can vary from approximately 0.3% to 0.6%. Those values are considered low. The required reinforcement ratios plotted in Fig. 4.2 were obtained using the ACI direct design method and the design data that is common for those lightly loaded buildings.

Therefore, the slab specimens were designed to cover this low range of reinforcement ratios as well as some of the higher range of reinforcement ratios to provide a complete set of data. The strengths of the concrete used in this set of slab specimens were more than 95 MPa. The objectives are:

- To investigate mainly the influence of flexural reinforcement ratios on the punching shear strength of HSC slabs, and as well as other aspects such as the yield line patterns and failure modes.

- To investigate and further confirm the effects of the column rectangularity on the punching shear strength of HSC slabs.
- To provide a new range of data for validating the author's proposed design method, and for verifying the applicability of existing design codes such as ACI 318, Eurocode 2 and as well as other available design methods.

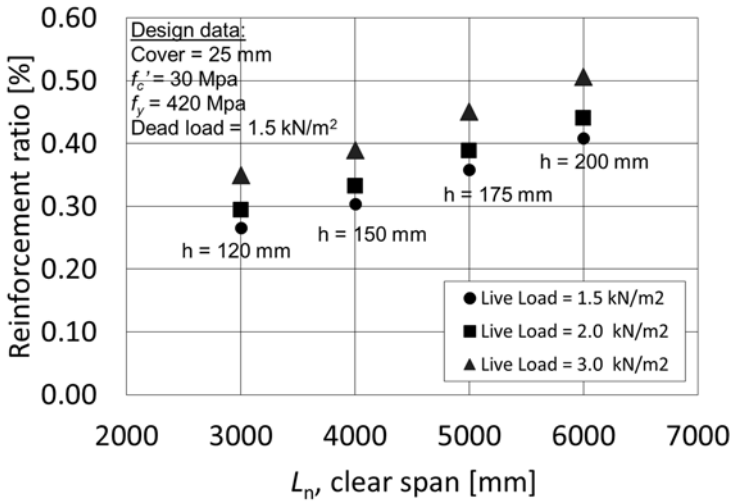

Fig.4. 2 – Flexural reinforcement ratios for a typical column strip of a slab in a flat plate building with various column spans and applied loading

4.1.2 Objectives of Steel fibre reinforced concrete (SFRC) slab tests

Past researches have shown that steel fibres have many applications and advantages on the overall structural performances of slabs. However, there is no available standard design Code for design of fibre reinforced concrete structure yet. Experimental data to support the development of design codes for FRP structures is considerably scarce, and most of the published data are limited to normal strength concrete.

This programme is a continuation to the HSC slab tests, it presents the punching shear tests of a new set of high strength SFRC slabs varying fibre contents. A new type of steel fibre, the double-hooked steel fibre, was used. The strengths of the concrete used in all the specimens in this test program were about 80 to 100 MPa. The objectives of this set of the experiment are:

- To investigate the influence of SFRC and a new fibre type, double-hooked end steel fibre, on the structural performances of HSC slabs such as cracking behaviours, failure behaviours and the emphasis is on the punching shear strength.
- To provide a new set of SFRC slab data for validating the author's proposed design methods, and for assessing the existing standard guidelines such as Model Code 2010, TR 34, ACI 544R and also other available design methods.

4.2 Specimen Details and Material Properties

4.2.1 Details of 12 HSC Slabs

Table 4.1 summarises important properties of the 12 specimens. Essentially, the varying parameters are (1) column aspect ratios, 1.0, 3.0, and 5.0; and (2) flexural reinforcement ratios, 0.28% to 1.43%. The specimen notation represents the main properties of the slab specimens. For example, specimen S13-143 indicates a slab specimen with column aspect ratio of 1:3 ($\beta = 3$) and flexural reinforcement ratio ρ of 1.43%.

The 12 slab specimens were categorised into three main groups: S11 series, S13 series, and S15 series, to represent their corresponding column aspect ratios c_2/c_1 of 1:1, 1:3 and 1:5, respectively. Figure 4.3 shows the general dimensions; The overall dimensions ($L_1 \times L_2 \times h$) of the slabs were 2.2 × 2.2 × 0.15 m for the S11 and S13 series and 2.7 × 2.2 × 0.15 m for the S15 series. The dimensions of column stubs were 200 mm × 200 mm for the S11 series, 600 mm × 200 mm for the S13 series, and 1000 mm × 200 mm for the S15 series.

Figure 4.4 shows the top (tension) reinforcement details of the 12 slab specimens, all top and bottom steel reinforcement bars were provided with 180-degree hooks at both ends to prevent any slippage. At least two reinforcing bars of the top and the bottom reinforcements were specifically placed to pass through the column core in both directions. The bottom reinforcements were designed to satisfy ACI 318-14 minimum requirement for reinforcement ratio of 0.18% or 10 mm bars at 260 mm spacing.

Table 4. 1 – Properties of 12 HSC slab specimens

	No.	Slab ID	Dimensions (m)	Column size (m)	d (mm)	f'_c (MPa)	f_y MPa	ρ (%)	Bar size @ spacing (mm)
(1)	**(2)**	**(3)**	**(4)**	**(5)**	**(6)**	**(7)**	**(8)**	**(9)**	**(10)**
S11 Series	1	S11-028	2.2×2.2×0.15	0.2×0.2	120	112.0	459	0.28	T10@ 260
	2	S11-050			117		537	0.50	T13@ 235
	3	S11-090			117		537	0.90	T13@ 118
	4	S11-139			114		501	1.39	T16@ 118
S13 Series	5	S13-028	2.2×2.2×0.15	0.6×0.2	120	114.0	459	0.28	T10@ 260
	6	S13-050			117		537	0.50	T13@ 235
	7	S13-090			117		537	0.90	T13@ 118
	8	S13-143			114		501	1.43	T16@ 118
S15 Series	9	S15-028	2.7×2.2×0.15	1.0×0.2	120	97.0	459	0.28	T10@ 260
	10	S15-050			117		537	0.50	T13@ 235
	11	S15-090			117		537	0.90	T13@ 118
	12	S15-143			114		501	1.43	T16@ 118

NOTE:
Concrete cover = 20 mm; maximum aggregate size = 20 mm
Same reinforcement is provided in both directions.
T10 @ 260 mm = 10 mm bars at 260 mm spacing
d = average effective depth
f_c' = cylinder compressive strength of concrete
f_y = yield strength of flexural reinforcement
ρ = average reinforcement ratio $A_s/(L\times d) = (\rho_x + \rho_y)/2$

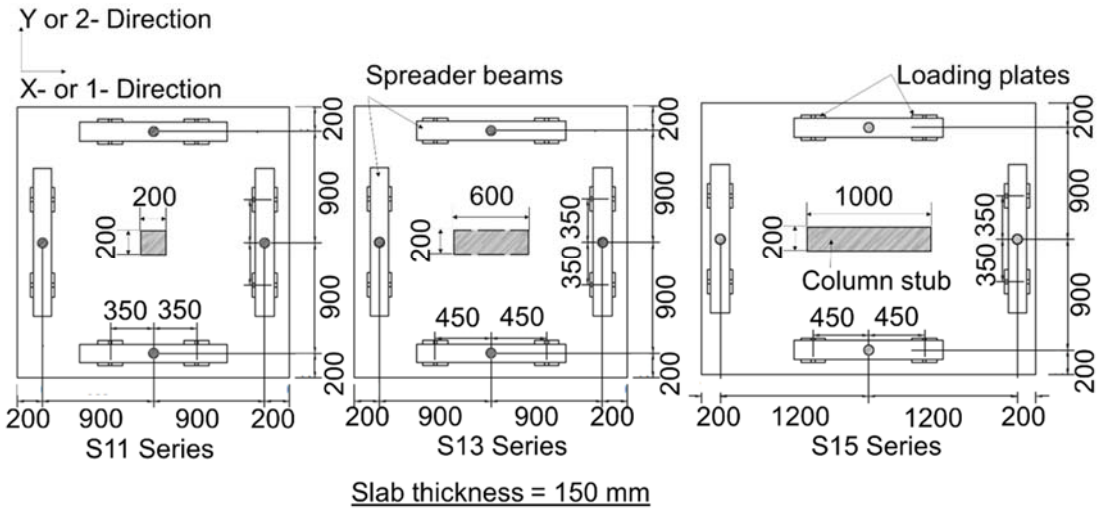

Fig.4. 3 – General dimensions and loading positions of the HSC slab specimens. Note the SFRC slabs have the same dimensions as S11 series slabs

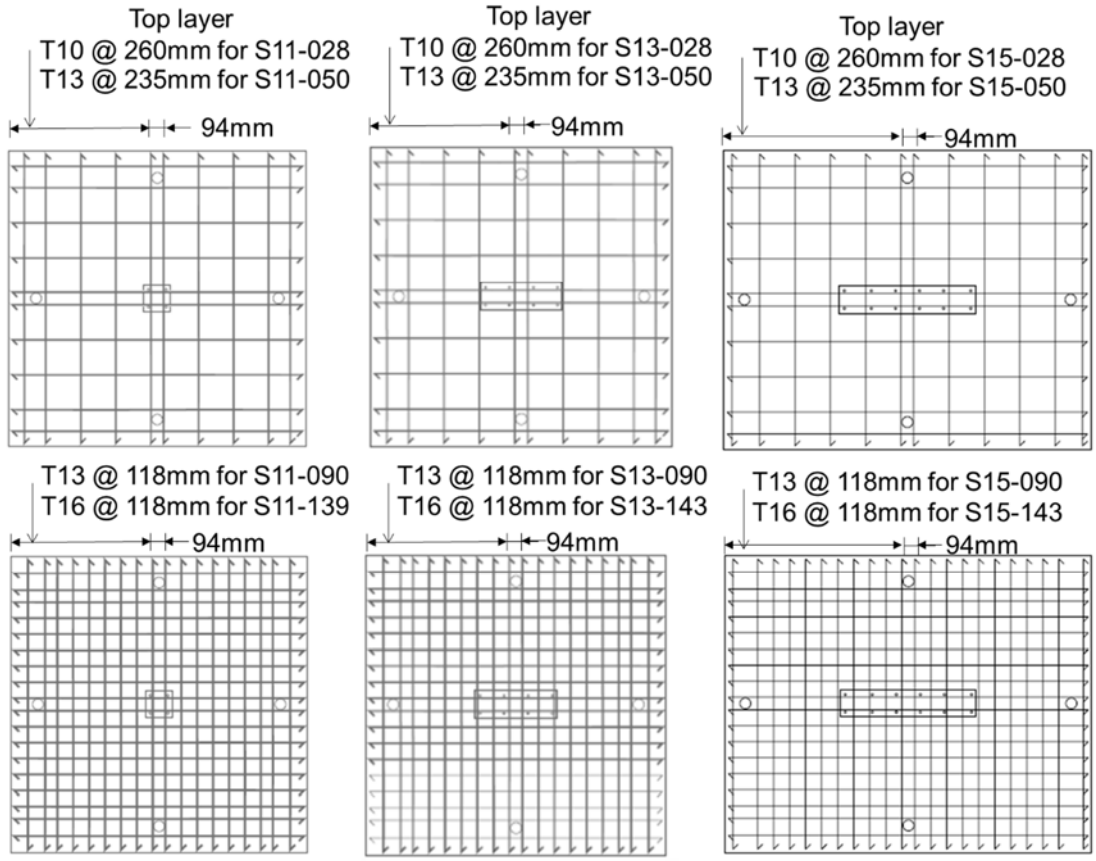

NOTE: Cover = 20 mm. The layout of the tension (Top) reinforcement is same in both directions. Compression (bottom) reinforcement for all specimens is T10 @ 260mm spacing

Fig.4. 4 – Top reinforcement details of the HSC slab specimens. Note F09 series and F14 series slabs have the same details as S11-090 and S11-139, respectively

4.2.2 Details of 10 SFRC Slabs

Table 4.2 summarises the properties of the 10 slab specimens. The 10 specimens were divided into two series (F09 and F14) depending on their reinforcement ratios. There are five specimens in each series. The label of each specimen (e.g. F*xx*-*yy*) indicates the actual values of its respective reinforcement ratio and fibre volume fraction, where *xx* represents the value of ρ (%) and *yy* represent the value of V_f (%). The overall dimensions ($L_1 \times L_2 \times h$) of these 10 slabs are identical to the S11-series slabs as shown in Fig. 4.3, that is 2.2 × 2.2 × 0.15 m. The F09 series slabs and F14 series have the same reinforcement layout as Specimens S11-090 and S11-143 as shown in Fig. 4.4, respectively. The main parameters being investigated are as follows:

(1) Fibre volume fraction (V_f) which is a ratio of the fibre content per one unit volume to the steel density (the steel density ≈ 7800 kg/m3). V_f was varied at 0%, 0.3%, 0.6%, 0.9%, and 1.2%; the equivalent fibre dosages are zero kg/m^3, 23.4 kg/m^3, 46.8 kg/m^3, 70.2 kg/m^3, and 93.6 kg/m^3, respectively.

(2) Flexural reinforcement ratio ($\rho = A_s/bd$). This has two values, 0.9% and 1.40%. The two values of reinforcement ratios were designed to ensure brittle punching shear failure for similar concrete specimens but without steel fibre

Table 4. 2 – Properties of 10 SFRC slabs

Series	ID	*c* (mm)	*d* (mm)	ρ (%)	f_y (MPa)	f_c' (MPa)	V_f (%)	Residual tensile strength of SFRC				*Rebar layout* (mm)
								f_{r1} (MPa)	f_{r2} (MPa)	f_{r3} (MPa)	f_{r4} (MPa)	
(1)	(2)	(3)	(4)	(5)	(6)	(7)	(8)	(9)	(10)	(11)	(12)	(13)
F09	F09-00	200	117	0.9	585	80	-	-	-	-	-	T13@118
	F09-03					89	0.3	4.2	6.0	6.5	5.8	
	F09-06					87	0.6	8.9	12.8	10.5	7.5	
	F09-09					90	0.9	16.0	17.5	16.3	13.5	
	F09-12					100	1.2	17.5	21.2	22.2	21.2	
F14	F14-00		114	1.4	575	80	-	-	-	-	-	T16@118
	F14-03					89	0.3	4.2	6.0	6.5	5.8	
	F14-06					87	0.6	8.9	12.8	10.5	7.5	
	F14-09					90	0.9	16.0	17.5	16.3	13.5	
	F14-12					100	1.2	17.5	21.2	22.2	21.2	

The maximum aggregate size (d_a) was 20 mm.

4.2.3 Material properties

4.2.3.1 Steel fibre properties

The new double hooked-end steel fibre [Dramix 5D fibre, BEKAERT] is shown in Fig. 4.5(a) and it has the following geometric properties: steel fibre length L_f is 60 mm, steel fibre diameter D_f is 0.9 mm, and the corresponding aspect ratio L_f /D_f is 65. The nominal tensile strength of the steel fibre is 2300 MPa and its modulus of elasticity is 210 GPa. For a comparison, the typical single hooked-end steel fibre is shown in Fig. 4.5(b).

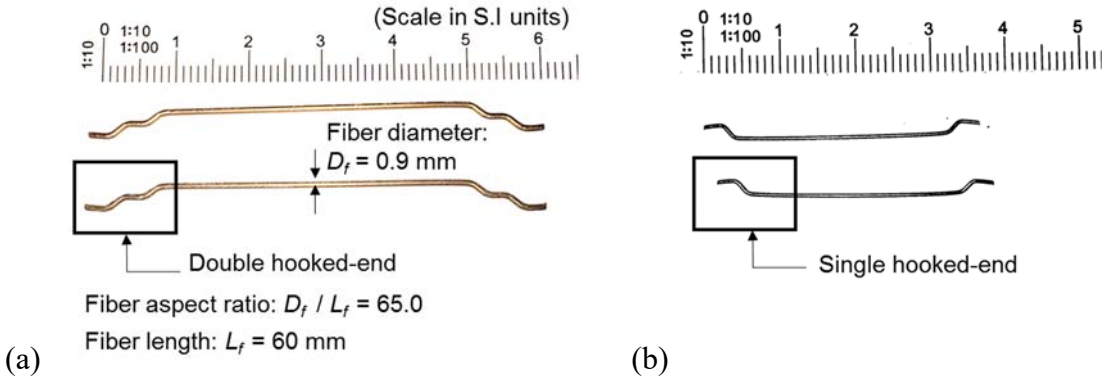

Fig.4. 5 – (a) Double hooked-end steel fibre and its geometric properties. (b) Single (normal) Hooked-end steel fibre

4.2.3.2 Reinforcing steel properties

Three sizes of deformed steel bars were used in the slab specimens such as. T10, T13 and T16 which have the normal diameters of 10 mm, 13 mm and 16 mm, respectively. Tensile tests of the reinforcement were conducted in accordance to the ASTM A184 standard. Three samples of each reinforcing steel were tested using an Instron Machine actuator test system.

Table 4.3 summarises the tensile test results of the steel bars, the stress-strain curves of each reinforcing bar are plotted in Fig. 4.6. The yield stress (f_y) obtained at the point where the stress-strain curve starts to develop a plastic-plateau before

strain hardening, the modulus of elasticity E_s was determined by calculating the slope of the curve at the elastic range, the yield-strain (ε_y) was approximated to be (f_y/E_s), the ultimate tensile strength (f_u) was maximum stress recorded before the rupture point. Note that the value of each parameter in Table 4.3 is an average value of three test samples.

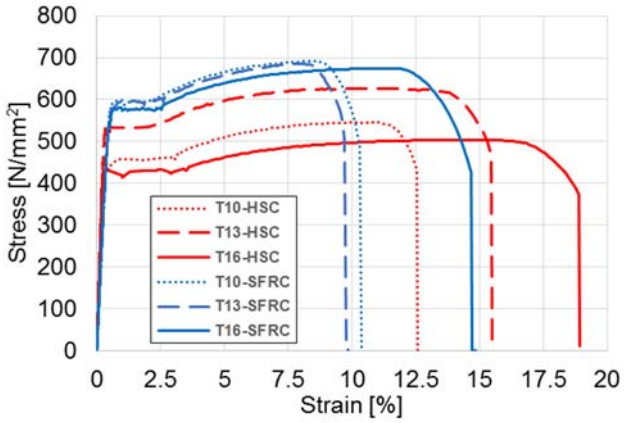

Fig.4. 6 – Stress-strain curves of steel bar specimens

Table 4. 3 – Properties of steel reinforcement

Steel ID	Steel Type	Nominal Diameter (mm)	E_s (GPa)	ϵ_y (%)	f_y (MPa)	f_u (MPa)	Remark
T10	Deformed	10.0	198.5	0.23	459	551	Used in HSC slab specimens
T13		13.0	220.0	0.24	537	627	
T16		16.0	218.5	0.23	501	575	
T10		10.0	191.0	0.30	595	698	Used in SFRC slab specimens
T13		13.0	195.0	0.33	585	686	
T16		16.0	200	0.28	575	575	

Table 4. 4 – Concrete mix design for HSC slab specimens

Mix ID	Water-to-binder ratio	Maximum Agg. Size	Water	Cement	Silica fume	GGBS	Fine Agg.	Coarse Agg	Water reducing admixture	Steel Fibre	
		(mm)	(Kg/m^3)							(%)	(Kg/m^3)
M1	0.25	20	150	360	60	180	790	790	6.0	-	-
M2	0.25		150	360	60	180	780	780	11.0	0.30	23.4
M3	0.25		150	360	60	180	775	775	11.0	0.60	46.8
M4	0.25		150	360	60	180	770	770	11.0	0.90	70.2
M5	0.25		150	360	60	180	765	765	11.0	1.20	93.6

4.2.3.3 Concrete properties

Table 4.4 summarises the proportion of materials used in the mix design of the concrete used in the construction of the specimens. The maximum aggregate size (d_a) was 20 mm. Note that during the actual batching, the proportions of fine aggregate, coarse aggregate, and water reducing admixture were adjusted to take into account of moisture content. Mix M1 is the mix design reference for the specimens S11, S13, S15 series and the non-fibrous slab specimens, F09-00 and F14-00. Mix M2 to M5 are for the specimens with fibre volume V_f ranging from 0.3% to 1.2%, respectively. The slump-flow diameters of the HSC were recorded at about 500 mm to 600 mm. The slump diameters of the SFRC reduced with an increase in the fibre content. Mix M4 (V_f = 0.9%) and M5 (V_f =1.2%) did not have slump-flow, they have typical concrete slumps with a slump height of about 120 mm to 200 mm.

Relevant properties of each concrete used in all specimens were tested. Concrete strength f'_c of the S11-series, S13-series, and S15-series slab specimens are listed in Table 4.1. Table 4.5 summarises the test results of concrete specimens used in the SFRC slab specimens. Each concrete property was tested near the dates of the punching shear test of each slab specimen (+- 3 days), and the punching shear tests were conducted around 60-100 days after concrete castings.

The failure mode of most concrete cylinder specimens tested under compressive loads was brittle. Photograph of the specimen and the test apparatus of the flexural tensile strength test (according to standard test EN 14651 (2007)) is shown in Fig. 4.7. Figure 4.8(a) shows the stress-CMOD response curves of the SFRC M2 to M5, CMOD is the crack mouth opening displacement as defined by EN 14651 (2007). The CMODs and their corresponding stresses are important properties for determining the ultimate strength of a cracked SFRC member.

Table 4. 5 – Mechanical properties of concrete specimens

Specimen	Mix ID	E_c (GPa)	f_c' (MPa)	f_{ct} (MPa)	f_R (MPa)	f_{r1} (MPa)	f_{r2} (MPa)	f_{r3} (MPa)	f_{r4} (MPa)
F09-00/F14-00	M1	33	80	5.3	5.5	-	-	-	-
F09-03/F14-03	M2	40	89	5.5	5.6	4.2	6.0	6.5	5.8
F09-06/F14-06	M3	38	87	- *	6.5	8.9	12.8	10.5	7.5
F09-09/F14-09	M4	38	90	-*	8.4	16.0	17.5	16.3	13.5
F09-12/F14-12	M5	40	100	-*	9.5	17.5	21.2	22.2	21.2

Note: * Unable to obtain experimental data due to unforeseen technical issue.
E_c = Modulus of elasticity
f_c' = cylinder compressive strength of concrete (age > 60-100 days)
f_{ct} = Split tensile strength of concrete (age > 60-100 days)
$f_{r,i}$ = residual stress for fibre reinforced concrete; f_{r1} at CMOD of 0.5 mm; f_{r2} at CMOD of 1.5 mm; f_{r3} at CMOD of 2.5 mm; f_{r4} at CMOD of 3.5 mm. (in accordance with EN 14651:2007)

Fig.4. 7 – Photograph from the notched beam test according to EN 14651:2007

Discussions of concrete properties:

The compressive strengths were shown to improve with an increase in the fibre content, the improvement is not so significant that is about 10% increment from V_f = 0% to V_f = 1.2%.

Figs. 4.8 (a) shows that even at a fibre content as low as 0.3% for the beam with double hooked-end steel fibres have better performance over unreinforced beams; this is not the case for beams with conventional single hooked-end fibres as shown in Fig. 4.8 (b).

As expected, the maximum flexural stress increases with an increase in fibre content. The stress-CMOD response curves M2 (V_f = 0.3%) and M3 (V_f = 0.6%) have similar behaviours as typical SFRC notched beams, where the load would drop suddenly after the maximum load at the linear portion of the curve is reached, then

the deflection hardening or softening would take place. The maximum load is normally reached shortly after the first crack occurs, this load is defined as the modulus of rupture f_R. In general, the deflection softening (the load drops as the displacement continues to increase) is common for SFRC using other typical types of steel fibre (see Fig. 4.8(b)). However, the results show that the deflection hardening is indeed dominant for all the curves in Fig. 4.8(a). This can be due to the better frictional pull-out resistance introduced by the double hooked-end fibres comparing to the single hooked-end fibres. In addition, high strength concrete has also been known to improve the bond strength of the fibre-concrete interface.

The curves M4 (V_f = 0.9%) and M5 (V_f=1.2%) in Fig. 4.8(a) have interesting behaviours that resemble the behaviours of lightly steel reinforced concrete beams. In comparison to the curves M2 and M3, the curves M4 and M5 have much higher flexural strengths as well as post-crack flexural stiffness. There are no drastic drops in the stresses at the ends of the linearity, this phenomenon (Blunt and Ostertag, 2009a, 2009b) may be explained by the presence of high volume of randomly orientated fibres at the cracked region, and the effective bond strengths of the fibres bridging cracks are greater than the tensile stresses induced by the bending moments. Eventually, the softening and frictional pull-out mechanisms took place, where the stresses reduced as the cracks widen.

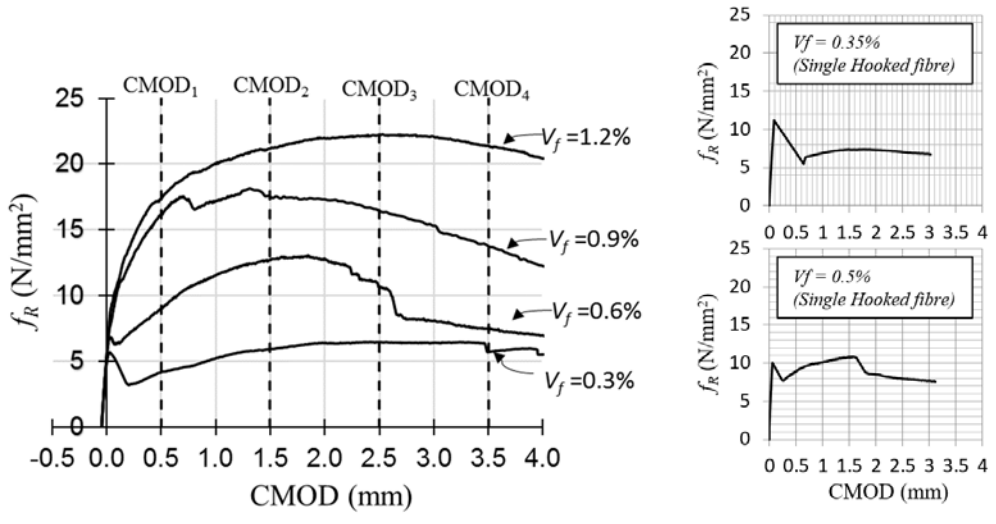

(a) (b) [Source: Teng et al. (2015)]

Fig.4. 8 – Flexural tensile stress - CMOD curves of (a) the current SFRC specimens for V_f = 0.3%, 0.6%, 0.9% and 1.2%; (b) the SFRC specimen (using single hooked fibres) obtained from Teng et al. (2015)

4.3 Specimen Preparations and Test Setup

4.3.1 Castings of specimens

All of the 22 slab specimens were cast horizontally as shown in Fig. 4.9(a). The specimens were cast upside down, meaning that the top surface faced the bottom of the formwork. The slab panels and the column stubs were monolithically cast to prevent construction joints. The workability of the SFRC was low compared to the flowing concrete of the HSC, thus to ensure the consistency of the concrete work, the concrete vibrators were used while pouring the SFRC onto the slab panels (see Fig. 4.9(a)). The column stubs were cast by carefully pouring the concrete into the formwork through the drilled holes of the base plates. Abundant of concrete samples from the same batch used for each slab were collected for concrete property tests. The samples are 100 × 200 mm cylinders, 150 × 300 mm cylinders for compression and modulus of elasticity test, 100 × 100 × 300 mm prisms for flexural strength test, and 150 × 150 × 650 mm prisms for the notched beam test or flexural tensile strength tests for SFRC.

Immediately after the concrete had reasonably settled, the slab specimens were covered with plastic sheets to prevent excessive loss of water through evaporation. Water was regularly splashed onto the slab specimens for the first seven days and kept in an enclosed environment. The hardened concrete samples were cured in water tanks throughout before the property tests. Note that there were some plastic shrinkage cracks in some of the SFRC specimens as shown in Fig. 4.9(b), especially for those specimens with the higher fibre contents. Even though steel fibre is known to reduce structural shrinkage cracks, but this case might be due to the low surface moisture, and high water demand for the SFRC. Nevertheless, it will be shown that these shrinkage cracks would have no effects on the structural behaviours and ultimate strengths of the specimens.

(a)

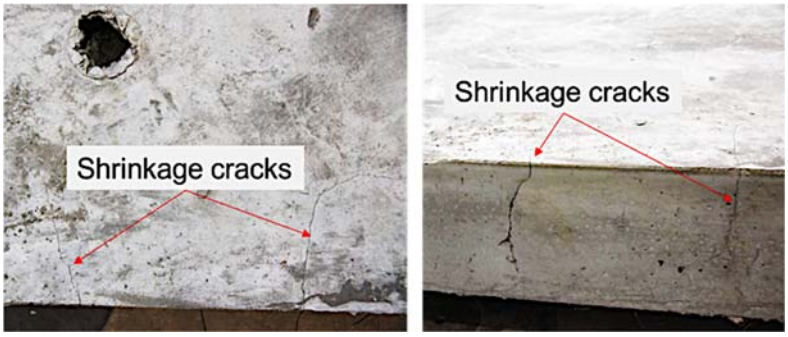

(b)

Fig.4. 9 – (a) photographs taken during casting of SFRC slab specimens; (b) photographs of some shrinkage cracks in SFRC slab specimens.

4.3.2 Test setup

The test set-up is identical for all the slab specimens, except for S15 series slabs where the positions of the loading points are slightly different as shown in Fig. 4.3. The positions of the spreader beams and loading points were determined such that the distributions of stresses near the column zone were close to those stress distributions in the same slab when loaded under uniform loading. Figure 4.10(a) and Fig. 4.10(b) show the details and the sequence of the test setup, respectively.

First, a very stiff steel block and hydraulic jack assemblies were positioned and secured onto the laboratory strong floor, the hydraulic jack assemblies were anchored to the strong floor by high-strength steel rods. Then, loading plates, steel rollers and spreader beams were installed on the specimen's top surface before

placing the specimen on the steel support block. The precision of the slab position was checked and adjusted carefully. The top surface was whitewashed for better visibility of cracks.

During testing, the specimen was statistically loaded downward through four hydraulic jacks. Each hydraulic jack would apply the loading by pulling down the steel rod which transferred the pulldown force to the spreader beams and then on to the loading plates (points) on the slab. The role of the rollers is to allow the slab edges to rotate freely, thus the in-plane forces were eliminated. One load cell was placed on top of each spreader beam to measure and monitor the real-time pulldown force. All the four jacks were connected to a single hydraulic pump.

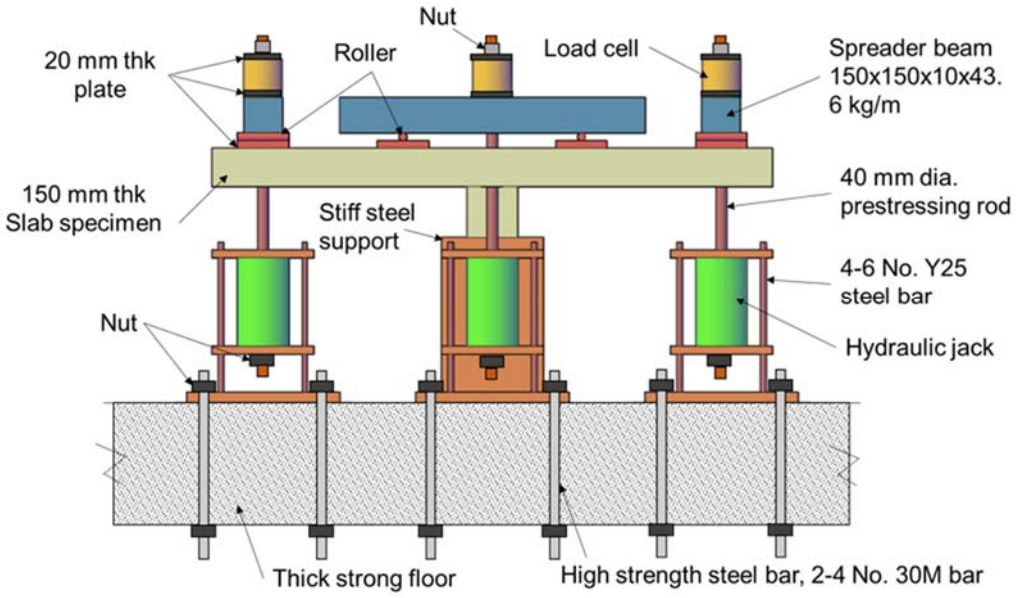

(a)

Fig.4. 10 – (a) Schematic drawings of test setup details; (b) photographs of the in-progress sequences of test setup of a slab specimen. Note Fig. 4.10(b) is placed in the next page.

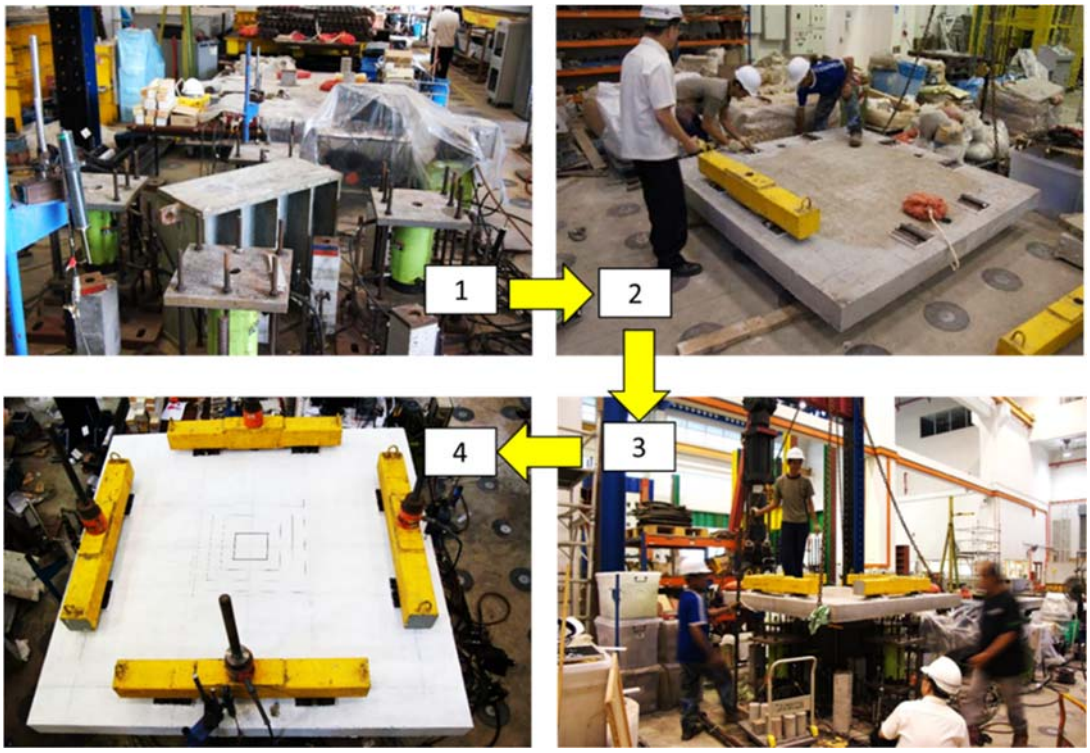

(b)

Fig. 4.10 (Continued)

4.4 Instrumentation

4.4.1 Steel strain gauges

The 5 mm steel strain gauges were carefully installed onto the top reinforcing bars in both directions (x and y directions) with strict compliances to appropriate procedures to avoid premature damages.

For presentation purposes, Fig. 4.11(a) shows the typical positions of strain gauges for the specimens that have 118 mm bar spacing arrangement (ρ = 0.9% and 1.4%), strain gauges' positions for the other specimens were arranged in a similar pattern. To study the effectiveness of the flexural reinforcement, the positions of the strain gauges were designed to measure the flexural strains in the reinforcement across a distance at 50 mm (the first vertical set, G11 to G61), 170 mm (the second vertical set, G12 to G52) and 290 mm (the third vertical set, G13 to G53) away from the line of column face. The strain gauges' labels represent their coordinates (row,

column), e.g. G23 represents the strain gauge that is positioned at the second row and the third column as shown in Fig. 4.11(a).

Since strain gauges are prone to damages especially during concrete casting. For redundancy, the same arrangement of strain gauges was also installed in the opposite quarter of each specimen. Note that the locations of strain gauges for each specimen is detailed in Appendix B. The (notations) labels of the strain gauges in Appendix B are not identical to those as shown in Fig. 4.11(a), nevertheless, they should not affect the clarity of the subsequent discussions of test results.

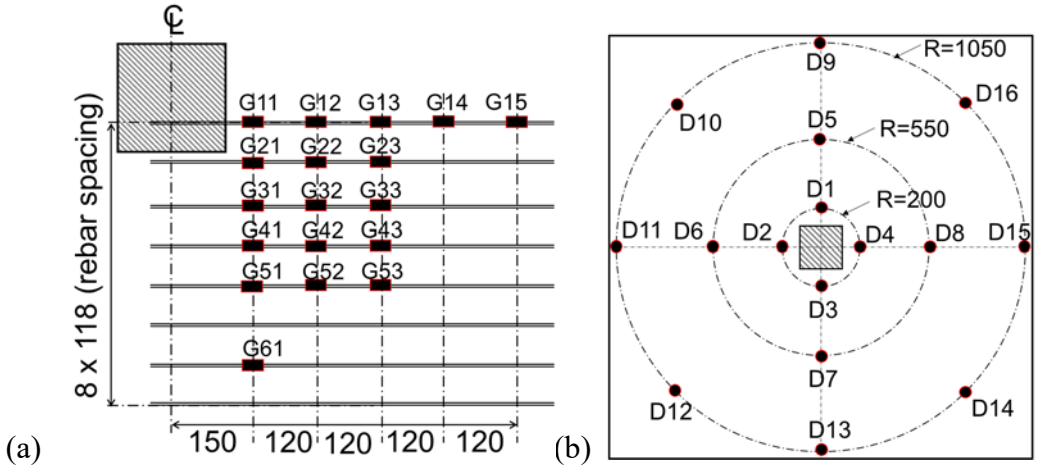

Fig.4. 11 – (a) Typical locations of steel strain gauges in the tension reinforcements; (b) Typical positions of LVDTs

4.4.2 Transducers (LVDTs)

Several linear variable differential transformers (LVDTs) were positioned below the slab specimens to measure the deflection profiles. For illustration, the typical locations of the LVDTs are shown in Fig. 4.11(b). The arrangement of LVDTs in Fig. 4.11(b) are for the second set of experiment (F09 series and F14 series SFRC slab specimens). Photographs of test equipment and instruments such as LVDTs and spreader beams are shown in Fig. 4.12.

Essentially, the LVDTs were designed to capture the vertical deflections at near column faces to the slab edges. The edge deflections (measured at about 1.0 m radius from the column centre) will be used most for discussions and calculations of energy absorption of the SFRC slabs. Each LVDT was sturdily attached on a stand which was laid and secured on the steel plate by magnetic forces. Note that the

actual LVDTs positions for the S11 series, S13 series, and S15 series specimens are given in Appendix B.

All the load cells, LVDTs, and steel strain gauges were connected to an electronic data logger which was also linked to a desktop computer. The real-time data could be monitored digitally and graphically by a software known as VisualLog. All test data were stored as raw file formats which were carefully pre-configured to match the stored data with the correct assignments in the files. The post analysis of the data were done through a software – Excel (Microsoft Office).

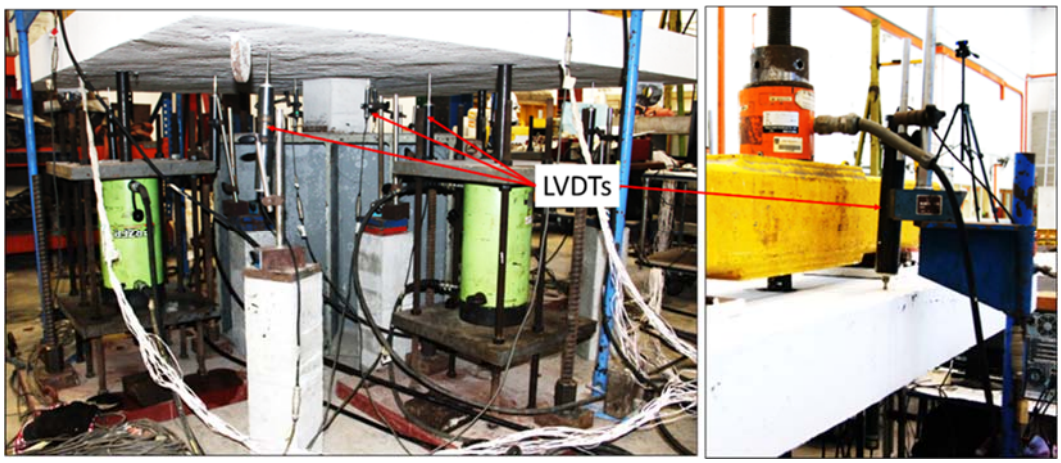

Fig.4. 12 – Photographs of test setup showing testing equipment and instruments

4.4.3 Test and post-test procedure

All the specimens were whitewashed first before testing for better visibility in tracing crack patterns. Each specimen was loaded at a slow rate at the beginning to observe first flexural cracks. After first flexural cracks were recorded, each specimen was loaded at about 20 kN load increment or approximately 5 kN increment for each jack. At every load increment, readings of vertical displacements from LVDTs, steel strains, and crack widths were recorded. All the first cracks were observed carefully and crack propagations were marked using colour markers at several load steps all the way to failure. Each slab was loaded to failure and the first indication of failure, either by yielding of steel bars or change of slope of load-deflection curves, was studied to ensure correct identification of the initiating failure mode. All slabs containing steel fibres were loaded beyond the maximum loads (failure loads) to capture the post-failure behaviours.

Video and photo documentations:

For the first set of the experiment programme (12 HSC specimens, S11, S13, and S15 series), video was recorded to capture the moment just before the failure occurred for each test. Testing equipment on top of each slab was removed to allow clearer photograph view of the surface crack patterns.

The second set of the experiment programme (10 SFRC specimens, F09 and F14-series) involves more graphical documentations, a set of high-definition webcams were set up to record the entire process of each test. A camera was mounted onto a high scaffold to capture an aerial view of a slab specimen. The camera was set to the time-lapse mode to capture a photo every 15 to 30 seconds automatically, this enables the real-time recording of crack propagation for each slab specimen. Time-lapse photoss of SFRC slab specimens are provided in Appendix A.3.

Post-test treatment of specimen:

The 12 HSC specimens (S11, S13, and S15 series) were carefully disposed after crack patterns have been photographed. A professional contractor did the disposal works.

To measure inclinations of the punching shear cracks, the 10 SFRC specimens (F09, and F 14 series) were cut using a pavement cutting machine at a distance about 100 mm away from a column face. The shear crack inclination was measured using an approximated straight-line measured from the bottom face of a slab to the intersection of the inclined shear crack with the tension steel. An average inclination of the two sides (left and right) of the cut section will be reported and summarised later in Chapter 6. After the measurements, the 10 slabs were carefully disposed by a professional contractor.

4.5 Summary

A total of 22 slab specimens were designed, constructed, and tested under punching loads. The experimental programmes were divided into two sets such as (1) the tests of 12 HSC slabs that mainly investigate the influences of low reinforcement ratios and column rectangularity on the punching shear strength of HSC slabs. (2) the tests of 10 high strength SFRC slabs that investigate the influence of a new type of fibres, the double hooked-end fibres, on the punching shear failure behaviours of high strength SFRC slabs.

This new experimental data will be used together with other published slab data to evaluate the existing design methods and also to support the development of the author's proposed shear equations.

5

HSC SPECIMENS – RESULTS AND DISCUSSIONS

5.1 Introduction

Experimental results of the 12 high strength concrete (HSC) slab specimens are presented in this chapter. The presented results are used to discuss the effects of low flexural reinforcement ratios and column rectangularity on punching shear strength of HSC slabs. Code methods such ACI 318-14 and Eurocode 2 are compared with the results, and their performances are evaluated. The presented results in the subsequent sections are carefully analysed and summarised for concise discussions that conform to the main objectives of this current work. Thus, not all collected data are reported in this chapter. For completeness or further investigation, complete data can be obtained in Appendix B.

5.2 Experimental results

5.2.1 Failure loads and failure modes

The failure loads of the 12 specimens are summarised in Column 4 of Table 5.1, the failure loads are the maximum loads recorded during the tests. The results showed that as the reinforcement ratio was varied from about 0.3% to 1.4%, the failure load continually increased from 260 kN to 435 kN (for S11 series slabs), 290 kN to 700 kN (for S13 series slabs), and 300 kN to 754 kN (for S15 series slabs).

Table 5.1 also shows the mode of failure of each slab specimen. Those slabs that failed abruptly with a sudden drop in their load-deflection curves are indicated to have failed in punching mode. Those slabs that failed in a more ductile manner or with widespread yielding of reinforcement before punching failure are indicated to have failed in flexural mode. All the slabs finally failed in what appears to be punching failure even though the slabs might have failed earlier in flexural mode.

Table 5. 1 – Failure loads and failure mode of the l2 specimens

Series	Slab ID	ρ (%)	Maximum Load (kN)	Maximum crack width (mm)	Observed failure mode
1	2	3	4	5	6
S11 Series	**S11-028**	**0.28**	260	1.50	Flexural
	S11-050	**0.50**	375	0.85	Flexural
	S11-090	**0.90**	420	0.80	Punching
	S11-139	**1.39**	435	0.60	Punching
S13 Series	**S13-028**	**0.27**	290	2.00	Flexural
	S13-050	**0.50**	400	4.00	Flexural
	S13-090	**0.90**	540	1.50	Punching
	S13-143	**1.43**	700	1.00	Punching
S15 Series	**S15-028**	**0.27**	300	1.60	Flexural
	S15-050	**0.50**	435	1.00	Flexural
	S15-090	**0.90**	635	0.80	Punching
	S15-143	**1.43**	754	1.60	Punching

Note: ρ is the reinforcement ratio. The first crack loads were not available for each specimen. The first longitudinal flexural crack appeared about 80 kN to l00 kN.

5.2.2 Crack Patterns and Characteristics

5.2.2.1 Crack patterns

Figures 5.1 to 5.3 show the photographs of the ultimate crack patterns of the S1l series, S13 series, and S15 series slabs, respectively. Note that the crack lines were digitally enhanced for better visibility and the camera angles were not perfectly orthogonal.

Figure 5.1 shows fairly clearly that slabs with low reinforcement ratios would have different crack patterns at failure compared to slabs with high reinforcement ratios. Typical crack patterns of slabs failing in normal punching are the patterns of the specimens S1l-090 and S1l-139 in Fig. 5.1. The crack pattern in each of these cases comprises a set of closely spaced radial cracks or circular fan type cracks with

the final circumferential crack that comes to the surface from the internal inclined shear cracks.

If the reinforcement ratio is low, however, the circular fan type of crack pattern does not occur as shown by the pattern of Slab S11-028 in Fig. 5.1, it can be seen that the crack pattern forms straight-line cracks nearly parallel to column lines in both directions with perhaps one diagonal crack from the column corner toward a corner of the slab. The parallel line crack pattern shows that widespread yielding of the reinforcement has occurred. In the end, the final failure of the slab would still be a punching failure but at a load no greater than the load that caused earlier yielding of the flexural reinforcement. Similar crack patterns can also be seen in other specimens with low reinforcement ratios such as S13-028 ($\rho = 0.28\%$) and S15-028 ($\rho = 0.28\%$) as shown in Figs. 5.2 and 5.3, respectively.

A slab with a slightly higher reinforcement ratio of 0.50% such as Specimen S11-050 is shown in Fig. 5.1. In this case, the crack pattern forms a transition between parallel-line and circular fan patterns, with additional cracks from the column corners to slab corners.

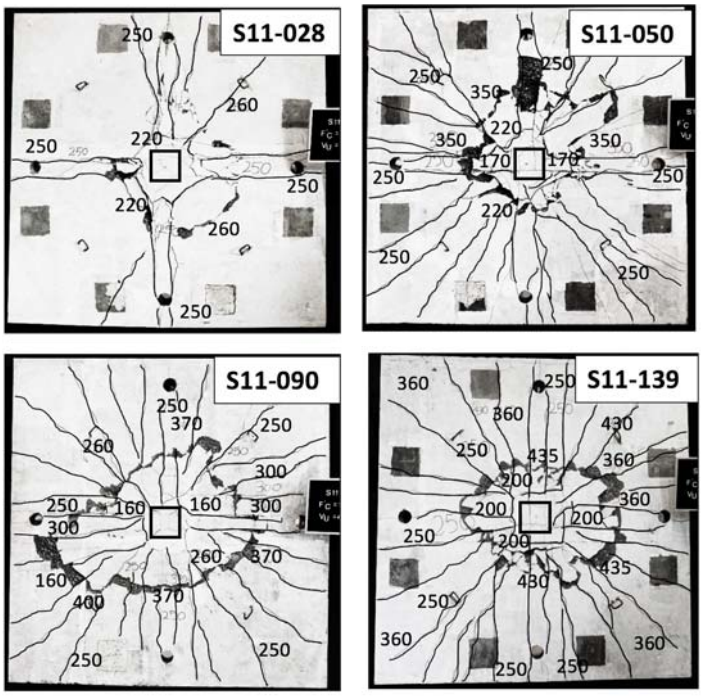

Fig.5. 1 – Photographs of ultimate crack patterns for S11 series slabs.

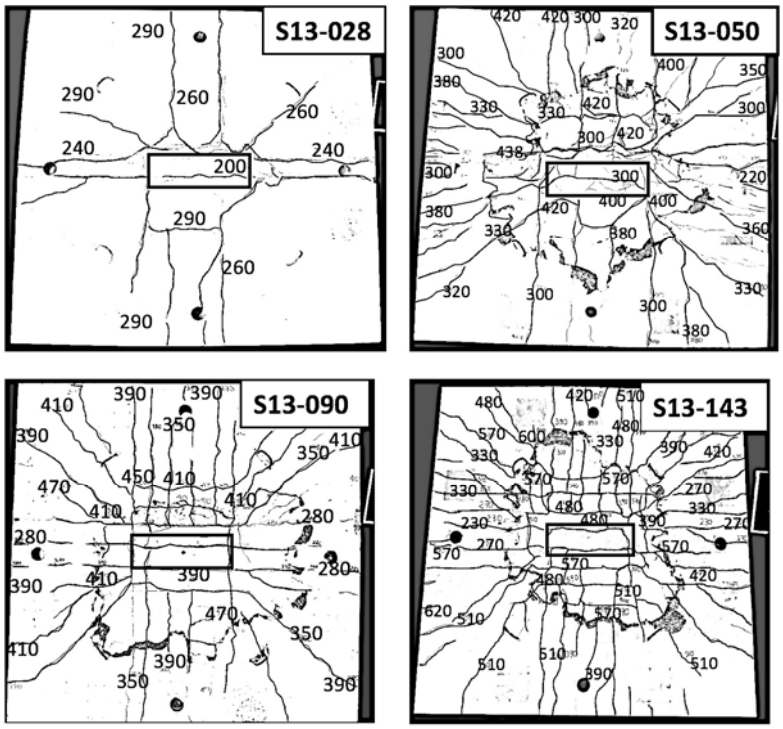

Fig.5. 2 – Photographs of ultimate crack patterns for S13 series slabs.

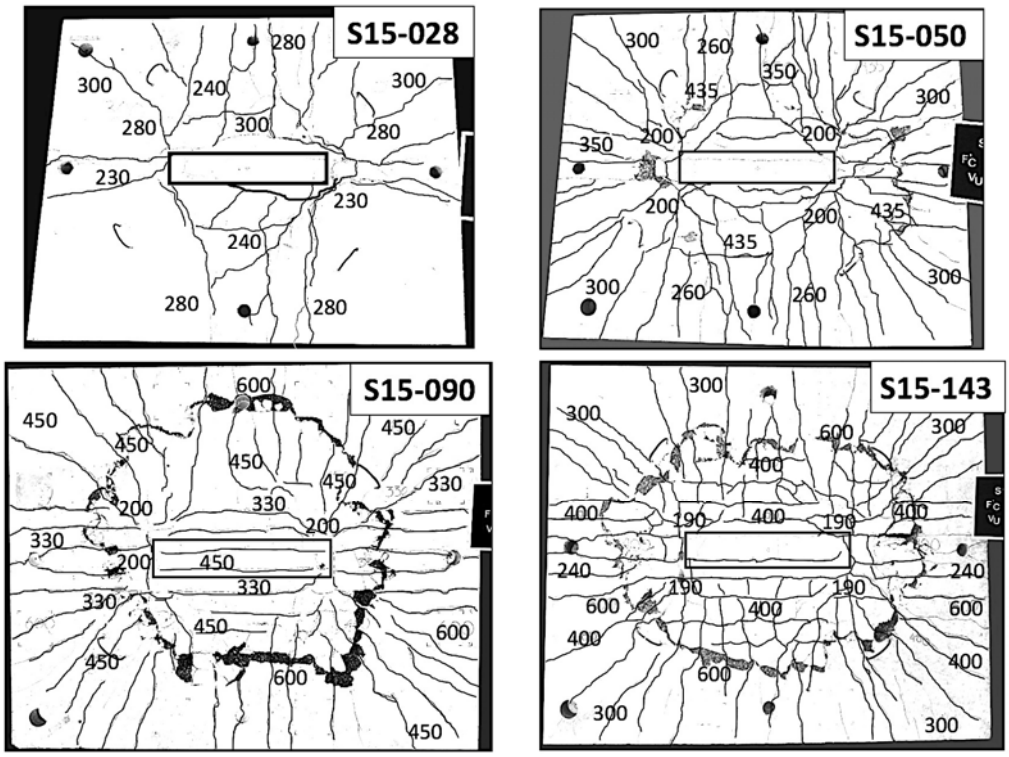

Fig.5. 3 – Photographs of ultimate crack patterns for S15 series slabs.

5.2.2.2 Crack characteristics

Table 5.1 also summarises the average (maximum) crack widths of all the specimens measured within *d* to 1.5*d* away from the column faces. Each maximum crack width was the crack width measured at the load stage very close to failure. It can be seen that the maximum crack width reduced with an increase in flexural reinforcement ratios.

Figure 5.4 represents the crack development in Specimen S11-028, it can also represent typical crack development in the slabs failed in flexure (S11-028, S13-028, and S15-028). Initiations of first cracks occurred at around the column perimeter due to the negative bending moments; the cracks continued to propagate longitudinally along the lines of column faces as shown in Fig. 5.4. While the applied loads approached the maximum loads, there were no significant development of new cracks. There were one or two radial cracks that extended from the corners of the column section. After reaching the peak load, the load was continuously applied and there was no more increase in the load resistance. Eventually, the slab failed by the punching mechanism as the secondary mode of failure, which caused the sudden development of the circumferential surface cracks.

In comparison with the ductile slabs discussed above, the circumferential cracks developed at earlier loading stages for the slabs with relatively higher reinforcement ratios as shown in Fig. 5.5. The cracks first occurred around the column perimeter at about 100 kN to 160 kN. These circumferential cracks were initiated by several inclined shear cracks that developed from the top surface and internally propagated toward the column faces at the bottom of the slab or the high compressive zones. The final inclined shear cracks that formed the punching cones were the outermost of these circumferential cracks which formed right before failure occurred.

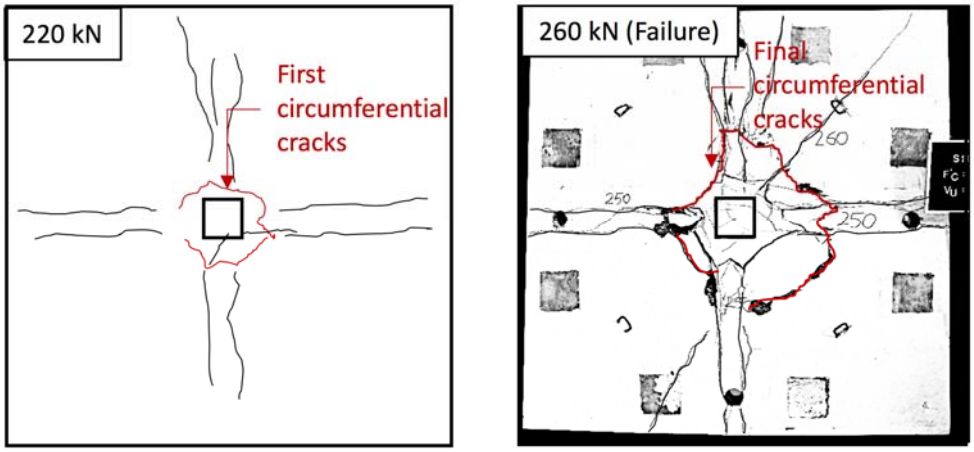

Fig.5. 4 – Development cracks om Specimen S11-028 (Flexural mode)

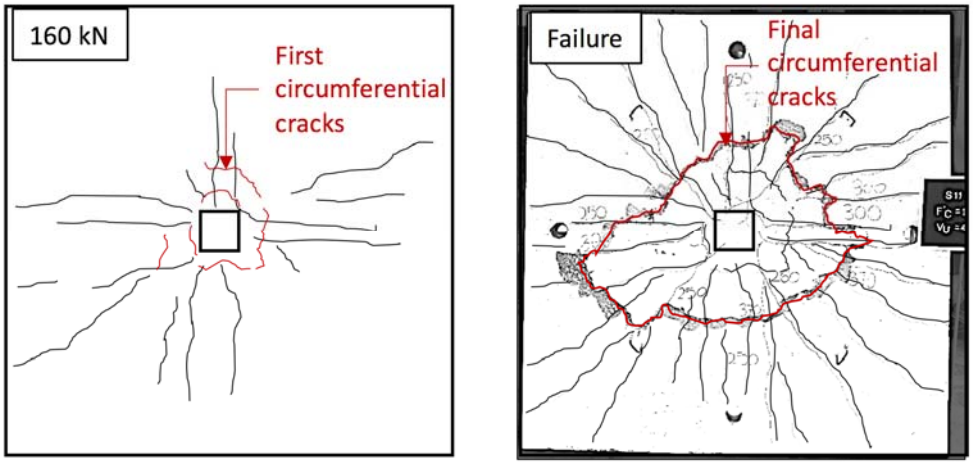

Fig.5. 5 – Development cracks om Specimen S11-028 (Punching shear mode)

5.2.3 Deflections

Figures 5.6(a, b and c) show the load-deflection curves of S11-series, S13-series, and S15-series, respectively. Before cracking, the relationship between the load and deflection is linear. After the first circumferential crack formed, the slope of the load-deflection curve would change slightly. Upon further loading, the change of slope becomes increasingly more significant as the flexural stiffness of the slab drops further due to more cracking or widening of cracks. As expected, the flexural stiffness of the slab with a higher reinforcement ratio will degrade less after cracking; that is, its load-deflection curves have steeper slopes compared to slabs with low reinforcement ratios.

From Figs. 5.6, it can also be seen that the slabs with lower reinforcement ratios are more ductile than the other slabs with higher reinforcement ratios. Upon reaching the maximum load, any further load increment to Specimen S11-028, S13-028, and S15-028 (very low reinforcement ratios) produces no additional increase in resistance (plastic plateau), but their deformations continue to increase until the final failure at the end. These slabs are the slabs that clearly failed in flexure. Specimen S11-050, S13-050 and S15-050 are also considered to fail in flexure, there is a short segment of the flat portion in their load-deflection curves as shown in Figs. 5.6. However, the curves are higher than those of the slabs with the lowest reinforcement ratios ($\rho = 0.28\%$). The slabs with high reinforcement ratios ($\rho > 0.9\%$) all failed in brittle punching failure. As expect, Specimens S11-139, S13-143, and S15-143 are the most brittle.

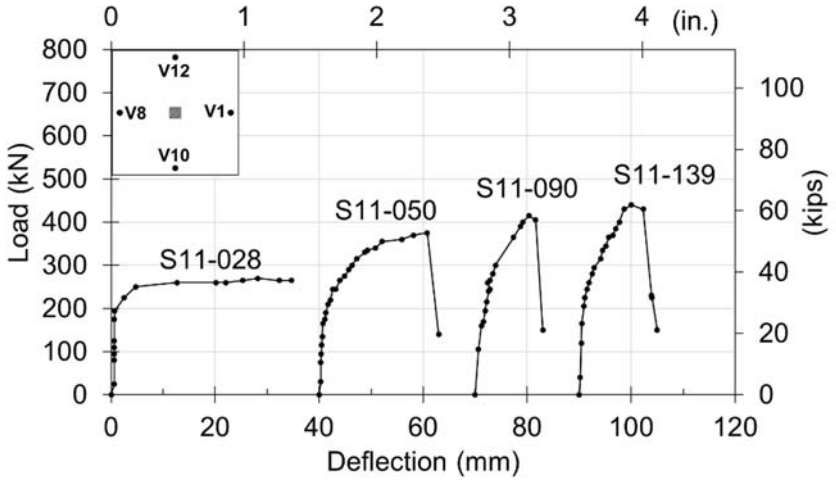

(a)

S11 series

Note: Deflection is the average of four deflections at V1,V8,V10 and V12

Fig.5. 6 – Load-deflection curves of the 12 slabs (a) S11 series, (b) S13 series, (c) S15 series. [Fig. 5.6(b) and Fig. 5.6(c) are placed in the next page]

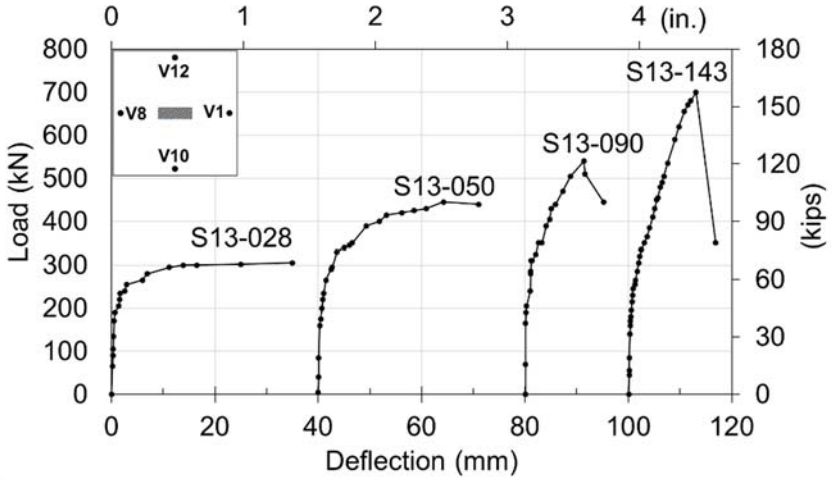

(b)

S13 series

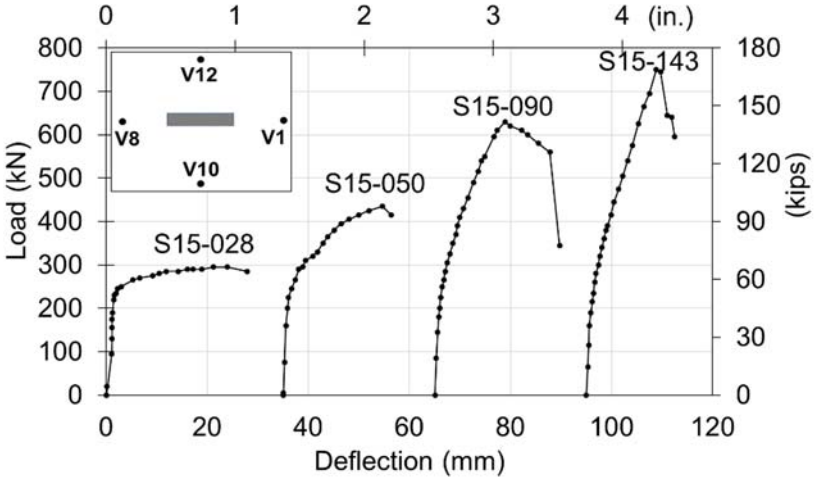

(c)

S15 series

Note: Deflection is the average of four deflections at V1,V8,V10 and V12

Fig. 5.6 (Continued)

5.2.4 Strains in flexural reinforcements

Figures 5.7 show the development of strains in flexural reinforcements at various loading stages for the S11-series slabs. Fig. 5.7(a) shows that the strains developments in Specimen S11-028 were very small even at the load of about 75% of maximum load (200 kN). The strains then increased quickly and reached the yield strain at the load very close to maximum load. Other slabs with higher reinforcement ratios showed gradual developments of the steel strains from early stage of loadings as shown in Figs. 5.7(b, c and d).

Figures 5.8 summarise steel strain distributions at the ultimate load stage in the S11-series, S13-series, and S15-series. From Fig. 5.8, it can be seen that in slabs with higher reinforcement ratios ($\rho \geq 0.9\%$ or Sxy-090 and Sxy-143), most of the steel strains drop considerably at locations beyond 1.5*h* away from the column face. In slabs with lower reinforcement ratios ($\rho \leq 0.5\%$ or Sxy-028 and Sxy-050), the initial failure mode is flexure, and most of the steel strains can remain high or greater than the yield strain even at locations near the edge of the slabs.

Figures 5.9 show the strain developments in reinforcements within the lines of column face and outside lines of columns faces of the slabs S13-143 and S15-143, respectively. The strain gauge positions are inset in the figures for better visualisation. It can be seen that the strains are low in the middle of the longer side of column section, the strain values are highest at the locations just outside the column face for both specimens. Significances of the strain results presented here are discussed in the next sections (Section. 5.3).

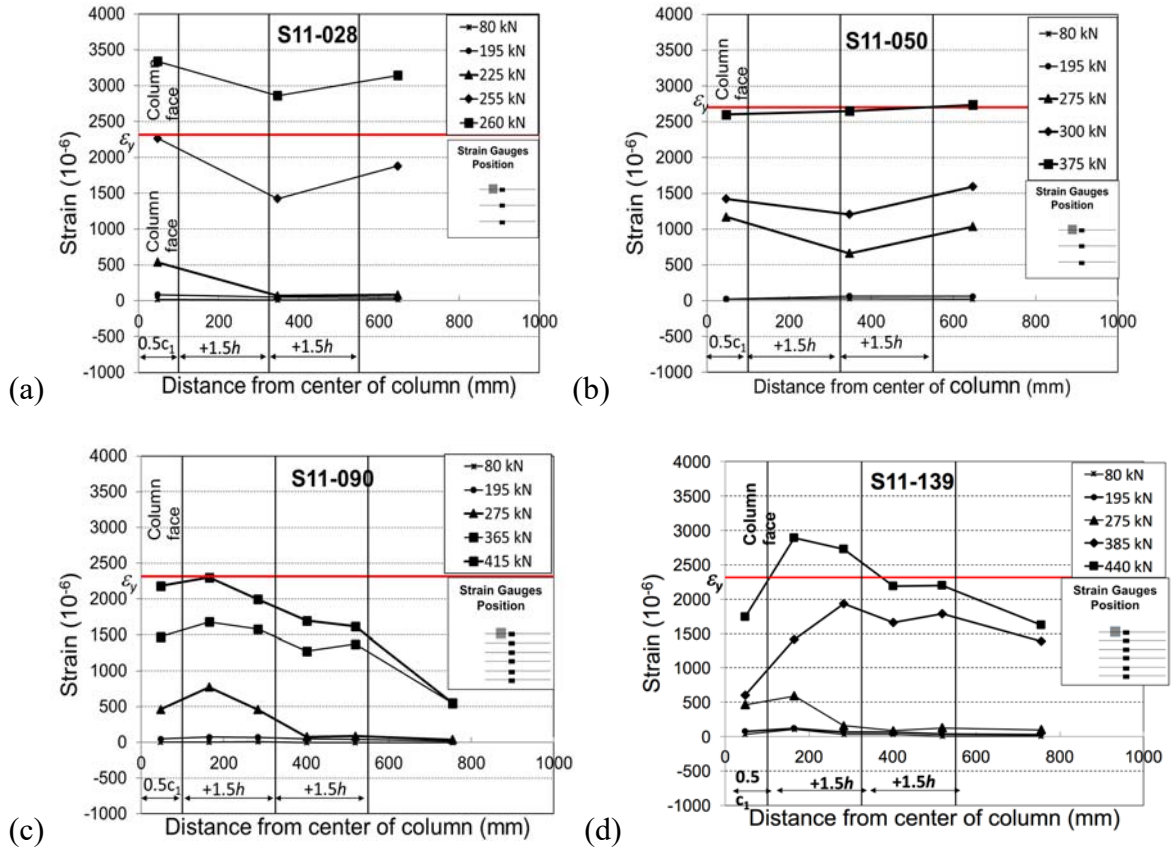

Fig.5. 7 – Development of strains in the reinforcements of Specimen (a) S11-028, (b) S11-050, (b) S11-090, and (d) S11-139

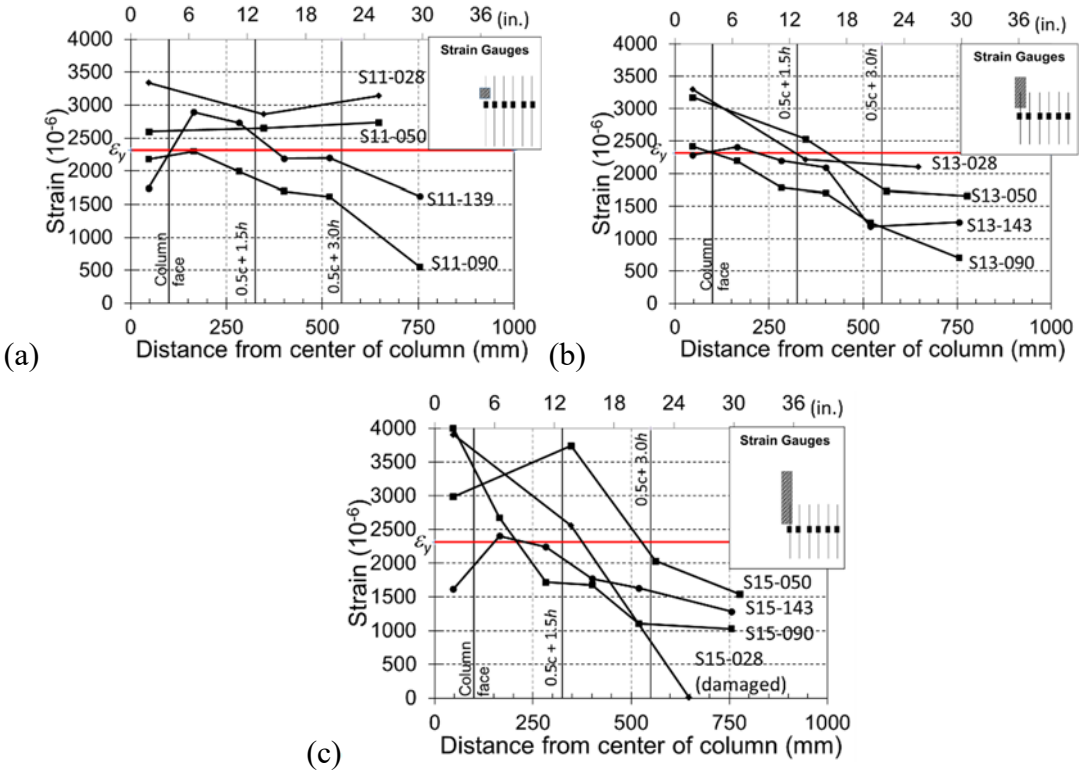

Fig.5. 8 – Steel strains in several reinforcing bars near the columns at failure loads for (a) S11 series slabs, (b) S13 series slabs, (c) S15 series slabs.

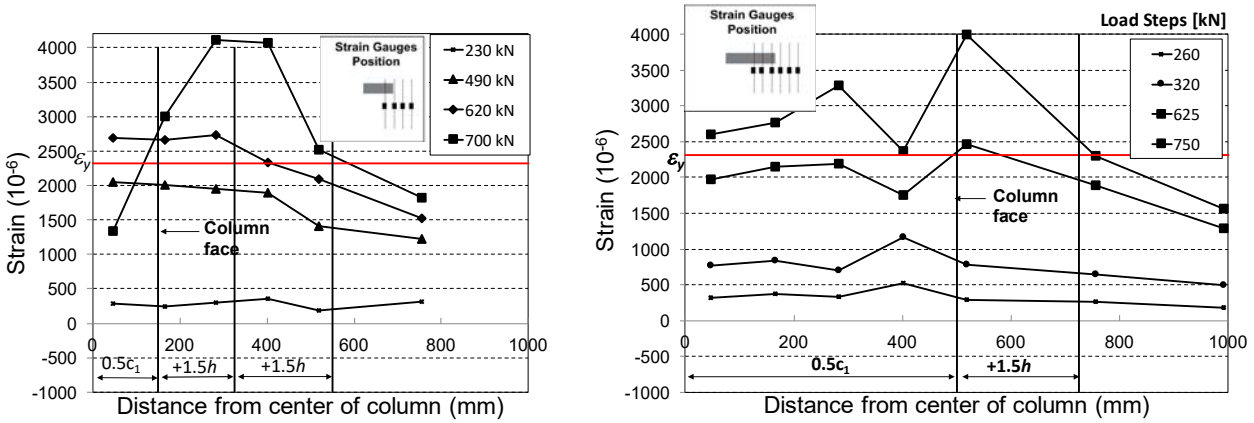

(a) **S13-143** (b) **S15-143**

Fig.5. 9 – Strain developments in reinforcements within the lines of column face and outside lines of columns faces of the slabs (a) S13-143, and (b) S15-143

5.3 Discussions

5.3.1 Comparisons of design equations with test results

For the purpose of these comparisons, all the load factors, materials safety factors and strength reduction factors are all set equal to 1.0. For comparison with design codes, maximum load of each specimen presented earlier in Table 5.1 was added with the self-weight of the slab outside the perimeter measured at *d* away from column faces and the weight of test equipment placed on top of the slab. Table 5.2 compares the punching shear strengths of the 12 HSC slabs with the predictions of the ACI 318 (ACI) method, Eurocode 2 (EC2) method and also the yield line theory (YTL). The evaluations of each design method are as follows.

Table 5. 2 – Comparisons of code equations with experimental results

					YLT	ACI	EC2	V_{exp}/V_{calc}		
	Slab ID	c_1/c_2	ρ (%)	V_{exp} (kN)	V_{flex} (kN)	V_C (kN)	V_C (kN)	**YLT** (5)/(6)	**ACI** (5)/(7)	**EC2** (5)/(8)
1	2	3	4	5	6	7	8	9	10	11
S11 Series	**S11-028**	1.0	0.28	279	132.8	428.4	292.2	2.10	0.65	0.95
	S11-050		0.50	394	225.9	413.7	340.0	1.74	0.95	1.16
	S11-090		0.90	439	469.4	413.7	413.6	0.93	1.06	1.06
	S11-139		1.39	454	635.4	399.3	458.3	0.71	1.14	0.99
S13 Series	**S13-028**	3.0	0.27	308	150.6	580.1	393.5	2.04	0.53	0.78
	S13-050		0.50	418	325.0	562.3	460.2	1.29	0.74	0.91
	S13-090		0.90	558	578.4	562.3	559.8	0.96	0.99	1.00
	S13-143		1.43	718	802.1	544.7	628.2	0.90	1.32	1.14
S15 Series	**S15-028**	5.0	0.27	321	165.5	655.1	494.9	1.94	0.49	0.65
	S15-050		0.50	456	351.0	655.1	579.7	1.30	0.70	0.79
	S15-090		0.90	656	623.6	655.1	705.3	1.05	1.00	0.93
	S15-143		1.43	775	864.5	635.6	794.0	0.90	1.22	0.98
							Minimum =	0.71	0.49	0.65
							Maximum =	2.10	1.32	1.16
							Average =	1.32	0.90	0.94
							Coefficient of variation, COV =	0.363	0.302	0.158

Note: YLT = the yield line theory method; V_{exp}/V_{calc} is the ratio of the failure load to the predicted punching shear strength

5.3.1.1 Performance of ACI 318-14:

The ACI 318-14's method is unconservative for predicting the strengths of the high-strength concrete slabs, Table 5.2 Column (10) shows the ratio of experimental load to calculated load V_{exp}/V_{calc}. The average value of V_{exp}/V_{calc} is only 0.90 (lowest among other methods), and the coefficient of variation (COV) is 0.30 that is considered high and inconsistent. The inconsistency is because the ACI method severely overestimates the shear strengths of the slab specimens with low reinforcement ratios (ρ = 0.28% and ρ = 0.5%) that failed in flexure. The overestimation is more obvious for the S13-series and S15-series specimens (β =3.0, 5.0), the minimum value of V_{exp}/V_{calc} is 0.49 which associates with Specimen S15-028. This analysis shows that the omission of the reinforcement ratios in the ACI punching shear equation can lead to serious design inadequacy issues. However, the ACI method becomes relatively more accurate when the reinforcement ratio was increased to be more than 0.9% such as the slabs Sxy-090, Sxy-139, and Sxy-143. It is important to note that the author applied the ACI 318's upper limit of $\sqrt{f'_c}$ to be 100 psi or 8.3 MPa in calculating shear strength for the slabs. So, if this limit is not considered, the analysis would show that the ACI method is unconservative for most of the HSC slabs here.

5.3.1.2 Performance of Eurocode 2:

Table 5.2 Column (11) shows that the Eurocode 2(EC2) 's method is more consistent than the ACI method, but it is still unconservative (Average of V_{exp}/V_{calc} = 0.94, and COV = 0.15). Even though the influence of flexural reinforcement is considered in the EC2's equation, this analysis shows that the equation overestimates the shear strength of the slabs that have the low reinforcement ratios (ρ = 0.28% and 0.50%). The EC2's performance over the slabs with rectangular columns is not desirable because the predictions are unconservative, particularly for the S15-series (β = 5.0). The minimum value of V_{exp}/V_{calc} is 0.65 which corresponds to Specimen S15-028. Thus, the applicability of Eurocode 2's method for HSC slabs supported on rectangular columns should be addressed. Also, the concrete strength f'_c was limited at 90 MPa for the Eurocode 2's method in this analysis. Similar to the case of the

ACI method discussed above, Eurocode 2 would be even more unconservative if the actual concrete strengths are used to calculate the punching shear strengths of these HSC slabs.

5.3.1.3 Performance of yield line theory:

The yield line theory method is very conservative for predicting the strengths of the slabs with low reinforcement ratios as shown in Column 9 of Table 5.2. Equation (3.14) associating with the yield line pattern given in Fig. 3.9(a) (in Section 3.4.3.2) is used to calculate V_{flex} of the slabs with the lowest rho (Specimens Sxy-028). For the other slabs, the author used Eq. (3.16) for calculating V_{flex} which was derived from a "circular fan" yield line pattern because the pattern is more suitable to represent the actual crack patterns of the slabs (discussed earlier in Section 5.2.2.1). Note that the circular fan pattern would give the lower bound values of V_{flex} for a case of concentric loading of a slab.

For the slabs with $\rho > 0.9\%$, the V_{flex} calculated using YLT is high and not conservative for predicting the failure loads of these slabs. This is expected because the failure mode is punching, so the shear strength governs and should be attained before the flexural strength V_{flex}. However, for the slabs with low reinforcement ratios, Table 5.2 shows that the yield line theory method becomes overly conservative. By comparing the values of V_{flex} in Column 6 of Table 5.2 with the loads in strain profiles shown in Figs. 5.7(a and b). It can be seen that the yield line theory method predicts the loads of Specimens S11-028 (V_{flex} = 133 kN) and S11-050 (V_{flex} = 226 kN) lower than the corresponding failure loads which are also the loads at first yielding of the reinforcement, that is 260 kN for S11-028, and about 375 kN for S11-050. The differences may be due to some influences of other factors that were not accounted for. One possibility is due to the complex failure mechanism that is different from yield line mechanism, it involves a combination of flexure, shear and even torsion. Torsion can occur mostly when the cracks are extensive and unsymmetrical. Another possibility, the ultimate moment capacity may be enhanced by the membrane actions that can take place in a lightly reinforced slab even without the lateral restraints, as suggested by Park and Gamble (2000) and supported by the works of Taylor [Park and Gamble (2000), pg. 687]. Moreover, it

is also a possibility of the inaccurate yield line pattern that does not represent the actual collapse mechanism.

The discussions above highlights some of the limitations of yield line theory in a design application. Technically speaking, using the yield line theory to design flat plates needs careful judgements in selecting admissible yield line patterns and loading configurations. Nevertheless, if correctly applied, the theory would be mostly conservative.

5.3.2 Influence of the reinforcement ratio

Observations from the experimental results presented above showed that HSC slabs with high reinforcement ratios (i.e. $\rho > 0.9\%$) are brittle and can fail in punching, the steel strains in those slabs can reach the yield strain but only near the column. So, the reinforcements that should be considered effective for resisting the punching load are those within about 1.5h from the column faces or within a width of $c + 3h$ for an interior column. This finding is consistent with past studies (discussed in Section 2.3.2) where concentration of reinforcement around column region (c_2+3h) was found to enhance the punching shear strength to some extents.

It is evident that the strength of a slab (both flexural and punching) increases as the reinforcement ratio increases. Discussed earlier in Section 2.3.2, the punching shear strength v_c can be a power function of reinforcement ratio ($v_c \propto \rho^N$) which can vary between a linear function (N=1) and a power function of ¼ (N = 1/4). The values of the power N are essentially empirical.

The yield line theory tends to be overly conservative for slabs with low reinforcement but not applicable for the slabs with high reinforcement ratios that failed in punching. The Eurocode 2 method uses a power function of 1/3 ($v \propto \rho^{1/3}$) but it tends to overestimate the strengths of slabs with very low reinforcement ratios. The ACI method does not consider the influence of flexural reinforcement in its punching shear equations, so a prediction by the ACI method can be unreliable for the design of lightly reinforced slabs.

The evaluations of other published slab data with low reinforcement ratios will be discussed separately in Chapter 7 where a new method to tackle this effect of low reinforcement ratios will be proposed.

5.3.3 Influence of the column rectangularity

Figure 5.10 shows the relationship between the normalised shear stress at failure $V_{exp}/[b_o d\sqrt{f'_c}]$ and the column aspect ratio β (= c_1/c_2), which is the ratio of long to short sides of the column. The comparing data are the author's current slab specimens and from the literature [References of the data are shown in Fig. 5.10]. Each of selected set of data comprises slab specimens with different column aspect ratios. The author's slab specimens were made of high strength concrete while those from the literature were made of normal strength concrete. It can be seen from the trend line for each set of data that the normalised shear stress decreases as the column aspect ratio increases. The trend lines are all similar to each other, including the one for the author's current high strength concrete slabs.

In Fig. 5.10 we can also see that the trend line for ACI 318 is reasonably close to those of the experiments. The ACI method, however, is unconservative for the author's high strength concrete specimens (S11, S13, and S15 series). This is due to the inaccuracy of the overall ACI's V_c equations which do not represent the influence of high strength concrete and reinforcement ratio well enough. It can also be seen from Fig. 5.10 that the ACI column rectangularity ratio (β) can be applied equally well for β of up to 5.0, even though β > 4.0 may fall into the category of walls rather than columns.

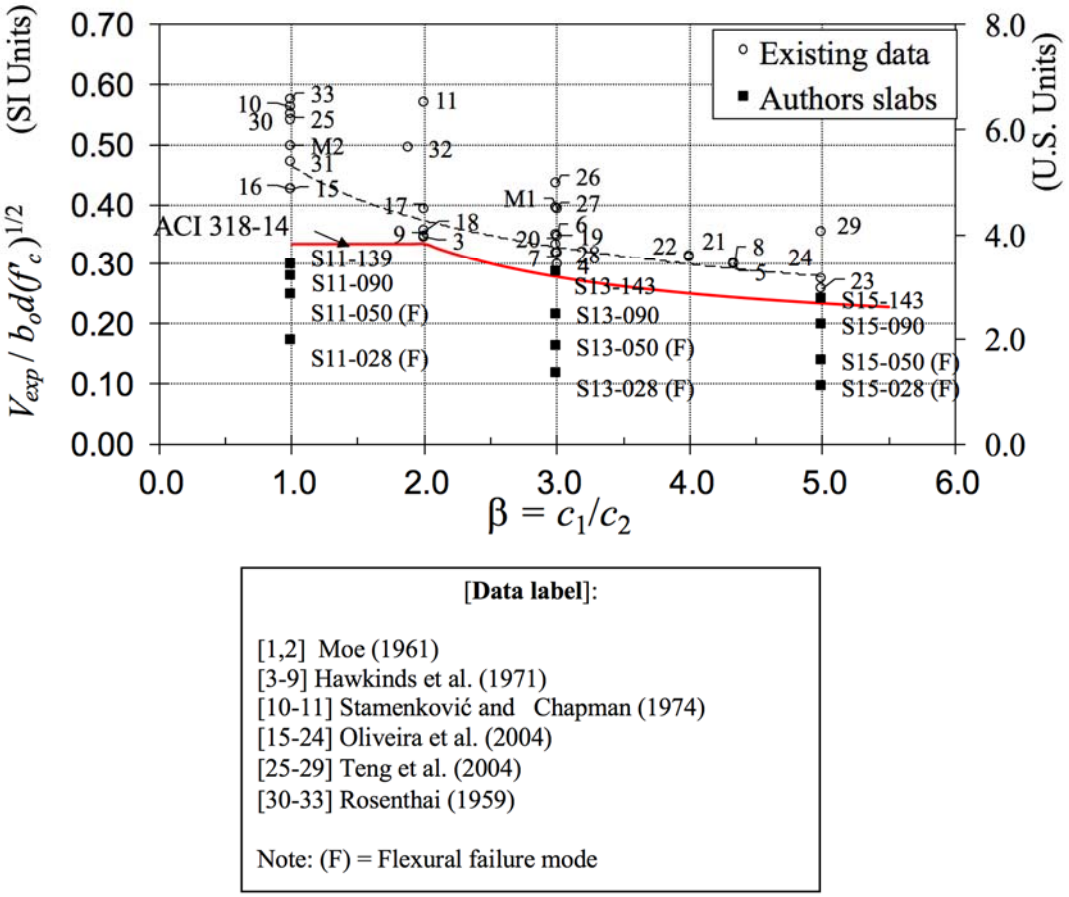

Fig.5. 10 – Performance of ACI 318 equation with respect to column aspect ratio (β = c_1/c_2)

5.3.4 Influences of the high strength concrete

The concrete strength f'_c is an important parameter in shear equations. Discussed earlier in Section 2.3.1, the shear strength of member is known to be a function of concrete strength raised to the power of 1/3 or 1/2 ($v_c \propto f'^{1/3}_c$ or $v_c \propto \sqrt{f'_c}$). Essentially, if the f'_c is increased from 40 MPa to 100 MPa, the shear strength would increase by about 58% for $v_c \propto \sqrt{f'_c}$, and about 35% for $v_c \propto f'^{1/3}_c$, provided that other variables are similar.

To study the influences of HSC on the punching shear strength, the results of the current HSC slabs S11-139, S13-143 and S15-143 can be compared directly with the normal strength concrete (NSC) slabs OC11, OC13, and OC15 as presented in the paper by Teng et al. (2004). Direct comparisons can be made because their test setup, loading conditions, and other basic parameters and geometry are identical (or

similar). Table 5.3 shows the comparison of their normalised failure loads ($V_{exp}/[b_o d(100\rho)^{1/3}]$), it can be seen that the punching shear strengths of the HSC slabs (average f'_c = 100 MPa) are only about 10% to 25% higher than the NSC slabs' strengths (average f'_c = 40 MPa). The increase is smaller for the slab with a square column. Compare this increment with the increment calculated in the previous paragraph, the use of $\sqrt{f'_c}$ for calculating the shear strength may be too high for HSC members. Therefore, the ACI 318's limiting value of $\sqrt{f'_c}$ (= 100 psi or 8.3 MPa) in its current form of shear equations should remain.

Nevertheless, the author also compared other structural aspects of the HSC slabs with the NSC slabs presented in the Teng et al. (2004)'s paper, such as the cracking behaviors and load-deflection response. The comparisons showed that the current HSC slabs have much higher first crack loads and flexural stiffness. So, in practice, where cracks, deflections and perhaps floor-to-floor height limits control the design, the use of HSC can be a more economical choice because the overall slab thickness as well as the concrete volume can be reduced substantially for the same design loads.

Table 5. 3 – Comparisons of current test results with data from Teng et al. (2004)

Slab ID	d (mm)	b_o (mm)	ρ (%)	f'_c (Mpa)	V_{exp} (kN)	$V_{exp}/[b_o d(100\rho)^{1/3}]$ Normalised
S11-139	114	1256	1.39	112	454	2.84
S13-143	114	2056	1.43	114	718	2.72
S15-143	114	2856	1.43	97	775	2.11
***OC11**	105	1256	1.80	36	423	2.64
***OC13**	105	2056	1.80	36	568	2.16
***OC15**	105	2856	1.80	40	649	1.78

Note: * data obtained from Teng et al. (2004)

5.4 Summary

Based on the author's experiments and the accompanying discussions, the following conclusions can be made and they are applicable to normal as well as high strength concrete slabs:

1. Under a punching load, a slab provided with a low reinforcement ratio (0.5% for the current 12 slabs) may fail in flexure first before it fails in what looks like punching failure in the end. The failure mode will be ductile and the failure load will be the load that causes yielding of the majority of the reinforcement. The failure load will be lower than predicted by ACI 318-14 equations for punching shear.

2. Slabs failing in pure punching shear mode will tend to form circular-fan type crack patterns at failure, while those failing in flexural mode will tend to form cracks parallel to column lines. In this case, the final circumferential crack tends to be very close to the column.

3. The higher the amount of reinforcement provided, the higher the failure load. However, only those reinforcements within the width of $1.5h$ from a column face (or total width of $c_2 + 3h$ for an interior column) will be fully effective in resisting punching shear stresses and, therefore, can be considered in influencing the punching shear strength.

4. The ACI 318 method is unconservative for the slabs with low reinforcement ratios (especially for $\rho < 0.9\%$). The EC2 method can be unconservative for slabs with very low reinforcement ratio and supported on rectangular columns.

5. The use of $\sqrt{f'_c}$ for calculating the shear strength may be too high for HSC members. Therefore, the ACI 318's limiting value of $\sqrt{f'_c}$ (= 100 psi or 8.3 MPa) in its current form of shear equations should remain. HSC slabs have higher first crack loads and flexural stiffness than NSC slabs. Therefore, the use of HSC can be a more economical choice.

6

SFRC SPECIMENS – RESULTS AND DISCUSSIONS

6.1 Introduction

This chapter presents the experimental programme of a new set of 10 SFRC slabs with varying flexural reinforcement ratios and varying fibre volume V_f up to 1.2%. The author investigated a new type of steel fibre (the double hooked-end steel fibre). The strengths of the concrete used in all the specimens in this test program were about 80 to 100 MPa. This study will show that inclusions of steel fibre can improve the overall structural performance of HSC slabs further.

The test results will be discussed and used to verify the applicability of the yield line theory, and the Model Code 2010's and TR 34's methods. Some useful design recommendations derived from this experiment will be given.

6.2 Experimental results

The main properties of the 10 slab specimens were presented earlier in Table 4.2. The concrete properties such as compressive strength f'_c, tensile flexural strengths f_r, modulus of elasticity E_c were summarised in Table 4.5 and Fig. 4.8.

6.2.1 Crack patterns and Characteristics

6.2.1.1 Crack patterns and propagations

Figure 6.1 shows the ultimate crack patterns of F09-series slabs. The crack patterns of F14 series slabs are similar to those of the F09 series slabs and are shown in Fig. 6.2. The crack patterns and crack propagations of the 10 slabs are somewhat similar to those of slabs failing in typical punching shear failure. First, one or two short lines of flexural longitudinal cracks appeared just across the column faces; these cracks were orthogonal to the orientation of the main reinforcement. As the load

was increased, more cracks developed in the SFRC slabs than in the non-fibrous HSC slabs. However, the widths of cracks are narrower in SFRC slabs than in non-fibrous slabs. As the applied load approached the failure load, a few circumferential cracks appeared. The internal inclined shear cracks (Fig. 6.3) formed the outermost ring of the circumferential cracks.

Note that crack widths were measured for those cracks that are within a region of 200 mm away from column faces at various load stages, and it was observed that the widths of surface cracks were narrower for the slabs containing higher fibre volume fractions V_f compared to those with lower V_f at all load stages. At certain load level, there were lesser cracks developed in the specimens with a higher V_f compared to the specimens with a lower V_f. For comparison purposes, the crack-width development charts for all the 10 specimens, and the time-lapse photographs showing crack propagation at various load stages in some of the specimens are provided in Appendix A.3.

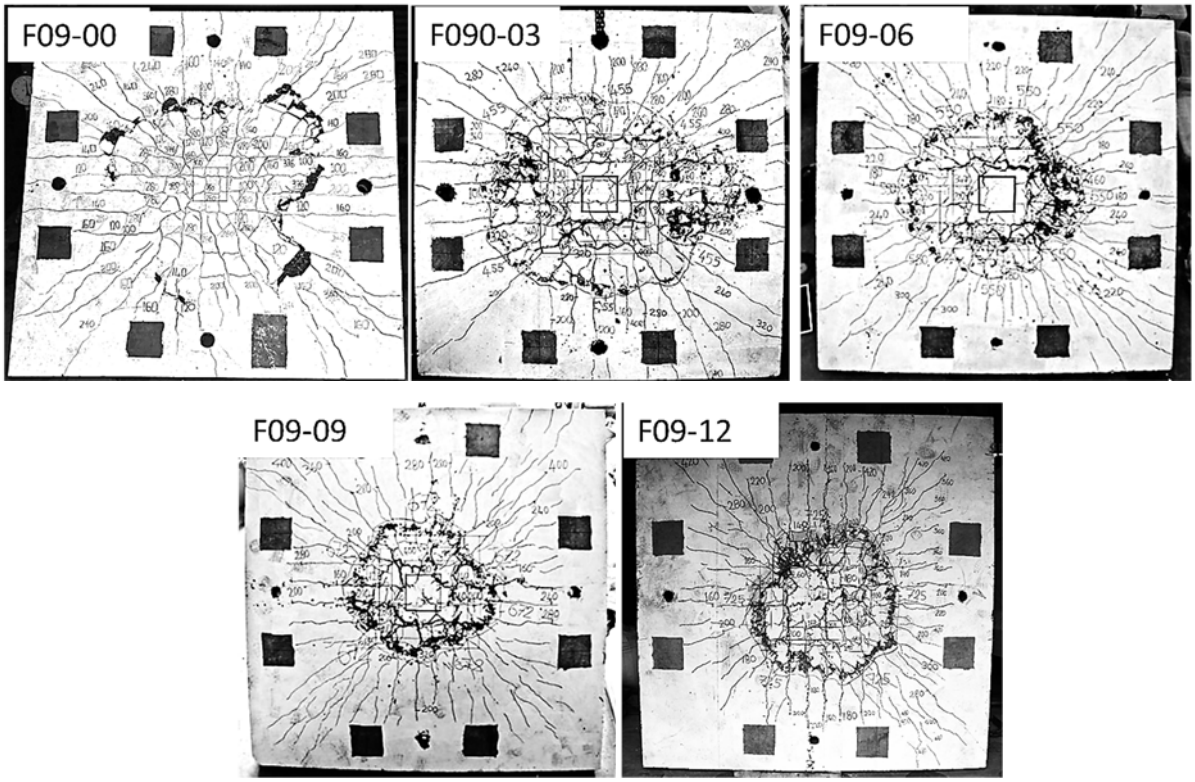

Note: Top left labels are the specimen IDs

Fig.6. 1 – Ultimate cracks patterns of the F09 series specimens

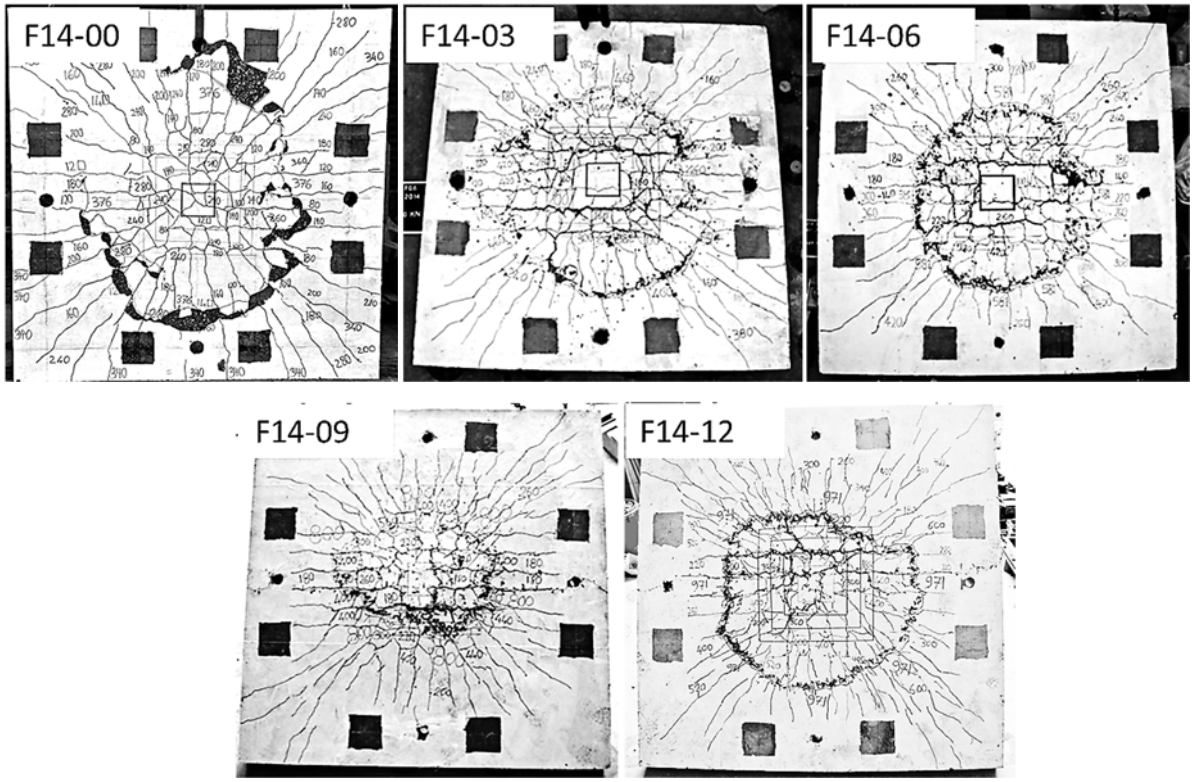

Note: Top left labels are the specimen IDs

Fig.6. 2 – Ultimate cracks patterns of the F14 series specimens

6.2.1.2 Shear crack inclinations

After tests, each slab was cut into half at a location near the column face in order to observe the inclinations of internal shear cracks (Fig. 6.3). Column 7 of Table 6.1 shows the average values of the shear crack angles (with respect to the horizontal plane) measured on the left and right sides of the cut sections. The angles seem to reduce with an increase in V_f as compared to the angles of the plain non-fibrous slabs. The shear crack angles for the non-fibrous HSC slabs (F09-00 and F14-00) were observed to be about 30° to 34°. The inclusion of the double hooked-end steel fibres can reduce the shear crack angles down to about 15° (see the row F09-06 in Table 6.1), a reduction in shear crack angle due to an inclusion of fibres has been reported in past experiments (Narayanan and Darwish, 1987; Theodorakopoulos and Swamy, 1993).

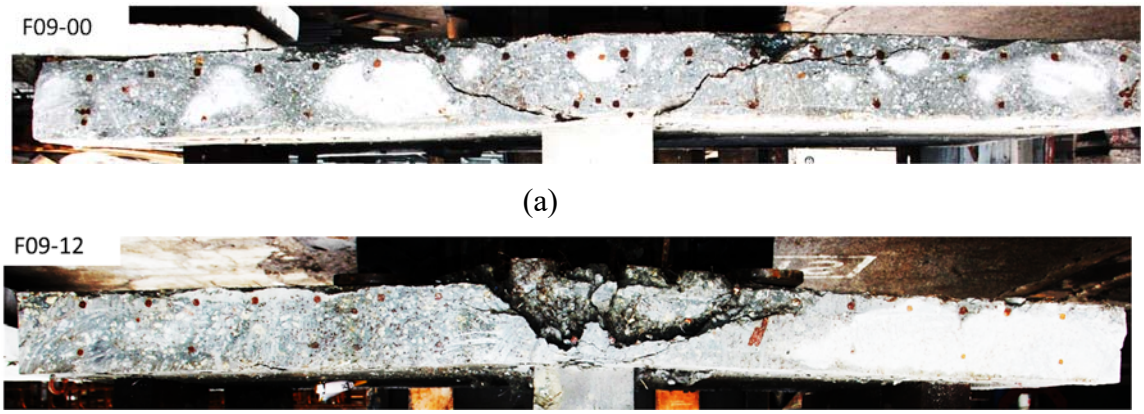

Fig.6. 3 – punching shear cracks of (a) Specimen F09-00, (b) Specimen F09-12

6.2.2 Ultimate failure loads and failure modes

6.2.2.1 Ultimate failure loads

Table 6.1 summarizes the loads at first cracks (Column 4) and the failure loads (Column 5). It can be seen that the load at first crack increased with an increase in in the fibre volume fraction, in particular for the series F09 slabs (ρ = 0.9%). The load for first crack development was between 100 kN to 120 kN; the addition of fibres 0.6% does not provide any further increase in the cracking load compared to the first cracking load of the slab with V_f of 0.6%.

Columns 5 of Table 6.1 shows that the ultimate failure loads of the 10 slabs were considerably influenced by the steel fibre content. By varying the fibre content from V_f of 0% to 1.2%, the failure loads increased by 1.9 times or from 382 kN to 731 kN for the F09-series slabs. The failure loads of the F14-series slabs are higher compared to the the F09-series slabs, with failure loads increasing by a factor 2.56 from 382 kN (85.9 kips) to 977 kN (219.6 kips). Between the F09 series (ρ = 0.9%) and F14 series (ρ = 1.4%) specimens, the failure load increment due to the addition of steel fibre is steeper for slabs with higher ρ (F14 series) compared to the slabs with lower ρ (F09 series) as shown in Column 6 of Table 6.1. Thus, the results highlight that the flexural reinforcement ratios influenced the failure loads (or the punching shear strengths) of the SFRC slabs.

6.2.2.2 Failure modes

Table 6.1 (Column 9) lists the observed failure modes of the slabs. The non-fibrous slabs (F09-00 and F14-00) failed suddenly after the peak loads were reached, so they had "brittle punching" failure mode. The four slabs with V_f = 0.3% and 0.6% also failed in clear punching but they were more ductile than the slabs without steel fibre, so the failure modes of these slabs were described as "ductile punching". The other four slabs with V_f = 0.9% and 1.2% had an interesting failure behavior; the punching occurred at the ultimate loads which were also their maximum loads. Their corresponding load-deflection curves (to be discussed in the following section) have some flat portions similar to a plastic plateau before reaching the ultimate failures. Therefore, the failure mode of these slabs is termed "Flexural-punching".

Table 6. 1 – Experimental results of SFRC specimens

ID	ρ (%)	V_f (%)	Load at first crack (kN)	Failure Load (kN)	Failure load increment (%)	Shear crack angle (Deg.)	Energy absorption (kN.mm) or (J)	Failure mode
1	2	3	4	5	6	7	8	9
F09-00	0.9	-	60	382	-	31.5	3452.5	Brittle Punching
F09-03		0.3	80	461	21	19.5	5422.3	Ductile Punching
F09-06		0.6	100	556	46	15.4	6290.7	Ductile Punching
F09-09		0.9	100	678	77	21.4	19091.6	Flexural-Punching
F09-12		1.2	120	731	91	24.2	21497.3	Flexural-Punching
F14-00	1.4	-	80	382	-	33.1	2705.6	Brittle Punching
F14-03		0.3	80	466	22	16.5	3555.2	Ductile Punching
F14-06		0.6	100	587	55	22.0	7405.7	Ductile Punching
F14-09		0.9	100	806	111	16.2	24063.3	Flexural-Punching
F14-12		1.2	100	977	156	19.6	23709.5	Flexural-Punching

Notes: V_{exp} in Col (5) is the failure load plus self-weight of the slab outside the perimeter measured at d away from column faces and weight of test equipment placed on top of the slab. The percentage increase in failure load for each series [in Col (6)] is calculated with respect to the plain HSC slabs (i.e. F09-00 and F14-00). Col (8) shows the energy absorption (the area under the load-deflection curve calculated up to the deflection corresponding to the ultimate failure load of each specimen).

6.2.3 Load-Deflection curves

The load-deflection curves of the specimens are shown in Figs. 6.4 and 6.5. Figure 6.4(a) shows the complete curves of the F09 series slabs while Fig. 6.4(b) shows the elastic region of Fig. 6.4(a) revealing the early stages of the corresponding load-deflection curves. Figures 6.5 (a and b) correspond to the F14 series slabs.

As expected, the slabs exhibit a linear-elastic behaviour prior to cracking. The slope of the load-deflection curve changes slightly (less steep) especially when the circumferential cracks formed. Upon further loading, the slopes of the curve becomes increasingly flat as the flexural stiffness of the slab continues to drop. As expected, the flexural stiffness of the slabs with the higher reinforcement ratio degrades less after cracking, and this is shown in Figs. 6.5 where the F14 series slabs exhibit steeper slopes compared to the F09 series slabs (Figs. 6.4). The flexural stiffness of the slabs after crack initiation increases with increasing fibre content as shown in the Fig. 6.4(b) and Fig. 6.5(b). This increase (for a given set of ρ) is due to the deflection hardening behaviour of SFRC that was also observed in the notched beam tests shown earlier in Fig. 4.8(a). Therefore, SFRC can indeed improve the slab performances at the service load level.

At about 80% to 90% of failure loads, any further load increment to Specimens F09-09, F09-12, F14-09, and F14-12 produces almost no additional increase in resistance, and the load-deflection curves become flat horizontal lines. These flat portions in the curves reveal yielding of the reinforcement as will be shown later.

The load-deflection curves of the slabs with lower V_f (= 0%, 0.3% and 0.6%) are similar to the typical curves of slabs failing in normal punching shear, where there are no flat portions in the curves upon reaching failure. However, the slabs with V_f = 0.3% and 0.6% are still relatively more ductile compared to the non-fibrous slabs (F09-00, F14-00). When punching finally occurred, Figs. 6.4(a) and 6.5(a) also show that the loads dropped less abruptly for the slabs containing the higher fibre contents (i.e. those slabs with V_f = 0.6%, 0.9% and 1.2%).

Figures. 6.4(a) and 6.5(a) show that the post failure load-resistances of the slabs containing steel fibres dropped to about 50% of their corresponding peak loads and retained the loads for a considerable amount of deformations.

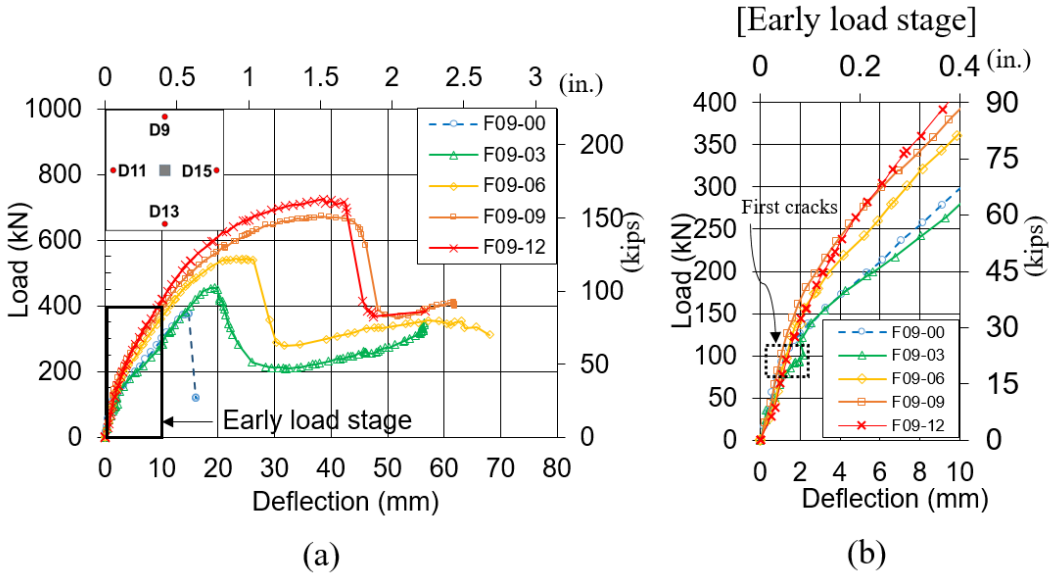

Note: Deflection is the average of four deflections at D9, D11, D13 and D15

Fig.6. 4 – Load deflection curves of F09 series slabs, (a) full curves, (b) early load stage

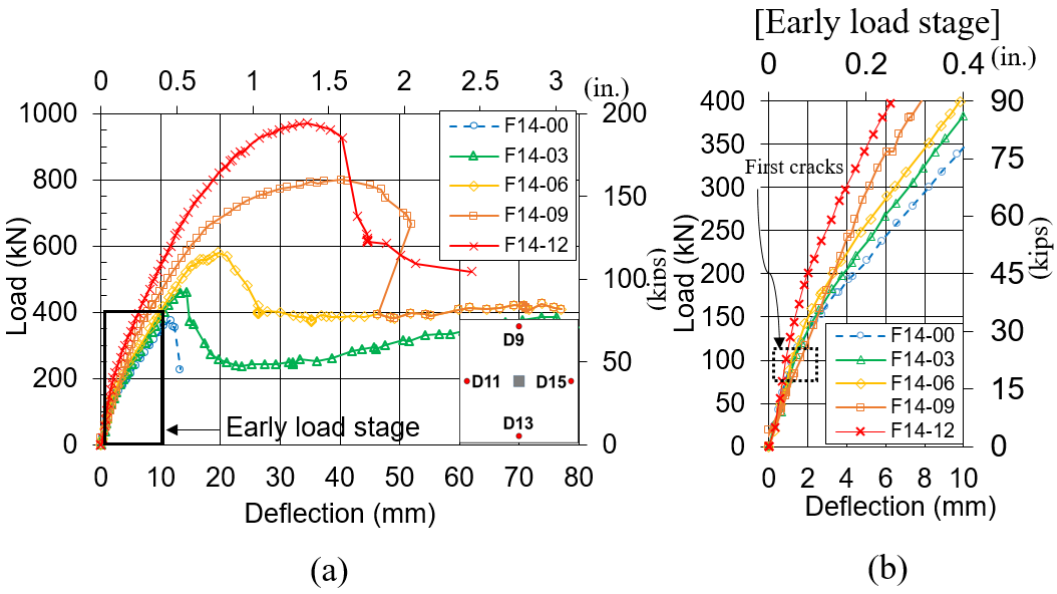

Note: Deflection is the average of four deflections at D9, D11, D13 and D15

Fig.6. 5 – Load deflection curves of F14 series slabs, (a) full curves, (b) early load stage

6.2.4 Energy absorptions

Another important attribute of SFRC is the toughness and energy absorption. Table 6.1 (Column 8) shows the values of the energy absorption (EA) of the slabs. Figure 6.6 shows the plot for the values of EA of each specimen. The average values of the

edge deflection δ_u at failure for the slab specimens are also indicated in Fig. 6.6. Note that the EA is determined by the area under the load-deflection curve of each slab calculated up to the failure load where the punching occurred. The EA increases mildly when V_f was varied from 0% to 0.6%; however, at V_f of 0.9% and 1.2%, the EA increases drastically with respect to the plain slabs without fibres. The EA are higher for the F09 series slabs than for the F14 series slabs when the fibre volume fraction V_f is less than 0.6% . This is expected because the slab with a lower reinforcement ratio would attain the yield strength faster than the one with higher reinforcement ratio, and the yielding leads to more ductile failures and, therefore, higher energy absorptions.

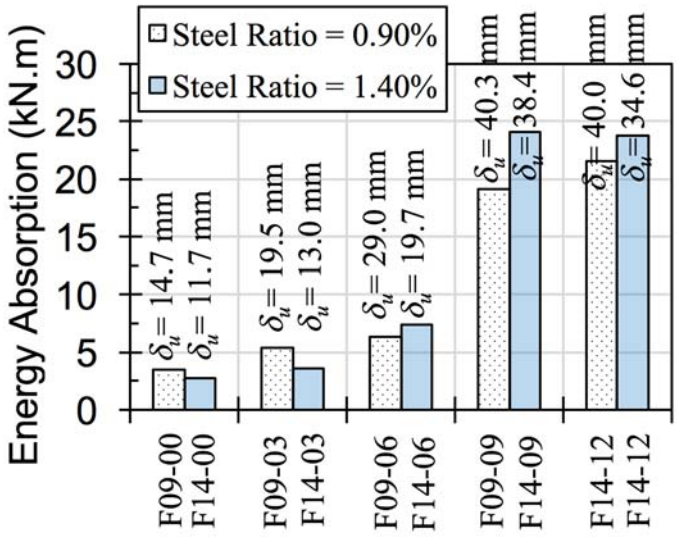

Note: δ_u is the (average) edge deflection at failure

Fig.6. 6 – Engery absorption of the 10 slab specimens

6.2.5 Strains in flexural reinforcements

Figures 6.7 and 6.8 show the strain in the flexural reinforcements of F09 series and F14 series slabs, respectively. Figures 6.7(a) and 6.8 (a) summarize the strain values at failures of the first set of the strain gauges (G11 to G61). Similarly, Figs. 6.7(b) and 6.8(b) show the strain values of the second set of the strain gauges (G12 to G52). These sets of strain gauges were intended to capture flexural strains in the high shear and high moment regions; that is at a distance about 50 mm to 170 mm or about 0.5*d* to 1.5*d* away from a line parallel to column face.

Figs. 6.7 and 6.8 reveal that only the reinforcement in the non-fibrous slabs (F09-00 and F14-00) and the slab F14-03 did not yield while the reinforcements in the other slabs with higher fibre contents yielded. The yielding of the flexural reinforcements became more widespread as the V_f increases from 0.3% to 1.2% as shown in Fig. 6.7(a) and 6.8(a). As expected, the reinforcements in the F09 series slabs (ρ = 0.9%) reached the yield strains at a lower load than the F14 series slabs, and the strain values at any loading stage (after first cracks) were also higher in the F09 series slabs than in the F14 series slabs. At failure, the strains in the reinforcements of slabs with V_f = 0.9% and 1.2%, exceeded the yield strain even at locations near the edge of the slabs. Therefore, it is clear that their initial failure modes are flexure, which were also indicated by the flat portions in the load-deflection curves shown earlier in Figs. 6.4 and 6.5.

Figures 6.7(b) and 6.8(b) show that some of the reinforcements at the location of the strain gauges G12 to G52 have yielded, especially in the slabs with high V_f(= 0.9% and 1.2%). The strain distribution confirms that the moments were distributed from yielded sections to adjacent unyielded sections which are located futher away from the column faces. The results highlight that the rotational and bending moment capcities of the SFRC slabs using the double hooked-end fibres (especially when $V_f \geq$ 0.9%) are significantly greater than those without fibres.

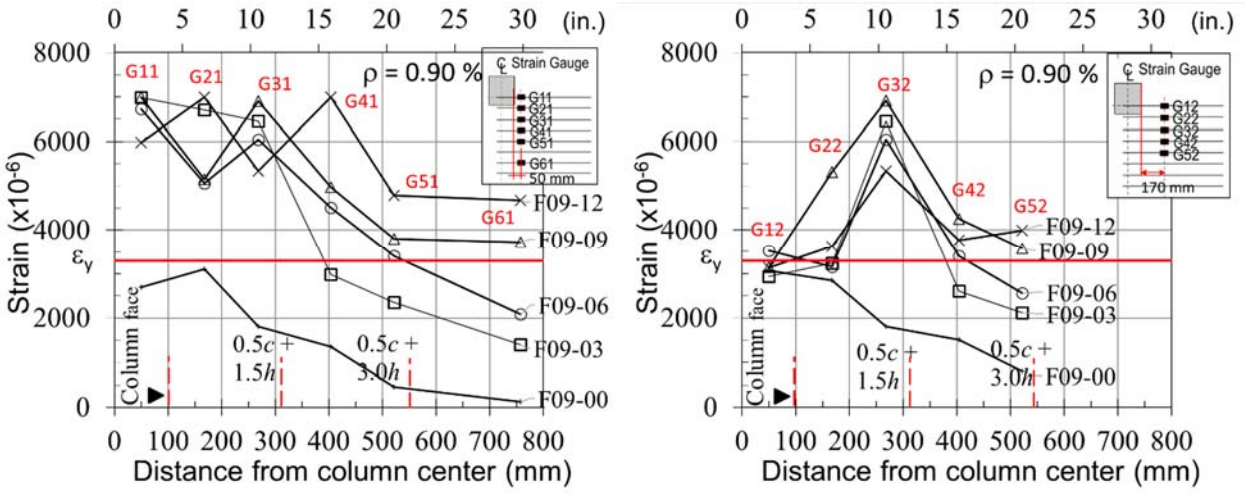

Fig.6. 7 – Strain profiles of F09 series slabs, (a) strain locations at 50 mm from a line of column face, (b)) strain locations at 170 mm from a line of column face

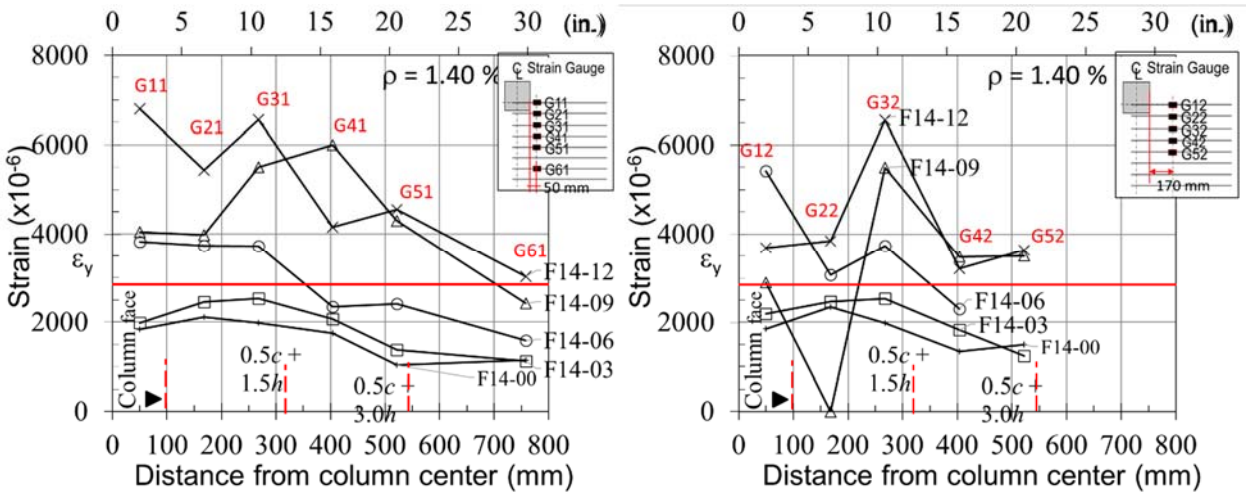

Fig.6. 8 – Strain profiles of F14 series slabs, (a) strain locations at 50 mm from a line of column face, (b)) strain locations at 170 mm from a line of column face

6.3 Discussions

6.3.1 Influence of SFRC using double hooked fibres

6.3.1.1 On crack and serviceability behaviours

Besides the serviceability issues such as visual appearance and durability problems, surface cracks can be an essential indicator of structural health and performances. Crack widths were observed to become smaller with an increase in fibre volume fraction V_f. Compared to normal RC slabs, SFRC slabs have better performance in terms of crack controls as the fibres can effectively delay the propagation of cracks; thus, it is possible for the SFRC slabs to be designed for higher service loads, depending on the amount of fibres used.

6.3.1.2 On ultimate failure load and comparison with other slabs using single hooked-end fibres

From the experimental results, it is clear that the inclusion of double hooked-end fibres can increase the failure loads or shear resistance of concrete slabs

significantly. The increase in the shear resistances of the slabs are proportional to the amount of the steel fibre added and the flexural reinforcement ratios ρ.

It is known that different types of fibres have different influences on the slabs' failure loads. Hence, to compare the effects of the two types of fibres on the punching shear strength; the chart in Fig. 6.9(a) was plotted to show the relationship between the normalized stress at failure $V_{exp}/(b_o d\sqrt{f'_c})$ in the y-axis and the fibre volume fraction V_f in the x-axis. Fig. 6.9(b) is similar to Fig. 6.9(a) but the y-axis (the normalized stress at failure) is $V_{exp}/[ud\sqrt[3]{(100\rho f'_c)}]$ instead. Note that b_o and u are the critical shear perimeters calculated according to ACI 318-14 (0.5d away from column faces) and Eurocode 2 (2d away from column faces with round corners), respectively. The data for comparison were obtained from Harajli et al. (1994), and Gouveia et al. (2014). Relevant properties of the concrete and slab specimens are also provided in the legend of Figs. 6.9. Note that the author used double hooked-end fibres while Harajli et al. (1994), and Gouveia et al. (2014) used single hooked fibres. The relationships (trend lines) shown in Figs. 6.9 confirms that the punching shear strength of a slab, in general, increases with an increase in fibre content. Fig. 6.9(a) and Fig. 6.9(b) also show the influence of fibre content (V_f) on the punching shear strength equations of ACI 318-14 and Eurocode 2 Codes, respectively, for rough comparison purposes. From Fig. 6.9 (a) and Fig. 6.9(b), it is also clear that a rise in the shear resistances of the current 10 slabs is particularly steeper than those of other slabs from Harajli et al. (1994) and Gouveia et al. (2014). This comparison shows that the double hooked-end steel fibres have stronger (positive) effects on the punching shear strength than the single hooked-end fibres.

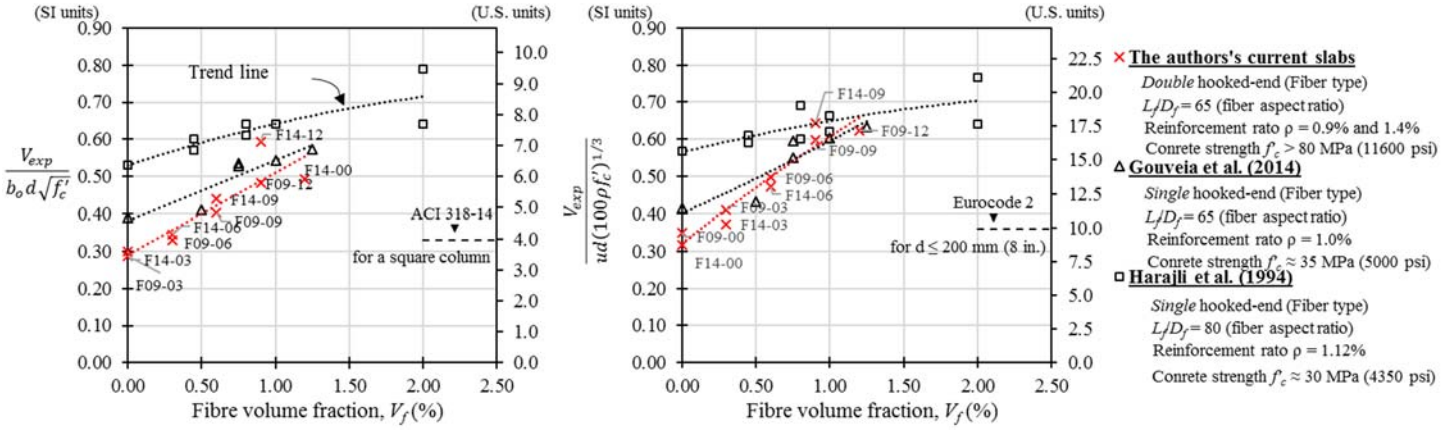

Fig.6. 9 – Relationship between the normalized punching shear stress at failure with fibre volume fraction V_f.

6.3.1.3 On post-punching behaviour

After punching occurred, the load carrying capacities of the slabs dropped to about 50% of the peak loads. The post-failure strength (Regan et al., 1979) that may remain is known to be contributed by the bottom reinforcement (or integrity reinforcement) that pass through the column core. It can be seen also that the post-failure strengths were higher for the slabs with higher steel fibre contents. Therefore, steel fibres, especially the double hooked-end fibres, improve the load resistance of slabs even after punching occurred. Therefore, incorporating SFRC in slabs where the bottom bars act as the integrity reinforcement can also be an effective enhancement for that integrity reinforcement.

6.3.1.4 On ductility and energy absorption

The ductility of a slab can be improved by an addition of steel fibres. One of the key indicators of slab ductility is the energy absorption. Energy absorption also signifies the rotational capacity and moment redistribution capacity of a slab. Shown earlier in Table 6.1 (Column 8), a drastic increase in the energy absorption of at least 450% with respect to non-fibrous slabs can be achieved when the fibre volume fraction V_f is greater than or equal to 0.9%. High EA can also be reflected by the widespread yielding of the reinforcement in slabs as shown earlier in Figs. 6.7 and 6.8, where almost the entire flexural reinforcements in the current SFRC slabs were activated to resist the moments and punching shear loads.

6.3.2 Comparisons of design methods with test results

Table 6.2 shows the comparisons of the performances of the Model Code 2010, TR 34 as well as the yield line theory (V_{flex}) with the current ten slabs. For the purpose of subsequent comparisons in this section, all the load factors, materials safety factors and strength reduction factors are all set to 1.0. The failure load of each specimen V_{exp} includes the self-weight of the slab outside the perimeter measured at d away from the column faces and the weight of test equipment placed on top of the slab. The performance of each method will be evaluated by the statistical analysis of the ratio of the failure load to the calculated load (V_{exp}/V_{calc}). For instance, a high value of an average V_{exp}/V_{calc} indicates the conservatism of a method while a low value of a COV (coefficient of variation) indicates a reliability of the method. So, a method that has an average value of V_{exp}/V_{calc} close to 1 (on the conservative side or > 1.0) and with a low COV should be considered as accurate.

The Model Code 2010 method, TR 34 method, and the yield line theory were described in Chapter 3. In this analysis, the calculated ultimate strength V_{calc} using the TR 34, Model Code 2010, and yield line theory are given by Eq. (3.5), Eq. (3.8) and Eq. (3.16), respectively.

6.3.2.1 Performance of yield line theory:

Columns 2 and 4 of Table 6.2 show the experimental failure loads V_{exp} and the calculated strength V_{flex} using yield line theory, respectively. The ratios of V_{exp}/V_{calc}, shown in Column 11, are shown to be lower than 1 with an average V_{exp}/V_{calc} of 0.71. Note that $V_{flex} = V_{calc}$. Thus, based on these results, the flexural strength of all the 10 slab specimens should be considered as not attained before failures. This is true for the slab specimens with $V_f \leq 0.6\%$ because there was no widespread yielding of reinforcements in these slabs. However, it is an interesting case for the specimens F09-09, F14-09, F09-12, and F14-12 (V_f = 0.9% and 1.2%). According to the yield line theory, the failure loads V_{exp} of these slabs should be at least equal or greater than the loads V_{flex} because most of the reinforcements in these slabs, indeed, yielded. But Column 10 of Table 6.2 shows that the failure loads V_{exp} of the slabs are smaller than V_{flex}. Therefore, the comparisons show that the failure mode of the

slabs with high reinforcement ratios and high fibre content such as Specimens F09-09, F09-12, F14-09, and F14-12 should not be treated as the flexural mode even though their failure behaviours were ductile and their reinforcements yielded.

Therefore, the yield line theory may not be an accurate method for calculating ultimate shear strength of SFRC slabs having parameters similar to the cases discussed above. Among the three methods compared in Table 6.2, the predictions by the yield line theory method are not conservative because the average V_{exp}/V_{calc} is 0.71 even though the COV is considerably low (about 14%).

6.3.2.2 Performance of TR34:

TR34 method is shown to perform best among the three methods, with a COV of only 12% and an average value of V_{exp}/V_{calc} of 0.99 (See Table 6.2 Column 12). The TR34's prediction of the shear strength increment V_{Rf} (see Column 6) due to an addition of fibres is quite consistent with the failure load increments ΔV (shown in Column 3). In Column 12 of Table 6.2, the TR34 method overestimates the punching shear strength of the slabs with low fibre contents, especially the slabs without fibre (F09-00 and F12-00). This is somewhat expected, because TR34 method is essentially the Eurocode 2's equation but with the term v_f. The author has evaluated the performance of Eurocode 2 (EC2) with current 12 HSC slabs in Chapter 5. In Chapter 7, it will be shown again that the EC2's equation tends to overestimate punching shear strength of slabs constructed with high strength concrete, especially for $f'_c > 80$ MPa.

6.3.2.3 Performance of Model Code 2010:

The performance of Model Code 2010 method is inaccurate compared to the other two methods. It has a COV of 44% and an average of V_{exp}/V_{calc} of 0.99 (See Table 6.2 Column 13). The highly scattered predictions are because the Model Code 2010 method underestimates the strengths of the slabs F09-00, F14-00 (Maximum of $V_{exp}/V_{calc} = 1.81$), but overestimates strengths of those slabs with fibres by large margins (Minimum of $V_{exp}/V_{calc} = 0.58$). The overly conservative prediction for the slabs F09-00 and F14-00 can be due to the use of the slab rotation ψ in Eq. (3.10) which is

the simplest form of approximation. More complex forms of the Model Code 2010 method are expected to solve this problem. In Column 8 of Table 6.2, the shear strength contribution from SFRC calculated using the Model Code 2010 method does not perform well. It can be seen that V_{Rf} (= $v_f \times b_o d$) are too high compared to the failure load increments ΔV (Column 3).

6.3.2.4 Summary of comparisons

It can be seen clearly that the use of double hooked-end fibres is significant in increasing certain properties of concrete slabs. These properties include: punching shear strength, flexural strength, ductility, post-failure strength and as well as first cracking load. So far, based on the results of current 10 slabs with double hooked-end fibres, only TR34 method seems to be able to predict the failure loads accurately. Yet, it is not known if the method will be accurate when more test data (with residual tensile strengths) become available.

Table 6. 2 – Comparisons of design methods with experimental results

ID	V_{exp}	ΔV	V_{flex} Eq.11	TR34			MC2010			V_{exp} / V_{calc}		
				V_c Eq. 2	V_{Rf} Eq. 3	V_{Rd} Eq.1 (5)+ (6)	V_c Eq.6	V_{Rf} Eq. 10	V_{Rd} Eq. 5 (8)+(9)	YLT (2)/ (3)	TR34 (2)/ (6)	MC 2010 (2)/ (9)
	kN (kips)	kN (kips)	kN (kips)	kN (kips)	kN (kips)	kN (kips)	kN (kips)	kN (kips)	kN (kips)			
1	**2**	**3**	**4**	**5**	**6**	**7**	**8**	**9**	**10**	**11**	**12**	**13**
F09-00	382	-	505.4	398	-	398	212.4	-	212.4	0.76	0.96	1.80
F09-03	461	79	623	412.4	89.6	502	212.4	300.8	513.2	0.74	0.92	0.90
F09-06	556	174	701.8	409.3	158.1	567.4	212.4	503.3	715.7	0.79	0.98	0.78
F09-09	678	296	868.2	413.9	252.1	666	212.4	799.1	1011.6	0.78	1.02	0.67
F09-12	731	349	992	428.7	327	755.7	212.4	1053.2	1265.6	0.74	0.97	0.58
F14-00	382	-	716.4	440.6	-	440.6	211.5	-	211.5	0.53	0.87	1.81
F14-03	466	84	842.9	456.6	85.9	542.4	211.5	290.7	502.3	0.55	0.86	0.93
F14-06	587	205	921.8	453.1	151.5	604.6	211.5	486.4	697.9	0.64	0.97	0.84
F14-09	806	424	1088.2	458.3	241.6	699.9	211.5	772.4	983.9	0.74	1.15	0.82
F14-12	977	595	1211.9	474.7	313.3	788	211.5	1017.9	1229.5	0.81	1.24	0.79
Minimum =										0.53	0.86	0.58
Maximum =										0.81	1.24	1.81
Average =										0.71	0.99	0.99
Coefficient of variation, COV =										0.139	0.120	0.44

Notes: V_{calc} is the calculated strength of a slab
$V_c = v_c \times (ud)$ or $v_c \times (b_o d)$ and $V_{Rf} = v_f \times (ud)$ or $v_f \times (b_o d)$

6.4 Summary

Based on the above experimental results and the accompanying discussions, the following conclusions can be drawn:

- The punching shear strength of a slab can be significantly enhanced by an inclusion of fibres. The test results showed that the punching shear strength of SFRC slab with double hooked-end fibres having volume fraction of 1.2% can be 156% higher than the strengths of plain HSC slabs, given the same reinforcement ratios. This is considerably higher than the increment introduced by normal hooked-end fibres, which can increase punching shear strength by about 45% to 65 %.
- The post-punching residual strength of a slab increases as the fibre volume fraction increases. The post-punching residual strength is about 50% of the corresponding peak load of each SFRC slab for the same fibre volume fraction.
- The addition of fibres can enhance the serviceability performance of the slabs. It can delay the occurrence of first flexural cracks because the concrete modulus of rupture is increased. Crack widths are reduced with an increase in the fibre contents at all stages of loadings
- When the fibre volume is about 0.9% (70.2 kg/m^3 fibre dosage) and higher, ductility and energy absorption of a slab are improved substantially because reinforcements outside the width of 1.5h from the column face become more active in resisting the moments. In other words, the addition of double hooked end fibres also leads to widespread yeilding of reinforcements that are located further away from the column section.
- The Concrete Society's TR34 method is accurate for current SFRC slabs. The Model Code 2010's method, using the first level of approximation, is inaccurate and unconservative for the current slabs. Since all the slabs were considered to ultimately fail in punching, the yield line theory method is not suitable for the current slabs. The analysis results showed that the yield line theory overestimates the ultimate strengths of all slabs.

7

PROPOSED SHEAR DESIGN METHOD FOR REINFORCED CONCRETE SLABS

7.1 Introduction

This chapter presents a reliable and accurate design method for predicting the punching shear strength of a reinforced concrete slab. A new attribute of the proposed method is its capability to address the influence of the effect of low reinforcement ratio. Other influencing factors, such as column rectangularity ratio, concrete strength, and size (thickness) effect are also addressed. The new experimental results presented in Chapter 5 will be combined with 355 existing published data. The data will be used to evaluate the accuracies and safety of the ACI 318-14 and Eurocode 2 methods for punching shear, as well as some other methods proposed by other researchers.

7.2 Derivation of the proposed equation

The proposed equation, shown in Eq. (7.6), is an extension of the punching shear strength formula that was previously introduced by Teng et al. (2004) shown earlier in Eq. (2.1) (in Chapter 2). New reduction factors to consider low reinforcement ratio and size effect are added.

7.2.1 Factor for low reinforcement ratio, k_{RR}

The effect of low reinforcement ratio is treated in the same way as in Peiris and Ghali's approach discussed in Section 2.5 in Chapter 2. If the reinforcement ratio is less than ρ_{fs}, then the failure mode changes from punching to flexural mode and a reduction factor for low ρ is activated. The author derived a reduction factor k_{RR} (Eq. 7.3) that accounts for the effect of low reinforcement ratio on the punching

shear strength of a reinforced concrete slab, the final form of the factor is a function of reinforcement ratio and expressed as:

$$k_{RR} = (\rho/\rho_{fs})^N$$

where ρ is the provided reinforcement ratio, and ρ_{fs} is the limiting reinforcement ratio. N is a suitable exponent calibrated from relevant test data. The complete derivation of this reduction factor k_{RR} is as follows:

By referring to the crack patterns of the slab specimens shown in Figs. 5.1 and 5.2 presented earlier in Chapter 5 of this thesis, Fig. 5.1 shows the crack pattern for slab S11-050 that failed by yielding of the flexural reinforcement and followed quickly by punching failure. The crack pattern of Specimen S11-090 is for the case of clear punching failure. Thus, the crack pattern or yield line pattern that can suitably represent the transition from the punching failure to flexural failure is in between the yield lines in the slabs S11-050 and S11-090. This is also true for the crack patterns for slabs S13 and S15 series shown in Fig. 5.2 (Chapter 5), as well as for a number of slab data from the literature (Guandalini et al. 2009, Guandalini 2005) whose yield lines are available. The idealized yield line pattern that can represent this transition phase is shown below in Fig. 7.1. The V_{flex} for the slab with that yield line pattern was presented earlier in Eq. 3.16 in Chapter 3 and shown here again as follows.

$$V_{flex} = \alpha_o m \qquad \text{(7.1a) or (3.16)}$$

where α_o is a dimensionless parameter that depends on the boundary and loading conditions of a slab and (for this case) expressed as:

$$\alpha_o = [2(c_1 + c_2)/r + 2\pi] \text{ and } m = 0.95\ \rho_{fs} f_y\ d^2 \qquad \text{(7.1b)}$$

where c_1 and c_2 are the lengths of long and short sides of column cross-section, respectively. r is the distance from the column face to the point load (for design purpose, r can be assumed to be $0.2L$, that is the distance from the column to the inflection point in a flat plate floor).

The limiting reinforcement ratio ρ_{fs} can be obtained by setting $V_{flex} = V_c$, that is, Eq. (7.1) = Eq. (2.1). Adding the reduction factors k_{CR} for column rectangularity ratio and k_{SZ} for size effect to Eq. (2.1) and setting Eq. (7.1) = Eq. (2.1), the following relationship is obtained (the reduction factors for the effect of column

rectangularity k_{CR}, and the size effect k_{SZ} will be discussed in the subsequent subsections below):

$$\alpha_o\,(0.95\,\rho_{fs} f_y\, d^2) = 0.6\, k_{CR}\, k_{SZ}\,(100\rho_{fs} f'_c)^{1/3} b_o d$$

From the above relationship, the limiting reinforcement ratio ρ_{fs} is then obtained as:

$$100\,\rho_{fs} = \left[\frac{0.6 k_{CR} k_{SZ} f_c'^{1/3} b_o d}{\alpha_o (0.95 f_y d^2)}(100)\right]^{3/2} \text{ (SI Units)}$$

$$= \left[\frac{16.6 k_{CR} k_{SZ} f_c'^{1/3} b_o d}{\alpha_o (0.95 f_y d^2)}(100)\right]^{3/2} \text{ (U.S. Units)} \qquad (7.2a)$$

The yield line pattern shown in Fig. 7.1 is to represent slabs supported on square as well as rectangular columns. The actual value of α_o [Eq. 7.1(b)] varies from about 8 for square columns to about 10 for rectangular columns.

Note, however, that the standard ρ_{fs} of Eq. (7.2a) can be simplified considerably, if desired. By assuming α_o to be equal to 8, the two reduction factors to be 1.0, f'_c = 40 MPa (5800 psi), f_y = 410 MPa (60 ksi), column size c_1 and c_2 = 350 mm (13.8 in.), d = 175 mm (7.9 in), the value of ρ_{fs} becomes 0.007 or

$$100\rho_{fs} = \left[\frac{0.6(1)(1)(40)^{1/3}(2100)(175)}{(8)(0.95)(410)(175)^2}(100)\right]^{3/2} \approx 0.7 \qquad (7.2b)$$

Therefore, if the ρ_{fs} is obtained from the standard Eq. (7.2a), the method is referred to the *Standard Method*. When ρ_{fs} is obtained from the simplified Eq. (7.2b), the method is called the *Simplified Method*.

The advantage of using the standard method comes in the form of more accurate predictions of failure modes; that is, either flexural mode, punching mode. The simplified method that uses ρ_{fs} of Eq. (7.2b) gives equally accurate predictions of failure loads as the standard method but with less accurate predictions of failure modes. This will be discussed subsequently in Section 7.3 "Comparison with experimental results".

For slabs with low reinforcement ratios or ρ less than ρ_{fs}, Fig. 7.2 was constructed. In Fig. 7.2, the x-axis is the reinforcement ratio ρ and the y-axis is

$V_{exp}/\{0.6\, k_{CR}\, k_{SZ}\, (f'_c)^{1/3}\, b_o d\}$ (SI units). Experimental slab data [References of data are given in Fig. 7.2] that failed in flexure are plotted in Fig. 7.2. The denominator is essentially V_c of Eq. (2.1) without the $\rho^{1/3}$ term. A solid line is also drawn from the origin to an arbitrary point of $\rho = 0.7\%$. Since, in Fig. 7.2, at $\rho = 0.7\%$ the y-axis is also equal to 1.0, this ρ is actually ρ_{fs} where $V_{flex} = V_c$. So, taking $\rho_{fs} = 0.7\%$ and assuming that the punching shear strength to be a linear function of ρ, for $\rho < \rho_{fs}$, produces the solid inclined line. Obviously, the assumption of the linear relationship leads to overly conservative predictions of failure loads for $\rho < \rho_{fs}$. A more suitable form for the relationship between failure load and ρ for the region of $\rho < \rho_{fs}$ would be a function of $(\rho/\rho_{fs})^{1/2}$ as shown by the curved line (Fig. 7.2).

Therefore, a reduction factor for low reinforcement ratio is needed for the region of $\rho < \rho_{fs}$. The punching shear strength of the slab would best be represented by $k_{RR}V_c$, where $k_{RR} = (\rho/\rho_{fs})^{1/2}$. Since the basic form of V_c itself (Eq. (2.1)) has already had $\rho^{1/3}$ term in it, the exponent in k_{RR} needs to be reduced by 1/3, which is the exponent of ρ in basic V_c, to become (1/2 –1/3) = 1/6, or

$$k_{RR} = (\rho/\rho_{fs})^{1/6} \tag{7.3}$$

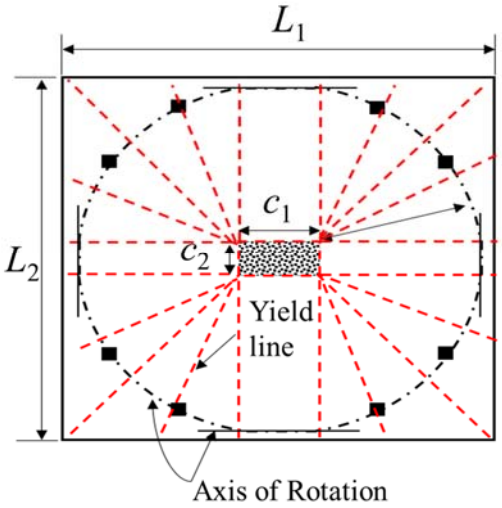

Reference: Park and Gamble[13]

External work done = Internal work done

(Neglecting the short yield lines beyond the Circular line and the negative reinforcement)

$V_{flex}\delta = 2(\delta/r)\,(c_1+c_2)m + 2\pi\delta m$

$V_{flex} = (2\,(c_1+c_2)/r + 2\pi)m$

where,

$r \approx 0.5(L_1-c_1)$

Fig.7. 1 – Idealized yield line pattern representing transition from punching failure mode to flexural failure mode.

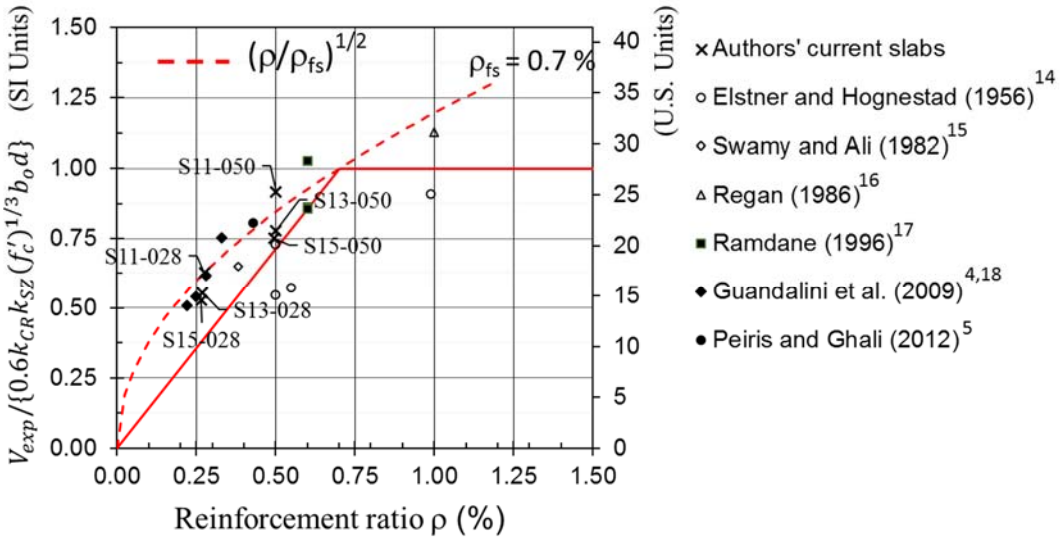

Fig.7. 2 – Relationship between V_{exp} and ρ for slabs with low reinforcement ratios.

7.2.2 Factors for size effect and column rectangularity ratio

Various approaches have been employed to study the size effect in concrete structures. Reviewed earlier in Section 2.3.4 of this thesis, a fracture mechanics-based approach pioneered by Bazant (1984) leads to a reduction factor that is proportional to $d^{-1/2}$. However, due to the variability of test results, properties of concrete members, and the influence of reinforcement, etc, an empirical approach is often used, and this can lead to a reduction factor that is proportional to $d^{-1/3}$ to $d^{-1/4}$ or others.

By observing the available experimental data and practical design considerations, the size-effect reduction factor k_{SZ} below is adopted for the proposed equation.

$$k_{SZ} = (300/d)^{1/2} \le 1.0 \quad \text{(SI units)}$$
$$= (12/d)^{1/2} \le 1.0 \quad \text{(U.S. units)} \qquad (7.4)$$

where k_{SZ} is chosen to be applicable for an effective depth $d > 300$ mm (12 in.) simply because the current basic equation for V_c is safe for d of up to 300 mm (12 in.). For $d \le 300$ mm (12 in.), $k_{SZ} = 1.0$. So, for the majority of slabs in practical structural design, the size effect factor can be disregarded.

For the column rectangularity ratio, β (= c_1/c_2), greater than 1.0, the corresponding reduction factor k_{CR} in Eq. (2.1), that was empirically derived, is retained with the exponent adjusted to 1/3 to suit more data.

$$k_{CR} = (b_2/b_1)^{1/3} \tag{7.5}$$

where b_1 and b_2 are the lengths of the long and short sides of the critical perimeter b_o respectively. Figure 7.3 shows the graph depicting the normalized shear stress at failure $V_{exp}/\{b_o d(100\rho f'_c)^{1/3}\}$ against β (the ratio of long to short sides of the column, or c_1/c_2) for the author's current slab specimens and other existing slab data from the literature [References of the comparing data are provided in Fig. 7.3]. Each of selected set of data comprises slab specimens with different column aspect ratios. The author's slab specimens were made of high strength concrete while those from the literature were made of normal strength concrete. It can be seen from the trend line for each set of data that the normalized shear stress decreases as the column aspect ratio increases. The trend lines are all similar to each other, including the one for the author's current high strength concrete slabs.

Figure 7.3 essentially shows the performance of the column rectangularity factor, k_{CR}, in comparison with experimental data. It can be seen that k_{CR} represents the trend line of the experimental data (including high strength concrete slabs) very well. The way ACI treats rectangular column is by the use of the β coefficient as shown in Eq. (3.1b). It cannot be shown together in Fig. 7.3 because ACI uses $\sqrt{f'_c}$ instead of $f'^{1/3}_c$ in its equation. Nevertheless, it has been discussed earlier in Section 5.3.3, the ACI method of treating rectangular columns as shown in Eq. (3.1b) (Chapter 3) also represents the experimental data very closely.

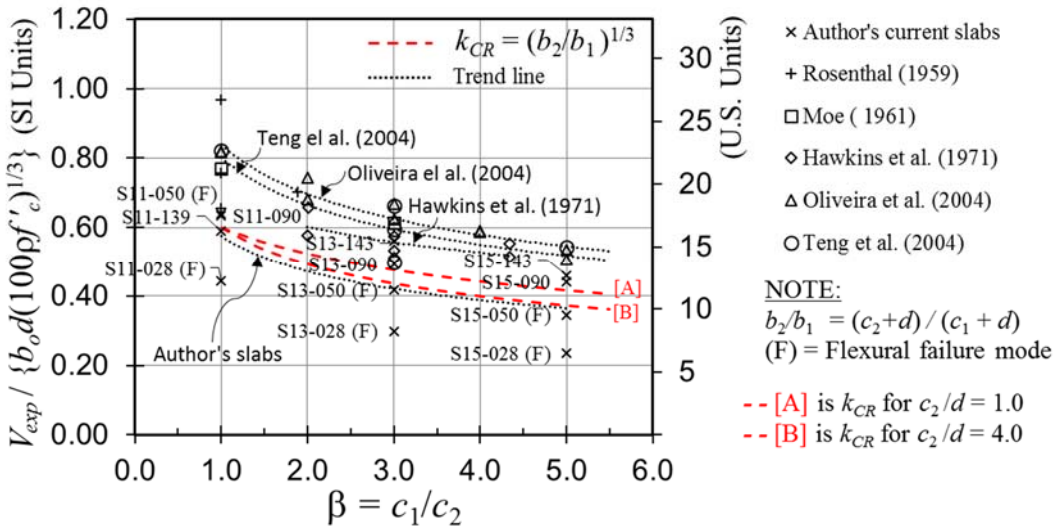

Fig.7. 3 – Performance of the proposed column rectangularity factor k_{CR}.

7.2.3 The Proposed Equation

The general form of the proposed equation can be written as:

$$V_C = 0.6 k_{RR} k_{CR} k_{SZ} (100\,\rho f_c')^{1/3} b_o d \quad \text{(SI units: MPa, mm);}$$

$$= 16.6 k_{RR} k_{CR} k_{SZ} (100\,\rho f_c')^{1/3} b_o d \quad \text{(U.S. units: psi, in.)} \qquad (7.6)$$

where k_{RR}, k_{CR}, and k_{SZ} are the reductions factors for reinforcement ratio, size effect and column rectangularity ratio, respectively [see Eqs. (7.3), (7.4), and (7.5)]. ρ is an average flexural reinforcement ratio in both directions (= A_s/bd) and should not be taken greater than 2.5%. b_o is the critical perimeter calculated at the distance $0.5d$ away from a column face (for both circular and rectangular columns). d is an average effective depth of a slab. Note that in most cases, the reduction factors need not be calculated as they will be equal to 1.0.

For commonly used slabs supported on square columns (c_1/c_2 =1) with reinforcement ratios ρ greater than 0.7%, and effective depths d of 300 mm or less; the proposed equation in Eq. (7.6) becomes simple as follows:

$$V_C = 0.6(100\,\rho f_c')^{1/3} b_o d \quad \text{(SI units: MPa, mm);}$$

$$= 16.6(100\,\rho f_c')^{1/3} b_o d \quad \text{(U.S. units: psi, in.)} \qquad (7.7)$$

Note if the ρ_{fs} (used in k_{RR}) is obtained from the standard Eq. (7.2a), the method is referred to the *Standard Method*. When ρ_{fs} is obtained from the simplified Eq. (7.2b), the method is called the *Simplified Method*.

7.3 Comparison with experimental results

7.3.1 Comparison with author's 12 new HSC slab specimens

For the purpose of these comparisons, all the load factors, materials safety factors and strength reduction factors are all set equal to 1.0. Shown in Table 7.1 are the punching shear strengths of the 12 high strength concrete slabs presented earlier in Chapter 5. Four existing (relevant) design methods are compared to the author's proposed standard method and simplified method, which are: ACI 318-14 [Eqs. (3.1), discussed in Section 3.2.1], Eurocode 2 [Eq. (3.2), discussed in Section 3.2.2], CSCT [Eqs. (2.3) and (2.4), discussed in Section 2.5.1], and the Peiris-Ghali's approach [discussed in Section 2.5.1]. Note that the performances of the ACI 318 method and Eurocode 2 method for the current 12 HSC slabs have been discussed earlier in Chapter 5 Section 5.3.1; they will be briefly discussed here again.

The predictions of the ACI Code method are unconservative (V_{exp}/V_{calc} < 1.0) for slabs with low reinforcement ratios of 0.28% or 0.5%, as expected (See Column 9 of Table 7.1). For slabs with higher ρ, such as Sxy-090 and Sxy-143 series, the ACI predictions are conservative. The corrections to ACI method that was introduced by Peiris and Ghali (2011) (Column 11 of Table 7.1) make the corrected ACI method very conservative for low reinforcement ratio cases. For the Eurocode 2 method (Column 10 of Table 7.1), the predictions are reasonably conservative, but it cannot take into account the reduction in punching shear strengths of slabs supported on rectangular columns (the S15 series slabs especially) and of slabs with very low reinforcement ratio of ρ < 0.3%, such as S11-028, S13-028, and S15-028. The CSCT method (Column 12 of Table 7.1) performs very well for these 12 slabs, with a coefficient of variation (COV) of only 8.4% and an average of V_{exp}/V_{calc} of 1.01.

The author's proposed standard method (Column 13 of Table 7.1) is the most accurate, with an average of V_{exp}/V_{calc} of 1.09 and a COV of only 8.2%. The failure modes of the slabs are predicted accurately. Column 8 shows the values of ρ/ρ_{fs} from the standard ρ_{fs} equation [Eq. 7.2a]. If the ρ/ρ_{fs} is less than 1.0, the corresponding slab would fail in flexural mode (F); otherwise, if ρ/ρ_{fs} is equal or

greater than 1.0, the failure mode is expected to be punching (P). The actual (observed) failure modes of the slabs are shown in Column 6 of Table 7.1. By comparing Column 8 and Column 6, it can be seen that the author's standard method predicts the actual failure modes very accurately; that is, all the failure modes are predicted correctly. In fact, both the standard and the simplified methods predict the failure modes of the 12 HSC slabs correctly. Note that the second best method is the author's proposed simplified method (see Column 14) that is when the limiting reinforcement ratio ρ_{fs} is simplified to be 0.007 (derived in Eq. (7.2b)). The coressponding values of an average of V_{exp}/V_{calc} and COV are 1.08 and 8.3%, respectively.

Table 7. 1 – Comparison of design methods with current test results of 12 HSC slabs

Slab ID	$c_2 \times c_1$ mm	d mm	ρ %	[1] V_{exp} kN	[2] Failure Mode	[3] ρ_{fs} %	[4] ρ/ρ_{fs} (4)/(7)	V_{exp}/V_{calc}					
								ACI 318-14	Eurocode 2	Peiris -Ghali	CSCT	Proposed Standard Method	Proposed Simplified Method
(1)	(2)	(3)	(4)	(5)	(6)	(7)	(8)	(9)	(10)	(11)	(12)	(13)	(14)
S11-028	200 × 200	120	0.28	280	F	0.96	0.29 (F)	0.65	0.96	1.92	1.12	1.19	1.13
S11-050		117	0.50	394	F	0.98	0.51 (F)	0.95	1.16	1.58	1.21	1.29	1.22
S11-090		117	0.90	440	P	0.78	1.16 (P)	1.06	1.06	1.06	0.99	1.06	1.06
S11-139		114	1.39	454	P	0.88	1.58 (P)	1.14	0.99	1.14	0.89	0.98	0.98
S13-028	200 × 600	120	0.28	308	F	0.98	0.27 (F)	0.53	0.79	2.18	0.99	1.07	1.01
S13-050		117	0.50	418	F	0.80	0.63 (F)	0.74	0.91	1.44	0.97	1.06	1.04
S13-090		117	0.90	558	P	0.80	1.13 (P)	0.99	1.00	1.08	0.96	1.08	1.08
S13-143		114	1.43	718	P	0.91	1.57 (P)	1.32	1.14	1.32	1.05	1.23	1.23
S15-028	200 × 1000	120	0.28	322	F	1.07	0.25 (F)	0.49	0.68	2.42	0.97	1.04	0.97
S15-050		117	0.50	458	F	0.85	0.58 (F)	0.70	0.79	1.59	0.95	1.04	1.00
S15-090		117	0.90	658	P	0.85	1.06 (P)	1.00	0.93	1.28	1.00	1.12	1.12
S15-143		114	1.43	776	P	0.97	1.47 (P)	1.22	0.98	1.22	0.99	1.17	1.17
Min =								0.49	0.68	1.06	0.89	0.98	0.97
Max =								1.32	1.16	2.42	1.21	1.29	1.23
Average =								0.90	0.95	1.52	1.01	1.11	1.08
COV=								0.30	0.15	0.29	0.084	0.082	0.083

NOTE: COV = Coefficient of variation

[1] V_{exp} = total failure load, including weight of specimen outside the distance of d from column face and weight of test equipment on top of the specimen.

[2] Observed Failure Mode: F = Flexural Failure; P = Punching Failure

[3] ρ_{fs} = proposed limiting reinforcement ratio, calculated using Eq. (7.2a), ρ_{fs} is taken to be 0.007 for the proposed Simplified Method as shown by Eq. (7.2b)

[4] For $\rho/\rho_{fs} > 1.0$, the predicted failure mode is punching; for $\rho/\rho_{fs} \leq 1.0$, the predicted failure mode is flexure. ρ_{fs} in Col (7) is for the proposed Standard Method and calculated using Eq. (7.2a)

7.3.2 Comparison with Slab Database of 367 specimens

Table 7.2 summarizes the punching shear strength predictions of the methods mentioned above for the 367 slabs in the database. The material properties and complete details of the 367 slab data and the detailed comparisons of the failure load of each slab with the predictions of all the methods are given in Appendix E (Table E.1).

The current database of 367 slab data was from the author's research group earlier database [Teng et al. (2004)] with the addition of slab data from the database of the ACI 445 - Subcommittee C (2011) and new slab data from the literature. All the slab data in the current database is selected to make sure that they satisfy all the relevant ACI design requirements. Slabs having unusual geometries, loading arrangements, or boundary conditions were excluded as their punching strengths would be quite different from those of normal slabs in typical construction and they deserve special treatment of their own.

The data are grouped according to three parameters (reinforcement ratio ρ, effective depth d, and compressive strength f'_c) and divided into three or four different divisions or ranges as detailed in Figs. 7.4 to 7.8 and also in Table 7.2. A good and reliable method is expected to perform well in all the different ranges or divisions.

Figures 7.4 and 7.5 show the comparison between the experimental failure load V_{exp} and ACI 318-14 and Eurocode 2 predictions (V_{calc}), respectively. The ratio of the experimental failure load to the calculated punching shear strength (V_{exp}/V_{calc}) is plotted in the y-axis, with the x-axis being three design parameters: ρ, d, and f'_c. Separate statistical analysis is done for each of the divisions A1, A, B, and C. The horizontal dashed line in each division shows the average values of the V_{exp}/V_{calc} for that division. Figures 7.6, 7.7, and 7.8 show the comparisons of the experimental results with the predictions of CSCT, Peiris-Ghali, and the author's standard methods, respectively. The statistical analysis results for each division are summarized in Table 7.2.

7.3.2.1 Influence of reinforcement ratio

The performance of the ACI equations with respect to reinforcement ratio is shown in in Fig. 7.4(a). It can be seen that as the reinforcement ratio increases, the average of V_{exp}/V_{calc} increases as well. Similarly, Table 7.2 shows for the ACI318-14 predictions, that as the reinforcement ratio increases from group A1 (Col 4 or $\rho <$ 0.6%) to C (Col 7 or $\rho > 2\%$) the average of the V_{exp}/V_{calc} increase from 0.86 to 1.61. This is caused by the neglect of the reinforcement ratio in the V_c formulas in the ACI 318-14. Note also that for the region A1($\rho <0.6\%$) in both Fig. 7.4(a) and Table 7.2, the average is 0.86 and most of the points are below the 1.0 line. This confirms the earlier conclusion from the 12 HSC slabs, that the ACI 318 method for punching shear is unconservative for slabs with low reinforcement ratio, specifically for ρ less than about 0.6% or 0.7%.

The correction procedure introduced by Peiris and Ghali (2011) to take care of possible flexural failure prior to punching failure is effective for the intended A1 region. From Table 7.2, in Peiris-Ghali rows, the average of V_{exp}/V_{calc} in division A1 increases from 0.86 (ACI average) to a healthy 1.15. However, the maximum V_{exp}/V_{calc} increases from 1.19 to 2.42. This shows that the correction can also lead to overconservatism of the method. Both the Eurocode-2 (EC2) method and the Muttoni et al's CSCT method give good predictions with the CSCT method having slightly lower coefficients of variations (average COV, that is, average of the 4 divisions = 0.16 compared to 0.18 for EC2). Figure 7.6(a**)** shows that CSCT predictions in terms of reinforcement ratio has narrower band (better) compared to Fig. 7.5(a) for EC2. Note, however, that both methods has *Minimum* V_{exp}/V_{calc} of 0.64 for EC2 and 0.57 for CSCT method. These are quite low.

The author's proposed method can be considered the best with respect to reinforcement ratio. The combined average of V_{exp}/V_{calc} of the four divisions (sum of 4 averages divided by 4) is about 1.2, with a combined average COV of about 0.15. Figure 7.8(a) shows the author's predictions using the standard method. The average of one division is close to the averages of the other three divisions, and the data are in a reasonably narrow band, indicating a low COV.

7.3.2.2 Influence of effective depth

The second chart (Figure b) of Figs. 7.4 and 7.8 and Columns 8 to 10 of Table 7.2 show the statistical analysis results as they are influenced by the effective depth *d*. It can be seen that the average of V_{exp}/V_{calc} of the ACI 318-14 becomes lower as the effective depth *d* increases. The ACI method can be unconservative for slabs having an effective depth of greater than 300 mm. Obviously, this is caused by the neglect of size effect in the ACI equations. The Peiris-Ghali's method, which is a correction to ACI method does not address size effect.

The EC2 equation, which has a size effect term, also does not perform well when *d* is greater than 300 mm. The CSCT method also does not predict well the punching shear strengths of slabs that are thicker than 300 mm.

Both the author's simplified and standard methods show very good agreements with the experimental results. The average lines from the author's standard method across the different divisions of effective depths as shown in Fig. 7.8(b) are very close to each other, indicating a very good match between the equations and actual failure behavior of the slabs. The average of the three divisions is about 1.2 and the average COV is about 0.11 for both the simplified and standard equations.

7.3.2.3 Influence of compressive strength of concrete

The third charts (Figure c) in Figs. 7.4(c) shows the performance of ACI method in terms compressive strength f'_c. It can be seen that the average of V_{exp}/V_{calc} in one division or range (represented by the horizontal dashed line) is nearly the same as that of the other divisions. This is true for the other four methods shown in Figs. 7.4-8(b). However, the ACI method has the widest spread of results with combined COV across the three divisions of 0.28. The CSCT method provides the best predictions with a combined average of V_{exp}/V_{calc} of 1.03 and with a combined COV of 0.14. The author's simplified and standard equations both have a combined average of 1.2 and a combined COV of 0.15. Both CSCT and the author's methods can be considered equally accurate. Table 7.2 (Column 13, for $f'_c > 90$ MPa) shows that the CSCT method predicts the punching shear strength of very HSC slabs ($f'_c >$ 90 MPa) very well with an average of 1.04 and a COV of 0.094. The next best

method for $f'c$ > 90 MPa (13,000 psi) is the author's Standard and Simplified methods with the COVs of 0.125 and 0.131, respectively, followed by the EC2, Peiris-Ghali, and ACI methods.

7.3.2.4 Other parameters, failure modes, and summary

It is understood that influencing parameters can be inter-related and they may also influence each other. Discussed earlier in Chapter 2, other parameters that might influence the punching shear strength include column size to slab thickness effect (c/d or b_o/d), maximum aggregate size (d_a), and also shear span to depth ratio (r/d or $0.2L/d$). However, those effects were considered to be insignificant.

From the comparative study above, it can be seen that the author's proposed Standard Method and the Simplified Method are accurate and reliable. The standard method predicts failure modes more accurately than the simplified method (see Table E.1 in the Appendix E). Of the 27 slabs that failed in Flexure, the standard method predicted correctly 20 of them (74% correct) while the simplified method predicts 21 correctly (78%). Of the 340 slabs failing in punching, the standard method predicts mode of failure correctly for 316 (93%) compared to 274 (81%) for the simplified method. Nevertheless, both methods predict the punching shear strength equally accurately and they give the closest predictions to the experimental failure loads compared to other methods. The simplified method is especially very simple to use.

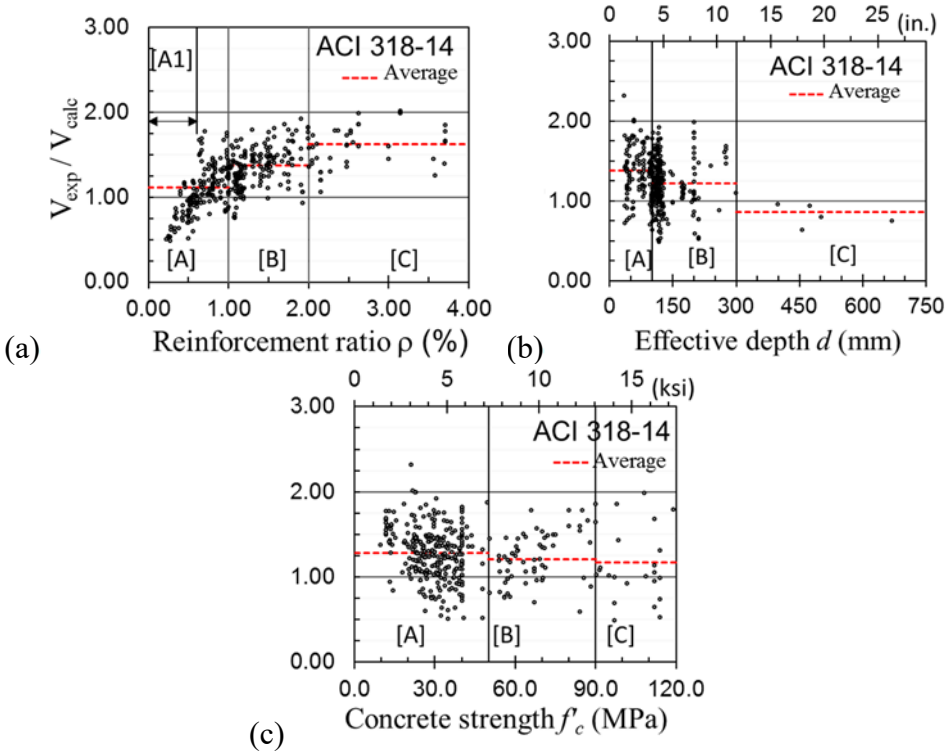

Fig.7. 4 – Failure load predictions of 367 test data by ACI 318-14 in term of (a) reinforcement ratio ρ; (b) Effective depth *d*; (c) Concrete strength f'_c

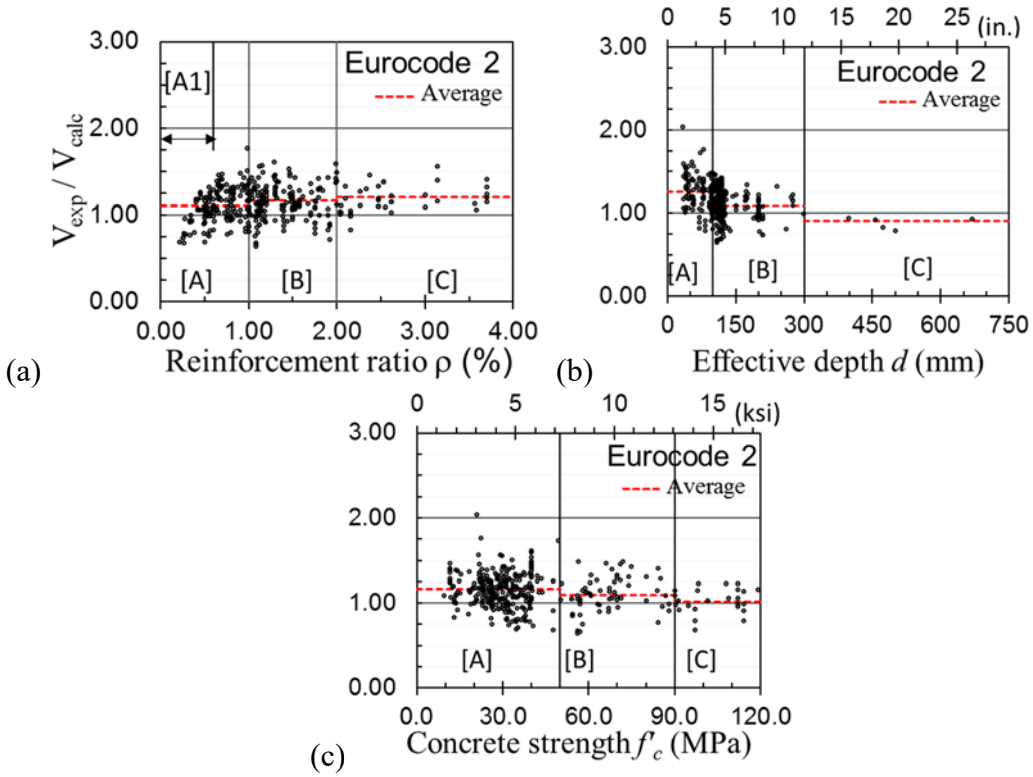

Fig.7. 5 – Failure load predictions of 367 test data by Eurocode 2 in term of (a) reinforcement ratio ρ; (b) Effective depth *d*; (c) Concrete strength f'_c

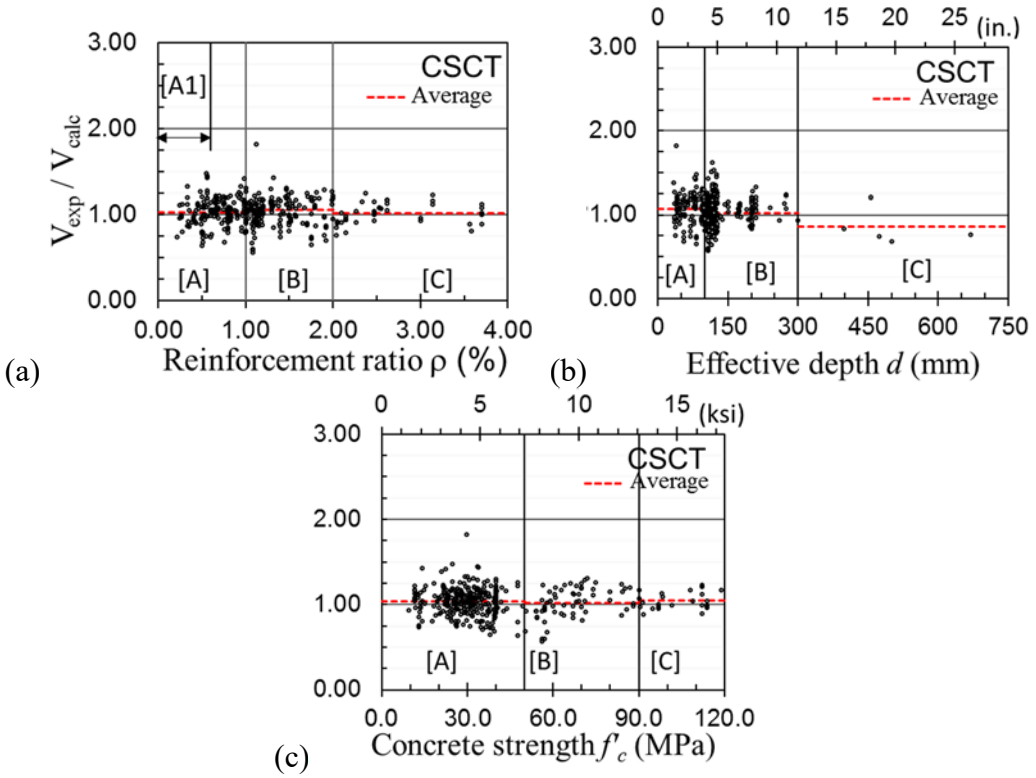

Fig.7. 6 – Failure load predictions of 367 test data by CSCT in term of (a) reinforcement ratio ρ; (b) Effective depth *d*; (c) Concrete strength f'_c

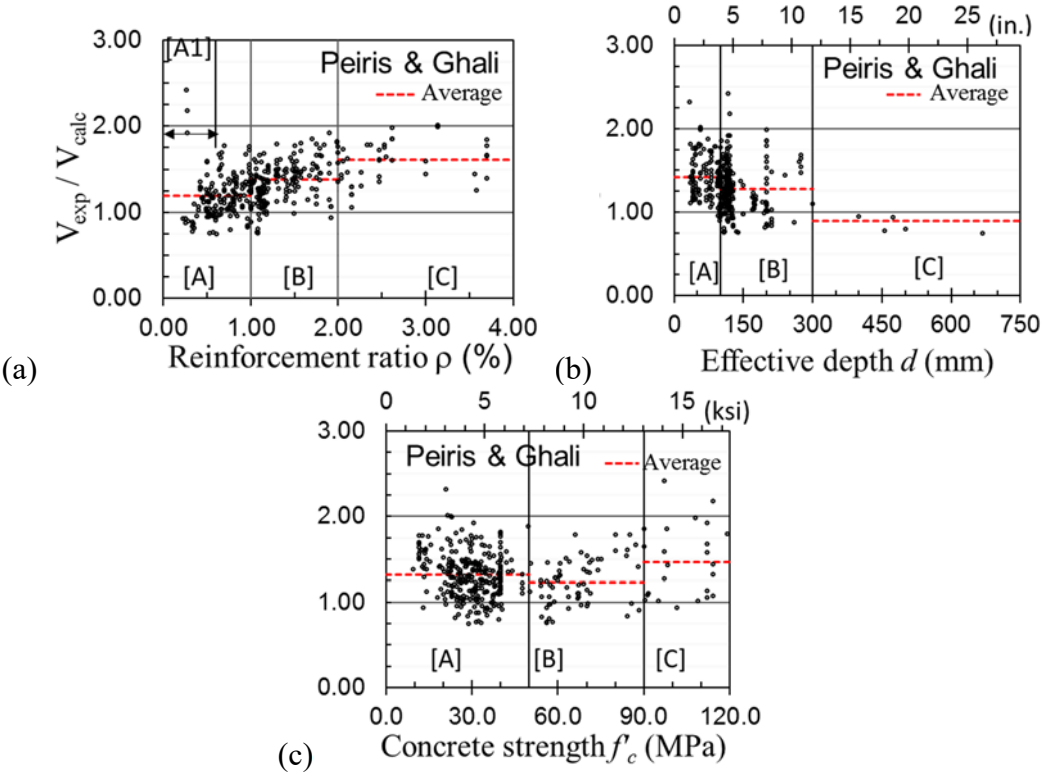

Fig.7. 7 – Failure load predictions of 367 test data by Peiris-Ghali's method in term of (a) reinforcement ratio ρ; (b) Effective depth *d*; (c) Concrete strength f'_c

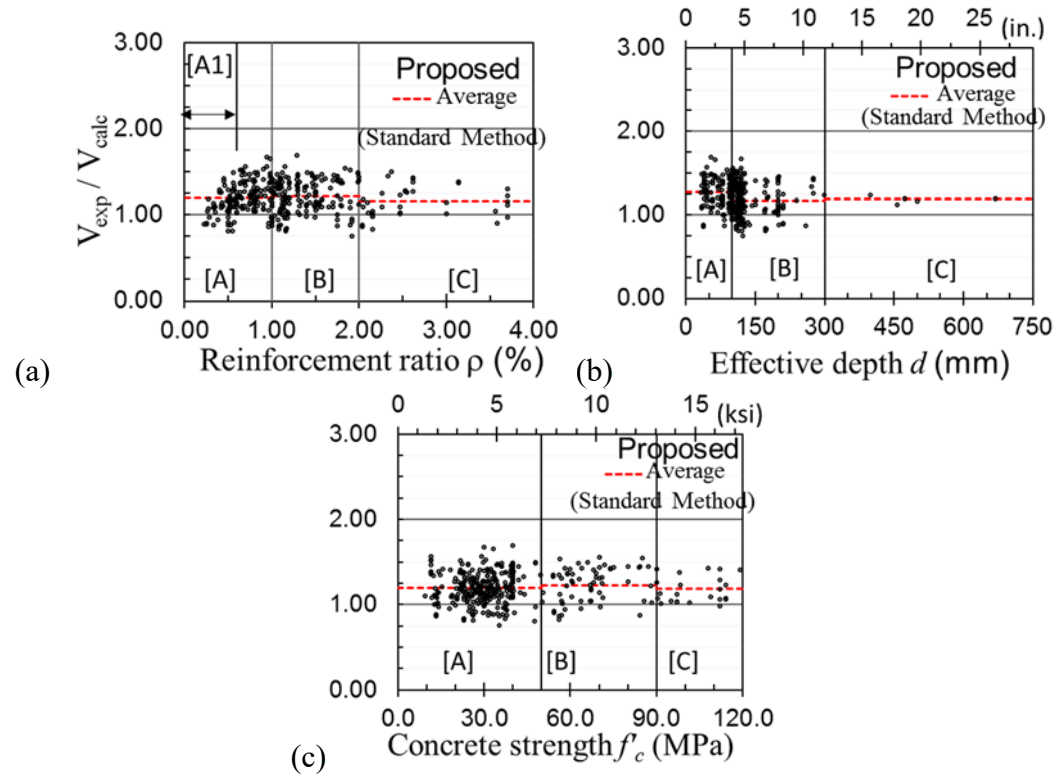

Fig.7. 8 – Failure load predictions of 367 test data by proposed Standard Method in terms of (a) reinforcement ratio ρ; (b) Effective depth d; (c) Concrete strength f'_c

Table 7. 2 – Comparison of Experimental and Calculated Failure Load by all methods

V_{exp}/V_{calc}		All data	Reinforcement ratio ρ (%)				Effective depth d (mm)			Concrete strength f'_c (MPa)		
Division (Units)			[A1] ρ < 0.6 (%)	[A] 0 < ρ ≤ 1.0 (%)	[B] 1.0 < ρ ≤ 2.0 (%)	[C] ρ > 2.0 (%)	[A] $d \leq 100$ (mm)	[B] 100 < d < 300 (mm)	[C] $d \geq 300$ (mm)	[A] $f'_c \leq 50$ (MPa)	[B] 50 < $f'_c \leq 90$ (MPa)	[C] $f'_c > 90$ (MPa)
Nos. of data:		367	57	160	175	41	114	247	6	279	63	25
(1)	(2)	(3)	(4)	(5)	(6)	(7)	(8)	(9)	(10)	(11)	(12)	(13)
V_{exp}/V_{calc} ACI 318-14	Min =	0.49	0.49	0.49	0.76	1.06	0.70	0.49	0.73	0.51	0.59	0.49
	Max=	2.32	1.19	1.78	1.92	2.32	2.32	1.98	2.32	2.32	1.79	1.98
	Average=	1.26	0.86	1.08	1.37	1.61	1.38	1.22	1.41	1.28	1.22	1.17
	COV=	0.249	0.233	0.258	0.171	0.167	0.223	0.247	0.231	0.240	0.236	0.366
V_{exp}/V_{calc} Eurocode 2	Min =	0.64	0.68	0.68	0.64	0.83	0.79	0.64	0.82	0.69	0.64	0.68
	Max=	2.04	1.32	1.77	2.01	2.04	2.04	1.48	2.04	2.04	1.48	1.23
	Average=	1.14	1.02	1.11	1.17	1.21	1.26	1.09	1.30	1.16	1.10	1.02
	COV=	0.174	0.169	0.175	0.183	0.179	0.158	0.156	0.155	0.171	0.181	0.138
V_{exp}/V_{calc} CSCT	Min =	0.57	0.64	0.64	0.57	0.76	0.65	0.57	0.68	0.64	0.57	0.89
	Max=	1.82	1.37	1.37	2.19	1.38	1.82	1.48	1.82	1.82	1.31	1.23
	Average=	1.04	1.02	1.03	1.06	1.02	1.07	1.02	1.09	1.04	1.02	1.04
	COV=	0.152	0.17	0.145	0.198	0.129	0.156	0.145	0.160	0.151	0.174	0.094
V_{exp}/V_{calc} Peiris-Ghali	Min =	0.75	0.76	0.75	0.76	1.06	0.90	0.76	1.06	0.75	0.76	0.94
	Max=	2.42	2.42	2.42	2.31	2.32	2.32	2.42	2.32	2.32	1.79	2.42
	Average=	1.31	1.15	1.19	1.37	1.61	1.42	1.28	1.46	1.32	1.23	1.47
	COV=	0.214	0.27	0.217	0.177	0.167	0.185	0.215	0.180	0.201	0.217	0.282
V_{exp}/V_{calc} Proposed Simplified Method	Min =	0.73	0.73	0.73	0.76	0.83	0.86	0.73	0.86	0.73	0.83	0.97
	Max=	1.69	1.55	1.67	1.69	1.50	1.69	1.67	1.69	1.69	1.56	1.43
	Average=	1.21	1.18	1.22	1.22	1.16	1.28	1.18	1.29	1.21	1.24	1.16
	COV=	0.151	0.151	0.151	0.151	0.153	0.127	0.158	0.124	0.150	0.160	0.131
V_{exp}/V_{calc} Proposed Standard Method	Min =	0.76	0.81	0.81	0.76	0.83	0.86	0.76	0.86	0.76	0.83	0.98
	Max=	1.69	1.49	1.67	1.69	1.50	1.69	1.67	1.69	1.69	1.56	1.43
	Average=	1.20	1.13	1.20	1.22	1.16	1.27	1.17	1.28	1.20	1.23	1.17
	COV=	0.152	0.143	0.151	0.153	0.153	0.129	0.158	0.126	0.151	0.164	0.125

NOTE: Regions A1, A, B, C correspond to the regions in Figs. 7.5 to 7.9.
COV = Coefficient of variation.
1 mm = 0.0394 in., 1 MPa = 145.0 psi.

7.4 Summary

New standard and simplified methods for calculating the punching shear strength of a reinforced concrete slab were derived and proposed. Influencing factors, such as column rectangularity ratio, concrete strength, and size (thickness) effect were addressed and considered in the proposed methods.

The author's new experimental results presented in Chapter 5 were combined with 355 existing published data to evaluate the accuracies and safety of the ACI 318-14 and Eurocode 2 methods for punching shear, as well as some relevant methods proposed by other researchers such as the critical shear crack theory (CSCT) method by Muttoni (2008) and the Peiris-Ghali method (2001). The comparisons of these methods with 367 slab data showed that:

- The ACI 318 method is unconservative for slabs with low reinforcement ratios (especially for $\rho < 0.7\%$). The correction procedure proposed by Peiris and Ghali fixes the problem but it may lead to over conservatism. The EC2 method can be unconservative for slabs with very low reinforcement ratio and supported on rectangular columns.
- The ACI 318, EC2, and CSCT methods may not be safe for slabs with an effective depth of more than 300 mm (12 in.) even though EC2 and CSCT do consider size effect. ACI needs to consider the inclusion of size effect into the equation.
- The author's proposed standard and simplified methods both have been shown to be most accurate and reliable with uniform averages of V_{exp}/V_{calc} and COV across different ranges of design parameters. The simplified method is especially simple to use.

8

PROPOSED SHEAR DESIGN METHOD FOR STEEL FIBRE REINFORCED CONCRETE SLABS

8.1 Introduction

From the review of various design methods for fibre reinforced concrete (FRC) slabs in Chapter 2 Section 2.5.2 and in Chapter 3, it is clear that most of the available models and methods for predicting the shear strength of FRC slabs are dependent on tensile strength of FRC composites. In general, there are two different approaches for calculating the shear strength of FRC slabs, such as:

(1) The approach that calculates the shear strength by using the residual tensile strengths obtained from the notched beam test as recommended in EN 14651 (2007).

(2) The approach that approximates the shear strength to be a function of semi-empirical and empirical fibre parameters, such as fibre geometry, fibre content, and various reduction factors. Some methods that use this approach were reviewed in Section 2.5.2.2.

The *first approach* has been adopted by some standard guidelines such as RILEM (2003), Model Code 2010 (fib Committee 65-66, 2012), and Technical Report 34 (The Concrete Society, 2015) as reviewed earlier in Section 2.5.2.1 and Section 3.3. In practice, the residual flexural tensile strengths (from bending test EN 14651) have already been the common standard properties for accrediting the design adequacy of FRC structures – particularly for the ultimate flexural design. In comparison, the *second approach* is relatively more empirical than the first one. As reviewed in Section 2.5.2.2, most existing design methods use statistical means to estimate the tensile strength of FRC; these methods include several semi-empirical or empirical factors to consider the highly heterogeneity of FRC materials.

Both approaches have their advantages and disadvantages. The advantages of the *first approach* are that the (bending) behaviours and stress conditions of actual FRC structures can be more realistically analysed without relying too much on statistics. However, the bending test itself can also contain several uncertainties that may lead to errors. For instance, the consistency and uniformity of fibres in the concrete may be different in the slabs and flexural tests. Unlike other properties of concrete, results of the bending tests can vary quite significantly from specimens to specimens. In consequence, the TR 34 method by the Concrete Society (2015) recommends at least 12 notched beam samples (EN 14651, 2007) from the same batch of FRC for a test set. Also, the process of the bending test and the preparation of the test samples can be much cumbersome and expensive than conventional concrete tests.

One of the advantages of the *second approach* over the first one is that, it does not contain variables that need to be obtained experimentally. Hence, it is straightforward and ideal for design purpose. It is also easier to be validated with existing test data from the literature because the results of bending test are not available in most of the references. Validations by various researchers with test data have shown that the design method using this approach can be quite accurate and reliable to some extent (Narayanan and Darwish, 1987; Theodorakopoulos and Swamy, 1999; Shaaban and Gesund, 1994; Harajli et al., 1995; Choi et al., 2007, Higashiyama et al., 2011; Maya et al., 2012; Nguyen-mind et al., 2012; Gouveia et al.,2014). However, some of the disadvantages include the predicted tensile strength are statistically dependent, so the tensile strength cannot realistically represent the stress in actual structure. It is also possible that a method using this approach can be highly unreliable if the fibres used in actual structures are not consistent and uniform throughout the slabs.

Hence, in this chapter, the author will derive and propose a new method for the punching shear design of SFRC slabs considering the advantages and disadvantages mentioned above. There are two shear design methods proposed in this work.

- First proposal (Section 8.2), the standard fibre reinforced concrete (FRC) method that was analytically derived using the first approach
- Second proposal (Section 8.3), the general method that was based on the standard FRC method but using the principles of the second approach.

The second proposal, the general method, will be combined with the proposed equation Eq. (7.7) presented earlier in Chapter 7 to become a general equation for the ultimate punching shear strength of reinforced concrete slabs with steel fibres (Section 8.4). Therefore, the new contribution of this proposed general method, is its treatment of the ultimate punching shear strength which considers the effects of low reinforcement ratio, large column rectangularity ratio, and size (thickness) that have been addressed in Chapter 7.

These new proposed methods, together with other existing methods for calculating punching shear strength of SFRC slabs, will be evaluated and compared with 148 slab data (Table E.2) collected from the literature. The comparison will show that the author's proposed methods are accurate and reliable for slabs with a broad range of parameters, especially with the new set of the current SFRC slab data tested by the author.

8.2 Proposed Standard FRC method

The ultimate punching shear V_u is expressed as

$$V_u = V_c + V_{Rf} \tag{8.1}$$

where V_c is the punching shear strength calculated by the proposed equation [Eq. (7.7)] presented in Chapter 7. The additional shear resistance due to the contribution of the fibre V_{Rf} is given in Eq. (8.14), which is subsequently derived based on the force diagram shown in Fig. 8.1 and the main assumptions and limitations as follows.

8.2.1 Main assumptions and limitations

- Inclination of the shear cracks is taken to be an angle α with respect to the horizontal *r*-axis. The tips of the inclined shear cracks end at the point O' or the depth of the compression zone as shown in the illustrating diagram in Fig.

8.1(a) [Similar to the approaches by Kinnunen and Nylander (1960), Hallgren (1996)].

- The crack width is linearly increasing from O' to the top of the slab (Fig. 8(b). The equivalent stresses are derived based on residual strength obtained from the notched beam tests (EN 14651,2007). The details are discussed subsequently.
- Tensile stresses develop across the inclined failure surface from Point O' to the top (tension) face of the slab. The equivalent tensile stress is taken to be a linear function of the distance along the crack (ξ) as shown in Fig. 8.2 [Similar to the Model Code 2010 approach as discussed in Section 3.3.3]. Note that the actual stress distribution is complex and nonlinear.
- Dowel action and aggregate interlock mechanism are not considered as individual shear resisting constituents, i.e. they are assumed to be incorporated into V_c.
- V_{Rf} is the vertical force component of tensile stress acting orthogonally across an inclined crack surface as shown in Fig. 8.1(a).

8.2.2 Derivation

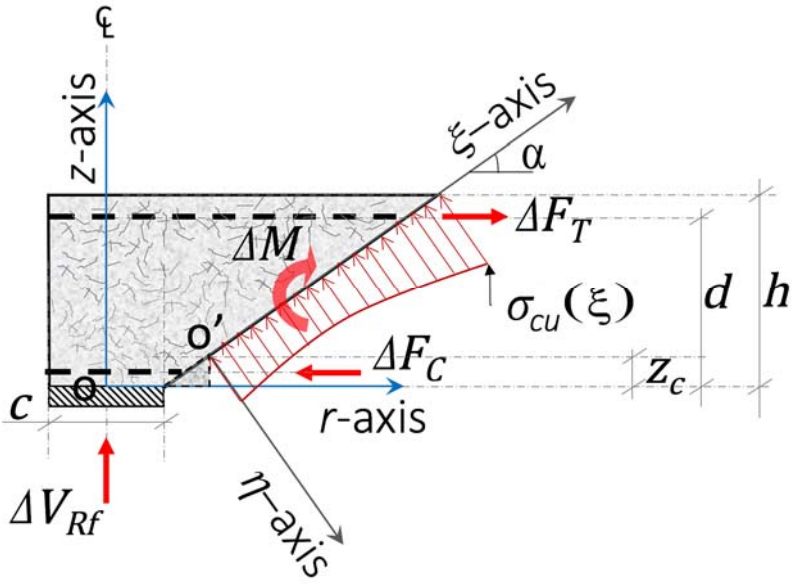

(a)

[Fig. 8.1 (Caption provided in the next page)]

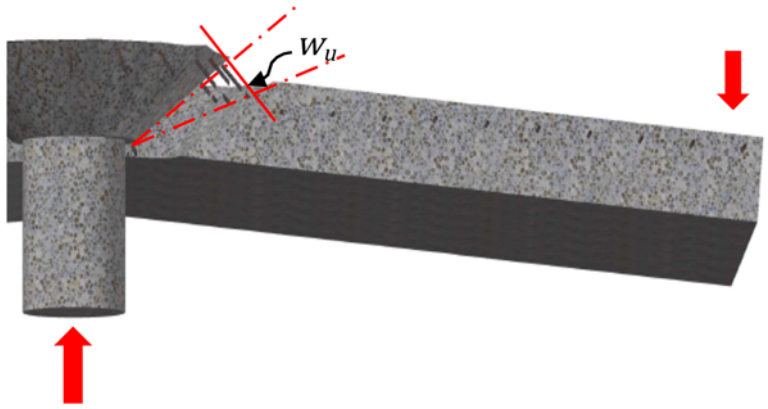

(b)

Fig.8. 1 – (a) Force diagram in the punching shear model of a fibre reinforced concrete slab; (b) Schematic model showing the crack-width opening increases linearly.

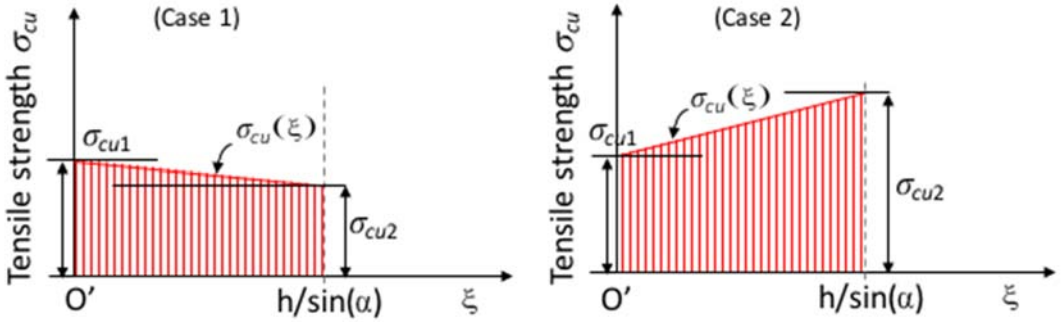

(a) (b)

Fig.8. 2 – Stress (linear) distribution along the plane of inclined shear cracks for (a) Case 1: Post-crack strain-softening behaviour; (b) Case 2: Post-crack strain-hardening behaviour.

Consider the force diagram of a slab section shown in Fig. 8.1 and assumptions listed above. Total shear contribution by the FRC V_{Rf} is the projected resultant force due to tensile stress σ_{cu}; where σ_{cu} is a function of ξ and it can be transposed to become a function of z. Thus, total resultant force can be calculated by integrating the tensile stress over failure surface from the height $z = h - z_c$ to h. The integral equation of V_{Rf} can be expressed as

$$V_{Rf} = \left(\int_{z=h-z_c}^{z=h} 2\pi(r_o + z\cos\alpha)\sigma_{cu}(z)\ dz \right) \cos\alpha \qquad (8.2)$$

where the term $(r_o + z \cos \alpha)$ represents a radius of a cone as z varies; r_o is the horizontal distance from the centroid of column to the Point O', or

$$r_o = 0.5c + z_c / \tan\alpha$$

where c is the length of the column; z_c is the depth of the compression zone. It is rather complicated to determine the depth of compression zone analytically because it is a function of many parameters, which needs an iterative analysis and satisfies overall equilibrium. In the past, several researchers have attempted to propose analytical methods to determine the depth of the compression zone [Kinnunen et al. (1960)'s group, Theodorakopoulos and Swamy (1999), Muttoni (2008)]. For cases where both concrete and reinforcement are in elastic state, the general form of this depth z_c, according to Hallgren (1997), can be expressed as:

$$z_c = \frac{\rho E_s}{k_E E_c}\left(\sqrt{1 + \frac{2k_E E_c}{\rho E_s}} - 1\right) d \tag{8.3}$$

where ρ is the tension reinforcement ratio, E_s is the Young's modulus of steel reinforcement, E_c is the elastic modulus of concrete; k_E (> 1.0) is the stiffness factor that accounts for bi-axial compression in the compression zone. Kinnunen et al.'s group (Hallgren, 1997) proposed this factor k_E to be a function of Poisson's ratio. So, if the Poisson's ratio of concrete is taken to be about 0.2, the k_E can be approximated as k_E = 1.15. Note also that in the derivation of CSCT (critical shear crack theory) by Muttoni (2008), the same equation of compression zone's depth [Eq. (8.3)] was also used, where the term ($1/k_E$) was defined by Muttoni (2008) as an efficiency factor that accounts for orthogonal layout of reinforcement and a reduction in the ratio between the torsion and bending stiffness of the slab after cracking. Muttoni (2008) suggested the ratio $1/k_E$ to be 0.6 or k_E = 1.67.

Nevertheless, in this proposal, the author assumes that the depth of compression zone to be a fraction of effective depth d, i.e. a simplified form of the Eq. (8.3):

$$z_c = \beta_c d \tag{8.4}$$

where, β_c is less than one and can vary from about 0.15 to 0.40. β_c approaches 0.40 when the concrete strength f'_c is very high (E_c is high) and the section is heavily reinforced. However, β_c is close to zero when concrete strength f'_c is small and reinforcement ratio is very low. For simplicity, the author proposes the ratio β_c to be

$\beta_c = 1/5$ for $f'_c < 60$ MPa (8.5a)

$\beta_c = 1/3$ for $f'_c \geq 60$ MPa (8.5b)

Figure 8.2(a) shows the Case 1 when an FRC member experiences post-crack softening as crack opening increases. It is the common case for an FRC member containing relatively low fibre volume fractions - particularly for the hooked end types of fibres. On the other hand, Fig. 8.2(b) is for the post-crack hardening case (Case 2). Case 2 occurs when the fibre volume fraction is high; it was shown by the results of the author's test programme presented in Fig. 4.8(a) (Chapter 4) that the notched beam containing the double hooked fibres with $V_f > 0.3\%$ already experienced post-crack hardening. Note that for other types of fibres, post-crack hardening could start at a higher value of fibre volume V_f, i.e. 0.5% for the conventional single hooked-end fibres as shown in Fig. 4.8(b).

By adopting similar principles used in RILEM (2003), TR34 (The Concrete Society, 2015) and Model Code 2010 (fib 65-66, 2012) as discussed earlier on in Chapter 2 and Chapter 3, the author assumes the equivalent ultimate tensile stress σ_{cu} to be distributed linearly along the plane of shear cracks as a linear function of ξ as shown in Figs. 8.2. The equation of σ_{cu} can be formulated as

$$\sigma_{cu}(\xi) = \sigma_{cu1} + \frac{\sigma_{cu2} - \sigma_{cu1}}{\xi_2 - \xi_1}(\xi) \tag{8.6}$$

where σ_{cu1} and σ_{cu2} are the tensile stresses at the tip and the opening of the inclined shear cracks, respectively. With good agreement with existing test data, the author proposed the values of σ_{cu1} and σ_{cu2} to be directly proportional to equivalent tensile stresses σ_{f1} and σ_{f2} as follows.

$$\sigma_{cu1} = n_s \sigma_{f1} \tag{8.7}$$

$$\sigma_{cu2} = n_s \sigma_{f2} \tag{8.8}$$

where n_s (= 0.41) is a strength reduction factor to account for several complexities and uncertainties pertaining FRC slabs under punching shear loads. Some of them can possibly be due to (1) the difference in fibre orientation and dispersion in actual structure and notched beam samples; (2) shear failure mechanism of FRC is different from flexural failure in bending test; (3) punching shear failure involves complex stress conditions (three-dimensional stresses) due to high shear – high

moment interaction. Therefore, the reduction factor is chosen to be 0.41, which is the same value as the orientation factor (n'_o) derived using the probabilistic function by Swamy et al. (1976)'s and Lim et al.'s (1987) groups as presented in Section 2.5.2.2.

According to RILEM's procedure (2003) (Section 2.5.2.1) which has been adopted by TR 34 method, the equivalent tensile stresses σ_{f1} and σ_{f2} are the adjusted values of residual strengths f_{r1} (at CMOD = 0.5 mm) and f_{r4} (at CMOD = 3.5 mm) obtained from the standard notched beam tests EN 14651 (2007). The purpose of the adjustment is to get more realistic tensile stresses for the FRC section. According to EN 14651:2007, since residual strength f_r at each stage of loading F_R is simply calculated using an uncracked section with a depth of h_{sp} as illustrated in Fig. 8.3, the corresponding linear-elastic stress diagrams can be represented by the left diagrams in Fig. 8.4. Knowing that these residual stresses are for the standard properties only, and cannot be the true values for the actual case. Therefore, to address this issue, the RILEM's procedure (2003) is adopted, that is, the neutral axis of the beam section is adjusted for different loading stages as follows.

The depth of tension zone is taken to be $0.66h_{sp}$ when the CMOD is 0.5 mm (shown in the right chart of Fig. 8.4(a)) and $0.9h_{sp}$ when the CMOD is 3.5 mm (shown in the right chart of Fig. 8.4(b)). The adjusted equivalent stress σ_{f1} and σ_{f2} are assumed to be uniform over the new depth of the tension zone.

The stress σ_{f1} and σ_{f2} are obtained directly by equating the moments M_1 to M_2, where M_1 and M_2 are the moments corresponding to the linear-elastic stress diagram (the left chart) and the adjusted diagram (the right chart) shown in Figs. 8.4(a) and 8.4(b), respectively. M_1 and M_2 can be determined by taking moments about the centroids of their respective compressive stresses. Therefore,

At CMOD = 0.5 mm [see Fig. 8.4(a)]

$$M_1 = \left(\frac{bh_{sp}^2}{6}\right) f_{r1}; \qquad M_2 = 0.37\, bh_{sp}^2 \sigma_{f1}; \qquad \text{Take } M_1 = M_2, \text{ thus}$$

$$\sigma_{f1} = 0.45 f_{r1} \tag{8.9}$$

At CMOD = 3.5 mm [see Fig. 8.4(b)]

M_1

$= \left(\frac{bh_{sp}^2}{6}\right) f_{r4}$; $\quad M_2 = 0.45\, bh_{sp}^2 \sigma_{f2}$; $\quad$ Take $M_1 = M_2$, thus

$$\sigma_{f2} = 0.37 f_{r4} \tag{8.10}$$

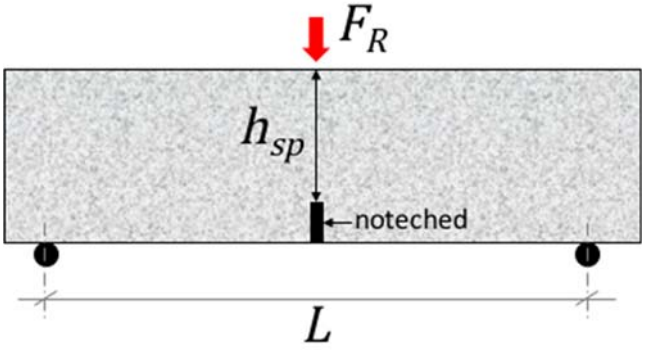

Stress at each load stage, $f_{r,1} = \frac{3F_R L}{2bh_{sp}^2}$

Fig.8. 3 – Schematic model of the notched beam (EN 14651,2007)

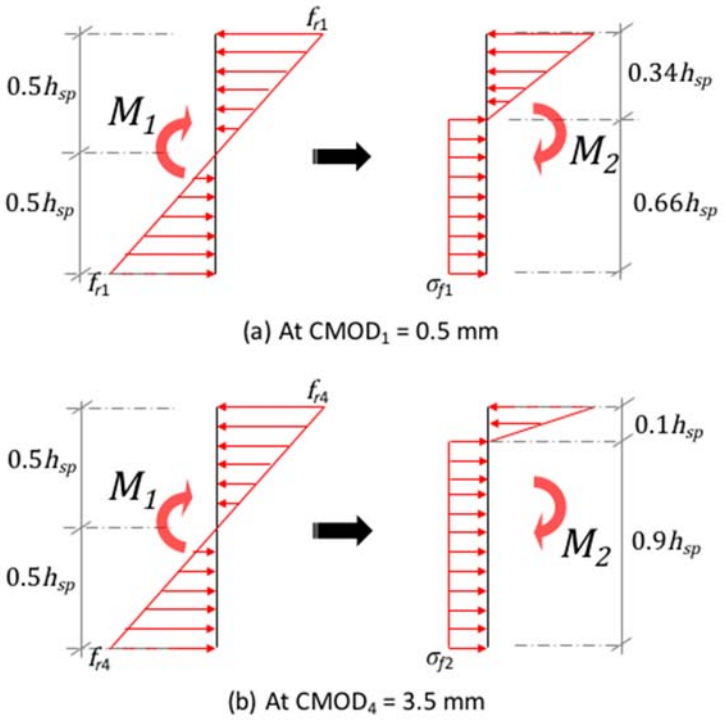

Note CMOD is crack mouth opening displacement

Fig.8. 4 – Idealised stress distribution at the middle section of the notched beam for (a) CMOD = 0.5 mm; (b) CMOD = 3.5 mm. [Modified from Fig. 2.7 (RILEM (2003))]

The equation of ultimate tensile stress σ_{cu} shown in Eq. (8.6) can be simply rearranged to be a function of variable z by transposing the ξ axis to the z-axis (see Fig. 8.1(a)). Note that the vector relationship between $\sigma(\xi)$ and $\sigma(z)$ can be expressed as

$$\vec{\sigma}(z) = \vec{\sigma}(\xi)\sin\alpha$$

Multiply sin α to Eq. (8.6), leads to

$$\sigma_{cu}(z) = \left(\sigma_{cu1} + \frac{\sigma_{cu2} - \sigma_{cu1}}{z_2 - z_1} z\right)\sin\alpha \tag{8.11}$$

where $z_2 = h$, $z_1 = z_c$ from Fig. 8.2(a).

Now the integral in the V_{Rf} equation (Eq. (8.2)) can be performed since the variable ξ was eliminated, and there is only one variable z in the equation. Since σ_{cu} is a linear function, without violating any mathematical rules, the solution of V_{Rf} in Eq. (8.2) can be simply replaced by a product of two components σ_{fV} (stress) and A_{fH} (area) as shown below.

$$V_{Rf} = \sigma_{fV} A_{fH}$$

where σ_{fV} is the average value of the vertical component of tensile stresses σ_{cu1} and σ_{cu2}, that is

$$\sigma_{fV} = 0.5(\sigma_{cu1} + \sigma_{cu2})/\cos\alpha$$

From Eqs. (8.7) to (8.10), σ_{cu1} and σ_{cu2} can be replaced. Thus, σ_{fV} becomes

$$\sigma_{fV} = 0.5 n_s (0.45 f_{r1} + 0.37 f_{r4})/\cos\alpha \tag{8.12}$$

A_{fH} is the projection of the failure cone surface to the (Horizon) r-axis, that is

$$\begin{aligned} A_{fH} &= \frac{\pi(h - z_c)}{\tan\alpha}\frac{(h - z_c)\cos\alpha}{\tan\alpha} \\ &= \pi(h - z_c)^2 \cot^2\alpha \cos\alpha \end{aligned} \tag{8.13}$$

where z_c ($=\beta_c d$) is the depth of compression zone. Note that the term cos α in Eq. (8.12) and Eq. (8.13) will cancel each other when combining together to obtain V_{Rf}.

8.2.3 Summary

Hence, the ultimate punching shear V_u is expressed as

$$V_u = V_c + V_{Rf} \qquad \text{[Eq. (8.1)]}$$

where V_c is the punching shear strength calculated by the proposed equation [Eq. (7.7)] presented in Chapter 7. The final form of V_{Rf} is,

$$V_{Rf} = v_f A_f \qquad (8.14)$$

where v_f and A_f are given in Eq. (8.15) and (8.16). They are actually the components σ_{fV} (stress) and A_{fH} (area) in Eqs. (8.12) and (8.13) but without the term cos α, respectively.

$$v_f = 0.5 n_s (0.45 f_{r1} + 0.37 f_{r4}) \qquad (8.15)$$

$$A_f = \pi (h - \beta_c d)^2 \cot^2 \alpha \qquad (8.16)$$

where the notations in the equations are summarised as follows

n_s = reduction factor, take as 0.41.

β_c = ratio of the depth of compression zone to effective depth or z_c/d, taken as 0.20 (for f'_c <60 MPa) and 0.34 (for $f'_c \geq 60$ MPa) [Eqs. (8.5)]

α = average shear crack angle, taken as 30°. This angle was also observed in the author's experimental programme presented in Chapter 6.

f_{r1}, f_{r4} = residual tensile strengths at CMODs of 0.5 mm and 3.5 mm, respectively. They are obtained from the standard notched beam test EN 14651 (2007).

h, d = slab thickness and effective depth, respectively.

8.3 Proposed General method

The general method uses the approach that approximates the shear strength increment due to the presence of fibres to be a function of semi-empirical and fibre parameters. According to the derivation of the above method shown in Eq. (8.14), shear strength v_f can be related to the residual tensile strength σ_{cu} ($v_f \propto \sigma_{cu}$) which is supported by the literature discussed in Section 2.5.2.2. Steel fibres function in a similar way to aggregate, as they prevent the propagation of cracks in a mortar matrix. This is because the fibres have greater modulus of elasticity than the matrix's. Thus they deform less and resist crack propagation by exerting a pinching force at the crack tip. The resistance of crack propagation becomes ineffective when failure occurs, that is, when the ultimate tensile strength of the composite σ_{cu} is attained. So, by Hooke's law, the following relationship is obtained

$$v_f \propto \sigma_{cu} \approx (\text{fibre stress}) \times V_f$$

Therefore, the tensile stress σ_{cu} is influenced by the fibre volume fraction V_f and the fibre stress which is known to be a function of basic fibre parameters such as fibre aspect ratio (L_f/D_f), and other fibre characteristics such as the fibre-matrix bond strength, and the randomness of fibre orientation. Therefore, based on the equations of σ_{cu} in Eq. (2.17) and Eq. (2.20) in Chapter 2, and by treating the shear strength v_f the same way as the tensile strength of a FRC composite, the general form of the proposed shear strength v_f can be expressed as

$$v_f = n_{fo} n_{fl} n_{fb} \tau_{fb} V_f \left(\frac{L_f}{D_f}\right) \tag{8.17}$$

where V_f is the fibre volume fraction, calculated as ratio of the fibre dosage per unit volume to the fibre density. L_f/D_f is the fibre aspect ratio or the ratio of the fibre length to the fibre cross-sectional diameter. Other variables such as fibre orientation factor n_{fo}, effective fibre length n_{fl}, fibre bond factor n_{fb}, and basic fibre-matrix interface bond strength τ_{fb} are defined and derived subsequently.

8.3.1 Fibre orientation factor

The fibre orientation factor n_{fo} is taken to be 0.41, this value of n_{fo} = 0.41 was also used by other researchers [Swamy et al.'s group - Theodorakopoulos and Swamy, 1999; Lim et al., 1987, Narayanan and Darwish, 1987]. The value can be mathematically derived based on the mean of the probability function by Eq. (2.22) in Section 2.5.2.2. The value n_{fo} = 0.41 is applicable for most practical cases in design. That is when the fibre length L_f is smaller than the thickness and width of the FRC member.

8.3.2 Effective fibre length factor

The effective fibre length factor n_{fl} is taken to be 0.5, the value of n_{fl} = 0.5 is obtained from the basic length efficiency factor n_l given by Law (1972),Swamy et al. (1974) and also Lim et al. (1987). From Eq. (2.18), the basic equation of n_l can be expressed in term of

$$n_l = \begin{cases} L_f/2L_c & \text{For } L_f \leq L_c \\ 1 - L_f/2L_c & \text{For } L_f > L_c \end{cases} \qquad \text{(8.18) or (2.18)}$$

where L_c is the critical length. In other words, it is the development length that will cause the fibre to yield. In most cases, the failure mechanism is not governed by the yielding of fibre. So, it can be assumed that the fibre length L_f is always lower than the critical length L_c, where L_c is a function of ultimate bond strength of the fibre and the fibre diameter. Since the bond strength and fibre diameter are already presented as independent variables in the proposed general form of v_f in Eq. (8.17), the ratio of L_f/L_c in n_l [Eq. (8.18)] can then be eliminated, thus n_l becomes 0.5 for $L_f \leq L_c$.; this is also a value proposed by Lim et al. (1987) [see Eq. (2.21)]. Therefore, to account for length efficiency, the author proposed the term called the effective fibre length factor, where n_{fl} = 0.5.

8.3.3 Fibre-matrix bond strength

The ultimate tensile strength of FRC is proportional to the bond strength τ_u, which can be obtained by fibre pull-out tests under uniaxial tension. It is known that different types and geometries of fibres have different influences on the pull-out

strength. Shown earlier by Fig. 2.9(a) [Lim et al. (1987)], the fibre-matrix bond strengths are typically greater or equal to 5.5 N/mm^2 for the hooked fibres, and lower than 4 N/mm^2 for round or straight fibres. Recent investigations also confirmed that the pullout strength is in a range of 5-7 N/mm^2 depending on fibre properties [Yassir Abbas and Khan, 2016; Garcia-Taengua et al., 2011]. Therefore, this ultimate bond strength can be written in term of

$$\tau_u = n_{fb}\tau_{fb} \tag{8.19}$$

where τ_{fb} (=5.5 N/mm^2) is the basic bond strength of single hooked end fibres. The author selected τ_{fb} to be 5.5 N/mm^2 to set the hooked end as a reference fibre, in which the bond factor n_{fb} for hooked fibre will be equal to 1. Note that Swamy et al. (1974) and Narayanan and Darwish (1987) proposed this basic bond strength (originally defined as the average bond strength) to be 4.15 N/mm^2, which was empirically obtained from available test data at that time.

Thus, the proposed bond factor n_{fb} is the correction factor to account for different types of fibres, i.e. n_{fb} is 1.0 for the single hooked end fibre. The proposed n_{fb} factor is empirical and is based on the general knowledge about the pull-out strength for different type of fibres, e.g. the bond strength is the highest for the hooked type of fibres and the lowest for the other fibre types. The following proposed values of n_{fb} were calibrated to best fit the existing SFRC slabs data, to ensure accuracy and conservatism. Essentially, there are four values of n_{fb} as follows:

n_{fb} = 0.25 for undeformed, round and straight fibres;
= 0.50 for crimped, paddled, corrugated and fibres;
= 1.00 for single hooked fibres;
= 2.25 for doubled hooked fibres.

8.3.4 Ultimate punching shear strength formula

The proposed formula [Eq. (8.30)] for the ultimate punching shear strength (v_u, V_u) of an SFRC slab (limited to steel fibre reinforce concrete SFRC) is an extension to the proposed equation presented in Chapter 7 for the case of non-fibrous reinforced concrete slabs [in Eq. (7.7)]. The general form of the ultimate punching shear equation is expressed as:

$$v_u = \frac{V_u}{b_o d} = \text{R.F} \times \left(v_{c,basic} + v_f\right) \quad (8.20)$$

where the basic shear strength $v_{c,basic}$ is taken as $v_{c,basic} = 0.6(100\rho f'_c)^{1/3}$; the shear strength increment due to the presence of fibres v_f was proposed and given earlier in Eq. (8.17). The term R.F in Eq. (8.20) represents all the reduction factors that account for the influences of various structural parameters as discussed previously in Chapter 7, i.e. the effects of low reinforcement ratio (k_{RR}), column rectangularity (k_{CR}), and size (k_{SZ}).

There has been no specific set of FRC slab data to investigate the influences of size effect and column rectangularity. In the current database (Appendix E Table E.2), the maximum slab thickness that has been tested is 155 mm (d = 138 mm). All 138 existing slabs have square columns ($c_1/c_2 = 1$). Without any validation with the test data, the reduction factors for rectangular columns k_{CR} and size effect k_{SZ} are to remain as proposed in Chapter 7. They are repeated here:

$k_{SZ} = (300/d)^{1/3}$ [or Eq.(7.4)] (8.21)

$k_{CR} = (b_2/b_1)^{1/3}$ [or Eq.(7.5)] (8.22)

The effect of low reinforcement ratio has not been addressed in any research on punching shear in FRC slabs; the author has discussed this issue previously for the case of reinforced concrete slabs. Based on the data collected in the database, there is a reasonable amount of FRC slab data with low reinforcement ratios. Thus, to investigate the effect for FRC slabs, a similar data analysis as presented previously by Fig. 7.2 (Section 7.2.1) is adopted here. Figure 8.5 shows a plot of slab data having low reinforcement ratio ($\rho \leq 0.8\%$) where the y-axis is the normalised failure load with the proposed terms but without the influence of the reinforcement $\{V_{exp}/[(0.6(f'_c)^{1/3} + v_f)\, b_o d]\}$ and the x-axis is the reinforcement ratio ρ (Note the terms k_{CR} and k_{SZ} are equal to 1.0 for the data plotted in the chart). From Fig. 8.5, the relationship between the strength of a slab and reinforcement ratio is similar to the one observed in Fig. 7.2. The relationship in Fig. 8.5 shows that a reduction factor for low reinforcement ratio is needed for the region of $\rho < \rho_{fs}$. Therefore, the ultimate punching shear strength of a SFRC slab can also be represented by

$$v_u \propto (\rho/\rho_{fs})^{1/2} \times [0.6(f'_c)^{1/3} + v_f] \quad (\text{for } \rho < \rho_{fs})$$

Since the basic shear strength ($v_{c,basic} = 0.6(100\rho f'_c)^{1/3}$) has already had the $\rho^{1/3}$ term in it, the exponent 1/2 in $(\rho/\rho_{fs})^{1/2}$ needs to be reduced by 1/3. So, the reduction factor $k_{RR,c}$ to be applied to the shear strength component V_c is,

$$k_{RR,c} = (\rho/\rho_{fs})^{1/6} \quad \text{(or Eq. 7.3)} \quad (8.23)$$

There is no reinforcement ratio ρ in the shear strength equation due to the presence of fibres v_f. Hence, its corresponding reduction factor $k_{RR,f}$ remains as:

$$k_{RR,f} = (\rho/\rho_{fs})^{1/2} \quad (8.24)$$

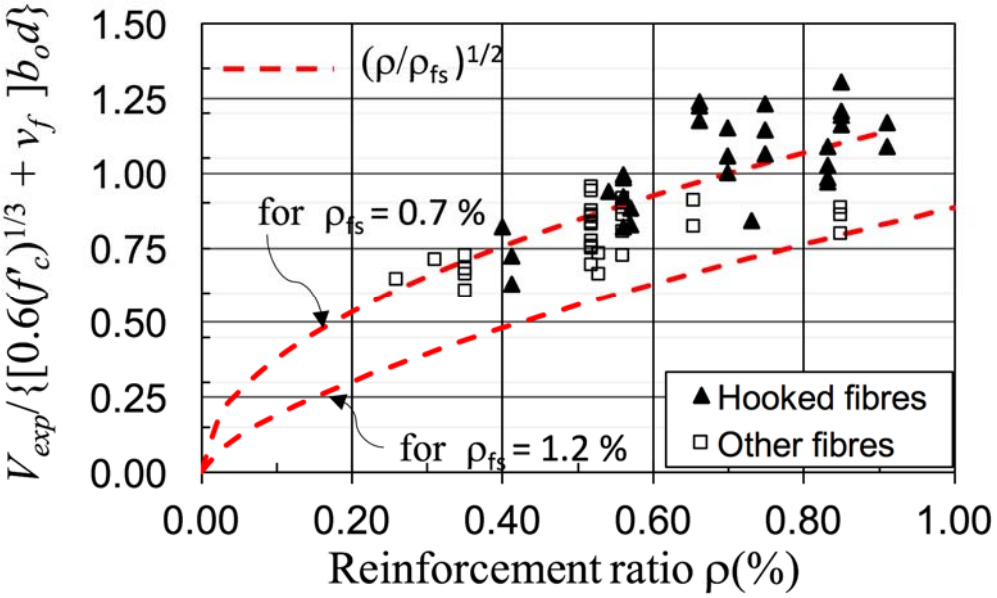

Note: Hooked fibres represent the type of single hooked end fibres. Other fibres represent various types of fibres such as round, straight, crimped, corrugated,or paddle fibres. Indication of fibre type for each data is also provided in the database presented in Appendix. Data source - Hooked fibres: [Ozden et al., 2006; Cheng and Parra-Montesinos, 2010; Higashiyama et al., 2011; Nguyen-Minh et al., 2012] Other fibres: [Swamy and Ali 1982; Alexander and Simmonds 1992; Theodorakopoulos and Swamy 1993]

Fig.8. 5 – Relationship between V_{exp} and ρ for SFRC slabs with low reinforcement ratios

Derivation of limiting reinforcement ratio ρ_{fs} *for a SFRC slab*

For the case of SFRC slabs, the limiting reinforcement ratio ρ_{fs} can be obtained by the derivations from Eqs. (7.1) to (7.2) presented in Section 7.2.1. The ratio ρ_{fs} is essentially obtained by setting $V_{flex} = V_u$ (Eq. (8.25)). Note that the contributions from the fibres needs to be considered in the equations of V_{flex} and V_u,. The load V_{flex} is obtained using the yield line analysis with a circular fan yield line pattern ($V_{flex} = \alpha_o m_u$ in Eq. (3.16)). V_u is taken as $V_u = k_{CR} k_{SZ} [0.6(100\rho f'_c)^{1/3} + v_f] b_o d$. Thus,

$$\alpha_o (m_u) = k_{CR} k_{SZ} [0.6(100\rho f'_c)^{1/3} + v_f] b_o d \quad (8.25a)$$

where m_u can be approximated by Eq. (3.19) or ACI 544.4R method which was first developed by Henager and Doherty (1976). An actual solution of ρ_{fs} needs an iterative procedure by solving for ρ in in Eq. (8.25a). However, the author proposes a simplified solution to calculate a standard form of ρ_{fs} as follows.

The ultimate moment capacity of per unit width of a FRC slab can be expressed as $m_u = m_c + m_f$, where m_c ($\approx 0.95\rho f_y d^2$) and m_f are the moments contributed by reinforced concrete and fibre components, respectively. From Eq. (8.25a), the term ρ from the left-hand side expression and the term $(100\rho)^{1/3}$ from the right-and side expression are brought together leading to Eq. (8.25b) as follows:

$$\rho\{\alpha_o [0.95 f_y d^2 + (m_f/\rho)]\} = (100\rho)^{1/3}\{k_{CR} k_{SZ} [0.6(f'_c)^{1/3} + (v_f/(100\rho)^{1/3})] b_o d \quad (8.25b)$$

Assume that the terms m_f/ρ and $v_f/(100\rho)^{1/3}$ on the left-hand side and the right-hand side of the expression Eq. (8.25b) are constants, where ρ is the flexural reinforcement ratio of a slab, rearrange to solve for the remaining variable ρ in both sides. Hence, the standard equation for calculating ρ_{fs} can be expressed as.

$$\rho_{fs} = \left(\frac{k_{CR} k_{sz} \left(0.6 f_c'^{\frac{1}{3}} + \frac{v_f}{(100\rho)^{\frac{1}{3}}} \right) b_o d}{\alpha_o \left(0.95 f_y d^2 + \frac{m_f}{\rho} \right)} 100 \right)^{3/2}$$

The ultimate moment m_u ($\approx 0.95\rho f_y d^2 + m_f$) can be substituted back to the denominator, leading to

$$\rho_{fs} = \left(\frac{k_{CR} k_{sz} \left(0.6 f_c'^{\frac{1}{3}} + \frac{v_f}{(100\rho)^{\frac{1}{3}}} \right) b_o d}{\alpha_o (m_u/\rho)} 100 \right)^{3/2} \tag{8.26}$$

The ACI 544.4R method [or the method proposed by Henager and Doherty (1976), in Eq. (3.19)] is adopted for calculating the ultimate moment capacity m_u of an FRC slab. The term m_u can be simplified as follows.

$$m_u = m_c + m_f \tag{8.27a}$$

where

$$m_c = \rho f_y d^2 \left(1 - 0.59 \frac{\rho f_y}{f_c'} \right) \approx 0.95 \rho f_y d^2 \tag{8.27b}$$

$$m_f = \frac{1}{2} \sigma_t (h - e)(h + e - 0.59 \frac{\rho f_y}{f_c'}) \tag{8.27c}$$

The term σ_t is the tensile stress on the tension side of the neutral axis (Eq. 8.28), while e is the distance calculated from the extreme compression fibre to the top of tensile stress block (assumed to be the compression side of the neutral axis, Eq. (8.29)); the equations of σ_t and e are given as follows:

$$\sigma_t = 0.008 F_{be} V_f (\frac{L_f}{D_f}) \tag{8.28}$$

$$e = \left(\sqrt{(n\rho)^2 + n\rho} - n\rho \right) d \tag{8.29}$$

where F_{be} is 1.2 for hooked-end fibres, and 1.0 for other fibres. V_f is the fibre volume fraction, L_f/D_f is the fibre aspect ratio, and n ($=E_s/E_c$) is the ratio of the steel of concrete moduli of elasticity.

For simplicity, the simplified ρ_{fs} (= 0.007) derived previously in Eq. (7.2b) can also be used for the FRC slab cases. Fig. 8.5 shows that most data with low reinforcement ratio can be represented by $(\rho/0.007)^{1/2}$.

Therefore, if the ρ_{fs} is obtained from the standard Eq. (8.26), the method is termed as the *Standard General Method*. If the simplified ρ_{fs} (=0.007) in Eq. (7.2b) is used, the method is termed as the *Simplified General Method*.

8.3.5 Summary

From the derivations, the proposed general method for calculating the ultimate punching shear strength of a SFRC slab is summarised as follows.

$$V_u = k_{SZ}k_{CR}\left(k_{RR,c}0.6(100\rho f_c')^{1/3} + k_{RR,f}v_f\right)b_o d \qquad (8.30)$$

where

$k_{SZ} = (300/d)^{1/3} \leq 1.0$ [Eq.(7.4) or (8.21)]

$k_{CR} = (b_2/b_1)^{1/3} \leq 1.0$ [Eq.(7.5) or (8.22)]

$k_{RR,c} = (\rho/\rho_{fs})^{1/6} \leq 1.0$ [Eq. 7.3] or (8.23)]

$k_{RR,f} = (\rho/\rho_{fs})^{1/2} \leq 1.0$ [Eq.(8.24)]

where k_{RR}, k_{CR}, and k_{SZ} are the reductions factors for reinforcement ratio, column rectangularity ratio, and size effect. The term ρ is an average flexural reinforcement ratio in both directions (= A_s/bd) and should not be taken greater than 2.5%. The term b_o is the critical perimeter calculated at a distance $0.5d$ away from a column face (for both circular and rectangular columns). b_1 and b_2 are the lengths of the long and short sides of the critical perimeter b_o respectively. d is an average effective depth of a slab. v_f is the shear strength increment due to the presence of fibres, or

$$v_f = n_{fo}n_{fl}n_{fb}\tau_{fb}V_f\left(\frac{L_f}{D_f}\right) \qquad \text{[Eq.(8.17)]}$$

and,

n_{fo} = 0.41, fibre orientation factor

n_{fl} = 0.50, fibre effective length factor

n_{fb} = 0.25 to 2.25 (see Table 8.1 below), bond factor

τ_{fb} = 5.5 N/mm^2, basic bond strength of fibre-matrix interface

V_f and (L_f/D_f) are the fibre volume fraction and the fibre aspect ratio, respectively. Table 8.1 summarises the proposed values of n_{fb} with sketches of each type of fibres.

Note that the proposed *Standard General Method* uses Eq. (8.26) to obtain the limiting reinforcement ratio ρ_{fs} for calculating the factors $k_{RR,c} = (\rho/\rho_{fs})^{1/6}$ and $k_{RR,f} = (\rho/\rho_{fs})^{1/2}$, whereas *Simplified General Method* assumes $\rho_{fs} = 0.007$.

Subsequent analysis and validations with test data will show that both of the *Standard* and *Simplified* methods are equally accurate and reliable for calculating punching shear strength. But the Standard General Method is more accurate for predicting the failure mode of a slab.

Table 8. 1 – values of bond factor for different types of steel fibres

Fibre type	Bond factor n_{fb}	Fibre types
Undeformed, straight, round	0.25	
Crimped	0.50	
Paddled	0.50	
Single Hooked	1.00	
Double Hooked	2.25	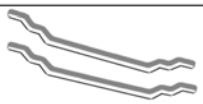

8.4 Comparison with experimental results

For the purpose of subsequent comparisons, all the load factors, materials safety factors and strength reduction factors are set to 1.0. The results of the current 10 FRC slabs that were presented in Chapter 6, and 138 relevant data obtained from Database will be used to verify the author's proposed methods. Other design methods will also be evaluated and compared, such as the TR 34 method (reviewed in Section 3.3.2), Model Code 2010 (reviewed in Section 3.3.3), and the other design methods (in Section 2.5) proposed by Narayanan and Darwish (1987), Shaaban and Gesund (1990), Higashiyama et al. (2011) and the CSCT+VEM method by Mutton el al.'s group (Muttoni and Ruiz 2010, Maya et al., 2012).

8.4.1 Comparison of design methods with author's 10 new SFRC slabs

Table 8.2 shows the comparisons of various design methods with the test results of the author's 10 SFRC slabs. Column 9 of Table 8.2 shows that the author's proposed Standard FRC method [Eq. (8.1)] gives the most accurate and consistent predictions of the 10 slabs among all the methods. The corresponding value of an average V_{exp}/V_{calc} is 1.01 with a coefficient of variation (COV) of 0.089 (lowest among all). The TR 34 method and Model Code 2010 method use similar approach to calculate the shear strength increment due to the presence of fibres. Note that the performances of TR34 and Model Code 2010 methods have been evaluated earlier with the 10 slabs in Section 6.3.2. In brief, the predictions of TR 34 method is accurate (Average V_{exp}/V_{calc} = 0.99 and COV = 0.120) but can be unconservative for HSC slabs. Model Code 2010 method is not accurate, the corresponding value of average V_{exp}/V_{calc} is 0.99 with a COV of 0.444. A more complex form of the Model Code 2010 method is expected to be better, which is essentially the CSCT method.

The predictions of the proposed general method [Eq. (3.30)] have an average V_{exp}/V_{calc} of 1.08 and a COV of 0.122 for both of the standard and simplified general methods (See Columns 10 and 11 of Table 8.2). The COV of the general method is very close to that of TR 34, which is the second best method. In comparison, the proposed general method is more conservative. The predictions of the other methods that use the similar approach as the proposed general method are shown in Columns 5 to 8 of Table 8.2. The method proposed by Narayanan and Darwish (1987) is unconservative for this set of slabs. The modifications made to the ACI equation by Shaaban and Gesund (1990) are conservative but not accurate. The predictions tend to be overly conservative as fibre content increases. The modifications made to the Japanese Code equation by Hagashiyama et al. (2011) are relatively accurate with a COV of 0.159 (Fifth best) but tend to be over-conservative for the slabs with high fibre volume fractions ($V_f \geq 0.9\%$). The CSCT+VEM method that incorporates VEM (Voo and Foster 2003) with CSCT (Muttoni 2008) performs well for this set of slabs, with a COV of 0.140 (fourth best) and an average of V_{exp}/V_{calc} of 1.12.

Table 8. 2 – Comparison of design methods with the SFRC slab specimens

Slab ID	V_{exp} (kN)	V_{exp}/V_{calc}								
		TR 34 Method	Model Code 2010 Method	Narayanan & Darwish Method	Shaaban & Gesund Method	Higashiyama et al. Method	CSCT+VEM Method	Proposed Standard FRC Method	Proposed (Standard) General Method	Proposed (Simplified) General Method
		Eq. (3.5)	Eq. (3.8)	Eq. (2.23)	Eq. (2.27)	Eq. (2.35)	Eqs. (2.3) + (2.33)	Eq. (8.1)	Eqs. (8.30) + (8.26)	Eqs. (8.30) + (7.2b)
(1)	(2)	(3)	(4)	(5)	(6)	(7)	(8)	(9)	(10)	(11)
F09-00	382	0.96	1.80	0.70	0.85	1.18	1.05	1.03	1.03	1.03
F09-03	461	0.92	0.90	0.67	0.97	1.19	1.05	0.96	1.01	1.01
F09-06	556	0.98	0.78	0.79	1.18	1.26	1.11	1.03	1.05	1.05
F09-09	678	1.02	0.67	0.95	1.42	1.40	1.18	1.01	1.13	1.12
F09-12	731	0.97	0.58	1.03	1.45	1.42	1.10	0.95	1.11	1.06
F14-00	382	0.87	1.81	0.68	0.88	1.06	0.91	0.92	0.92	0.92
F14-03	466	0.86	0.93	0.67	1.02	1.08	0.95	0.89	0.93	0.93
F14-06	587	0.97	0.84	0.83	1.29	1.19	1.08	1.00	1.03	1.03
F14-09	806	1.15	0.82	1.13	1.75	1.50	1.33	1.12	1.25	1.25
F14-12	977	1.24	0.79	1.38	2.01	1.71	1.41	1.19	1.34	1.34
Minimum=		0.86	0.58	0.67	0.85	1.06	0.91	0.89	0.92	0.92
Maximum=		1.24	1.81	1.38	2.01	1.71	1.41	1.19	1.34	1.34
Average=		0.99	0.99	0.88	1.28	1.30	1.12	1.01	1.08	1.08
COV =		0.120	0.444	0.270	0.299	0.159	0.140	0.089	0.122	0.122

NOTE: COV = Coefficient of variation

Material properties and geometry details of the 10 slabs are given in Table 4.2

Col(2) V_{exp} = total failure load, including weight of specimen outside the distance of d from column face and weight of test equipment on top of the specimen.

8.4.2 Validation of the proposed standard FRC method with other data

Most of the existing slab data (138 data) do not contain available information on residual tensile strength (obtained using the standard test EN 14651, 2007). Thus, it is not possible for the proposed standard FRC method [Eq. (8.1)] (or other methods that use residual tensile strength, i.e. TR34 and Model Code 2010) to be validated with all the available data. However, there are five SFRC slab data tested by Gouveia et al. (2014) that had residual tensile strengths. This test data from Gouveia et al. (2014) is combined with the author's 10 data to validate the proposed standard FRC method, as well as the TR34 and Model Code 2010 methods.

The residual tensile strengths (from EN 14651 test) for the 13 SFRC slabs are given in Table 8.3. Note that Gouveia et al. (2014) used single hooked-end steel fibre. The predictions of the three methods including the proposed method are given in Columns 8 to 10 of Table 8.3.

Table 8.3 confirms that the proposed standard FRC method [Eq. (8.1)] also performs very well with the additional data from Gouviea et al. (2014). The results show that the proposed FRC method is the most accurate, with a mean value of V_{exp}/V_{calc} of 1.06 and a COV of 0.103 (lowest among all). The TR34 method is more conservative for slabs with single hooked end fibres, and its predictions for all 16 slabs are also consistent (average V_{exp}/V_{calc} = 1.07, COV = 0.138). As expected, Model Code 2010 method does not perform well for the Gouviea et al. (2014)'s data either (average V_{exp}/V_{calc} = 1.03, COV = 0.372). If only the six Gouviea et al.' slabs were considered in the comparisons as shown in Table 8.3, then statistics show that the COVs are 0.0801 for the proposed standard FRC method (average V_{exp}/V_{calc} =1.14), 0.090 for the TR34 method (average V_{exp}/V_{calc} = 1.19), and 0.272 for the Model Code 2010 method (average V_{exp}/V_{calc} = 1.09).

Table 8. 3 – Comparison of design methods with results of 16 slabs that have their residual flexural tensile strength available

Specimen information							V_{exp}/V_{calc}		
Slab ID	V_{exp} (kN)	V_f (%)	f_{r1} (MPa)	f_{r2} (MPa)	f_{r3} (MPa)	f_{r4} (MPa)	**TR 34 Method**	**Model Code 2010 Method**	**Proposed Standard FRC Method**
							Eq. (3.5)	**Eq. (3.8)**	**Eq. (8.1)**
(1)	**(2)**	**(3)**	**(4)**	**(5)**	**(6)**	**(7)**	**(8)**	**(9)**	**(10)**
Gouveia et al. (2014)									
ND0 (-)	289.2	-	-	-	-	-	1.14	1.68	1.18
ND1 (0.5%)	296.0	0.50	4.64	4.16	3.2	2.7	1.00	0.96	0.97
ND2 (0.75%)	369.3	0.75	5.60	5.60	5.1	4.5	1.19	0.98	1.14
ND3 (0.75%)	450.7	0.75	8.00	6.24	5.12	4.64	1.28	1.05	1.19
ND4 (1.00%)	456.0	1.00	7.36	7.20	5.60	4.48	1.29	1.04	1.23
ND5 (1.25%)	474.7	1.25	10.08	9.60	8.80	7.04	1.23	0.84	1.15
						Minimum=	1.00	0.84	0.97
						Maximum=	1.29	1.68	1.23
						Average=	1.19	1.09	1.14
						COV =	0.090	0.272	0.080
Author's current slabs									
F09-00	382	-	-	-	-	-	0.96	1.80	1.03
F09-03	461	0.3	4.2	6.0	6.5	5.8	0.92	0.90	0.96
F09-06	556	0.6	8.9	12.8	10.5	7.5	0.98	0.78	1.03
F09-09	678	0.9	16.0	17.5	16.3	13.5	1.02	0.67	1.01
F09-12	731	1.2	17.5	21.2	22.2	21.2	0.97	0.58	0.95
F14-00	382	-	-	-	-	-	0.87	1.81	0.92
F14-03	466	0.3	4.2	6.0	6.5	5.8	0.86	0.93	0.89
F14-06	587	0.6	8.9	12.8	10.5	7.5	0.97	0.84	1.00
F14-09	806	0.9	16.0	17.5	16.3	13.5	1.15	0.82	1.12
F14-12	977	1.2	17.5	21.2	22.2	21.2	1.24	0.79	1.19
						Minimum=	0.86	0.58	0.89
						Maximum=	1.24	1.81	1.19
						Average=	0.99	0.99	1.01
						COV =	0.120	0.444	0.089
Combined results									
						Minimum=	0.86	0.58	0.89
						Maximum=	1.29	1.81	1.23
						Average=	1.07	1.03	1.06
						COV =	0.138	0.374	0.103

Note: Dimension and properties of the ND-series slabs [Gouveia et al. (2014)] are 1650 × 1650 × 125 mm (c = 200 mm, d = 103 mm, ρ = 1.0%, f'_c = 32 MPa to 44.5 MPa). The type of fibre is single hooked fibre. Complete details are provided in Appendix E (Table E.1)

8.4.3 Comparison of design methods with existing data from Database

This section compares the performance of design methods with 138 slab data combing with the author's 10 current SFRC slabs. The material properties and complete details of the 148 slab data and the detailed comparisons of the failure load of each slab with the predictions of all the methods are given in Appendix E (Table E.2).

The data are grouped according to two parameters (fibre volume fraction V_f, and reinforcement ratio ρ) and divided into two or three different divisions as detailed in Figs. 8.6 to 8.10 and also in Table 8.4. In each chart, four different markers are used which represent (1) data without fibres, (2) data with single-hooked fibre, (3) data with other types of fibres, and (4) data from the current experiment. A good and reliable method is expected to perform well in all the different ranges or divisions for all types of fibres.

Note that in Figs. 8.6 to 8.10, and Table 8.4, the word Other fibres represent various types of fibres such as round, straight, crimped, corrugated, paddle fibres. Indication of fibre type for each data is also provided in Database Table E.2 in Appendix E.

Figures 8.6, 8.7, 8.8, 8.9 and 8.10 show the comparisons of experimental results with the predictions of Narayanan and Darwish method, Shaaban and Gesund method, Higashiyama et al. method, CSCT+VEM method, and the proposed (standard) general method, respectively. The ratio of experimental failure load to calculated punching shear strength (V_{exp}/V_{calc}) is plotted in the y-axis, while the x-axis has two parameters: V_f (Chart (a) of each Fig.) and ρ (Chart (b) of each Fig.) Separate statistical analysis is conducted for each of the divisions A, B, or C. Horizontal (red) dashed line and solid line in each division shows the average values of V_{exp}/V_{calc} of the data using hooked end fibre and other fibres, respectively, for that division. The statistical analysis results for each division are summarised in Table 8.4.

8.4.3.1 Influence of fibre volume fractions

Columns 4 to 9 of Table 8.4 show the statistical analysis results for each division of fibre volume fraction V_f. Distributions of predicted data with respect to fibre volume fractions are plotted in Charts (a) of Figs. 8.6 to 8.10. Evaluation of each method is as follows.

Figure 8.6(a) shows the performance of Narayanan and Dawish method with respect to fibre content. It can be seen that the method is not conservative, with an average of $V_{exp}/V_{calc} < 1.0$ for the regions A and B where $V_f < 1.0\%$. As V_f increases to very high values, the Narayanan and Dawish method become more conservative especially for the data with hooked fibres. Figure 8.7(a) shows the performance of Shaaban and Gesund method; the predicted data are scattered above the y-axis $V_{exp}/V_{calc} = 1$, showing a high conservatism. However, the results in Table 8.4 show that the COVs of the method by Shaaban and Gesund (1990) are also the highest in all divisions compared to the other methods. Hence, this highlights that the approach that uses only the relative weight of fibres [in Eq. (2.27)]] to calculate the shear strength increment due to the presence of fibre is not accurate.

Figure 8.8(a) shows the performance of the Higashiyama et al. (2011)'s method. The results in Table 8.4 show that the method performs reasonably well especially for slabs using other types of fibres (not hooked end fibres). The performance of the CSCT+VEM method is shown in Fig. 8.9(a). The results in Table 8.4 show that the method is accurate; the incorporation of CSCT with VEM to consider the influence of FRC on the punching shear strength is effective. However, both Higashiyama et al. (2011)'s and CSCT+VEM methods have *Minimum* V_{exp}/V_{calc} of 0.66, and 0.67, respectively. These are considered to be too low.

Figure 8.10(a) and the results in Table 8.4 show that the author's proposed general and simplified methods are the most accurate yet conservative. The proposed shear strength increment v_f [in Eq. (8.17)] shows good agreement with experimental results. The combined average of V_{exp}/V_{calc} of the two divisions (Columns 10 to 13 of Table 8.4) is about 1.22 (conservative), with a combined average COV of about 0.12 (lowest among all)

8.4.3.2 Influence of reinforcement ratios

Columns 10 to 13 of Table 8.4 show the statistical analysis results for each division of reinforcement ratio ρ. Distributions of predicted data with respect to reinforcement ratio are plotted in Charts (b) of Figs. 8.6 to 8.10. Evaluation of each method is as follows.

Figure 8.6(b) shows the performance of the method by Narayan and Darwish (1987) with respect to the reinforcement ratio. Note that the method uses an exponent of 1 for reinforcement ratio in its punching shear equation ($V_u \propto \rho$). It can be seen that a number of data predicted by the method fall below the y-axis V_{exp}/V_{calc} =1.0 in the range ρ < 0.8%, which makes the method unconservative. Hence, the use of $V_u \propto \rho$ is not suitable for this range. However, as reinforcement ratio ρ increases, Narayanan and Dawish method becomes more conservative.

Figure 8.7(b) shows the performance of the method by Shaaban and Gesund (1990), the method is essentially an extension of the ACI punching shear equation. For the region A (ρ < 0.8%), the method is conservative only for the SFRC slabs (see the corresponding average of V_{exp}/V_{calc} in Table 8.4). But as expected, the method is shown to overestimate the strengths of the non-fibrous slabs (V_{exp}/V_{calc} < 1.0). This can be due to the neglect of the reinforcement ratio in the punching shear formula.

Figure 8.8(b) shows that the Higashiyama et al.'s (2011) method performs better than the two methods above, the method uses the exponent of 1/3 for reinforcement ratio ($V_u \propto \rho^{1/3}$), and it can be seen that the predictions are accurate for high reinforcement ratios (ρ > 0.8%), but for the region A (ρ< 0.8%), the method tends to overestimate the strengths of the slabs. This can be due to the effect of low reinforcement ratios which was not considered by the method.

The CSCT+VEM method is accurate and better than the three methods compared above as shown by Fig. 8.9(b), this is expected because it has been discussed earlier in Chapter 7 that the CSCT method is able to perform well for both low and high ranges of reinforcement ratios. The results in Table 8.4 show that the values of COV for CSCT+VEM are low for both divisions of ρ. However, in term of conservatism, the CSCT+VEM method may not be the best option because there are a considerable number of data with V_{exp}/V_{calc} < 1.0 with *Minimum* V_{exp}/V_{calc} of

0.67. This concerns the safety issue of the design. On top of that, the method is complicated to apply in design practice.

Among all the methods, the author's proposed standard general method can be considered the best with respect to reinforcement ratio. This highlights that the proposed treatment of low reinforcement ratio can be extended to SFRC slabs. The combined average of V_{exp}/V_{calc} of the two divisions (Columns 10 to 13 of Table 8.4) is about 1.22 (conservative), with a COV of about 0.12 (lowest among all). The data are narrowly distributed around the mean values greater than $V_{exp}/V_{calc} = 1$, indicating a low COV and conservative predictions (see Fig. 8.10(b)). Note also that the proposed simplified general method has almost identical predictions to the standard method as shown in Table 8.4.

8.4.3.3 Influence of fibre types

The performance of each method with respect to different fibre types is also summarised in Table 8.4. The horizontal (red) dashed lines and solid lines drawn in Figs. 8.6 to 8.10 represent the average of V_{exp}/V_{calc} of test data using hooked end fibre and other types of fibres, respectively. The comparisons (Figs. 8.6 to 8.10) show that most of the methods including the author's proposed method tend to predict higher values of V_{exp}/V_{calc} for the slabs using hooked end fibres compared to the slabs with other types of fibres, indicating that all the methods are relatively more conservative when hooked end fibres are used.

All methods, except the method by Shaaban and Gesund (1990), have very close 'y' values for horizontal dashed lines and solid lines in all divisions. The reason for the Shaaban and Gesund method to have deviating values of average of V_{exp}/V_{calc} for hooked end fibres and other types of fibres is that, the method does not consider the influence of fibre-matrix bond behaviours for different types of fibres. Other methods tackle this influence by introducing a fibre bond factor to their shear equations which vary with shapes or types of fibres. Note that the region A in Chart (a) of Figs. 8.6 to 8.10 show that horizontal solid and dashed lines are not as close. The reason is that there are there are very few data available in this region (7 data for hooked end fibres, 3 for other type of fibres). Some other parameters (besides the fibre types) may influence the failure loads of these slabs in this region.

By comparing the author's proposed method (in Fig. 8.10) with the other methods (in Figs. 8.6 to 8.9), it can be seen that the average of V_{exp}/V_{calc} of the author's proposed method in one division (represented by the horizontal dashed and solid lines) is almost identical as that of the other divisions. This confirms that the proposed bond strength factor to account for the influence of different fibre types in Eq. (8.19) is reasonably accurate.

8.4.3.4 Concrete strength, failure modes, and summary

The performances of all methods with respect to concrete strength are shown in Figs. 8.11(a to e). Fig. 8.11(e) shows that the proposed general method performs very well and conservative throughout a broad range of concrete strength f'_c up to about 100 MPa. Column 3 of Table 8.4 shows the statistical analysis results of all the 148 data combined. Therefore, based on COV criteria, the methods can be reanked as follows: the 1st rank is the author's proposed (Standard and Simplified) general methods with a COV of about 13%, the 2nd rank is CSCT+VEM method with a COV of 14.6%, the 3rd rank is the Higashiyama et al. (2011)'s method with a COV of 19.1%, the 4th rank is the Shaaban and Gesund (1990)'s Method with a COV of 23.8% and the last rank is the Narayanan and Darwish (1987)'s method with a COV of 25.0.%

From the comparative study above, the author's proposed general methods are the most accurate and reliable. The simplified general method (that uses $\rho_{fs} = 0.7\%$ as the limiting reinforcement ratio for the low reinforcement ratio effect factor) is especially very simple to apply because of simpler calculation effort. However, in terms of failure mode prediction, the standard general method predicts failure modes more accurately than the simplified method (See Table E2 in Appendix E for comparison). Of the 8 slabs out of 148 slabs that failed in Flexure, the standard general method predicted correctly for all 8 of them (100% correct) while the simplified method also predicts 100% correctly. However, of the 140 slabs failing in punching (including ductile punching), the standard method predicts the mode of failure correctly for 115 slabs (82%), while the simplified method only predicts correctly for 93 slabs (66%).

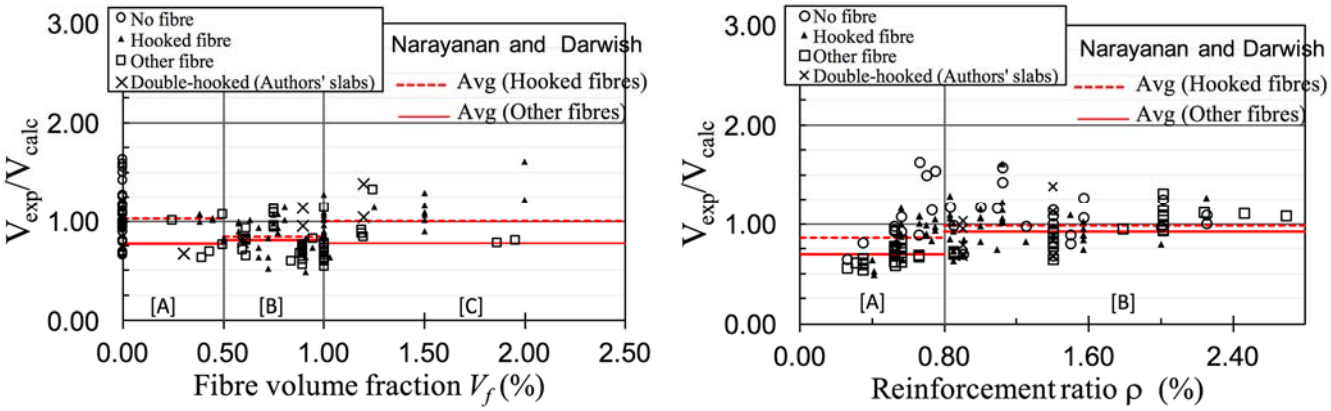

Fig.8. 6 – Failure load predictions of 148 test data by Narayanan and Darwish Method in term of (a) fibre volume fraction; (b) reinforcement ratio ρ

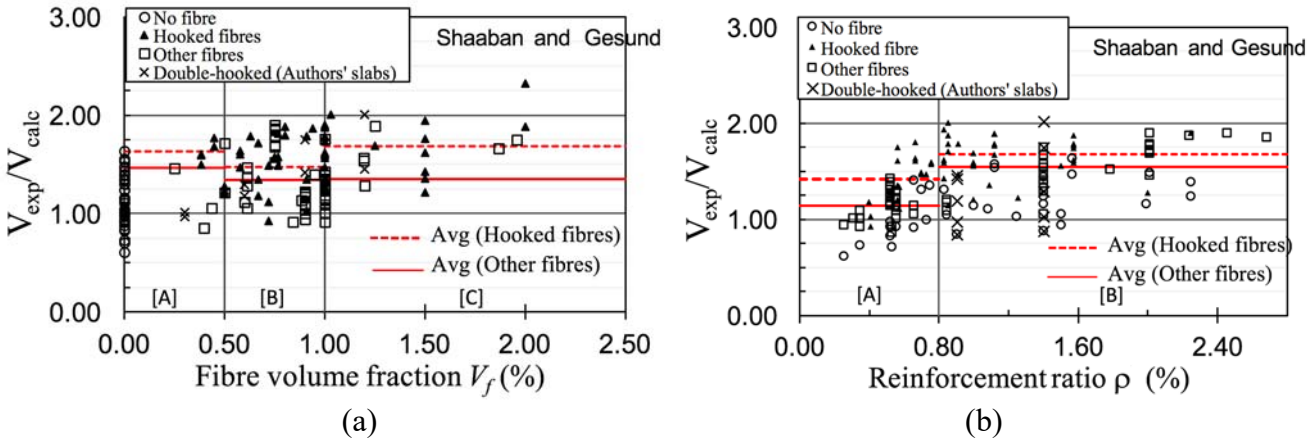

Fig.8. 7 – Failure load predictions of 148 test data by Shaaban and Gesund Method in term of (a) fibre volume fraction; (b) reinforcement ratio ρ

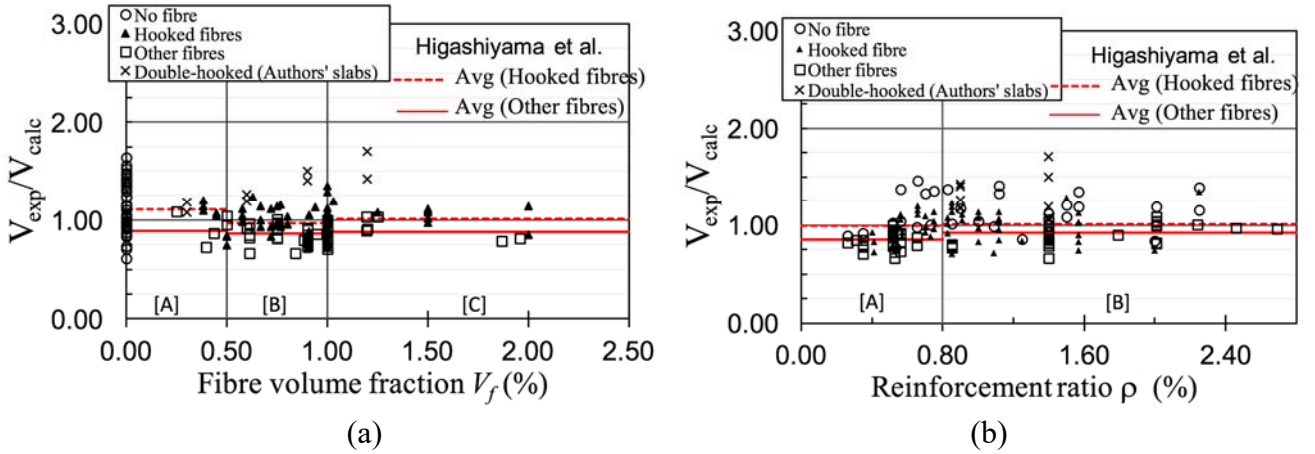

Fig.8. 8 – Failure load predictions of 148 test data by Hagashiyama et al. Method in term of (a) fibre volume fraction; (b) reinforcement ratio ρ

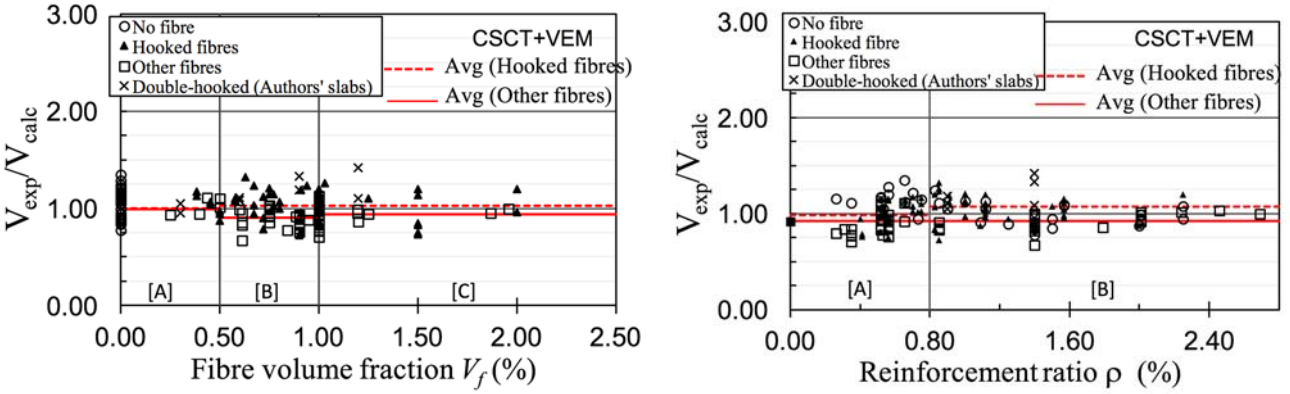

Fig.8. 9 – Failure load predictions of 148 test data by CSCT+VEM Method in term of (a) fibre volume fraction; (b) reinforcement ratio ρ

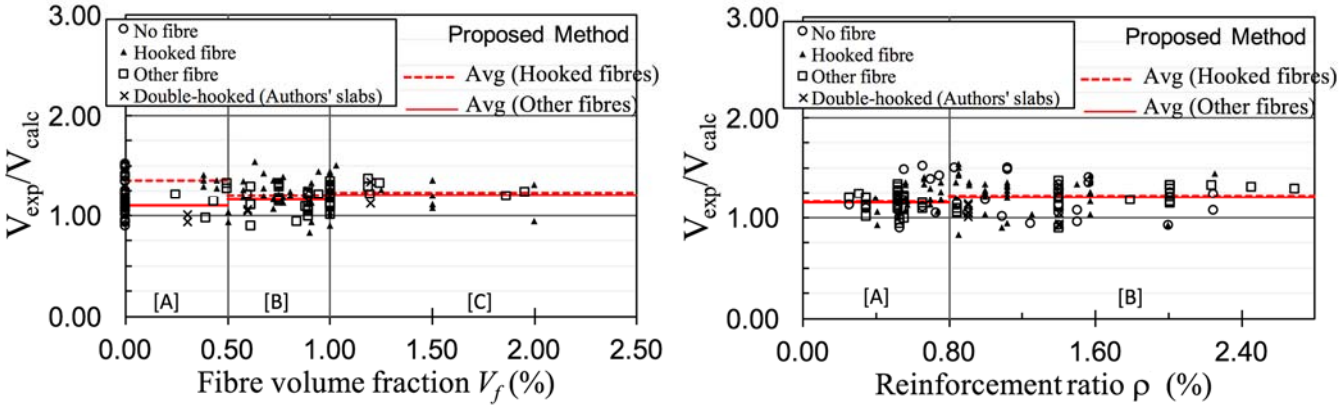

Fig.8. 10 – Failure load predictions of 148 test data by proposed (Standard) General Method in term of (a) fibre volume fraction; (b) reinforcement ratio ρ

Table 8. 4 – Comparison of Experimental and Calculated Failure Load by all methods

V_{exp}/V_{calc}		All data	Fibre volume fraction V_f (%)						Reinforcement ratio ρ (%)			
Division (Units)			[A]		[B]		[C]		[A]		[B]	
			$0 < V_f < 0.5$ (%)		$0.5 \le V_f < 1.0$ (%)		$V_f \ge 1.0$ (%)		$0 < \rho < 0.8$ (%)		$\rho \ge 0.8$ (%)	
Type of fibres			Hooked	Other	Hooked	Other	Hooked	Other	Hooked	Other	Hooked	Other
Nos. of data:		148	7	3	29	26	28	21	21	27	43	23
(1)	(2)	(3)	(4)	(5)	(6)	(7)	(8)	(9)	(10)	(11)	(12)	(13)
V_{exp}/V_{calc} Narayanan and Darwish Eq. (2.23)	Min =	0.49	0.67	0.62	0.49	0.56	0.63	0.54	0.49	0.54	0.63	0.65
	Max=	1.63	1.07	1.00	1.15	1.12	1.61	1.32	1.16	0.84	1.61	1.32
	Average=	0.92	0.93	0.77	0.86	0.81	1.02	0.78	0.86	0.69	0.97	0.92
	COV=	0.250	0.190	0.267	0.202	0.217	0.212	0.228	0.223	0.112	0.210	0.185
V_{exp}/V_{calc} Shaaban and Gesund Eq. (2.27)	Min =	0.61	0.97	0.85	0.92	0.92	1.21	0.92	0.92	0.85	0.97	1.05
	Max=	2.32	1.76	1.46	1.88	1.90	2.32	1.89	1.81	1.43	2.32	1.90
	Average=	1.38	1.45	1.12	1.46	1.34	1.69	1.35	1.42	1.14	1.62	1.55
	COV=	0.238	0.222	0.274	0.186	0.233	0.150	0.200	0.166	0.136	0.179	0.170
V_{exp}/V_{calc} Higashiya-ma et al. Eq. (2.35)	Min =	0.66	1.05	0.72	0.70	0.66	0.72	0.71	0.73	0.66	0.70	0.66
	Max=	1.71	1.20	1.08	1.50	1.04	1.71	1.03	1.20	1.00	1.71	1.08
	Average=	1.00	1.11	0.89	1.02	0.86	1.05	0.88	0.99	0.85	1.07	0.90
	COV=	0.191	0.054	0.20	0.185	0.117	0.199	0.103	0.126	0.098	0.196	0.125
V_{exp}/V_{calc} CSCT +VEM Eq. (2.3) + Eq. (2.33)	Min =	0.67	0.95	0.93	0.73	0.67	0.73	0.70	0.73	0.70	0.73	0.67
	Max=	1.41	1.17	1.11	1.33	1.10	1.41	1.13	1.17	1.13	1.41	1.03
	Average=	1.01	1.08	0.99	1.05	0.90	1.05	0.94	0.99	0.92	1.08	0.92
	COV=	0.146	0.073	0.101	0.146	0.108	0.153	0.122	0.151	0.136	0.141	0.089
V_{exp}/V_{calc} Proposed General Method Eq. (8.30) (Simplified)	Min =	0.84	0.93	1.01	0.84	0.89	0.90	1.10	0.99	0.96	0.84	0.89
	Max=	1.55	1.44	1.21	1.55	1.35	1.52	1.40	1.44	1.40	1.55	1.38
	Average=	1.19	1.24	1.12	1.22	1.18	1.23	1.27	1.25	1.23	1.22	1.20
	COV=	0.130	0.155	0.10	0.135	0.110	0.134	0.069	0.110	0.100	0.146	0.099
V_{exp}/V_{calc} Proposed General Method Eq. (8.30) (Standard)	Min =	0.84	0.93	0.97	0.84	0.89	0.90	1.00	0.94	0.93	0.84	0.89
	Max=	1.55	1.42	1.21	1.55	1.32	1.52	1.38	1.42	1.34	1.55	1.38
	Average=	1.22	1.24	1.10	1.20	1.16	1.23	1.21	1.21	1.16	1.22	1.20
	COV=	0.129	0.152	0.12	0.140	0.103	0.128	0.079	0.112	0.089	0.145	0.099

NOTE: Regions A, B, C correspond to the regions in Figs. 8.6 to 8.10.
COV = Coefficient of variation.
Hooked = Hooked end fibre type
Other = Other types of fibres

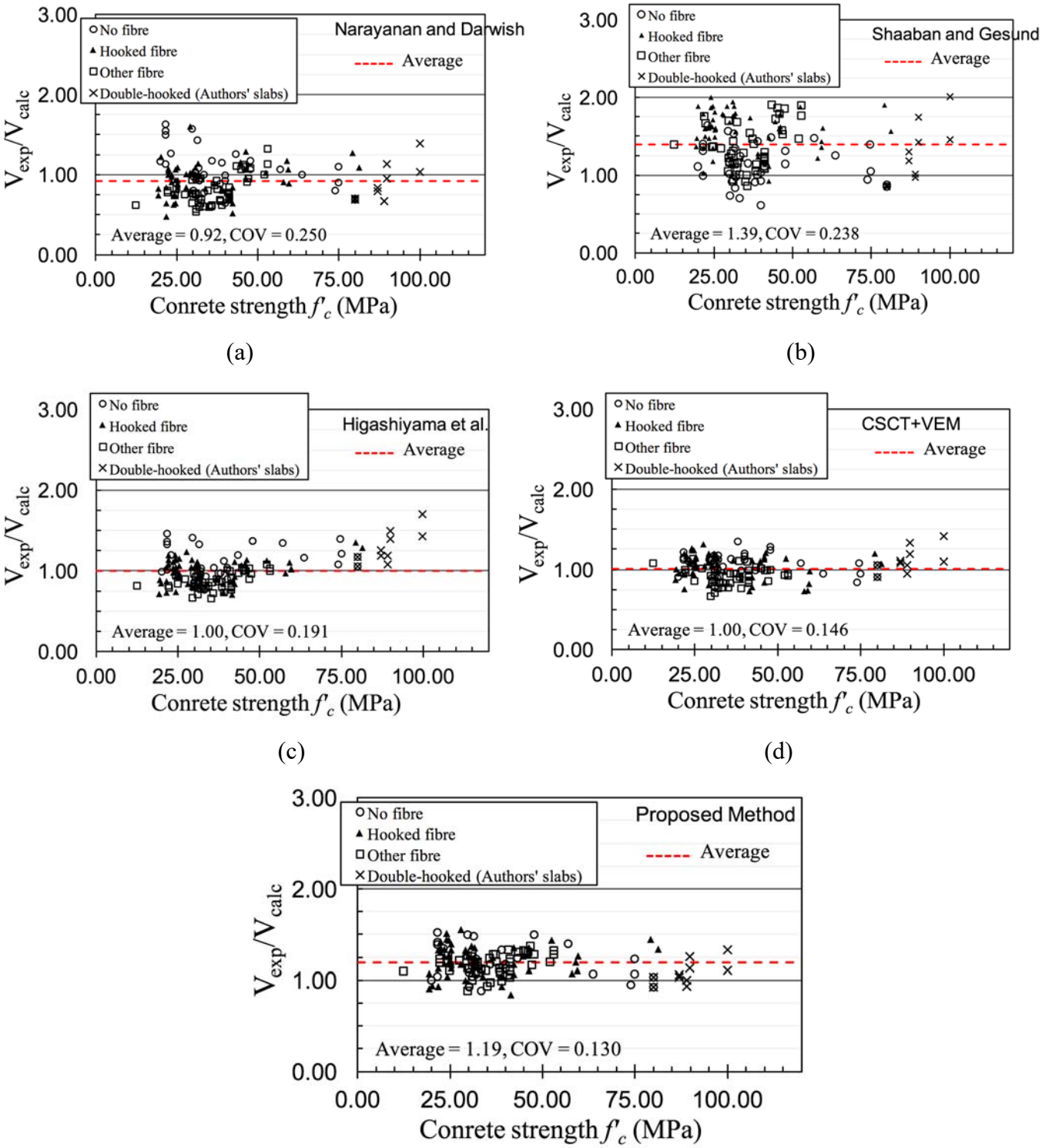

Fig.8. 11 – Performances with respect to concrete strength of (a) Narayanan and Darwish method; (b) Shaaban and Gesund method; (c) Hagashiyama et al. Method; (d) CSCT+VEM method; and (e) The proposed (standard) general method.

8.5 Summary

Two new approaches of calculating the punching shear strength increment due to the presence of fibres were derived and proposed based on theoretical basis. The first approach calculates shear strength by incorporating residual tensile strengths obtained from the notched beam test EN 14651 (2007). The second approach approximates the shear strength to be a function of semi-empirical and empirical fibre parameters, such as fibre geometry, fibre content, and various reduction factors.

The author's proposed method that uses the first approach is referred to the *Standard FRC* method (in Section 8.2). The second method (in Section 8.3) uses the second approach which is referred as the (standard) *General* method. The second method or the general method can be simplified further to be referred to the *simplified* general method. The simplification is the same as the one made to the proposed method for reinforced concrete slabs presented in Chapter 7.

Both proposed methods were validated with the author's current test results of the SFRC slabs and also with existing 138 data from literature. The other design methods that were used to compare in this study are the TR 34 punching shear equation (Concrete Society 2015), Model Code 2010 (2012), and the methods proposed by Narayanan and Darwish (1987), Shaaban and Gesund (1990), Higashiyama et al. (2011) and CSCT+VEM method by Mutton el al.'s group (Muttoni and Ruiz 2010, Maya et al. 2012) in which the VEM (variable engagement model) was proposed by Voo and Foster (2003).

Among all the methods compared, the validation with a set of 16 slab data that were provided with the properties of residual tensile strengths showed that the author's proposed FRC method has the best performances with the lowest COV which is about 10%. The comparisons with 148 data showed that the proposed general methods (both standard and simplified) are the most accurate and reliable. The predictions have conservative values of V_{exp}/V_{calc} (≈1.2) and low values of COV (≤ 0.14) across different ranges of design parameters. The simplified general method requires less calculation effort, which is, therefore, suitable for design purpose.

9

GENERAL CONCLUSIONS

9.1 Conclusions

Conclusions are summarised at the end of each chapter of this thesis, and they are presented here again to highlight some key findings drawn from this research.

Experimental works

A total of full-scale 22 slab specimens were tested under punching loads. The experimental programmes were divided into two sets such as (1) the punching shear tests of 12 HSC slabs to mainly investigate the effects of low reinforcement ratio and column rectangularity. (2) the punching shear tests of 10 high strength concrete and steel fibre reinforced concrete (SFRC) slabs to investigate the influence of a new type of fibres (the double hooked-end fibres).

The key findings drawn from the 1st set of this experimental programme:

- Under a punching load, a slab that is provided with a low reinforcement ratio ($\rho = 0.5\%$ for the current 12 slabs) may fail in flexure first before it fails in what looks like punching failure in the end. The failure load will be lower than that predicted by ACI 318-14 for punching shear.
- Slabs that fail in punching will tend to form circular-fan shape of crack patterns at failure, while those failing in flexure will tend to form cracks parallel to column lines.
- The higher the amount of reinforcement provided, the higher is the failure load. However, only those reinforcements within the width of $1.5h$ from a column face (or total width of $c_2 + 3h$ for an interior column) will be fully effective in resisting punching shear stresses and, therefore, can be considered in influencing punching shear strength.

- ACI 318 method is unconservative for high strength cocnrete slabs with low reinforcement ratios (especially for $\rho < 0.9\%$). Eurocode 2 method can be unconservative for high strength concrete slabs with very low reinforcement ratio and supported on rectangular columns.

The key findings drawn from the 2nd set of experiment

- The punching shear strength of a slab can be significantly enhanced by the inclusion of fibres. Th use of double hooked-end fibres is better than normal hooked-end fibres. The results showed that the punching shear strength of SFRC slab with double hooked-end fibres having volume fraction of 1.2% can be 156% higher than the strengths of plain HSC slabs, given the same reinforcement ratios. This is considerably higher than the increment introduced by normal hooked-end fibres, which can increase punching shear strength by about 40-65 %.
- The post-punching residual strength of a slab also increases as the fibre volume fraction increases. The post-punching residual strength is about 50% of the corresponding peak load of each SFRC slab. Hence, the use of double hooked-end steel fibres can be an effective enhancement.
- The addition of fibres can enhance the serviceability performance of the slabs. It can delay the initiation of flexural cracks because the concrete modulus of rupture is increased. The crack widths are reduced with an increase in the fibre contents at all stages of loadings
- When the fibre volume is about 0.9% (70.2 kg/m^3 fibre dosage) and higher, ductility and energy absorption of a slab are improved substantially. The Concrete Society's TR34 method is accurate for the author's current SFRC slabs.
- Model Code 2010's method, using the first level of approximation, is inaccurate and unconservative for the current slabs. Since all the slabs were considered to ultimately fail in punching, yield line theory method is not suitable for the current slabs. The analysis results showed that the yield line theory overestimates the strengths of all the slabs.

Proposal and Analytical works

Proposed method for reinforced concrete (RC) slabs

New methods for calculating the punching shear strength of a reinforced concrete slab were derived and proposed. Influencing factors, such as column rectangularity ratio, concrete strength, and size (thickness) effect were addressed and considered in the proposed methods.

The author's new experimental results presented in Chapter 5 were combined with 355 existing published data to evaluate the accuracy and safety of ACI 318-14 and Eurocode 2 equations, as well as some relevant methods proposed by other researchers such as the critical shear crack theory (CSCT) method by Muttoni (2008) and the Peiris-Ghali method (2011). The comparisons of these methods with 367 slab data showed that:

- The ACI 318 and EC 2 codes can be unconservative for slabs with low reinforcement ratios (especially for $\rho < 0.7\%$). The correction procedure proposed by Peiris and Ghali (2011) fixes the problem but it may lead to over conservatism. The EC 2 code can be unconservative for high strength concrete slabs (especially for $f'_c > 80$ MPa).
- The ACI 318, EC2, and CSCT methods may not be safe for slabs with an effective depth of more than 300 mm, even though EC2 and CSCT do consider size effect. ACI needs to consider the inclusion of size effect into the equation.
- The author's proposed standard and simplified methods (in Chapter 7) have been shown to be most accurate and reliable with a uniform averages of V_{exp}/V_{calc} and COV across different ranges of design parameters. The simplified method is especially simple to use.
- The author's proposed standard method has been shown to be accurate in terms of failure mode prediction for RC slabs.

Proposed method for steel fibre reinforced concrete (SFRC) slabs

The author's proposed methods (in Chapter 8) and other available methods were validated and compared with the test results of the author's current SFRC slabs and also with existing 138 data from the literature.

Among all the compared methods, the validation with 16 slab data (with available data of the concrete residual tensile strengths) showed that the author's proposed FRC method performs best with the lowest COV of about 10%. The comparisons with 148 data showed that the proposed general methods (both standard and simplified) are the most accurate and reliable. The predictions have conservative values of average V_{exp}/V_{calc} (≈ 1.2) and low values of COV (≤ 0.14) across different ranges of design parameters. The simplified general method requires less calculation effort, which is, therefore, suitable for design purpose.

The author's proposed standard general method has also been shown to predict failure modes of SFRC slabs accurately.

9.2 Final remarks and contributions

New data of 12 high strength concrete slabs with various flexural reinforcement ratios and column aspect ratios have been presented. This work has shown that the effect of low reinforcement ratio can be treated by the author's proposed approach. Standard and Simplified equations for calculating the limiting reinforcement ratio ρ_{fs} were proposed, the simplified ρ_{fs} has also been proposed and can be taken as 0.7%. A slab having the reinforcement ratio $\rho < \rho_{fs}$ is expected to fail in flexure. Its strength can be represented very well by the relationship as $V_{exp} = (\rho/\rho_{fs})^{1/2} v_{c,basic}$, where $v_{c,basic}$ is the basic shear strength proposed by Teng et al. (2004) but without the term ρ. The author hopes that the current works and proposals can help to improve the current design methods of two-way slabs (flat plates and flat slabs).

The accuracy of existing methods for designing against punching shear has been verified, such as those of the ACI 318, Eurocode 2, and several researchers. It is found that most of those methods including the ACI method and Eurocode 2 can be unconservative for slabs with low flexural reinforcement ratios. Hence, extra caution is required for designing slabs with low ranges of reinforcement ratios.

New Experimental data of 10 high strength concrete SFRC slabs utilising a new type of steel fibres has been investigated and presented. The experimental results have been discussed and presented in details. There has not been any standard code provision for designing a structure member using SFRC yet. The author believes that this study provides an important set of data and new discussions for the on-going development of SFRC slabs, especially for research on the double-hooked end steel fibres.

New design methods have been proposed and shown to be very reliable and accurate for both reinforced concrete and steel fibre reinforced concrete slabs. The proposed general method (the second proposal for SFRC slabs, Section 8.3) is simple to use and suitable for practical design purpose.

9.3 Suggestions for future works

The current work was limited to interior RC and SFRC slabs. Future research on the effects of low reinforcement ratios can be extended to edge, and corner slab-column connections. In Chapter 8, the author has also proposed a reduction factor to account for the influence of low reinforcement ratio on ultimate punching shear strength of SFRC slabs based on the data analysis of existing data. However, so far, there has not been a specific test to investigate this parameter for SFRC slabs yet.

Based on the current database, there has not been any SFRC slab data with varying column aspect ratios; all existing slab data only have square columns. Thus, the influence of column rectangularity for SFRC slabs has yet to be investigated in the future. The author's current results of SFRC slabs seem to be the only set of data in the database that use the double hooked-end fibres. More research on the influence of double hooked-end fibres on various structural performances even including the flexural strength of flat plates are still in demand.

One of the influencing parameters that has not been constructively concluded is the size effect. There are very limited slab data that have large thicknesses; the maximum thickness, especially for the existing SFRC slab data, is less or equal to 150 mm. Tests to investigate size effect are needed for both RC and SFRC slabs.

References

ACI 318-14 (ACI Committee 318). (2014). Building Code Requirements for Structural Concrete (ACI 318-14) and Commentary (318R-14) American Concrete Institute (Vol. 524 pp). Farmington Hills, Michigan

ACI 445C Database (Collected by Ospina, B., and Kuchma). (2011). ACI 445C - Punching Shear - Collected Databank. https://nees.org/resources/3660/

ACI 544.4R (ACI Committee 544). (1988 (Reapproved 2009)). Design Considerations for Steel Fiber Reinforced Concrete.

ACI 544.3R-08 (ACI Comittee 544). Guide for specifying, Proportioning, and Production of Fiber-Reinforced Concrete. (2008).

ACI 544.6R-15 (ACI Committee 544). (2015). Report on Design and Construction of Steel Fiber-Reinforced Concrete Elevated Slabs (pp. 38).

ASTM A184. Standard Specification for Welded Deformed Steel Bar Mats for Concrete Reinforcement. (2011).

Alexander, S. D. B., & Simmonds, S. H. (1992). "Bond Model for Concentric Punching Shear". ACI Structural Journal, 89(3), 325-334.

Alexander, S. D. B., & Simmonds, S. H. (1992). "Punching Shear Tests of Concrete Slab-Column Joints Containing Fiber Reinforcement". ACI Structural Journal, Vol. 89(4), 425-432.

Alexander, S. D. B., & Simmonds, S. H. (1992). "Test of Column-Flat Plate Connections". ACI Structural Journal, 89(5), 495-502.

Anggadjaja, E., & Teng, S. (2008). "Edge-column slab connections under gravity and lateral loading". ACI Structural Journal, 105(5), 541-551.

AS 3600 (Standards Australia International). (2001). Concrete Structures (pp. 176). Sydeny, New South Wales.

Banthia, N., Trottier, J. F., Soroushian, P., & Bayasi, Z. (1992). "Fiber-Type Effects on the Performance of Steel Fiber Reinforced-Concrete - Discussion". Aci Materials Journal, 89(1), 106-107.

Base. (1966). "Data obtained from databank collected by ACI committee 445C (2011)".

Bažant, Z. (1984). "Size Effect in Blunt Fracture: Concrete, Rock, Metal". ASCE Journal of Engineering Mechanics, 110(4), 518-535. doi:10.1061/(ASCE)0733-9399(1984)110:4(518)

Bažant, Z. P., & Cao, Z. (1987). "Size Effect in Punching Shear Failure of Slabs". ACI Structural Journal, 84(1), 44-53.

Bažant, Z. P., Qiang Yu, Walter Gerstle, James Hanson, & Ju, J. W. (2007). "Justification of ACI 446 Proposal for Updating ACI Code Provisions for Shear Design of Reinforced Concrete Beams". ACI Structural Journal, V. 104(No. 5, Sep-Oct).

BEKAERT. (Dramix) 5D fibres Datasheet. in www.bekaert.com (Brochure_Dramix_5D4D3D.PDF)

Bortolotti, L. (1990). "Punching Shear Strength in Concrete Slabs". ACI Structural Journal, 84(2), 208-219.

Bræstrup, M. W., Nielsen, M. P., Jensen, B. C., & Bach, F. (1976). "Axisymmetric Punching of Plain and Reinforced Concrete". Report R75, Structural Research Laboratory, Technical University of Denmark, Copenhagen, Denmark.

Brom, C. E. (2016). "Tangential Strain Theory for Punching Failure of Flat Slabs". ACI Structural Journal, 113(1), 95-104.

Broms, C. E. (1990). "Punching of Flat Plates – A Question of Concrete Properties in Biaxial Compression and Size Effect". ACI Structural Journal, 87(3), 292-304.

Broms, C. E. (2000). "Elimination of Flat Plate Punching Failure Mode". ACI Structural Journal, V. 97, No. 1, Jan.-Feb., pp. 94-101.

BS 8110 (British Standards). (1997). Structural Use of Concrete: Part 1: Code of practice for design and construction (BS 8110-1:1997) (pp. 168 pp). British Standards Institution, London, UK.

CEB-Bulletin 168 (Comite Euro-Interational Du Beton). (1985). Punching shear in Reinforced Concrete.

Chandler, J. & Neal, F. The Design of Ground-Supported Concrete Industrial FLoor Slabs. Interim Technical Note 11, Cement and Concrete Association, UK, 16 pp (1988).

Cheng, M.-Y., & Parra-Montesinos, G. J. (2010a). "Evaluation of Steel Fiber Reinforcement for Punching Shear Resistance in Slab-Column Connections—Part I: Monotonically Increased Load". ACI Structural Journal, Vol. 107(1), 101-109.

Choi, K.-K., Reda Taha, M. M., Park, H.-G. & Maji, A. K. Punching shear strength of interior concrete slab–column connections reinforced with steel fibers. Cement and Concrete Composites 29, 409-420,

Collins, M. P., Bentz, E. C., & Sherwood, E. G. (2008). "Where is Shear Reinforcement Required? Review of Research Results and Design Procedures". ACI Structural Journal, 105(5), 590-600.

Corley, W. G., & Jirsa, J. O. (1970). "Equivalent frame analysis for slab design". ACI Journal, Proceedings, 67(11), 875-884.

Corley, W. G., Sozen, M. A., & Siess, C. P. (1961). The Equivalent Frame Analysis For Reinforced Concrete Slabs (Vol. 218): University of Illinois Urbana, Illinois.

CP 65-1 (Singapore Standards). (1997). Structural Use of Concrete: Part 1: Code of practice for design and construction (pp. 168 pp).

Criswell, M. E. (1974). Static and Dynamic Response of Reinforced Concrete Slab-Column Connections. ACI Special Publication SP-42

CSA-A23.3 (Canadian Standards Association). (2004). Design of Concrete Structures (pp. 214). Canada.

De Hanai, J. B., & Holanda, K. M. A. (2008). "Similarities between punching and shear strength of steel fibre reinforced concrete (SFRC) slabs and beams.". IBRACON Structures and Materials Journal, 1(1), 1-16.

Destrée, X., & Mandl, J. r. (2008). "Steel fibre only reinforced concrete in free suspended elevated slabs: Case studies, design assisted by testing route, comparison to the latest SFRC standard documents". ailor Made Concrete Structures – Walraven & Stoelhorst (eds), 437-443.

Dilger, W., Birkle, G., & Mitchell, D. (2005). "Effect of Flexural Reinforcement on Punching Shear Resistance". Punching Shear in Reinforced Concrete Slabs, SP-232, M. A. Polak, ed., American Concrete Institutem, Farmington Hills, MI, 57-73.

Elstner, R. C., and Hognestad, E. (1956). "Shearing Strength of Reinforced Concrete Slabs". ACI Journal, Proceedings, V. 53(No. 1), pp. 29-58.

EN 14651 (BS). (2007). Test method for metallic fibre concrete - measuring the flexural tensile strength (limit of proportionality (LOP), residual) (EN 14651:2005+A1:2007).

Eurocode 2 (CEN Committee). (2004). Design of Concrete Structures: Part 1-1-General Rules and Rules for Buildings EN 1992-1-1, Brussels, Belgium,2004, 225 pp.

fib bulletin 12. (2001). Punching of structural concrete slabs (fib, Bulltetin 12- Féd. Int. du Béton Technical report). In S. Kinnunen (Ed.).

fib bulletin 57. (2010). Shear and punching shear in RC and FRC elements, (Technical report) [15-16 Oct Workshop, in Salo, Italy]

fib bulletin 65. (2012). Model Code 2010 final draft fib, Bulletin 65- Féd. Int. du Béton Technical report (Vol. 1). Lausanne: CEB.FIP.

fib bulletin 66. (2012). Model Code 2010 final draft fib, Bulletin 65- Féd. Int. du Béton Technical report (Vol. 2). Lausanne: CEB.FIP.

Forssell, C., & Holmberg, E. (1946). "Concentrated Loads on Concrete Slabs". Betong, V. 31(No. 2), pp. 95-123.

Foster, S. (2010). Design of FRC beams for shear using the VEM and the draft Model Code approach. Paper presented at the FIB Bulletin 57: shear and punching shear in RC and FRC elements. , Salo (Italy).

Garcia-Taengua, E., Marti-Vargas, J. R. & Serna-Ros, P. (2011), "Statistical Approach to Effect of Factors Involved in Bond Performance of Steel Fiber-Reinforced Concrete". ACI Structural Journal 108

Gardner, N. J. (1990). "Relationship of the Punching Shear Capacity of Reinforced Concrete Slabs with Concrete Strength". ACI Structural Journal, 87(1), 66-71.

Gardner, N. J., & Shao, X.-Y. (1996). "Punching Shear of Continuous Flat Reinforced Concrete Slabs". ACI Structural Journal, V. 93, No. 2, Mar.-Apr., pp. 218-228.

Gasparini, D. A. (2002). "Contributions of C.A.P. Turner to Developent of Reinforced Concrete Flat Slabs 1905-1909". Journal of Structural Engineering (ASCE), 1243. doi:10.1061/(ASCE)0733-9445(2002)128:10(1243)

Geng, J., & Teng S. (Supervisor). (2004). Strength of Slab-Column Connections With Opening Transfering Biaxial Unbalanced Moments. (PhD's thesis), Nanyang Technological University, Singapore.

Georgopoulos, T. (1989). "Punching-force and punching-angle of a flat slab without shear-reinforcement". Durchstanzlast und Durchstanzwinkel punktfoermig gestuetzter, 64(4), 187-191.

Gesund, H., & Dikshit, O. P. (1971). "Yield Line Analysis of the Punching Problem at Slab/Column Intersections, Cracking, Deflection, and Ultimate Load of Concrete Slab Systems". Special Publication ACI, 30, 177-201.

Ghannoum, C. M. (1998). Effect of high-strength concrete on the performance of slabcolumn specimens. (Masters Thesis), Mc Gill University, Montreal, Canada.

Gouveia, N. D., Fernandes, N. A. G., Faria, D. M. V., Ramos, A. n. M. P., & Lúcio, V. l. J. G. (2014). "SFRC flat slabs punching behaviour – Experimental research". Composites: Part B (Elsevier Journal), 63, 161-171.

Graf, O. (1938). "Versuche über die Widerstandsfähigkeit von allseitig aufliegenden dicken Eisenbetonplatten unter Einzellasten". Deutscher Ausschuß für Eisenbeton, Heft 88, Berlin, 26p.

Guandalini, S., Burdet, O. L., & Muttoni, A. (2009). "Punching tests of slabs with low reinforcement ratios". ACI Structural Journal, 106(1), 87-95.

Hallgren, M. (1996). Punching Shear Capacity of Reinforced High Strength Concrete Slabs. (Doctoral Thesis), Royal Institute of Technology, Stockholm,Sweden.

Harajli, M. H., Maalouf, D., & Khatib, H. (1995). "Effect of fibres on the punching shear strength of slab-column connections". Cement and Concrete Composites, 17(2), 161-170. doi:http://dx.doi.org/10.1016/0958-9465(94)00031-S

Hawkins, N. M., Fallsen, H. B., & Hinojosa, R. C. (1971). Influence of Column Rectangularity on the Behaviour of Flat Plate Structures. Paper presented at the SP-30, Cracking, Deflection, and Ultimate Load of Concrete Slab Systems,, American Concrete Institute, Detroit.

Henager, C. H., & Doherty, T. J. (1976). "Analysis of Reinforced Fibrous Concrete Beams". Journal of the Structural Division-Asce, 102(1), 177-188.

Henager, C.H. Steel Fibrous Ductile Concrete Joint for Seismic Resistant Structures. Reinforced Concrete Structures in Seismic Zones, ACI SP-53, 371-386 (1977).

Himawan, A., & Teng, S. (2014). "Cycli Behavior of Post-Tensioned Slab-Rectangular Column Connections". ACI Structural Journal, 111(1), 177-188.

Hiroshi Higashiyama, A. O., & Mutsumi, M. "Design Equation for Punching Shear Capacity of SFRC Slabs". IJCSM, 5(1).

Ingerslev, A. (1923). "The Strength of Rectangular Slabs". J. Inst. Struct. Eng., 1(1), 3-14.

Johansen, K. W. (1962). "Yield-Line Theory". Cement and Concrete Association,London, 181.

JSCE. (2007). Standard Specifications for Concrete Structures (Concrete Committee of Japan Society of Civil Engineers).

King, S., & Delatte, N. J. (2004). "Collapse of 2000 commonwealth avenue: Punching shear case study". Journal of Performance of Constructed Facilities, 18(1), 54-61. doi:Doi 10.1061/(Asce)0887-3828(2004)18:1(54)

Kinnunen, S., & Nylander, H. (1960). "Punching of Concrete Slabs without Shear Reinforcement". Transaction No. 158, Royal Institute of Technology, Stockholm, Sweden, 112 pp.

Kinnunen, S., Nylander, H., & Tolf, P. (1980). "Plattjocklekens inverkan på betongplattors hållfasthet vid genomstansning. Försök med rektangulära plattor". Bulletin 137, Department of Structural Mechanics and Engineering, Royal Institute of Technology, Sweden (Obtained from ACI subcomittee ACI 445C(2011)), 73.

Kukorlo, J. D. (2009). Harbour Cay Condomimiumns. Retrieved from http://failures.wikispaces.com/Harbour+Cay+Condominiums - x-Causes

Ladner, M., Schaeidt, W., & Gut, S. (1977). "Experimentelle Untersuchungen an Stahlbeton-Flachdecken". Eidgenössische Materialprüfungs- und Versuchsanstalt, Bericht Nr. 205, Dübendorf, Switzerland.

Laws, V. (1971), The efficiency of fibrous reinforcement of brittle matrices. Journal of Applied Physics 4, 1737-1746

Li, K. K. L. (2000). Influence of Size on Punching Shear Strength of Concrete Slabs. (M. Eng.), McGill University, Montreal,Quebec.

Li, V. C. (2002). "Large Volume, High-Performance Applications of FIbers in Civil Engineering". Jounral of Applied Polymer Science, 83, 660-686.

Lim T.Y., Paramasivam. P., & Lee, S. L. (1987) "Analytical Model for Tensile Behavior of Steel-Fiber Concrete". Materials Journal, 84(4). doi:10.14359/1454

Lovrovich, J. S., & Mclean, D. I. (1990). "Punching Shear Behavior of Slabs Varying Span-Depth Ratios". ACI Structural Journal, V. 87(No. 5, Sep.-Oct), pp. 507-511.

MacGregor, J. G., & Wight, J. K. (2005). Reinforced Concrete Mechanics and Design (4th Edition in SI Units).

Marti, P., & Thürlimann, B. (1977). "Fliessbedingung für Stahlbeton mit Berücksichtigung der Betonzugfestigkeit, (in German)". BuStb 72, H. 1(7-12).

Marzouk, H., Emam, M., & Hilal, M. S. (1996). "Effect of High-Strength Concrete Columns on the Behavior of Slab-Column Connections". ACI Structural Journal, V. 93(No. 5), pp. 1-8.

Marzouk, H., Emam, M., & Hilal, M. S. (1998). "Effect of high-strength concrete slab on the behavior of slab-column connections". ACI Structural Journal, 95(3), 227-237.

Marzouk, H., & Hussein, A. (1991). "Punching Shear Analysis of Reinforced High-Strength Concrete Slabs". Canadian Journal of Civil Engineering, V. 18, No. 6, Dec., pp. 954-963.

Marzouk, H. R., E.; and Tiller, R. (2010). "Design of Shear Reinforcement Using a Strut and Tie Model". Canadian Journal of Civil Engineering, 37(2), pp. 181-194.

Maya, L. F., Ruiz, M. F. n., Muttoni, A., & Foster, S. J. (2012). "Punching shear strength of steel fibre reinforced concrete slabs". Engineering Structures (Elsevier Journal), 40, 83-94.

McHarg, P. J., Cook, W. D., Mitchell, D., & Yoon, Y. S. (2000). "Benefits of Concentrated Slab Reinforcement and Steel Fibers on Performance of Slab-Column Connections". ACI Structural Journal, V. 97, No. 2, Mar.-Apr., pp. 225-234.

Mobasher, B. & Destree, X. Design and Construction Aspects of Steel Fiber-Reinforced Concrete Elevated Slabs. ACI Special Publication 274. (2010)

Moe, J. (1961). Shearing Strength of Reinforced Concrete Slabs and Footings Under Concentrated Loads. Paper presented at the Bulletin D47, Portland Cement Association, Research and Development Laboratories, Skokie, IL.

Mokhatar, A. (1982). Design of Stud Shear Reinforcement for Concrete Flat Plates. (PhD Thesis), University of Calgary.

Muttoni, A. (2008). "Punching shear strength of reinforced concrete slabs without transverse reinforcement". ACI Structural Journal, 105(4), 440-450.

Muttoni, A., & Ruiz, M. F. (2010). MC2010: the critical shear crack theory as a mechanical model for punching shear design and its application to code

provisions. . Paper presented at the FIB Bulletin 57: shear and punching shear in RC and FRC elements. , Salo (Italy).

Muttoni, A., & Schwartz, J. (1991). "Behaviour of Beams and Punching in Slabs without Shear Reinforcement". IABSE Colloquium, Zurich,Switzerland, 62, 703-708.

Narayanan, R., & Darwish, I. Y. S. (1987). "Punching shear tests on steel-fibre reinforced micro-concrete slabs". Magazine of Concrete Research, 39(138), 42-50.

NEMA. (2004). Collapse of Sampoong Department Store. Retrieved from http://www.nema.go.kr/eng/m4_samp.jsp

Nguyen-Minh, L., Rovňák, M., & Tran-Quoc, T. (2012). "Punching Shear Capacity of Interior SFRC Slab-Column Connections". Journal of Structural Engineering, 138(5), 613-624.

Nichols, J. R. (1914). "Statical Limitations upon the Steel Requirements in Reinforced Concrete Flat Slab FLoors". Transactions ASCE, 77, 1670-1681.

NZS 3101 (Standards New Zealand). (2006). Concrete Structures Standard. Wellington, New Zealand.

Oliveira, D. R. C., Regan, P. E., & Melo. (2004). "Punching Resistance of RC Slabs with Rectangular Columns". Magazine of Concrete Research, V. 56, No. 3, Apr., pp. 123-138.

Osman, M., Marzouk, H., & Helmy, S. (2000). "Behavior of High-Strength Lightweight Concrete Slabs under Punching Loads". ACI Structural Journal, V. 97, No. 3, May-June 2000, pp. 492-498.

Ospina, C. E., & Hawkins, N. M. (2013). Addressing Punching Failure: Considerations to Prevent Premature Concentric Punching Shear Failure in Reinforced Concrete (RC) Two-way Slabs. Structure Magazine, 14-16.

Ozden, S., & Ersoy, U. O., T. (2006). "Punching Shear Tests of Normal-and High-strength Concrete Flat Plates". Can. Ji. Civ. Eng, NRC Canada, 33. doi:10.1139/L06-089

Park, R., & Gamble, W. L. (2000). Reinforced Concrete Slabs: John Wiley & Sons.

Peiris, C., & Ghali, A. (2012). "Flexural reinforcement essential for punching shear resistance of slabs". Special Publication ACI, 287(SP287-06), 1-16.

Perkins, S. A. (2009). Skyline Plaza - Bailey's Crossroads. Retrieved from http://failures.wikispaces.com/Bailey%27s+Crossroads+-+Skyline+Plaza

Pralong, J., Brändli, W., & Thürlimann, B. (1979). "Durchstanzversuche an Stahlbetonund Spannbetonplatten (in German)". Institut für Baustatik und Konstruktion, ETH Zürich, No. 7305-3, 89p.

Rankin, G. I. B., & Long, A. E. (1987). "Predicting the Enhanced Punching Strength of Interior Slab-Column Connections". Institution of Civil Engineers, Proceedings, V. 82(No. 3), pp 1165-1186.

Regan, P.E., Walker, P.R. & Zakaria, K.A.A. Tests of Reinforced Concrete Flat Slabs. in CIRIA Project RP 220 217 pp (Polytechnic of Central London, London, Uk, 1979).

Regan, P. E. (1981). Behaviour of Reinforced Concrete Flat Slabs. Retrieved from CIRIA, London:

Regan, P. E. (1986). "Symmetrical Punching of Reinforced Concrete Slabs". Magazine of Concrete Research, V. 38, No. 136, Sept., pp. 115-128.

Regan, P. E., Al-Hussaini, A., Ramdane, K. E., & Xue, H. Y. (1993). Behaviour of High Strength Concrete Slabs. Paper presented at the Concrete 2000 Proc. of the International Conference, E&FN Spon, Cambridge, U.K.

Regan, P. E., & Braestrup, M. W. (1985). Punching Shear in Reinforced Concrete: A State of the Art Report (Bulletin D'Information, No. 168, Comité Euro-International du Béton, Lausanne, Switzerland, Jan., 232 pp).

Richart, F. E. (1948). "Reinforced Concrete Wall and Column Footings, Part 1". JOurnal of the American Concrete Institute, Proc., 45(2), 97-127.

RILEM. (2003). "Final recommendation of TC 162-TDF: Test and design methods for steel fibre reinforced concrete". Materials and Structures, 36(262), 560-565.

Rizk, E., Marzouk, H., & Tiller, R. (2012). "Design of Thick Concrete Plates Using Strut-and-Tie Model". ACI Structural Journal, 109(5).

Roll, F., Zaidi, S. T. H., Sabnis, G., & Chuang, K. (1971). "Shear Resistance of Perforated Reinforced Concrete Slabs". ACI Publication, Cracking, Deflection and Ultimate Load of Concrete Slab Systems, V. SP-30, pp. 77-101.

Romualdi, J.P. & Mandel, J.A. Tensile Strength of Concrete Affected by Uniformly Distributed and Closely Spaced Short Lengths of Wire Reinforcement. Journal Proceedings 61. (1964)

Rosenthal, I. (1959). "Experimental Investigation of Flat Plate Floors". Journal of the American Concrete Institute, Proceedings, V. 56(No. 12), pp. 153-166.

Schaefers, U. (1984). "Konstruktion, Bemessung und Sicherheit gegen Durchstanzen von balkenlosen Stahlbetondecken im Bereich der Innenstützen". Deutscher Ausschuss für Stahlbeton, Heft 357, Berlin, 72p.

Schaeidt, W., & Ladner, M. (1970). "Berechnung von Flachdecken auf Durchstanzen ". Schriftenreihe der Schweizerischen Zement-Industrie, Wildegg, Switzerland.

Shaaban, A. M., & Gesund, H. (1994). "Punching Shear Strength of Steel Fiber Reinforced Concrete Flat Plates". ACI Structural Journal, Vol. 91(3), 406-414.

Shehata, I. A. E. M. (1990). "Simplified Model for Estimating The Punching Resistance of Reinforced Concrete Slabs". Materials and Structures, 23(5), 364-371.

Soroushian, P., & Bayasi, Z. (1991). "Fiber-Type Effects on the Performance of Steel Fiber Reinforced-Concrete". Aci Materials Journal, 88(2), 129-134.

Sozen, M. E., & Siess, C. P. (1963). "Investigation of Multiple Panel Reinforced Concrete Floor Slabs:Design Methods - THeir Evolution and Comparison". ACI Journal, Proceedings, 60(8), 999-2017.

Stein, T., Ghali, A., & Dilger, W. (2007). "Distinction between Punching and Flexural Failure Modes of Flat Plates". ACI Structural Journal, 104(3), 357-365.

Swamy, R. N., & Ali, S. A. R. (1982). "Punching Shear Behavior of Reinforced Slab-Column Connections Made with Steel Fiber Concrete". ACI Journal, Proceedings V. 79, No. 5, Sept.-Oct., pp. 392-406.

Swamy, R. N., & Mangat, P. S. (1974). "A theory for the flexural strength of steel fibre reinforced concrete". Cement and Concrete Research, 4, 313-325.

Talbot, A. N. (1913). Reinforced Concrete Wall Footings and Column Footings (Bulletin No. 67). University of Illinois Engineering Experiment Station.

Taylor, R., & Hayes, B. (1965). " Some Tests on the Effect of Edge Restraint on Punching Shear in Reinforced Concrete Slab". Magazine of Concrete Research, 17(50), 39-44.

Teng, S., Cheong, H. K., Kuang, K. L., & Geng, J. Z. (2004). "Punching shear strength of slabs with openings and supported on rectangular columns". ACI Structural Journal, 101(5), 678-687.

Teng, S., & Tan, Y. (2005). " Interior Slab-Rectangular Column Connections under Biaxial Lateral Loadings". American Concrete Institute, Farmington Hills, Michigan, SP-232-9, pp. 147-174.

Teng Susanto, et.al. "Ultra-high performance concrete, Part 1", Final Research Report, Report for the National Research Foundation, Singapore, 2015

The Concrete Society: TR 34. (2003). Concrete industrial ground floors: a guide to design and construction.

The Concrete Society: TR 34. (2015). Concrete industrial ground floors (4th edition): a guide to design and construction.

Theodorakopoulos, D., & Swamy, N. (1993). "Contribution of Steel Fibers to the Strength Characteristics of Lightweight Concrete Slab-Column Connections Failing in Punching Shear". ACI Structural Journal, Vol. 90(4), 342-355.

Theodorakopoulos, D., & Swamy, N. (1999). "Ultimate Punching Shear Strength Analysis of Slab-Column Connections With Steel Fibers". ACI Special Publication, Vol. 182, 181-214.

Theodorakopoulos, D. D., & Swamy, R. N. (2003). "A Design Method for Punching Shear Strength of Steel Fiber Reinforced Concrete Slabs". ACI Special Publication, vol.216, 181-202.

Tiller, R. (1995). Strut-and-Tie Model for Punching Shear of Concrete Slabs. (master's thesis), Memorial University of Newfoundland, St. John’s, NL, Canada.

Tolf, P. (1988). "Plattjocklekens inverkan på betongplattors hållfasthet vid genomestansning. Försök med cikulära plattor". Department of Structural Mechanics and Engineering, Royal Institute of Technology, Stockholm, Sweden, Bulletin No. 146, 64 pp.

Tomaszewicz, A. (1993). "High Strength Concrete: SP2 - Plates and ShellsReport 2.3 Punching Shear Capacity of Reinforced Concrete Slabs". Report No. STF70 A93082, SINTEF Structures and Concrete, Trondheim, Norway, July, 36 pp.

Vanderbilt, M. D. (1972). "Shear Strength of Continuous Plates". Journal of Structural Division (ASCE), V. 98, (No. ST5,), 961-973.

Vecchio, F. J., & Collins, M. P. (1986). "The Modified-Field Compression Theory for Reinforced Concrete Elements Subjected to Shear". ACI Structural Journal, 83(2), pp.219-231.

Voo, Y. L., & Foster, S. (2003). Variable Engagement Model for the Design of Fibre Reinforced Concrete Structures. Paper presented at the Advanced Materials for Construction of Bridges, Buildings, and Other Structures III (Engineering Conferences International).

Walraven, J. C. (1994). Size effects: Their Nature and Their Recognition in Building codes. Paper presented at the Proc. of the Japan Concrete Institute International Workshop: Size effect in Concrete Structures., E&FN Spon.

Widianto, Bayrak, O., & Jirsa, J. O. (2009). "Two-way shear strength of slab-column connections: Reexamination of ACI 318 provisions". ACI Structural Journal, 106(2), 160-170.

Widjaja, S., & Teng S. (Supervisor). (2008). Behavior of Corner Slab-Column Connections in Irregular Flat Plate Floors under Gravity and Bidirectional Lateral Loading. (PhD thesis), Nanyang Technological University (NTU).

Yassir Abbas & Khan, M. I. Fiber-Matrix Interfacial Behavior of Hooked-End Steel Fiber-Reinforced Concrete. Journal of Material in Civil Engineering (ASCE) (2016).

Yitzhaki, D. (1966). "Punching Strength of Reinforced Concrete Slabs". ACI Journal, Proceedings V. 63, No. 5, May, pp. 527-542.

Appendix A

PHOTOGRAPHS FROM EXPERIMENTS

A.1 Specimen preparations

S11-028

S11-050

S11-090

S11-139

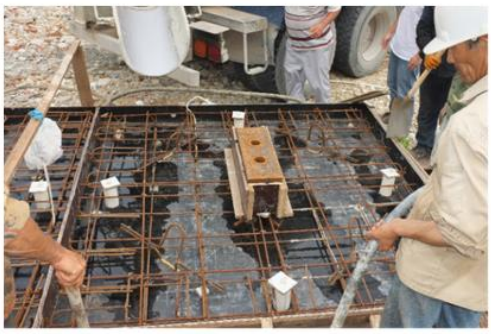

S13-028

S3-050

Fig. A.1 – Steel cages and form works of some HSC slab specimens

(a)

(b)

(c)

(d)

(e)

Fig. A.2 – (a) Steel cages and form works, (b) concrete cast of a SFRC specimen, (c) concrete flow diameter, (d) concrete samples for mechanical property tests, and (e) a typical slump of fibrous concrete with fibre volume fraction of 1.2%.

(a)

(b)

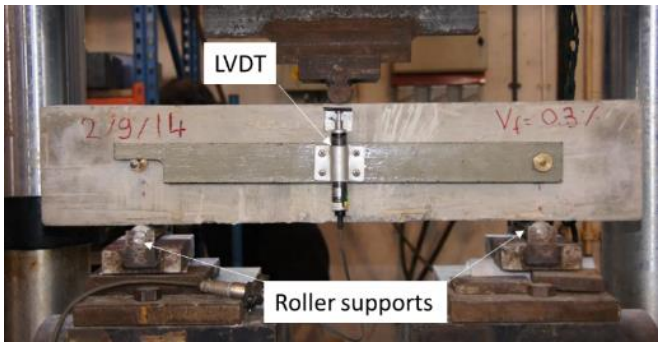

(c)

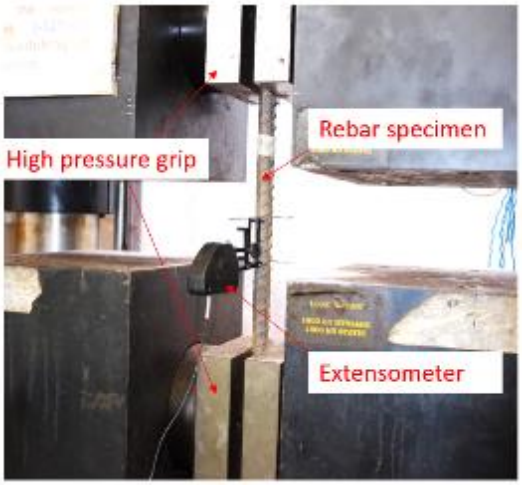

(e)

Fig. A.3 – (a) Concrete compressive strength test, (b) concrete split tensile test, (c) notched beam test or flexural tensile test, and (d) Steel tensile strength test

(a)

(b)

(c)

Fig. A.4 – (a) Precise positioning of a slab specimen (b) positioning of LVDTs below a specimen, (c) test equipment above a slab specimen

A.2 Post-test photographs

(a)

(b)

Fig. A.5 – (a) Concrete cylinder specimen after compression test., (b) Concrete prism specimens after flexural tensile tests.

S1-028

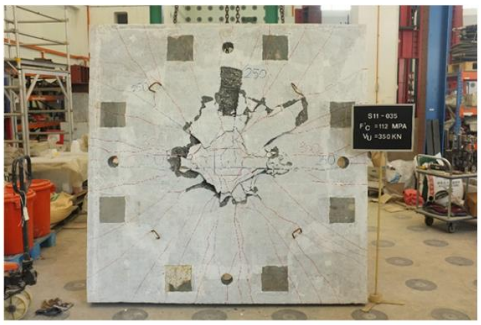

S1-050

S1-090

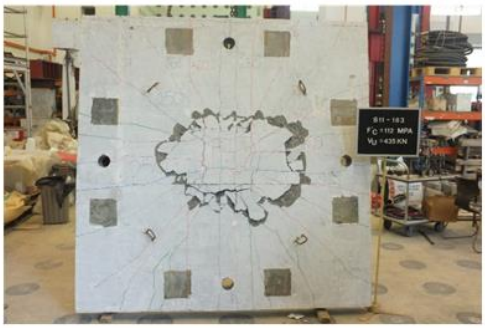

S1-139

Fig. A.6 – Photos of S1-series specimens without digital enhancement of cracks

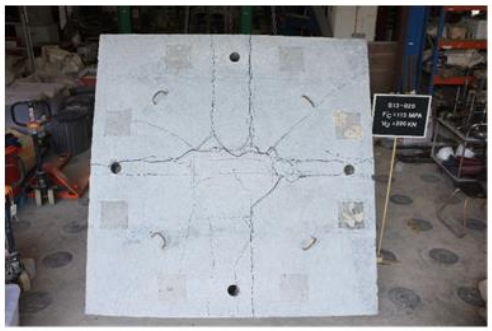

S13-028

S13-050

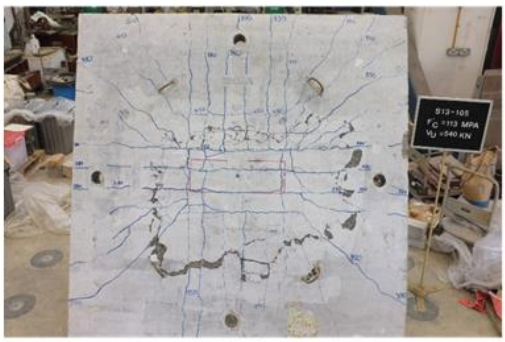

S13-090

S13-143

Fig. A.7 – Photos of S13-series specimens without digital enhancement of cracks

S15-028

S15-050

S15-090

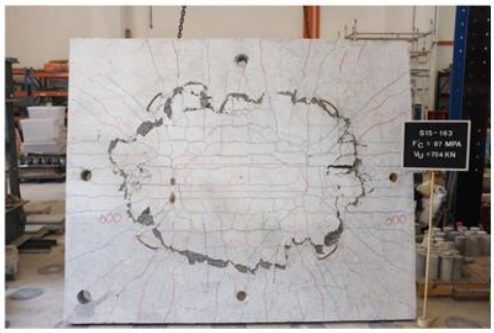

S15-143

Fig. A.8 – Photos of S15-series specimens without digital enhancement of cracks

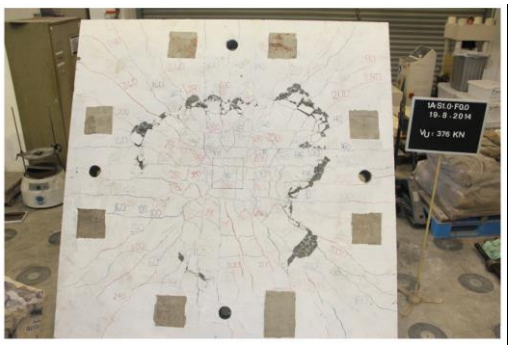

F09-00

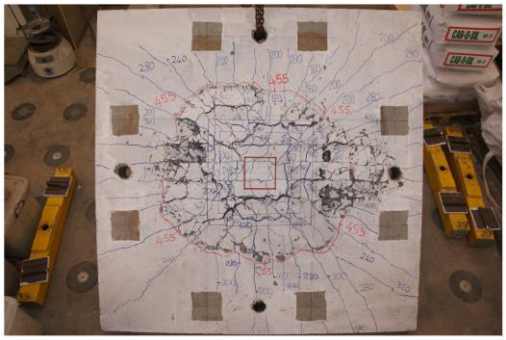

F09-03

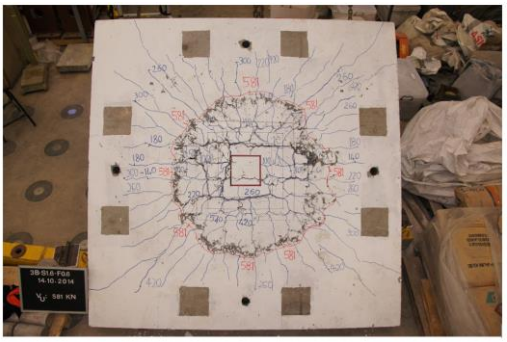

F09-06

F09-09

Fig. A.9 – Unedited photos of F09-series specimens

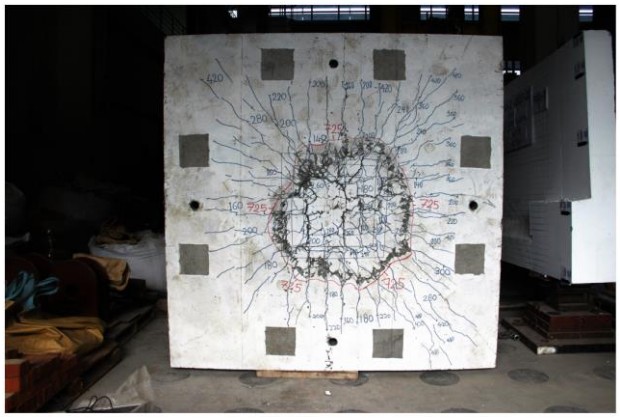

F09-12

Fig. A.10 (continued)

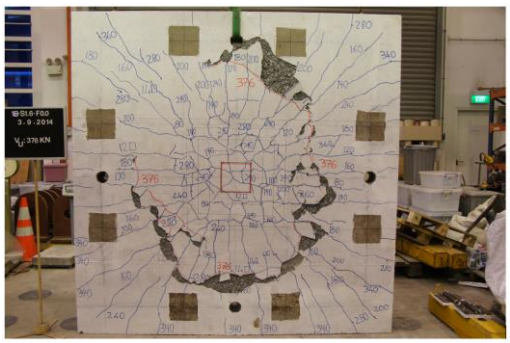

F14-00

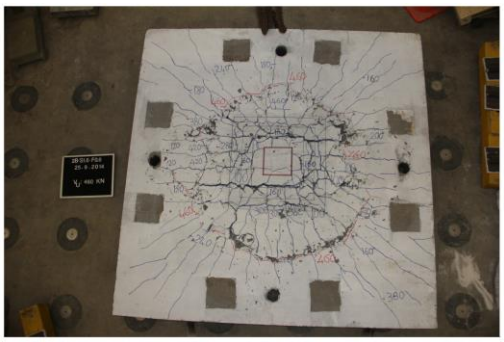

F14-03

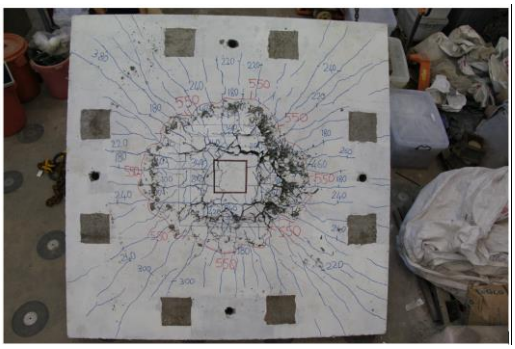

F14-06

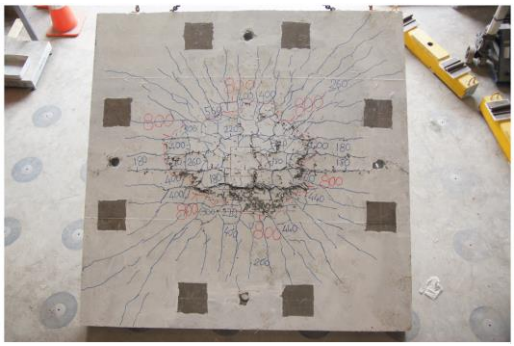

F14-09

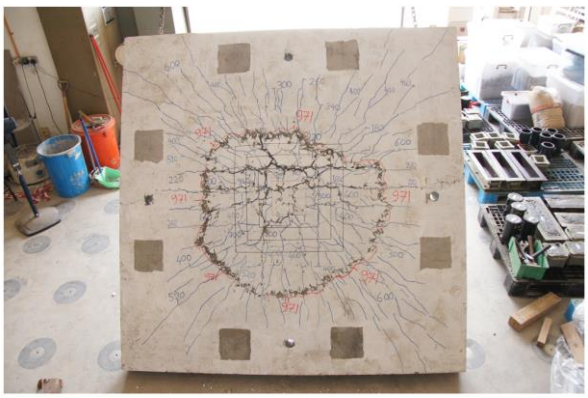

F14-12

Fig. A.11 – Unedited photos of F14-series specimens

F09-00

F09-03

F09-06

F09-09

F09-12

Fig. A.12 – Sawn sections of F09-series specimens

F14-00

F14-03

F14-06

F14-09

F14-09

Fig. A.13 – Sawn sections of F09-series specimens

A.3 Time-lapsed photos of SFRC specimens for crack development observations

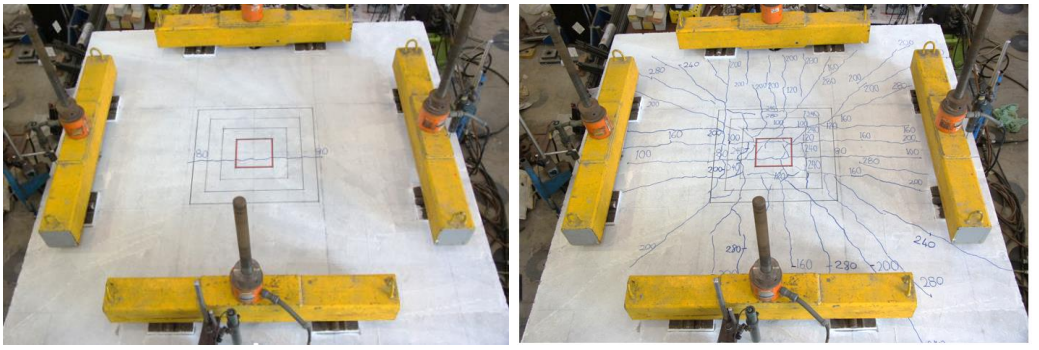

F = 80 kN F=280 kN

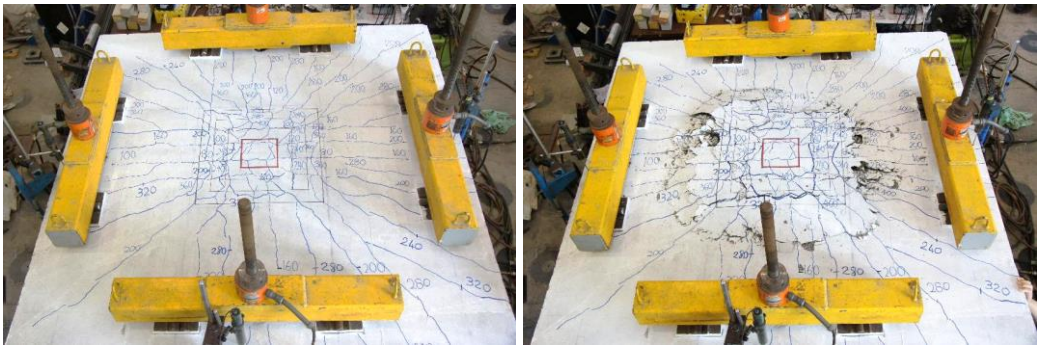

F = 320 kN Maximum Load

Fig. A.14 – Time-lapsed photos of Specimen F09-03

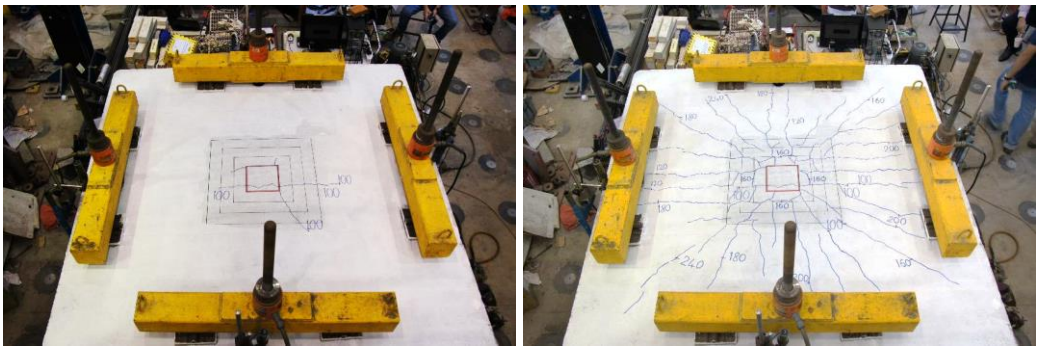

F = 100 kN F=240 kN

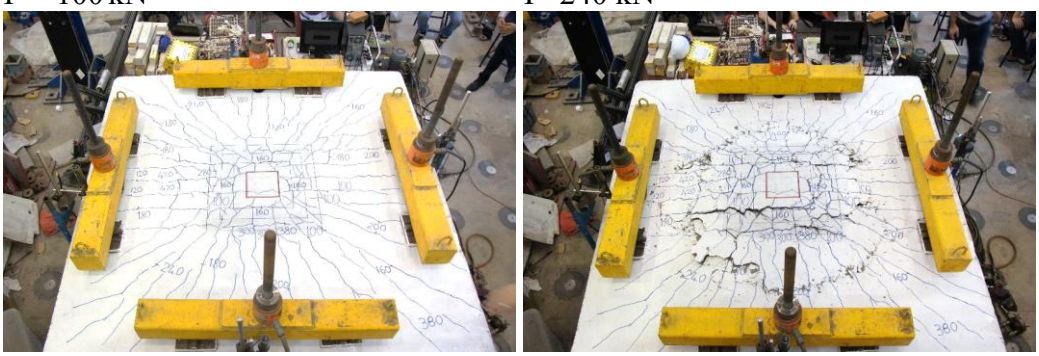

F = 380 kN Maximum Load

Fig. A.15 – Time-lapsed photos of Specimen F14-03

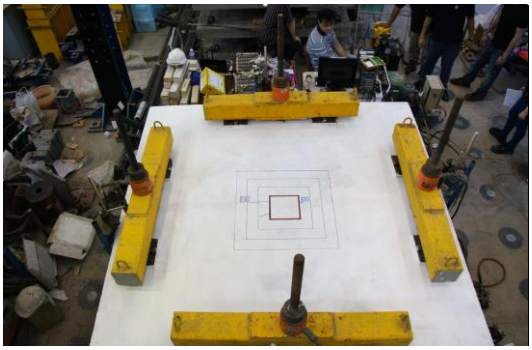
F = 100 kN

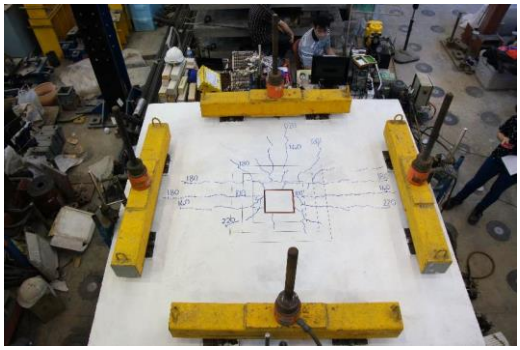
F=220 kN

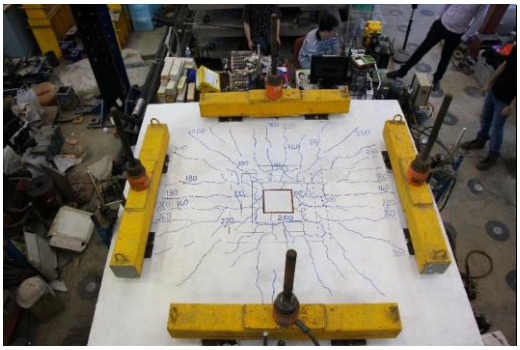
F =320 kN


Maximum Load

Fig. A.16 – Time-lapsed photos of Specimen F09-06

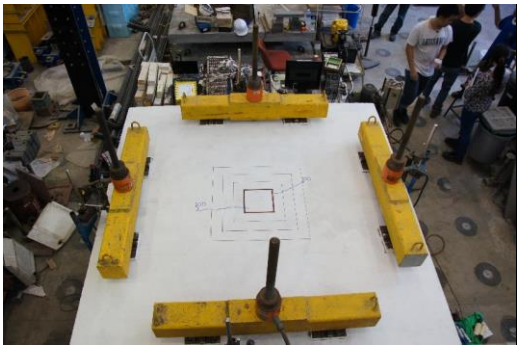
F = 100 kN

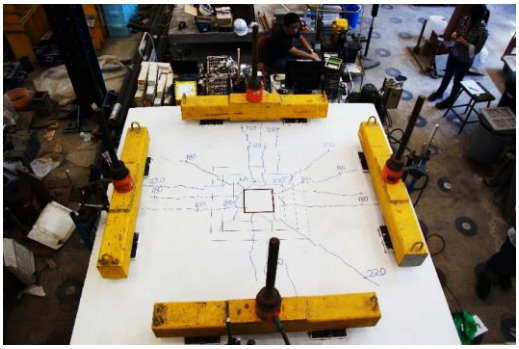
F=220 kN

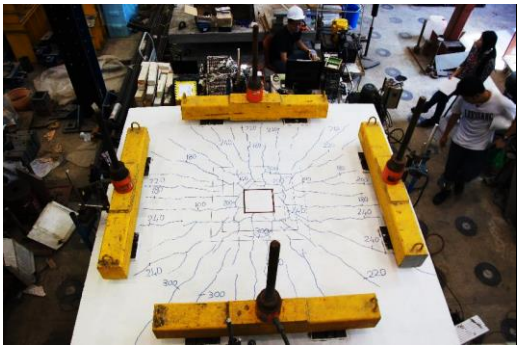
F =320 kN


Maximum Load

Fig. A.17 – Time-lapsed photos of Specimen F14-06

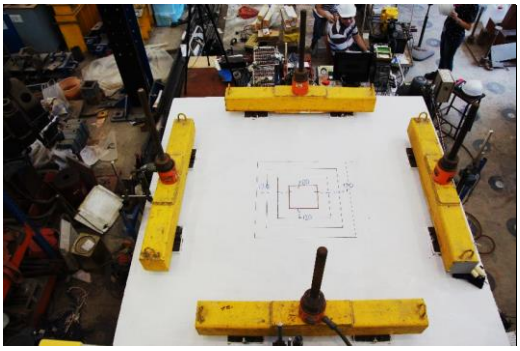

F = 120 kN

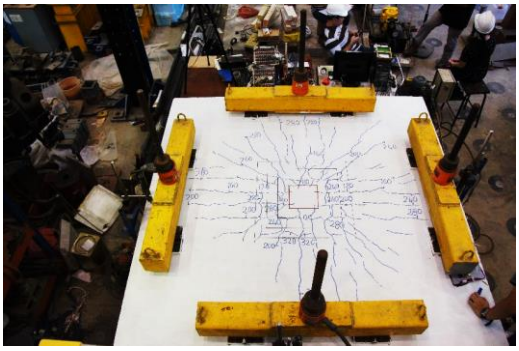

F= 320 kN

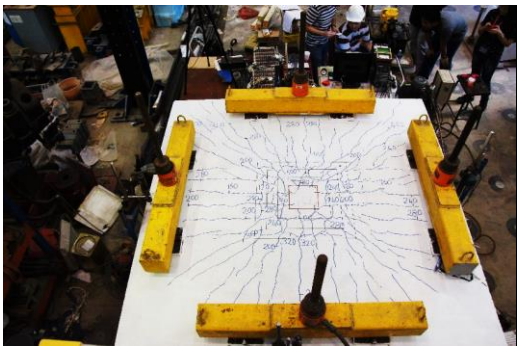

F = 420 kN

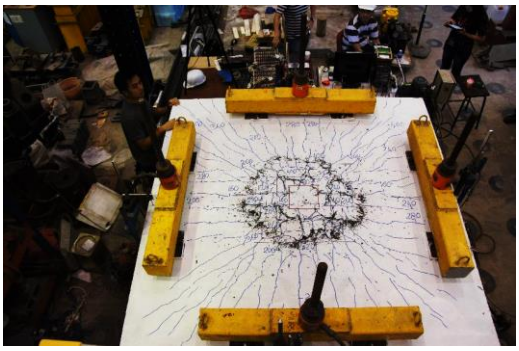

Maximum Load

Fig. A.18 – Time-lapsed photos of Specimen F09-09

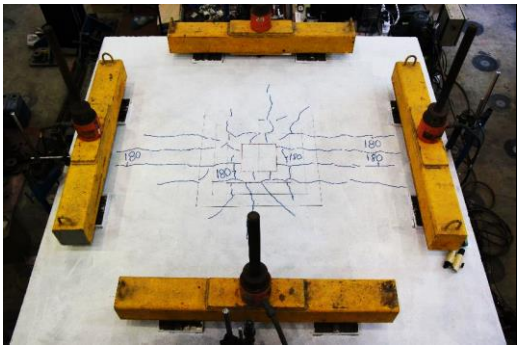

F = 180 kN

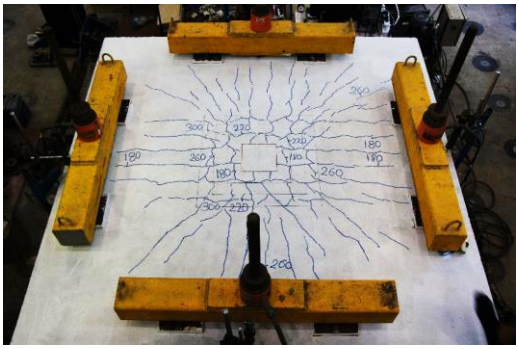

F= 320 kN

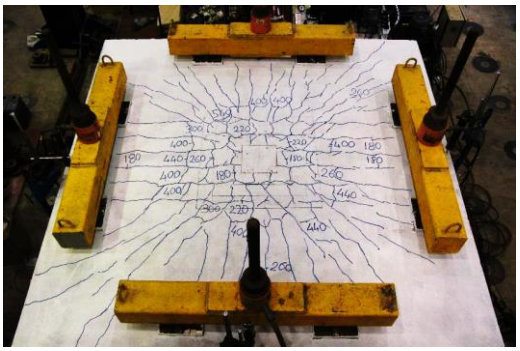

F = 560 kN

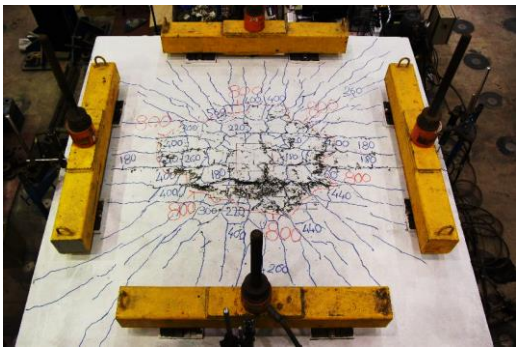

Maximum Load

Fig. A.19 – Time-lapsed photos of Specimen F14-09

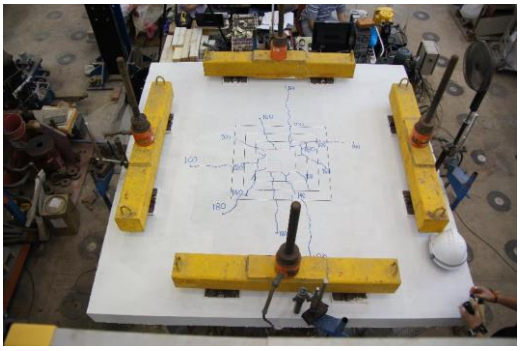
F = 180 kN

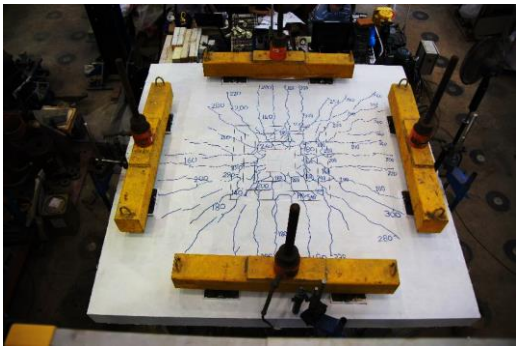
F= 360 kN

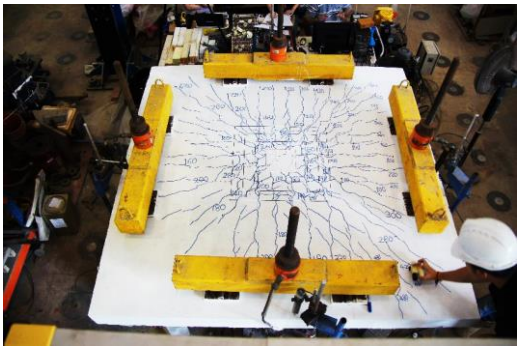
F = 560 kN

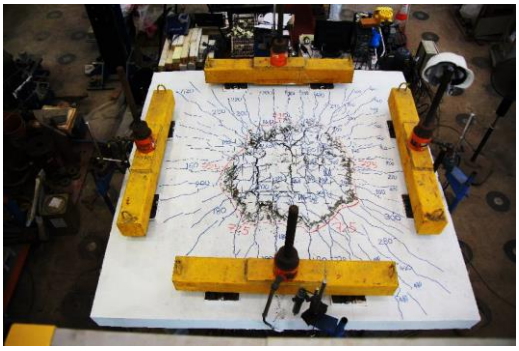
Maximum Load

Fig. A.20 – Time-lapsed photos of Specimen F09-12

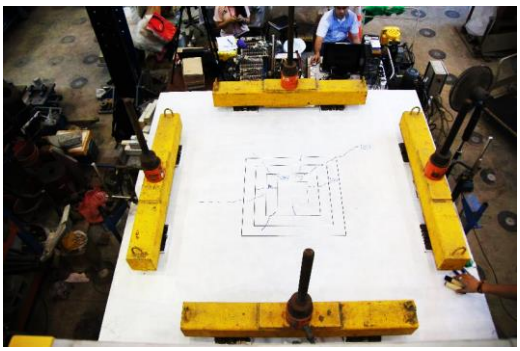
F = 180 kN

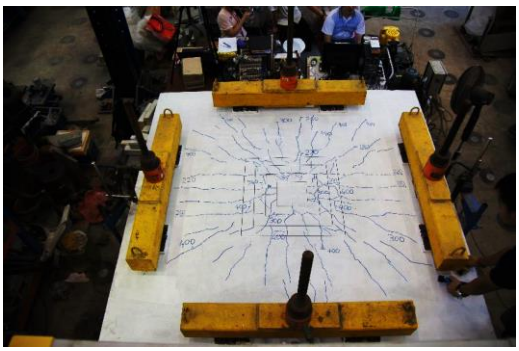
F= 400 kN

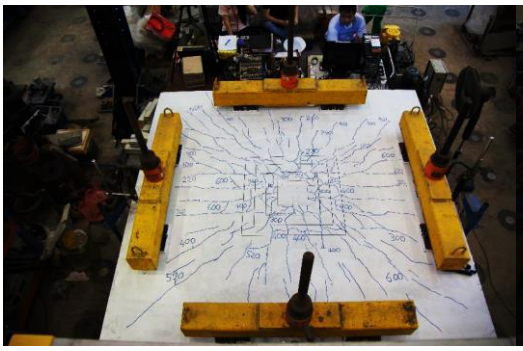
F = 600 kN

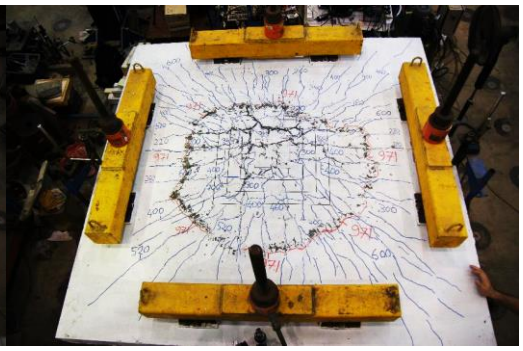
Maximum Load

Fig. A.21 – Time-lapsed photos of Specimen F14-12

Appendix B

EXPERIMENTAL DATA

Appendix B contains numerical experimental data obtained from each test of the specimen, the following data were analysed and presented in graphical and tabular formats as shown in the main thesis.

B.1 Crack width measurements

Figs. B.1 to B.2 show the load vs crack width relationships of all 22 specimens. The crack widths were measured in a region about 100 mm away from a column face.

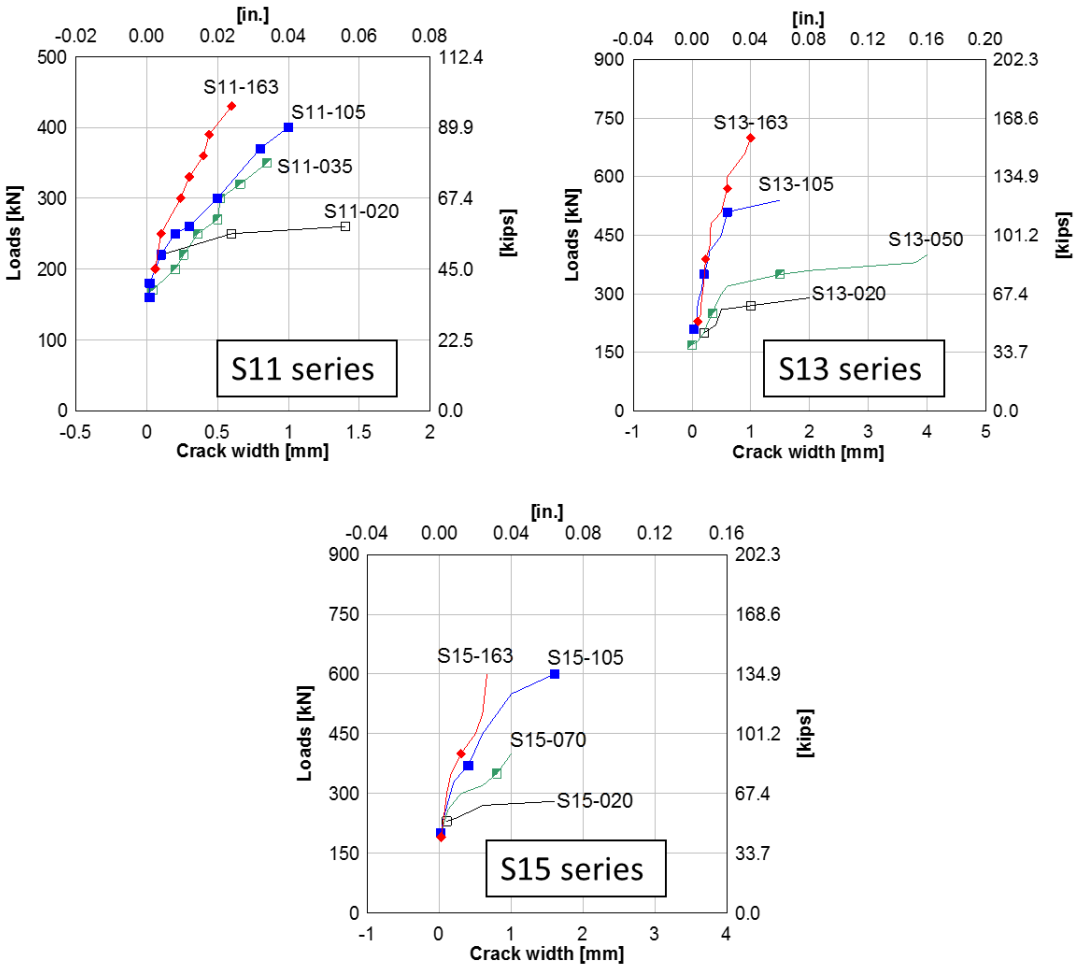

Fig. B.1 – Load-vs-crack width curves of S11 series, S13 series, and S15 series slabs.

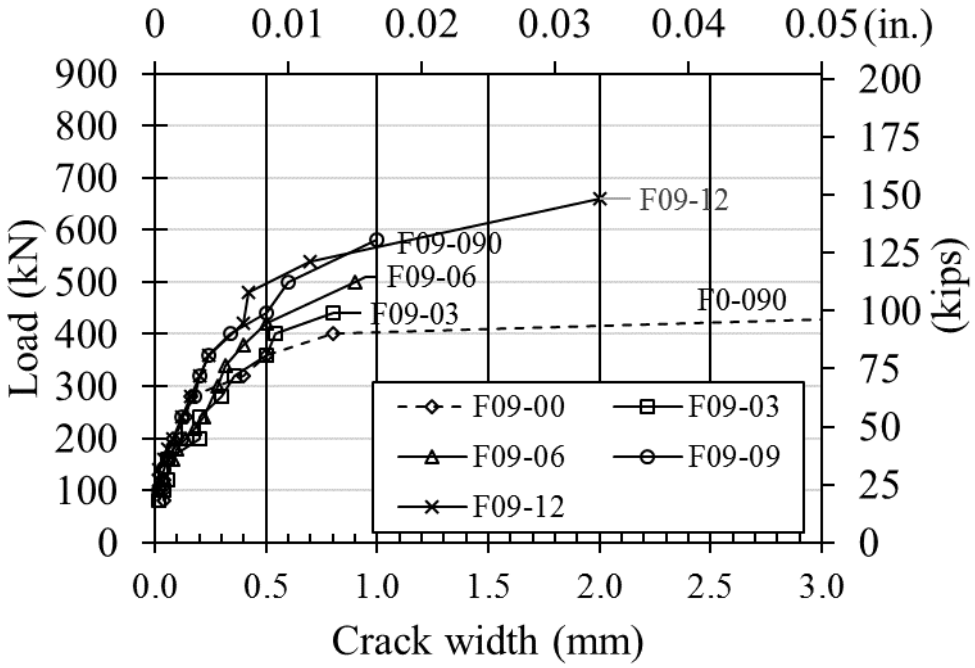

(a)

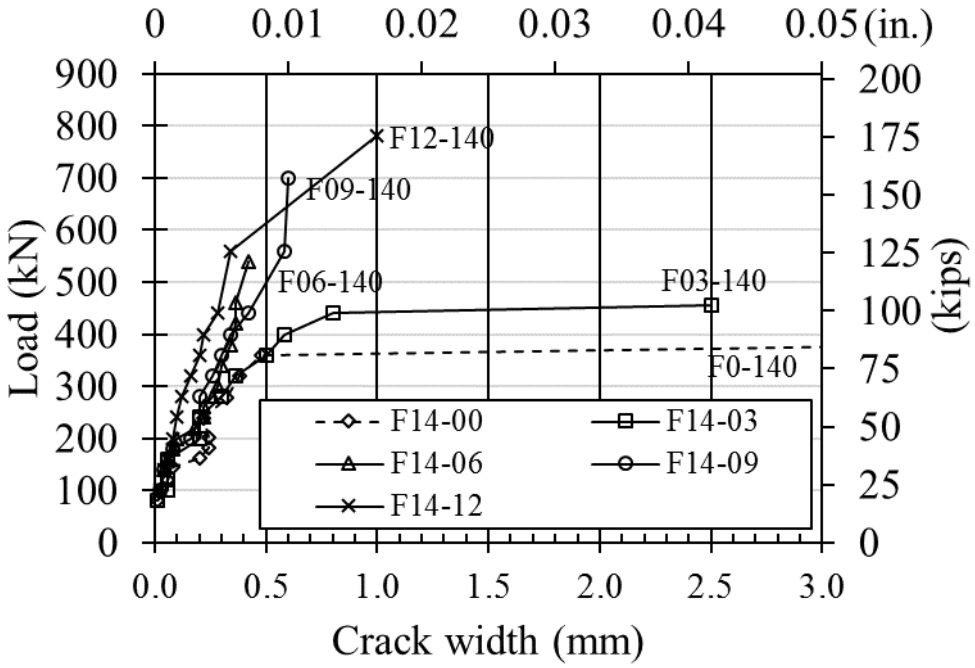

(b)

Fig. B.2 – (a) Load-vs-crack width curves of F09 series slabs, (b) Load-vs-crack width curves of F14 series slabs.

B.2 Strain gauge data for the 12 HSC slabs

Figs. B.3 to B.6 show the positions and labels of strain gauges in the reinforcements. Table B.1 to B.12 show the strain gauge data of the 12 HSC slab specimens (S11 series, S13 series, S15 series sabs).

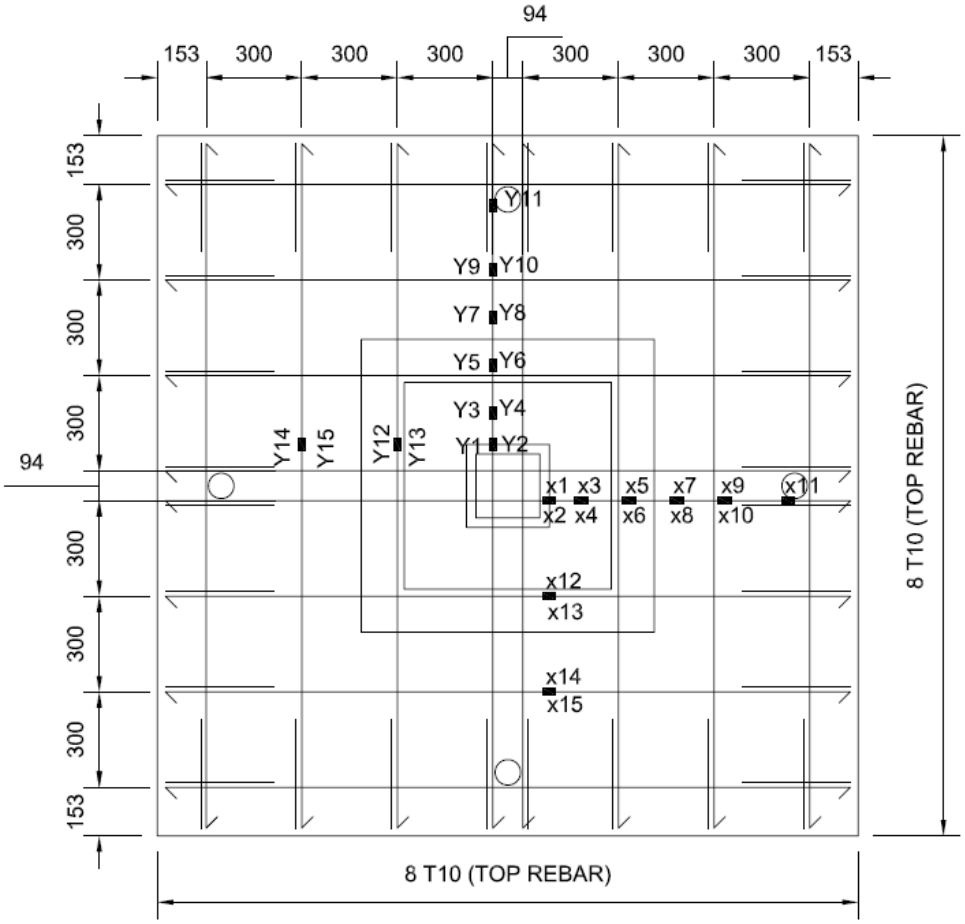

Fig. B.3 – Typical strain gauges' locations and labels for Specimen S11-028, S11-050 (ρ = 0.28% and 0.50%)

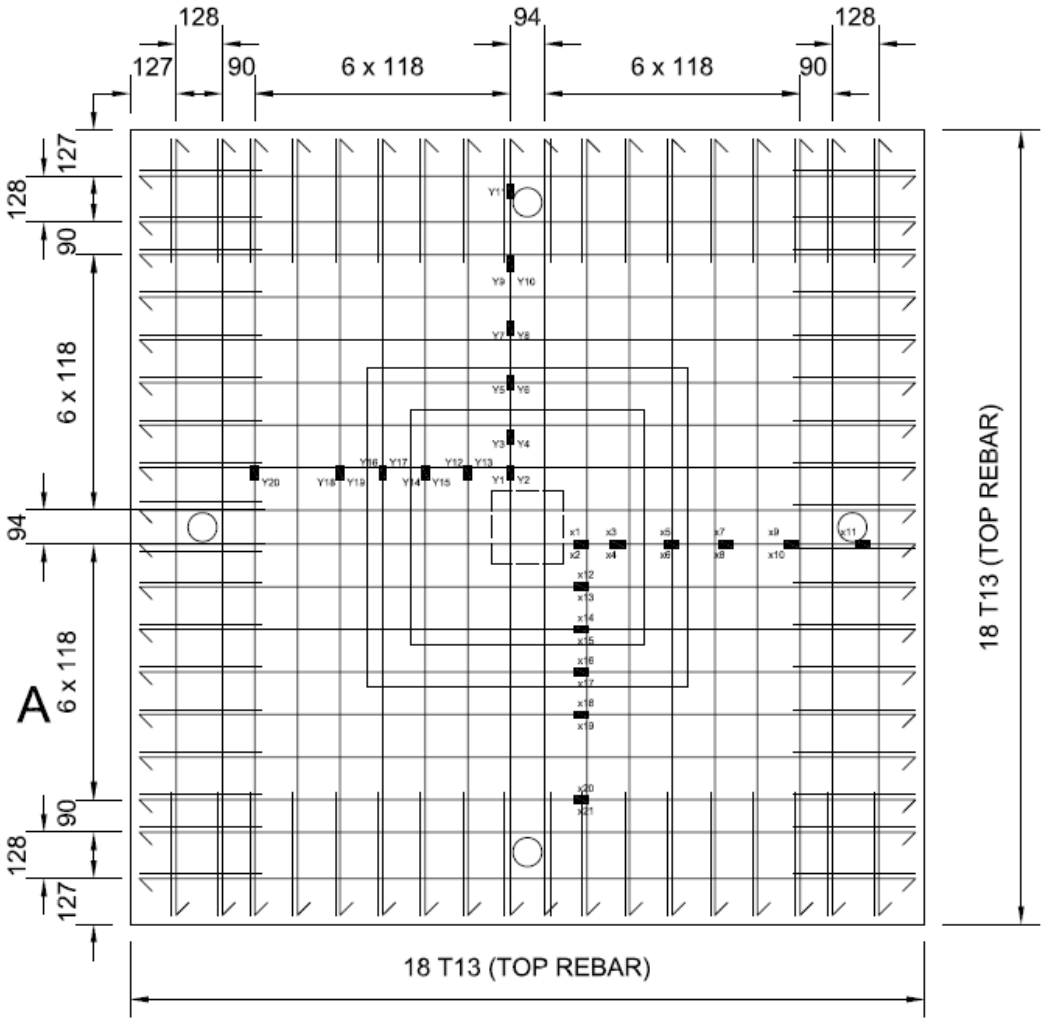

Fig. B.4 – Typical strain gauges' locations and labels for Specimen S11-028, S11-050 (ρ = 0.28% and 0.50%)

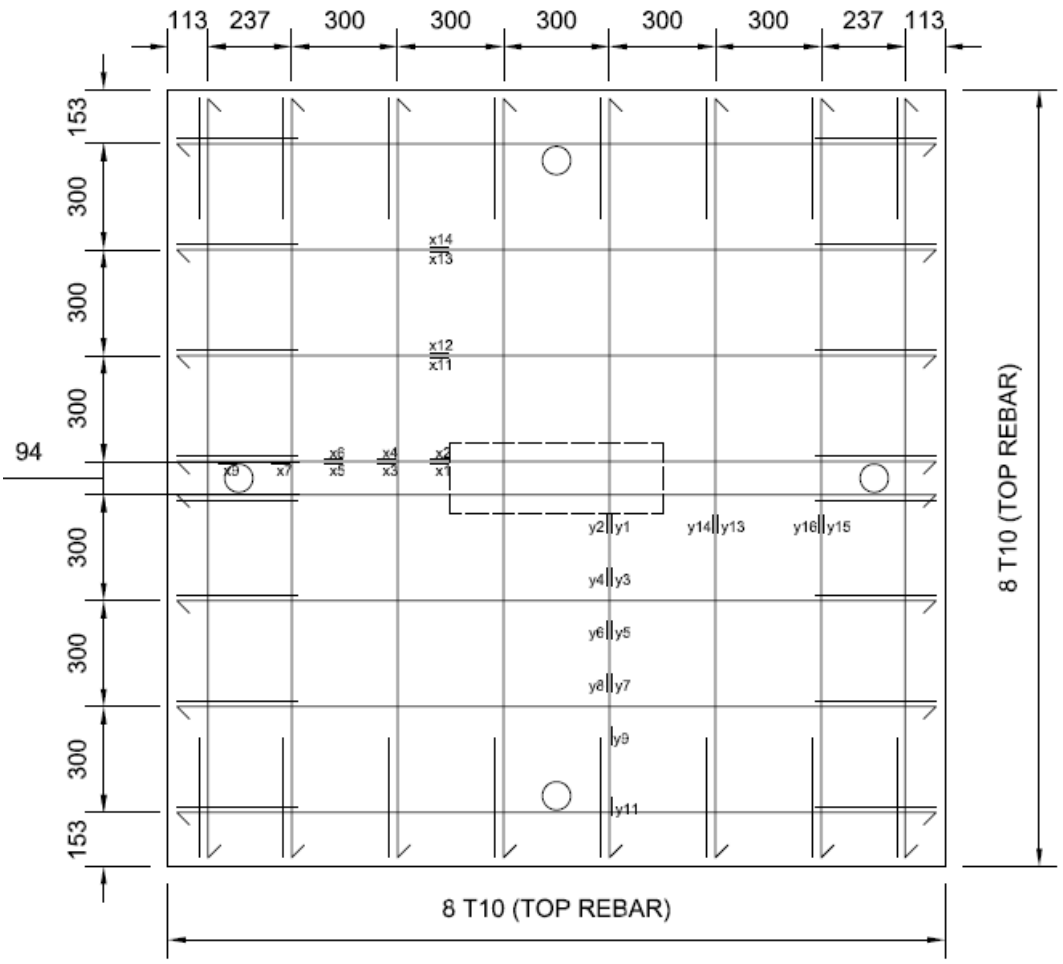

Fig. B.5 – Typical strain gauges' locations and labels for Specimen S13/15-028, S13/15-050 (ρ = 0.28% and 0.50%)

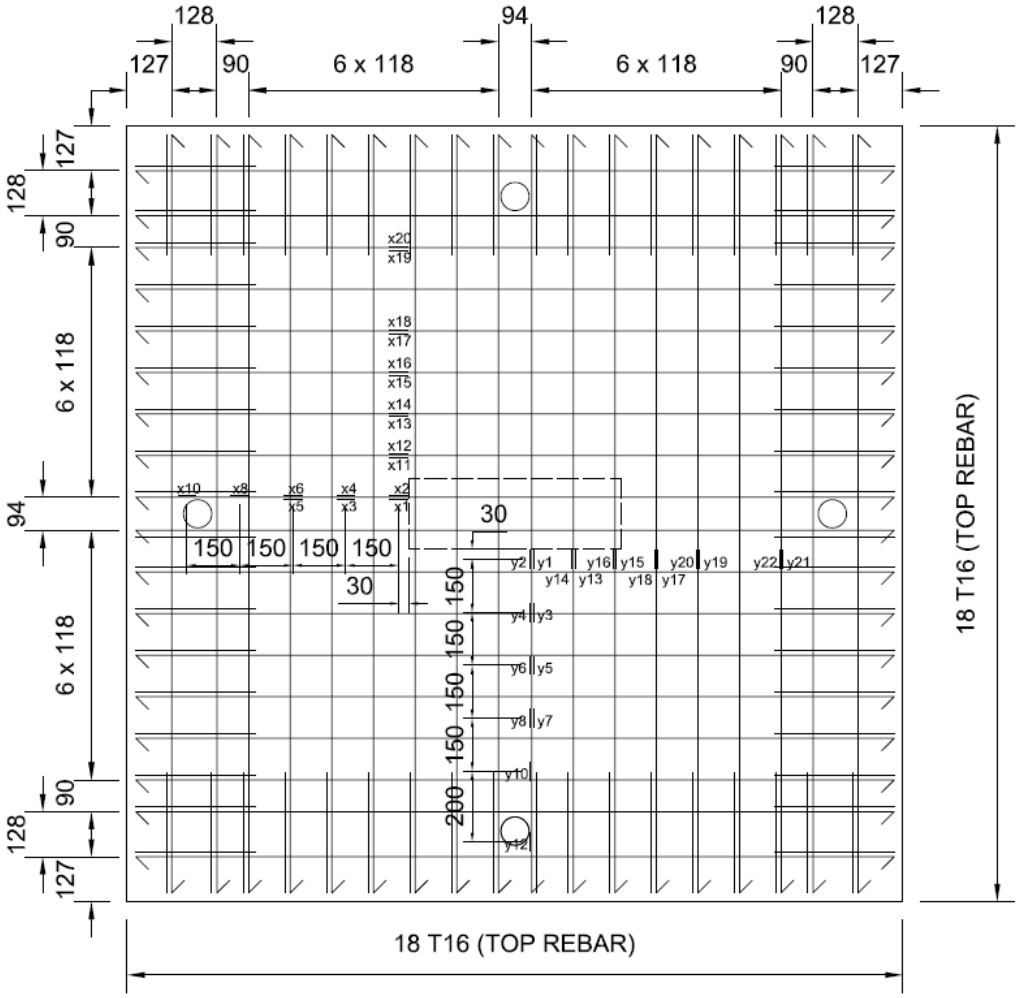

Fig. B.6 – Typical strain gauges' locations and labels for Specimen S13/15-090, S13/15-139/143 (ρ = 0.90% and 0.139% or 0.143%)

Table B.1 – Strain gauge data of Specimen S11-028

Type of strains		Radial strains											Tangential strains					
Location from column centre (mm)		130	230	380	530	680	30	130	280	430	580	780	47	347	647	47	347	647
Step	Load	x1x2	x3x4	x5x6	x7x8	x9x10	y1y2	y3y4	y5y6	y7y8	y9y10	y11	x1x2	x12x13	x14x15	y1y2	y12y13	y14y15
	kN	($\times10^{-6}$)	($\times10^{-6}$)	($\times10^{-6}$)	($\times10^{-6}$)	($\times10^{-6}$)	($\times10^{-6}$)	($\times10^{-6}$)	($\times10^{-6}$)	($\times10^{-6}$)	($\times10^{-6}$)	($\times10^{-6}$)	($\times10^{-6}$)	($\times10^{-6}$)	($\times10^{-6}$)	($\times10^{-6}$)	($\times10^{-6}$)	($\times10^{-6}$)
1	**0**	0	0	0	0	0	0	0	0	0	0	0	0	0	0	0	0	0
2	**10**	4	-0.5	-3	0	-1.5	12	4.5	2	2.5	0.5	5	4	0.5	5	12	-2	4
3	**25**	10.5	1.5	-0.5	0.5	-1	18.5	8	3.5	4.5	1	6	10.5	5.5	11	18.5	1	7
4	**80**	20	6	0.5	2	0.5	24.5	12.5	4.5	5.5	0	6	20	11.5	15	24.5	5	10
5	**95**	30	10	3.5	2.5	0	31	16.5	7	6	0	5	30	17	19	31	11	14
6	**110**	39.5	14.5	7	4.5	0.5	37	21.5	9.5	7	0.5	5	39.5	24.5	24	37	16.5	18
7	**125**	45.5	14	6	1.5	-4	39.5	22.5	6.5	4	-3.5	1	45.5	26	24.5	39.5	18.5	17.5
8	**175**	68.5	24.5	14	6	-1	54.5	32	11.5	8.5	-2	5	68.5	41	35.5	54.5	30.5	26.5
9	**195**	86	32	20	9	0	66	39.5	15.5	8.5	-0.5	6	86	53	45	66	40	33
10	**215**	138	83	71.5	55	-22	96	19.5	-2	-3.5	-8.5	3	138	58.5	53	96	49	67
11	**225**	537	12.5	159.5	-25	-31	793	289	-23.5	52.5	22	29	537	67	83	793	499	521.5
12	**250**	946.5	274	188	-47	-2	1013.5	437	-75	89	17.5	66	946.5	76	93	1013.5	786	821
13	**250**	942	543.5	226	-59.5	-17	1210	544	-52	76	23.5	73	942	82.5	99.5	1210	913	989.5
14	**250**	1321	779.5	312	-46.5	-22	1595	1084	16	120	18.5	74	1321	86.5	103.5	1595	923	986
15	**260**	1487	1091.5	430.5	-15.5	-11	1756	1872.5	1700.5	359	305.5	69	1487	101	124	1756	1145	1029.5
16	**265**	1506	1156.5	496.5	-22.5	22	0	2261	2154	1867	1756	125	1506	137	133.5	0	1342	1100.5
17	**260**	1799	1362	703	14.5	69.5	0	2296.5	2304	2122	2105.5	172	1799	752.5	142	0	1347	1087.5
18	**255**	2268	1425	1881	551.5	164.5		2337	2627	2360.5	2338	214	2268	2664	3222	0	1360.5	1069.5
19	**260**	3340	1854	2501.5	1738	545.5	0	2390	3384	2655	2662.5	265	3340	2862.5	3142.5	0	1435.5	1099.5
20	**260**	5421	2073.5	2798	2075	780		2351	3437	2729.5	2813	294	5421	2919.5	3120.5	0	1455	1105
21	**265**	0	2422.5	3042.5	2413.5	1028	0	2075	3456	2761	2989	335	0	2992	3026	0	1498.5	1121.5
22	**270**		2391.5	3082	2542.5	1146	0	1835	3513	2818	3069.5	355	0	2972	3059.5	0	1512	1130.5
23	**265**	0	2463	3326	2689	1300	0	0	3532	2839	3118.5	341	0	3128	3089	0	1520.5	1125
24	**265**	0	1810	3380.5	2756	1440.5	0	0	0	2867.5	3127.5	338	0	3528.5	3044	0	1535	1128.5
25	**250**	0	2553.5	5668.5	3068	1927	0	0	0	3014.5	3269	372	0	4667	3100.5	0	1543.5	1130

Table B.2 – Strain gauge data of Specimen S11-090

Type of strains		Radial strains												Tangential strains					
Location from column centre (mm)		130	230	380	530	680	880	30	130	280	430	580	780	47	347	647	47	347	647
Step	Load	x1x2	x3x4	x5x6	x7x8	x9x10	x11	y1y2	y3y4	y5y6	y7y8	y9y10	y11	x1x2	x12x13	x14x15	y1y2	y12y13	y14y15
	kN	($\times10^{-6}$)	($\times10^{-6}$)	($\times10^{-6}$)	($\times10^{-6}$)	($\times10^{-6}$)	$\times10^{6}$	($\times10^{-6}$)	($\times10^{-6}$)	($\times10^{-6}$)	($\times10^{-6}$)	($\times10^{-6}$)	($\times10^{-6}$)	($\times10^{-6}$)	($\times10^{-6}$)	($\times10^{-6}$)	($\times10^{-6}$)	($\times10^{-6}$)	($\times10^{-6}$)
1	0	0.5	3.5	0	1	1.5	0	3.5	0	3.5	2.5	5.5	4.5	0.5	3	3.5	3.5	6.5	3.5
2	30	6.5	10.5	3	3	1	-17	11.5	29	11.5	7.5	11	7.5	6.5	12	10.5	11.5	19	8
3	75	16.5	18	8	4	2	-15	16	66	16	10	12	8	16.5	19	18	16	25	14.5
4	95	24.5	23.5	11	5	2	-18	22	73	22	12	12.5	8	24.5	27	24	22	30.5	18.5
5	115	34	31	17	6.5	1	-26	27	85	27	16	14	8	34	35	32	27	37	20
6	135	40.5	35.5	21	8.5	1	-33	32.5	94	32.5	19	16	9	40.5	43	37.5	32.5	45	21
7	165	45	45	26	13.5	-0.5	-36	18.5	80	18.5	10	11	5	45	49	45.5	18.5	52.5	34.5
8	175	28.5	7.5	-1	48	5	-53	31.5	103	31.5	15	13	6	28.5	53	50.5	31.5	46	23.5
9	190	23.5	6.5	10	59	19.5	-54	36.5	121	36.5	16.5	14	5.5	23.5	65	62	36.5	53.5	31.5
10	210	47.5	19.5	85	63.5	20	-68	44	142	44	11	6	-3	47.5	52	65.5	44	64	35.5
11	220	141.5	66.5	123	68.5	15	-72	34.5	236	34.5	2	-0.5	-8	141.5	68	74.5	34.5	71.5	43
12	245	338	115.5	167	86	0.5	-72	47	440	47	-2.5	-10.5	-13.5	338	86	92.5	47	80.5	54.5
13	245	532	147	215	67.5	-3	-105	96	860	96	15	9	6.5	532	99	106	96	126	55.5
14	265	745.5	674	414	169.5	-10	-28	227.5	1234	227.5	31.5	-2.5	-2.5	745.5	95	104.5	227.5	167.5	72
15	275	1171	873.5	521	194	-11	-47	621	1505	621	60.5	17	-8.5	1171	663	1036	621	631	531
16	290	1396	1287.5	739	206	-2.5	-96	1010	2069	1010	107.5	35	-2.5	1396	1078	1489	1010	1275	1036
17	300	1422	1488	914	227	40.5	-84	1233	2251	1233	166	55	10.5	1422	1207	1592.5	1233	1339.5	1058.5
18	315	1687	1755	1206	262.5	54	-99	1584.5	2544	1584.5	309	73	18.5	1687	1646	1951	1584.5	1632	1365.5
19	330	2286	2212	1514	445.5	123	-66	1818.5	2775	1818.5	472.5	101.5	35.5	2286	2287	1986.5	1818.5	1704	1575.5
20	335	2236	2191	1369	843.5	351	-28	1901.5	2911	1901.5	467	140	44	2236	2375	2090	1901.5	1672.5	1728
21	340	2431	25115	1576	1175.5	601	34	2192.5	3347	2192.5	579	176	49	2431	2646	2244.5	2192.5	1715	2362
22	355	2518	2913	1837	1520	892.5	51	2624	3363	2624	767	248	61.5	2518	2756	2420.5	2624	15915	2552
23	360	0	1363	0	2101.5	1390.5	231	3036.5	3856	3036.5	1164	447	116	0	2578	2416	3036.5	1578	2633.5
24	370	0	1397.5	0	2524	1899.5	642	3096.5	3937	3096.5	1460.5	537	153	0	2580	2597.5	3096.5	1674.5	3021
25	375	0	0	0	2733	2241	516	3448.5	4060	3448.5	1944.5	791.5	250.5	2600	2650	2735	3448.5	1999.5	3088.5

Table B.3 – Strain gauge data of Specimen S11-090

Type of strains		Radial strains											
Location from column centre (mm)		130	230	380	530	680	880	30	130	280	430	580	780
Step	Load	x1x2	x3x4	x5x6	x7x8	x9x10	x11	y1y2	y3y4	y5y6	y7y8	y9y10	y11
	kN	($\times10^{-6}$)	($\times10^{-6}$)	($\times10^{-6}$)	($\times10^{-6}$)	($\times10^{-6}$)	$\times10^{6}$	($\times10^{-6}$)	($\times10^{-6}$)	($\times10^{-6}$)	($\times10^{-6}$)	($\times10^{-6}$)	($\times10^{-6}$)
1	0	0.5	3.5	0	1	1.5	0	0	0	0	0	0	0
2	30	6.5	10.5	3	3	1	20	13	11	5.5	13	12	12
3	75	16.5	18	8	4	2	20	12.5	10.5	7	12	12	11
4	95	24.5	23.5	11	5	2	35	6	4	3	1	0	-1
5	115	34	31	17	6.5	1	105	23	17	11	5	0	-5
6	135	40.5	35.5	21	8.5	1	155	31.5	25.5	16	7	0	-9
7	165	45	45	26	13.5	-0.5	160	30.5	31.5	16.5	7	-1	-10
8	175	28.5	7.5	-1	48	5	170	37.5	48.5	11	8	-2	-13
9	190	23.5	6.5	10	59	19.5	195	48	79.5	28.5	-24	-1	-23
10	210	47.5	19.5	85	63.5	20	215	68.5	108.5	40.5	-47	1	-97
11	220	141.5	66.5	123	68.5	15	240	101.5	132	54	-87	4	-148
12	245	338	115.5	167	86	0.5	245	120.5	142	58	-100	6	-170
13	245	532	147	215	67.5	-3	260	283.5	202	67.5	-115	7	-198
14	265	745.5	674	414	169.5	-10	265	371.5	232.5	67	-100	3	-175
15	275	1171	873.5	521	194	-11	280	460	296	77	-106	4	-151
16	290	1396	1287.5	739	206	-2.5	300	549	342.5	91.5	-111	3	-144
17	300	1422	1488	914	227	40.5	295	570	364.5	107.5	-122	4	-133
18	315	1687	1755	1206	262.5	54	300	584	382	116.5	-126	5	-117
19	330	2286	2212	1514	445.5	123	365	1473	959	564.5	-63	20	-77
20	335	2236	2191	1369	843.5	351	390	1879	1387	761.5	-27	26	-55
21	340	2431	25115	1576	1175.5	601	400	2007	1601	819	-16	27	-53
22	355	2518	2913	1837	1520	892.5	415	2180	1827.5	960	47	32	-40
23	360	0	1363	0	2101.5	1390.5	400	2182	1863	976	70	33	-37
24	370	0	1397.5	0	2524	1899.5	400	2181	1863.5	977	70	33	-37
25	375	0	0	0	2733	2241	400	2181	1863	976.5	70	33	-37
26	140	0	0	0	1919.5	1868.5	405	2169	2081.5	1153.5	218	32	-27
27	165	0	0	0	1967.5	1872	215	1088	1105.5	656.5	2111	263	17

Table B.3 – Strain gauge data of Specimen S1-090 (Continued)

Type of strains		**Tangential strains**											
Location from column centre (mm)		**65**	**183**	**301**	**419**	**537**	**773**	**65**	**183**	**301**	**419**	**537**	**773**
Step	x1x2	**x12x13**	**x14x15**	**x16x17**	**x18x19**	**x20x21**	**y1y2**	**y12y13**	**y14y15**	**y16y17**	**y18y19**	**y20**	**y11**
	kN	**(×10^{-6})**	**(×10^{-6})**	**(×10^{-6})**	**(×10^{-6})**	**(×10^{-6})**	**×10^{6}**	**(×10^{-6})**	**(×10^{-6})**	**(×10^{-6})**	**(×10^{-6})**	**(×10^{-6})**	**(×10^{-6})**
1	0	0	0	1	0	1	1	0	-0.5	-0.5	0	0	0
2	30	13	9	0	-25	-25.5	-26	13.5	0.5	11.5	13	0.5	9
3	75	12.5	8	-1.5	-23.5	-23	-21.5	13	1	11	12.5	0.5	9
4	95	6	5	9.5	0	0	-2	10	5.5	5.5	5.5	2	2
5	115	23	27	26	16	15	2.5	24	18.5	17.5	17.5	11.5	9
6	135	31.5	39	37	25	23.5	5.5	37.5	30.5	28	27	18.5	17
7	165	30.5	46	41.5	30.5	27	7.5	40	31	39.5	38.5	25.5	19
8	175	37.5	53	47.5	33	29	6.5	85	36.5	39.5	46.5	33.5	26
9	190	48	75	69.5	50	44.5	13.5	168.5	60.5	54	58.5	55	57
10	210	68.5	96	88	69	63	22.5	264.5	110.5	87	79	73.5	82
11	220	101.5	174	99	77	60.5	23.5	539	258	177	153.5	165	145
12	245	120.5	246	127.5	70	66	24	615	301.5	202.5	180.5	201	182
13	245	283.5	546	306.5	68	71.5	33.5	813	475	218	199.5	242	242
14	265	371.5	622	354.5	70.5	77.5	37	979	597	264	244	295	305
15	275	460	773	457	79	87	39.5	1358	775.5	318	274.5	324	334
16	290	549	888	543.5	86	97.5	46	1724.5	878	364.5	311	353.5	356
17	300	570	961	615	83.5	102	45	1937.5	1412	979	1166	1110.5	925
18	315	584	982	637	85.5	104.5	47.5	2131	1657	1162	1396.5	1294.5	1055
19	330	1473	1678	1578.5	1274	1372.5	547	3024.5	2463	1727.5	1866	1533	1233
20	335	1879	1978	1752.5	1538	1657.5	535.5	6192.5	2995	1940	2088.5	1673	1312
21	340	2007	2120	1889.5	1644.5	1639.5	554	8724.5	3190	2001.5	2168	1723.5	1347
22	355	2180	2298	1995	1695	1615.5	548.5	4579.5	4071	2123.5	2310	1802.5	1401
23	360	2182	2317	2011	1698	1607	546.5	4144	3999.5	2033	2222.5	1724.5	1339
24	370	2181	2316	2005.5	1692.5	1604	544	4140.5	3999.5	2032	2221.5	1724.5	1339
25	375	2181	2316	2005.5	1693.5	1605.5	545.5	4138	3999	2031.5	2221.5	1724	1340
26	140	2169	2504	2126	1791	1688	566.5	4283	6618.5	2086	2285	1746	1380
27	165	1088	919	1240.5	1137.5	1066.5	344.5	4008.5	5821	1349	1345	1064	869

Table B.4 – Strain gauge data of Specimen S11-139

Type of strains		Radial strains											
Location from column centre (mm)		130	230	380	530	680	880	30	130	280	430	580	780
Step	Load	x1x2	x3x4	x5x6	x7x8	x9x10	x11	y1y2	y3y4	y5y6	y7y8	y9y10	y11
	kN	($\times10^{-6}$)	($\times10^{-6}$)	($\times10^{-6}$)	($\times10^{-6}$)	($\times10^{-6}$)	$\times10^{6}$	($\times10^{-6}$)	($\times10^{-6}$)	($\times10^{-6}$)	($\times10^{-6}$)	($\times10^{-6}$)	($\times10^{-6}$)
1	0	0	0	0	1	0	0	0	0	0.5	0	-0.5	0
2	20	3	3.5	1.5	4.5	8	0	1	5.5	2	0.5	0.5	2
3	40	11.5	14.5	4	7	7	1	10	15	5.5	2	1	0
4	120	34.5	37	10	16	8	2	48	30.5	11.5	5.5	1	0
5	165	47	51.5	12.5	25.5	10	0	74	40	15	8.5	0	0
6	205	76	98	18.5	45	8	15	81	29	10	5	-6	-5
7	225	91.5	142.5	17	16.5	9	26	161	155	12	10.5	-3.5	-7
8	245	156.5	184.5	23	15	2	30	414	68.5	5	27	-3.5	-7
9	260	350	332.5	23.5	17	-6	27	604	179	2.5	41	-7	21
10	280	465.5	411.5	24.5	32	-12	33	769.5	267.5	12.5	72.5	-7.5	47
11	295	594.5	491	11.5	58	-8	33	908	346	17	68.5	5.5	57
12	315	919	934	-2.5	111.5	-5	36	1530	725.5	65.5	38	20	63
13	335	975	1007.5	20	162.5	-3	37	1637.5	813	76	71.5	19	73
14	345	499	1090	45.5	217	5	37	1821	1017.5	156.5	45.5	40.5	121
15	365	542	1168.5	84	241	8	37	1798.5	1155	200	79.5	40.5	116
16	370	577	1326	177	310	36	48	2090	1390.5	299.5	114.5	54	131
17	385	604	1411	230	346	33	37	2196.5	1513	364.5	121	55	140
18	400	679	1553	306	393.5	54	57	2439.5	1741	505	143	62.5	138
19	430	746	1644	449.5	458.5	82	82	2702	2085	614	176	69	159
20	440	1743	1902.5	628.5	832	177	145	3380.5	2537	793	289	85	163
21	435	1734	1898.5	625.5	835.5	178	146	3418.5	2172	803	295	86	163
22	430	1142	1229.5	627.5	842	211	173	3501.5	5094	2026	740.5	106.5	133
23	230	1073	1127.5	622.5	831	211	177	3019	435	1271.5	733.5	105.5	132
24	225	1049	1163	644.5	834	215	180	3172	-61	1333.5	735.5	106.5	131
25	240	1013	1335	563.5	885	228	192	4040	-1387	2562	796	113	131

Table B.4 – Strain gauge data of Specimen S11-139 (Continued)

Type of strains		**Tangential strains**											
Location from column centre (mm)		**65**	**183**	**301**	**419**	**537**	**773**	**65**	**183**	**301**	**419**	**537**	**773**
Step	x1x2	**x12x13**	**x14x15**	**x16x17**	**x18x19**	**x20x21**	**y1y2**	**y12y13**	**y14y15**	**y16y17**	**y18y19**	**y20**	**y11**
	kN	**($\times10^{-6}$)**	**($\times10^{-6}$)**	**($\times10^{-6}$)**	**($\times10^{-6}$)**	**($\times10^{-6}$)**	**$\times10^{6}$**	**($\times10^{-6}$)**	**($\times10^{-6}$)**	**($\times10^{-6}$)**	**($\times10^{-6}$)**	**($\times10^{-6}$)**	**($\times10^{-6}$)**
1	0	0	30	0.5	-4.5	0	0	0	-1	0	0	0	0
2	20	3	72.5	0	6.5	-18.5	-12.5	1	-1	3.5	0.5	0	0
3	40	11.5	88.5	8.5	14.5	-9	-4.5	10	8	9	4.5	1.5	5
4	120	34.5	106.5	31.5	33	9	9	48	31	29	14	0.5	16
5	165	47	112.5	46.5	43.5	18.5	13	74	49	38	35.5	3	26
6	205	76	116.5	69.5	62.5	36.5	32	81	53	38.5	35.5	4	44
7	225	91.5	118	71.5	64.5	40.5	44.5	161	87	59	29.5	9	107
8	245	156.5	269.5	72.5	78	57	69.5	414	220	607.5	352	21.5	151
9	260	350	639.5	106	76.5	67	88	604	458	1207.5	629.5	194.5	161
10	280	465.5	594	157.5	86	125.5	97.5	769.5	601	1342.5	676	384	205
11	295	594.5	628	212.5	98.5	144.5	139	908	883	15105	749.5	421	264
12	315	919	1565	1306.5	1163	1277.5	111.55	1530	1301	1625	828.5	532	397
13	335	975	1619	1490	1321.5	1468	1261	1637.5	1446	1737	879.5	564.5	438
14	345	499	1516	1670	1458	1638.5	1328	1821	1612	1806	918	623	473
15	365	542	1528.5	1798	1577.5	1749.5	1383.5	1798.5	1785	1934	968	661	512
16	370	577	1329.5	1891	1617.5	1763	1367.5	2090	2152	2080.5	1024	714.5	542
17	385	604	1412.5	1936	1661.5	1791	1386	2196.5	2310	2185	1061	739	567
18	400	679	2331	2168.5	1828	1927	1436.5	2439.5	2578	2336	1136.5	817	630
19	430	746	2522	2373.5	1959	2055	1540.5	2702	2805	2467.5	1175	869.5	697
20	440	1743	2893	2731.5	2188.5	2198	1623	3380.5	3280	2866.5	1351.5	1237.5	1632
21	435	1734	2900	2736	2201	22115	1629	3418.5	3284	2867.5	1346	1233.5	1626
22	430	1142	2582	1488.5	1306	1403.5	930	3501.5	6544	1767	847.5	938	1083
23	230	1073	2668	1404	1212.5	1316	881	3019	9171	1663	800	901.5	1019
24	225	1049	2793	1352.5	1169	1276.5	842.5	3172	10995	1600.5	780.5	888	999
25	240	1013	3379	1228	1094.5	1204	779	4040	12674	1529.5	768	870.5	970

Table B.5 – Strain gauge data of Specimen S13-028

Type of strains		Radial strains											Tangential strains					
Location from column centre (mm)		130	230	380	530	680	30	130	280	430	580	780	47	347	647	47	347	647
Step	Load	x1x2	x3x4	x5x6	x7x8	x9x10	y1y2	y3y4	y5y6	y7y8	y9y10	y11	x1x2	x11x12	x13x14	y1y2	y13y14	y15y16
	kN	($\times10^{-6}$)	($\times10^{-6}$)	($\times10^{-6}$)	($\times10^{-6}$)	($\times10^{-6}$)	($\times10^{-6}$)	($\times10^{-6}$)	($\times10^{-6}$)	($\times10^{-6}$)	($\times10^{-6}$)	($\times10^{-6}$)	($\times10^{-6}$)	($\times10^{-6}$)	($\times10^{-6}$)	($\times10^{-6}$)	($\times10^{-6}$)	($\times10^{-6}$)
1	0	0	0	0	0	0	0	0	0	0	0	0	0	0	N/A	0	0	0
2	65	30.5	15	5	0	22	13.5	9.5	9.5	3	1	30.5	21	13	N/A	22	18.5	13
3	90	43.5	19	5	0	31	20.5	13	10.5	4	2	43.5	28	18	N/A	31	25.5	18
4	105	54	23	6	-1	36	21.5	14.5	12	5	2	54	33	20	N/A	36	29.5	20
5	135	73.5	26	2	-4	47	27.5	17	12.5	3	0	73.5	41	24	N/A	47	36	24
6	170	88.5	28	3	-7	57	31.5	18.5	14	2	-2	88.5	47	29	N/A	57	44.5	25
7	190	73	206	-43	-16	71	29.5	16	9	-1	-5	73	53	33	N/A	71	36	26
8	205	-18	233	-57	-165	150	36	17	10.5	-2	-6	-18	66	39	N/A	150	52.5	33
9	220	9	234	-72	-187	239	36	17.5	10	-4	-8	9	72	42	N/A	239	62.5	37
10	235	72.5	254	-90	-191	315	34.5	14	6.5	-9	-11	72.5	81	45	N/A	315	69	40
11	240	214	352	-93	-35	2187	55.5	9	4	-12	-14	214	98	63	N/A	2187	588	73
12	255	235.5	378	-84	6	2542	83	9.5	5	-15	-14	235.5	104	67	N/A	2542	765.5	81
13	265	1460.5	1339	33	-31	20975	1659	476	71.5	-76	10	1460.5	102	69	N/A	20975	1227.5	571
14	280	1810.5	1691	101	-30	19089	2510.5	939.5	192.5	-73	71	1810.5	113	70	N/A	19089	1300	618
15	295	2719.5	1890	1737	230	21005	3467	1573.5	486	29	77	2719.5	127	83	N/A	21005	1487	835
16	300	2809.5	1874	1975	261	13426	3766	1610.5	614.5	72	70	2809.5	127	82	N/A	13426	1618	941
17	300	3297	2227	2474	79	13401	5457.5	1906	1527.5	826	97	3297	129	86	N/A	13401	1684	986
18	305	0	0	0	0	13582	3808	2816	2948	2311	222	0	125	85	N/A	13582	2056.5	1402
19	300	0	0	0	0	13566	5291	0	2998.5	2368	238	0	125	87	N/A	13566	2157	1444

Table B.6 – Strain gauge data of Specimen S13-050

Type of strains		Radial strains											Tangential strains						
Location from column centre (mm)		130	230	380	530	680	30	130	280	430	580	780	47	347	647	777	47	347	647
Step	Load	x1x2	x3x4	x5x6	x7x8	x9x10	y1y2	y3y4	y5y6	y7y8	y9y10	y11	x1x2	x11x12	x13x14	x15x16	y1y2	y13y14	y15y16
	kN	(×10^{-6})	(×10^{-6})	(×10^{-6})	(×10^{-6})	(×10^{-6})	(×10^{-6})	(×10^{-6})	(×10^{-6})	(×10^{-6})	(×10^{-6})	(×10^{-6})	(×10^{-6})	(×10^{-6})	(×10^{-6})	(×10^{-6})	(×10^{-6})	(×10^{-6})	(×10^{-6})
1	5	0	0	0	0	0	0	0	0	0	0	0	0	0	0	0	0	0	0
2	40	3	0.5	0	0	0	11.5	4	2.5	1	0	-2	3	2	1	2	11.5	11.5	3
3	85	6	1	0	-2	-3	25	10	6.5	3	0	-2	6	5	4	3.5	25	25	8.5
4	160	11.5	2.5	-0.5	-7	-6	58.5	19	10.5	5.5	0	-4	11.5	10.5	8.5	7.5	58.5	46.5	23.5
5	175	39	56	-4.5	-36	-22	368.5	21.5	10.5	4.5	-3	-7	39	26.5	21.5	17.5	368.5	333	18.3
6	200	52.5	64	-4	-30	-4	555	31	16.5	8.5	-2	-8	52.5	36	28.5	21	555	532.5	286
7	220	82.5	73.5	-2.5	-32	0	674	36	19	9.5	-3	-8	82.5	49.5	37	28	674	653.5	351
8	235	110	77.5	-3	-37	-1	796.5	53	22.5	10.5	-5	-9	110	60.5	44.5	32	796.5	809	441
9	265	446	64.5	-11.5	-53	-8	1183	93	32.5	14	-7	-11	446	132	77	49	1183	1417.5	782
10	290	823.5	171	237.5	74	-44	2008.5	642	64	97.5	163	-192	823.5	752.5	450	304	2008.5	2190.5	993.5
11	340	1659	597.5	555	186	89	3933	1487.5	680	208.5	314	-184	1659	1714.5	1276.5	1246.5	3933	3590	1279
12	370	2151.5	1493.5	1203	265	171	6356	2105.5	2511	397.5	352	-142	2151.5	2077	1507	1446	6356	6936	1421
13	390	2352	1707.5	1322.5	307	155	6200	2091.5	2670.5	405.5	348	-129	2352	1880.5	1309.5	1288.5	6200	6666	1489
14	400	2905	2361.5	1725.5	511	156	6423	2265	3779	460.5	358	-54	2905	2074.5	1457.5	1431.5	6423	7031	1699
15	420	3241	2615.5	2156	1512	-131	6728	2618	5312.5	637	381	-20	3241	2371	1640.5	1567.5	6728	7234	1771.5
16	425	3268	2696.5	2297	1832	-281	6748	2867.5	5877	691	375	-7	3268	2437	1678	1617	6748	7302	1683.5
17	430	3177	2626	2484.5	1709	196	6846	3001.5	6059	726.5	375	-3	3177	2532	1732	1660.5	6846	7393	1738.5
18	445	0	2568.5	2922.5	1756	865	0	3289	6202	754	377	-2	0	2728.5	1768	1664.5	0	7569	0
19	360	0	0	0	1515	9928	0	7834	0	2019.5	1218	32	0	3241.5	2007.5	1652	0	6683	0
20	275	0	0	0	1641	8965	0	0	0	1528.5	1183	37	0	3359	0	0	0	6104	0
21	75	0	0	0	2194	8427	0	0	0	1408	1086	58	0	0	0	0	0	0	0
22	5	0	0	0	1703	6386	0	0	0	1021.5	871	78	0	0	0	0	0	0	0

Table B.7(a) – Strain gauge data of Specimen S13-090

Type of strains		Radial strains											
Location from column centre (mm)		30	180	330	480	630	780	30	180	330	480	630	830
Step	x1x2	x3x4	x5x6	x7x8	x9x10	x11	y1y2	y3y4	y5y6	y7y8	y9y10	y11y12	y11
	($\times10^{-6}$)	($\times10^{-6}$)	($\times10^{-6}$)	($\times10^{-6}$)	($\times10^{-6}$)	($\times10^{-6}$)	($\times10^{-6}$)	($\times10^{-6}$)	($\times10^{-6}$)	($\times10^{-6}$)	($\times10^{-6}$)	($\times10^{-6}$)	($\times10^{-6}$)
1	0	0	0	0	0	0	0	0	0	0	0	0	0
2	30	2	1.5	0	0	0	5	4	2	1	1	1.5	12
3	65	3	1.5	0.5	-2	0	115	7	4	9.5	9	1.5	11
4	85	5.5	2.5	1	-3	0	20.5	13	7	9.5	8	1.5	-1
5	130	9	3	0	-7	0	34	21	12	12	8.5	1.5	-5
6	155	27	14	3.5	-11	-2	39.5	25	13.5	10.5	6	-0.5	-9
7	190	30.5	13	-4	-22	-9	40	24	11	7	0.5	-7.5	-10
8	205	48.5	9.5	-5.5	-38	-8	37	23	10	5	-1.5	-9	-13
9	240	84.5	-7.5	-4.5	-50	-28	53.5	25	9	1.5	-9	-14	-23
10	280	141.5	-5	-1.5	-209	-126	638	155	12	-1	-16.5	-20	-97
11	310	261.5	3.5	8	-254	-112	1019.5	408	17	17	-7	-16	-148
12	325	337	5.5	15	-296	-102	1146	605	28	4.5	-24	-33	-170
13	350	669.5	82.5	19	-308	-81	1445	767	118.5	25	-17.5	-37	-198
14	390	1322.5	414.5	71	-363	-103	2039	1301	384.5	54.5	-10.5	-34.5	-175
15	405	1601	597.5	131	-353	-118	2260	1661	645	86.5	-7.5	-41	-151
16	430	1738.5	992.5	283.5	-317	-130	2490	1941	836	121.5	-0.5	-42	-144
17	440	1736	1061.5	338	-287	-123	2585.5	2047	912	138.5	3.5	-41.5	-133
18	470	1910	1318	509.5	-246	-116	2826.5	2377	1218	205	31	-40.5	-117
19	505	2148.5	1773	758.5	-182	-101	2912	2693	1467.5	300	78	-29	-77
20	535	2418	2087.5	977.5	-74	-77	2921	2923	1623	429	171	-13	-55
21	510	2372	2155.5	1177.5	-28	-65	0	4108	1504.5	483.5	208.5	-3.5	-53
22	445	2054.5	1944.5	1472.5	84	-26	0	4408	1465	469.5	210	0.5	-40
23	310	1556.5	1552.5	1570.5	300	137	0	4237	1163.5	368.5	180	23	-37
24	265			850	2194	8427	0	1757	4911	1408	1219	572	-37
25	75			432	1803	6701	0	1532	4697	1052.5	982.5	482	-37
26	60			381	1703	6386	0	1506	4681	1021.5	962	474.5	-27
27	5			328	1624	6089	0	1471	4657	999.5	946	469.5	17

Table B.7(b) – Strain gauge data of Specimen S13-090 (Continued)

Type of strains		Tangential strains											
Location from column centre (mm)		47	165	283	401	519	755	47	165	283	401	519	755
Step	x1x2	x11x12	x13x14	x15x16	x17x18	x19x20	y1y2	y13y14	y15y16	y17y18	y19y20	y21y22	y11
	($\times10^{-6}$)	($\times10^{-6}$)	($\times10^{-6}$)	($\times10^{-6}$)	($\times10^{-6}$)	($\times10^{-6}$)	($\times10^{-6}$)	($\times10^{-6}$)	($\times10^{-6}$)	($\times10^{-6}$)	($\times10^{-6}$)	($\times10^{-6}$)	($\times10^{-6}$)
1	0	0	0	0	0	0	0	0	0	0	0	0	0
2	30	2	1.5	0	0	0	5	4	2	1	1	1.5	12
3	65	3	1.5	0.5	-2	0	11.5	7	4	9.5	9	1.5	11
4	85	5.5	2.5	1	-3	0	20.5	13	7	9.5	8	1.5	-1
5	130	9	3	0	-7	0	34	21	12	12	8.5	1.5	-5
6	155	27	14	3.5	-11	-2	39.5	25	13.5	10.5	6	-0.5	-9
7	190	30.5	13	-4	-22	-9	40	24	11	7	0.5	-7.5	-10
8	205	48.5	9.5	-5.5	-38	-8	37	23	10	5	-1.5	-9	-13
9	240	84.5	-7.5	-4.5	-50	-28	53.5	25	9	1.5	-9	-14	-23
10	280	141.5	-5	-1.5	-209	-126	638	155	12	-1	-16.5	-20	-97
11	310	261.5	3.5	8	-254	-112	1019.5	408	17	17	-7	-16	-148
12	325	337	5.5	15	-296	-102	1146	605	28	4.5	-24	-33	-170
13	350	669.5	82.5	19	-308	-81	1445	767	118.5	25	-17.5	-37	-198
14	390	1322.5	414.5	71	-363	-103	2039	1301	384.5	54.5	-10.5	-34.5	-175
15	405	1601	597.5	131	-353	-118	2260	1661	645	86.5	-7.5	-41	-151
16	430	1738.5	992.5	283.5	-317	-130	2490	1941	836	121.5	-0.5	-42	-144
17	440	1736	1061.5	338	-287	-123	2585.5	2047	912	138.5	3.5	-41.5	-133
18	470	1910	1318	509.5	-246	-116	2826.5	2377	1218	205	31	-40.5	-117
19	505	2148.5	1773	758.5	-182	-101	2912	2693	1467.5	300	78	-29	-77
20	535	2418	2087.5	977.5	-74	-77	2921	2923	1623	429	171	-13	-55
21	510	2372	2155.5	1177.5	-28	-65	0	4108	1504.5	483.5	208.5	-3.5	-53
22	445	2054.5	1944.5	1472.5	84	-26	0	4408	1465	469.5	210	0.5	-40
23	310	1556.5	1552.5	1570.5	300	137	0	4237	1163.5	368.5	180	23	-37
24	265			850	2194	8427	0	1757	4911	1408	1219	572	-37
25	75			432	1803	6701	0	1532	4697	1052.5	982.5	482	-37
26	60			381	1703	6386	0	1506	4681	1021.5	962	474.5	-27
27	5			328	1624	6089	0	1471	4657	999.5	946	469.5	17

Table B.8(a) – Strain gauge data of Specimen S13-090

Type of strains		Radial strains											
Location from column centre (mm)		30	180	330	480	630	780	30	180	330	480	630	830
Step	Load	x1x2	x3x4	x5x6	x7x8	x9x10	x11	y1y2	y3y4	y5y6	y7y8	y9y10	y11y12
	kN	($\times 10^{-6}$)	($\times 10^{-6}$)	($\times 10^{-6}$)	($\times 10^{-6}$)	($\times 10^{-6}$)	($\times 10^{-6}$)	($\times 10^{-6}$)	($\times 10^{-6}$)	($\times 10^{-6}$)	($\times 10^{-6}$)	($\times 10^{-6}$)	($\times 10^{-6}$)
1	0	5	-1	-1	-1	0	1	0	-115	0	0	-3	0
2	45	6	-0.5	-2.5	0	0	10	5	2.5	0	0	-2	0
3	85	17	3.5	-0.5	0	0	14	9	4.5	0	0	-1	0
4	140	21.5	4	-1.5	-4	0	29.5	17	10	0	0	-2	0
5	160	23	3.5	-1.5	-5	-2	36.5	20	14.5	0	0	-2	0
6	170	22.5	4	-2	-6	-2	42.5	25	15	0	0	-3	0
7	180	42.5	12.5	-2.5	-9	-5	71	18	9.5	0	0	-6	0
8	195	56	17	0	-13	-13	151.5	23	12	0	0	-7	0
9	215	100.5	20.5	2	-14	-20	207	29	13.5	0	0	-9	0
10	230	114	24	6.5	-13	-15	288.5	41	15.5	0	0	-10	0
11	245	124	18.5	7.5	-23	-15	347	53	16	0	0	-11	0
12	255	156	13	36.5	-97	-27	666	92	11.5	0	0	-17	0
13	265	176	12.5	-2.5	-190	-26	753	106	13.5	0	0	-18	0
14	305	306.5	30.5	-4	-225	-20	980.5	371	16	0	0	-34	0
15	320	352.5	49.5	-8.5	-203	-8	1033.5	726	18	0	0	-23	0
16	410	1000.5	751	106.5	-84	18	1636.5	1466	442.5	0	0	59	0
17	430	1068.5	861.5	140	-84	21	1736	1562	551	0	0	64	0
18	450	1154	966	169	-80	25	1855	1676	668.5	0	0	66	0
19	480	1264	1117	223.5	-57	29	1967.5	1778	785.5	0	0	67	0
20	490	1321.5	1195.5	248	-48	32	2050.5	1855	855.5	0	0	71	0
21	505	1407	1306	281	-40	33	2165.5	1975	952	0	0	73	0
22	535	15145	1059.5	331	0	39	2298.5	2081	1054.5	0	0	72	0
23	590	1747	1044.5	426	103	54	2514	2244	1251.5	0	0	75	0
24	620	1953.5	1181	496.5	184	53	2693.5	2351	1317	0	0	68	0
25	655	2090	1258	549	253	74	2889	2473	1385.5	0	0	62	0
26	670	2180.5	1319.5	592.5	315	85	2872.5	2461	1357	0	0	62	0
27	700	2284.5	1537.5	692.5	456	90	1346	2573	1313.5	0	0	65	0

Table B.8(b) – Strain gauge data of Specimen S13-090 (Continued)

Type of strains		Tangential strains											
Location from column centre (mm)		47	165	283	401	519	755	47	165	283	401	519	755
Step	Load	x1x2	x11x12	x13x14	x15x16	x17x18	x19x20	y1y2	y13y14	y15y16	y17y18	y19y20	y21y22
	kN	($\times10^{-6}$)	($\times10^{-6}$)	($\times10^{-6}$)	($\times10^{-6}$)	($\times10^{-6}$)	($\times10^{-6}$)	($\times10^{-6}$)	($\times10^{-6}$)	($\times10^{-6}$)	($\times10^{-6}$)	($\times10^{-6}$)	($\times10^{-6}$)
1	0	5	3	1	-1	0	-19	1	-0.5	-6	-3	1	0
2	45	6	4	2	0.5	0	-17.5	10	44	2	5	9	6
3	85	17	13	9	7.5	0	-11.5	14	48	6	8	12	9
4	140	21.5	17	12.5	10.5	6	-9.5	29.5	64.5	23	23	26	18
5	160	23	18	15	13	9	-12	36.5	73.5	32	31	32.5	25
6	170	22.5	19	15.5	14	8	-11.5	42.5	79	31	37	38.5	29
7	180	42.5	36	29.5	25	17	-4	71	106.5	50	66	51	45
8	195	56	46	37.5	32	23	0.5	151.5	147	95	200	88	83
9	215	100.5	54	45	38	27	4	207	189.5	214	275	130.5	133
10	230	114	63	53	46	30	9.5	288.5	244.5	294	351	190	308
11	245	124	74	61.5	52.5	32	9.5	347	292.5	352	403	229	368
12	255	156	93	79	66	46	55	666	611.5	603	670	409	528
13	265	176	94	102	79.5	47	25	753	704.5	670	750	455	566
14	305	306.5	174	217	180	61	62	980.5	943.5	848	946	568	689
15	320	352.5	213	317	349	89	121.5	1033.5	1006	882	984	607.5	738
16	410	1000.5	1152	706.5	748.5	299	223	1636.5	1614	1388	1396	989.5	1033
17	430	1068.5	1243	843.5	806.5	328	352	1736	1709.5	1575	1493	1090.5	1090
18	450	1154	1351	955.5	907.5	403	620.5	1855	1818.5	1708	1584	1193.5	1115
19	480	1264	1513	1093	974	459	725.5	1967.5	1929	1863	1791	1341	1184
20	490	1321.5	1573	1135.5	10125	468	743.5	2050.5	2007.5	1950	1893	1413.5	1220
21	505	1407	1649	1207	1085	506	793	2165.5	2120.5	2078	2004	1510	1273
22	535	15145	1742	1336	1205.5	561	851	2298.5	2262.5	2219	2147	1656.5	1345
23	590	1747	1889	1610.5	1502.5	710	930	2514	2455.5	2472	2373	1970	1492
24	620	1953.5	2034	1809.5	1698.5	881	1028.5	2693.5	2655.5	2733	2335	2098.5	1519
25	655	2090	2172	1939.5	1826	984	1104.5	2889	2832	3213	2797	2268	1639
26	670	2180.5	2260	2025.5	19155	1046	1148.5	2872.5	2829.5	3821	3344	2412	1718
27	700	2284.5	2408	2198	2093	1189	1254	1346	0	4116	4067	2514	1822

Table B.9 – Strain gauge data of Specimen S15-028

Type of strains		Radial strains											Tangential strains					
Location from column centre (mm)		30	180	330	530	680	30	180	330	480	630	830	47	347	647	47	327	607
Step	x1x2	x3x4	x5x6	x7	x9	y1y2	y3y4	y5y6	y7y8	y9	y11	x1x2	x11x12	x13x14	y1y2	y13y14	y15y16	y15y16
	kN	(×10^{-6})	(×10^{-6})	(×10^{-6})	(×10^{-6})	(×10^{-6})	(×10^{-6})	(×10^{-6})	(×10^{-6})	(×10^{-6})	(×10^{-6})	(×10^{-6})	(×10^{-6})	(×10^{-6})	(×10^{-6})	(×10^{-6})	(×10^{-6})	(×10^{-6})
1	0	0	0	0	-1	0	-0.5	-1	-0.5	0	-2	0	0	7	1.5	-0.5	-0.5	-0.5
2	20	7.5	7	4	3	8	-4	-5	-2	6.5	-6	-2	7.5	5	7.5	-4	2	1
3	0	0	0	3.5	0	0	4	4	2	0	3	4	0	2	0.5	4	2.5	2
4	95	27	16	11	2	-2	20	16	5.5	3	2	0	27	12	6	20	19	19
5	130	36	21.5	13.5	1	-4	27.5	21.5	7	5	2	0	36	16	7	27.5	24.5	27
6	155	46	27	15.5	0	-5	34.5	26.5	9	7	2	0	46	18	7.5	34.5	31.5	34
7	175	56.5	34	20	0	-7	37.5	29	9	7.5	1	-1	56.5	21.5	9	37.5	35.5	39.5
8	190	66.5	40	24.5	1	-8	42.5	32.5	10	9	0	-3	66.5	25.5	8.5	42.5	40	45.5
9	220	139	42	23.5	-3	-12	63	44.5	13.5	11.5	0	-4	139	35.5	10	63	58.5	54.5
10	230	214	37.5	39	-4	-14	100	60	14.5	11	-2	-6	214	41.5	10.5	100	77	52
11	235	393.5	56	11	176	9	279.5	134	9.5	5.5	-11	-12	393.5	47.5	11.5	279.5	330.5	63
12	245	526.5	143	-19	214	-31	571	304.5	18	6.5	-12	-17	526.5	49	13.5	571	557.5	76
13	250	859	227	147	606	-5	834	432.5	20.5	-31.5	-6	-19	859	45.5	10.5	834	759	92
14	240	944	246.5	175	426	129	1214	795.5	21.5	-13.5	-331	-239	944	41.5	9	1214	1191.5	186.5
15	265	937	335.5	219.5	452	155	1775	1572	131	22.5	-29	-276	937	40.5	10.5	1775	2264.5	637.5
16	270	1067	486	306	332	231	2032	1890.5	259	49.5	33	-259	1067	40	11.5	2032	2558	733
17	275	1626	971.5	506	376	301	2322	2297	672	67	82	-174	1626	45.5	13	2322	1341.5	1007.5
18	280	1876	1268	573	356	310	2375	2440	924	80.5	105	-145	1876	47	15	2375	780.5	1115.5
19	285	2211	1662	671.5	279	289	2415	2316	2176	119.5	169	-135	2211	45.5	12	2415	786	1184.5
20	285	3907	2300	853	266	279	2515	2400	2448	147.5	295	-186	3907	50	13	2515	823.5	1265.5
21	290	1333	2320	973.5	217	255	1334.5	2474	5067	173.5	453	-221	1333	54	11.5	1334.5	881.5	1283
22	290	1367	2283.5	994.5	203	238	0	2495	6486	185.5	530	-235	1367	60.5	13	0	887.5	1299
23	290	1353	2234	918	175	190	0	2841	8090	208.5	649	-293	1353	62.5	11.5	0	882	1343.5
24	295	1444	2310.5	977.5	166	158	0	2879	5049.5	219.5	767	-347	1444	65.5	11	0	866	1390
25	295	1701	2546	944	167	125	0	2907	5761	227.5	842	-366	1701	138	12	0	835.5	1446.5
26	285	1560	2543.5	2467	279	164	0	2910.5	5907	203.5	889	-387	1560	123	11	0	832	1421.5

Table B.10 – Strain gauge data of Specimen S15-050

Type of strains		Radial strains										Tangential strains							
Location from column centre (mm)		130	230	380	530	30	130	280	430	580	780	47	347	647	777	47	347	647	752
Step	Load	x1x2	x3x4	x5x6	x7x8	y1y2	y3y4	y5y6	y7y8	y9y10	y11	x1x2	x11x12	x13x14	x15x16	y1y2	y13y14	y15y16	y17y18
	kN	(×10^{-6})	(×10^{-6})	(×10^{-6})	(×10^{-6})	(×10^{-6})	(×10^{-6})	(×10^{-6})	(×10^{-6})	(×10^{-6})	(×10^{-6})	(×10^{-6})	(×10^{-6})	(×10^{-6})	(×10^{-6})	(×10^{-6})	(×10^{-6})	(×10^{-6})	(×10^{-6})
1	0	0	0	-0.5	0	0	0	0	0	0	0	0	-1	0	0	0	0	0	2
2	5	-2	3	-4	2	22.5	-3	3	-8	-6	-5	-2	-9	-12.5	-8.5	22.5	2	1	7
3	75	17	11	1.5	1	34	7	9	-5	-5.5	-8	17	4	1.5	0	34	2.5	2	3
4	160	62.5	29.5	8.5	1	52.5	26.5	20.5	0	-3.5	-10	62.5	34	20.5	15.5	52.5	19	19	12
5	200	1B.5	71.5	9.5	0	76	45.5	29.5	0	-2.5	-14	1B.5	54	35.5	27.5	76	24.5	27	15.5
6	225	163	109.5	6	-2	97.5	56.5	36.5	-1	-6.5	-20	163	53	37	30	97.5	31.5	34	19
7	245	466	288	7	1	111	201	75.5	0	-7.5	-34	466	56	49	41.5	111	35.5	39.5	21.5
8	265	811	319	5	33	117	445.5	140.5	90	16.5	59	811	53	51.5	45	117	40	45.5	27
9	290	1090.	440	28.5	54	124	619.5	198.5	245	29	74	1090.	69	61	56	124	58.5	54.5	31
10	295	1457.5	672	59	56	141	717	246.5	356	42.5	77	1457.	383	123	70	141	77	52	36.5
11	310	1639.5	995.5	130.5	66	189.5	738.5	278	434	50	77	1639.	669	221	86.5	189.5	330.5	63	30
12	320	2191.5	1515	495.5	110	318.5	894.5	374.5	882	77.5	86	2191.	1570	1075	704	318.5	557.5	76	35
13	330	2471	1736	687.5	125	396	996	476.5	1195	109	85	2471	1711	1166.5	794	396	759	92	39.5
14	350	2816.5	2063	945.5	164	593	1050.5	550	1355	182	93	2816.	1970	1283	912	593	1191.5	186.5	82
15	365	2699	2278.	1186	235	791	1124	598.5	1447	214.5	94	2699	2139	1340	967	791	2264.	637.5	193
16	380	3489	2498.	1388.5	282	1057.5	1272	762.5	1562	267.5	-6	3489	2243	1393.5	1028	1057.5	2558	733	216
17	395	4109	2591.5	1496	308	1253	1418.5	954.5	1682	435.5	86	4109	2598	1501.5	1091	1253	1341.5	1007.5	398
18	405	4287	2723.5	1573	319	1527.5	1618.5	1171	1762	568	105	4287	3015	1642.5	1226	1527.5	780.5	1115.5	459
19	415	3079	3042	1734	363	2012.5	1695	1460	1891	671	129	3079	3425	1790.5	1386	2012.5	786	1184.5	505
20	425	2967	3271.5	1903.5	424	2227.5	1837	1654	2009	896	159	2967	3600	1986.5	1501.5	2227.5	823.5	1265.5	569
21	435	2987	3919	2085.	489	2392.5	1957	1875	2042	1017.5	180	2987	3739	2033.5	1543.5	2392.5	881.5	1283	580
22	415	2980	4030.	2083.	483	2369	1989	1854	1895	1002	190	2980	3915	2078.	1579.5	2369	887.5	1299	587.
23	400	2893	3928.	2054	475	2422	2390.5	1881	1577	895.5	185	2893	3837	2046.	1568	2422	882	1343.5	590
24	390	2784	3736	1999	474	2618	49376	1857	1458	819	188	2784	3702	1986	1543	2618	866	1390	601
25	430	2857	4638	2254	686	0	0	2027	1458	560	0	2857	4807	2114	1646	0	835.5	1446.5	607

Table B.11(a) – Strain gauge data of Specimen S15-090

Type of strains		**Radial strains**									
Location from column centre (mm)		**30**	**180**	**330**	**680**	**47**	**197**	**347**	**497**	**647**	**847**
Step	**Load**	**x1x2**	**x3x4**	**x5x6**	**x10**	**y1y2**	**y3y4**	**y5y6**	**y7y8**	**y9y10**	**y11**
	kN	**($\times10^{-6}$)**	**($\times10^{-6}$)**	**($\times10^{-6}$)**	**($\times10^{-6}$)**	**($\times10^{-6}$)**	**($\times10^{-6}$)**	**($\times10^{-6}$)**	**($\times10^{-6}$)**	**($\times10^{-6}$)**	**($\times10^{-6}$)**
1	0	-0.5	0	0	0	-0.5	0	0	0	0	-1
2	85	28.5	12.5	5.5	3	15.5	16.5	11.5	6	2	-2
3	145	152.5	4.5	11	5	37	35.5	25	12.5	4	-1
4	180	305.5	2.5	47	13	92.5	59.5	35.5	16.5	7	-1
5	200	381	4.5	46.5	13	130	69.5	42	19	9	40
6	225	475.5	6.5	52	17	189	198	45	19.5	7	40
7	250	611	16	57	17	282	347.5	53	20.5	8	40
8	265	684	26	58	16	358	463	66.5	23	9	40
9	285	792	49.5	54.5	16	453	627.5	101.5	27.5	17	40
10	305	912.5	83	72.5	21	572.5	788	156	34.5	14	45
11	325	1122	159	93	28	699.5	1004	255.5	52	22	68
12	350	1316	227.5	107	31	813	1158	341.5	70	21	82
13	370	1554.5	343.5	125.5	34	950	1281.5	473.5	102	29	88
14	390	1619.5	408.5	136.5	33	998	1320.5	525.5	117	23	91
15	410	1817.5	536.5	157	34	1109	1463	643.5	160	33	100
16	430	2040.5	722.5	203	40	1264	1684	795	219.5	42	106
17	455	2290.5	929	281.5	48	1421.5	1909.5	951.5	292.5	50	117
18	490	2621	1185.5	411.5	53	1652.5	2269	1171	409.5	69	142
19	515	3000	1382	525	62	1812	2506	1322	503	81	153
20	540	3467	1516	616.5	70	1941	2670	1443.5	583.5	97	164
21	595	18658.5	1733	791.5	116	2401	3172.5	1784.5	856	151	206
22	610	20033.5	1790	842.5	134	2574	3343	1891.5	957	173	215
23	630	13697	1796.5	969	171	2724	3521	2027.5	1093	205	224
24	620	13055.5	1791.5	1004	180	2732.5	3536	2028	1114	219	225
25	610	12293	1762.5	1002	175	2759	3582	1931	1152	256	223
26	580	11903	1520.5	961	166	2806.5	3544.5	1680.5	1017	257	196
27	560	11726	1252.5	903	161	2956.5	3890	1733	1051.5	220	182

Table B.11(b) – Strain gauge data of Specimen S13-090 (Continued)

Type of strains		Tangential strains												
Location from column centre (mm)		47	165	283	401	519	755	47	165	283	401	519	755	991
Step	Load	x1x2	x11x12	x13	x15x16	x17x18	x19x20	y1y2	y12y13	y15	y16y17	y18y19	y20y21	y22y23
	kN	($\times10^{-6}$)	($\times10^{-6}$)	($\times10^{-6}$)	($\times10^{-6}$)	($\times10^{-6}$)	($\times10^{-6}$)	($\times10^{-6}$)	($\times10^{-6}$)	($\times10^{-6}$)	($\times10^{-6}$)	($\times10^{-6}$)	($\times10^{-6}$)	($\times10^{-6}$)
1	0	-0.5	0	0	0	-0.5	0	0	0	0	-1	-0.5	-0.5	0
2	85	28.5	12.5	5.5	3	15.5	16.5	11.5	6	2	-2	28.5	25.5	20
3	145	152.5	4.5	11	5	37	35.5	25	12.5	4	-1	152.5	76	45
4	180	305.5	2.5	47	13	92.5	59.5	35.5	16.5	7	-1	305.5	157.5	109
5	200	381	4.5	46.5	13	130	69.5	42	19	9	40	381	199	167
6	225	475.5	6.5	52	17	189	198	45	19.5	7	40	475.5	246	205
7	250	611	16	57	17	282	347.5	53	20.5	8	40	611	327.5	252
8	265	684	26	58	16	358	463	66.5	23	9	40	684	419.5	267
9	285	792	49.5	54.5	16	453	627.5	101.5	27.5	17	40	792	539	296
10	305	912.5	83	72.5	21	572.5	788	156	34.5	14	45	912.5	643.5	329
11	325	1122	159	93	28	699.5	1004	255.5	52	22	68	1122	791.5	435
12	350	1316	227.5	107	31	813	1158	341.5	70	21	82	1316	972	505
13	370	1554.5	343.5	125.5	34	950	1281.5	473.5	102	29	88	1554.5	1194.5	638
14	390	1619.5	408.5	136.5	33	998	1320.5	525.5	117	23	91	1619.5	1268	689
15	410	1817.5	536.5	157	34	1109	1463	643.5	160	33	100	1817.5	1437	763
16	430	2040.5	722.5	203	40	1264	1684	795	219.5	42	106	2040.5	1639.5	904
17	455	2290.5	929	281.5	48	1421.5	1909.5	951.5	292.5	50	117	2290.5	1873	1080
18	490	2621	1185.5	411.5	53	1652.5	2269	1171	409.5	69	142	2621	2189.5	1328
19	515	3000	1382	525	62	1812	2506	1322	503	81	153	3000	2411	1506
20	540	3467	1516	616.5	70	1941	2670	1443.5	583.5	97	164	3467	2571	1623
21	595	18658.5	1733	791.5	116	2401	3172.5	1784.5	856	151	206	18658.5	3424	2143
22	610	20033.5	1790	842.5	134	2574	3343	1891.5	957	173	215	20033.5	4709	2347
23	630	13697	1796.5	969	171	2724	3521	2027.5	1093	205	224	13697	10091.5	2675
24	620	13055.5	1791.5	1004	180	2732.5	3536	2028	1114	219	225	13055.5	11592	2800
25	610	12293	1762.5	1002	175	2759	3582	1931	1152	256	223	12293	11608.5	2755
26	580	11903	1520.5	961	166	2806.5	3544.5	1680.5	1017	257	196	11903	11220	2552
27	560	11726	1252.5	903	161	2956.5	3890	1733	1051.5	220	182	11726	10892	2272

Table B.12(a) – Strain gauge data of Specimen S15-090

Type of strains		Radial strains									
Location from column centre (mm)		30	180	330	680	47	197	347	497	647	847
Step	Load	x1x2	x3x4	x5x6	x10	y1y2	y3y4	y5y6	y7y8	y9y10	y11
	kN	($\times10^{-6}$)	($\times10^{-6}$)	($\times10^{-6}$)	($\times10^{-6}$)	($\times10^{-6}$)	($\times10^{-6}$)	($\times10^{-6}$)	($\times10^{-6}$)	($\times10^{-6}$)	($\times10^{-6}$)
1	0	-1	0	0	0	0	0	-1	0	0	0
2	65	145	9	3	0	1	8.5	6	4.5	2	0
3	115	47	16	11	0	4	24.5	185	13	6	0
4	160	126.5	28	23	69	20	42.5	34	20	9	-1
5	190	263	42	39	84	12	127	178	27.5	12	0
6	215	386.5	55	41	65	16	252	287	33	13	0
7	235	464	66	40	54	23	323	362.5	36.5	13	-1
8	260	555	89	37	33	35	456.5	453	41	15	-3
9	280	621.5	164	37	20	46	558	539	49.5	19	-4
10	300	710.5	272	40	-2	57	666.5	646	72.5	25	-4
11	320	765	352	43	-15	65	763	712	108	32	-7
12	340	8115	422	51	-23	69	824.5	785.5	160	32	-8
13	360	835.5	498	230	-25	70	913	875	233.5	36	-9
14	380	841.5	580	338	-18	73	1000	955.5	308.5	46	-5
15	390	944	641	383	-9	76	1051.5	1003	360	56	-4
16	415	1001	836	526	20	83	1174	1110	491	93	1
17	445	1032	1046	628	52	91	1273.5	1211	585.5	132	1
18	475	1206	1345	741	126	100	1395.5	1324	687.5	194	2
19	505	1441.5	1613	834	262	115	1515	1438.5	788	278	1
20	540	1609.5	1859	935	416	149	1651.5	1536.5	906	412	17
21	575	1755	4858	1038	544	182	1784	1651	1021.5	534	37
22	625	1933.5	2506	1191	689	220	1977	1797.5	1168.5	690	80
23	665	1480	2553	1321	819	262	2163	1922.5	1300	823	95
24	695	1558	2597	1450	932	310	2373	2072.5	1433.5	956	111
25	750	1616	2656	1598	1032	394	2594	2351.5	1559	1082	121
26	745	1392	2672	1770	1152	482	2737	3278.5	1631	1129	127
27	645	0	2750	2055	1170	491	3374	4953	1436	1006	117

Table B.12(b) – Strain gauge data of Specimen S13-090 (Continued)

Type of strains		Tangential strains												
Location from column centre (mm)		47	165	283	401	519	755	47	165	283	401	519	755	991
Step	Load	x1x2	x11x12	x13	x15x16	x17x18	x19x20	y1y2	y12y13	y15	y16y17	y18y19	y20y21	y22y23
	kN	($\times10^{-6}$)	($\times10^{-6}$)	($\times10^{-6}$)	($\times10^{-6}$)	($\times10^{-6}$)	($\times10^{-6}$)	($\times10^{-6}$)	($\times10^{-6}$)	($\times10^{-6}$)	($\times10^{-6}$)	($\times10^{-6}$)	($\times10^{-6}$)	($\times10^{-6}$)
1	0	-1	0	0	0	0	0	-1	0	0	0	-1	0	0
2	65	14.5	9	3	0	1	8.5	6	4.5	2	0	14.5	15	12.5
3	115	47	16	11	0	4	24.5	18.5	13	6	0	47	38	32.5
4	160	126.5	28	23	69	20	42.5	34	20	9	-1	126.5	62	51
5	190	263	42	39	84	12	127	178	27.5	12	0	263	89	79
6	215	386.5	55	41	65	16	252	287	33	13	0	386.5	159	135.5
7	235	464	66	40	54	23	323	362.5	36.5	13	-1	464	277	133.5
8	260	555	89	37	33	35	456.5	453	41	15	-3	555	373	152.5
9	280	621.5	164	37	20	46	558	539	49.5	19	-4	621.5	450.5	167.5
10	300	710.5	272	40	-2	57	666.5	646	72.5	25	-4	710.5	519.5	190
11	320	765	352	43	-15	65	763	712	108	32	-7	765	581	225.5
12	340	8115	422	51	-23	69	824.5	785.5	160	32	-8	8115	647	262
13	360	835.5	498	230	-25	70	913	875	233.5	36	-9	835.5	739.5	328.5
14	380	841.5	580	338	-18	73	1000	955.5	308.5	46	-5	841.5	834	418
15	390	944	641	383	-9	76	1051.5	1003	360	56	-4	944	895.5	480.5
16	415	1001	836	526	20	83	1174	1110	491	93	1	1001	1046	658.5
17	445	1032	1046	628	52	91	1273.5	1211	585.5	132	1	1032	1168	816
18	475	1206	1345	741	126	100	1395.5	1324	687.5	194	2	1206	1299	1008
19	505	1441.5	1613	834	262	115	1515	1438.5	788	278	1	1441.5	1444.5	1189.5
20	540	1609.5	1859	935	416	149	1651.5	1536.5	906	412	17	1609.5	1609	1365.5
21	575	1755	4858	1038	544	182	1784	1651	1021.5	534	37	1755	1771	1525.5
22	625	1933.5	2506	1191	689	220	1977	1797.5	1168.5	690	80	1933.5	1969.5	1743.5
23	665	1480	2553	1321	819	262	2163	1922.5	1300	823	95	1480	2122.5	1938.5
24	695	1558	2597	1450	932	310	2373	2072.5	1433.5	956	111	1558	2258	2091
25	750	1616	2656	1598	1032	394	2594	2351.5	1559	1082	121	1616	2404	2243
26	745	1392	2672	1770	1152	482	2737	3278.5	1631	1129	127	1392	2120	2151
27	645	0	2750	2055	1170	491	3374	4953	1436	1006	117	0	2118.5	2096

B.3 Strain gauge data for the 10 SFRC slabs

Figs. B.7 shows the typical positions and labels of strain gauges in the reinforcements of the 10 SFRC specimens (F09 series and F14 series slabs). Tables B.13 to B22 show the strain gauge data of the 10 specimens.

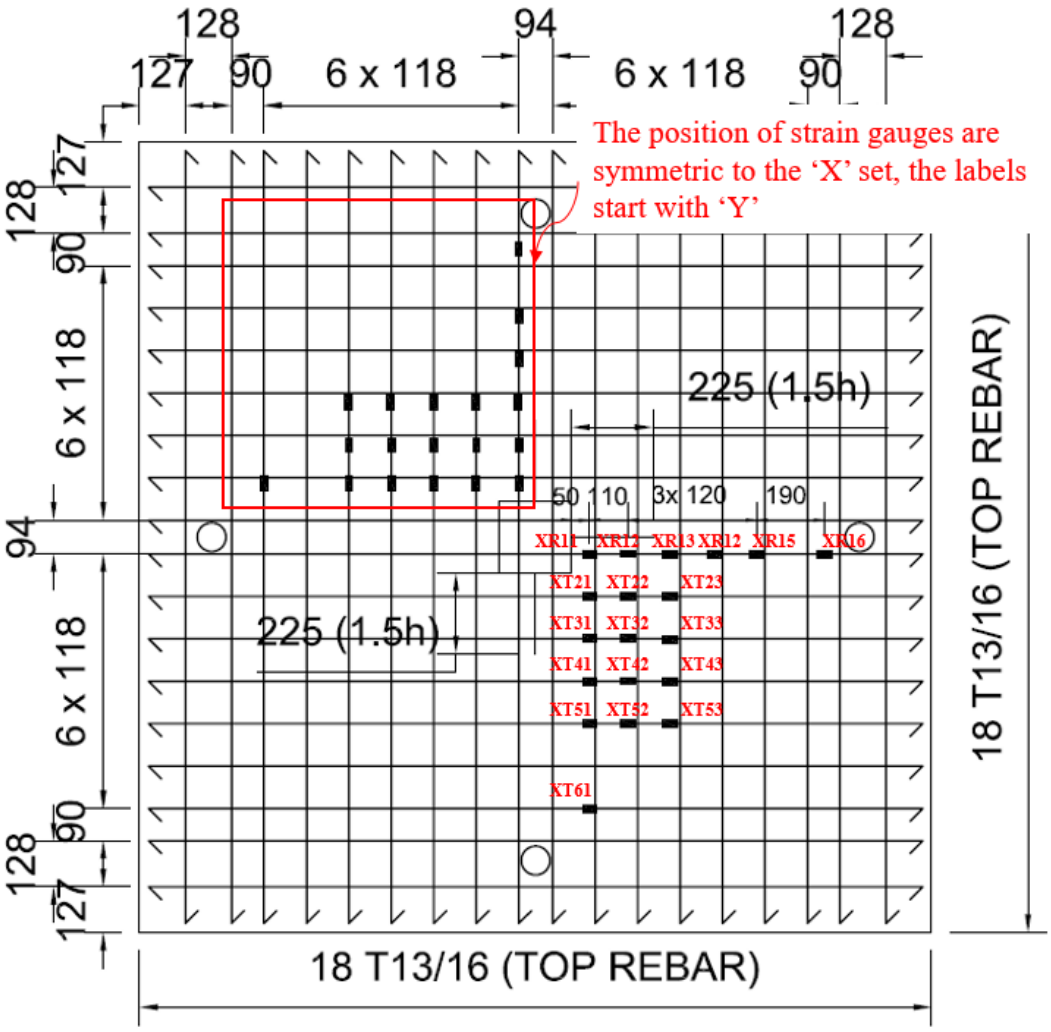

Fig. B.7 – Typical strain gauges' locations and labels for F09-series and F14-series slabs. Distances between strain gauges are also indicated in the drawing.

Table B.13 (a) – (X-set) Strain gauge data of Specimen F09-00

Step	Load	Strains in reinforcements																		
		XR11	XR12	XR13	XR14	XR15	XR16	XT21	XT22	XT23	XT31	XT32	XT33	XT41	XT42	XT43	XT51	XT52	XT53	XT61
	kN	(×10^{-6})	(×10^{-6})	(×10^{-6})	(×10^{-6})	(×10^{-6})	(×10^{-6})	(×10^{-6})	(×10^{-6})	(×10^{-6})	(×10^{-6})	(×10^{-6})	(×10^{-6})	(×10^{-6})	(×10^{-6})	(×10^{-6})	(×10^{-6})	(×10^{-6})	(×10^{-6})	(×10^{-6})
1	**0.0**	0	0	0	0	0	1	0	0	0	0	0	0	0	0	1	0	0	1	0
2	**-0.3**	0	0	1	0	0	0	1	1	1	1	0	1	0	0	1	0	0	0	0
3	**16.5**	2	62	35	35	20	15	1	9	24	2	3	6	2	4	4	-2	0	2	0
4	**32.3**	10	80	47	46	29	20	3	17	32	0	4	9	6	10	6	-3	0	5	0
5	**56.2**	41	117	69	65	46	33	16	35	53	3	7	25	20	23	14	-6	4	12	14
6	**74.5**	60	172	126	90	61	43	19	44	69	5	10	35	37	31	18	-14	4	17	28
7	**92.5**	119	286	327	183	89	65	50	54	87	-19	7	51	40	32	17	-28	2	16	48
8	**108.7**	186	448	552	291	108	97	127	92	151	-38	10	60	34	27	15	-49	1	6	62
9	**118.1**	234	555	673	382	125	131	171	135	206	-44	12	64	31	29	12	-55	-3	8	66
10	**125.8**	291	667	807	502	216	245	223	186	267	-46	15	77	35	33	10	-68	-12	16	62
11	**138.0**	376	779	927	603	289	396	306	320	318	20	37	117	37	35	55	-84	-28	22	63
12	**135.9**	392	788	941	615	307	423	319	352	326	-32	45	123	39	37	61	-83	-29	21	63
13	**156.6**	603	1001	1144	761	502	719	581	612	513	46	307	413	60	51	142	-95	-36	27	76
14	**172.2**	819	1165	1265	880	604	833	809	801	635	146	494	542	75	77	241	-61	-35	66	87
15	**198.7**	1158	1446	1540	1064	741	941	1146	1116	863	366	748	688	158	160	456	-38	-38	158	84
16	**213.7**	1390	1675	1735	1137	823	988	1352	1318	1003	502	924	775	236	224	572	-20	-27	254	84
17	**236.2**	1747	1989	2053	1261	1068	1088	1608	1563	1207	652	1155	884	344	309	688	2	-9	360	91
18	**257.9**	1947	2254	2284	1367	1451	1196	1867	1825	1412	886	1442	1039	553	449	839	55	37	498	97
19	**278.9**	2146	2474	2505	1524	1657	1283	2141	2053	1647	1074	1735	1219	704	623	967	109	110	718	100
20	**299.7**	2312	2647	2722	1670	1797	1369	2461	2253	1861	1276	1990	1422	845	824	1101	165	235	842	105
21	**317.4**	2424	2754	2965	1775	1925	1426	2711	2448	2039	1455	2207	1616	972	1026	1235	222	367	963	109
22	**337.3**	2554	2890	3198	1914	2062	1483	2960	2651	2259	1643	2403	1823	1128	1241	1381	317	541	1097	116
23	**357.1**	2695	3072	3580	2126	2260	1565	3107	2843	2511	1804	2619	2078	1352	1513	1564	459	797	1232	123
24	**370.5**	2823	3394	4075	2238	2361	1615	3301	3000	2673	1881	2780	2236	1488	1662	1686	573	952	1313	128
25	**372.1**	2853	3524	4730	2265	2391	1627	3406	3064	2728	1930	2840	2287	1561	1702	1724	636	1026	1343	131
26	**375.8**	2829	3534	6133	2303	2426	1643	3557	3094	2800	2107	2926	2348	1667	1713	1751	788	1168	1394	138
27	**373.9**	2839	3508	6194	2303	2416	1637	3588	3078	2762	2130	2941	2388	1680	1678	1742	876	1276	1457	139
28	**118.5**	1600	2058	5150	1439	1212	724	2013	1670	0	2834	3292	1076	0	574	288	613	642	757	99

Table B.13 (b) – (Y-set) Strain gauge data of Specimen F09-00 (Continued)

Step	Load	Strains in reinforcements																		
		YR11	YR12	YR13	YR14	YR15	YR16	YT21	YT22	YT23	YT31	YT32	YT33	YT41	YT42	YT43	YT51	YT52	YT53	YT61
	kN	(×10^{-6})	(×10^{-6})	(×10^{-6})	(×10^{-6})	(×10^{-6})	(×10^{-6})	(×10^{-6})	(×10^{-6})	(×10^{-6})	(×10^{-6})	(×10^{-6})	(×10^{-6})	(×10^{-6})	(×10^{-6})	(×10^{-6})	(×10^{-6})	(×10^{-6})	(×10^{-6})	(×10^{-6})
1	**0.0**	-12	-9	-8	-6	-5	-5	-4	-4	-3	-3	-2	-2	-2	-2	-3	-2	-2	-2	-2
2	**-0.3**	-9	-7	-6	-5	-3	-4	-3	-3	-3	-2	-1	-2	-1	-1	-2	-2	-1	-1	-1
3	**16.5**	-16	-13	-28	-11	-13	-12	14	-10	0	10	7	-7	3	8	2	1	2	1	1
4	**32.3**	-12	-11	-27	-10	-12	-14	25	-4	5	19	15	-2	11	15	8	7	8	6	7
5	**56.2**	-3	-11	-30	-11	-15	-18	54	7	10	38	31	4	28	31	17	18	18	15	16
6	**74.5**	14	-12	-36	-16	-18	-23	253	21	12	87	81	7	35	74	31	37	41	32	32
7	**92.5**	52	-15	-45	-32	-31	-44	527	56	10	128	203	19	51	141	60	54	53	65	59
8	**108.7**	155	-7	-52	-61	-44	-82	720	119	13	200	327	40	76	221	93	80	78	107	103
9	**118.1**	261	17	-50	-65	-50	-91	849	169	16	264	414	66	98	294	125	97	102	138	131
10	**125.8**	382	49	-41	-66	-55	-98	1010	229	25	393	514	97	299	366	155	136	162	172	246
11	**138.0**	592	133	-12	-54	-54	-108	1248	326	50	626	647	157	601	436	193	247	285	220	470
12	**135.9**	610	148	-8	-53	-54	-109	1248	336	53	636	647	162	605	433	193	250	288	221	473
13	**156.6**	921	375	41	-14	-60	-129	1591	580	130	928	867	281	878	573	294	381	437	341	619
14	**172.2**	1236	632	110	20	-64	-140	1948	819	332	1182	1104	489	1070	755	418	491	547	467	726
15	**198.7**	1522	935	282	72	-70	-148	2300	1284	605	1477	1378	872	1312	1010	594	611	663	738	851
16	**213.7**	1629	1068	375	111	-50	-154	2457	1486	751	1674	1525	1026	1519	1139	696	658	764	925	884
17	**236.2**	1746	1195	476	183	-27	-158	2646	1691	942	1867	1693	1199	1726	1276	813	729	876	1070	938
18	**257.9**	1954	1410	639	306	-16	-162	2943	1947	1176	2147	1940	1376	2010	1500	1001	883	1035	1239	1031
19	**278.9**	2096	1581	776	405	1	-172	3081	2136	1397	2365	2104	1520	2215	1679	1165	1006	1148	1389	1086
20	**299.7**	2355	1852	961	544	23	-176	3379	2380	1655	2611	2327	1695	2451	1856	1349	1139	1287	1536	1181
21	**317.4**	2649	2186	1207	716	69	-177	3871	2615	1931	2862	2576	1892	2660	1990	1519	1256	1409	1659	1267
22	**337.3**	2966	2493	1442	863	130	-177	5531	2879	2206	3142	2834	2118	2919	2157	1725	1420	1559	1770	1363
23	**357.1**	2999	2522	1511	905	190	-177	7306	2993	2342	3434	2990	2269	3206	2290	1902	1561	1685	1900	1435
24	**370.5**	3024	2547	1565	933	228	-175	9117	3049	2409	3629	3097	2361	3405	2404	2037	1673	1782	1989	1496
25	**372.1**	3059	2563	1585	948	248	-174	11642	3094	2456	3737	3164	2412	3475	2458	2112	1732	1829	2026	1521
26	**375.8**	3081	2539	1573	943	255	-176	16118	3266	2502	3933	3265	2495	3570	2554	2229	1816	1912	2086	1567
27	**373.9**	3074	2509	1557	932	256	-178	16681	3259	2498	3942	3269	2504	3599	2578	2267	1845	1939	2101	1576
28	**118.5**	1813	1622	1406	1640	207	-24	14589	2288	5278	2889	3110	2292	2233	1767	1686	796	2505	1239	968

Table B.14 (a) – (X-set) Strain gauge data of Specimen F14-00

Step	Load	Strains in reinforcements																		
		XR11	XR12	XR13	XR14	XR15	XR16	XT21	XT22	XT23	XT31	XT32	XT33	XT41	XT42	XT43	XT51	XT52	XT53	XT61
	kN	(×10^{-6})	(×10^{-6})	(×10^{-6})	(×10^{-6})	(×10^{-6})	(×10^{-6})	(×10^{-6})	(×10^{-6})	(×10^{-6})	(×10^{-6})	(×10^{-6})	(×10^{-6})	(×10^{-6})	(×10^{-6})	(×10^{-6})	(×10^{-6})	(×10^{-6})	(×10^{-6})	(×10^{-6})
1	**0.0**	0	1	0	1	1	0	1	1	0	1	1	0	0	-1	0	0	1	0	1
2	**23.5**	0	4	2	2	0	-3	14	11	4	11	12	8	10	10	6	8	7	6	8
3	**42.7**	-15	-7	-11	-1	0	-8	25	20	13	19	23	14	18	17	13	15	14	11	14
4	**62.9**	-45	7	-17	-3	2	-14	46	30	17	38	42	19	33	30	23	26	23	19	25
5	**82.1**	-35	19	-31	-12	1	-35	74	39	12	58	63	22	49	45	35	38	33	28	36
6	**97.4**	25	22	-44	-22	-7	-60	182	56	1	146	117	14	71	69	84	56	48	47	50
7	**115.1**	116	78	-52	-30	-14	-110	265	87	6	221	171	18	85	189	117	64	107	66	70
8	**122.1**	143	123	-59	-40	-26	-100	284	98	12	264	208	23	97	231	134	72	134	73	84
9	**146.2**	278	376	-33	-36	-5	-118	427	318	41	346	344	35	141	341	227	99	206	107	172
10	**156.5**	372	478	22	-22	5	-129	517	440	57	426	432	54	197	414	291	150	270	129	308
11	**152.9**	384	487	31	-19	7	-129	524	455	61	432	437	58	206	414	314	155	275	133	323
12	**161.8**	403	522	38	-18	8	-139	552	492	66	445	487	63	215	422	359	160	282	146	335
13	**178.5**	517	661	98	0	17	-159	670	635	126	491	653	135	308	512	511	233	373	209	458
14	**178.2**	530	678	112	4	20	-160	679	656	143	486	673	153	318	516	533	239	379	218	460
15	**194.1**	647	811	194	31	33	-172	817	787	249	560	823	277	400	602	678	298	456	273	535
16	**197.1**	694	861	255	46	40	-175	863	854	307	565	868	430	409	600	680	304	456	270	539
17	**215.1**	843	1011	403	123	67	-182	986	1002	473	647	989	590	503	670	736	357	534	301	591
18	**237.8**	1007	1129	519	192	99	-206	1125	1152	621	774	1067	756	639	762	811	429	651	361	645
19	**258.8**	1182	1248	672	303	143	-217	1305	1339	809	943	1155	905	807	848	882	519	787	435	705
20	**278.7**	1337	1350	817	420	197	-225	1464	1536	951	1135	1256	1053	954	927	948	610	895	494	775
21	**300.7**	1469	1464	961	554	271	-227	1624	1744	1095	1317	1408	1224	1113	1024	1056	690	1037	586	826
22	**318.0**	1571	1559	1077	655	324	-223	1741	1900	1199	1454	1526	1346	1229	1102	1125	754	1134	644	895
23	**338.2**	1673	1654	1219	789	410	-209	1876	2049	1348	1624	1632	1502	1388	1157	1191	829	1236	703	959
24	**358.7**	1758	1725	1388	926	498	-197	1980	2179	1483	1758	1748	1610	1522	1227	1258	903	1325	762	1031
25	**376.3**	1834	1843	1771	1263	749	-165	2117	2345	1814	1984	1944	1788	1750	1344	1362	1029	1498	870	1141
26	**356.2**	1842	1835	1823	1379	845	-143	2126	2399	1919	2023	1958	1810	1765	1355	1369	1041	1515	881	1140
27	**355.0**	1855	1844	1826	1454	904	-128	2154	2421	2032	2058	1962	1828	1796	1391	1390	1070	1564	906	1154
28	**227.0**	1310	1315	1279	1364	978	-61	1598	1945	1814	1908	1301	1423	1302	1263	1256	953	1067	962	1007

Table B.14 (b) – (Y-set) Strain gauge data of Specimen F14-00 (Continued)

Step	Load	Strains in reinforcements																		
		YR11	YR12	YR13	YR14	YR15	YR16	YT21	YT22	YT23	YT31	YT32	YT33	YT41	YT42	YT43	YT51	YT52	YT53	YT61
	kN	(×10^{-6})	(×10^{-6})	(×10^{-6})	(×10^{-6})	(×10^{-6})	(×10^{-6})	(×10^{-6})	(×10^{-6})	(×10^{-6})	(×10^{-6})	(×10^{-6})	(×10^{-6})	(×10^{-6})	(×10^{-6})	(×10^{-6})	(×10^{-6})	(×10^{-6})	(×10^{-6})	(×10^{-6})
1	**0.0**	0	1	0	1	1	0	1	1	0	1	1	0	0	-1	0	0	1	0	1
2	**23.5**	0	4	2	2	0	-3	14	11	4	11	12	8	10	10	6	8	7	6	8
3	**42.7**	-15	-7	-11	-1	0	-8	25	20	13	19	23	14	18	17	13	15	14	11	14
4	**62.9**	-45	7	-17	-3	2	-14	46	30	17	38	42	19	33	30	23	26	23	19	25
5	**82.1**	-35	19	-31	-12	1	-35	74	39	12	58	63	22	49	45	35	38	33	28	36
6	**97.4**	25	22	-44	-22	-7	-60	182	56	1	146	117	14	71	69	84	56	48	47	50
7	**115.1**	116	78	-52	-30	-14	-110	265	87	6	221	171	18	85	189	117	64	107	66	70
8	**122.1**	143	123	-59	-40	-26	-100	284	98	12	264	208	23	97	231	134	72	134	73	84
9	**146.2**	278	376	-33	-36	-5	-118	427	318	41	346	344	35	141	341	227	99	206	107	172
10	**156.5**	372	478	22	-22	5	-129	517	440	57	426	432	54	197	414	291	150	270	129	308
11	**152.9**	384	487	31	-19	7	-129	524	455	61	432	437	58	206	414	314	155	275	133	323
12	**161.8**	403	522	38	-18	8	-139	552	492	66	445	487	63	215	422	359	160	282	146	335
13	**178.5**	517	661	98	0	17	-159	670	635	126	491	653	135	308	512	511	233	373	209	458
14	**178.2**	530	678	112	4	20	-160	679	656	143	486	673	153	318	516	533	239	379	218	460
15	**194.1**	647	811	194	31	33	-172	817	787	249	560	823	277	400	602	678	298	456	273	535
16	**197.1**	694	861	255	46	40	-175	863	854	307	565	868	430	409	600	680	304	456	270	539
17	**215.1**	843	1011	403	123	67	-182	986	1002	473	647	989	590	503	670	736	357	534	301	591
18	**237.8**	1007	1129	519	192	99	-206	1125	1152	621	774	1067	756	639	762	811	429	651	361	645
19	**258.8**	1182	1248	672	303	143	-217	1305	1339	809	943	1155	905	807	848	882	519	787	435	705
20	**278.7**	1337	1350	817	420	197	-225	1464	1536	951	1135	1256	1053	954	927	948	610	895	494	775
21	**300.7**	1469	1464	961	554	271	-227	1624	1744	1095	1317	1408	1224	1113	1024	1056	690	1037	586	826
22	**318.0**	1571	1559	1077	655	324	-223	1741	1900	1199	1454	1526	1346	1229	1102	1125	754	1134	644	895
23	**338.2**	1673	1654	1219	789	410	-209	1876	2049	1348	1624	1632	1502	1388	1157	1191	829	1236	703	959
24	**358.7**	1758	1725	1388	926	498	-197	1980	2179	1483	1758	1748	1610	1522	1227	1258	903	1325	762	1031
25	**376.3**	1834	1843	1771	1263	749	-165	2117	2345	1814	1984	1944	1788	1750	1344	1362	1029	1498	870	1141
26	**356.2**	1842	1835	1823	1379	845	-143	2126	2399	1919	2023	1958	1810	1765	1355	1369	1041	1515	881	1140
27	**355.0**	1855	1844	1826	1454	904	-128	2154	2421	2032	2058	1962	1828	1796	1391	1390	1070	1564	906	1154
28	**227.0**	1310	1315	1279	1364	978	-61	1598	1945	1814	1908	1301	1423	1302	1263	1256	953	1067	962	1007

Table B.15 (a) – (X-set) Strain gauge data of Specimen F09-03

Step	Load	Strains in reinforcements																		
		XR11	XR12	XR13	XR14	XR15	XR16	XT21	XT22	XT23	XT31	XT32	XT33	XT41	XT42	XT43	XT51	XT52	XT53	XT61
	kN	($\times 10^{-6}$)	($\times 10^{-6}$)	($\times 10^{-6}$)	($\times 10^{-6}$)	($\times 10^{-6}$)	($\times 10^{-6}$)	($\times 10^{-6}$)	($\times 10^{-6}$)	($\times 10^{-6}$)	($\times 10^{-6}$)	($\times 10^{-6}$)	($\times 10^{-6}$)	($\times 10^{-6}$)	($\times 10^{-6}$)	($\times 10^{-6}$)	($\times 10^{-6}$)	($\times 10^{-6}$)	($\times 10^{-6}$)	($\times 10^{-6}$)
1	**0**	0	1	1	0	-1	0	0	0	1	-2	1	1	0	1	1	1	1	-1	0
2	**0**	0	1	0	0	1	0	0	1	0	1	1	0	0	1	1	0	0	2	0
3	**35**	31	23	17	8	5	0	28	22	16	29	20	19	24	24	19	21	21	18	18
4	**24**	16	13	7	1	0	0	15	12	7	16	11	8	13	13	10	11	11	9	9
5	**51**	26	22	12	0	-3	0	20	20	12	30	20	15	24	22	16	20	21	13	17
6	**94**	164	40	-28	-7	-51	0	206	46	19	197	44	19	71	114	28	62	87	41	50
7	**101**	176	38	-35	-11	-59	0	217	46	16	212	43	16	73	126	24	61	91	41	50
8	**122**	274	69	-32	-17	-68	0	312	67	19	286	57	20	91	184	29	72	136	61	65
9	**154**	653	148	-3	-20	-118	0	540	275	29	499	97	85	134	346	252	96	304	118	94
10	**282**	2200	1526	936	209	-85	0	2011	1527	774	1837	847	1107	1260	987	1237	1085	1140	466	846
11	**302**	2278	1747	1092	314	-46	0	2214	1669	866	2019	982	1241	1418	1096	1359	1207	1230	531	922
12	**320**	2440	1989	1248	447	-16	0	2420	1890	983	2228	1142	1390	1596	1254	1464	1350	1342	626	1000
13	**324**	2530	2095	1322	513	9	0	2517	2002	1086	2355	1244	1488	1693	1373	1579	1376	1396	850	976
14	**341**	2598	2189	1419	606	29	0	2605	2110	1171	2476	1337	1566	1780	1435	1627	1432	1436	976	1006
15	**360**	2781	2363	1591	779	99	0	2806	2348	1320	2738	1509	1704	1993	1638	1750	1599	1536	1190	1080
16	**380**	3054	2524	1806	1001	206	0	2983	2586	1512	2950	1692	1914	2121	1755	1914	1694	1586	1270	1124
17	**400**	3386	2641	1989	1163	293	0	3173	2764	1680	3143	1866	2002	2284	1915	2023	1818	1684	1397	1183
18	**418**	3726	2748	2208	1357	432	0	3619	2930	1883	3379	2062	2126	2451	2079	2135	1951	1776	1505	1246
19	**434**	4848	2843	2387	1518	556	0	3916	3070	2056	3673	2233	2254	2615	2244	2266	2067	1880	1663	1281
20	**444**	9289	2854	2434	1571	617	0	4163	3123	2135	4103	2315	2317	2697	2325	2327	2131	1929	1719	1305
21	**453**	18214	2897	2478	1639	717	0	5330	3233	2271	5002	2501	2457	2891	2516	2441	2283	2051	1825	1364
22	**455**	6989	2930	2513	1676	775	0	6709	3238	2291	6453	2567	2507	2987	2600	2491	2355	2114	1875	1398
23	**450**	21153	2923	2529	1688	799	0	6784	3218	2287	7362	2591	2518	3060	2669	2521	2406	2160	1913	1427
24	**422**	20956	2867	2641	1792	894	0	6554	3103	2372	7189	2486	2491	2942	2570	2437	2333	2078	1844	1376
25	**418**	20938	2855	2627	1786	909	0	6535	3088	2360	7160	2472	2483	2919	2565	2431	2327	2074	1837	1371
26	**412**	20915	2822	2597	1775	927	0	6497	3048	2328	7099	2451	2475	2911	2580	2461	2349	2106	1837	1385
27	**399**	20866	2786	2583	1761	933	0	6445	3001	2291	7037	2419	2469	2854	2530	2453	2329	2111	1813	1379
28	**371**	20760	2705	2595	1675	945	0	6342	2893	2187	6820	2298	2448	2702	2375	2348	2210	2103	1762	1343

Table B.15 (b) – (Y-set) Strain gauge data of Specimen F09-03 (Continued)

Step	Load	Strains in reinforcements																		
		YR11	YR12	YR13	YR14	YR15	YR16	YT21	YT22	YT23	YT31	YT32	YT33	YT41	YT42	YT43	YT51	YT52	YT53	YT61
	kN	(×10^{-6})	(×10^{-6})	(×10^{-6})	(×10^{-6})	(×10^{-6})	(×10^{-6})	(×10^{-6})	(×10^{-6})	(×10^{-6})	(×10^{-6})	(×10^{-6})	(×10^{-6})	(×10^{-6})	(×10^{-6})	(×10^{-6})	(×10^{-6})	(×10^{-6})	(×10^{-6})	(×10^{-6})
1	**0**	0	1	1	0	-1	0	0	0	1	-2	1	1	0	1	1	1	1	-1	0
2	**0**	0	1	0	0	1	0	0	1	0	1	1	0	0	1	1	0	0	2	0
3	**35**	31	23	17	8	5	0	28	22	16	29	20	19	24	24	19	21	21	18	18
4	**24**	16	13	7	1	0	0	15	12	7	16	11	8	13	13	10	11	11	9	9
5	**51**	26	22	12	0	-3	0	20	20	12	30	20	15	24	22	16	20	21	13	17
6	**94**	164	40	-28	-7	-51	0	206	46	19	197	44	19	71	114	28	62	87	41	50
7	**101**	176	38	-35	-11	-59	0	217	46	16	212	43	16	73	126	24	61	91	41	50
8	**122**	274	69	-32	-17	-68	0	312	67	19	286	57	20	91	184	29	72	136	61	65
9	**154**	653	148	-3	-20	-118	0	540	275	29	499	97	85	134	346	252	96	304	118	94
10	**282**	2200	1526	936	209	-85	0	2011	1527	774	1837	847	1107	1260	987	1237	1085	1140	466	846
11	**302**	2278	1747	1092	314	-46	0	2214	1669	866	2019	982	1241	1418	1096	1359	1207	1230	531	922
12	**320**	2440	1989	1248	447	-16	0	2420	1890	983	2228	1142	1390	1596	1254	1464	1350	1342	626	1000
13	**324**	2530	2095	1322	513	9	0	2517	2002	1086	2355	1244	1488	1693	1373	1579	1376	1396	850	976
14	**341**	2598	2189	1419	606	29	0	2605	2110	1171	2476	1337	1566	1780	1435	1627	1432	1436	976	1006
15	**360**	2781	2363	1591	779	99	0	2806	2348	1320	2738	1509	1704	1993	1638	1750	1599	1536	1190	1080
16	**380**	3054	2524	1806	1001	206	0	2983	2586	1512	2950	1692	1914	2121	1755	1914	1694	1586	1270	1124
17	**400**	3386	2641	1989	1163	293	0	3173	2764	1680	3143	1866	2002	2284	1915	2023	1818	1684	1397	1183
18	**418**	3726	2748	2208	1357	432	0	3619	2930	1883	3379	2062	2126	2451	2079	2135	1951	1776	1505	1246
19	**434**	4848	2843	2387	1518	556	0	3916	3070	2056	3673	2233	2254	2615	2244	2266	2067	1880	1663	1281
20	**444**	9289	2854	2434	1571	617	0	4163	3123	2135	4103	2315	2317	2697	2325	2327	2131	1929	1719	1305
21	**453**	18214	2897	2478	1639	717	0	5330	3233	2271	5002	2501	2457	2891	2516	2441	2283	2051	1825	1364
22	**455**	6989	2930	2513	1676	775	0	6709	3238	2291	6453	2567	2507	2987	2600	2491	2355	2114	1875	1398
23	**450**	21153	2923	2529	1688	799	0	6784	3218	2287	7362	2591	2518	3060	2669	2521	2406	2160	1913	1427
24	**422**	20956	2867	2641	1792	894	0	6554	3103	2372	7189	2486	2491	2942	2570	2437	2333	2078	1844	1376
25	**418**	20938	2855	2627	1786	909	0	6535	3088	2360	7160	2472	2483	2919	2565	2431	2327	2074	1837	1371
26	**412**	20915	2822	2597	1775	927	0	6497	3048	2328	7099	2451	2475	2911	2580	2461	2349	2106	1837	1385
27	**399**	20866	2786	2583	1761	933	0	6445	3001	2291	7037	2419	2469	2854	2530	2453	2329	2111	1813	1379
28	**371**	20760	2705	2595	1675	945	0	6342	2893	2187	6820	2298	2448	2702	2375	2348	2210	2103	1762	1343

Table B.16 (a) – (X-set) Strain gauge data of Specimen F14-03

Step	Load	Strains in reinforcements																		
		XR11	XR12	XR13	XR14	XR15	XR16	XT21	XT22	XT23	XT31	XT32	XT33	XT41	XT42	XT43	XT51	XT52	XT53	XT61
	kN	(×10^{-6})	(×10^{-6})	(×10^{-6})	(×10^{-6})	(×10^{-6})	(×10^{-6})	(×10^{-6})	(×10^{-6})	(×10^{-6})	(×10^{-6})	(×10^{-6})	(×10^{-6})	(×10^{-6})	(×10^{-6})	(×10^{-6})	(×10^{-6})	(×10^{-6})	(×10^{-6})	(×10^{-6})
1	**0**	0	1	0	-1	0	0	1	0	-1	-2	0	1	1	0	0	1	0	1	0
2	**26**	7	6	4	2	0	-3	19	9	7	15	11	8	16	13	9	12	9	9	9
3	**40**	15	-2	-34	-10	-27	-11	33	15	9	27	19	14	26	21	15	19	16	13	16
4	**66**	22	-34	-45	-27	-39	-30	55	19	10	52	31	20	47	39	22	33	25	20	26
5	**79**	37	-65	-39	-43	-32	-43	75	21	4	72	41	28	66	52	26	42	32	25	32
6	**107**	77	-78	-34	-68	-9	-70	136	32	5	129	81	40	155	104	33	102	52	37	58
7	**121**	125	-99	-32	-53	8	-70	203	49	17	170	116	39	212	166	45	165	61	52	86
8	**141**	208	-86	-27	-61	8	-85	294	90	33	248	158	47	269	256	60	243	77	78	145
9	**158**	298	-58	-9	-71	11	-106	378	134	53	316	197	68	297	318	79	277	92	101	169
10	**183**	439	39	61	-71	26	-126	499	230	96	446	320	120	395	431	161	388	120	134	228
11	**198**	538	134	111	-67	38	-138	623	347	144	538	417	183	449	472	369	427	138	151	256
12	**222**	690	318	197	-58	55	-143	808	547	246	686	535	294	556	557	538	508	174	193	301
13	**243**	801	490	298	-35	76	-146	961	680	382	805	648	388	643	673	610	562	246	265	334
14	**267**	935	670	406	16	105	-149	1125	833	527	948	784	484	762	788	725	652	308	315	421
15	**282**	1027	811	504	71	132	-153	1243	957	647	1063	884	565	845	872	838	714	355	351	557
16	**306**	1145	1000	654	174	183	-154	1429	1154	827	1229	1042	660	966	999	964	787	476	409	643
17	**322**	1221	1094	712	201	210	-155	1526	1272	905	1322	1133	702	1029	1056	1024	830	526	439	685
18	**357**	1456	1347	868	281	279	-153	1758	1572	1115	1556	1376	831	1187	1157	1150	915	687	494	779
19	**383**	1616	1552	996	374	356	-146	1928	1779	1257	1752	1575	918	1349	1246	1258	1000	832	555	849
20	**400**	1715	1691	1075	445	408	-141	2050	1928	1348	1872	1718	995	1465	1325	1328	1065	913	612	897
21	**421**	1835	1844	1159	529	466	-137	2173	2082	1430	2006	1857	1088	1566	1409	1406	1118	976	678	945
22	**441**	1934	1989	1252	622	527	-128	2299	2238	1515	2138	1992	1183	1674	1516	1467	1174	1028	767	994
23	**459**	2042	2166	1444	802	638	-111	2478	2452	1640	2333	2207	1339	1845	1656	1560	1270	1130	871	1071
24	**457**	2019	2175	1465	837	662	-104	2483	2468	1682	2394	2275	1398	1903	1704	1590	1299	1159	902	1084
25	**460**	1980	2194	1440	892	690	-92	2455	2464	1753	2532	2429	1493	2075	1824	1653	1377	1239	998	1119
26	**374**	1725	1953	1338	1183	866	-54	2132	2316	1465	1992	2235	1692	1825	1690	1647	1308	1190	933	1072
27	**364**	1707	1941	1362	1200	923	-44	2107	2306	1440	1923	2248	1664	1817	1597	1676	1302	1244	941	1098
28	**306**	1530	1767	1353	1227	1310	12	1939	2256	1419	1559	2194	1773	1795	1209	1395	1195	1137	947	1052

Table B.16 (b) – (Y-set) Strain gauge data of Specimen F14-03 (Continued)

Step	Load	Strains in reinforcements																		
		YR11	YR12	YR13	YR14	YR15	YR16	YT21	YT22	YT23	YT31	YT32	YT33	YT41	YT42	YT43	YT51	YT52	YT53	YT61
	kN	(×10^{-6})	(×10^{-6})	(×10^{-6})	(×10^{-6})	(×10^{-6})	(×10^{-6})	(×10^{-6})	(×10^{-6})	(×10^{-6})	(×10^{-6})	(×10^{-6})	(×10^{-6})	(×10^{-6})	(×10^{-6})	(×10^{-6})	(×10^{-6})	(×10^{-6})	(×10^{-6})	(×10^{-6})
1	**0**	0	1	0	-1	0	0	1	0	-1	-2	0	1	1	0	0	1	0	1	0
2	**26**	7	6	4	2	0	-3	19	9	7	15	11	8	16	13	9	12	9	9	9
3	**40**	15	-2	-34	-10	-27	-11	33	15	9	27	19	14	26	21	15	19	16	13	16
4	**66**	22	-34	-45	-27	-39	-30	55	19	10	52	31	20	47	39	22	33	25	20	26
5	**79**	37	-65	-39	-43	-32	-43	75	21	4	72	41	28	66	52	26	42	32	25	32
6	**107**	77	-78	-34	-68	-9	-70	136	32	5	129	81	40	155	104	33	102	52	37	58
7	**121**	125	-99	-32	-53	8	-70	203	49	17	170	116	39	212	166	45	165	61	52	86
8	**141**	208	-86	-27	-61	8	-85	294	90	33	248	158	47	269	256	60	243	77	78	145
9	**158**	298	-58	-9	-71	11	-106	378	134	53	316	197	68	297	318	79	277	92	101	169
10	**183**	439	39	61	-71	26	-126	499	230	96	446	320	120	395	431	161	388	120	134	228
11	**198**	538	134	111	-67	38	-138	623	347	144	538	417	183	449	472	369	427	138	151	256
12	**222**	690	318	197	-58	55	-143	808	547	246	686	535	294	556	557	538	508	174	193	301
13	**243**	801	490	298	-35	76	-146	961	680	382	805	648	388	643	673	610	562	246	265	334
14	**267**	935	670	406	16	105	-149	1125	833	527	948	784	484	762	788	725	652	308	315	421
15	**282**	1027	811	504	71	132	-153	1243	957	647	1063	884	565	845	872	838	714	355	351	557
16	**306**	1145	1000	654	174	183	-154	1429	1154	827	1229	1042	660	966	999	964	787	476	409	643
17	**322**	1221	1094	712	201	210	-155	1526	1272	905	1322	1133	702	1029	1056	1024	830	526	439	685
18	**357**	1456	1347	868	281	279	-153	1758	1572	1115	1556	1376	831	1187	1157	1150	915	687	494	779
19	**383**	1616	1552	996	374	356	-146	1928	1779	1257	1752	1575	918	1349	1246	1258	1000	832	555	849
20	**400**	1715	1691	1075	445	408	-141	2050	1928	1348	1872	1718	995	1465	1325	1328	1065	913	612	897
21	**421**	1835	1844	1159	529	466	-137	2173	2082	1430	2006	1857	1088	1566	1409	1406	1118	976	678	945
22	**441**	1934	1989	1252	622	527	-128	2299	2238	1515	2138	1992	1183	1674	1516	1467	1174	1028	767	994
23	**459**	2042	2166	1444	802	638	-111	2478	2452	1640	2333	2207	1339	1845	1656	1560	1270	1130	871	1071
24	**457**	2019	2175	1465	837	662	-104	2483	2468	1682	2394	2275	1398	1903	1704	1590	1299	1159	902	1084
25	**460**	1980	2194	1440	892	690	-92	2455	2464	1753	2532	2429	1493	2075	1824	1653	1377	1239	998	1119
26	**374**	1725	1953	1338	1183	866	-54	2132	2316	1465	1992	2235	1692	1825	1690	1647	1308	1190	933	1072
27	**364**	1707	1941	1362	1200	923	-44	2107	2306	1440	1923	2248	1664	1817	1597	1676	1302	1244	941	1098
28	**306**	1530	1767	1353	1227	1310	12	1939	2256	1419	1559	2194	1773	1795	1209	1395	1195	1137	947	1052

Table B.17 (a) – (X-set) Strain gauge data of Specimen F09-06

Step	Load	Strains in reinforcements																		
		XR11	XR12	XR13	XR14	XR15	XR16	XT21	XT22	XT23	XT31	XT32	XT33	XT41	XT42	XT43	XT51	XT52	XT53	XT61
	kN	(×10^{-6})	(×10^{-6})	(×10^{-6})	(×10^{-6})	(×10^{-6})	(×10^{-6})	(×10^{-6})	(×10^{-6})	(×10^{-6})	(×10^{-6})	(×10^{-6})	(×10^{-6})	(×10^{-6})	(×10^{-6})	(×10^{-6})	(×10^{-6})	(×10^{-6})	(×10^{-6})	(×10^{-6})
1	**0**	-1	0	0	0	0	1	0	0	0	-1	0	0	1	0	0	0	0	0	0
2	**24**	17	8	4	1	-2	-4	13	9	5	13	8	6	10	9	7	9	8	6	8
3	**44**	28	14	6	1	-4	-8	23	15	8	23	16	8	18	16	11	16	14	9	13
4	**58**	38	19	8	2	-6	-9	31	20	11	30	21	12	23	22	15	23	19	12	19
5	**81**	-1	-11	8	-8	-15	-15	52	31	22	46	31	19	37	32	23	34	27	19	28
6	**98**	-15	-12	-4	-19	-29	-32	76	41	27	69	47	26	55	47	33	49	39	27	40
7	**123**	34	-8	-11	-29	-42	-39	89	45	25	83	53	24	79	57	39	81	54	35	57
8	**156**	235	136	-21	-63	-60	-67	163	111	16	115	135	41	141	101	67	146	138	47	102
9	**180**	449	260	8	-45	-44	-92	382	167	49	307	239	74	275	147	89	220	256	78	192
10	**242**	1137	774	94	-14	-40	-115	1248	629	149	853	628	324	795	407	302	439	548	546	471
11	**260**	1364	951	169	5	-33	-121	1465	793	218	970	726	362	892	576	369	508	698	644	493
12	**282**	1585	1113	285	24	-24	-141	1716	1019	265	1094	853	424	1026	731	471	603	816	718	551
13	**302**	1773	1250	383	57	-9	-147	1925	1185	323	1272	1048	484	1165	841	644	716	921	859	610
14	**420**	2829	2165	1400	897	338	-160	2541	2240	1154	2457	1906	961	2011	1605	1276	1358	1459	1343	1023
15	**440**	3064	2329	1619	1104	453	-154	2638	2384	1371	2691	2095	1072	2183	1785	1405	1502	1574	1443	1096
16	**484**	3763	2702	2191	1651	758	-129	3141	2658	1814	3537	2511	1354	2663	2331	1719	1926	1892	1646	1248
17	**501**	5658	2833	2343	1838	863	-111	3427	2736	1978	4390	2611	1475	2836	2531	1845	2115	2004	1739	1345
18	**519**	12221	3067	2487	2009	956	-94	3418	2787	2101	5708	2732	1599	3009	2749	2025	2288	2101	1865	1450
19	**537**	19974	3245	2612	2176	1070	-46	3945	2955	2240	8605	2826	1686	3588	2947	2192	2550	2287	2013	1650
20	**540**	22183	3256	2687	2232	1101	-34	5714	2982	2286	12030	2865	1713	3731	2999	2250	2680	2381	2083	1763
21	**538**	22958	3278	2680	2229	1110	-25	8228	2966	2348	13742	2879	1716	3806	3014	2273	2748	2418	2118	1813
22	**543**	25119	3375	2727	2332	1160	-8	13281	3010	2527	15797	3237	1814	4132	3075	2325	2897	2519	2187	1950
23	**540**	25477	3414	2748	2401	1222	10	13285	3063	2483	16272	3252	1827	4140	3072	2289	3046	2459	2169	1928
24	**541**	26023	3487	2795	2438	1246	20	14315	3122	2491	16920	3287	1867	4225	3119	2330	3194	2508	2209	1971
25	**543**	6735	3519	2810	2451	1265	23	5062	3156	2471	6045	3409	1911	4503	3397	2375	3399	2554	2264	2082
26	**540**	26947	3512	2807	2446	1281	31	14945	3133	2441	18159	3379	1896	4496	3393	2357	3381	2524	2252	2060
27	**358**	27235	3403	2728	2531	1922	111	15014	3242	2578	17169	2456	1796	3782	2829	2164	2926	1900	1968	1719
28	**288**	26970	3208	2611	2510	2054	159	14578	3187	2147	16546	1949	1430	3315	2396	1796	2569	1529	1667	1482

Table B.17 (b) – (Y-set) Strain gauge data of Specimen F09-06 (Continued)

Step	Load	Strains in reinforcements																		
		YR11	YR12	YR13	YR14	YR15	YR16	YT21	YT22	YT23	YT31	YT32	YT33	YT41	YT42	YT43	YT51	YT52	YT53	YT61
	kN	(×10^{-6})	(×10^{-6})	(×10^{-6})	(×10^{-6})	(×10^{-6})	(×10^{-6})	(×10^{-6})	(×10^{-6})	(×10^{-6})	(×10^{-6})	(×10^{-6})	(×10^{-6})	(×10^{-6})	(×10^{-6})	(×10^{-6})	(×10^{-6})	(×10^{-6})	(×10^{-6})	(×10^{-6})
1	**0**	-1	0	0	0	0	1	0	0	0	-1	0	0	1	0	0	0	0	0	0
2	**24**	17	8	4	1	-2	-4	13	9	5	13	8	6	10	9	7	9	8	6	8
3	**44**	28	14	6	1	-4	-8	23	15	8	23	16	8	18	16	11	16	14	9	13
4	**58**	38	19	8	2	-6	-9	31	20	11	30	21	12	23	22	15	23	19	12	19
5	**81**	-1	-11	8	-8	-15	-15	52	31	22	46	31	19	37	32	23	34	27	19	28
6	**98**	-15	-12	-4	-19	-29	-32	76	41	27	69	47	26	55	47	33	49	39	27	40
7	**123**	34	-8	-11	-29	-42	-39	89	45	25	83	53	24	79	57	39	81	54	35	57
8	**156**	235	136	-21	-63	-60	-67	163	111	16	115	135	41	141	101	67	146	138	47	102
9	**180**	449	260	8	-45	-44	-92	382	167	49	307	239	74	275	147	89	220	256	78	192
10	**242**	1137	774	94	-14	-40	-115	1248	629	149	853	628	324	795	407	302	439	548	546	471
11	**260**	1364	951	169	5	-33	-121	1465	793	218	970	726	362	892	576	369	508	698	644	493
12	**282**	1585	1113	285	24	-24	-141	1716	1019	265	1094	853	424	1026	731	471	603	816	718	551
13	**302**	1773	1250	383	57	-9	-147	1925	1185	323	1272	1048	484	1165	841	644	716	921	859	610
14	**420**	2829	2165	1400	897	338	-160	2541	2240	1154	2457	1906	961	2011	1605	1276	1358	1459	1343	1023
15	**440**	3064	2329	1619	1104	453	-154	2638	2384	1371	2691	2095	1072	2183	1785	1405	1502	1574	1443	1096
16	**484**	3763	2702	2191	1651	758	-129	3141	2658	1814	3537	2511	1354	2663	2331	1719	1926	1892	1646	1248
17	**501**	5658	2833	2343	1838	863	-111	3427	2736	1978	4390	2611	1475	2836	2531	1845	2115	2004	1739	1345
18	**519**	12221	3067	2487	2009	956	-94	3418	2787	2101	5708	2732	1599	3009	2749	2025	2288	2101	1865	1450
19	**537**	19974	3245	2612	2176	1070	-46	3945	2955	2240	8605	2826	1686	3588	2947	2192	2550	2287	2013	1650
20	**540**	22183	3256	2687	2232	1101	-34	5714	2982	2286	12030	2865	1713	3731	2999	2250	2680	2381	2083	1763
21	**538**	22958	3278	2680	2229	1110	-25	8228	2966	2348	13742	2879	1716	3806	3014	2273	2748	2418	2118	1813
22	**543**	25119	3375	2727	2332	1160	-8	13281	3010	2527	15797	3237	1814	4132	3075	2325	2897	2519	2187	1950
23	**540**	25477	3414	2748	2401	1222	10	13285	3063	2483	16272	3252	1827	4140	3072	2289	3046	2459	2169	1928
24	**541**	26023	3487	2795	2438	1246	20	14315	3122	2491	16920	3287	1867	4225	3119	2330	3194	2508	2209	1971
25	**543**	6735	3519	2810	2451	1265	23	5062	3156	2471	6045	3409	1911	4503	3397	2375	3399	2554	2264	2082
26	**540**	26947	3512	2807	2446	1281	31	14945	3133	2441	18159	3379	1896	4496	3393	2357	3381	2524	2252	2060
27	**358**	27235	3403	2728	2531	1922	111	15014	3242	2578	17169	2456	1796	3782	2829	2164	2926	1900	1968	1719
28	**288**	26970	3208	2611	2510	2054	159	14578	3187	2147	16546	1949	1430	3315	2396	1796	2569	1529	1667	1482

Table B.18 (a) – (X-set) Strain gauge data of Specimen F14-06

Step	Load	Strains in reinforcements																		
		XR11	XR12	XR13	XR14	XR15	XR16	XT21	XT22	XT23	XT31	XT32	XT33	XT41	XT42	XT43	XT51	XT52	XT53	XT61
	kN	(×10^{-6})	(×10^{-6})	(×10^{-6})	(×10^{-6})	(×10^{-6})	(×10^{-6})	(×10^{-6})	(×10^{-6})	(×10^{-6})	(×10^{-6})	(×10^{-6})	(×10^{-6})	(×10^{-6})	(×10^{-6})	(×10^{-6})	(×10^{-6})	(×10^{-6})	(×10^{-6})	(×10^{-6})
1	**0**	516	219	79	-53	-156	-111	545	316	83	502	314	203	435	270	102	406	0	167	346
2	**19**	847	538	176	-21	-173	-143	883	568	184	747	526	346	639	468	207	593	0	296	569
3	**48**	947	668	225	2	-174	-153	962	662	229	836	599	393	708	534	256	657	0	359	624
4	**70**	1126	901	347	69	-167	-166	1101	841	329	972	714	477	811	615	358	749	0	447	700
5	**103**	1349	1114	487	140	-167	-183	1306	1016	433	1158	880	592	953	731	453	862	0	549	764
6	**122**	1597	1386	701	247	-159	-192	1557	1239	562	1359	1079	745	1085	838	574	977	0	623	854
7	**160**	1779	1648	901	358	-112	-203	1802	1457	680	1611	1298	863	1280	991	696	1152	0	729	941
8	**179**	1970	1888	1104	468	-39	-208	2015	1642	851	1858	1503	979	1463	1152	795	1325	0	837	1010
9	**200**	2126	2093	1372	587	42	-192	2187	1804	1074	2050	1680	1111	1605	1273	881	1441	0	910	1070
10	**214**	2255	2248	1508	678	108	-181	2317	1921	1225	2200	1814	1216	1723	1380	955	1539	0	969	1125
11	**264**	2585	2531	1720	842	263	-156	2611	2131	1485	2464	2040	1408	1917	1565	1090	1697	0	1065	1211
12	**301**	3007	2750	1862	1008	396	-131	2937	2318	1723	2737	2271	1643	2092	1757	1241	1880	0	1172	1300
13	**317**	3092	2843	1893	1050	426	-122	3053	2354	1790	2812	2328	1715	2129	1810	1275	1936	0	1194	1329
14	**351**	3240	2994	1909	1127	479	-111	3225	2414	1848	2900	2409	1827	2174	1901	1327	1994	0	1220	1348
15	**371**	3470	3214	1976	1276	563	-98	3426	2511	1919	2995	2503	1970	2222	2019	1453	2114	0	1273	1421
16	**385**	3462	3256	1972	1350	619	-78	3408	2516	1884	3064	2487	1982	2196	2009	1476	2109	0	1266	1403
17	**419**	3551	3792	2029	1580	767	-52	3435	2742	1859	3233	2562	2028	2251	2142	1697	2266	0	1337	1489
18	**445**	3663	4140	2034	1657	833	-35	3474	2818	1868	3417	2595	2047	2269	2166	1776	2286	0	1353	1496
19	**477**	3810	7791	2016	2035	1181	35	4000	3459	1856	3831	2727	2196	2357	2281	2151	2395	0	1450	1607
20	**503**	3619	7943	2066	2173	1432	80	3898	3748	1811	3799	2708	2201	2242	2093	2274	2234	0	1489	1593
21	**521**	3436	7936	2028	2335	1609	126	3682	3869	1868	3712	2681	2157	2132	1913	2312	2154	0	1579	1602
22	**541**	3278	8709	2059	1507	1577	161	3433	3949	1543	3431	2537	1753	1795	1516	2178	1885	0	1482	1477
23	**560**	3249	8844	2036	1468	1570	163	3404	3930	1515	3407	2528	1732	1772	1496	2167	1867	0	1469	1465
24	**557**	3244	8863	2030	1463	1569	164	3399	3923	1510	3403	2525	1728	1768	1492	2164	1864	0	1467	1463
25	**560**	3240	8881	2027	1458	1568	164	3396	3918	1506	3399	2523	1724	1764	1489	2163	1861	0	1464	1460
26	**570**	3239	8903	2023	1452	1568	164	3393	3915	1503	3395	2519	1719	1761	1485	2162	1857	0	1463	1458
27	**581**	3282	11917	2024	1552	1601	171	3408	4641	2443	3417	2484	1785	1738	1405	2263	1870	0	1487	1476
28	**569**	3333	15605	2100	1731	1661	190	3411	5958	0	3481	2440	2117	1675	1292	2395	1881	0	1501	1511

Table B.18 (b) – (Y-set) Strain gauge data of Specimen F14-06 (Continued)

Step	Load	Strains in reinforcements																		
		YR11	YR12	YR13	YR14	YR15	YR16	YT21	YT22	YT23	YT31	YT32	YT33	YT41	YT42	YT43	YT51	YT52	YT53	YT61
	kN	($\times10^{-6}$)	($\times10^{-6}$)	($\times10^{-6}$)	($\times10^{-6}$)	($\times10^{-6}$)	($\times10^{-6}$)	($\times10^{-6}$)	($\times10^{-6}$)	($\times10^{-6}$)	($\times10^{-6}$)	($\times10^{-6}$)	($\times10^{-6}$)	($\times10^{-6}$)	($\times10^{-6}$)	($\times10^{-6}$)	($\times10^{-6}$)	($\times10^{-6}$)	($\times10^{-6}$)	($\times10^{-6}$)
1	**0**	914	444	28	-10	1	-33	684	481	62	598	386	200	464	296	195	365	266	270	455
2	**19**	1205	786	107	6	19	-29	917	836	147	833	600	398	668	433	326	506	367	397	600
3	**48**	1287	888	158	19	28	-24	1003	949	194	927	683	455	755	484	370	559	436	453	659
4	**70**	1413	1029	247	40	38	-25	1133	1131	269	1080	821	556	901	599	444	644	587	543	739
5	**103**	1654	1266	395	84	56	-26	1348	1408	387	1295	1008	686	1066	781	544	747	727	621	814
6	**122**	1978	1588	623	184	81	-27	1654	1788	567	1591	1246	849	1294	1055	707	900	916	743	947
7	**160**	2077	1720	762	245	108	-26	1799	1997	691	1753	1361	932	1419	1245	785	999	1036	850	1027
8	**179**	2194	1846	896	307	131	-28	1926	2189	813	1901	1489	1016	1570	1407	863	1097	1143	974	1123
9	**200**	2511	2101	1109	429	160	-28	2182	2481	1007	2116	1696	1153	1773	1597	984	1225	1285	1114	1237
10	**214**	2770	2253	1253	525	184	-28	2358	2620	1132	2225	1812	1241	1881	1697	1051	1291	1352	1195	1285
11	**264**	3301	2515	1510	699	233	-27	2907	2935	1388	2497	2085	1443	2165	1937	1208	1466	1523	1378	1404
12	**301**	3963	2735	1747	861	292	-25	4121	3220	1633	2803	2326	1634	2459	2180	1364	1645	1695	1547	1524
13	**317**	4016	2741	1779	893	304	-26	4207	3239	1659	2842	2337	1649	2477	2196	1374	1650	1701	1559	1520
14	**351**	4216	2790	1954	1195	386	-22	4660	3348	1892	2901	2418	1835	2609	2300	1427	1724	1765	1617	1581
15	**371**	4376	2885	1982	1349	440	-23	4961	3419	1954	2979	2452	1958	2671	2351	1470	1761	1798	1653	1602
16	**385**	4718	3156	2034	1537	495	-20	5443	3564	2027	3102	2526	2049	2816	2437	1543	1844	1870	1711	1673
17	**419**	4858	3265	2008	1782	615	-19	5561	3611	2040	3341	2526	2044	2856	2474	1646	1867	1886	1750	1674
18	**445**	4920	3469	2039	1915	724	-13	5602	3768	2259	3678	2565	2118	2932	2579	1767	1948	1964	1792	1736
19	**477**	4767	3918	2047	2187	1315	15	5364	4815	2366	4811	3460	2086	2999	2675	2153	2062	2055	1824	1776
20	**503**	4426	3902	1786	2236	1817	45	5235	6512	2257	-1019	3578	2191	2876	2504	2169	2010	2012	1776	1750
21	**521**	4079	4387	1849	1936	1932	65	5088	8593	1720	0	3354	2263	2570	2269	2020	1840	1844	1653	1622
22	**541**	3885	5357	1079	1083	1751	74	4599	9114	972	0	2803	1932	2245	1947	1732	1624	1605	1426	1425
23	**560**	3875	5353	1044	1042	1739	74	4568	9035	945	0	2774	1908	2219	1925	1715	1606	1590	1409	1410
24	**557**	3873	5355	1038	1035	1735	75	4564	8992	942	0	2768	1904	2214	1921	1712	1604	1587	1408	1408
25	**560**	3868	5361	1032	1037	1737	76	4559	8968	936	0	2763	1899	2210	1917	1707	1601	1583	1404	1405
26	**570**	3867	5368	1029	1025	1735	76	4554	8968	934	0	2758	1895	2206	1913	1703	1597	1580	1401	1403
27	**581**	3941	6503	871	877	1736	79	4538	8972	854	0	2573	1905	2151	1877	1672	1568	1542	1359	1369
28	**569**	3949	8398	628	631	1702	82	4319	9166	745	0	2375	1869	2024	1767	1587	1474	1450	1269	1275

Table B.19 (a) – (X-set) Strain gauge data of Specimen F09-09

Step	Load	Strains in reinforcements																		
		XR11	XR12	XR13	XR14	XR15	XR16	XT21	XT22	XT23	XT31	XT32	XT33	XT41	XT42	XT43	XT51	XT52	XT53	XT61
	kN	(×10^{-6})	(×10^{-6})	(×10^{-6})	(×10^{-6})	(×10^{-6})	(×10^{-6})	(×10^{-6})	(×10^{-6})	(×10^{-6})	(×10^{-6})	(×10^{-6})	(×10^{-6})	(×10^{-6})	(×10^{-6})	(×10^{-6})	(×10^{-6})	(×10^{-6})	(×10^{-6})	(×10^{-6})
1	**0**	0	0	2	0	1	0	1	0	0	0	1	0	0	-1	0	0	-1	1	0
2	**20**	11	6	4	2	1	-2	10	8	0	9	8	5	8	6	5	8	6	6	6
3	**44**	26	14	8	4	0	-4	24	17	0	21	17	10	18	14	10	17	14	12	14
4	**66**	32	18	8	5	-2	-8	45	27	0	38	28	18	31	23	17	28	23	19	23
5	**82**	32	21	6	4	-5	-11	59	29	0	47	34	22	39	29	20	36	29	23	28
6	**101**	57	26	-7	4	-12	-19	83	41	0	74	54	29	59	44	29	53	42	32	41
7	**126**	77	23	-8	-11	-28	-58	98	63	0	122	75	34	89	58	36	74	56	40	57
8	**145**	92	24	-7	-3	-48	-102	128	78	0	210	83	38	136	68	39	110	68	47	78
9	**161**	131	36	-5	3	-57	-134	180	87	0	287	106	50	167	77	58	163	73	55	127
10	**180**	192	50	-5	3	-64	-144	213	103	0	401	147	62	229	93	71	224	152	58	162
11	**197**	350	73	-3	5	-62	-155	321	172	0	566	230	86	440	114	108	391	219	65	249
12	**256**	799	344	78	24	-40	-208	738	472	0	1025	502	219	852	342	307	743	601	89	535
13	**277**	965	479	160	62	-32	-246	902	612	0	1157	634	302	975	444	416	844	722	146	602
14	**280**	999	509	177	71	-30	-246	944	643	0	1195	665	322	1011	470	439	877	752	162	627
15	**340**	1510	1213	508	352	36	-245	1580	1180	0	1629	980	824	1367	870	734	1170	985	649	831
16	**359**	1670	1417	609	450	68	-237	1771	1366	0	1812	1092	942	1523	1016	830	1316	1103	753	906
17	**380**	1838	1583	700	532	100	-234	1919	1523	0	1948	1202	1045	1639	1127	926	1412	1189	838	949
18	**393**	1970	1715	780	602	133	-232	2050	1663	0	2067	1306	1130	1738	1237	1010	1496	1281	912	984
19	**402**	2045	1785	821	638	149	-234	2127	1733	0	2126	1359	1176	1788	1295	1051	1535	1322	946	1008
20	**422**	2228	1971	934	743	217	-235	2307	1912	0	2268	1487	1272	1907	1427	1143	1626	1414	1039	1056
21	**465**	2624	2393	1204	1001	374	-209	2785	2338	0	2683	1816	1499	2264	1729	1361	1915	1670	1267	1246
22	**578**	4886	3108	1965	1752	876	-55	13632	3058	0	7553	2750	2237	3782	2801	2260	3385	2668	1975	1886
23	**616**	11772	3148	2149	1947	1085	11	18515	3240	0	12716	2968	2467	4679	3051	2534	6809	3190	2302	2284
24	**625**	12418	3127	2166	1996	1130	25	19018	3242	0	13625	2987	2491	4805	3175	2564	7964	3463	2353	2373
25	**664**	17274	3126	2334	2491	1791	619	20991	3610	0	15701	3351	2745	20047	3645	2780	12668	6042	2712	3825
26	**668**	17700	3146	2370	2555	1864	660	21146	3632	0	15908	3437	2787	20668	3731	2822	13510	7854	2755	4184
27	**672**	5976	3139	2385	2578	1905	687	7000	3626	0	5336	3526	2822	6992	3762	2843	4784	9506	2768	4673
28	**670**	18496	3178	2402	2604	1948	712	21162	3591	0	16030	3534	2811	21010	3716	2808	14626	9984	2734	4783

Table B.19 (b) – (Y-set) Strain gauge data of Specimen F09-09 (Continued)

Step	Load	Strains in reinforcements																		
		YR11	YR12	YR13	YR14	YR15	YR16	YT21	YT22	YT23	YT31	YT32	YT33	YT41	YT42	YT43	YT51	YT52	YT53	YT61
	kN	($\times10^{-6}$)	($\times10^{-6}$)	($\times10^{-6}$)	($\times10^{-6}$)	($\times10^{-6}$)	($\times10^{-6}$)	($\times10^{-6}$)	($\times10^{-6}$)	($\times10^{-6}$)	($\times10^{-6}$)	($\times10^{-6}$)	($\times10^{-6}$)	($\times10^{-6}$)	($\times10^{-6}$)	($\times10^{-6}$)	($\times10^{-6}$)	($\times10^{-6}$)	($\times10^{-6}$)	($\times10^{-6}$)
1	**0**	-3	0	0	0	-1	-1	0	0	-1	-1	-1	0	0	0	-1	-2	0	0	N/A
2	**20**	10	0	0	0	4	3	0	0	7	11	11	0	10	9	8	8	9	8	N/A
3	**44**	22	0	0	0	4	0	0	0	9	20	19	0	19	17	14	19	14	12	N/A
4	**66**	35	0	0	0	3	-7	0	0	11	28	24	0	26	23	19	25	20	15	N/A
5	**82**	62	0	0	0	4	-11	0	0	14	39	31	0	35	31	23	34	25	20	N/A
6	**101**	94	0	0	0	-8	-28	0	0	19	53	39	0	45	39	29	42	33	23	N/A
7	**126**	134	0	0	0	-23	-53	0	0	12	69	45	0	76	51	38	82	48	34	N/A
8	**145**	170	0	0	0	-33	-73	0	0	11	80	61	0	119	54	61	115	64	40	N/A
9	**161**	211	0	0	0	-47	-100	0	0	8	98	88	0	172	58	95	164	72	49	N/A
10	**180**	275	0	0	0	-64	-114	0	0	-2	126	110	0	239	66	195	224	81	73	N/A
11	**197**	353	0	0	0	-67	-128	0	0	1	173	110	0	336	82	237	314	98	96	N/A
12	**256**	751	0	0	0	-86	-152	0	0	105	608	260	0	712	209	470	636	262	233	N/A
13	**277**	979	0	0	0	-96	-156	0	0	234	798	381	0	867	329	600	762	392	333	N/A
14	**280**	991	0	0	0	-96	-156	0	0	248	810	398	0	876	344	615	769	407	348	N/A
15	**340**	1372	0	0	0	-69	-113	0	0	567	1302	795	0	1285	709	894	1089	685	638	N/A
16	**359**	1490	0	0	0	-51	-69	0	0	662	1458	914	0	1417	829	967	1193	770	746	N/A
17	**380**	1750	0	0	0	-29	-45	0	0	777	1663	1072	0	1555	971	1066	1312	875	843	N/A
18	**393**	1917	0	0	0	-8	-25	0	0	854	1801	1189	0	1647	1068	1130	1392	946	910	N/A
19	**402**	2000	0	0	0	1	-17	0	0	890	1878	1250	0	1696	1116	1167	1435	981	945	N/A
20	**422**	2298	0	0	0	31	0	0	0	1015	2140	1450	0	1878	1289	1303	1601	1114	1074	N/A
21	**465**	2715	0	0	0	85	29	0	0	1205	2526	1770	0	2177	1558	1529	1861	1322	1243	N/A
22	**578**	3742	0	0	0	368	84	0	0	1670	3838	2825	0	3299	2471	2484	3432	2287	2115	N/A
23	**616**	3933	0	0	0	496	110	0	0	1787	4326	3049	0	3454	2642	2725	3942	2548	2384	N/A
24	**625**	3919	0	0	0	531	116	0	0	1801	4398	3086	0	3490	2682	2769	4349	2612	2445	N/A
25	**664**	15639	0	0	0	694	192	0	0	1922	4864	3411	0	3656	2973	3021	13529	2973	2782	N/A
26	**668**	19466	0	0	0	699	194	0	0	1904	5095	3467	0	3662	3203	3065	14485	3029	2835	N/A
27	**672**	20787	0	0	0	698	197	0	0	1876	5314	3492	0	3659	3282	3085	14978	3106	2845	N/A
28	**670**	21515	0	0	0	704	208	0	0	1864	5668	3542	0	3672	3443	3112	15780	3251	2884	N/A

Table B.20 (a) – (X-set) Strain gauge data of Specimen F14-09

Step	Load	Strains in reinforcements																		
		XR11	XR12	XR13	XR14	XR15	XR16	XT21	XT22	XT23	XT31	XT32	XT33	XT41	XT42	XT43	XT51	XT52	XT53	XT61
	kN	($\times 10^{-6}$)	($\times 10^{-6}$)	($\times 10^{-6}$)	($\times 10^{-6}$)	($\times 10^{-6}$)	($\times 10^{-6}$)	($\times 10^{-6}$)	($\times 10^{-6}$)	($\times 10^{-6}$)	($\times 10^{-6}$)	($\times 10^{-6}$)	($\times 10^{-6}$)	($\times 10^{-6}$)	($\times 10^{-6}$)	($\times 10^{-6}$)	($\times 10^{-6}$)	($\times 10^{-6}$)	($\times 10^{-6}$)	($\times 10^{-6}$)
1	**0**	-1	0	0	1	0	0	0	0	-1	-1	0	0	-1	0	0	-2	1	0	0
2	**19**	2	-8	-8	-3	-4	-3	0	0	-5	1	0	-5	2	-1	-1	-2	4	-3	1
3	**44**	46	6	-6	-2	-6	-8	0	0	2	42	26	4	35	24	24	23	29	15	26
4	**58**	81	23	1	-3	-8	-13	0	0	8	71	45	11	58	44	42	39	47	29	43
5	**62**	96	31	4	-1	-8	-13	0	0	12	84	55	16	69	54	49	48	55	37	52
6	**81**	146	58	16	-1	-10	-20	0	0	25	127	85	29	105	83	75	72	81	58	75
7	**103**	209	95	34	2	-13	-27	0	0	44	180	120	47	147	119	108	105	114	85	106
8	**180**	418	226	100	12	-20	-48	0	0	115	383	258	119	323	260	230	242	242	198	233
9	**202**	479	264	118	15	-22	-54	0	0	134	437	296	139	367	297	264	278	275	226	265
10	**246**	597	346	159	19	-29	-68	0	0	178	563	379	183	472	379	343	358	347	293	332
11	**286**	712	417	195	32	-29	-71	0	0	222	679	455	224	567	458	408	439	416	353	402
12	**302**	760	455	221	45	-23	-68	0	0	253	745	495	249	618	500	450	477	452	386	433
13	**323**	829	501	249	60	-19	-67	0	0	286	816	541	277	672	544	491	518	489	421	465
14	**381**	1100	720	400	147	30	-41	0	0	454	1101	730	423	896	745	654	682	650	554	579
15	**382**	1105	728	407	151	32	-40	0	0	460	1107	734	427	900	747	659	683	653	556	577
16	**402**	1222	837	480	195	55	-30	0	0	541	1231	824	510	1000	838	736	759	723	614	622
17	**481**	1647	1267	760	410	181	11	0	0	856	1715	1184	838	1358	1211	1004	1064	1024	851	793
18	**503**	1753	1381	839	474	221	22	0	0	940	1831	1293	937	1453	1301	1085	1140	1101	919	837
19	**563**	2055	1753	1094	672	346	66	0	0	1184	2204	1599	1238	1747	1583	1317	1380	1327	1118	982
20	**603**	2383	1986	1257	803	421	86	0	0	1339	2481	1798	1421	1989	1796	1490	1573	1497	1270	1103
21	**664**	2963	2322	1598	1073	580	139	0	0	1585	2994	2097	1679	2548	2192	1837	1914	1809	1593	1303
22	**701**	3652	2585	1756	1370	714	189	0	0	1699	3317	2253	1805	3182	2631	2101	2236	2096	1872	1501
23	**719**	4211	2701	1818	1608	783	217	0	0	1747	3439	2314	1860	3628	2817	2227	2403	2249	2013	1604
24	**795**	7145	2865	2068	2549	1367	503	0	0	2041	6307	2502	2040	14968	3369	2764	6073	3374	2613	2411
25	**796**	7142	2868	2104	2550	1445	567	0	0	2106	6732	2776	2170	15197	3409	2838	6341	3409	2647	2420
26	**801**	7091	2895	2127	2585	1544	659	0	0	2212	5500	3143	2346	6000	3484	3037	4300	3505	2905	2512
27	**797**	7100	2922	2163	2612	1582	684	0	0	2281	9152	3186	2394	15653	3453	3086	6824	3501	2911	2540
28	**784**	6979	2904	2248	2743	1762	779	0	0	2443	9405	3256	2522	15702	3508	3164	6853	3497	2920	2504

Table B.20 (b) – (Y-set) Strain gauge data of Specimen F14-09 (Continued)

Step	Load	Strains in reinforcements																		
		YR11	YR12	YR13	YR14	YR15	YR16	YT21	YT22	YT23	YT31	YT32	YT33	YT41	YT42	YT43	YT51	YT52	YT53	YT61
	kN	($\times10^{-6}$)	($\times10^{-6}$)	($\times10^{-6}$)	($\times10^{-6}$)	($\times10^{-6}$)	($\times10^{-6}$)	($\times10^{-6}$)	($\times10^{-6}$)	($\times10^{-6}$)	($\times10^{-6}$)	($\times10^{-6}$)	($\times10^{-6}$)	($\times10^{-6}$)	($\times10^{-6}$)	($\times10^{-6}$)	($\times10^{-6}$)	($\times10^{-6}$)	($\times10^{-6}$)	($\times10^{-6}$)
1	**0**	-3	-3	-1	-2	-2	-2	0	-2	-3	-3	-2	-3	-4	-3	-3	0	-4	-3	-4
2	**19**	-13	-16	-11	-14	-17	-17	0	-15	-16	-12	-9	-11	-13	-11	-11	0	-13	-10	-13
3	**44**	18	-3	-8	-15	-20	-22	0	21	0	-8	21	14	1	21	13	0	17	8	8
4	**58**	53	13	-1	-15	-21	-23	0	59	19	1	50	40	17	52	39	0	45	29	29
5	**62**	55	11	-1	-15	-22	-25	0	61	18	0	51	40	18	53	39	0	45	29	31
6	**81**	112	41	10	-13	-24	-30	0	122	51	12	100	83	43	100	79	0	89	62	64
7	**103**	250	74	25	-11	-27	-35	0	190	88	26	154	130	72	156	124	0	138	99	100
8	**180**	475	192	79	-2	-37	-52	0	426	212	74	345	283	173	346	276	0	308	225	231
9	**202**	547	234	98	2	-38	-56	0	502	253	91	406	332	206	406	326	0	361	265	272
10	**246**	713	333	149	14	-38	-63	0	680	353	135	552	454	285	551	443	0	491	364	370
11	**286**	808	380	170	15	-46	-73	0	781	400	155	633	514	327	629	506	0	561	419	424
12	**302**	871	420	195	21	-46	-77	0	849	441	176	697	563	361	689	555	0	615	468	464
13	**323**	948	468	223	29	-48	-81	0	931	493	202	771	623	401	759	614	0	679	527	510
14	**381**	1249	688	393	101	-37	-89	0	1233	744	364	1082	865	582	1018	847	0	896	769	680
15	**382**	1264	704	408	110	-35	-88	0	1251	762	378	1102	884	596	1035	870	0	909	791	700
16	**402**	1367	787	483	147	-28	-92	0	1349	859	451	1211	968	670	1116	952	0	976	853	728
17	**481**	1843	1199	870	348	18	-84	0	1814	1328	795	1754	1360	985	1532	1355	0	1353	1218	972
18	**503**	1982	1318	973	408	33	-74	0	1954	1462	897	1911	1474	1080	1652	1465	0	1463	1322	1049
19	**563**	2424	1626	1270	593	85	-54	0	2518	1793	1168	2348	1795	1338	2015	1785	0	1784	1609	1268
20	**603**	2856	1804	1440	711	119	-44	0	2983	1979	1317	2585	1987	1506	2277	2013	0	1995	1807	1421
21	**664**	3400	1924	1691	886	177	-27	0	5258	2147	1489	3317	2214	1740	3254	2441	0	2472	2219	1744
22	**701**	3979	1976	1912	1085	283	-6	0	8270	2226	1571	4032	2334	1898	6467	2899	0	3114	2562	2058
23	**719**	4439	2016	1970	1161	333	5	0	9416	2239	1629	4785	2466	1955	8554	3092	0	3348	2899	2171
24	**795**	10555	2455	2211	1590	839	161	0	15074	2594	2130	6360	2684	2138	17699	3646	0	6816	3419	2774
25	**796**	11489	2466	2238	1636	887	187	0	15651	2646	2228	7073	2680	2177	18605	3886	0	8767	3446	2842
26	**801**	12370	2478	2301	1717	960	237	0	15980	2758	2381	8906	2692	2286	19796	4446	0	10722	3500	2884
27	**797**	12665	2457	2298	1737	996	269	0	15989	2775	2401	9363	2668	2317	20055	4533	0	11006	3474	2857
28	**784**	13932	2516	2363	1854	1106	345	0	16170	3001	2601	11688	2596	2377	21840	4766	0	12622	3503	2861

Table B.21 (a) – (X-set) Strain gauge data of Specimen F09-12

Step	Load	Strains in reinforcements																		
		XR11	XR12	XR13	XR14	XR15	XR16	XT21	XT22	XT23	XT31	XT32	XT33	XT41	XT42	XT43	XT51	XT52	XT53	XT61
	kN	(×10^{-6})	(×10^{-6})	(×10^{-6})	(×10^{-6})	(×10^{-6})	(×10^{-6})	(×10^{-6})	(×10^{-6})	(×10^{-6})	(×10^{-6})	(×10^{-6})	(×10^{-6})	(×10^{-6})	(×10^{-6})	(×10^{-6})	(×10^{-6})	(×10^{-6})	(×10^{-6})	(×10^{-6})
1	**0**	0	-1	-1	1	0	0	1	0	0	0	0	0	-1	0	-1	1	-1	0	0
2	**0**	1	0	0	0	0	0	0	0	0	0	1	0	1	0	0	0	0	0	-1
3	**1**	0	0	-1	0	0	0	-1	1	0	-1	-1	0	0	0	-1	-1	-1	0	0
4	**28**	15	-1	0	-2	-3	-7	14	10	3	12	6	7	8	10	6	8	8	6	8
5	**68**	59	-13	5	-13	-27	-30	177	17	-11	58	36	18	33	43	21	31	26	17	24
6	**124**	209	-28	13	-70	-31	-82	539	29	-68	262	101	39	173	115	39	129	71	38	72
7	**156**	367	8	60	-83	-40	-121	672	112	-80	368	219	54	241	146	101	238	103	59	150
8	**199**	669	85	104	-79	-55	-170	810	156	-41	514	354	51	393	188	170	336	131	87	268
9	**215**	797	122	134	-86	-54	-184	863	196	9	545	397	114	472	206	204	406	144	94	325
10	**282**	1442	727	330	-86	-28	-166	1385	552	181	816	707	358	799	520	378	719	280	255	677
11	**304**	1626	882	400	-85	-13	-147	1558	706	248	987	834	427	941	642	430	791	430	295	727
12	**321**	1840	1044	471	-67	0	-142	1739	870	325	1162	987	514	1040	749	468	862	536	345	799
13	**360**	2215	1403	716	51	56	-126	2147	1294	570	1453	1357	757	1322	957	824	993	723	596	937
14	**401**	2580	1739	970	170	107	-114	2554	1656	765	1750	1729	973	1572	1157	986	1145	893	762	1091
15	**444**	2940	2170	1316	361	171	-102	2985	2041	1036	2115	2080	1202	1845	1389	1203	1322	1076	965	1256
16	**464**	3090	2364	1471	461	221	-89	3143	2208	1147	2269	2235	1302	1996	1509	1305	1398	1158	1045	1329
17	**480**	3357	2505	1618	573	269	-71	3294	2369	1262	2417	2381	1405	2148	1649	1392	1477	1239	1126	1403
18	**507**	3695	2695	1842	750	349	-43	3883	2596	1417	2674	2622	1573	2372	1862	1522	1603	1376	1239	1507
19	**597**	5368	2944	2508	2040	710	78	3126	3000	1766	3347	3511	2224	3530	2809	2164	2226	2024	1864	1988
20	**597**	5549	2927	2515	2093	722	87	6230	2988	1748	12647	3497	2222	3656	2816	2161	2215	2024	1867	1972
21	**624**	7455	2980	2632	2389	802	131	7583	3105	1838	19736	3674	2377	3985	3040	2361	2470	2295	2092	2171
22	**673**	18861	2960	2792	4495	1185	531	9170	3385	2064	23180	4847	2638	11884	3478	2678	2972	2856	2624	2619
23	**702**	25079	3010	2840	5138	1759	1101	11000	3925	2269	23933	11258	2728	15448	3857	2984	3397	3360	2926	3006
24	**707**	25800	3056	2871	5216	1876	1237	11172	4020	2271	23967	12683	2749	16109	3920	3100	3508	3400	2951	3078
25	**718**	27756	3101	2884	5421	2090	1473	12142	4677	2287	24114	15529	2810	18822	4132	3468	3836	3539	3098	3600
26	**725**	7000	3146	2930	5504	2184	1562	5151	5319	2267	6913	16255	2825	4967	4246	3548	3801	3576	3167	3728
27	**708**	29379	3129	2992	5494	2285	1688	10235	5856	2213	24266	17037	2825	18716	4351	3582	3779	3578	3189	3760
28	**715**	29643	3368	3094	5722	2393	1765	10473	6451	2188	24457	17298	2823	18696	4377	3611	3808	3604	3220	3786

Table B.21 (b) – (Y-set) Strain gauge data of Specimen F09-12 (Continued)

Step	Load	Strains in reinforcements																		
		YR11	YR12	YR13	YR14	YR15	YR16	YT21	YT22	YT23	YT31	YT32	YT33	YT41	YT42	YT43	YT51	YT52	YT53	YT61
	kN	($\times 10^{-6}$)	($\times 10^{-6}$)	($\times 10^{-6}$)	($\times 10^{-6}$)	($\times 10^{-6}$)	($\times 10^{-6}$)	($\times 10^{-6}$)	($\times 10^{-6}$)	($\times 10^{-6}$)	($\times 10^{-6}$)	($\times 10^{-6}$)	($\times 10^{-6}$)	($\times 10^{-6}$)	($\times 10^{-6}$)	($\times 10^{-6}$)	($\times 10^{-6}$)	($\times 10^{-6}$)	($\times 10^{-6}$)	($\times 10^{-6}$)
1	**0**	0	0	-1	-1	0	1	0	-1	0	0	-1	0	-1	-1	-1	-1	0	-1	0
2	**0**	0	1	0	1	0	1	0	0	1	0	1	0	1	0	1	1	1	1	0
3	**1**	0	0	0	1	0	1	0	1	0	1	0	0	0	1	0	1	0	0	0
4	**28**	15	5	2	0	-5	-2	0	8	4	10	8	6	8	8	5	8	7	5	7
5	**68**	43	7	-1	-2	-18	-8	0	28	11	37	27	17	33	26	15	27	22	17	20
6	**124**	168	69	-19	-57	-66	-24	0	90	8	128	115	38	173	60	35	115	52	38	77
7	**156**	283	108	-27	-92	-117	-66	0	145	7	177	249	48	241	99	84	185	71	121	158
8	**199**	493	223	11	-104	-177	-86	0	252	23	373	378	65	393	145	175	300	100	243	251
9	**215**	608	301	26	-100	-177	-84	0	320	53	481	434	72	472	175	221	372	118	292	300
10	**282**	1118	822	202	-61	-208	-39	0	782	272	963	839	253	799	675	418	618	630	442	499
11	**304**	1318	1060	324	-34	-198	-35	0	991	394	1153	963	373	941	823	523	747	749	531	593
12	**321**	1444	1238	427	-10	-192	-29	0	1141	484	1290	1070	477	1040	916	622	842	824	657	647
13	**360**	1848	1752	793	95	-170	-38	0	1620	793	1649	1416	780	1322	1212	901	1105	1101	899	829
14	**401**	2189	2170	1092	225	-131	-42	0	2046	1053	1958	1703	1028	1572	1553	1116	1330	1339	1088	944
15	**444**	2528	2550	1376	436	-69	-46	0	2464	1331	2224	1995	1284	1845	1863	1350	1542	1593	1271	1062
16	**464**	2700	2725	1530	550	-34	-45	0	2668	1493	2358	2156	1426	1996	2023	1474	1653	1726	1362	1138
17	**480**	2875	2877	1670	666	11	-45	0	2857	1639	2509	2310	1561	2148	2173	1588	1768	1845	1453	1232
18	**507**	3193	3080	1867	849	85	-39	0	3079	1818	2776	2550	1753	2372	2397	1761	1948	2035	1595	1384
19	**597**	21941	6093	2346	1538	485	20	0	3963	2209	6320	3707	2374	3530	3410	2621	2748	2874	2328	1975
20	**597**	23826	6341	2372	1570	515	24	0	4024	2227	8037	3766	2395	3656	3502	2674	2820	2982	2385	2028
21	**624**	30328	7397	2426	1794	719	51	0	4152	2244	11737	8721	2428	3985	3930	2870	3058	3422	2596	2168
22	**673**	35814	9264	2644	2180	1215	141	0	5854	2302	15042	17933	2560	11884	15165	3307	5727	13016	3036	2723
23	**702**	36797	10026	2689	2286	1475	188	0	6708	2262	16651	18680	2627	15448	21804	3691	15274	18847	3238	3240
24	**707**	37581	11138	2711	2304	1520	193	0	6930	2315	16797	18952	2630	16109	22068	3726	16207	19019	3240	3384
25	**718**	41294	15541	2968	2366	1682	208	0	13836	2409	17221	19262	2682	18822	22123	3785	18091	19352	3312	3758
26	**725**	44188	18880	3142	2413	1744	209	0	21460	2427	17327	19450	2691	19867	22125	3775	19292	19459	3334	3829
27	**708**	46918	13496	3532	2507	1851	234	0	26146	2524	17216	19564	2731	18716	22149	3748	20123	19637	3316	3868
28	**715**	48578	15313	7034	2627	1929	234	0	27276	2788	17499	20211	2777	18696	22102	3660	20415	19589	3234	3891

Table B.22 (a) – (X-set) Strain gauge data of Specimen F14-12

Step	Load	Strains in reinforcements																		
		XR11	XR12	XR13	XR14	XR15	XR16	XT21	XT22	XT23	XT31	XT32	XT33	XT41	XT42	XT43	XT51	XT52	XT53	XT61
	kN	(×10^{-6})	(×10^{-6})	(×10^{-6})	(×10^{-6})	(×10^{-6})	(×10^{-6})	(×10^{-6})	(×10^{-6})	(×10^{-6})	(×10^{-6})	(×10^{-6})	(×10^{-6})	(×10^{-6})	(×10^{-6})	(×10^{-6})	(×10^{-6})	(×10^{-6})	(×10^{-6})	(×10^{-6})
1	**0**	0	0	1	1	-1	0	0	1	1	1	0	1	1	0	0	0	0	1	1
2	**22**	8	5	5	2	0	-3	8	8	4	8	5	5	10	7	4	7	6	4	5
3	**56**	11	7	8	-1	-3	-10	17	15	8	18	12	9	22	14	8	15	13	8	10
4	**76**	22	22	14	0	-2	-12	34	24	13	32	22	15	35	23	15	25	23	14	19
5	**101**	38	82	67	-14	-3	-23	69	34	19	51	31	22	51	31	20	36	32	18	23
6	**201**	208	199	101	-23	-18	-92	302	67	52	331	88	29	316	85	54	184	108	56	95
7	**397**	1398	1201	600	145	10	-239	1055	909	463	1101	722	331	987	755	324	793	465	420	633
8	**427**	1553	1394	711	189	24	-239	1190	1063	543	1230	854	386	1107	852	394	887	615	479	700
9	**440**	1617	1507	786	222	31	-238	1251	1151	602	1285	921	414	1157	891	419	933	671	507	731
10	**502**	1943	1873	1031	389	88	-236	1548	1518	843	1577	1255	610	1401	1087	585	1138	872	699	881
11	**523**	2045	1971	1124	454	109	-232	1634	1626	919	1671	1349	667	1474	1143	617	1185	935	748	916
12	**545**	2170	2078	1224	517	143	-231	1744	1756	1008	1796	1463	743	1562	1210	657	1248	1006	805	964
13	**631**	2653	2479	1655	774	414	-205	2148	2248	1347	2269	1932	1010	1881	1497	842	1508	1298	1032	1146
14	**640**	2715	2530	1712	813	441	-194	2208	2318	1403	2341	2008	1060	1939	1547	870	1554	1375	1065	1178
15	**702**	3024	2774	2006	1068	623	-168	2659	2641	1666	2733	2431	1351	2230	1807	1095	1793	1620	1273	1319
16	**729**	3461	2857	2127	1173	718	-153	2835	2755	1751	2887	2595	1487	2375	1921	1201	1901	1728	1362	1389
17	**799**	3968	3016	2476	1532	1015	-40	3633	3043	1990	3642	2990	1832	2887	2331	1522	2254	2118	1701	1600
18	**821**	4256	3074	2563	1637	1098	-4	3825	3111	2055	4067	3091	1919	3055	2466	1628	2403	2262	1815	1691
19	**885**	7386	3442	2710	1865	1345	115	5435	3547	2158	8953	3674	2114	3957	2819	1899	3063	2732	2163	2013
20	**888**	9211	3445	2708	1892	1390	146	5710	3557	2154	10812	3690	2127	4106	2844	1929	3252	2782	2199	2026
21	**939**	17445	3549	2799	2071	1619	240	14577	3708	2244	21996	3869	2248	5764	2998	2131	7367	3349	2495	2446
22	**940**	18088	3551	2803	2102	1698	269	15575	3733	2268	22435	3888	2262	6036	3004	2141	8186	3390	2512	2468
23	**952**	19163	3610	2851	2187	1802	315	16994	3774	2321	23376	3949	2311	6780	3021	2176	10838	3520	2559	2573
24	**958**	20354	3638	2877	2244	1861	346	17910	3799	2365	24271	4031	2347	7133	3024	2196	13247	3590	2591	2672
25	**963**	21382	3656	2886	2292	1925	356	18401	3831	2400	24932	4120	2387	7442	3024	2208	15147	3621	2609	2743
26	**968**	22409	3654	2880	2336	1992	357	18732	3829	2440	25486	4120	2448	7797	3003	2202	16634	3624	2609	2794
27	**971**	6807	3691	2908	2429	2063	377	5439	3841	2507	6562	4149	2545	4161	3220	2199	4556	3634	2611	3025
28	**960**	25366	3735	2938	2529	2121	397	19588	3855	2622	27871	4462	2715	9877	3332	2153	20642	3665	2578	3267

Table B.22 (b) – (Y-set) Strain gauge data of Specimen F14-12 (Continued)

Step	Load	Strains in reinforcements																		
		YR11	YR12	YR13	YR14	YR15	YR16	YT21	YT22	YT23	YT31	YT32	YT33	YT41	YT42	YT43	YT51	YT52	YT53	YT61
	kN	($\times10^{-6}$)	($\times10^{-6}$)	($\times10^{-6}$)	($\times10^{-6}$)	($\times10^{-6}$)	($\times10^{-6}$)	($\times10^{-6}$)	($\times10^{-6}$)	($\times10^{-6}$)	($\times10^{-6}$)	($\times10^{-6}$)	($\times10^{-6}$)	($\times10^{-6}$)	($\times10^{-6}$)	($\times10^{-6}$)	($\times10^{-6}$)	($\times10^{-6}$)	($\times10^{-6}$)	($\times10^{-6}$)
1	**0**	-4	-3	-3	-2	-2	-3	-3	0	-1	-1	-2	-2	-2	-1	-2	-2	-1	-1	0
2	**22**	9	6	5	4	3	3	13	0	7	8	7	7	8	7	5	7	7	6	0
3	**56**	23	9	9	6	5	2	45	0	14	24	20	16	22	18	13	19	18	14	0
4	**76**	28	4	4	2	-1	-3	57	0	11	31	23	15	26	21	13	22	20	15	0
5	**101**	61	-4	2	0	-2	-6	104	0	11	73	31	21	49	35	22	38	34	23	0
6	**201**	442	37	-13	-23	-23	-19	369	0	11	303	168	64	282	85	126	166	133	67	0
7	**397**	1847	1010	534	131	-70	4644	3040	0	673	1325	862	529	1066	621	0	649	634	477	0
8	**427**	2021	1175	664	173	-66	4607	3398	0	805	1494	1003	620	1178	716	0	737	701	542	0
9	**440**	2146	1287	753	202	-54	4620	3620	0	901	1605	1094	700	1268	782	0	815	754	580	0
10	**502**	2569	1688	1038	331	-33	4708	4189	0	1201	2000	1404	958	1527	1096	0	1048	945	739	0
11	**523**	2737	1826	1133	401	-21	4739	4335	0	1299	2139	1516	1041	1647	1187	0	1174	1014	787	0
12	**545**	2902	1965	1230	463	-9	4765	4465	0	1405	2271	1630	1132	1754	1281	0	1264	1088	839	0
13	**631**	3789	2491	1628	700	39	4819	5061	0	1825	2819	2112	1540	2193	1686	0	1645	1444	1039	0
14	**640**	3873	2542	1673	731	51	4819	5103	0	1870	2872	2157	1584	2234	1742	0	1679	1476	1057	0
15	**702**	5764	2821	1917	874	109	4833	5812	0	2147	3459	2486	1905	2623	2173	0	2006	1757	1244	0
16	**729**	7191	2885	1988	933	146	4845	7479	0	2247	3862	2624	2064	2807	2369	0	2175	1919	1362	0
17	**799**	9722	2965	2142	1060	220	4865	7646	0	2394	5141	3148	2400	3881	2871	0	2737	2472	1769	0
18	**821**	16851	2952	2183	1097	242	4868	7521	0	2428	5663	3201	2467	4036	2952	0	2867	2602	1869	0
19	**885**	25438	3055	2359	1340	397	4861	7539	0	2612	7779	3614	2702	6923	3473	2364	3425	2995	2258	0
20	**888**	25663	3063	2367	1413	455	5575	3094	0	2631	8075	3621	2731	8397	3682	2412	3494	3057	2334	0
21	**939**	27192	3187	2470	1656	666	5594	3310	0	2797	11619	3869	2889	15421	4093	2584	4137	3628	2536	0
22	**940**	27665	3223	2499	1698	691	8811	3379	0	2816	14811	3965	2921	17159	4340	2625	4389	3760	2577	0
23	**952**	28285	3228	2533	1741	732	8817	3426	0	2841	17157	4094	2935	18487	4599	2647	4592	3990	2590	0
24	**958**	28630	3493	2585	1793	787	8828	3460	0	2880	18401	4132	2933	19429	4849	2658	4785	4070	2604	0
25	**963**	29276	3566	2636	1850	839	8836	3580	0	2916	19239	4043	2934	20628	5246	2678	4894	4171	2633	0
26	**968**	29840	3614	2694	1905	881	8843	3694	0	2942	19858	4001	2937	21820	5662	2677	4853	4231	2646	0
27	**971**	30675	3648	2772	1979	933	8851	3813	0	2957	20460	4010	2960	23220	6058	2687	4815	4302	2668	0
28	**960**	31586	3720	3044	2104	1051	8874	3903	0	3031	21495	4031	2990	24425	6245	2657	4813	4426	2651	0

B.4 LVDT (deflection) data for 12 HSC slabs

Figs. B.8 shows the typical positions and labels of LVDTs to measure the vertical deflections of the 12 HSC specimens. Tables B.23 to B.34 show the LVDT data of the 12 HSC specimens.

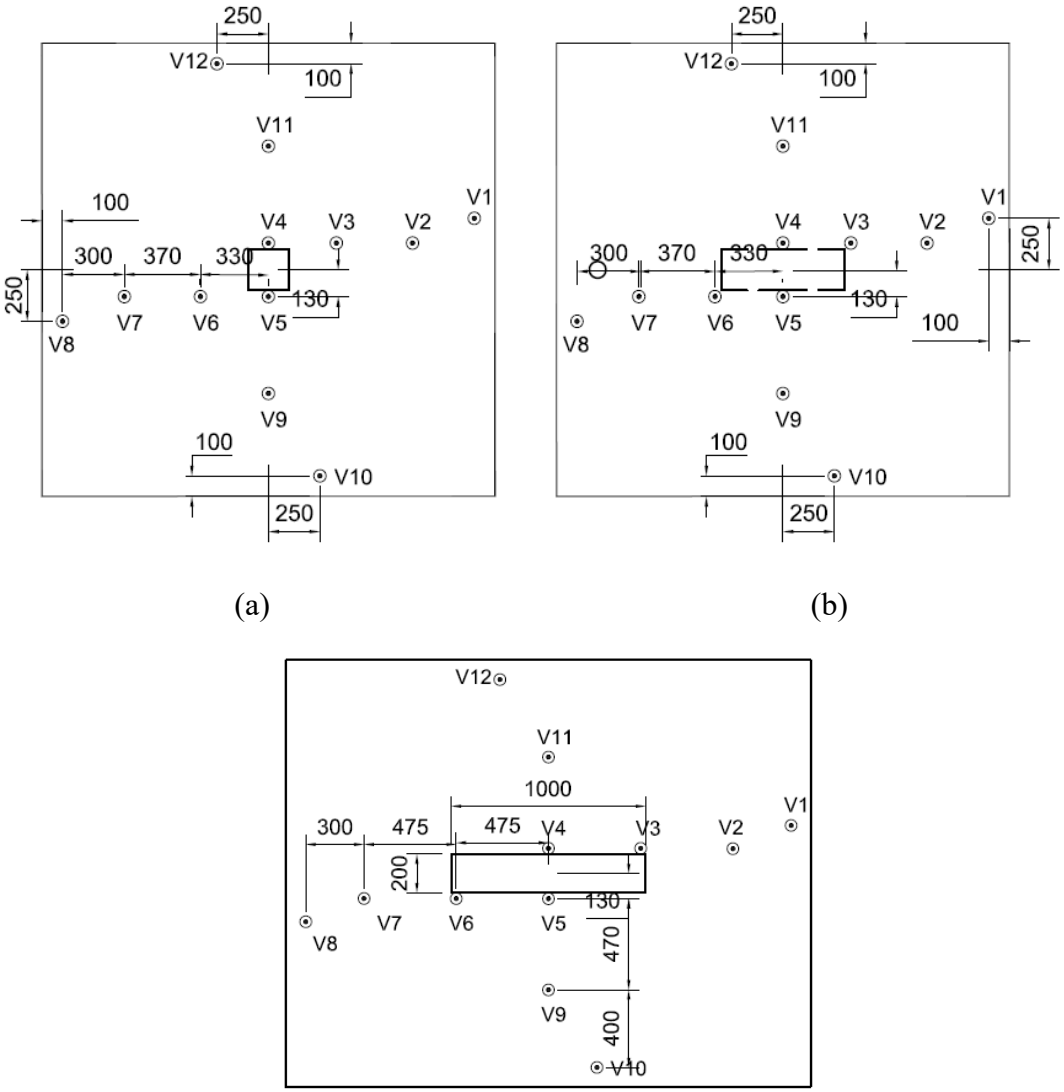

Fig. B.8 – Typical s typical positions and labels of LVDTs for 12 HSC slab specimens.

Table B.23 – LVDT data (Deflection) of Specimen S11-028

Load (kN)	Deflection (mm)											
	Group1			Group2			Group3			Group4		
	v3	v2	v1	v6	v7	v8	v4	v11	v12	v5	v9	v10
0	0	0	0	0	0	0	0	0	0	0	0	0
25	0.02	0.11	0.13	0.19	0.27	0.45	0.03	0.32	0.62	0.21	0.56	0.97
80	0.02	0.1	0.15	0.23	0.38	0.61	0.03	0.27	0.52	0.23	0.61	0.99
95	0	0.11	0.12	0.26	0.44	0.72	0.04	0.21	0.44	0.25	0.66	1.05
110	0.04	0.15	0.02	0.28	0.49	0.77	0.07	0.11	0.3	0.26	0.68	1.04
125	0.06	0.21	0.05	0.3	0.52	0.82	0.1	0.02	0.18	0.27	0.7	1.07
175	0.13	0.32	0.24	0.33	0.58	0.9	0.15	0.13	0.01	0.31	0.77	1.14
195	0.19	0.42	0.42	0.34	0.61	0.93	0.18	0.25	0.15	0.33	0.81	1.19
225	0.38	1.71	2.84	0.52	1.18	1.91	0.26	0.86	1.99	0.46	1.64	3.11
250	0.61	3.23	5.74	0.52	2.14	3.55	0.33	1.61	3.83	0.5	2.67	5.56
260	1.42	10.18	16.44	0.88	4.08	7.99	0.39	2.73	6.5	0.97	8.68	19.51
260	5.86	19.79	31.12	1.53	6.61	11.99	3.17	7.61	14.18	2.29	11.22	23.5
260	6.81	21.41	34.42	1.72	7.46	13.27	3.93	8.89	16.33	2.49	11.79	24.31
265	8.87	24.65	39.48	2.06	8.93	15.41	5.37	11.19	20.11	2.96	12.97	26.09
270	10.91	28.13	44.38	2.36	10.06	16.72	6.91	13.07	22.55	3.63	15.33	29.15
265	13.91	32.02	51.43	3.53	11.32	17.64	9.23	16.04	25.46	5.19	18.88	34.62
265	16.05	32.01	55.23	7.3	12.01	17.9	11.17	17.4	26.54	7.21	21.77	38.96

Table B.24 – LVDT data (Deflection) of Specimen S11-050

Load (kN)	Deflection (mm)											
	Group1			Group2			Group3			Group4		
	v3	v2	v1	v6	v7	v8	v4	v11	v12	v5	v9	v10
0	0	0	0.03	0	0.01	0	0	0	0	0	0	0.01
30	0.08	0.28	0.5	0.01	-0.08	-0.18	0.02	0	0.13	0.09	0.18	0.42
75	0.08	0.29	0.5	0.05	0.01	-0.01	0.05	0.07	0	0.11	0.21	0.44
95	0.09	0.31	0.5	0.1	0.13	0.18	0.09	0.19	0.18	0.14	0.25	0.48
115	0.12	0.33	0.54	0.15	0.25	0.38	0.14	0.32	0.41	0.16	0.27	0.47
135	0.16	0.36	0.57	0.18	0.34	0.52	0.19	0.44	0.62	0.18	0.29	0.45
165	0.2	0.43	0.65	0.22	0.46	0.69	0.24	0.68	0.98	0.21	0.3	0.43
175	0.28	0.47	0.8	0.27	0.57	0.85	0.31	1.19	1.85	0.23	0.4	0.57
190	0.33	0.53	0.94	0.28	0.64	0.99	0.37	1.48	2.36	0.23	0.42	0.55
210	0.42	0.65	1.14	0.3	0.84	1.3	0.47	1.95	3.72	0.21	0.41	0.44
220	0.47	0.93	1.67	0.35	1.19	1.89	0.5	2.17	4.24	0.19	0.46	0.61
245	0.57	1.24	2.21	0.39	1.41	2.27	0.59	2.6	4.98	0.19	0.57	0.79
245	0.72	1.77	3.16	0.41	1.47	2.46	0.68	2.98	5.58	0.2	0.93	1.48
265	0.81	2.11	3.76	0.5	1.96	3.4	0.72	3.38	6.39	0.23	1.36	2.27
275	0.91	2.61	4.65	0.6	2.57	4.47	0.77	3.75	7.1	0.25	1.74	3.13
290	0.97	2.87	5.11	0.66	3.15	5.55	0.79	3.97	7.66	0.28	2.32	4.28
300	1.06	3.17	5.65	0.7	3.39	5.97	0.86	4.41	8.5	0.29	2.62	4.99
315	1.16	3.42	6.1	0.8	3.86	6.81	0.93	4.97	9.72	0.34	3.15	6.01
330	1.31	4.38	7.88	0.94	4.82	8.49	1	6.04	1183	0.38	3.59	6.78
335	1.35	4.59	8.26	0.97	5.13	9.03	1.04	6.31	1238	0.39	3.79	7.19
340	1.42	5.08	9.18	1.1	5.87	10.35	1.11	7.14	14	0.47	4.9	9.39
355	1.51	5.35	9.68	1.26	6.72	1183	1.2	8.01	15.72	0.58	5.68	10.83
360	1.98	6.95	12.57	1.68	8.71	15.28	1.56	1148	21.26	0.79	7.5	14.29
370	2.41	7.95	14.29	1.95	9.86	17.33	1.93	13.39	24.74	0.89	8.46	15.89
375	3.27	9.54	16.76	2.42	115	20.03	2.72	15.72	28.58	1.06	9.54	17.5
140	12.54	153	19.81	1164	17.18	22.65	12.07	21.42	30.94	10.78	14.61	18.51

Table B.25 – LVDT data (Deflection) of Specimen S11-090

Load (kN)	Deflection (mm)											
	Group1			Group2			Group3			Group4		
	v3	v2	v1	v6	v7	v8	v4	v11	v12	v5	v9	v10
0	0	0	0	0	0	-0.01	0	0	0	0	0	0
105	0	0.18	0.13	0.17	0.27	0.49	-	-	0.78	0.15	0.47	0.78
160	0.01	0.46	0.48	0.29	0.29	0.5	-	-	1.84	0.31	1	1.84
170	0.03	0.46	0.44	0.39	0.41	0.71	-	-	2.44	0.41	1.33	2.44
195	0.02	0.69	0.74	0.44	0.45	0.77	-	-	3.04	0.48	1.67	3.04
215	0	0.77	0.84	0.5	0.61	1.06	-	-	3.4	0.52	1.89	3.4
240	0.07	0.82	0.93	0.56	0.96	1.65	-	-	3.76	0.51	2.14	3.76
245	0.07	0.98	1.17	0.58	1.02	1.67	-	-	4.09	0.54	2.29	4.09
260	0.08	1.33	1.73	0.65	1.09	1.86	0	0.31	0.97	0.63	2.74	5
265	0.1	1.55	2.07	0.68	1.14	2.01	0.01	0.33	1.02	0.69	3.13	5.73
280	0.11	1.87	2.57	0.75	1.19	2.25	0.03	0.38	1.18	0.8	4.03	7.55
300	0.12	2.19	3.08	0.79	1.27	2.38	0.06	0.45	1.37	0.86	4.49	8.47
365	0.14	3.46	5.06	1.52	3.35	6.37	0.09	0.86	2.02	1.39	8.56	15.82
390	0.12	3.87	5.7	1.87	4.53	8.53	0.12	0.96	2.13	1.57	10.02	18.36
400	0.06	4	5.91	2	5	9.39	0.28	1.02	2.17	1.62	10.54	19.23
415	0.03	4.3	6.42	2.28	5.79	10.8	0.3	1.07	2.17	1.77	11.87	21.6
405	0.02	4.89	7.18	2.95	6.69	12.35	0.27	1.02	2.33	2.47	13.78	24.37

Table B.26 – LVDT data (Deflection) of Specimen S11-139

Load (kN)	Deflection (mm)											
	Group1			Group2			Group3			Group4		
	v3	v2	v1	v6	v7	v8	v4	v11	v12	v5	v9	v10
0	0	0	-0.01	0	0	0.01	0	0	0	0	0	-0.01
40	0.01	0.1	0.1	0.05	0.09	0.14	0	0.03	0.02	0.06	0.15	0.27
120	0.09	0.3	0.34	0.11	0.23	0.36	0.07	0.17	0.24	0.12	0.28	0.44
165	0.15	0.41	0.54	0.14	0.28	0.45	0.11	0.33	0.43	0.13	0.33	0.51
205	0.25	0.75	1.09	0.2	0.46	0.7	0.17	0.62	0.83	0.15	0.41	0.67
225	0.34	1.04	1.59	0.2	0.54	0.78	0.24	0.88	1.2	0.16	0.41	0.71
245	0.42	1.28	1.99	0.22	0.88	1.35	0.29	1.12	1.61	0.16	0.43	0.81
260	0.49	1.56	2.47	0.26	1.16	1.85	0.33	1.41	2.03	0.17	0.59	1.03
280	0.54	1.88	3.05	0.32	1.49	2.34	0.39	1.78	2.69	0.23	0.83	1.56
295	0.6	2.18	3.6	0.36	1.71	2.7	0.43	2.11	3.28	0.24	0.95	1.86
315	0.74	2.8	4.71	0.43	2.47	4.07	0.52	2.77	4.43	0.3	1.6	3.01
335	0.76	2.95	4.97	0.48	2.71	4.52	0.53	2.99	4.81	0.31	1.81	3.37
345	0.82	3.35	5.75	0.54	3.04	5.1	0.57	3.3	5.45	0.39	2.08	3.99
365	0.89	3.67	6.36	0.57	3.29	5.53	0.6	3.81	6.25	0.4	2.23	4.29
370	1.01	4.17	7.33	0.64	3.75	6.4	0.68	4.35	7.24	0.43	2.5	4.83
385	1.06	4.52	7.86	0.67	3.99	6.8	0.7	4.72	7.85	0.46	2.71	5.26
400	1.14	4.79	8.35	0.75	4.55	7.78	0.76	5.21	8.74	0.51	3.07	5.92
430	1.27	5.31	9.28	0.85	5.12	8.76	0.83	5.8	9.85	0.56	3.34	6.35
440	1.51	6.34	10.48	1.13	6.41	10.95	1	6.73	11.38	0.69	3.91	7.19
430	3.61	7.64	11.32	3.88	9.38	13.86	3.66	11.99	15.96	3.03	6.77	7.81
230	9.14	11.45	13.86	8.06	11.92	14.63	8.81	14.77	19.14	7.35	7.46	7.6
225	10.64	12.95	15.57	9.2	12.85	15.22	10.39	16.78	21.45	8.65	7.97	7.64
240	17.98	20.1	23.27	14.82	18.32	19.65	17.82	27.55	35.77	14.35	10.06	6.89

Table B.27 – LVDT data (Deflection) of Specimen S13-028

Load (kN)	Deflection (mm)											
	Group1			Group2			Group3			Group4		
	v3	v2	v1	v6	v7	v8	v4	v11	v12	v5	v9	v10
0	0	0	0	0	0	0	0	0	0	0	0	0
65	-	-	-	0.26	0.32	0.62	-0.01	-0.11	-0.17	0.13	0.26	0.46
90	-	-	-	0.26	0.37	0.66	0.04	0.09	0.17	0.1	0.26	0.28
105	-	-	-	0.25	0.39	0.73	0.08	0.21	0.37	0.08	0.25	0.17
135	0	-0.06	-0.11	0.29	0.48	0.86	0.11	0.34	0.55	0.09	0.29	0.18
170	0.04	0.09	0.04	0.3	0.5	0.83	0.13	0.36	0.54	0.11	0.3	0.33
190	0.06	0.2	0.16	0.35	0.58	0.94	0.13	0.42	0.64	0.17	0.35	0.69
205	0.18	0.4	0.61	0.38	0.64	1.06	0.21	1.31	2.67	0.21	0.38	1.1
220	0.21	0.46	0.71	0.4	0.69	1.15	0.23	1.43	2.89	0.22	0.4	1.34
235	0.24	0.52	0.79	0.43	0.77	1.28	0.25	1.55	3.11	0.24	0.43	1.59
240	0.37	0.88	1.4	0.49	0.96	1.73	0.31	1.97	3.83	0.27	0.49	3.18
255	0.38	1.01	1.6	0.54	1.05	1.92	0.31	2.04	3.95	0.31	0.54	3.81
265	0.65	2.17	3.69	0.93	2.58	4.79	0.31	2.99	6.28	0.47	0.93	9.18
280	0.66	2.65	4.37	1.16	3.22	5.96	0.29	2.85	6.27	0.58	1.16	10.76
295	0.73	3.95	6.51	2.13	6.34	11.94	0.14	2.17	5.93	0.94	2.13	20.3
300	0.72	4.11	6.79	2.66	7.58	15.44	0.1	2.02	5.8	1.21	2.66	27.19
300	0.79	5	8.24	3.45	9.77	19.54	-0.01	1.6	5.48	1.43	3.45	32.65

Table B.28 – LVDT data (Deflection) of Specimen S13-050

Load (kN)	Deflection (mm)											
	Group1			Group2			Group3			Group4		
	v3	v2	v1	v6	v7	v8	v4	v11	v12	v5	v9	v10
5	0	0	0	0	0	0	0	0	0	0	0	0
40	-0.01	0.11	0.13	0.02	0.03	0.04	-0.05	-0.23	-0.33	0.06	0.23	0.19
85	0.04	0.27	0.31	0.03	0.04	-0.04	-0.05	-0.27	-0.43	0.09	0.39	0.45
160	0.12	0.58	0.71	0	-0.05	-0.2	-0.05	-0.31	-0.62	0.14	0.63	0.95
175	-0.45	-0.07	-0.32	0.27	0.35	1	-0.41	-1.86	-3.02	0.41	2.25	4.02
200	-0.52	-0.17	-0.48	0.35	0.52	1.4	-0.41	-1.97	-3.18	0.47	2.7	4.83
220	-0.57	-0.27	-0.45	0.44	0.7	1.79	-0.41	-2.01	-3.22	0.5	2.98	5.29
235	-0.62	-0.35	-0.63	0.51	0.86	2.12	-0.41	-2.08	-3.34	0.55	3.32	5.87
265	-0.73	-0.55	-0.97	0.64	1.23	2.9	-0.41	-2.25	-3.62	0.64	4.18	7.39
290	-0.58	0.28	0.23	0.68	1.52	3.47	-0.41	-2.27	-3.8	0.67	5.35	9.76
295	-0.57	0.47	0.57	0.71	1.65	3.7	-0.41	-2.28	-3.84	0.68	5.58	10.23
330	-0.61	0.7	0.89	0.82	2.15	4.77	-0.41	-2.42	-4.12	0.77	6.85	12.75
340	-0.74	0.92	1.26	0.98	3	6.52	-0.41	-2.55	-4.18	0.85	8.55	16.29
345	-0.77	1.05	1.44	1.07	3.51	7.63	-0.41	-2.59	-4.25	0.91	9.92	19.02
350	-0.78	1.14	1.55	1.13	3.81	8.27	-0.41	-2.61	-4.27	0.94	10.74	20.59
390	0.53	3.05	4.82	1.09	4.89	9.77	0.26	1.67	2.79	0.61	10.41	19.73
400	0.72	3.5	5.53	1.3	6.33	12.6	0.37	2.95	5.69	0.67	12.16	23.01
415	0.78	3.76	5.98	1.45	6.9	13.93	0.41	3.39	6.56	0.75	13.91	26.12
420	0.92	4.22	6.8	1.82	7.95	16.42	0.49	4.05	7.77	1.02	18.02	33.5
425	0.98	4.57	7.37	2.13	8.74	18.32	0.5	4.38	8.39	1.24	21.05	39.68
430	1.01	4.72	7.62	2.52	9.68	20.65	0.51	4.76	9.12	1.49	24.56	46.1
445	1.04	4.89	7.91	3.19	11.03	23.79	0.54	5.25	10.09	1.86	29.89	54.82
440	1.87	8.09	12.54	5.07	12.83	27.49	0.67	6.11	11.07	3.29	40.07	72.69
425	2.93	10.34	15.32	7.77	15.32	31.06	0.74	6.54	11.4	4.01	46.67	-8.41
360	4.16	12	17.03	10.97	18.26	34.59	0.84	6.95	11.38	4.34	0	-8.42
275	7.25	13.01	16.84	16.68	22.86	38.52	1.03	8.19	11.62	4.29	0	-8.41
265	16.15	17.06	17.65	0	32.41	48.47	0.58	12.31	12.24	4.82	0	-8.42

Table B.29 – LVDT data (Deflection) of Specimen S13-090

Load (kN)	Deflection (mm)											
	Group1			Group2			Group3			Group4		
	v3	v2	v1	v6	v7	v8	v4	v11	v12	v5	v9	v10
0	0	0.47	0.04	-0.25	-0.35	-0.56	0.38	1.05	1.64	-0.23	-0.67	-3.59
0	0	0.64	0.05	-0.24	-0.35	-0.57	0.39	1.07	1.55	-0.19	-0.53	-3.33
70	0	0.88	0.05	-0.15	-0.23	-0.4	0.42	1.15	1.57	-0.09	-0.3	-2.88
165	0	0.94	0.07	-0.12	-0.17	-0.31	0.43	1.22	1.68	-0.07	-0.24	-2.8
190	0	0.99	0.13	-0.08	-0.1	-0.22	0.44	1.29	1.79	-0.04	-0.17	-2.65
205	0	1.09	0.24	0	0.02	-0.03	0.41	1.31	1.8	0.04	0.05	-2.22
240	0	1.41	0.72	0.08	0.11	0.17	0.42	1.48	1.99	0.15	0.93	-0.51
280	0	1.37	0.64	0.13	0.24	0.46	0.44	1.57	2.19	0.13	1.07	-0.29
285	0	1.47	0.77	0.22	0.39	0.71	0.41	1.5	2.06	0.2	1.53	0.62
310	0	1.53	0.88	0.25	0.46	0.85	0.4	1.48	2.03	0.21	1.61	0.82
310	0	1.67	1.05	0.32	0.56	1.04	0.37	1.43	1.94	0.27	1.88	1.4
325	0	1.96	1.48	0.5	1.02	1.84	0.28	1.33	1.9	0.36	2.54	2.86
350	0	2.15	1.7	0.6	1.39	2.48	0.17	1.17	1.77	0.44	3.19	4.23
350	0	2.53	2.28	0.77	1.92	3.39	0.06	0.94	1.54	0.52	4.01	5.94
390	0	2.99	3.03	0.88	2.37	4.17	0.04	1.03	1.75	0.56	4.67	7.28
405	0	3.3	3.43	1.02	2.88	5.08	-0.05	0.86	1.53	0.61	5.42	8.82
430	0	3.43	3.63	1.09	3.11	5.46	-0.13	0.76	1.42	0.64	5.78	9.54
440	0	3.86	4.28	1.25	3.68	6.48	-0.25	0.59	1.2	0.73	6.78	11.64
470	0	4.4	5.09	1.49	4.48	7.93	-0.37	0.41	1.01	0.83	8.46	15.1
505	0	4.94	5.91	1.74	5.25	9.39	-0.47	0.24	0.82	0.94	10.33	18.74
540	0	8.38	10.2	2.5	5.69	9.95	-0.18	0.57	0.68	2.91	13.76	24.38
510	0	8.69	10.36	3.26	5.98	10.14	0.19	0.81	0.58	7.08	14.69	25.02
445	0	15.23	16.59	8.67	8.77	11.68	6.07	3.44	-0.21	2.33	21.81	32.58
310	0	17.05	16.91	0	32.73	48.6	0.59	13.19	13.6	-	-	-
265	0	14.08	9.16	0	29.79	42.82	0.78	13.87	15.5	-	-	-

Table B.30 – LVDT data (Deflection) of Specimen S13-143

Load (kN)	Deflection (mm)											
	Group1			Group2			Group3			Group4		
	v3	v2	v1	v6	v7	v8	v4	v11	v12	v5	v9	v10
0	0.09	0.17	0.25	0	0.03	-0.03	0.82	0.14	0.23	0.01	-0.03	-0.05
45	0.05	0.25	0.27	0.05	0.06	0.01	0.85	-0.01	-0.09	0.08	0.18	0.4
55	0.04	0.18	0.2	0.07	0.1	0.12	0.88	0	-0.04	0.08	0.18	0.36
85	0.02	0.19	0.14	0.13	0.16	0.23	0.88	-0.06	-0.15	0.12	0.29	0.56
140	0.02	0.39	0.35	0.16	0.18	0.22	0.88	-0.21	-0.51	0.2	0.56	1.12
160	0.03	0.49	0.47	0.17	0.17	0.18	0.89	-0.28	-0.62	0.25	0.69	1.39
170	0.03	0.56	0.54	0.16	0.19	0.15	0.89	-0.34	-0.75	0.26	0.76	1.56
180	-0.01	0.36	0.21	0.32	0.39	0.66	0.93	-0.29	-0.58	0.32	0.86	1.65
195	-0.03	0.36	0.14	0.39	0.5	0.87	0.93	-0.35	-0.69	0.32	1.07	2.01
215	-0.07	0.36	0.08	0.44	0.6	1.07	0.92	-0.4	-0.75	0.35	1.26	2.36
230	-0.09	0.37	0.03	0.49	0.68	1.25	0.91	-0.45	-0.82	0.38	1.49	2.67
245	-0.12	0.37	0.01	0.54	0.77	1.39	0.9	-0.5	-0.89	0.41	1.68	3.04
255	-0.09	0.43	0.14	0.58	0.9	1.68	0.92	-0.3	-0.56	0.43	2.07	3.71
265	-0.12	0.46	0.17	0.6	0.98	1.82	0.92	-0.29	-0.49	0.45	2.26	4.07
285	0.03	0.68	0.61	0.52	0.93	1.73	1.06	0.19	0.25	0.39	2.19	3.93
305	0.01	0.75	0.72	0.57	1.09	2.08	1.03	0.19	0.29	0.43	2.5	4.56
320	0.13	0.96	1.03	0.54	1.12	2.15	1.14	0.57	0.93	0.39	2.53	4.67
335	0.12	1.08	1.21	0.59	1.34	2.55	1.11	0.55	0.92	0.42	2.81	5.28
350	0.17	1.42	1.77	0.62	1.62	3.04	1.14	1.03	1.82	0.43	3.04	5.76
365	0.13	1.57	1.99	0.69	1.91	3.61	1.09	1.01	1.92	0.46	3.39	6.5
385	0.09	1.73	2.24	0.78	2.29	4.32	1.05	0.98	2.02	0.51	3.87	7.47
410	0.27	2.17	2.99	0.73	2.52	4.72	1.2	1.78	3.38	0.46	3.85	7.44
430	0.32	2.45	3.45	0.75	2.73	5.12	1.23	2.07	3.95	0.46	4.05	7.87
450	0.31	2.6	3.69	0.82	3.01	5.63	1.19	2.08	4.01	0.49	4.43	8.61
455	0.33	2.72	3.88	0.83	3.08	5.76	1.19	2.14	4.13	0.49	4.51	8.79
480	0.51	3.16	4.62	0.79	3.24	6.01	1.34	2.88	5.47	0.44	4.47	8.67
490	0.5	3.3	4.84	0.84	3.42	6.36	1.31	2.89	5.53	0.47	4.74	9.22
505	0.49	3.48	5.08	0.9	3.68	6.85	1.29	2.9	5.62	0.5	5.07	9.94
535	0.6	3.91	5.8	0.9	3.95	7.34	1.37	3.47	6.66	0.48	5.28	10.34
590	0.99	4.95	7.55	0.83	4.43	8.14	1.69	5.09	9.56	0.43	5.3	10.56
620	1.03	5.57	8.4	0.96	4.99	9.11	1.61	5.26	10.05	0.53	5.68	1151
655	1.05	6.19	9.18	1.15	5.54	10.13	1.56	5.13	9.82	0.62	6.86	13.77
670	1.17	6.7	9.84	1.28	5.95	10.91	1.54	5.08	9.67	0.69	7.85	15.57
680	1.3	7.11	10.32	1.39	6.21	1143	1.54	5.05	9.57	0.74	8.58	16.88
700	1.65	8.16	1139	1.56	6.67	12.28	1.53	5.05	9.42	0.86	9.8	19.01
350	9.7	14.37	16.52	9.4	1178	15.29	7.24	9.11	9.94	9.13	17.49	25.74
0	0.09	0.17	0.25	0	0.03	-0.03	0.82	0.14	0.23	0.01	-0.03	-0.05

Table B.31 – LVDT data (Deflection) of Specimen S15-028

Load (kN)	Deflection (mm)											
	Group1			Group2			Group3			Group4		
	v3	v2	v1	v6	v7	v8	v4	v11	v12	v5	v9	v10
0	0	-0.02	-0.01	0.01	0.01	0.03	-0.01	-0.07	-0.14	0.01	0.05	0.12
95	-0.33	-0.22	-0.52	0.38	0.64	1.09	-0.3	-1.2	-2.2	0.48	1.33	2.67
130	-0.32	-0.12	-0.41	0.41	0.71	1.2	-0.29	-1.15	-2.16	0.51	1.39	2.77
155	-0.19	0.03	-0.13	0.42	0.76	1.23	-0.16	-0.8	-1.57	0.47	1.28	2.41
175	-0.07	0.17	0.12	0.44	0.76	1.25	-0.08	-0.55	-1.18	0.43	1.17	2.15
190	-0.04	0.25	0.23	0.46	0.83	1.35	-0.06	-0.53	-1.16	0.44	1.22	2.25
220	0	0.38	0.42	0.51	0.96	1.57	-0.05	-0.5	-1.11	0.48	1.34	2.46
230	0.05	0.5	0.62	0.51	1	1.61	0	-0.35	-0.87	0.46	1.3	2.4
235	0.08	0.56	0.79	0.55	1.2	2.02	0.02	-0.23	-0.59	0.45	1.57	2.95
245	0.12	0.63	0.95	0.59	1.39	2.4	0.06	-0.11	-0.36	0.45	1.83	3.55
250	0.14	0.72	1.13	0.68	1.93	3.48	0.06	-0.12	-0.17	0.45	2.05	4.19
265	0.31	1.84	3.3	0.9	2.86	5.56	0.07	-0.11	0.5	0.47	3.14	6.92
270	0.47	3.06	5.6	0.99	3.28	6.45	0.07	-0.11	0.99	0.48	3.54	7.86
275	0.64	4.25	8.03	1.24	4.22	8.5	0.08	0	1.97	0.47	4.72	10.8
280	0.76	5.08	9.66	1.38	4.68	9.5	0.09	0.05	2.42	0.46	5.3	12.28
285	0.86	5.89	11.33	1.52	5.2	10.55	0.09	0.17	3.08	0.49	5.83	13.72
285	1.11	7.17	13.84	1.66	6.14	12.46	0.12	0.55	4.5	0.46	6.86	16.4
290	1.24	7.94	15.41	1.86	7.43	14.79	0.12	0.76	5.22	0.46	7.56	18.09
290	1.34	8.48	16.51	1.98	7.99	15.85	0.12	0.95	5.74	0.47	7.97	19.14
290	1.5	8.93	17.44	2.6	9.62	18.54	0.15	1.48	6.68	0.45	8.5	20.45
295	1.61	9.5	18.54	3.43	11.66	22.15	0.15	1.69	7.12	0.44	9.51	22.8
295	1.72	10.2	19.92	4.5	14.16	26.4	0.15	1.82	7.43	0.43	10.72	25.52
285	1.8	10.61	20.66	6.86	19.99	35.49	0.14	1.9	7.95	0.44	11.34	27.35

Table B.32 – LVDT data (Deflection) of Specimen S15-050

Load (kN)	Deflection (mm)											
	Group1			Group2			Group3			Group4		
	v3	v2	v1	v6	v7	v8	v4	v11	v12	v5	v9	v10
0	0	0	0.01	0	0	0.01	0	0	0	0	0	0
5	0	0.02	0.03	0.03	0.05	0.11	0.01	0.02	0.03	0.02	0.05	0.1
75	-0.03	0.08	-0.03	0.2	0.33	0.6	-0.08	-0.3	-0.6	0.16	0.06	0.98
160	0.02	0.37	0.4	0.29	0.59	0.97	-0.02	0.05	-0.05	0.17	0.07	0.98
200	0.16	0.65	0.84	0.3	0.73	1.16	0.05	0.36	0.47	0.16	0.05	0.85
225	0.24	0.8	1.11	0.32	0.81	1.31	0.11	0.52	0.77	0.16	0.09	0.82
245	0.4	1.16	1.89	0.37	1.06	1.74	0.16	1	1.93	0.16	0.09	1.1
265	0.54	1.55	2.65	0.47	1.49	2.52	0.2	1.23	2.66	0.17	0.23	1.67
290	0.68	1.95	3.41	0.54	1.93	3.26	0.21	1.49	3.4	0.17	0.34	2.04
295	0.85	2.53	4.61	0.57	2.45	4.12	0.27	1.81	4.35	0.18	0.37	2.33
310	0.93	2.77	5.09	0.63	2.99	5.02	0.28	2.01	4.97	0.18	0.46	2.57
320	1.05	3.55	6.51	0.75	4.11	6.96	0.31	2.56	6.34	0.19	0.71	3.47
330	1.17	4.15	7.64	0.82	4.82	8.17	0.32	2.87	7.2	0.19	0.84	4.05
350	1.33	4.78	8.82	0.91	5.61	9.51	0.34	3.19	8.1	0.19	1.17	4.96
365	1.46	5.52	10.17	1.01	6.22	10.6	0.38	3.48	8.82	0.2	1.41	5.62
380	1.66	6.48	12.05	1.1	6.87	117	0.38	3.78	9.69	0.21	1.81	6.66
395	1.82	7.3	13.61	1.25	8.08	13.72	0.4	4.24	10.94	0.21	2.1	7.55
405	2	8.3	15.51	1.39	9.28	15.79	0.41	4.72	12.15	0.23	2.57	8.76
415	2.24	9.74	18.18	1.53	10.53	17.85	0.43	5.38	13.82	0.24	2.96	9.97
425	2.57	11.47	21.44	1.74	11.79	19.93	0.43	5.96	15.44	0.24	3.26	11.05
435	3.18	14.18	26.47	2.03	13.68	23.02	0.44	6.43	16.79	0.24	3.66	12.5
415	4.67	16.74	30.12	2.2	14.66	24.14	0.43	6.68	17.78	0.26	3.93	13.31

Table B.33 – LVDT data (Deflection) of Specimen S15-090

Load (kN)	Deflection (mm)											
	Group1			Group2			Group3			Group4		
	v3	v2	v1	v6	v7	v8	v4	v11	v12	v5	v9	v10
0	0	0	0	0	0	0	0	0	0.01	0	0	0
85	-0.05	0.19	0.16	0.17	0.31	0.45	-0.1	-0.57	-1.16	0.35	0.8	1.67
145	0.08	0.44	0.53	0.21	0.45	0.64	-0.02	-0.32	-0.71	0.36	0.82	1.69
180	0.2	0.66	0.91	0.21	0.57	0.83	0.06	0	-0.14	0.3	0.78	1.55
200	0.28	0.79	1.13	0.21	0.63	0.94	0.11	0.19	0.2	0.26	0.8	1.56
225	0.34	0.93	1.36	0.21	0.71	1.1	0.15	0.36	0.51	0.24	0.86	1.68
250	0.39	1.08	1.63	0.24	0.85	1.35	0.18	0.52	0.83	0.25	1.04	2.07
265	0.42	1.22	1.87	0.26	0.95	1.56	0.2	0.64	1.06	0.27	1.2	2.39
285	0.47	1.37	2.13	0.29	1.09	1.81	0.22	0.83	1.47	0.28	1.37	2.79
305	0.52	1.52	2.47	0.32	1.24	2.13	0.25	1.06	1.97	0.28	1.55	3.19
325	0.58	1.8	3.03	0.36	1.5	2.63	0.28	1.32	2.59	0.29	1.75	3.72
350	0.65	2.09	3.56	0.4	1.78	3.19	0.3	1.55	3.13	0.29	1.93	4.16
370	0.72	2.41	4.2	0.44	2.14	3.89	0.33	1.81	3.76	0.29	2.13	4.7
390	0.74	2.58	4.53	0.47	2.33	4.28	0.35	1.92	4.03	0.31	2.25	4.95
410	0.78	2.87	5.09	0.52	2.63	4.83	0.36	2.11	4.55	0.31	2.42	5.41
430	0.87	3.28	5.87	0.58	3.05	5.64	0.38	2.36	5.19	0.31	2.67	6.09
455	0.95	3.7	6.71	0.64	3.54	6.61	0.41	2.63	5.91	0.31	2.92	6.79
490	1.09	4.39	7.79	0.76	4.15	7.95	0.41	3.04	6.98	0.3	3.29	7.82
515	1.17	4.88	8.75	0.83	4.66	8.95	0.43	3.31	7.74	0.3	3.55	8.58
540	1.23	5.33	9.6	0.9	5.09	9.8	0.45	3.61	8.42	0.3	3.75	9.21
550	1.3	5.61	10.13	0.94	5.36	10.32	0.46	3.76	8.84	0.3	3.89	10.31
595	1.5	6.57	11.97	1.1	6.35	12.26	0.5	4.35	10.35	0.3	4.45	11.91
610	1.59	6.98	12.76	1.17	6.76	13.05	0.51	4.62	11.03	0.3	4.72	12.63
630	1.9	7.91	14.43	1.35	7.48	14.53	0.54	5.13	12.17	0.32	5.41	14.43
620	2.53	9.48	16.14	1.44	7.71	15.02	0.54	5.48	12.8	0.32	5.83	15.46
610	5.32	14.26	22.54	1.46	7.6	14.81	0.53	6.26	13.59	0.35	6.71	17.86
600	7.3	16.98	25.99	1.44	7.34	14.34	0.52	6.86	14.27	0.39	7.06	18.77
580	10.66	21.49	32.33	1.39	6.78	13.27	0.87	8.39	16.38	0.48	7.58	19.94
560	15.02	27.16	39.28	1.32	5.98	11.67	2.56	11.33	18.74	0.74	8.45	21.51
345	19.23	32.17	42.59	7.01	8.28	8.45	14.31	24.73	34.31	10.29	8.21	13.12

Table B.34 – LVDT data (Deflection) of Specimen S15-090

Load (kN)	Deflection (mm)											
	Group1			Group2			Group3			Group4		
	v3	v2	v1	v6	v7	v8	v4	v11	v12	v5	v9	v10
0	0	0	-0.01	0	0	0	0	0	0	0	0	0
65	-0.08	0.01	-0.04	0.22	0.31	0.53	-0.04	-0.35	-0.66	0.23	0.54	1.02
115	-0.01	0.12	0.17	0.31	0.49	0.81	0	-0.25	-0.5	0.26	0.68	1.21
160	0.03	0.22	0.32	0.37	0.62	1.04	0.01	-0.18	-0.37	0.29	0.8	1.4
190	0.08	0.36	0.54	0.43	0.78	1.32	0.04	-0.08	-0.2	0.32	0.96	1.72
215	0.14	0.53	0.81	0.48	0.94	1.64	0.07	0.06	0.09	0.34	1.15	2.1
235	0.17	0.62	0.98	0.51	1.04	1.82	0.08	0.16	0.29	0.35	1.26	2.32
260	0.22	0.79	1.24	0.54	1.18	2.13	0.11	0.33	0.64	0.36	1.42	2.64
280	0.26	0.9	1.46	0.56	1.3	1.93	0.12	0.48	0.98	0.37	1.56	2.94
300	0.32	1.07	1.79	0.6	1.5	2.78	0.14	0.7	1.46	0.37	1.79	3.45
320	0.36	1.27	2.06	0.63	1.65	3.1	0.17	0.87	1.83	0.39	1.92	3.81
340	0.4	1.43	2.38	0.66	1.8	3.43	0.18	0.97	2.11	0.4	2.05	4.13
360	0.46	1.66	2.78	0.7	2.02	3.87	0.21	1.16	2.59	0.4	2.2	4.51
380	0.51	1.85	3.18	0.73	2.24	4.31	0.23	1.34	3.05	0.4	2.35	4.89
390	0.54	2	3.49	0.76	2.39	4.61	0.24	1.44	3.33	0.4	2.45	5.15
415	0.62	2.4	4.27	0.84	2.82	5.47	0.27	1.68	3.94	0.42	2.66	5.78
445	0.66	2.73	4.91	0.89	3.17	6.16	0.3	1.91	4.55	0.42	2.84	6.27
475	0.74	3.14	5.69	0.98	3.52	7.04	0.32	2.15	5.2	0.43	3.05	7.52
505	0.81	3.55	6.51	1.06	3.98	7.93	0.34	2.44	5.95	0.44	3.26	8.17
540	0.89	4.08	7.51	1.16	4.55	9.06	0.37	2.77	6.83	0.44	3.55	9.02
575	0.95	4.55	8.42	1.26	5.1	10.16	0.38	3.1	7.72	0.44	3.81	9.78
625	1.08	5.2	9.73	1.39	5.8	1155	0.41	3.53	8.86	0.44	4.2	10.85
665	1.2	5.86	10.91	1.53	6.38	12.87	0.45	3.91	9.87	0.47	4.6	1194
695	1.32	6.45	12.02	1.64	6.99	14.05	0.45	4.26	10.83	0.46	4.97	12.86
750	1.48	7.18	13.4	1.84	7.76	15.52	0.48	4.69	1192	0.48	5.53	14.31
745	1.52	7.45	13.75	2.15	8.87	17	0.48	4.93	12.62	0.48	6.02	15.28
645	1.36	6.65	12.08	6.21	14.02	23.07	0.49	5.12	13.2	0.59	6.69	15.36
640	1.3	6.44	1161	7.56	15.88	26.2	0.5	5.24	13.51	0.62	7.29	15.91
595	1.29	5.93	10.62	9.69	18.13	28.81	0.56	5.44	13.75	1.22	8.53	16.57

B.5 LVDT (deflection) data for 10 SFRC slabs

Figs. B.9 shows the typical positions and labels of LVDTs to measure the vertical deflections of the 10 SFRC specimens. Tables B.35 to B.44 show the LVDT data of the 10 SFRC specimens.

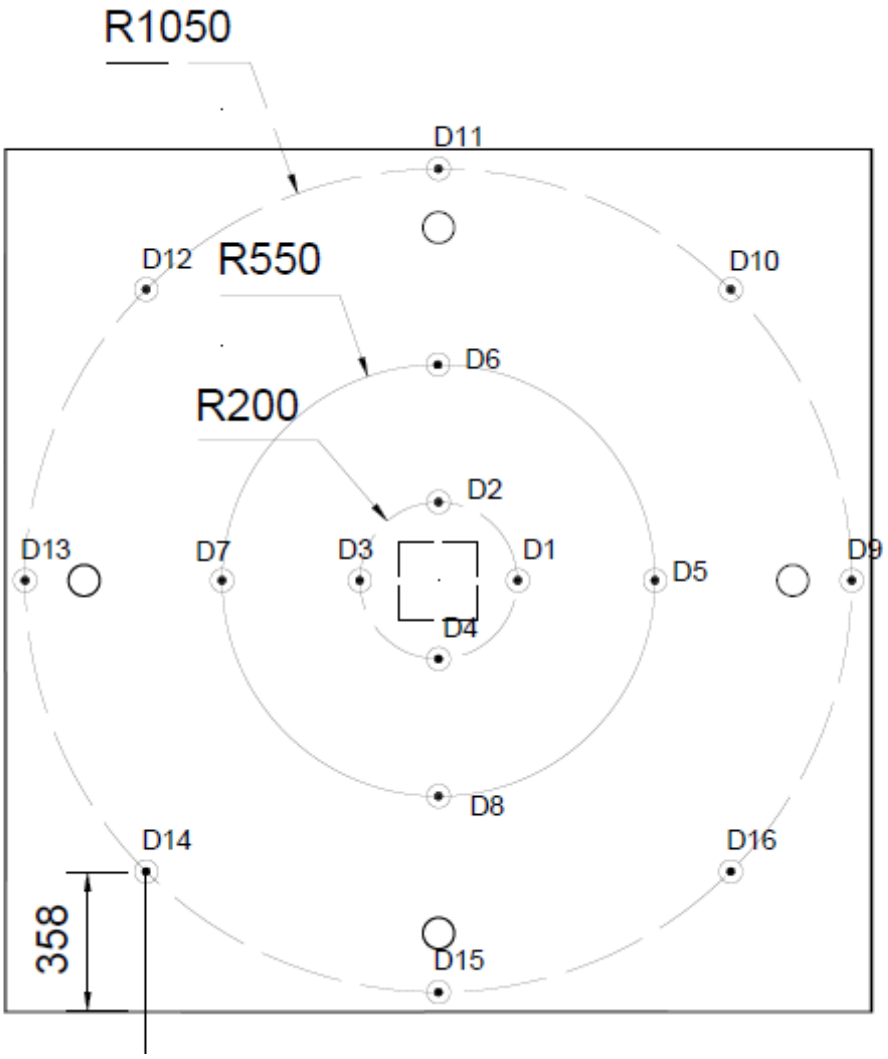

Fig. B.9 – Typical s typical positions and labels of LVDTs for 10 SFRC slab specimens.

Table B.35 – LVDT data (Deflection) of Specimen F09-00

Load	Deflection (mm)															
(kN)	D1	D2	D3	D4	D5	D6	D7	D8	D9	D10	D11	D12	D13	D14	D15	D16
0	0.00	0.00	0.00	0.00	0.00	0.01	0.00	0.00	-0.01	0.00	0.00	0.00	0.00	0.00	0.00	-0.01
0	0.00	0.00	0.00	0.00	0.00	0.00	0.00	0.00	0.00	0.00	-0.01	0.00	0.00	0.00	-0.01	0.00
16	0.05	0.05	0.05	0.06	0.18	0.00	0.03	0.26	0.34	0.04	-0.16	-0.17	0.05	0.28	0.64	0.49
32	0.08	0.04	0.08	0.10	0.24	-0.04	0.08	0.42	0.43	-0.01	-0.25	-0.22	0.15	0.51	1.77	0.74
56	0.10	0.17	0.14	0.07	0.30	0.30	0.22	0.29	0.57	0.46	0.40	0.37	0.39	0.44	1.59	0.54
74	0.11	0.31	0.21	0.08	0.35	0.68	0.38	0.21	0.63	0.89	1.07	1.00	0.64	0.43	1.45	0.36
92	0.21	0.44	0.22	0.08	0.60	1.02	0.38	0.20	1.15	1.59	1.71	1.34	0.60	0.28	1.47	0.61
109	0.28	0.57	0.25	0.07	0.85	1.41	0.44	0.20	1.65	2.37	2.48	1.86	0.68	0.25	1.57	0.86
118	0.33	0.63	0.27	0.08	1.01	1.61	0.48	0.22	1.98	2.82	2.91	2.14	0.75	0.30	1.66	1.06
126	0.37	0.69	0.30	0.09	1.16	1.84	0.56	0.30	2.29	3.28	3.37	2.48	0.90	0.47	1.85	1.31
138	0.40	0.81	0.35	0.06	1.29	2.33	0.74	0.27	2.57	4.10	4.40	3.29	1.21	0.60	1.86	1.35
136	0.41	0.81	0.36	0.07	1.32	2.34	0.76	0.31	2.64	4.15	4.41	3.31	1.28	0.68	1.94	1.43
157	0.56	0.98	0.44	0.03	1.72	3.04	1.09	0.33	3.58	5.60	5.90	4.48	1.97	0.91	2.11	1.87
172	0.65	1.16	0.50	-0.02	2.05	3.69	1.35	0.37	4.32	6.92	7.44	5.69	2.54	1.16	2.27	2.11
199	0.82	1.12	0.65	0.30	2.63	3.74	1.84	1.54	5.57	7.45	7.77	5.97	3.68	3.12	5.01	4.23
214	0.90	1.08	0.73	0.50	3.05	3.71	2.16	2.29	6.53	7.76	7.82	6.05	4.45	4.33	6.69	5.57
236	0.97	1.06	0.81	0.70	3.58	3.68	2.52	3.10	7.69	8.12	7.86	6.16	5.37	5.64	8.51	7.17
258	1.03	1.07	0.91	0.91	4.11	3.84	2.93	3.99	8.84	8.74	8.39	6.54	6.35	7.11	10.55	8.83
279	1.11	1.11	1.01	1.06	4.59	4.06	3.33	4.66	9.93	9.30	8.84	7.00	7.31	8.22	12.08	10.19
300	1.18	1.25	1.11	1.14	5.07	4.65	3.72	5.01	10.97	10.50	10.20	7.92	8.19	8.96	12.90	10.97
317	1.26	1.30	1.21	1.09	5.45	5.59	4.09	4.92	11.85	12.04	12.20	9.32	8.93	9.06	12.77	11.05
337	1.39	1.82	1.34	0.98	5.88	6.70	4.53	4.82	12.82	13.85	14.56	11.10	9.81	9.14	12.61	11.10
357	1.54	1.76	1.53	1.35	6.45	6.54	5.02	6.17	13.99	13.95	14.29	11.00	10.92	11.24	15.51	13.34
371	1.63	1.77	1.72	1.61	6.84	6.59	5.44	7.03	14.77	14.20	14.41	11.18	11.74	12.60	17.28	14.71
372	1.67	1.88	1.85	1.65	6.97	6.93	5.68	7.08	15.03	14.71	15.13	11.79	12.11	12.77	17.29	14.72
376	1.73	2.08	2.06	1.69	7.11	7.50	6.05	7.11	15.26	15.44	16.28	12.79	12.67	12.98	17.24	14.63
374	1.77	2.16	2.22	1.88	7.18	7.73	6.28	7.25	15.32	15.64	16.66	13.25	13.08	13.23	17.26	14.60
121	9.56	9.37	9.40	8.54	12.11	12.42	10.99	12.15	16.52	17.07	17.31	14.84	14.03	14.77	18.06	15.87
119	9.73	9.53	9.57	8.69	12.21	12.53	11.12	12.26	16.52	17.09	17.33	14.91	14.11	14.83	18.07	15.88
118	9.81	9.62	9.67	8.79	12.26	12.61	11.23	12.32	16.52	17.09	17.34	14.97	14.17	14.87	18.08	15.88

Table B.36 – LVDT data (Deflection) of Specimen F14-00

Load	Deflection (mm)															
(kN)	D1	D2	D3	D4	D5	D6	D7	D8	D9	D10	D11	D12	D13	D14	D15	D16
0	0.00	0.00	0.00	0.00	0.00	0.00	0.00	0.01	0.00	0.01	0.00	0.01	0.00	0.00	0.00	0.00
0	0.00	0.00	0.00	0.00	0.00	0.00	0.00	0.00	0.00	0.00	0.00	0.00	0.00	0.00	0.01	0.00
0	0.00	0.00	0.00	0.00	0.00	0.00	0.00	-0.01	0.00	0.00	0.00	-0.01	0.00	-0.01	0.00	0.00
24	0.08	0.16	0.01	-0.06	0.18	0.38	0.00	-0.24	0.35	0.68	0.74	0.43	-0.04	-0.39	0.25	-0.16
43	0.14	0.16	0.02	0.01	0.30	0.34	0.01	-0.09	0.60	0.75	0.71	0.35	-0.03	-0.24	0.83	0.16
63	0.20	0.16	0.04	0.08	0.41	0.33	0.06	0.10	0.82	0.82	0.68	0.32	0.08	0.00	1.27	0.48
82	0.25	0.15	0.07	0.18	0.52	0.30	0.13	0.36	1.03	0.84	0.62	0.28	0.23	0.39	1.95	0.90
97	0.27	0.14	0.12	0.27	0.58	0.30	0.23	0.61	1.19	0.86	0.61	0.34	0.48	0.81	2.48	1.27
115	0.29	0.13	0.17	0.38	0.65	0.30	0.38	0.99	1.33	0.86	0.61	0.46	0.78	1.44	3.28	1.80
122	0.30	0.13	0.18	0.45	0.69	0.32	0.44	1.22	1.43	0.91	0.65	0.52	0.92	1.84	3.78	2.16
146	0.34	0.10	0.25	0.62	0.84	0.34	0.72	1.88	1.77	1.04	0.75	0.88	1.63	3.09	5.22	3.16
157	0.35	0.11	0.30	0.70	0.94	0.39	0.90	2.17	1.99	1.16	0.85	1.15	2.05	3.61	5.87	3.64
153	0.35	0.11	0.30	0.70	0.95	0.39	0.91	2.19	2.01	1.18	0.87	1.15	2.06	3.63	5.89	3.68
162	0.37	0.09	0.30	0.75	1.02	0.38	0.94	2.39	2.16	1.22	0.90	1.15	2.13	3.91	6.34	4.00
178	0.46	0.09	0.32	0.87	1.35	0.48	1.05	2.84	2.92	1.72	1.14	1.28	2.47	4.58	7.34	5.07
178	0.46	0.09	0.33	0.90	1.36	0.49	1.08	2.95	2.95	1.75	1.19	1.32	2.52	4.74	7.62	5.24
194	0.51	0.10	0.37	0.99	1.57	0.58	1.29	3.32	3.45	2.10	1.41	1.59	3.07	5.46	8.42	5.85
197	0.53	0.09	0.38	1.03	1.65	0.62	1.35	3.49	3.63	2.22	1.53	1.63	3.23	5.73	8.84	6.17
215	0.60	0.19	0.45	1.08	1.96	1.00	1.62	3.77	4.34	2.94	2.37	2.44	3.94	6.20	9.52	6.86
238	0.65	0.44	0.53	1.02	2.25	1.83	1.91	3.65	5.03	4.26	4.15	3.82	4.57	6.20	9.39	6.89
259	0.72	0.69	0.60	0.97	2.58	2.68	2.21	3.52	5.81	5.70	6.01	5.20	5.32	6.30	9.25	6.89
279	0.80	0.77	0.66	1.05	2.91	3.05	2.50	3.86	6.58	6.40	6.85	6.01	6.05	6.85	10.09	7.67
301	0.89	0.83	0.73	1.19	3.23	3.36	2.79	4.35	7.31	7.03	7.58	6.58	6.82	7.74	1127	8.60
318	0.98	0.82	0.77	1.33	3.55	3.38	3.02	4.87	8.05	7.30	7.67	6.79	7.43	8.48	1240	9.64
338	1.04	1.08	0.83	1.27	3.89	4.33	3.26	4.72	8.81	8.84	9.74	8.27	7.98	8.36	1224	9.67
359	1.13	1.10	0.90	1.46	4.21	4.43	3.53	5.40	9.51	9.13	10.04	8.58	8.66	9.40	1375	10.87
376	1.29	1.12	1.21	1.97	4.71	4.50	4.23	6.67	10.50	9.41	10.16	8.96	9.98	1140	1612	1264
356	1.57	1.23	1.62	2.66	4.93	4.52	4.72	7.42	10.69	9.28	9.94	8.99	10.49	1238	1710	1332
355	1.70	1.27	1.86	2.96	5.02	4.51	5.06	7.82	10.77	9.17	9.83	9.11	10.99	1305	1764	1367
227	4.90	4.22	4.98	5.82	7.25	6.58	7.47	9.90	1157	10.02	10.49	10.49	1241	1457	1852	1479

Table B.37 – LVDT data (Deflection) of Specimen F09-03

Load	Deflection (mm)															
(kN)	D1	D2	D3	D4	D5	D6	D7	D8	D9	D10	D11	D12	D13	D14	D15	D16
0	0.00	0.00	0.00	0.00	0.00	-	0.00	0.00	0.00	-	-	-	0.00	-0.01	0.01	0.01
0	0.00	0.00	0.00	0.00	0.00	-	0.00	0.00	0.00	-	-	-	0.00	0.00	0.00	0.00
0	0.00	0.00	0.00	0.00	0.00	-	-0.01	-0.01	0.00	-	-	-	0.00	0.00	0.00	0.00
35	0.20	0.01	-0.08	0.00	0.46	-	-0.23	0.20	0.94	-	-	-	-0.40	-0.15	0.40	0.79
24	0.15	0.01	-0.07	0.00	0.34	-	-0.21	0.17	0.68	-	-	-	-0.38	-0.14	0.58	0.61
51	0.22	-0.01	-0.03	0.00	0.46	-	-0.15	0.45	0.89	-	-	-	-0.29	0.23	1.81	1.06
66	0.23	-0.02	0.03	0.00	0.48	-	-0.05	0.63	0.91	-	-	-	-0.08	0.57	2.28	1.27
79	0.23	-0.04	0.08	0.00	0.49	-	0.09	0.88	0.92	-	-	-	0.19	1.03	2.83	1.56
86	0.24	-0.06	0.13	0.07	0.49	-	0.19	1.06	0.95	-	-	-	0.39	1.35	3.15	1.76
91	0.25	-0.09	0.15	0.12	0.51	-	0.23	1.20	0.99	-	-	-	0.50	1.59	3.45	1.97
92	0.25	-0.09	0.16	0.14	0.51	-	0.24	1.25	0.98	-	-	-	0.52	1.65	3.55	2.03
94	0.24	-0.10	0.17	0.21	0.52	-	0.28	1.44	0.99	-	-	-	0.62	1.94	3.94	2.27
93	0.24	-0.11	0.17	0.22	0.52	-	0.28	1.45	0.99	-	-	-	0.63	1.97	3.98	2.30
101	0.25	-0.14	0.19	0.28	0.52	-	0.31	1.63	0.99	-	-	-	0.67	2.22	4.43	2.52
117	0.26	0.02	0.20	0.17	0.63	-	0.37	1.34	1.26	-	-	-	0.76	1.84	3.86	2.23
122	0.28	0.00	0.21	0.20	0.66	-	0.39	1.43	1.31	-	-	-	0.79	1.97	4.09	2.39
139	0.32	-0.03	0.25	0.31	0.79	-	0.49	1.74	1.63	-	-	-	1.04	2.48	4.75	2.95
154	0.37	-0.08	0.30	0.47	0.98	-	0.60	2.22	2.00	-	-	-	1.30	3.23	5.85	3.79
177	0.47	-0.15	0.34	0.68	1.37	-	0.76	2.92	2.88	-	-	-	1.72	4.28	7.36	5.15
195	0.58	-0.24	0.36	0.88	1.78	-	0.92	3.59	3.79	-	-	-	2.16	5.26	8.91	6.62
199	0.60	-0.27	0.37	0.94	1.86	-	0.97	3.81	3.96	-	-	-	2.29	5.61	9.41	7.01
217	0.68	-0.36	0.40	1.16	2.18	-	1.18	4.58	4.69	-	-	-	2.85	6.87	1108	8.36
242	0.82	-0.40	0.43	1.36	2.74	-	1.44	5.36	5.93	-	-	-	3.52	8.03	12.89	9.97
264	0.96	-0.40	0.48	1.53	3.28	-	1.74	6.04	7.15	-	-	-	4.31	9.08	14.44	1149
281	1.05	-0.28	0.54	1.60	3.71	-	1.96	6.47	8.06	-	-	-	4.83	9.72	15.52	12.42
282	1.07	-0.27	0.54	1.60	3.77	-	2.00	6.49	8.19	-	-	-	4.95	9.70	15.58	12.53
302	1.14	-0.04	0.64	1.53	4.08	-	2.31	6.41	8.90	-	-	-	5.60	9.78	15.48	12.57
319	1.20	-0.07	0.70	1.69	4.34	-	2.58	6.99	9.50	-	-	-	6.22	10.79	16.80	13.55
320	1.23	-0.06	0.70	1.70	4.44	-	2.60	7.02	9.74	-	-	-	6.30	10.84	16.84	13.69
324	1.29	-0.03	0.71	1.72	4.67	-	2.65	7.14	10.25	-	-	-	6.40	10.93	17.12	14.10
341	1.34	0.03	0.75	1.79	4.88	-	2.83	7.43	10.66	-	-	-	6.80	1145	17.88	14.63
360	1.43	0.10	0.83	1.88	5.27	-	3.17	7.81	1156	-	-	-	7.63	12.22	18.72	15.43
380	1.53	0.20	0.92	2.03	5.71	-	3.53	8.41	12.53	-	-	-	8.44	13.25	20.09	16.44
400	1.63	0.29	1.02	2.19	6.12	-	3.87	8.96	13.44	-	-	-	9.16	14.19	21.30	17.45
418	1.75	0.42	1.14	2.30	6.59	-	4.21	9.38	14.49	-	-	-	9.91	14.88	22.23	18.40
434	1.84	0.55	1.25	2.41	7.02	-	4.55	9.82	15.41	-	-	-	10.62	15.59	23.23	19.28
444	1.90	0.60	1.32	2.52	7.25	-	4.75	10.23	15.89	-	-	-	1103	16.21	24.14	19.93
453	2.09	0.75	1.58	2.91	7.86	-	5.26	1110	17.03	-	-	-	1196	17.47	25.70	21.30
455	2.26	0.85	1.82	3.26	8.18	-	5.69	1172	17.54	-	-	-	12.68	18.46	26.71	22.01
450	2.41	1.05	2.14	3.55	8.34	-	6.12	12.01	17.76	-	-	-	13.28	18.99	26.99	22.23
422	3.09	1.75	2.83	4.18	8.79	-	6.72	12.58	17.87	-	-	-	13.68	19.51	27.46	22.59
418	3.17	1.83	2.93	4.26	8.84	-	6.80	12.64	17.88	-	-	-	13.71	19.54	27.47	22.60
412	3.60	2.38	3.76	4.87	8.99	-	7.78	13.26	17.72	-	-	-	14.97	20.66	28.00	22.72

Table B.38 – LVDT data (Deflection) of Specimen F14-03

Load	Deflection (mm)															
(kN)	D1	D2	D3	D4	D5	D6	D7	D8	D9	D10	D11	D12	D13	D14	D15	D16
0	0.00	0.00	0.00	0.00	0.00	0.00	0.00	0.01	0.00	-	-	-	0.00	0.00	0.00	0.00
26	0.09	0.03	0.10	0.15	0.11	-0.03	0.15	0.29	0.16	-	-	-	0.26	0.42	0.71	0.40
40	0.18	-0.05	0.14	0.33	0.24	-0.26	0.18	0.70	0.35	-	-	-	0.34	0.94	2.51	1.04
66	0.25	-0.03	0.19	0.43	0.37	-0.23	0.27	0.93	0.56	-	-	-	0.51	1.24	3.06	1.41
79	0.29	-0.05	0.24	0.53	0.42	-0.28	0.36	1.17	0.62	-	-	-	0.68	1.61	3.59	1.75
107	0.31	-0.04	0.39	0.70	0.47	-0.30	0.70	1.64	0.61	-	-	-	1.39	2.60	4.56	2.27
121	0.28	-0.07	0.50	0.82	0.40	-0.35	1.00	2.07	0.44	-	-	-	2.04	3.58	5.44	2.72
141	0.28	-0.08	0.64	0.95	0.37	-0.33	1.35	2.55	0.36	-	-	-	2.83	4.63	6.41	3.23
158	0.27	-0.09	0.75	1.09	0.40	-0.31	1.68	3.05	0.32	-	-	-	3.53	5.66	7.51	3.82
183	0.26	-0.09	0.93	1.24	0.44	-0.28	2.23	3.67	0.42	-	-	-	4.73	7.10	8.85	4.49
198	0.28	-0.05	1.01	1.33	0.60	-0.14	2.51	4.04	0.75	-	-	-	5.36	7.88	9.67	5.06
213	0.34	-0.03	1.06	1.41	0.83	-0.05	2.69	4.37	1.30	-	-	-	5.80	8.47	10.44	5.68
222	0.37	-0.02	1.09	1.44	0.94	0.00	2.80	4.47	1.55	-	-	-	6.06	8.71	10.67	5.91
243	0.45	0.02	1.16	1.58	1.20	0.16	3.07	5.06	2.12	-	0.17	-	6.66	9.66	12.03	6.89
267	0.53	0.12	1.26	1.65	1.52	0.44	3.39	5.34	2.89	-	0.81	-	7.41	10.30	12.67	7.47
282	0.58	0.20	1.33	1.70	1.75	0.72	3.62	5.59	3.43	-	1.46	-	7.92	10.81	13.27	7.95
306	0.68	0.42	1.45	1.75	2.13	1.31	3.98	5.80	4.32	-	-	-	8.69	11.30	13.80	8.43
322	0.73	0.66	1.54	1.72	2.34	1.92	4.23	5.70	4.78	-	4.07	-	9.12	11.26	13.63	8.35
342	0.81	0.90	1.64	1.70	2.65	2.49	4.51	5.63	5.52	-	5.34	-	9.67	11.33	13.53	8.41
357	0.85	1.15	1.73	1.66	2.85	3.16	4.76	5.51	6.00	-	6.82	-	10.09	11.30	13.38	8.34
383	0.92	1.43	1.87	1.64	3.20	3.99	5.21	5.49	6.87	-	8.67	-	10.95	11.54	13.45	8.48
400	0.99	1.43	1.97	1.77	3.44	4.02	5.54	6.01	7.41	-	8.78	-	11.76	12.53	14.56	9.26
421	1.06	1.46	2.05	1.93	3.73	4.16	5.82	6.52	7.99	-	9.19	-	12.42	13.39	15.69	10.10
441	1.13	1.54	2.16	2.06	4.00	4.46	6.18	7.00	8.55	-	9.88	-	13.22	14.29	16.73	10.84
459	1.32	1.68	2.33	2.36	4.45	4.80	6.66	7.71	9.34	-	10.59	-	14.19	15.40	18.06	11.89
457	1.42	1.75	2.51	2.52	4.61	4.89	6.90	8.02	9.59	-	10.71	-	14.57	15.84	18.50	12.26
460	1.73	1.89	3.10	3.13	4.92	5.07	7.72	9.14	9.83	-	10.85	-	15.90	17.65	20.33	13.38
374	3.30	3.63	4.96	4.65	5.92	6.39	9.32	10.27	10.09	-	11.31	-	16.96	18.58	20.66	13.81
364	3.92	4.27	5.84	5.45	6.22	6.91	10.51	11.22	10.00	-	11.47	-	18.67	20.21	21.67	14.22
306	6.51	7.03	9.19	8.54	7.58	8.94	14.21	14.23	9.80	-	11.96	-	22.92	24.30	24.36	15.54

Table B.39 – LVDT data (Deflection) of Specimen F09-06

Load	Deflection (mm)															
(kN)	D1	D2	D3	D4	D5	D6	D7	D8	D9	D10	D11	D12	D13	D14	D15	D16
0	0.00	-	0.00	0.00	0.00	0.00	0.00	0.00	0.00	0.00	0.00	0.00	0.00	0.00	0.00	0.00
0	0.00	-	0.00	0.00	0.00	0.00	-0.01	0.01	0.01	0.00	0.00	0.00	0.00	0.00	0.00	0.00
24	0.20	-	0.03	0.16	0.32	-0.07	-0.11	0.31	0.58	-0.20	-0.14	0.41	-0.22	0.12	1.26	0.75
44	0.26	-	0.14	0.34	0.35	-0.25	0.07	0.70	0.57	0.13	-0.53	0.54	0.15	0.76	2.76	1.18
58	0.29	-	0.18	0.39	0.38	-0.23	0.15	0.79	0.66	0.13	-0.51	0.46	0.33	0.94	2.96	1.29
81	0.32	-	0.26	0.50	0.42	-0.24	0.31	1.04	0.69	0.26	-0.62	0.39	0.68	1.42	3.50	1.59
98	0.38	-	0.34	0.63	0.50	-0.32	0.46	1.39	0.83	0.41	-0.83	0.44	1.03	1.97	4.19	2.06
123	0.44	-	0.39	0.74	0.61	-0.37	0.57	1.66	1.03	0.42	-0.88	0.44	1.32	2.38	4.81	2.50
173	0.68	-	0.46	1.06	1.19	-0.44	0.85	2.72	2.10	-	-0.91	0.40	2.58	4.04	7.07	4.59
175	0.69	-	0.47	1.09	1.22	-0.44	0.86	2.83	2.15	-	-0.91	0.40	2.60	4.19	7.34	4.77
180	0.71	-	0.46	1.11	1.28	-0.44	0.87	2.92	2.27	-	-0.90	0.41	2.68	4.31	7.55	4.96
197	0.80	-	0.48	1.22	1.52	-0.47	0.98	3.36	2.75	-	-0.87	0.37	3.13	4.99	8.52	5.86
219	0.95	-	0.50	1.40	1.93	-0.46	1.17	4.05	3.59	-	-0.74	0.20	3.84	6.04	10.07	7.25
242	1.05	-	0.60	1.49	2.33	-0.03	1.60	4.51	4.48	-	0.33	-0.72	4.91	7.06	1110	8.14
260	1.04	0.24	0.74	1.40	2.53	0.73	2.04	4.40	4.96	-	1.93	-	5.74	7.25	10.96	8.03
279	1.00	0.55	0.90	1.32	2.65	1.55	2.51	4.25	5.25	-	3.68	-	6.59	7.49	10.73	7.77
282	1.00	0.60	0.92	1.31	2.67	1.69	2.58	4.24	5.31	-	3.99	-	6.71	7.52	10.71	7.74
302	0.96	0.88	1.07	1.25	2.80	2.45	3.11	4.13	5.66	-	5.62	-	7.69	7.82	10.52	7.55
400	1.30	1.30	1.53	1.70	4.32	4.18	5.09	6.21	9.00	-	9.88	-	12.13	12.31	15.34	1110
420	1.37	1.42	1.62	1.76	4.65	4.53	5.45	6.53	9.74	-	10.72	-	12.91	12.99	16.05	1176
420	1.37	1.48	1.63	1.75	4.67	4.69	5.48	6.51	9.77	-	1107	-	12.92	12.94	16.04	1172
440	1.40	1.78	1.75	1.70	4.99	5.60	5.93	6.43	10.52	-	13.07	-	13.74	13.16	15.91	1168
459	1.42	2.13	1.88	1.65	5.29	6.64	6.46	6.33	1121	-	15.36	-	14.71	13.47	15.74	1154
463	1.45	2.26	1.92	1.64	5.43	7.04	6.60	6.29	1153	-	16.25	-	14.92	13.48	15.70	1153
479	1.55	2.40	2.05	1.77	5.83	7.60	7.13	6.78	12.40	-	17.45	-	16.07	14.51	16.73	12.33
484	1.61	2.39	2.09	1.87	6.00	7.58	7.28	7.15	12.74	-	17.45	-	16.44	15.09	17.51	12.94
501	1.80	2.34	2.21	2.19	6.56	7.58	7.84	8.45	13.82	-	17.51	-	17.78	17.21	20.31	15.07
519	1.99	2.38	2.34	2.48	7.18	7.74	8.44	9.63	15.00	-	17.90	-	19.16	19.16	22.85	17.10
537	2.36	2.46	2.55	2.97	8.18	8.01	9.25	1157	16.77	-	18.48	-	20.96	22.04	26.87	20.33
540	2.62	2.52	2.68	3.19	8.83	8.11	9.50	12.24	17.85	-	18.62	-	21.46	22.86	28.13	21.67
538	2.90	2.57	2.80	3.53	9.38	8.14	9.68	13.03	18.67	-	18.62	-	21.71	23.66	29.52	23.00
543	3.49	2.69	2.94	4.01	10.55	8.24	9.90	14.04	20.62	-	18.65	-	22.12	24.63	31.26	25.18
540	3.89	2.73	3.12	4.74	1107	8.18	10.10	15.59	21.12	-	18.52	-	22.37	26.20	34.23	27.24
541	4.10	2.79	3.17	4.87	1147	8.23	10.13	15.76	21.85	-	18.55	-	22.39	26.24	34.44	27.80
543	4.50	2.92	3.42	5.29	12.16	8.32	10.50	16.48	22.93	-	18.55	-	22.99	27.09	35.63	29.10
540	4.68	3.02	3.61	5.61	12.30	8.33	10.68	17.12	22.97	-	18.50	-	23.14	27.79	36.79	29.81
539	5.22	3.31	4.22	6.43	12.96	8.46	1148	18.26	23.75	-	18.35	-	24.39	29.30	38.28	31.11

Table B.40 – LVDT data (Deflection) of Specimen F14-06

Load	Deflection (mm)															
(kN)	D1	D2	D3	D4	D5	D6	D7	D8	D9	D10	D11	D12	D13	D14	D15	D16
0	0.00	0.00	0.00	0.00	0.00	0.00	0.01	0.00	0.00	-	0.00	0.01	0.00	0.00	0.00	0.01
0	0.00	0.00	0.00	0.00	0.00	0.00	0.00	0.00	-0.01	-	0.00	0.00	0.00	0.00	0.00	0.00
19	0.04	-0.01	0.07	0.12	0.04	-0.10	0.12	0.26	0.05	-	-0.20	0.05	0.23	0.44	1.04	0.32
48	0.15	-0.09	0.16	0.40	0.23	-0.44	0.22	0.90	0.31	-	-0.87	0.53	0.50	1.29	2.48	1.26
70	0.24	-0.08	0.22	0.55	0.38	-0.53	0.31	1.29	0.58	-	-1.10	0.68	0.70	1.80	3.32	1.83
88	0.28	-0.06	0.26	0.61	0.45	-0.50	0.39	1.42	0.72	-	-1.03	0.61	0.83	2.00	3.57	2.03
103	0.33	-0.05	0.32	0.70	0.54	-0.51	0.49	1.63	0.88	-	-1.05	0.56	1.03	2.36	4.00	2.36
122	0.34	-0.04	0.42	0.84	0.57	-0.53	0.77	2.04	0.92	-	-1.16	0.33	1.59	3.24	4.86	2.81
143	0.38	-0.04	0.49	0.96	0.66	-0.56	0.95	2.40	1.13	-	-1.22	0.20	1.99	3.91	5.57	3.33
160	0.41	-0.06	0.57	1.08	0.73	-0.58	1.18	2.78	1.26	-	-1.25	-0.02	2.48	4.67	6.38	3.86
200	0.56	-0.07	0.64	1.39	1.22	-0.62	1.53	3.79	2.36	-	-1.27	-0.25	3.40	6.35	8.70	5.69
214	0.64	-0.07	0.66	1.50	1.48	-0.59	1.61	4.15	2.89	-	-1.22	-0.30	3.67	6.90	9.54	6.43
248	0.82	0.31	0.74	1.40	2.06	0.54	1.85	3.99	4.17	-	1.07	-1.95	4.17	6.65	9.40	6.66
264	0.92	-0.04	0.77	1.35	2.38	1.37	1.98	3.87	4.85	-	2.39	-2.86	4.37	6.51	9.28	6.77
289	1.07	-0.30	0.82	1.27	2.91	2.72	2.13	3.71	6.07	-	4.46	-	4.67	6.28	9.15	7.05
301	1.15	-0.35	0.87	1.40	3.16	2.62	2.22	4.13	6.60	-	4.31	-	4.96	6.84	10.10	7.86
317	1.20	-0.39	0.93	1.54	3.34	2.57	2.44	4.63	7.01	-	4.26	-	5.55	7.74	1127	8.69
351	1.37	-0.45	1.01	1.85	3.90	2.59	2.78	5.74	8.19	-	4.38	-	6.48	9.45	13.86	10.66
385	1.52	-0.08	1.10	1.78	4.49	3.77	3.12	5.59	9.53	-	6.84	-	7.18	9.36	13.71	10.89
399	1.59	0.09	1.14	1.74	4.77	4.31	3.29	5.50	10.14	-	8.01	-	7.47	9.30	13.64	10.98
477	2.09	0.23	1.37	2.29	6.21	5.03	4.14	7.45	13.12	-	9.61	-	9.59	12.32	18.05	14.70
503	2.26	0.30	1.43	2.49	6.74	5.26	4.38	8.10	14.23	-	10.14	-	10.16	13.24	19.50	15.99
539	2.56	0.43	1.54	2.82	7.62	5.76	4.74	9.13	15.97	-	1126	-	1102	14.60	21.74	18.01
541	2.64	0.47	1.55	2.87	7.86	5.84	4.80	9.22	16.46	-	1139	-	1116	14.69	21.88	18.31
557	3.96	1.20	2.13	4.15	10.26	6.63	5.37	1166	20.41	-	12.38	-	1186	16.91	26.24	22.91
560	4.13	1.30	2.29	4.34	10.52	6.73	5.57	1196	20.91	-	12.46	-	12.15	17.29	26.73	23.46
570	4.47	1.47	2.57	4.80	10.99	6.87	5.91	12.83	21.48	-	12.55	-	12.64	18.35	28.20	24.62
581	5.00	1.72	2.82	5.38	1187	7.05	6.23	13.84	22.94	-	12.65	-	13.12	19.40	29.90	26.46
569	6.56	2.71	3.73	7.04	13.90	7.44	6.80	15.85	25.54	-	12.53	-	13.48	20.83	32.54	29.68
526	8.64	4.15	5.43	9.34	16.20	7.94	7.55	18.55	28.05	-	12.19	-	13.65	22.76	36.04	33.37
482	1169	6.38	7.74	12.46	19.68	8.69	8.74	22.06	32.06	-	1157	-	13.78	24.86	40.20	38.40

Table B.41 – LVDT data (Deflection) of Specimen F09-09

Load	Deflection (mm)															
(kN)	D1	D2	D3	D4	D5	D6	D7	D8	D9	D10	D11	D12	D13	D14	D15	D16
0	0.00	0.00	0.00	0.00	0.01	0.00	0.00	0.00	0.00	0.00	0.00	0.00	0.00	0.00	0.00	0.00
20	0.09	0.02	0.02	0.10	0.18	0.00	-0.01	0.17	0.34	-0.14	-0.03	0.15	-0.06	0.12	0.72	0.41
44	0.20	-0.05	0.02	0.25	0.39	-0.21	-0.07	0.51	0.77	-0.07	-0.41	0.60	-0.21	0.46	2.03	1.12
66	0.26	-0.03	0.04	0.31	0.54	-0.18	-0.05	0.64	1.05	-0.21	-0.38	0.64	-0.19	0.57	2.40	1.45
82	0.30	-0.05	0.07	0.38	0.61	-0.24	0.00	0.81	1.19	-0.16	-0.47	0.71	-0.11	0.82	2.86	1.73
101	0.32	-0.03	0.13	0.44	0.66	-0.21	0.15	0.93	1.32	-0.20	-0.43	0.54	0.21	1.12	3.15	1.90
126	0.34	0.03	0.21	0.49	0.72	-0.07	0.33	1.10	1.46	-0.36	-0.17	0.21	0.58	1.48	3.58	2.12
145	0.36	0.21	0.28	0.45	0.79	0.31	0.46	0.98	1.60	-0.93	0.62	-0.46	0.89	1.40	3.39	1.92
180	0.40	0.56	0.46	0.38	0.93	1.15	0.92	0.78	1.95	-2.11	2.23	-2.09	1.89	1.52	3.06	1.60
197	0.45	0.75	0.53	0.34	1.17	1.67	1.13	0.67	2.50	-3.09	3.28	-3.07	2.41	1.58	2.87	1.65
280	0.67	0.50	0.89	0.66	2.08	3.15	2.43	1.85	4.66	-5.37	5.62	-5.94	5.37	4.55	5.69	4.06
320	0.71	1.10	1.10	0.54	2.54	4.88	3.22	1.54	5.79	-8.14	9.32	-9.21	7.22	4.85	5.28	3.79
320	0.73	1.11	1.11	0.54	2.61	4.90	3.25	1.56	5.97	-8.24	9.38	-9.26	7.30	4.90	5.31	3.88
340	0.82	1.40	1.14	0.47	3.06	5.79	3.47	1.42	7.04	-9.98	1142	-10.69	7.90	4.73	5.15	4.07
380	0.96	1.45	1.37	0.70	3.57	6.42	4.25	2.23	8.25	-1120	12.91	-12.23	9.66	6.60	7.08	5.52
402	1.01	1.39	1.50	0.90	3.85	6.40	4.75	2.97	8.95	-1126	12.95	-12.69	10.79	8.15	8.71	6.78
482	1.36	1.92	1.76	1.15	5.64	8.51	6.05	4.24	13.09	-15.85	17.76	-16.38	13.86	10.78	1182	9.84
498	1.36	2.20	1.89	1.12	5.81	9.46	6.54	4.12	13.56	-17.23	19.75	-18.21	14.97	1106	1167	9.65
501	1.36	2.29	1.93	1.11	5.91	9.79	6.67	4.10	13.77	-17.71	20.45	-18.79	15.29	1112	1163	9.63
523	1.48	2.67	2.02	1.06	6.58	1115	7.11	3.97	15.31	-20.26	23.39	-20.96	16.35	1114	1147	9.91
576	2.06	2.10	2.42	2.29	8.98	10.91	8.85	8.66	20.32	-21.49	23.21	-21.35	19.97	18.78	21.51	18.48
613	2.49	2.44	2.60	2.57	1100	13.17	9.71	10.02	24.62	-26.23	27.93	-24.53	22.01	20.89	24.60	22.11
646	2.85	2.81	2.98	2.54	12.88	16.19	1139	10.10	28.80	-32.15	34.26	-30.20	25.90	22.15	24.79	23.63
660	3.34	3.79	3.46	2.54	15.03	20.96	13.18	10.17	33.25	-40.84	44.15	-38.08	29.81	23.28	24.99	24.93
664	3.74	4.67	3.54	2.62	16.58	23.89	13.40	10.38	36.48	-46.91	50.47	-41.96	30.39	23.08	25.44	26.50
668	3.87	4.85	3.59	2.63	16.95	24.34	13.54	10.45	37.10	-47.92	51.48	-42.66	30.64	23.18	25.56	26.84
668	4.02	4.78	3.71	2.68	17.40	25.26	13.83	10.54	37.94	-49.63	53.44	-44.15	31.20	23.37	25.70	27.23
672	4.28	5.42	4.08	2.76	17.97	26.66	14.76	10.62	38.90	-51.64	55.82	-46.73	33.02	24.21	25.70	27.50
670	4.82	6.21	4.28	2.88	18.95	28.50	14.98	10.71	40.36	-54.81	59.34	-48.95	33.23	23.89	25.70	28.10
668	5.58	7.12	4.58	3.15	20.30	30.05	15.13	1100	42.63	-57.81	61.86	-50.30	33.23	23.58	25.91	29.39
665	6.84	8.37	5.03	3.55	22.71	31.73	15.31	1126	46.53	-61.66	64.43	-51.35	33.15	22.92	25.88	31.64
656	8.16	9.67	5.94	3.98	24.88	33.38	15.52	1158	49.87	-65.01	66.72	-52.27	32.97	22.24	25.87	33.53

Table B.42 – LVDT data (Deflection) of Specimen F14-09

Load	Deflection (mm)															
(kN)	D1	D2	D3	D4	D5	D6	D7	D8	D9	D10	D11	D12	D13	D14	D15	D16
1	0.00	-0.05	0.00	0.05	0.00	-0.14	0.00	0.11	0.01	-	-0.13	0.11	0.00	0.09	0.14	0.10
11	-0.02	-0.02	0.04	0.09	-0.01	-0.08	0.07	0.22	-0.57	-	-0.08	-0.01	0.09	0.29	0.33	0.14
40	0.01	0.15	0.05	0.06	0.35	0.37	0.04	0.11	0.16	-	0.83	-0.47	-0.03	-0.10	1.44	0.35
58	0.09	0.19	0.05	0.10	0.58	0.49	0.04	0.23	0.66	-	1.09	-0.54	-0.03	-0.04	1.79	0.78
81	0.18	0.23	0.07	0.16	0.81	0.61	0.10	0.43	1.29	-	1.37	-0.71	0.11	0.22	2.31	1.31
103	0.25	0.26	0.09	0.22	0.99	0.73	0.19	0.64	1.75	-	1.65	-0.91	0.33	0.53	2.87	1.81
140	0.28	0.36	0.21	0.27	1.15	1.12	0.56	0.86	2.19	-	2.42	-1.88	1.21	1.26	3.47	2.17
180	0.34	0.40	0.29	0.37	1.36	1.29	0.85	1.25	2.77	-	2.82	-2.40	1.90	2.09	4.42	2.92
220	0.40	0.45	0.37	0.47	1.57	1.51	1.14	1.62	3.36	-	3.37	-2.99	2.61	2.89	5.35	3.62
246	0.44	0.51	0.44	0.53	1.69	1.80	1.36	1.88	3.64	-	4.07	-3.62	3.08	3.47	6.08	4.04
286	0.50	0.56	0.50	0.6	1.93	2.01	1.64	2.14	4.29	-	4.51	-4.21	3.80	4.12	6.68	4.62
341	0.62	0.68	0.65	0.78	2.35	2.78	2.21	3.01	5.34	-	6.35	-5.80	5.06	5.86	8.85	6.09
362	0.68	0.70	0.67	0.79	2.57	2.82	2.35	3.05	5.95	-	6.40	-6.02	5.52	6.06	8.89	6.42
381	0.72	0.76	0.70	0.83	2.73	3.12	2.54	3.25	6.37	-	7.08	-6.61	5.96	6.49	9.42	6.81
402	0.79	0.82	0.74	0.87	3.02	3.46	2.75	3.52	7.11	-	7.84	-7.27	6.48	6.99	10.10	7.46
462	0.94	1.01	0.92	1.01	3.65	4.54	3.61	4.35	8.73	-	10.17	-9.55	8.50	8.98	12.16	9.03
481	1.00	1.02	0.97	1.11	3.89	4.68	3.86	4.76	9.35	-	10.56	-9.95	9.12	9.79	13.10	9.82
503	1.06	1.08	1.03	1.18	4.13	5.01	4.16	5.13	9.94	-	11.33	-10.65	9.80	10.57	13.98	10.50
585	1.31	1.38	1.33	1.45	5.14	6.66	5.55	6.60	12.45	-	14.85	-14.07	13.02	13.86	17.41	13.07
603	1.36	1.40	1.40	1.55	5.34	6.81	5.91	7.01	12.97	-	15.20	-14.61	13.85	14.78	18.28	13.76
664	1.59	1.79	1.73	1.80	6.29	8.79	7.45	8.32	15.16	-	19.20	-18.68	17.27	17.90	21.17	15.83
701	1.82	2.09	2.22	2.30	7.00	10.39	9.34	10.11	16.67	-	22.35	-22.52	21.34	22.06	24.85	18.14
719	1.90	2.20	2.47	2.44	7.30	11.34	10.30	10.75	17.33	-	24.14	-24.77	23.36	23.81	26.14	18.89
755	2.17	2.85	3.32	3.12	8.09	14.17	13.32	13.26	18.98	-	29.38	-31.45	29.52	30.00	31.03	21.67
777	2.33	3.98	4.48	3.69	8.37	17.70	16.70	14.81	19.31	-	35.58	-39.80	36.30	35.55	33.58	22.27
784	2.46	4.72	4.99	3.96	8.60	20.28	17.94	15.58	19.61	-	40.30	-44.51	38.58	37.81	34.98	22.68
795	2.58	5.29	5.55	4.11	8.90	22.38	19.33	15.87	20.08	-	43.84	-48.74	41.30	39.50	35.24	22.65
789	2.78	6.06	6.03	4.33	9.08	24.00	20.01	16.30	20.16	-	46.54	-51.25	42.36	40.56	35.95	22.88
796	3.08	6.73	6.52	4.46	9.40	25.76	20.78	16.38	20.51	-	49.22	-54.11	43.71	41.13	35.85	22.72
801	3.90	8.71	8.09	5.01	10.36	30.38	22.70	16.61	21.67	-	56.83	-61.36	46.94	42.51	35.58	22.37
797	4.45	9.63	8.91	5.38	10.8	32.16	23.76	16.72	22.15	-	59.08	-63.86	48.50	43.24	35.35	22.22
784	6.12	12.98	11.63	6.41	12.19	39.16	26.95	17.10	22.92	-	69.48	-73.97	53.35	45.38	34.60	20.92

Table B.43 – LVDT data (Deflection) of Specimen F09-12

Load	Deflection (mm)															
(kN)	D1	D2	D3	D4	D5	D6	D7	D8	D9	D10	D11	D12	D13	D14	D15	D16
0	0.00	0.00	0.00	0.00	0.01	-0.01	0.00	0.00	0.00	-	0.00	-	0.00	0.00	0.01	0.00
1	0.00	-0.01	0.00	0.00	0.00	-0.02	-0.01	0.01	0.01	-	-0.05	-	0.00	0.04	0.04	0.03
28	0.07	0.25	0.14	0.00	0.11	0.50	0.19	-0.17	0.29	-	0.82	-	0.39	-0.13	0.71	-0.31
39	0.07	0.33	0.31	0.08	0.01	0.57	0.53	-0.03	0.00	-	0.95	-	0.96	0.38	1.08	-0.38
68	0.10	0.43	0.42	0.12	0.05	0.73	0.70	0.02	0.12	-	1.22	-	1.32	0.63	1.38	-0.38
78	0.10	0.47	0.47	0.14	0.04	0.79	0.80	0.07	0.09	-	1.32	-	1.50	0.78	1.57	-0.38
95	0.10	0.56	0.62	0.17	-0.04	0.92	1.09	0.13	-0.10	-	1.56	-	2.05	1.18	1.75	-0.53
122	0.04	0.85	0.93	0.20	-0.21	1.37	1.73	0.06	-0.49	-	2.42	-	3.34	1.83	1.66	-1.04
144	0.05	1.09	1.07	0.20	-0.26	1.65	2.04	-0.01	-0.49	-	3.14	-	3.98	2.08	1.60	-1.32
156	0.04	1.33	1.22	0.17	-0.24	2.08	2.31	-0.22	-0.51	-	4.06	-	4.58	2.12	1.26	-1.63
184	0.05	1.56	1.41	0.13	-0.13	2.57	2.62	-0.37	-0.21	-	5.11	-	5.36	2.29	1.01	-1.79
199	0.11	1.71	1.47	0.10	0.07	2.89	2.75	-0.48	0.25	-	5.86	-	5.67	2.25	0.87	-1.73
215	0.18	1.86	1.52	0.07	0.32	3.24	2.91	-0.57	0.86	-	6.61	-	6.04	2.26	0.73	-1.58
223	0.22	1.86	1.54	0.11	0.43	3.23	3.00	-0.44	1.13	-	6.59	-	6.23	2.54	0.99	-1.26
343	0.72	2.23	1.85	0.53	2.31	4.44	4.45	1.22	5.45	-	9.60	-	9.44	6.12	4.95	2.94
360	0.81	2.28	1.92	0.61	2.66	4.67	4.77	1.55	6.22	-	10.14	-	10.16	6.81	5.74	3.75
392	0.91	2.38	2.04	0.73	3.08	5.07	5.24	2.06	7.21	-	1113	-	1123	7.89	6.96	4.81
401	0.98	2.38	2.04	0.78	3.37	5.11	5.35	2.24	7.85	-	1124	-	1146	8.19	7.37	5.39
523	1.71	2.82	2.44	1.33	6.05	6.89	7.22	4.55	13.65	-	15.45	-	15.37	12.50	12.59	10.96
583	2.31	3.18	2.83	1.80	8.35	8.15	8.87	6.42	18.75	-	18.23	-	18.81	16.05	16.63	15.53
597	2.41	3.28	2.94	1.93	8.71	8.43	9.31	6.95	19.47	-	18.86	-	19.65	17.11	17.84	16.50
679	4.15	3.75	3.82	3.24	14.91	10.25	12.91	11.91	32.53	-	22.83	-	26.49	25.79	28.17	29.56
709	6.62	4.02	4.50	4.56	22.32	11.11	14.93	16.26	46.88	-	24.41	-	30.16	31.75	36.38	43.47
714	7.21	4.06	4.62	4.96	23.83	11.26	15.17	17.22	49.65	-	24.62	-	30.50	32.73	38.10	46.28
718	7.90	4.13	4.75	5.47	25.56	11.41	15.41	18.22	52.75	-	24.89	-	30.86	33.79	39.94	49.40
725	8.80	4.20	4.87	6.01	27.59	11.57	15.62	19.44	56.42	-	25.11	-	31.08	34.84	42.10	53.29
713	9.16	4.22	4.95	6.24	28.25	11.58	15.70	19.87	57.34	-	25.02	-	31.13	35.21	42.64	54.04
720	9.81	4.26	5.03	6.60	29.76	11.61	15.79	20.61	60.28	-	24.99	-	31.15	35.70	43.90	56.79
712	10.31	4.28	5.14	6.93	30.69	11.60	15.88	21.16	61.58	-	24.78	-	31.20	36.15	44.66	58.09
708	10.49	4.33	5.20	7.04	30.98	11.64	15.93	21.34	62.12	-	24.79	-	31.19	36.23	44.96	0.00
715	11.95	4.65	5.49	8.07	33.67	11.85	16.02	22.86	66.62	-	24.80	-	30.99	36.84	47.00	0.00
698	12.74	4.96	5.77	8.66	34.60	11.90	16.16	23.55	67.55	-	24.51	-	31.00	37.23	47.63	0.00
413	-0.57	14.14	15.04	-1.46	-0.47	15.61	20.57	35.14	74.72	-	21.82	-	29.32	41.32	56.62	0.00

Table B.44 – LVDT data (Deflection) of Specimen F14-12

Load	Deflection (mm)															
(kN)	D1	D2	D3	D4	D5	D6	D7	D8	D9	D10	D11	D12	D13	D14	D15	D16
0	0.00	0.00	0.00	0.00	0.00	0.01	0.00	0.00	0.00	0.00	0.00		0.00	0.00	0.00	0.01
22	0.10	0.05	0.06	0.00	0.10	-0.01	0.07	0.15	0.19	-0.09	-0.04		0.07	0.31	1.01	0.30
56	0.19	-0.04	0.16	0.00	0.20	-0.34	0.18	0.71	0.28	0.38	-0.65		0.15	1.09	2.49	1.09
76	0.22	-0.03	0.22	0.00	0.25	-0.37	0.28	0.86	0.40	0.44	-0.73		0.34	1.39	2.80	1.29
101	0.26	-0.04	0.29	0.00	0.30	-0.44	0.39	1.14	0.45	0.58	-0.91		0.51	1.82	3.50	1.67
127	0.30	-0.04	0.37	0.00	0.36	-0.46	0.55	1.40	0.53	0.70	-0.91		0.80	2.29	4.04	1.99
165	0.33	0.08	0.53	0.00	0.41	-0.23	0.90	1.63	0.60	0.57	-0.47		1.55	2.88	4.49	2.12
187	0.35	0.16	0.58	0.00	0.49	-0.05	1.05	1.72	0.76	0.31	-0.13		1.84	3.12	4.74	2.28
201	0.37	0.26	0.62	0.00	0.56	0.20	1.16	1.67	0.97		0.36		2.09	3.16	4.65	2.24
238	0.48	0.55	0.69	0.00	0.88	0.94	1.39	1.53	1.75		1.93		2.69	3.29	4.43	2.26
285	0.62	0.74	0.78	0.00	1.31	1.49	1.74	1.84	2.82		3.18		3.46	4.08	5.01	2.95
298	0.66	0.76	0.81	0.00	1.40	1.59	1.84	2.02	3.02		3.46		3.66	4.46	5.49	3.28
322	0.72	0.82	0.87	0.06	1.62	1.81	2.05	2.27	3.57		4.01		4.17	5.07	6.07	3.81
397	0.96	1.03	1.02	0.24	2.40	2.59	2.71	3.10	5.45		5.82		5.65	6.92	8.08	5.52
427	1.05	1.13	1.08	0.29	2.69	2.94	2.98	3.34	6.16		6.61		6.26	7.53	8.62	6.10
502	1.27	1.42	1.25	0.45	3.47	3.99	3.62	4.08	8.10		9.11		8.05	9.28	10.39	7.66
523	1.32	1.50	1.31	0.49	3.65	4.29	3.86	4.31	8.56		9.82		8.58	9.86	10.98	8.05
600	1.61	1.76	1.50	0.70	4.55	5.35	4.58	5.22	10.73		12.27		10.44	11.92	13.01	9.87
681	1.85	2.01	1.74	0.96	5.41	6.38	5.55	6.36	12.72		14.65		12.62	14.41	15.68	11.84
702	1.94	2.05	1.83	1.10	5.73	6.57	5.77	6.86	13.39		15.07		13.34	15.45	16.71	12.72
741	2.10	2.17	2.00	1.33	6.28	7.10	6.30	7.77	14.63		16.23		14.73	17.29	18.72	14.25
777	2.29	2.34	2.19	1.61	6.93	7.77	7.04	8.86	16.00		17.67		16.31	19.45	21.02	16.04
799	2.40	2.43	2.30	1.80	7.29	8.13	7.46	9.59	16.73		18.49		17.20	20.76	22.54	17.16
821	2.53	2.52	2.41	1.95	7.77	8.49	7.92	10.17	17.77		19.24		18.18	21.97	23.78	18.29
856	2.77	2.64	2.61	2.31	8.54	9.06	8.67	11.54	19.36		20.55		19.71	24.49	26.66	20.56
888	3.17	2.90	2.88	2.75	9.76	10.04	9.69	13.22	21.81		22.66		21.74	27.52	30.19	23.60
939	3.91	3.21	3.29	3.49	11.89	11.31	11.20	15.77	26.08		25.24		24.88	32.19	35.34	28.60
940	4.11	3.30	3.36	3.73	12.31	11.61	11.37	16.57	26.79		25.92		25.16	33.34	37.00	29.94
952	4.43	3.41	3.47	4.04	12.99	11.97	11.67	17.54	28.05		26.62		25.75	34.77	38.85	31.87
958	4.73	3.51	3.71	4.32	13.68	12.32	11.97	18.30	29.36		27.28		26.37	35.94	40.34	33.53
963	5.04	3.67	3.87	4.60	14.33	12.79	12.22	19.15	30.59		28.32		26.80	37.17	42.08	35.12
968	5.49	3.91	4.05	5.08	15.17	13.36	12.42	20.33	31.86		29.36		27.09	38.57	44.18	37.14
971	6.14	4.23	4.30	5.77	16.24	13.90	12.67	21.94	33.53		30.27		27.38	40.50	47.16	39.98
960	7.64	4.91	4.81	7.20	18.47	14.59	12.92	24.24	36.92		31.17		27.38	42.66	51.13	44.71
951	9.28	5.53	5.49	8.68	20.90	15.06	12.81	26.58	40.44		31.56		26.91	44.48	54.84	49.23
691	11.96	13.24	14.22	20.13	32.32	18.00	16.23	37.83	50.49		29.94		25.64	49.75	65.52	59.97

Appendix C

Analysis and Derivations

C.1 Design Procedure for ACI direct design method

Comprehensive design examples using the ACI direct design method are provided in a text book by McGregor and Wight (2000) and converted in to SI units by Teng and Irawan. Thus, the authors used some of the figures in the textbook in this section for illustration purposes. The procedure of the direct design method is summarised by the following steps:

Step 1: **Total factored static moment for a span**

- Calculate the total factored static moment M_o for a strip (Column strip and Middle strip). M_o is given by

$$M_o = \frac{q_u l_2 l_n^2}{8}$$

where q_u is the factored load per unit area. As illustrated by Fig. 3.#, l_2 is the width transverse span, l_n is the clear span length and should be at least $0.65l_1$, l_1 is the column-to-column span length.

Step 2: **Distribution of total factored static moment**

- In an interior span, distribute $0.65M_o$ to negative moment (negative M_u = $0.65M_o$) and $0.35M_o$ to positive moment (positive M_u = $0.35M_o$).
- In an end span, M_o should be distributed in accordance with Table C.1 or ACI 318-14 Table 8.10.4.2 as shown below

Step 3: **Divide the moments between the column and middle strips**

- *For the negative moments*, distribute 0.75 of negative M_u obtained in Step 2 to become the interior negative moment in column strip, the remaining $0.25M_u$ should be proportionally assigned to corresponding half middle strips.
- *For the positive moments,* distribute 0.60 of negative M_u obtained in Step 2 to become the interior negative moment in column strip, the remaining $0.40M_u$ should be proportionally assigned to corresponding half middle strips.

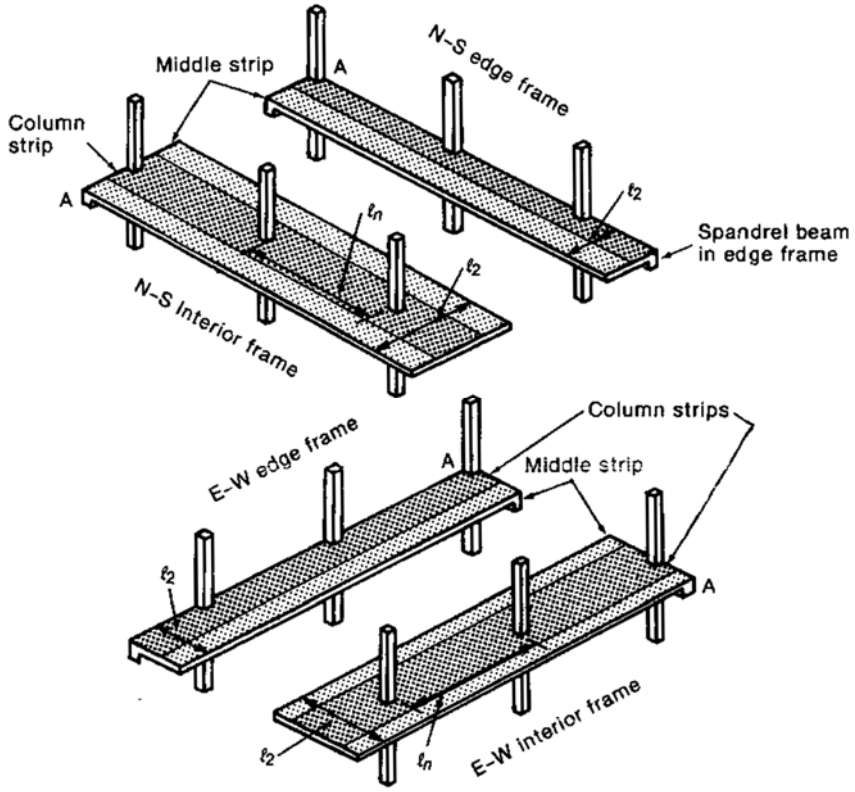

Fig. C.1 – Division of slab info frames for design (McGregor and Wight (2000))

Table C.1 - Distribution coefficients for end spans (ACI 318-14)

	Exterior edge unrestrained	Slab with beams between all supports	Slab without beams between interior supports		Exterior edge fully restrained
			Without edge beam	With edge beam	
Interior negative	0.75	0.70	0.70	0.70	0.65
Positive	0.63	0.57	0.52	0.50	0.35
Exterior negative	0	0.16	0.26	0.30	0.65

C.2 Derivations of flexural strength (Shear load) V_{flex} using Yield Line Analysis

This section of the appendix presents the derivation works of the Eqs. (3.14) to (3.16) of the ultimate load V_{flex} corresponding to the three yield line patterns as shown in Fig. 3.9 (Section 3.4.3.2). The three equations and the figure are also shown below.

$$V_{flex} = m_u \left(\frac{4 + 2\left(\frac{c_2}{c_1} - 1\right)\frac{c_2}{L_2}}{\frac{\sqrt{2}}{2}\cos\frac{\pi}{8} - \frac{c_2}{L_2}} \right) \quad \text{(For Fig. 3.9(a))} \tag{3.14}$$

$$V_{flex} = m_u \left(\frac{4L_1}{L_2 - c_2} + \frac{4L_2}{L_1 - c_1} \right) \quad \text{(For Fig. 3.9(b))} \tag{3.15}$$

$$V_{flex} = m_u \left(\frac{2(c_1 + c_2)}{r} + 2\pi \right) \quad \text{(For Fig. 3.9(c))} \tag{3.16}$$

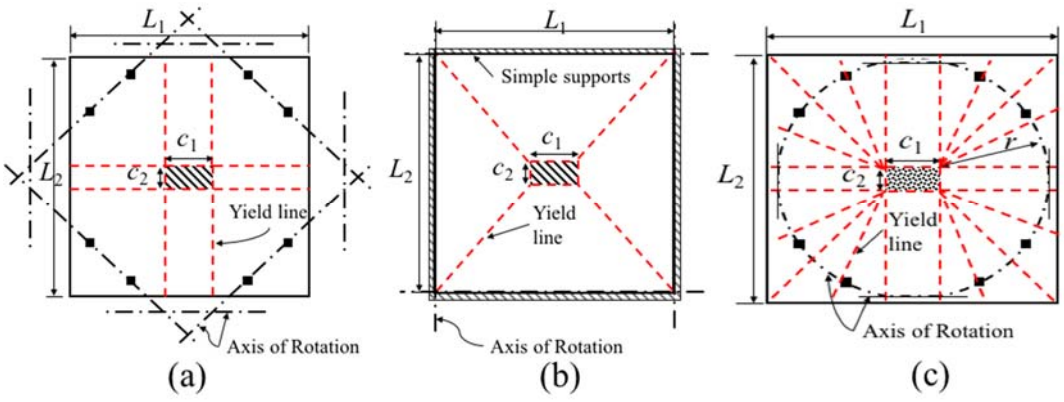

Fig. 3.9 — (a) yield line pattern a ductile slab loaded around the edges; (b) yield line pattern for a simply supported ductile slab; (c) circular fan yield line pattern.

Derivation of Equation (3.14)

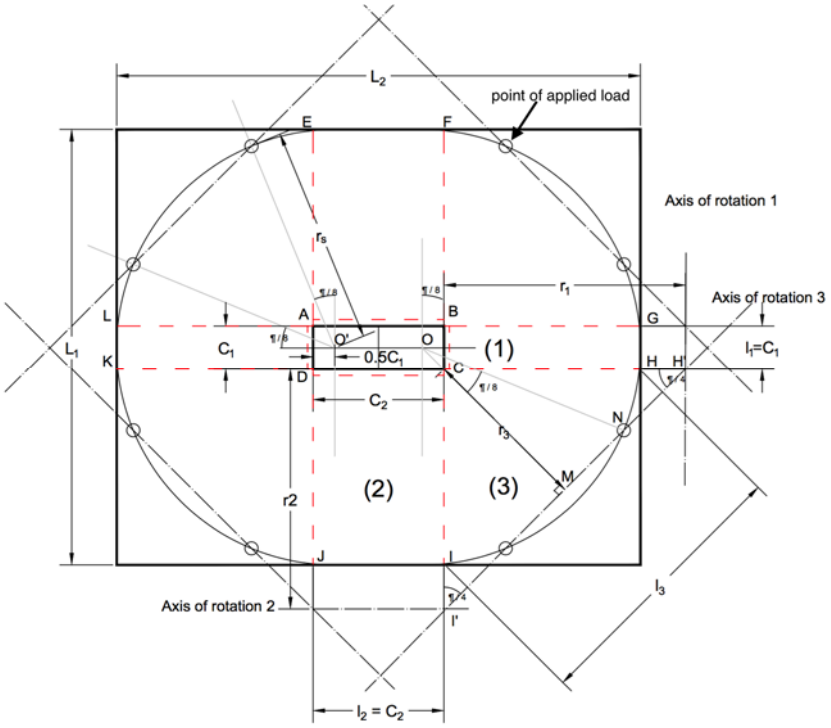

(a)

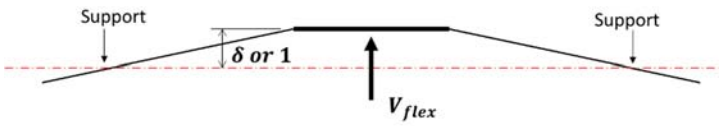

(b)

(Note that for this derivation, the longer side of columns and slab dimensions are denoted as L_2 instead of L_1)

Fig. C.1 – (a) Yield line for a slab supported on rectangular column. (b) idealised geometry of a slab rotation

Based on the yield line pattern shown in Fig. C.1 and Consider the virtual work method as described in Section 3.4.3.2, the solution of V_{flex} can be derived as follows.

Total external work (due to applied load) = Total internal work (done by the moments along yield lines)

$$U_E = U_I \qquad \text{(c1)}$$

Consider the downward loads applied at the 8 points on two half-circles whose centres are located at a distance of $0.5C_l$ from the centre of each short side of the column toward the column centre, and the radius is r_s or $0.5L_l$ as shown in Fig. C.1(a). At failure, the overall reaction force is V_{flex} and it acts at the centre of the column. To aid in visualization, we assume that the 8 point-loads provides 8 support points for the column. Thus, the 8 support points are assumed to have zero deflection. We also assume that the rigid column (providing an upward reaction of V_{flex}) deflects upward by an amount of δ or 1 (Fig. C.1(b)). Therefore, total external work U_E can be expressed by Eq. (c2).

$$U_E = V_{flex}.1 \qquad \text{(c2)}$$

Owing to symmetry, the total internal work done by the moments is equal to 2 times the internal work done by moments along yield lines in segment-1, $U_{I,1}$, and segment-2, $U_{I,2}$, plus 4 times the internal work done the by moments along yield lines in segment-3, $U_{I,3}$. Thus,

$$U_I = 2\left(U_{I,1} + U_{I,2}\right) + 4U_{I,3} \qquad \text{(c3)}$$

The internal work along each yield line is equal to the bending moment along the yield line per unit length times the length of the yield line times the amount of rotation that the moment undergoes along that yield line.

For segment-1, the internal work occurs along yield line BC only, the yield lines BG and CH do not contribute any internal work done to this segment because they are orthogonal to the axis of rotation-1. Since the segment rotates about axis of rotation-1, we have

$$U_{I,1} = ml_1\theta_1$$

where,

$l_1 = C_1$, and $\theta_1 = 1/r_1$

$r_1 = CH'$,

from triangle CH'M, the following relationship can be derived:

$CH' = \sqrt{2}CM$

from triangle OMN, the following relationship can be derived:

$CM = (ON)\cos\left(\frac{\pi}{8}\right) - \frac{\sqrt{2}}{2}C_1$, where ON = r_s

$$= r_s \cos(\tfrac{\pi}{8}) - \tfrac{\sqrt{2}}{2} C_1$$

then,

$$r_1 = CH' = \sqrt{2}CM$$

$$= \sqrt{2}\cos(\tfrac{\pi}{8})\, r_s - C_1$$

thus,

$$U_{I,1} = ml_1\theta_1 = mC_1 1/r_1$$

$$= \frac{mC_1}{\sqrt{2}\cos(\frac{\pi}{8})r_s - C_1} \qquad \text{(c4)}$$

For segment-2, the internal work occurs along yield line DC only, the yield lines CG and DJ do not contribute any internal work done to this segment because they are orthogonal to the axis of rotation-2. Since the segment rotates about axis of rotation-2, we have

$$U_{I,2} = ml_2\theta_2$$

where,

$l_2 = C_2$, and $\theta_2 = 1/r_2$

$r_2 = CI'$,

from triangle CH'I', the following relationship can be derived:

$CI' = CH' = \sqrt{2}CM$ (Determined previously in segment-1 case)

and this leads to:

$$r_2 = r_1 = \sqrt{2}\cos(\tfrac{\pi}{8})\, r_s - C_1$$

thus,

$$U_{I,2} = ml_2\theta_2 = mC_2 1/r_2$$

$$= \frac{mC_2}{\sqrt{2}\cos(\frac{\pi}{8})r_s - C_1} \qquad \text{(c5)}$$

For segment-3, the internal work occurs along yield lines CH and CI. Since the segment rotates about axis of rotation-2, we have

$$U_{I,3} = m[(CH)\cos\left(\tfrac{\pi}{4}\right) + (CI)\cos(\tfrac{\pi}{4})]\theta_3$$

or

$$U_{I,3} = ml_3\theta_3$$

where

from triangle CH'M and CI'M, the following relationship can be expressed as:

$l_3 = I\,H$

and,

$I\,H\ = (CI)\cos\left(\frac{\pi}{4}\right) + (CH)\cos\left(\frac{\pi}{4}\right)$

and, $CI = CH = \frac{L1-C1}{2}$

so, $l_3 = \frac{\sqrt{2}}{2}(L_1 - C_1)$

$\theta_3 = 1/r_3$

And,

$r_3 = CM = r_s\cos(\frac{\pi}{8}) - \frac{\sqrt{2}}{2}C_1$ (Determined previously)

Therefore,

$U_{I,3} = ml_3\theta_3$

$= \frac{m\frac{\sqrt{2}}{2}(L_1-C_1)}{r_s\cos(\frac{\pi}{8})-\frac{\sqrt{2}}{2}C_1}$

$= \frac{m(L_1-C_1)}{\sqrt{2}r_s\cos(\frac{\pi}{8})-C_1}$ (c6)

Substitute Eq. (c4) to (c6) into Eq. (c3) and the relationship in Eq. (c1) leads to:

$V_{flex}.1 = 2\left(U_{I,1} + U_{I,2}\right) + 4U_{I,3}$

Therefore,

$V_{flex} = 2\frac{mC_1}{\sqrt{2}\cos(\frac{\pi}{8})r_s-C_1} + 2\frac{mC_2}{\sqrt{2}\cos(\frac{\pi}{8})r_s-C_1} + 4\frac{m(L_1-C_1)}{\sqrt{2}r_s\cos(\frac{\pi}{8})-C_1}$

$= m\,(\frac{4L_1-2C_1+2C_2}{\sqrt{2}\cos(\frac{\pi}{8})r_s-C_1})$

substitute $r_s = 0.5L_1$ and $C_2 = \beta C_1$, where β is a ratio of long to short side of column face as defined by ACI 318. We are able to obtain the following expression:

$V_{flex} = 2m\,(\frac{2L_1+(\beta-1)C_1}{\frac{\sqrt{2}}{2}\cos(\frac{\pi}{8})L_1-C_1})$ (c7)

Or, to be consistent with the main thesis, swap the notations of L_1 with L_2, and c_1 with c_2, therefore

$$V_{flex} = m_u\left(\frac{4 + 2\left(\frac{c_2}{c_1} - 1\right)\frac{c_2}{L_2}}{\frac{\sqrt{2}}{2}\cos\frac{\pi}{8} - \frac{c_2}{L_2}}\right) \quad \text{(For Fig. 3.9(a))} \qquad (3.14)$$

Derivation of Equation (3.15)

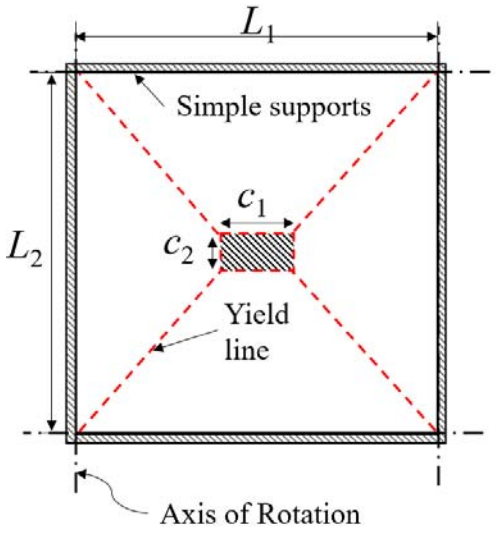

Fig. C.2 – Yield line for a slab supported around the four edges and loaded through on rectangular column

The derivation of V_{flex} for this case is simpler than the previous case. Consider the virtual work method as described in Section 3.4.3.2, the solution of V_{flex} can be derived as follows.

The total internal work, which is the work done by the plastic rotation along each yield line about the axis of rotation, the axis of rotations are the lines of supports along the edges as shown in Fig. C.2. Thus,

$$U_I = 2\times[m\times L_1\times 1/(L_2-c_2) + m\times L_2\times\delta\ (L_1-c_1)\ ]$$

The external work done is the same as the case for the V_{flex} in Eq. (3.14) that is:

$$U_E = V_{flex}\times\delta$$

Take $U_E = U_I$, therefore,

$$V_{flex} = m_u\left(\frac{4L_1}{L_2-c_2}+\frac{4L_2}{L_1-c_1}\right) \quad \text{(For Fig. 3.9(b))} \qquad (3.15)$$

Derivation of Equation (3.15)

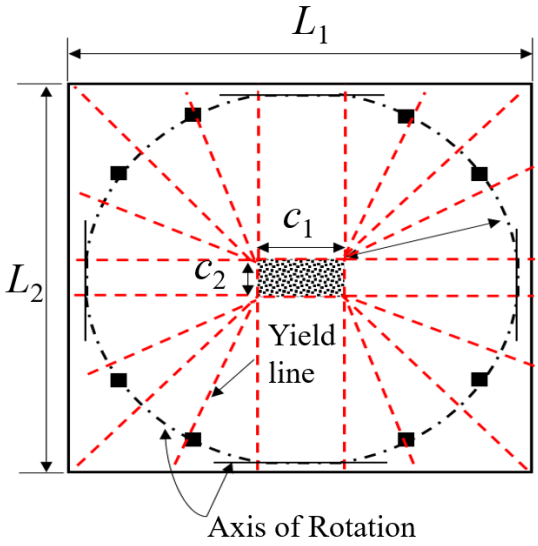

Fig. C.3 – Circular fan

The detailed derivation of V_{flex} for this case can also be obtained in the book by Park and Gamble (2000). Consider the virtual work method as described in Section 3.4.3.2, the solution of V_{flex} can be derived as follows.

The total internal work, which is the work done by the plastic rotation along each yield line about the axis of rotation, the axis of rotations are the lines of supports along the edges as shown in Fig. C.3. Thus,

$$U_I = 2(\delta/r)\ (c_1+c_2)m + (2\pi r)(\ \delta/r)\ m$$

The external work done is the same as the previous cases for the V_{flex} in Eq. (3.14) and Eq. (3.15) that is:

$$U_E = V_{flex} \times \delta$$

(Neglecting the short yield lines beyond the circular line and the negative reinforcement), Take $U_E = U_I$, therefore,

$$V_{flex} = m_u\left(\frac{2(c_1 + c_2)}{r} + 2\pi\right) \quad \text{(For Fig. 3.9(c))} \qquad (3.16)$$

where,

$r \approx 0.5(L_1\text{-}c_1)$

Appendix D

MS-EXCEL SUB-ROUTINES CODES FOR DESIGN METHODS AND ANALYSIS

VBA (Visual Basic for Applications) is the programming language of Excel and other Office programs. Following sections are the VBA codes of the relevant design methods evaluated in this thesis.

D.1 Authors' proposed methods

```
Sub ProposedMethod()
For i = 6 To Cells(3, "A").Value + 5
'*** read input
    ls1 = Cells(i, "G").Value 'distance between supports in x direction
    ls2 = Cells(i, "h").Value 'distance between supports in y direction
    l1 = Cells(i, "AK").Value ' length of slab in x direction
    l2 = Cells(i, "AL").Value ' length of slab in y direction
    h = Cells(i, "i").Value  ' thickness
    d = Cells(i, "O").Value  ' effective depth
    c1 = Cells(i, "k").Value ' longer length of column side
    c2 = Cells(i, "l").Value ' shorter length of column side
    fc = Cells(i, "m").Value ' compressive strength of concrete
    Col = Cells(i, "j").Value ' Column shape
    rho = Cells(i, "ad").Value ' average flexural reinforcement ratio
    dg = Cells(i, "n").Value  ' max aggregate size
    fy = Cells(i, "aj").Value ' yield strength of reinforcement
    fr1 = Cells(i, "as").Value ' residual strength fr1
    fr2 = Cells(i, "at").Value ' residual strength fr1
    fr3 = Cells(i, "au").Value ' residual strength fr1
    fr4 = Cells(i, "av").Value ' residual strength fr1
    FType = Cells(i, "AM").Value ' fibre type
    Lf = Cells(i, "AN").Value ' fibre length
    FRatio = Cells(i, "Ao").Value ' fibre type aspect ratio
    vf = Cells(i, "AP").Value ' fibre volume faction
    Vexp = Cells(i, "be").Value 'Observed failure load
'Convert rho
    rho100 = rho    '100As/bd
    rho = rho / 100 'As/bd
'*** Assumption for unknown parameter
    Es = 200 'in GPa,
    Ec = 4.7 * (fc) ^ 0.5   'in GPa ACI method
    If fy = 0 Then
        fy = 500 'MPa
    End If
    If dg = 0 And d < 50 Then ' for thin slab with d<50 mm that do have reported dg
        dg = 10
    End If
    If dg = 0 And d >= 50 Then ' for slab with d>= 50mm that do have reported dg
        dg = 20
    End If
    rs = 0.5 * ls1 ' assign the notation B, length of slab, to be used in Vflex
    If ls1 > ls2 Then
        rs = 0.5 * ls2
    End If
'*** Calculation
    bo = 2 * (c1 + c2) + 4 * d 'rectangular critical perimeter for circular columns
    b1 = c1 + 1# * d
    b2 = c2 + 1# * d
```

```
'Column rectangularity effect
    kC = Application.WorksheetFunction.Min((b1 / b2), (b2 / b1)) ^ (1 / 3)
'size effect factor
    d_o = 300
    kZ = (d_o / d) ^ (0.5)
    If kZ > 1 Then
        kZ = 1
    End If
 Coeff = 0.6 ' Coeff. for Vc basic
'*** Proposed Simplified Method for RC slabs in Chapter 7
    'alpha_o = 8
    fcc1 = fc ' set limit for f'c for calculation of rho_fs
    Vc_teng = kZ * kC * Coeff * (fcc1) ^ (1 / 3) * bo * d
    rho100_fs = 0.7
    kR = (rho100 / rho100_fs) ^ (1 / 6)
    If kR > 1# Then
        kR = 1
    End If
   'Limit rho for Vc calculation
    rho100_1 = rho100
    If rho100_1 > 2.5 Then
        rho100_1 = 2.5
    End If
    vcc = kb * kR * kC * kZ * Coeff * (fc) ^ (1 / 3) * (rho100_1) ^ (1 / 3)
    Vc = vcc * bo * d   ' Apply correction factor of 0.7
'Write output
Cells(i, "CF").Value = rho100 / rho100_fs  '
Cells(i, "CH").Value = Vexp / (Vc / 1000) ' Convert Vc to kN
'*** Proposed Standard Method for RC slabs in Chapter 7
    r = Application.WorksheetFunction.Min(0.5 * (ls1 - c1), 0.5 * (ls2 - c2)) ' the
        radius of the slab for Vflex calculation
    alpha_o = (2 / r * (c1 + c2) + 6.28)
    rho100_2 = rho100
    If rho100_2 > 2.5 Then
        rho100_2 = 2.5
    End If
    fcc2 = fc
    Vc_teng = kZ * kC * Coeff * (fcc2) ^ (1 / 3) * bo * d
    rho100_fs = (Vc_teng / (0.95 * alpha_o * fy * d ^ 2) * 100) ^ (3 / 2) 'times 100
        to Vc_basic to make rho in both sides in % unit
    'rho100_fs = (Vc_teng / (alpha_o * m / rho) * 100) ^ (3 / 2) 'times 100 to
        Vc_basic to make rho in both sides in % unit
    kR = (rho100 / rho100_fs) ^ (1 / 6)
    If kR > 1# Then
        kR = 1
    End If
    vcc = kR * kC * kZ * Coeff * (fc) ^ (1 / 3) * (rho100_2) ^ (1 / 3)
    Vc = vcc * bo * d    'Apply correction factor of 0.7
'Write output for Vc
Cells(i, "CG").Value = rho100 / rho100_fs 'Apply correction factor of 0.8
Cells(i, "CI").Value = Vexp / (Vc / 1000) ' Covert Vc to kN
Cells(i, "Cu").Value = Vexp / (kC * kZ * Coeff * (fc) ^ (1 / 3) * bo * d / 1000)
'****** Standard SFRC method for SFRC slabs Eq. (8.1)
    alpha = 30 * (3.1416 / 180)
    ns = 0.41
    bs = 0.2
    If fc > 60 Then
        bs = 0.34
    End If
    z_c = bs * d
    vff = 0.5 * ns * (0.45 * fr1 + 0.37 * fr4)
    Af = (3.1416) * (h - (z_c)) ^ 2 * (Cos(alpha) / Sin(alpha)) ^ 2
    VRf = vff * Af
    Vu = Vc + VRf
'Output for Vu standard FRC method Eq. (8.1)
    Cells(i, "DK").Value = Vc / 1000
    Cells(i, "DL").Value = VRf / 1000
    Cells(i, "DM").Value = Vu / 1000
    Cells(i, "DN").Value = Vexp / (Vu / 1000)
'******* Proposed standard general method in EQ. (8.30)
    nb = Switch(FType = 0, 0, FType = "RO", 0.25, FType = "ST", 0.25, FType = "JA",
        0.5, FType = "PA", 0.5, FType = "CO", 0.5, FType = "CR", 0.5, FType = "SH",
        1#, FType = "DH", 2.25)
    no = 0.41 'orientation factor
```

```
    nl = 0.5 'length factor
    tau_basic = 5.5   'basic bond strength
    vff = no * nl * nb * tau_basic * FRatio * (vf / 100)
    'VRf = vff * bo * d
    If vf = 0 Then
        VRf = 0
    End If
'*** Yield line parameter
    r = Application.WorksheetFunction.Min(0.5 * (ls1 - c1), 0.5 * (ls2 - c2)) ' the
        radius of the slab for Vflex calculation
    alpha_o = (2 / r * (c1 + c2) + 6.28)
   '*** ACI 544 method for m
    Fbe = Switch(FType = 0, 0, FType = "RO", 1, FType = "ST", 1, FType = "JA", 1,
        FType = "PA", 1, FType = "CO", 1, FType = "CR", 1, FType = "SH", 1.2, FType
        = "DH", 2.25)
    sigma_t = 0.008 * (FRatio) * vf * Fbe
    n_E = Es / Ec
    e = d * (((n_E * rho) ^ 2 + 2 * n_E * rho) ^ 0.5 - n_E * rho) '2 / 3 * d 'z_c
    a = 0.59 * d * (rho * fy / fc)
    m_f = sigma_t * (h - e) * (1 / 2) * (h + e - a)
    m_c = rho * fy * d ^ 2 * (1 - 0.59 * (rho * fy / fc))
    m = m_c + m_f
    If vf = 0 Then
        m = rho * fy * d ^ 2 * (1 - 0.59 * (rho * fy / fc))
    End If
    rho100_2 = rho100
    If rho100_2 > 2.5 Then
        rho100_2 = 2.5
    End If
    fcc2 = fc
    Vc_teng = kZ * kC * (Coeff * (fcc2) ^ (1 / 3) + vff / (rho100) ^ (1 / 3)) * bo *
        d
    'rho100_fs = (Vc_teng / (0.95 * alpha_o * fy * d ^ 2) * 100) ^ (3 / 2) 'times
        100 to Vc_basic to make rho in both sides in % unit
    rho100_fs = (Vc_teng / (alpha_o * m / rho) * 100) ^ (3 / 2) 'times 100 to
        Vc_basic to make rho in both sides in % unit
    kRc = (rho100 / rho100_fs) ^ (1 / 6)
    If kRc > 1# Then
        kRc = 1
    End If
    kRf = (rho100 / rho100_fs) ^ (1 / 2)
    If kRf > 1# Then
        kRf = 1
    End If
    Vc = kC * kZ * kRc * Coeff * (fc * rho100) ^ (1 / 3) * bo * d
    VRf = kC * kZ * (kRf * vff) * bo * d
   vuf = kC * kZ * (kRc * Coeff * (fc) ^ (1 / 3) * (rho100_2) ^ (1 / 3) + kRf * vff)
   Vu = vuf * bo * d
'Output 2 for Vu general method SFRC
    Cells(i, "DP").Value = rho100 / rho100_fs
    Cells(i, "DR").Value = Vexp / (Vu / 1000)

'**** simplified general method Eq. (8.30) with the limiting ratio, rhofs = 0.7%
    rho100_fs = 0.7
    kRc = (rho100 / rho100_fs) ^ (1 / 6)
    If kRc > 1# Then
        kRc = 1
    End If
    kRf = (rho100 / rho100_fs) ^ (1 / 2)
    If kRf > 1# Then
        kRf = 1
    End If
    Vc = kC * kZ * kRc * Coeff * (fc * rho100) ^ (1 / 3) * bo * d
    VRf = kC * kZ * (kRf * vff) * bo * d
   vuf = kC * kZ * (kRc * Coeff * (fc) ^ (1 / 3) * (rho100_2) ^ (1 / 3) + kRf * vff)
   Vu = vuf * bo * d
'output
    Cells(i, "DO").Value = rho100 / rho100_fs
    Cells(i, "DQ").Value = Vexp / (Vu / 1000)
Next i
'MsgBox "Proposed Method Done!"
End Sub
```

D.2 ACI 318-14

```
Sub ACI()
For i = 6 To Cells(3, "A").Value + 5
'*** read input
    d = Cells(i, "O").Value  ' effective depth
    c1 = Cells(i, "k").Value ' longer length of column side
    c2 = Cells(i, "l").Value ' shorter length of column side
    fc = Cells(i, "m").Value ' compressive strength of concrete
    Col = Cells(i, "j").Value ' Column shape
    Vexp = Cells(i, "be").Value 'Observed failure load
'**** calculation
    If fc > 70 Then  'to limit concrete strength for calculating vc by code
        fc_aci = 70
    Else
        fc_aci = fc
    End If
        alpha = 40 ' for interior slab
        b1 = c1 + d
        b2 = c2 + d
        bo = 2 * (b1 + b2)
        beta = Application.WorksheetFunction.Max(c2 / c1, c1 / c2)
    If Col = "C" Then ' ACI 318-14, R22.6.4.1.2
        c1 = 0.5 * c1 * (3.1416) ^ 0.5 ' convert to equivalent square column
        bo = 4 * (c1 + d)
        beta = 1
    End If
    ' calculate the 3 equations of punching shear strength, choose the minimum of
            the 3.
    vc1 = (1 + 2 / beta) * fc_aci ^ 0.5 / 6
    vc2 = (2 + alpha * d / bo) * fc_aci ^ 0.5 / 12
    vc3 = fc_aci ^ 0.5 / 3
    Vc = Application.WorksheetFunction.Min(vc1, vc2, vc3)
    Vc = Vc * bo * d / 1000
'*** Output
Cells(i, "BO").Value = Vexp / Vc
Next i
MsgBox "ACI Done!"
End Sub
```

D.3 Eurocode 2

```
Sub Eurocode2()

For i = 6 To Cells(3, "A").Value + 5

'*** read input

    'l1 = Cells(i, "G").Value ' length of slab in x direction
    'l2 = Cells(i, "h").Value ' length of slab in y direction
    d = Cells(i, "O").Value  ' effective depth
    c1 = Cells(i, "k").Value ' longer length of column side
    c2 = Cells(i, "l").Value ' shorter length of column side
    fc = Cells(i, "m").Value ' compressive strength of concrete
    Col = Cells(i, "j").Value ' Column shape
    rho = Cells(i, "ad").Value ' average flexural reinforcement ratio
    'dg = Cells(i, "n").Value  ' max aggregate size
    'fy = Cells(i, "aj").Value ' yield strength of reinforcement
    Vexp = Cells(i, "be").Value 'Observed failure load

'**** calculation

    If fc > 90 Then
        fc = 90
    End If

    k = 1 + (200 / d) ^ 0.5 'size effect
    If k > 2 Then
        k = 2
```

```
    End If

    If rho > 2 Then
        rho = 2
    End If

    u = 2 * (c1 + c2) + 3.14 * (4 * d) ' critical perimeter at 2d away from column
    If Col = "C" Then
        u = 3.14 * (c1 + 4 * d)
    End If


    vmin = 0.035 * k ^ 1.5 * fc ^ 0.5
    vRdc = Application.WorksheetFunction.Max(0.18 * k * (rho * fc) ^ (1 / 3), vmin)
    Vc = vRdc * u * d / 1000

'*** Output
Cells(i, "BS").Value = Vexp / Vc

Next i
MsgBox "EC2 Done!"
End Sub
```

D.4 Yield line theory

```
Sub Vflex_YLT()

For i = 6 To Cells(3, "A").Value + 5

'*** read input
    ls1 = Cells(i, "G").Value ' distance between supports in x direction
    ls2 = Cells(i, "h").Value ' distance between supports in y direction
    l1 = Cells(i, "G").Value ' length of slab in x direction
    l2 = Cells(i, "h").Value ' length of slab in y direction
    h = Cells(i, "i").Value ' slab thickness
    d = Cells(i, "O").Value  ' effective depth
    c1 = Cells(i, "k").Value ' longer length of column side
    c2 = Cells(i, "l").Value ' shorter length of column side
    fc = Cells(i, "m").Value ' compressive strength of concrete
    Es = Cells(i, "ai").Value ' compressive strength of concrete
    fy = Cells(i, "aj").Value ' compressive strength of concrete
    Col = Cells(i, "j").Value ' Column shape
    rho = Cells(i, "ad").Value ' average flexural reinforcement ratio
    dg = Cells(i, "n").Value  ' max aggregate size
    vf = Cells(i, "ap").Value ' fiber volume fraction
    fr1 = Cells(i, "as").Value ' residual strength fr1
    fr2 = Cells(i, "at").Value ' residual strength fr1
    fr3 = Cells(i, "au").Value ' residual strength fr1
    fr4 = Cells(i, "av").Value ' residual strength fr1
    Vexp = Cells(i, "be").Value 'Observed failure load

'**** conversion and assumption
    Es = Es * 1000 'convert to MPa
    If Es = 0 Then
        Es = 200 * 1000
    End If

    rho = (rho / 100) 'convert to decimal

'**** calculation

' TR34 method for m
    sig_r1 = 0.45 * fr1
    sig_r4 = 0.29 * fr4
    m = (h ^ 2) * (0.29 * sig_r4 + 0.16 * sig_r1) + rho * fy * (d ^ 2) * (1 - 0.048
* h / d)

If vf = 0 Then
    m = rho * fy * d ^ 2 * (1 - 0.59 * (rho * fy / fc))
End If
```

```
'Yeild line

    r = Application.WorksheetFunction.Min(0.5 * (ls1 - c1), 0.5 * (ls2 - c2)) ' the
radius of the slab for Vflex calculation
    alpha_o = (2 / r * (c1 + c2) + 6.28)

    Vflex = m * alpha_o / 1000 'convert to kN

'*** Output

Cells(i, "ck").Value = Vflex
Cells(i, "cl").Value = Vexp / Vflex

Next i
MsgBox "Vflex Done!"
End Sub
```

D.5 TR 34

```
Sub TR34()
For i = 6 To Cells(3, "A").Value + 5
'*** read input

    'l1 = Cells(i, "G").Value ' length of slab in x direction
    'l2 = Cells(i, "h").Value ' length of slab in y direction
    d = Cells(i, "O").Value  ' effective depth
    c1 = Cells(i, "k").Value ' longer length of column side
    c2 = Cells(i, "l").Value ' shorter length of column side
    fc = Cells(i, "m").Value ' compressive strength of concrete
    Col = Cells(i, "j").Value ' Column shape
    rho = Cells(i, "ad").Value ' average flexural reinforcement ratio
    'dg = Cells(i, "n").Value  ' max aggregate size
    fr1 = Cells(i, "as").Value ' residual strength fr1
    fr2 = Cells(i, "at").Value ' residual strength fr1
    fr3 = Cells(i, "au").Value ' residual strength fr1
    fr4 = Cells(i, "av").Value ' residual strength fr1
    Vexp = Cells(i, "be").Value 'Observed failure load

'**** calculation
    'If fc > 90 Then
        'fc = 90
    'End If
    k = 1 + (200 / d) ^ 0.5 'size effect
    If k > 2 Then
        k = 2
    End If

    If rho > 2 Then
        rho = 2
    End If

    u = 2 * (c1 + c2) + 3.14 * (4 * d) ' critical perimeter at 2d away from column
    If Col = "C" Then
        u = 3.14 * (c1 + 4 * d)
    End If
    vmin = 0.035 * k ^ 1.5 * fc ^ 0.5
    vRdc = Application.WorksheetFunction.Max(0.18 * k * (rho * fc) ^ (1 / 3), vmin)
    Vc = vRdc * u * d / 1000
    '*** Vf shear contribution from SFRC
    fr = (fr1 + fr2 + fr3 + fr4) / 4 'average residual strength
    vf = 0.5 * 0.12 * fr
    VRf = vf * u * d / 1000

    Vu = Vc + VRf
'*** Output
Cells(i, "DD").Value = Vexp / Vu
Next i
MsgBox "TR34 Done!"
End Sub
```

D.6 MC2010

```
Sub MC2010()

For i = 6 To Cells(3, "A").Value + 5

'*** read input

    l1 = Cells(i, "G").Value ' length of slab in x direction
    l2 = Cells(i, "h").Value ' length of slab in y direction
    d = Cells(i, "O").Value  ' effective depth
    c1 = Cells(i, "k").Value ' longer length of column side
    c2 = Cells(i, "l").Value ' shorter length of column side
    fc = Cells(i, "m").Value ' compressive strength of concrete
    Es = Cells(i, "ai").Value ' compressive strength of concrete
    fy = Cells(i, "aj").Value ' compressive strength of concrete
    Col = Cells(i, "j").Value ' Column shape
    rho = Cells(i, "ad").Value ' average flexural reinforcement ratio
    dg = Cells(i, "n").Value  ' max aggregate size
    fr1 = Cells(i, "as").Value ' residual strength fr1
    fr2 = Cells(i, "at").Value ' residual strength fr1
    fr3 = Cells(i, "au").Value ' residual strength fr1
    fr4 = Cells(i, "av").Value ' residual strength fr1
    Vexp = Cells(i, "be").Value 'Observed failure load

'**** conversion and assumption
    Es = Es * 1000 'convert to MPa
    If Es = 0 Then
        Es = 200 * 1000
    End If

'**** calculation
'*** Vc

      r = 0.5 * l1
      Phi = 1.5 * (r / d) * fy / (Es)

      If fc > 70 Then
          dg = 0
      End If
      k_dg = 32 / (16 + dg)
      If k_dg < 0.75 Then
           k_dg = 0.75
      End If
      If dg < 16 Then
            k_dg = 1
      End If

      k_phi = 1 / (1.5 + 0.9 * k_dg * Phi * d)
      If k_phi > 0.6 Then
           k_phi = 0.6
      End If

       bo = 2 * (c1 + c2) + 3.1416 * d

       If Col = "C" Then
            bo = (c1 + d) * 3.1416
       End If

       fc_mod = fc
       If fc >= 64 Then 'maximum allowable sqrt(fc) = 8MPa
            fc = 64
       End If
    Vc = k_phi * (fc) ^ 0.5 * bo * d / 1000
    Vc_mod = k_phi * (fc_mod) ^ 0.5 * bo * d / 1000

'*** Vf
    vf = 0.45 * fr1 - 0.6 * (0.45 * fr1 - 0.5 * fr3 + 0.2 * fr1) ' linear model
    'vf = fr3 / 3 ' regid model
    If vf < 0 Then
        vf = 0
```

```
    End If
    VRf = vf * bo * d / 1000
    Vu = Vc + VRf
    Vu_mod = Vc_mod + 0.25 * VRf
'*** Output

Cells(i, "DE").Value = Vc
Cells(i, "DF").Value = VRf
Cells(i, "DG").Value = Vu
Cells(i, "DH").Value = Vexp / Vu
Cells(i, "Di").Value = Vexp / Vu_mod

Next i
MsgBox "MC2010 Done!"
End Sub
```

D.7 CSCT and CSCT+VEM

```
Sub CSCTVEM()

For i = 6 To Cells(3, "A").Value + 5

'*** read input *****

    ls1 = Cells(i, "G").Value ' distance between supports in x direction
    ls2 = Cells(i, "h").Value ' distance between supports in y direction
    l1 = Cells(i, "AK").Value  ' slab length in x direction
    l2 = Cells(i, "AL").Value  ' slab length in x direction
    h = Cells(i, "i").Value  ' thickness
    d = Cells(i, "O").Value  ' effective depth
    c1 = Cells(i, "k").Value ' longer length of column side
    c2 = Cells(i, "l").Value ' shorter length of column side
    fc = Cells(i, "m").Value ' compressive strength of concrete
    rho = Cells(i, "ad").Value ' average flexural reinforcement ratio
    dg = Cells(i, "n").Value  ' max aggregate size
    fy = Cells(i, "aj").Value ' yield strength of reinforcement
    rq = Cells(i, "bc").Value ' rotational length of a slab
    FType = Cells(i, "AM").Value ' fibre type
    Lf = Cells(i, "AN").Value ' fibre lenght
    FRatio = Cells(i, "Ao").Value ' fibre type aspect ratio
    vf = Cells(i, "AP").Value ' fibre volume faction
    Vexp = Cells(i, "be").Value 'Observed failure load

'Convert rho

    rho100 = rho    '100As/bd
    rho = rho / 100 'As/bd

'*** Assumption for unknown parameter
    Ec = 4.7 * (fc) ^ 0.5 ' in GPa
    Es = 200 'in GPa,
    If fy = 0 Then
        fy = 500 'MPa
    End If

    If dg = 0 And d < 50 Then ' for thin slab with d<50 mm that do have reported dg
        dg = 10
    End If

    If dg = 0 And d >= 50 Then ' for slab with d>= 50mm  that do have reported dg
        dg = 20
    End If

'**** Solution of Vcsct using Eq.5+Eq.8 (in Muttoni 2008) or Eq. A2+Eq.A3 (in
Guandalini,Burdet,Muttoni 2009) ************************

    b0 = 2 * (c1 + c2) + 3.14 * d ' calcualted a 0.5d away from column faces with
round corners
    If Col = "C" Then
        b0 = 3.14 * (c1 + d)
    End If
```

```
'*** YL load for a slab supported on 8 points around the slab edges according to
Guandalini et al paper
   ' ACI 544 method for m
    Fbe = Switch(FType = 0, 0, FType = "RO", 1, FType = "ST", 1, FType = "JA", 1,
FType = "PA", 1, FType = "CO", 1, FType = "CR", 1, FType = "SH", 1.2, FType = "DH",
1.2)

    sigma_t = 0.008 * (FRatio) * vf * Fbe
    n_E = Ec / Es
    e = d * (((n_E * rho) ^ 2 + 2 * n_E * rho) ^ 0.5 - n_E * rho) '2 / 3 * d 'z_c
    a = 0.59 * d * (rho * fy / fc)
     m_f = sigma_t * (h - e) * (1 / 2) * (h + e - a)
     m_c = rho * fy * d ^ 2 * (1 - 0.59 * (rho * fy / fc))
     mR = m_c + m_f
'***
     m_muttoni = 1# * rho * fy * d ^ 2 * (1 - 0.5 * rho * fy / fc)        ' ultimate
flexural strength per unit width
        cosA = Cos(3.1416 / 8)
        sina = Sin(3.1416 / 8)
        tana = sina / cosA
        B = l1 ' assign the notation B, length of slab, to be used in Vflex
        If l1 > l2 Then
            B = l2
        End If
        c = c1 ' assign the notataion c, column side, to be used in Vflex
    'Vflex_8ptGuan = 4 * m_muttoni * (B ^ 2 - B * c - 0.25 * c ^ 2) / ((B - c) * (rq
* (cosa + sina) - c))  'Vflex2 , use Equation by Guandalini in ref 3. Cracks along
column faces
'*** Vflex
    rs = 0.5 * ls1
    rq = 0.5 * l1
    c = c1
    If vf = 0 Then
       mR = m_muttoni
    End If
  Vflex = 2 * 3.14 * rs / (rq - c) * mR

'*** Iteration procedure, Using Newton-Raphson Method
    j = 0.005 ' set intial value for iteration
    delphii = 1000000 'initial value
    rs = 0.5 * Application.WorksheetFunction.Min(l1, l2) ' the radius of the slab as
defined by the muttoni, Guandalini et al.

    Do While delphii > 0.000000001

    ' set j as the rotational angle Phi
    ' f1 and f2 are the normalized load (V/bodfc^0.5) Equation A(2), A(3) in
Guandalini et al.

        f1 = (3 / 4) / (1 + 15 * j * d / (16 + dg))
        f2 = Vflex / (b0 * d * fc ^ 0.5) * (j * d * Es * 1000 / (1.5 * rs * fy)) ^
(2 / 3)

        df1 = -0.75 * (15 * d / (16 + dg)) * (1 + 15 * j * d / (16 + dg)) ^ -2 '
first derivative of f1
        df2 = 2 / 3 * j ^ (-1 / 3) * Vflex / (b0 * d * fc ^ 0.5) * (d * Es * 1000 /
(1.5 * rs * fy)) ^ (2 / 3)  ' first derivative of f2

        F = f1 - f2
        dF = df1 - df2
        phii = j
        j = j - F / dF

        delphii = Abs(j - phii) / phii
    Loop

    Vc = f1 * (b0 * d * fc ^ 0.5) ' from iteration

'**** VRf
    kb = Switch(FType = 0, 0, FType = "RO", 0.4, FType = "ST", 0.4, FType = "JA",
0.6, FType = "PA", 0.6, FType = "CO", 0.6, FType = "CR", 0.6, FType = "SH", 0.8,
FType = "DH", 0.8)
```

```
    tau_b = kb * (fc) ^ 0.5
    alpha_i = 0
    If FRatio > 0 Then
        alpha_i = 1 / (3.5 * FRatio)
    End If

    w = phii * d / 6
    Kf = 0
    If vf > 0 Then
        Kf = (1 / 3.1416) * Atn(w / (alpha_i * Lf)) * (1 - 2 * w / Lf) ^ 2
        If Kf > (0.5 - 0.645 / (FRatio) ^ 0.45) Then
            Kf = 0.5 - 0.645 / (FRatio) ^ 0.45
        End If
    End If
   f_tf = Kf * FRatio * (vf / 100) * tau_b 'tensile strength
   A_p = (3.14 / 4) * ((c + 2 * d) ^ (2) - c ^ (2))
   VRf = f_tf * A_p

  Vu = Vc + VRF

'****Output
Cells(i, "DV").Value = Vexp / (Vu / 1000)     'convert Vc into kN

 Next i
 MsgBox "CSCT+VEM Done!"
End Sub
```

D.8 Peiris-Ghali

```
Sub PeirisGhali()

For i = 6 To Cells(3, "A").Value + 5

'*** read input

    'l1 = Cells(i, "G").Value ' length of slab in x direction
    'l2 = Cells(i, "h").Value ' length of slab in y direction
    d = Cells(i, "O").Value  ' effective depth
    c1 = Cells(i, "k").Value ' longer length of column side
    c2 = Cells(i, "l").Value ' shorter length of column side
    fc = Cells(i, "m").Value ' compressive strength of concrete
    Col = Cells(i, "j").Value ' Column shape
    rho = Cells(i, "ad").Value ' average flexural reinforcement ratio
    'dg = Cells(i, "n").Value  ' max aggregate size
    fy = Cells(i, "aj").Value ' yield strength of reinforcement
    Vexp = Cells(i, "be").Value 'Observed failure load

'*** Assumption for unknown parameter
    Es = 200 'in GPa,
    If fy = 0 Then
        fy = 500 'MPa
    End If

'**** calculation
' calculate Vc aci first

    If fc > 70 Then  'to limit concrete strength for calculating vc by code
        fc_aci = 70
    Else
        fc_aci = fc
    End If

        alpha = 40 ' for interior slab
        b1 = c1 + d
        b2 = c2 + d
        bo = 2 * (b1 + b2)
        beta = Application.WorksheetFunction.Max(c2 / c1, c1 / c2)

    If Col = "C" Then ' ACI 318-14, R22.6.4.1.2
        c1 = 0.5 * c1 * (3.1416) ^ 0.5 ' convert to equivalent square column
        bo = 4 * (c1 + d)
```

```
        beta = 1
    End If
    ' calculate the 3 equations of punching shear strength, choose the minimum of
the 3.
    vc1 = (1 + 2 / beta) * fc_aci ^ 0.5 / 6
    vc2 = (2 + alpha * d / bo) * fc_aci ^ 0.5 / 12
    vc3 = fc_aci ^ 0.5 / 3
    Vc = Application.WorksheetFunction.Min(vc1, vc2, vc3)
    Vc = Vc * bo * d / 1000

'calculate rho_fs and governing V ( min of Vflex & Vaci)

    a_depth = 1 / 0.85 * (rho / 100 * fy / fc)
    a_bal = 0.85 * (600 / (600 * fy)) * d

    If (1 - 0.5 * (a_depth)) < 0 Then 'take compressive dept to be balance depth,
the limit of tension control
        a_depth = a_bal
    End If
    m = rho / 100 * fy * d ^ 2 * (1 - 0.5 * (a_depth)) ' ultimate flexural strength
    Vflex = 8 * m / 1000
    alpha1 = Vflex * 1000 / (bo * d * fc ^ (1 / 2) * (rho / 100))
    rho_fs = (Vc * 1000 / (bo * d * fc ^ 0.5)) / alpha1 * 100

' Vc is assumed to be Vaci directly for rho > 3%
    If rho < rho_fs And rho < 3 Then
        Vc = Vflex
    End If

'*** Output
Cells(i, "CP").Value = Vexp / Vc

Next i
MsgBox "Peiris & Ghali Done!"
End Sub
```

D.9 Narayanan and Darwish

```
Sub NarayananMethod()

For i = 6 To Cells(3, "A").Value + 5
'*** read input
    ls1 = Cells(i, "G").Value ' distance between supports in x direction
    ls2 = Cells(i, "h").Value ' distance between supports in y direction
    l1 = Cells(i, "AK").Value ' length of slab in x direction
    l2 = Cells(i, "AL").Value ' length of slab in y direction
    h = Cells(i, "i").Value  ' thickness
    d = Cells(i, "O").Value  ' effective depth
    c1 = Cells(i, "k").Value ' longer length of column side
    c2 = Cells(i, "l").Value ' shorter length of column side
    fc = Cells(i, "m").Value ' compressive strength of concrete
    Col = Cells(i, "j").Value ' Column shape
    rho = Cells(i, "ad").Value ' average flexural reinforcement ratio
    dg = Cells(i, "n").Value  ' max aggregate size
    fy = Cells(i, "aj").Value ' yield strength of reinforcement
    SSpan = Cells(i, "BI").Value ' shear span
    fr1 = Cells(i, "as").Value ' residual strength fr1
    fr2 = Cells(i, "at").Value ' residual strength fr1
    fr3 = Cells(i, "au").Value ' residual strength fr1
    fr4 = Cells(i, "av").Value ' residual strength fr1
    FType = Cells(i, "AM").Value ' fibre type
    Lf = Cells(i, "AN").Value ' fibre lenght
    FRatio = Cells(i, "Ao").Value ' fibre type aspect ratio
    vf = Cells(i, "AP").Value ' fibre volume faction
    Vexp = Cells(i, "be").Value 'Observed failure load

'Convert rho

    rho100 = rho    '100As/bd
    rho = rho / 100 'As/bd
```

```
'*** Calculation
    fcube = fc / 0.8 'approximate
    nf = Switch(FType = 0, 0, FType = "RO", 0.5, FType = "ST", 0.5, FType = "JA",
0.75, FType = "PA", 0.75, FType = "CO", 0.75, FType = "CR", 0.75, FType = "SH", 1,
FType = "DH", 1)

    F = FRatio * (vf / 100) * nf
    vff = 0.41 * (4.15) * F
        'f_spt = 0
    'If Vf > 0 Then
        f_spt = fcube / (20 - (F) ^ (0.5)) + 0.7 + (F) ^ 0.5
    'End If
    e = 1.4
    bof = (2 * (c1 + c2) + 3 * (3.1415) * h) * (1 - 0.55 * F)

    Vu = e * (0.24 * f_spt + 16 * rho + vff) * bof * d

'****Output
Cells(i, "DW").Value = Vexp * 1000 / (Vu)
 Next i
 MsgBox "Narayanan and Darwish Method Done!"
End Sub
```

D.10 Shaaban and Gesund

```
Sub ShaabanMethod()

For i = 6 To Cells(3, "A").Value + 5
'*** read input
    ls1 = Cells(i, "G").Value ' distance between supports in x direction
    ls2 = Cells(i, "h").Value ' distance between supports in y direction
    l1 = Cells(i, "AK").Value ' length of slab in x direction
    l2 = Cells(i, "AL").Value ' length of slab in y direction
    h = Cells(i, "i").Value  ' thickness
    d = Cells(i, "O").Value  ' effective depth
    c1 = Cells(i, "k").Value ' longer length of column side
    c2 = Cells(i, "l").Value ' shorter length of column side
    fc = Cells(i, "m").Value ' compressive strength of concrete
    Col = Cells(i, "j").Value ' Column shape
    rho = Cells(i, "ad").Value ' average flexural reinforcement ratio
    dg = Cells(i, "n").Value  ' max aggregate size
    fy = Cells(i, "aj").Value ' yield strength of reinforcement
    SSpan = Cells(i, "BI").Value ' shear span
    fr1 = Cells(i, "as").Value ' residual strength fr1
    fr2 = Cells(i, "at").Value ' residual strength fr1
    fr3 = Cells(i, "au").Value ' residual strength fr1
    fr4 = Cells(i, "av").Value ' residual strength fr1
    FType = Cells(i, "AM").Value ' fibre type
    Lf = Cells(i, "AN").Value ' fibre lenght
    FRatio = Cells(i, "Ao").Value ' fibre type aspect ratio
    vf = Cells(i, "AP").Value ' fibre volume faction
    Vexp = Cells(i, "be").Value 'Observed failure load

'Convert rho

    rho100 = rho    '100As/bd
    rho = rho / 100 'As/bd

'*** Calculation
    Wf = 7859 * (vf / 100) / (2400)
    bo = (2 * (c1 + c2) + 4 * d)
    Vu = (1 / 12) * 0.6 * (0.3 * Wf + 6.8 * fc ^ (0.5)) * bo * d

'****Output
Cells(i, "Dx").Value = Vexp * 1000 / (Vu)
 Next i
 MsgBox "Shaaban and Gesund Done!"
End Sub
```

D.11 Higashiyama et al.

```
 Sub HigashiyamaMethod()

For i = 6 To Cells(3, "A").Value + 5
'*** read input
    ls1 = Cells(i, "G").Value ' distance between supports in x direction
    ls2 = Cells(i, "h").Value ' distance between supports in y direction
    l1 = Cells(i, "AK").Value ' length of slab in x direction
    l2 = Cells(i, "AL").Value ' length of slab in y direction
    h = Cells(i, "i").Value  ' thickness
    d = Cells(i, "O").Value  ' effective depth
    c1 = Cells(i, "k").Value ' longer length of column side
    c2 = Cells(i, "l").Value ' shorter length of column side
    fc = Cells(i, "m").Value ' compressive strength of concrete
    Col = Cells(i, "j").Value ' Column shape
    rho = Cells(i, "ad").Value ' average flexural reinforcement ratio
    dg = Cells(i, "n").Value  ' max aggregate size
    fy = Cells(i, "aj").Value ' yield strength of reinforcement
    SSpan = Cells(i, "BI").Value ' shear span
    fr1 = Cells(i, "as").Value ' residual strength fr1
    fr2 = Cells(i, "at").Value ' residual strength fr1
    fr3 = Cells(i, "au").Value ' residual strength fr1
    fr4 = Cells(i, "av").Value ' residual strength fr1
    FType = Cells(i, "AM").Value ' fibre type
    Lf = Cells(i, "AN").Value ' fibre lenght
    FRatio = Cells(i, "Ao").Value ' fibre type aspect ratio
    vf = Cells(i, "AP").Value ' fibre volume faction
    Vexp = Cells(i, "be").Value 'Observed failure load

'Convert rho

    rho100 = rho    '100As/bd
    rho = rho / 100 'As/bd

'*** Calculation

    u = 2 * (c1 + c2)
    fpc = 0.2 * (fc) ^ 0.5
    If fpc > 1.2 Then
        fpc = 1.2
    End If

    nf = Switch(FType = 0, 0, FType = "RO", 0.5, FType = "ST", 0.5, FType = "JA",
            0.75, FType = "PA", 0.75, FType = "CO", 0.75, FType = "CR", 0.75, FType
            = "SH", 1, FType = "DH", 1)

    F = FRatio * (vf / 100) * nf
    vff = 0.41 * (4.15) * F
    up = (u + (3.1415) * d) * (1 - 0.32 * F)

    Bd = (1000 / d) ^ 0.25
    If Bd > 1.5 Then
        Bd = 1.5
    End If

    Bp = (rho100) ^ (1 / 3)
    If Bp > 1.5 Then
        Bp = 1.5
    End If

    Br = 1 + 1 / (1 + 0.25 * u / d)

    Vu = Bd * Bp * Br * (fpc + vff) * up * d

'****Output
Cells(i, "DY").Value = Vexp * 1000 / (Vu)

 Next i
 MsgBox "Higashiyama et al Method Done!"
End Sub
```

D.12 Calculation of the area under a load-CMOD curve (Energy absorption)

```
Sub CalArea()
'
' CalArea Macro
'
' Read number of rows

RowNum = Cells(1, "B")

'Set index
Area_sum = 0
n = 1000 ' number of division
For i = 4 To 3 + RowNum

y_1 = Cells(i, "A")
y_0 = Cells(i - 1, "A")
x_1 = Cells(i, "B")
x_0 = Cells(i - 1, "B")

    If i = 4 Then
        y_0 = 0
        x_0 = 0
    End If

' Set X&Y interval

delx = (x_1 - x_0) / n
dely = (y_1 - y_0) / n

Area_i = (n * y_0 + n ^ (2) / 2 * dely) * delx
Area_sum = Area_sum + Area_i

Next

Cells(2, "E").Value = Area_sum

MsgBox "Calculation complete!", vbOKOnly, "Slabs Analysis"
'
End Sub
```

Appendix E

SLAB DATABASE

E.1 Property and analysis results of 367 RC slab specimens

Table E.1 (Columns (2) to (15)) shows the original slab ID, material properties, observed failure mode and failure load V_{exp} of 367 slab data including the current 12 high strength concrete slabs. Columns (16) and (17) of Table E.1 show the failure mode predictions by the proposed simplified and standard methods, respectively. Columns (18) to (23) show the ratio of the failure load to the calculated punching shear strength V_{exp}/V_{calc} of each design method such as ACI 318-14, Eurocode 2, Critical Shear Crack Theory by Muttoni (2008), Peiris and Ghali (2011) and the proposed simplified and standard methods, respectively.

All the slab data in Table E.1 was constructed without shear reinforcement and tested under punching shear loads to failures. They were selected to make sure that they satisfy all the relevant ACI design requirements. Slabs having unusual geometries, loading arrangements, or boundary conditions were excluded as their punching strengths would be quite different from those of normal slabs in typical construction and they deserve special treatment of their own. The ranges of the parameters of the 367 slab data can be summarized as follows:

- The slab lengths L_1 and L_2 range from 483 to 6000 mm (1.60 to 19.70 ft).
- The column dimensions (c_1, c_2) range from 50 to 1000 mm (2.0 to 39.4 in.), which include column shapes such as square (denoted as "S"), rectangular ("R") and circular s ("C").
- The average effective depth d ranges from 33 to 669 mm (1.3 to 26.4 in.).
- The average reinforcement ratio ρ ranges from 0.22 to 7.30%.
- The (cylinder) concrete strength f'_c ranges from 9.5 to 119 MPa (1378 to 17260 psi).
- The yield strength of the reinforcement f_y ranges from 255 to 749 MPa (37 to 110 ksi).

Table E.1 - Property and analysis results of 367 RC slab specimens

No.	Slab ID	L_1 (mm)	L_2 (mm)	c_1 (mm)	c_2 (mm)	Column Shape	d (mm)	f'_c (MPa)	f_y (MPa)	ρ (%)	V_{exp} (kN)	Failure mode	ρ/ρ_{fs} Simplified Method	ρ/ρ_{fs} Standard Method	V_{exp}/V_{calc}					
															ACI 318-14	Eurocode 2	CSCT	Peiris-Ghali	Proposed Simple Method	Proposed Standard Method
(1)	(2)	(3)	(4)	(5)	(6)	(7)	(8)	(9)	(10)	(11)	(12)	(13)	(14)	(15)	(16)	(17)	(18)	(19)	(20)	(21)
Graf, O (1938)																				
1	1362	1700	1700	300	300	S	271	12.3	270	1.04	1165	P	1.49	2.55	1.61	1.19	1.13	1.61	1.34	1.34
2	1375	1700	1700	300	300	S	473	13.1	270	0.60	1659	P	0.86	2.94	0.94	0.83	0.74	0.94	1.23	1.20
Forssell, C. and E. Holmberg (1946)																				
3	1	1200	1200	140	140	C	101	115	350	0.70	183.0	P	1.00	1.83	1.78	1.47	1.22	1.78	1.56	1.56
4	2	1200	1200	140	140	C	111	115	350	0.64	177.0	P	0.91	1.81	1.50	1.24	1.05	1.50	1.38	1.36
5	3	1200	1200	140	140	C	106	115	350	0.67	172.0	P	0.95	1.82	1.56	1.29	1.08	1.56	1.40	1.39
6	4	1200	1200	140	140	C	110	115	350	0.64	177.0	P	0.92	1.81	1.52	1.26	1.06	1.52	1.40	1.38
7	5	1200	1200	140	140	C	111	115	350	0.64	198.0	P	0.91	1.81	1.68	1.39	1.17	1.68	1.55	1.52
8	6	1200	1200	140	140	C	107	115	350	0.66	183.0	P	0.94	1.82	1.63	1.35	1.13	1.63	1.48	1.47
9	7	1200	1200	140	140	C	106	115	350	0.67	187.0	P	0.95	1.82	1.69	1.40	1.17	1.69	1.53	1.51
Elstner, R. C., and Hognestad, E. (1956)																				
10	A-1a	1829	1829	254	254	S	118	14.1	332	1.15	302.5	P	1.64	1.73	1.38	1.13	1.04	1.38	1.14	1.14
11	A-1b	1829	1829	254	254	S	118	25.2	332	1.15	364.7	P	1.64	1.29	1.25	1.13	1.02	1.25	1.13	1.13
12	A-1c	1829	1829	254	254	S	118	29.0	332	1.15	355.8	P	1.64	1.20	1.13	1.05	0.95	1.13	1.05	1.05
13	A-1d	1829	1829	254	254	S	118	36.8	332	1.15	351.4	P	1.64	1.07	0.99	0.96	0.87	0.99	0.96	0.96
14	A-1e	1829	1829	254	254	S	118	20.3	332	1.15	355.8	P	1.64	1.44	1.36	1.18	1.08	1.36	1.19	1.19
15	A-2a	1829	1829	254	254	S	114	13.7	321	2.47	333.6	P	3.53	3.48	1.61	1.10	1.02	1.61	1.02	1.02
16	A-2b	1829	1829	254	254	S	114	19.5	321	2.47	400.3	P	3.53	2.91	1.62	1.17	1.04	1.62	1.09	1.09
17	A-2c	1829	1829	254	254	S	114	37.4	321	2.47	467.0	P	3.53	2.10	1.36	1.10	0.93	1.36	1.02	1.02
18	A-7b	1829	1829	254	254	S	114	27.9	321	2.47	5115	P	3.53	2.44	1.73	1.33	1.15	1.73	1.23	1.23
19	A-3a	1829	1829	254	254	S	114	12.8	321	3.70	355.8	P	5.29	5.39	1.77	1.20	1.08	1.77	1.11	1.11
20	A-3b	1829	1829	254	254	S	114	22.6	321	3.70	444.8	P	5.29	4.05	1.67	1.24	1.01	1.67	1.15	1.15
21	A-3c	1829	1829	254	254	S	114	26.5	321	3.70	533.8	P	5.29	3.74	1.85	1.41	1.12	1.85	1.31	1.31
22	A-3d	1829	1829	254	254	S	114	34.5	321	3.70	547.1	P	5.29	3.28	1.66	1.32	1.03	1.66	1.23	1.23
23	A-4	1829	1829	356	356	S	118	26.1	332	1.15	400.3	P	1.64	1.00	1.06	1.05	0.95	1.06	0.96	0.96
24	A-5	1829	1829	356	356	S	114	27.8	321	2.47	533.8	P	3.53	1.92	1.41	1.19	1.00	1.41	1.01	1.01
25	A-6	1829	1829	356	356	S	114	25.0	321	3.70	498.2	P	5.29	3.03	1.39	1.15	0.89	1.39	0.97	0.97

No.	Slab ID	L_1 (mm)	L_2 (mm)	c_1 (mm)	c_2 (mm)	Column Shape	d (mm)	f'_c (MPa)	f_y (MPa)	ρ (%)	V_{exp} (kN)	Failure mode	ρ/ρ_{fs} Simplified Method	ρ/ρ_{fs} Standard Method	V_{exp}/V_{calc}					
															ACI 318-14	Eurocode 2	CSCT	Peiris-Ghali	Proposed Simple Method	Proposed Standard Method
26	A-9	1829	1829	254	254	S	114	29.9	321	3.56	444.8	P	5.09	3.39	1.45	1.13	0.89	1.45	1.05	1.05
27	A-10	1829	1829	356	356	S	114	29.7	321	3.58	489.3	P	5.11	2.69	1.25	1.07	0.82	1.25	0.90	0.90
28	A-13	1829	1829	356	356	S	121	26.2	294	0.55	235.7	F	0.79	0.41	0.60	0.76	0.75	1.30	0.73	0.81
29	B-1	1829	1829	254	254	S	114	14.2	324	0.50	178.4	F	0.71	0.70	0.84	0.92	0.81	1.13	0.97	0.98
30	B-2	1829	1829	254	254	S	114	47.6	321	0.50	200.2	F	0.71	0.38	0.52	0.69	0.64	1.22	0.73	0.81
31	B-4	1829	1829	254	254	S	114	47.7	303	0.99	333.6	F	1.41	0.68	0.86	0.92	0.79	1.10	0.91	0.97
32	B-9	1829	1829	254	254	S	114	43.9	341	2.00	504.8	P	2.86	1.72	1.36	1.13	0.95	1.36	1.12	1.12
33	B-11	1829	1829	254	254	S	114	13.5	409	3.00	329.2	P	4.29	6.11	1.60	1.09	0.96	1.60	1.01	1.01
34	B-14	1829	1829	254	254	S	114	50.5	325	3.00	578.2	P	4.29	2.24	1.45	1.23	0.93	1.45	1.14	1.14
Rosenthal, I. (1959)																				
35	II/1	1143	1143	229	229	C	80	13.7	456	1.34	181.0	P	1.91	2.94	1.62	1.38	1.15	1.62	1.16	1.16
36	II/2	1702	1702	229	229	C	80	12.7	372	1.32	152.0	P	1.89	1.87	1.41	1.20	1.11	1.41	1.00	1.00
37	II/3	1702	1702	432	229	R	80	14.2	490	1.32	245.0	P	1.89	2.53	1.50	1.38	1.43	1.50	1.38	1.38
38	II/4	1143	1143	229	229	C	80	22.3	490	0.98	245.0	P	1.40	1.88	1.72	1.77	1.42	1.72	1.48	1.48
Kinnunen, S. and H. Nylander (1960)																				
39	IA15a-5	1840	1840	150	150	C	117	27.9	441	0.80	255.0	P	1.14	1.90	1.24	1.11	0.93	1.24	1.21	1.21
40	IA15a-6	1840	1840	150	150	C	118	25.8	454	0.80	275.0	P	1.14	2.07	1.37	1.21	1.01	1.37	1.32	1.32
41	IA15c-11	1840	1840	150	150	C	121	31.4	436	1.80	334.0	P	2.57	4.06	1.45	1.00	0.88	1.45	1.11	1.11
42	IA15c-12	1840	1840	150	150	C	122	28.8	439	1.70	332.0	P	2.43	4.08	1.49	1.03	0.90	1.49	1.14	1.14
43	IA30a-24	1840	1840	300	300	C	128	25.9	456	1.00	430.0	P	1.43	1.76	1.26	1.24	0.96	1.26	1.11	1.11
44	IA30a-25	1840	1840	300	300	C	124	24.6	451	1.10	408.0	P	1.57	1.89	1.28	1.22	0.94	1.28	1.08	1.08
45	IA30c-30	1840	1840	300	300	C	120	29.5	436	2.10	491.0	P	3.00	3.02	1.46	1.19	0.92	1.46	1.03	1.03
46	IA30c-31	1840	1840	300	300	C	119	29.5	448	2.10	540.0	P	3.00	3.12	1.63	1.33	1.02	1.63	1.14	1.14
47	IA30d-32	1840	1840	300	300	C	123	25.8	448	0.50	258.0	P	0.71	0.82	0.80	1.00	0.81	1.00	0.93	0.91
48	IA30d-33	1840	1840	300	300	C	125	26.2	462	0.50	258.0	P	0.71	0.87	0.77	0.97	0.78	0.94	0.91	0.88
49	IA30e-34	1840	1840	300	300	C	120	26.9	461	1.00	332.0	P	1.43	1.64	1.04	1.05	0.80	1.04	0.92	0.92
50	IA30e-35	1840	1840	300	300	C	122	24.6	459	1.00	332.0	P	1.43	1.73	1.06	1.05	0.81	1.06	0.92	0.92
Moe, J. (1961)																				
51	H1	1830	1830	254	254	S	114	26.1	328	1.15	375.0	P	1.64	1.21	1.31	1.20	1.02	1.31	1.19	1.19
52	S1-60	1830	1830	254	254	S	114	23.3	399	1.06	389.2	P	1.51	1.58	1.44	1.33	1.11	1.44	1.32	1.32
53	S2-60	1830	1830	254	254	S	114	22.1	399	1.03	355.8	P	1.47	1.58	1.35	1.24	1.04	1.35	1.24	1.24
54	S3-60	1830	1830	254	254	S	114	22.6	399	1.02	363.6	P	1.46	1.55	1.36	1.27	1.06	1.36	1.26	1.26

No.	Slab ID	L_1 (mm)	L_2 (mm)	c_1 (mm)	c_2 (mm)	Column Shape	d (mm)	f'_c (MPa)	f_y (MPa)	ρ (%)	V_{exp} (kN)	Failure mode	ρ/ρ_{fs} Simplified Method	ρ/ρ_{fs} Standard Method	V_{exp}/V_{calc}					
															ACI 318-14	Eurocode 2	CSCT	Peiris-Ghali	Proposed Simple Method	Proposed Standard Method
55	S4-60	1830	1830	254	254	S	114	23.9	399	1.13	333.6	P	1.61	1.67	1.22	1.10	0.92	1.22	1.10	1.10
56	S1-70	1830	1830	254	254	S	114	24.5	482	1.06	392.3	P	1.51	2.05	1.41	1.31	1.08	1.41	1.31	1.31
57	S3-70	1830	1830	254	254	S	114	25.4	482	1.02	378.1	P	1.46	1.94	1.34	1.27	1.04	1.34	1.26	1.26
58	S4-70	1830	1830	254	254	S	114	35.2	482	1.13	373.6	P	1.61	1.82	1.12	1.08	0.89	1.12	1.08	1.08
59	S4A-70	1830	1830	254	254	S	114	20.5	482	1.13	311.4	P	1.61	2.39	1.23	1.08	0.90	1.23	1.08	1.08
60	S5-60	1830	1830	203	203	S	114	22.2	399	1.06	342.5	P	1.52	1.91	1.50	1.29	1.10	1.50	1.37	1.37
61	S5-70	1830	1830	203	203	S	114	24.3	482	1.06	378.1	P	1.52	2.42	1.59	1.38	1.16	1.59	1.47	1.47
62	R-1	1830	1830	457	152	R	114	27.6	328	1.38	393.6	P	1.97	1.87	1.41	1.08	1.11	1.41	1.32	1.32
63	R-2	1830	1830	152	152	S	114	26.5	328	1.38	311.4	P	1.97	2.07	1.49	1.11	1.19	1.49	1.28	1.28
64	M1A	1830	1830	305	305	S	114	23.0	481	1.50	432.8	P	2.14	2.62	1.41	1.22	1.01	1.41	1.16	1.16
Taylor, R. and B. Hayes (1965)																				
65	2S2	889	889	51	51	S	57	25.9	376	1.57	71.7	P	2.24	3.81	1.71	1.10	1.07	1.71	1.41	1.41
66	2S3	889	889	76	76	S	57	24.5	376	1.57	91.1	P	2.25	3.03	1.81	1.28	1.17	1.81	1.47	1.47
67	2S4	889	889	102	102	S	57	23.2	376	1.57	85.8	P	2.25	2.55	1.47	1.12	0.98	1.47	1.19	1.19
68	2S5	889	889	127	127	S	57	22.1	376	1.57	96.5	P	2.24	2.22	1.46	1.17	1.01	1.46	1.17	1.17
69	2S6	889	889	152	152	S	57	18.4	376	1.57	96.5	P	2.24	2.14	1.41	1.15	0.99	1.41	1.09	1.09
70	3S2	889	889	51	51	S	57	22.8	376	3.14	78.4	P	4.49	8.12	1.99	1.16	1.12	1.99	1.37	1.37
71	3S4	889	889	102	102	S	57	22.6	376	3.14	115.2	P	4.49	5.16	2.00	1.40	1.17	2.00	1.38	1.38
72	3S6	889	889	152	152	S	57	21.6	376	3.14	149.9	P	4.49	3.95	2.02	1.56	1.23	2.02	1.38	1.38
Base (1966)																				
73	A1/M1	1370	1370	203	203	S	114	15.5	255	1.10	316.0	F	1.57	1.30	1.67	1.33	1.22	1.67	1.42	1.42
74	A1/M2	1370	1370	203	203	S	117	14.7	282	1.50	339.0	P	2.14	2.17	1.77	1.26	1.17	1.77	1.34	1.34
75	A1/M3	1370	1370	203	203	S	121	13.5	282	1.90	301.0	P	2.71	2.96	1.57	1.01	0.98	1.57	1.09	1.09
76	A1/T1	1370	1370	203	203	S	124	13.3	432	1.00	254.0	P	1.43	3.04	1.29	1.01	0.91	1.29	1.10	1.10
77	A1/T2	1370	1370	203	203	S	117	20.0	432	1.20	339.0	P	1.71	2.82	1.52	1.22	1.08	1.52	1.31	1.31
78	A2/M1	1370	1370	203	203	S	124	33.6	255	1.00	401.0	F	1.43	0.87	1.28	1.17	1.08	1.34	1.28	1.31
79	A2/M2	1370	1370	203	203	S	117	31.2	282	1.50	411.0	P	2.14	1.49	1.47	1.19	1.07	1.47	1.27	1.27
80	A2/M3	1370	1370	203	203	S	121	30.9	282	1.90	422.0	P	2.71	1.96	1.45	1.07	0.98	1.45	1.15	1.15
81	A2/T1	1370	1370	203	203	S	124	37.3	432	1.00	411.0	P	1.43	1.82	1.24	1.16	1.01	1.24	1.26	1.26
82	A2/T2	1370	1370	203	203	S	124	39.3	432	1.70	431.0	P	2.43	3.01	1.27	1.00	0.88	1.27	1.09	1.09
83	A3/M1	1370	1370	203	203	S	124	17.9	255	1.00	242.0	P	1.43	1.19	1.06	0.88	0.81	1.06	0.95	0.95
84	A3/M2	1370	1370	203	203	S	102	18.3	282	1.70	330.0	P	2.43	1.92	1.86	1.36	1.25	1.86	1.40	1.40
85	A3/M3	1370	1370	203	203	S	117	25.9	282	1.90	292.0	P	2.71	2.07	1.15	0.83	0.76	1.15	0.89	0.89

No.	Slab ID	L_1 (mm)	L_2 (mm)	c_1 (mm)	c_2 (mm)	Column Shape	d (mm)	f'_c (MPa)	f_y (MPa)	ρ (%)	V_{exp} (kN)	Failure mode	ρ/ρ_{fs} Simplified Method	ρ/ρ_{fs} Standard Method	V_{exp}/V_{calc}					
															ACI 318-14	Eurocode 2	CSCT	Peiris-Ghali	Proposed Simple Method	Proposed Standard Method
86	A3/T1	1370	1370	203	203	S	121	19.6	432	1.00	322.0	P	1.43	2.45	1.39	1.18	1.03	1.39	1.27	1.27
87	A3/T2	1370	1370	203	203	S	119	15.2	432	1.20	292.0	P	1.71	3.29	1.47	1.12	1.01	1.47	1.21	1.21
88	A4/M1	1370	1370	203	203	S	114	36.4	255	1.10	254.0	P	1.57	0.85	0.87	0.81	0.74	0.91	0.86	0.88
89	A4/M2	1370	1370	203	203	S	119	27.7	282	1.50	335.0	P	2.14	1.60	1.24	0.98	0.89	1.24	1.05	1.05
90	A4/M3	1370	1370	203	203	S	117	30.6	322	1.90	531.0	P	2.71	2.32	1.92	1.43	1.29	1.92	1.53	1.53
91	A4/T1	1370	1370	203	203	S	114	31.2	432	1.10	377.0	P	1.57	2.02	1.40	1.26	1.09	1.40	1.34	1.34
92	A4/T2	1370	1370	203	203	S	117	27.8	432	1.20	394.0	P	1.71	2.39	1.50	1.27	1.11	1.50	1.36	1.36
Corley, W. G. and N. M. Hawkins (1968)																				
93	AN-1	2134	2134	254	254	S	111	18.7	403	1.54	334.0	P	2.20	2.52	1.42	1.13	1.10	1.42	1.12	1.12
94	BN-1	2134	2134	254	254	S	111	20.1	444	1.03	265.5	P	1.47	1.87	1.09	1.00	0.97	1.09	0.99	0.99
Schaeidt, W. and M. Ladner (1970)																				
95	P1	2900	2900	500	500	C	240	27.9	544	1.31	1662.	P	1.87	3.36	1.44	1.32	1.09	1.44	1.17	1.17
Hawkins, N. M., H. B. Fallsen and R. C. Hinojosa (1971)																				
96	1	2134	2134	305	305	S	117	30.3	412	1.12	383.9	F	1.60	1.37	1.06	1.05	1.17	1.06	1.00	1.00
97	2	2134	2134	406	203	R	117	26.3	412	1.12	351.4	S	1.60	1.92	1.04	1.01	1.12	1.04	1.13	1.13
98	3	2134	2134	457	152	R	117	32.0	412	1.12	333.2	S	1.60	2.01	1.08	0.89	1.00	1.08	1.10	1.10
99	4	2134	2134	495	114	R	117	31.0	412	1.12	330.5	S	1.60	2.30	1.24	0.90	1.00	1.24	1.18	1.18
100	5	2134	2134	457	152	R	117	26.9	412	1.44	355.0	S	2.06	2.82	1.25	0.93	1.01	1.25	1.14	1.14
101	6	2134	2134	457	152	R	117	22.7	412	1.12	335.8	F	1.60	2.39	1.29	1.01	1.12	1.29	1.24	1.24
102	7	2134	2134	457	152	R	117	25.9	412	0.87	319.8	S	1.24	1.74	1.15	1.00	1.14	1.15	1.23	1.23
103	8	2134	2134	495	114	R	121	26.1	414	0.81	314.5	S	1.16	1.89	1.23	0.95	1.09	1.23	1.27	1.27
104	9	2134	2134	305	152	R	121	29.5	414	0.77	315.4	S	1.10	1.55	1.03	1.05	1.21	1.03	1.27	1.27
Roll, F., S. T. H. Zaidi, G. Sabnis and K. Chuang (1971)																				
105	AS000-0-0-2	737	737	102	102	S	46	35.1	359	1.15	65.4	P	1.65	1.18	1.23	1.18	0.95	1.23	1.18	1.18
106	AS-000-0-0-3	737	737	102	102	S	46	28.9	359	1.15	63.2	P	1.65	1.30	1.31	1.22	0.99	1.31	1.22	1.22
107	AS000-0-0-4	737	737	102	102	S	46	28.9	359	1.15	61.0	P	1.65	1.30	1.26	1.18	0.95	1.26	1.17	1.17
108	AS000-0-0-5	737	737	102	102	S	46	29.0	359	1.15	63.6	P	1.65	1.30	1.32	1.22	0.99	1.32	1.22	1.22
109	BS-000-0-0-1	737	737	102	102	S	46	31.4	368	2.53	88.2	P	3.61	2.84	1.75	1.38	1.08	1.75	1.28	1.28
110	B-S-00-0-0-2	737	737	102	102	S	46	29.6	462	2.53	87.0	P	3.61	4.13	1.78	1.38	1.08	1.78	1.28	1.28
111	H-0-a	737	737	102	102	S	46	30.3	374	1.15	67.1	P	1.65	1.35	1.36	1.27	1.03	1.36	1.27	1.27
112	H-0-b	737	737	102	102	S	46	29.0	440	1.15	81.4	P	1.65	1.77	1.68	1.57	1.25	1.68	1.56	1.56

No.	Slab ID	L_1 (mm)	L_2 (mm)	c_1 (mm)	c_2 (mm)	Column Shape	d (mm)	f'_c (MPa)	f_y (MPa)	ρ (%)	V_{exp} (kN)	Failure mode	ρ/ρ_{fs} Simplified Method	ρ/ρ_{fs} Standard Method	V_{exp}/V_{calc}					
															ACI 318-14	Eurocode 2	CSCT	Peiris-Ghali	Proposed Simple Method	Proposed Standard Method
Ladner, M. (1973)																				
113	M	1400	1400	226	226	C	109	39.6	541	1.32	362.0	P	1.89	2.83	1.28	1.19	0.85	1.28	1.10	1.10
Ladner, M., W. Schaeidt and S. Gut (1977)																				
114	DA6	1260	1260	100	100	S	80	30.0	550	1.79	183.0	P	2.56	5.91	1.74	1.20	1.11	1.74	1.40	1.40
115	DA7	1260	1260	200	200	S	80	33.5	550	1.79	288.0	P	2.56	3.53	1.67	1.42	1.19	1.67	1.37	1.37
116	DA10	1260	1260	240	240	S	80	32.0	550	1.79	281.0	P	2.56	3.22	1.46	1.29	1.08	1.46	1.19	1.19
117	DA11	1260	1260	320	320	S	80	30.4	550	1.79	324.0	P	2.56	2.84	1.38	1.30	1.10	1.38	1.11	1.11
Marti, P., and Thürlimann, B. (1977)																				
118	P2	2750	2750	300	300	C	143	34.6	558	1.48	628.0	P	2.11	3.00	1.37	1.20	1.13	1.37	1.11	1.11
Pralong, J., W. Brändli and B. Thürlimann (1979)																				
119	P5	2750	2750	300	300	C	171	26.2	515	1.18	628.0	P	1.69	2.91	1.23	1.05	1.02	1.23	1.04	1.04
Kinnunen, S., Nylander, H., and Tolf, P.(1980)																				
120	S1	5820	4680	800	800	C	669	28.7	622	0.61	4915.	P	0.87	5.51	0.75	0.93	0.77	0.75	1.23	1.20
Mokhatar, A. (1982)																				
121	AB1	1900	1900	249	249	S	114	36.2	515	1.40	407.9	P	2.00	2.45	1.23	1.10	1.00	1.23	1.11	1.11
Swamy, R. N. and S. A. R. Ali (1982)																				
122	S1	1800	1800	150	150	S	100	40.1	462	0.57	197.7	P	0.81	1.05	0.94	1.04	1.12	0.98	1.20	1.16
123	S7	1800	1800	150	150	S	100	37.4	462	0.76	221.7	P	1.09	1.46	1.09	1.09	1.13	1.09	1.21	1.21
124	S19	1800	1800	150	150	S	100	37.6	462	0.38	130.7	F	0.54	0.73	0.64	0.81	0.91	0.95	0.99	0.95
Schaefers, U. (1984)																				
125	0	1960	1960	210	210	C	113	23.1	420	0.83	280.0	P	1.18	1.55	1.29	1.24	1.01	1.29	1.19	1.19
126	3	1960	1960	210	210	C	170	23.3	450	0.55	460.0	P	0.79	1.64	1.18	1.15	0.99	1.18	1.32	1.27
Regan, P. E. (1986)																				
127	I/1	2000	2000	200	200	S	77	25.8	500	1.20	194.0	P	1.72	1.89	1.34	1.26	1.17	1.34	1.21	1.21
128	I/2	2000	2000	200	200	S	77	23.4	500	1.20	176.0	P	1.72	1.98	1.28	1.18	1.10	1.28	1.13	1.13
129	I/3	2000	2000	200	200	S	77	27.4	500	0.92	194.0	P	1.31	1.40	1.30	1.35	1.26	1.30	1.29	1.29
130	I/4	2000	2000	200	200	S	77	32.3	500	0.92	194.0	P	1.31	1.29	1.20	1.28	1.20	1.20	1.22	1.22
131	I/5	2000	2000	200	200	S	79	28.2	480	0.75	165.0	P	1.07	1.09	1.06	1.17	1.12	1.06	1.13	1.13
132	I/6	2000	2000	200	200	S	79	21.9	480	0.75	165.0	P	1.07	1.24	1.20	1.27	1.21	1.20	1.23	1.23
133	I/7	2000	2000	200	200	S	79	30.4	480	0.80	186.0	F	1.14	1.12	1.15	1.26	1.20	1.15	1.21	1.21
134	II/1	3000	3000	250	250	C	200	34.9	530	0.98	825.0	P	1.40	2.81	1.24	1.07	1.07	1.24	1.18	1.18

No.	Slab ID	L_1 (mm)	L_2 (mm)	c_1 (mm)	c_2 (mm)	Column Shape	d (mm)	f'_c (MPa)	f_y (MPa)	ρ (%)	V_{exp} (kN)	Failure mode	ρ/ρ_{fs} Simplified Method	ρ/ρ_{fs} Standard Method	V_{exp}/V_{calc}					
															ACI 318-14	Eurocode 2	CSCT	Peiris-Ghali	Proposed Simple Method	Proposed Standard Method
135	II/2	2000	2000	160	160	C	128	33.3	485	0.98	390.0	P	1.40	2.51	1.47	1.26	1.14	1.47	1.38	1.38
136	II/3	2000	2000	160	160	C	128	34.3	485	0.98	365.0	P	1.40	2.47	1.35	1.16	1.15	1.35	1.28	1.28
137	II/4	1000	1000	80	80	C	64	33.3	480	0.98	117.0	P	1.40	2.47	1.76	1.51	1.17	1.76	1.66	1.66
138	II/5	1000	1000	80	80	C	64	34.3	480	0.98	105.0	P	1.40	2.44	1.56	1.34	1.11	1.56	1.47	1.47
139	II/6	1000	1000	80	80	C	64	36.2	480	0.98	105.0	P	1.40	2.37	1.52	1.31	1.15	1.52	1.44	1.44
140	III/1	1500	1500	150	150	C	95	23.2	494	0.83	197.0	P	1.19	2.23	1.42	1.29	1.06	1.42	1.32	1.32
141	III/2	1500	1500	150	150	C	95	9.5	494	0.83	123.0	P	1.19	3.48	1.38	1.09	0.93	1.38	1.11	1.11
142	III/3	1500	1500	150	150	C	95	37.8	494	0.83	214.0	P	1.19	1.75	1.21	1.19	0.98	1.21	1.21	1.21
143	III/4	1500	1500	150	150	C	93	119	464	1.52	154.0	P	2.17	5.08	1.59	1.07	0.96	1.59	1.08	1.08
144	III/5	1500	1500	150	150	C	93	26.8	464	1.52	214.0	P	2.17	3.39	1.48	1.13	0.95	1.48	1.15	1.15
145	III/6	1500	1500	150	150	C	93	42.6	464	1.52	248.0	P	2.17	2.69	1.36	1.13	0.92	1.36	1.14	1.14
146	V/1	1600	1600	54	54	C	118	34.3	628	0.80	170.0	P	1.14	5.14	1.11	0.80	0.79	1.11	1.16	1.16
147	V/2	1600	1600	170	170	C	118	32.2	628	0.80	280.0	P	1.14	2.86	1.17	1.11	0.91	1.17	1.16	1.16
148	V/3	1600	1600	110	110	C	118	32.4	628	0.80	265.0	P	1.14	3.73	1.37	1.15	1.01	1.37	1.39	1.39
149	V/4	1600	1600	102	102	S	118	36.2	628	0.80	285.0	P	1.14	3.68	1.37	1.16	1.08	1.37	1.49	1.49
150	V/5	1600	1600	150	150	C	118	32.9	628	0.80	285.0	P	1.14	3.06	1.26	1.16	0.97	1.26	1.26	1.26
Rankin, G. I. B. and A. E. Long (1987)																				
151	1	700	700	100	100	S	41	40.0	530	0.42	36.4	FP	0.60	0.67	0.76	1.07	0.92	1.30	1.14	1.11
152	2	700	700	100	100	S	41	40.0	530	0.55	49.1	P	0.79	0.89	1.02	1.32	1.10	1.33	1.33	1.30
153	3	700	700	100	100	S	41	40.0	530	0.69	56.6	P	0.99	1.11	1.18	1.41	1.15	1.24	1.37	1.37
154	4	700	700	100	100	S	41	40.0	530	0.82	56.2	P	1.17	1.32	1.17	1.32	1.06	1.17	1.29	1.29
155	5	700	700	100	100	S	41	40.0	530	0.88	57.3	P	1.25	1.41	1.19	1.32	1.06	1.19	1.28	1.28
156	6	700	700	100	100	S	41	40.0	530	1.04	65.6	P	1.48	1.67	1.37	1.43	1.14	1.37	1.39	1.39
157	7	700	700	100	100	S	41	40.0	530	1.16	70.9	P	1.66	1.86	1.48	1.49	1.18	1.48	1.45	1.45
158	8	700	700	100	100	S	41	40.0	530	1.29	71.7	P	1.84	2.07	1.49	1.45	1.15	1.49	1.41	1.41
159	9	700	700	100	100	S	41	40.0	530	1.45	78.6	P	2.08	2.34	1.64	1.53	1.21	1.64	1.49	1.49
160	10	700	700	100	100	S	41	40.0	530	0.52	43.6	P	0.74	0.83	0.91	1.20	1.00	1.26	1.22	1.20
161	11	700	700	100	100	S	41	40.0	530	0.80	55.0	P	1.14	1.28	1.15	1.31	1.05	1.15	1.27	1.27
162	12	700	700	100	100	S	41	40.0	530	1.12	67.1	P	1.59	1.79	1.40	1.43	1.13	1.40	1.39	1.39
163	13	700	700	100	100	S	41	40.0	530	0.60	49.4	P	0.85	0.96	1.03	1.29	1.07	1.25	1.29	1.26
164	14	700	700	100	100	S	41	40.0	530	0.69	52.5	P	0.99	1.11	1.09	1.31	1.07	1.15	1.27	1.27
165	15	700	700	100	100	S	41	40.0	530	1.99	84.8	P	2.85	3.21	1.77	1.49	1.20	1.77	1.44	1.44
166	1A	700	700	100	100	S	47	40.0	530	0.44	45.2	FP	0.62	0.81	0.79	1.06	0.90	1.17	1.15	1.10

No.	Slab ID	L_1 (mm)	L_2 (mm)	c_1 (mm)	c_2 (mm)	Column Shape	d (mm)	f'_c (MPa)	f_y (MPa)	ρ (%)	V_{exp} (kN)	Failure mode	ρ/ρ_{fs} Simplified Method	ρ/ρ_{fs} Standard Method	V_{exp}/V_{calc}					
															ACI 318-14	Eurocode 2	CSCT	Peiris-Ghali	Proposed Simple Method	Proposed Standard Method
167	2A	700	700	100	100	S	47	40.0	530	0.69	66.2	P	0.99	1.29	1.15	1.33	1.08	1.15	1.34	1.34
168	3A	700	700	100	100	S	47	40.0	530	1.29	89.7	P	1.85	2.40	1.56	1.46	1.17	1.56	1.47	1.47
169	4A	700	700	100	100	S	47	40.0	530	1.99	97.4	P	2.85	3.70	1.70	1.37	1.12	1.70	1.38	1.38
170	1B	700	700	100	100	S	35	40.0	530	0.42	28.9	FP	0.61	0.58	0.73	1.06	0.92	1.36	1.08	1.09
171	2B	700	700	100	100	S	35	40.0	530	0.69	37.6	P	0.99	0.95	0.94	1.18	0.96	1.11	1.10	1.11
172	3B	700	700	100	100	S	35	40.0	530	1.29	56.7	P	1.84	1.77	1.42	1.44	1.14	1.42	1.34	1.34
173	4B	700	700	100	100	S	35	40.0	530	1.99	72.5	P	2.84	2.73	1.82	1.59	1.27	1.82	1.49	1.49
174	1C	700	700	100	100	S	54	40.0	530	0.42	62.7	FP	0.60	0.90	0.91	1.18	1.01	1.27	1.35	1.26
175	2C	700	700	100	100	S	54	40.0	530	0.69	87.9	P	0.99	1.48	1.27	1.41	1.15	1.27	1.48	1.47
176	3C	700	700	100	100	S	54	40.0	530	1.29	124.1	P	1.85	2.76	1.79	1.61	1.30	1.79	1.69	1.69
177	4C	700	700	100	100	S	54	40.0	530	1.99	125.9	P	2.84	4.25	1.82	1.42	1.18	1.82	1.49	1.49
Tolf, P. (1988)																				
178	S2.1	2540	2540	250	250	C	200	24.2	657	0.80	603.0	P	1.14	3.92	1.09	0.95	0.83	1.09	1.04	1.04
179	S2.2	2540	2540	250	250	C	199	22.9	670	0.80	600.0	P	1.14	4.13	1.12	0.97	0.85	1.12	1.06	1.06
180	S2.3	2540	2540	250	250	C	200	25.4	668	0.34	489.0	P	0.49	1.67	0.86	1.00	0.92	0.86	1.24	1.10
181	S2.4	2540	2540	250	250	C	197	24.2	664	0.35	444.0	P	0.50	1.72	0.82	0.94	0.86	0.82	1.16	1.03
182	S1.1	1270	1270	125	125	C	100	28.6	706	0.80	216.0	P	1.14	4.02	1.44	1.28	1.04	1.44	1.41	1.41
183	S1.2	1270	1270	125	125	C	99	22.9	701	0.80	194.0	P	1.14	4.40	1.46	1.26	1.03	1.46	1.38	1.38
184	S1.3	1270	1270	125	125	C	98	26.6	720	0.40	145.0	P	0.57	2.11	1.03	1.15	0.95	1.03	1.38	1.26
185	S1.4	1270	1270	125	125	C	99	25.1	712	0.40	148.0	P	0.57	2.16	1.07	1.18	0.97	1.07	1.41	1.29
Gardner, N. J. (1990)																				
186	5	483	483	102	102	C	38	13.1	550	2.04	33.0	P	2.91	7.16	1.39	1.01	0.76	1.39	0.86	0.86
187	7	787	787	102	102	C	38	13.1	550	2.04	34.0	P	2.91	5.45	1.44	1.04	0.85	1.44	0.89	0.89
188	8	1219	1219	102	102	C	76	22.9	414	2.05	129.0	P	2.93	4.73	1.59	1.03	0.90	1.59	1.10	1.10
189	9	787	787	102	102	C	76	21.5	414	2.05	136.0	P	2.93	5.52	1.73	1.11	0.92	1.73	1.18	1.18
190	18	610	610	203	203	C	33	21.0	450	7.31	89.0	P	10.44	7.49	2.32	2.04	1.38	2.32	1.27	1.27
191	26	991	991	203	203	C	73	49.5	450	5.01	323.0	P	7.16	6.85	1.88	1.73	0.98	1.88	1.35	1.35
Lovrovich, J. S. and D. I. Mclean (1990)																				
192	F3	914	914	102	102	C	83	38.0	531	1.75	149.0	P	2.50	5.73	1.27	0.91	0.73	1.27	1.01	1.01

No.	Slab ID	L_1 (mm)	L_2 (mm)	c_1 (mm)	c_2 (mm)	Column Shape	d (mm)	f'_c (MPa)	f_y (MPa)	ρ (%)	V_{exp} (kN)	Failure mode	ρ/ρ_{fs} Simplified Method	ρ/ρ_{fs} Standard Method	V_{exp}/V_{calc}					
															ACI 318-14	Eurocode 2	CSCT	Peiris-Ghali	Proposed Simple Method	Proposed Standard Method
193	F4	1118	1118	102	102	C	83	38.0	531	1.75	129.0	P	2.50	5.24	1.10	0.79	0.65	1.10	0.87	0.87
194	F5	1524	1524	102	102	C	83	38.0	531	1.75	139.0	P	2.50	4.80	1.18	0.85	0.74	1.18	0.94	0.94
Marzouk, H. and A. Hussein (1991)																				
195	HS1	1700	1700	150	150	S	95	67.0	490	0.49	178.0	P	0.70	0.75	0.70	0.91	0.90	1.05	1.06	1.04
196	HS2	1700	1700	150	150	S	95	70.0	490	0.84	249.0	P	1.20	1.26	0.96	1.04	0.97	0.96	1.15	1.15
197	HS3	1700	1700	150	150	S	95	69.0	490	1.47	356.0	P	2.10	2.21	1.38	1.24	1.12	1.38	1.37	1.37
198	HS4	1700	1700	150	150	S	90	66.0	490	2.37	418.0	P	3.39	3.47	1.79	1.46	1.25	1.79	1.50	1.50
199	HS5	1700	1700	150	150	S	125	68.0	490	0.64	365.0	P	0.91	1.23	0.97	1.06	1.03	0.97	1.28	1.26
200	HS6	1700	1700	150	150	S	120	70.0	490	0.94	489.0	P	1.34	1.73	1.35	1.33	1.24	1.35	1.56	1.56
201	HS7	1700	1700	150	150	S	95	74.0	490	1.19	356.0	P	1.70	1.73	1.37	1.30	1.18	1.37	1.43	1.43
202	HS8	1700	1700	150	150	S	120	69.0	490	1.11	436.0	P	1.59	2.05	1.22	1.13	1.05	1.22	1.32	1.32
203	HS9	1700	1700	150	150	S	120	74.0	490	1.61	543.0	P	2.30	2.88	1.50	1.21	1.12	1.50	1.42	1.42
204	HS10	1700	1700	150	150	S	120	80.0	490	2.33	645.0	P	3.33	4.00	1.78	1.31	1.15	1.78	1.45	1.45
205	HS11	1700	1700	150	150	S	70	70.0	490	0.95	196.0	FP	1.36	1.06	1.14	1.30	1.19	1.14	1.31	1.31
206	HS12	1700	1700	150	150	S	70	75.0	490	1.52	258.0	P	2.17	1.63	1.50	1.43	1.26	1.50	1.44	1.44
207	HS13	1700	1700	150	150	S	70	68.0	490	2.00	267.0	P	2.86	2.26	1.58	1.39	1.22	1.58	1.40	1.40
208	HS14	1700	1700	220	220	S	95	72.0	490	1.47	498.0	P	2.10	1.64	1.49	1.48	1.31	1.49	1.47	1.47
209	HS15	1700	1700	300	300	S	95	71.0	490	1.47	560.0	P	2.10	1.32	1.34	1.45	1.29	1.34	1.32	1.32
210	NS1	1700	1700	150	150	S	95	42.0	490	1.47	320.0	P	2.10	2.84	1.59	1.32	1.20	1.59	1.45	1.45
211	NS2	1700	1700	150	150	S	120	30.0	490	0.94	396.0	P	1.34	2.64	1.67	1.43	1.33	1.67	1.67	1.67
Alexander, S. D. B. and S. H. Simmonds (1992)																				
212	P11FO	2750	2750	200	200	S	138	33.2	438	0.53	257.0	P	0.76	1.02	0.72	0.78	0.95	0.76	0.92	0.88
213	P38FO	2750	2750	200	200	S	111	38.1	438	0.66	264.0	P	0.94	0.96	0.93	1.03	1.22	0.98	1.10	1.10
214	P11S150	2750	2750	200	200	S	134	31.5	438	0.56	257.0	P	0.81	1.08	0.77	0.82	0.98	0.77	0.95	0.92
215	P38S150	2750	2750	200	200	S	107	33.8	438	0.56	264.0	P	0.81	0.84	1.04	1.20	1.43	1.22	1.30	1.29
216	P19S150	2750	2750	200	200	S	125	24.7	438	0.56	258.0	P	0.81	1.14	0.96	1.01	1.19	0.96	1.14	1.10
217	P19S75	2750	2750	200	200	S	125	24.7	438	0.49	258.0	P	0.69	0.98	0.96	1.06	1.27	1.03	1.23	1.16
218	P19S50	2750	2750	200	200	S	125	24.7	438	0.55	319.0	P	0.79	1.12	1.19	1.25	1.48	1.19	1.43	1.37
219	P19RE	2750	2750	200	200	S	125	33.5	438	0.56	304.0	P	0.81	0.98	0.97	1.07	1.29	1.03	1.22	1.18
220	P19RC	2750	2750	200	200	S	125	33.5	438	0.56	282.0	P	0.81	0.98	0.90	1.00	1.19	0.96	1.13	1.09
221	P19RB	2750	2750	200	200	S	125	33.5	438	0.56	343.0	P	0.81	0.98	1.10	1.21	1.45	1.17	1.37	1.33
Theodorakopoulos, D. and N. Swamy (1993)																				

No.	Slab ID	L_1 (mm)	L_2 (mm)	c_1 (mm)	c_2 (mm)	Column Shape	d (mm)	f'_c (MPa)	f_y (MPa)	ρ (%)	V_{exp} (kN)	Failure mode	ρ/ρ_{fs} Simplified Method	ρ/ρ_{fs} Standard Method	V_{exp}/V_{calc}					
															ACI 318-14	Eurocode 2	CSCT	Peiris-Ghali	Proposed Simple Method	Proposed Standard Method
222	FS-1	1800	1800	150	150	S	100	30.9	460	0.52	173.5	P	0.74	1.09	0.94	1.03	1.10	0.95	1.20	1.15
223	FS-10	1800	1800	200	200	S	100	31.9	460	0.52	191.4	P	0.74	0.87	0.85	1.01	1.09	1.05	1.10	1.07
224	FS-19	1800	1800	150	150	S	100	30.2	460	0.35	136.5	P	0.50	0.74	0.75	0.93	1.05	1.09	1.16	1.09
225	FS-8	1800	1800	100	100	S	100	32.1	460	0.52	150.3	P	0.74	1.41	0.99	0.99	1.08	0.99	1.29	1.23
Tomaszewicz, A. (1993)																				
226	ND65-1-1	3000	3000	200	200	S	275	64.0	500	1.49	2050	P	2.13	4.21	1.47	1.15	1.23	1.47	1.43	1.43
227	ND65-2-1	2600	2600	150	150	S	200	70.0	500	1.75	1200	P	2.50	4.53	1.54	1.08	1.20	1.54	1.44	1.44
228	NG95-1-1	3000	3000	200	200	S	275	84.0	500	1.49	2250	P	2.13	3.67	1.54	1.15	1.23	1.54	1.43	1.43
229	ND95-1-3	3000	3000	200	200	S	275	90.0	500	2.55	2400	P	3.64	6.07	1.65	1.09	1.08	1.65	1.26	1.26
230	ND95-2-1	2600	2600	150	150	S	200	88.0	500	1.75	1100	P	2.50	4.04	1.41	0.92	1.01	1.41	1.22	1.22
231	ND95-2-1D	2600	2600	150	150	S	200	87.0	500	1.75	1300	P	2.50	4.06	1.66	1.09	1.20	1.66	1.45	1.45
232	ND95-2-3	2600	2600	150	150	S	200	90.0	500	2.62	1450	P	3.74	5.98	1.86	1.15	1.17	1.86	1.42	1.42
233	ND95-2-3D	2600	2600	150	150	S	200	80.0	500	2.62	1250	P	3.74	6.34	1.60	1.03	1.05	1.60	1.27	1.27
234	ND95-2-3D+	2600	2600	150	150	S	200	98.0	500	2.62	1450	P	3.74	5.73	1.86	1.15	1.13	1.86	1.38	1.38
235	ND95-3-1	1500	1500	100	100	S	88	85.0	500	1.84	330.0	P	2.63	3.35	1.79	1.28	1.19	1.79	1.54	1.54
236	ND115-1-1	3000	3000	200	200	S	275	112.0	500	1.49	2450	P	2.13	3.18	1.68	1.23	1.23	1.68	1.42	1.42
237	ND115-2-1	2600	2600	150	150	S	200	119.0	500	1.75	1400	P	2.50	3.47	1.79	1.16	1.17	1.79	1.41	1.41
238	ND115-2-3	2600	2600	150	150	S	200	108.0	500	2.62	1550	P	3.74	5.45	1.98	1.23	1.17	1.98	1.43	1.43
Hallgren, M. (1996)																				
239	A1	3180	3180	100	100	S	39	29.6	501	1.12	62.5	P	1.60	1.84	1.59	1.56	1.82	1.59	1.50	1.50
Shaaban, A. M. and H. Gesund (1994)																				
240	SFO-1	1600	1600	64	64	S	70	33.4	420	1.40	90.0	P	2.00	3.33	1.26	0.89	0.80	1.26	1.13	1.13
241	SFO-2	1600	1600	64	64	S	70	39.1	420	1.40	112.5	P	2.00	3.08	1.46	1.05	0.94	1.46	1.34	1.34
242	SFO-3	1600	1600	64	64	S	70	31.1	420	1.40	81.0	P	2.00	3.46	1.18	0.82	0.74	1.18	1.04	1.04
243	SFO-4	1600	1600	64	64	S	70	31.7	420	1.40	94.5	P	2.00	3.42	1.36	0.95	0.86	1.36	1.20	1.20
Banthia, N., J. F. Trottier, P. Soroushian and Z. Bayasi (1992)																				
244	I	600	600	100	100	C	55	39.0	448	0.51	65.0	P	0.73	0.98	0.99	1.20	0.79	1.21	1.23	1.17
245	II	600	600	100	100	C	55	50.3	448	0.51	61.0	P	0.73	0.86	0.82	1.04	0.68	1.13	1.06	1.03
246	IV	600	600	100	100	C	55	39.0	448	0.51	60.0	P	0.73	0.98	0.91	1.11	0.73	1.12	1.14	1.08
Gardner, N. J. and X.-Y. Shao (1996)																				
247	1	2400	2400	254	254	S	120	21.5	460	0.66	311.0	FP	0.94	1.63	1.12	1.18	1.21	1.12	1.20	1.19
Hallgren, M. (1996)																				

No.	Slab ID	L_1 (mm)	L_2 (mm)	c_1 (mm)	c_2 (mm)	Column Shape	d (mm)	f'_c (MPa)	f_y (MPa)	ρ (%)	V_{exp} (kN)	Failure mode	ρ/ρ_{fs} Simplified Method	ρ/ρ_{fs} Standard Method	V_{exp}/V_{calc}					
															ACI 318-14	Eurocode 2	CSCT	Peiris-Ghali	Proposed Simple Method	Proposed Standard Method
248	HSC0	2540	2540	250	250	C	200	90.3	643	0.80	965.0	P	1.14	1.96	1.03	0.98	0.97	1.03	1.07	1.07
249	HSC1	2540	2540	250	250	C	200	91.3	627	0.80	1021	P	1.14	1.88	1.09	1.03	1.03	1.09	1.13	1.13
250	HSC2	2540	2540	250	250	C	194	85.7	620	0.82	889.0	P	1.17	1.90	0.99	0.96	0.95	0.99	1.04	1.04
251	HSC4	2540	2540	250	250	C	200	91.6	596	1.19	1041	P	1.70	2.59	1.11	0.92	0.89	1.11	1.01	1.01
252	HSC6	2540	2540	250	250	C	201	108.8	633	0.60	960.0	P	0.86	1.31	1.01	1.06	1.04	1.01	1.12	1.10
253	N/HSC8	2540	2540	250	250	C	198	94.9	631	0.80	944.0	P	1.14	1.84	1.02	0.97	0.95	1.02	1.05	1.05
254	HSC9	2540	2540	250	250	C	202	84.1	634	0.33	565.0	FP	0.47	0.83	0.59	0.77	0.87	0.84	0.97	0.88
Marzouk, H., M. Emam and M. S. Hilal (1996)																				
255	N.H.Z.S.1.0	1900	1900	250	250	S	119	32.2	460	1.00	475.5	P	1.43	1.63	1.43	1.40	1.31	1.43	1.42	1.42
256	N.N.Z.S.1.0	1900	1900	250	250	S	119	37.2	460	1.00	484.8	P	1.43	1.52	1.36	1.36	1.27	1.36	1.38	1.38
Ramdane, K. E. (1996)																				
257	1	1700	1700	150	150	C	98	88.2	550	0.60	224.0	F	0.86	1.00	0.89	0.99	0.99	0.90	1.05	1.02
258	2	1700	1700	150	150	C	98	56.2	550	0.60	212.0	FP	0.86	1.25	0.94	1.09	1.06	0.94	1.15	1.12
259	3	1700	1700	150	150	C	98	26.9	550	0.60	169.0	P	0.86	1.81	1.08	1.11	1.04	1.08	1.18	1.15
260	4	1700	1700	150	150	C	98	58.7	550	0.60	233.0	F	0.86	1.22	1.01	1.18	1.15	1.01	1.25	1.22
261	6	1700	1700	150	150	C	98	101.6	550	0.60	233.0	F	0.86	0.93	0.92	1.03	0.99	0.94	1.04	1.03
262	12	1700	1700	150	150	C	98	60.4	550	1.30	319.0	P	1.86	2.61	1.36	1.24	1.12	1.36	1.28	1.28
263	13	1700	1700	150	150	C	98	43.6	550	1.30	297.0	P	1.86	3.07	1.49	1.29	1.16	1.49	1.33	1.33
264	14	1700	1700	150	150	C	98	60.8	550	1.30	341.0	P	1.86	2.60	1.45	1.32	1.20	1.45	1.36	1.36
265	16	1700	1700	150	150	C	98	98.4	550	1.30	362.0	FP	1.86	2.05	1.43	1.23	1.09	1.43	1.23	1.23
266	21	1700	1700	150	150	C	98	41.9	650	1.30	286.0	P	1.86	4.03	1.46	1.26	1.03	1.46	1.29	1.29
267	22	1700	1700	150	150	C	98	84.2	650	1.30	405.0	P	1.86	2.84	1.60	1.41	1.15	1.60	1.45	1.45
268	23	1700	1700	150	150	C	100	56.4	650	0.90	341.0	P	1.29	2.45	1.46	1.48	1.23	1.46	1.53	1.53
269	25	1700	1700	150	150	C	100	32.9	650	1.20	244.0	P	1.71	4.27	1.37	1.15	1.04	1.37	1.19	1.19
270	26	1700	1700	150	150	C	100	37.6	650	1.20	294.0	P	1.71	4.00	1.54	1.33	1.10	1.54	1.38	1.38
271	27	1700	1700	150	150	C	102	33.7	650	1.00	227.0	P	1.43	3.59	1.22	1.09	0.91	1.22	1.14	1.14
Sistonen, E., M. Lydman and S. Houinen (1997)																				
272	L1	1770	1770	202	202	C	172	31.1	621	0.46	503.0	P	0.66	2.02	1.12	1.20	1.07	1.12	1.44	1.34
273	L2	1770	1770	202	202	C	176	31.1	621	0.45	537.0	P	0.64	2.01	1.16	1.24	1.11	1.16	1.50	1.40
274	L3	1770	1770	201	201	C	173	31.1	621	0.45	530.0	P	0.64	1.99	1.17	1.26	1.13	1.17	1.53	1.42
275	L4	1970	1970	402	402	C	170	31.1	612	0.67	686.0	P	0.96	1.86	1.03	1.20	1.02	1.03	1.08	1.07
276	L5	1970	1970	399	399	C	172	31.1	612	0.66	696.0	P	0.94	1.86	1.04	1.20	1.02	1.04	1.09	1.08

No.	Slab ID	L_1 (mm)	L_2 (mm)	c_1 (mm)	c_2 (mm)	Column Shape	d (mm)	f'_c (MPa)	f_y (MPa)	ρ (%)	V_{exp} (kN)	Failure mode	ρ/ρ_{fs} Simplified Method	ρ/ρ_{fs} Standard Method	V_{exp}/V_{calc}					
															ACI 318-14	Eurocode 2	CSCT	Peiris-Ghali	Proposed Simple Method	Proposed Standard Method
277	L6	1970	1970	406	406	C	175	31.1	612	0.65	799.0	P	0.93	1.85	1.15	1.34	1.14	1.15	1.22	1.20
278	L7	1970	1970	201	201	C	177	22.9	586	0.64	478.0	P	0.91	2.99	1.19	1.07	0.98	1.19	1.23	1.22
279	L8	2470	2470	899	899	C	174	22.9	576	1.16	1110	P	1.66	2.13	1.09	1.19	1.06	1.09	0.83	0.83
280	L9	2470	2470	897	897	C	172	22.9	576	1.17	1107.0	P	1.67	2.12	1.10	1.20	1.07	1.10	0.84	0.84
281	L10	2470	2470	901	901	C	173	22.9	576	1.16	1079.	P	1.66	2.12	1.06	1.16	1.04	1.06	0.81	0.81
Marzouk, H., M. Emam and M. S. Hilal (1998)																				
282	H.H.Z.S.1.0	1900	1900	250	250	S	119	67.2	460	1.00	5115	P	1.43	1.13	1.07	1.18	1.12	1.07	1.19	1.19
Ghannoum, C. M. (1998)																				
283	S1-U	2300	2300	225	225	S	127	35.3	445	0.96	301.0	P	1.37	1.59	0.85	0.82	0.81	0.85	0.87	0.87
284	S1-B	2300	2300	225	225	S	123	35.3	445	1.92	317.0	P	2.74	3.08	0.93	0.72	0.70	0.93	0.76	0.76
285	S2-U	2300	2300	225	225	S	127	54.2	445	0.96	363.0	P	1.37	1.28	0.83	0.85	0.86	0.83	0.91	0.91
286	S2-B	2300	2300	225	225	S	123	54.2	445	1.92	447.0	P	2.74	2.49	1.06	0.88	0.85	1.06	0.92	0.92
287	S3-U	2300	2300	225	225	S	127	63.7	445	0.96	443.0	P	1.37	1.18	0.93	0.99	1.00	0.93	1.05	1.05
288	S3-B	2300	2300	225	225	S	123	63.7	445	1.92	485.0	P	2.74	2.29	1.06	0.90	0.87	1.06	0.95	0.95
Broms, C. E. (2000)																				
289	9	2600	2600	250	250	S	150	26.9	500	0.52	408.0	P	0.74	1.30	0.98	1.09	1.16	0.98	1.24	1.18
290	9a	2600	2600	250	250	S	150	21.0	500	0.52	360.0	P	0.74	1.47	0.98	1.04	1.10	0.98	1.18	1.13
McHarg, P. J., Cook, W. D., Mitchell, D., & Yoon, Y. S. (2000)																				
291	NU	2300	2300	225	225	S	110	30.0	444	1.11	306.0	P	1.58	1.75	1.14	1.05	1.03	1.14	1.08	1.08
292	NB	2300	2300	225	225	S	110	30.0	444	2.15	349.0	P	3.07	3.39	1.30	0.99	0.94	1.30	0.98	0.98
Osman, M., H. Marzouk and S. Helmy (2000)																				
293	NSNW0.5P	1900	1900	250	250	S	120	37.8	450	0.49	310.2	F	0.70	0.73	0.85	1.08	1.10	1.26	1.17	1.16
Li, K. K. L. (2000)																				
294	P100	925	925	201	201	S	99	39.3	488	0.97	330.0	P	1.39	2.25	1.33	1.34	1.03	1.33	1.38	1.38
295	P150	1190	1190	201	201	S	150	39.3	464	0.90	582.7	P	1.29	2.40	1.33	1.23	1.04	1.33	1.41	1.41
296	P200	1450	1450	201	201	S	201	39.3	464	0.83	902.9	P	1.19	2.55	1.34	1.18	1.08	1.34	1.46	1.46
297	P300	1975	1975	201	201	S	300	39.3	468	0.76	1378.9	P	1.09	2.79	1.10	0.99	0.94	1.10	1.23	1.23
298	P400	1975	1975	300	300	S	399	39.3	433	0.76	2224.	P	1.09	3.22	0.95	0.94	0.83	0.95	1.24	1.24
299	P500	1975	1975	300	300	S	500	39.3	433	0.76	2682.	P	1.09	4.38	0.80	0.79	0.68	0.80	1.16	1.16

No.	Slab ID	L_1 (mm)	L_2 (mm)	c_1 (mm)	c_2 (mm)	Column Shape	d (mm)	f'_c (MPa)	f_y (MPa)	ρ (%)	V_{exp} (kN)	Failure mode	ρ/ρ_{fs} Simplified Method	ρ/ρ_{fs} Standard Method	V_{exp}/V_{calc}					
															ACI 318-14	Eurocode 2	CSCT	Peiris-Ghali	Proposed Simple Method	Proposed Standard Method
Oliveira, D. R., G. S. Melo and P. E. Regan (2000)																				
300	1	2400	2400	120	120	S	93	60.9	695	1.50	270.0	P	2.14	4.63	1.31	1.09	1.08	1.31	1.26	1.26
301	2	1700	1700	120	120	S	97	62.9	695	1.40	335.0	P	2.00	4.41	1.51	1.27	1.17	1.51	1.49	1.49
Oliveira, D. R. C., P. E. Regan and Melo (2004)																				
302	L1a	2280	1680	120	120	S	107	57.0	749	1.09	240.0	FP	1.56	4.20	0.98	0.86	0.79	0.98	1.04	1.04
303	L1b	2280	1680	120	120	S	108	59.0	749	1.08	322.4	P	1.54	4.31	1.28	1.13	1.04	1.28	1.37	1.37
304	L1c	2280	1680	120	120	S	107	59.0	749	1.09	318.0	P	1.56	4.32	1.28	1.13	1.04	1.28	1.36	1.36
305	L2a	2280	1680	240	120	R	109	58.0	749	1.07	246.0	FP	1.53	3.84	0.77	0.76	0.67	0.77	0.95	0.95
306	L2b	2280	1680	240	120	R	106	58.0	749	1.10	361.0	P	1.57	4.17	1.17	1.15	1.02	1.17	1.43	1.43
307	L2c	2280	1680	240	120	R	107	57.0	749	1.09	330.8	P	1.56	4.11	1.07	1.05	0.93	1.07	1.31	1.31
308	L3a	2280	1680	360	120	R	108	56.0	749	1.08	240.6	FP	1.54	3.66	0.77	0.68	0.60	0.77	0.86	0.86
309	L3b	2280	1680	360	120	R	107	60.0	749	1.09	400.0	P	1.56	3.97	1.25	1.12	0.98	1.25	1.42	1.42
310	L3c	2280	1680	360	120	R	106	54.0	749	1.10	357.6	P	1.57	3.96	1.19	1.05	0.92	1.19	1.33	1.33
311	L4a	2280	1680	480	120	R	108	56.0	749	1.08	250.8	FP	1.54	3.49	0.76	0.64	0.57	0.76	0.83	0.83
312	L4b	2280	1680	480	120	R	106	54.0	749	1.10	395.0	P	1.57	4.16	1.25	1.05	0.92	1.25	1.35	1.35
313	L4c	2280	1680	480	120	R	107	56.0	749	1.09	404.0	P	1.56	3.66	1.24	1.05	0.92	1.24	1.35	1.35
314	L5a	2280	1680	600	120	R	108	57.0	749	1.08	287.4	FP	1.54	3.35	0.81	0.67	0.60	0.81	0.88	0.88
315	L5b	2280	1680	600	120	R	108	67.0	749	1.08	426.4	P	1.54	3.84	1.10	0.94	0.84	1.10	1.23	1.23
316	L5c	2280	1680	600	120	R	109	63.0	749	1.07	446.4	P	1.53	3.28	1.18	0.99	0.89	1.18	1.30	1.30
Teng, S., Cheong, H. K., Kuang, K. L., Geng, J. Z., (2004)																				
317	OC11	2200	2200	200	200	S	105	36.0	461	1.81	423.0	P	2.59	2.95	1.65	1.31	1.26	1.65	1.37	1.37
318	OC13	2200	2200	600	200	R	107	35.8	461	1.71	568.0	P	2.44	2.61	1.57	1.27	1.21	1.57	1.46	1.46
319	OC13-1.6	2200	2200	600	200	R	110	33.0	461	1.67	508.0	P	2.39	2.72	1.42	1.13	1.08	1.42	1.31	1.31
320	OC13-0.63	2200	2200	600	200	R	111	39.7	461	1.65	455.0	P	2.36	2.48	1.15	0.94	0.90	1.15	1.09	1.09
321	OC15	2700	2200	1000	200	R	103	40.2	461	1.76	649.0	P	2.51	2.13	1.52	1.15	1.16	1.52	1.39	1.39
Ozden, S. and U. O. Ersoy, T. (2006)																				
322	NR1E0F0	1500	1500	200	200	S	100	20.5	507	0.73	188.0	P	1.04	1.94	1.04	1.03	0.90	1.04	1.06	1.06
323	NR2E0F0	1500	1500	200	200	S	100	19.0	507	1.09	202.0	P	1.56	3.03	1.16	0.99	0.87	1.16	1.02	1.02
324	HR1E0F0	1500	1500	200	200	S	100	70.3	471	1.49	331.0	P	2.14	1.93	0.99	0.95	0.82	0.99	0.97	0.97
325	HR1E0F0r	1500	1500	200	200	S	100	71.3	471	1.49	371.0	P	2.14	1.92	1.11	1.06	0.91	1.11	1.09	1.09
326	HR2E0F0	1500	1500	200	200	S	100	60.5	471	2.26	405.0	P	3.23	3.15	1.30	1.11	0.92	1.30	1.09	1.09
327	HR2E0F0r	1500	1500	200	200	S	100	71.0	471	2.26	489.0	P	3.23	2.91	1.46	1.27	1.05	1.46	1.25	1.25

No.	Slab ID	L_1 (mm)	L_2 (mm)	c_1 (mm)	c_2 (mm)	Column Shape	d (mm)	f'_c (MPa)	f_y (MPa)	ρ (%)	V_{exp} (kN)	Failure mode	ρ/ρ_{fs} Simplified Method	ρ/ρ_{fs} Standard Method	V_{exp}/V_{calc}					
															ACI 318-14	Eurocode 2	CSCT	Peiris-Ghali	Proposed Simple Method	Proposed Standard Method
Birkle, G. and W. H. Dilger (2008)																				
328	1	2400	2400	250	250	S	124	36.2	488	1.54	483.0	P	2.20	2.71	1.30	1.11	1.13	1.30	1.14	1.14
329	7	3400	3400	300	300	S	190	35.0	531	1.30	825.0	P	1.86	3.16	1.12	0.94	1.07	1.12	1.03	1.03
330	10	4200	4200	350	350	S	260	31.4	524	1.00	1046	P	1.43	2.85	0.88	0.81	0.94	0.88	0.87	0.87
Lee, J.-H., Y.-S. Yoon, S.-H. Lee, W. D. Cook and D. Mitchell (2008)																				
331	30U	2300	2300	225	225	S	110	30.0	434	1.11	306.0	P	1.58	1.69	1.14	1.05	1.03	1.14	1.08	1.08
332	30B	2300	2300	225	225	S	110	30.0	434	2.15	349.0	P	3.07	3.28	1.30	0.99	0.95	1.30	0.98	0.98
333	35U	2300	2300	225	225	S	110	37.2	445	1.18	301.0	P	1.69	1.68	1.00	0.94	0.92	1.00	0.96	0.96
334	35B	2300	2300	225	225	S	110	37.2	445	2.15	317.0	P	3.07	3.05	1.06	0.83	0.79	1.06	0.83	0.83
335	55U	2300	2300	225	225	S	110	57.1	445	1.18	363.0	P	1.69	1.35	0.98	0.99	0.97	0.98	1.01	1.01
336	55B	2300	2300	225	225	S	110	57.1	445	2.15	447.0	P	3.07	2.47	1.20	1.02	0.95	1.20	1.02	1.02
337	65U	2300	2300	225	225	S	110	67.1	445	1.18	443.0	P	1.69	1.25	1.10	1.14	1.13	1.10	1.17	1.17
338	65B	2300	2300	225	225	S	110	67.1	445	2.15	485.0	P	3.07	2.27	1.21	1.05	0.98	1.21	1.05	1.05
Guandalini, S., Burdet, O.L. and Muttoni, A (2009)																				
339	PG-1	3000	3000	260	260	S	210	27.6	573	1.50	1023	P	2.14	5.52	1.48	1.08	1.17	1.48	1.25	1.25
340	PG-2b	3000	3000	260	260	S	210	40.6	552	0.25	440.0	F	0.36	0.72	0.52	0.74	0.96	0.92	1.02	0.91
341	PG-3	6000	6000	520	520	S	456	32.4	520	0.33	2153.	P	0.47	1.43	0.64	0.92	1.21	0.78	1.28	1.13
342	PG-4	3000	3000	260	260	S	210	32.2	541	0.25	408.0	F	0.36	0.78	0.55	0.74	1.12	0.88	1.02	0.90
343	PG-5	3000	3000	260	260	S	210	29.3	555	0.33	550.0	F	0.47	1.12	0.77	0.94	1.33	0.88	1.24	1.09
344	PG-6	1500	1500	130	130	S	96	34.7	526	1.50	238.0	P	2.14	4.01	1.40	1.07	0.99	1.40	1.22	1.22
345	PG-7	1500	1500	130	130	S	100	34.7	550	0.75	241.0	P	1.07	2.22	1.33	1.27	1.17	1.33	1.47	1.47
346	PG-8	1500	1500	130	130	S	117	34.7	525	0.28	140.0	F	0.40	0.88	0.62	0.78	0.80	0.89	1.10	0.97
347	PG-9	1500	1500	130	130	S	117	34.7	525	0.22	115.0	F	0.31	0.69	0.51	0.70	0.74	0.93	1.02	0.90
348	PG-10	3000	3000	260	260	S	210	28.5	577	0.33	540.0	F	0.47	1.21	0.77	0.93	1.12	0.84	1.22	1.08
349	PG-11	3000	3000	260	260	S	210	31.5	570	0.75	763.0	P	1.07	2.56	1.03	0.97	1.06	1.03	1.12	1.12
Cheng, M.-Y. and G. J. Parra-Montesinos (2010)																				
350	S1	1500	1500	152	152	S	127	47.7	471	0.83	433.0	P	1.19	1.81	1.33	1.26	1.22	1.33	1.49	1.49
351	S2	1500	1500	152	152	S	127	47.7	471	0.56	379.0	P	0.80	1.22	1.16	1.26	1.26	1.16	1.55	1.49
Nguyen-Minh, L., M. Rovňák and T. Tran-Quoc (2012)																				
352	A0	1050	1050	200	200	S	105	21.7	492	0.66	284.0	P	0.94	1.81	1.43	1.46	1.15	1.43	1.54	1.52
353	B0	1350	1350	200	200	S	105	21.7	492	0.75	275.0	P	1.07	1.88	1.38	1.35	1.14	1.38	1.41	1.41
354	C0	1650	1650	200	200	S	105	21.7	492	0.70	264.0	P	1.00	1.66	1.33	1.33	1.18	1.33	1.39	1.39

No.	Slab ID	L_1 (mm)	L_2 (mm)	c_1 (mm)	c_2 (mm)	Column Shape	d (mm)	f'_c (MPa)	f_y (MPa)	ρ (%)	V_{exp} (kN)	Failure mode	ρ/ρ_{fs} Simplified Method	ρ/ρ_{fs} Standard Method	V_{exp}/V_{calc}					
															ACI 318-14	Eurocode 2	CSCT	Peiris-Ghali	Proposed Simple Method	Proposed Standard Method
Author's current slab specimens																				
355	S-1	1800	1800	249	249	S	117	28.4	433	0.43	252.2	F	0.61	0.68	0.83	1.06	1.05	1.29	1.16	1.14
356	S11-028	2200	2200	200	200	S	120	112.0	459	0.28	278.6	F	0.39	0.29	0.65	0.96	1.12	1.92	1.13	1.19
357	S11-050	2200	2200	200	200	S	117	112.0	459	0.50	393.6	F	0.72	0.51	0.95	1.16	1.21	1.58	1.22	1.29
358	S11-090	2200	2200	200	200	S	117	112.0	537	0.90	438.6	P	1.29	1.16	1.06	1.06	0.99	1.06	1.06	1.06
359	S11-139	2200	2200	200	200	S	114	112.0	501	1.39	453.6	P	1.99	1.58	1.14	0.99	0.89	1.14	0.98	0.98
360	S13-028	2200	2200	600	200	R	120	114.0	459	0.27	308.0	F	0.38	0.27	0.53	0.79	0.99	2.18	1.01	1.07
361	S13-050	2200	2200	600	200	R	117	114.0	537	0.50	418.0	F	0.72	0.63	0.74	0.91	0.97	1.44	1.04	1.06
362	S13-090	2200	2200	600	200	R	117	114.0	537	0.90	558.0	P	1.29	1.13	0.99	1.00	0.96	1.08	1.08	1.08
363	S13-143	2200	2200	600	200	R	114	114.0	501	1.43	718.0	P	2.04	1.57	1.32	1.14	1.05	1.32	1.23	1.23
364	S15-028	2700	2200	1000	200	R	117	97.0	459	0.27	321.3	F	0.38	0.25	0.49	0.68	0.97	2.42	0.97	1.04
365	S15-050	2700	2200	1000	200	R	117	97.0	537	0.50	456.3	F	0.71	0.58	0.70	0.79	0.95	1.59	1.00	1.04
366	S15-090	2700	2200	1000	200	R	117	97.0	537	0.90	656.3	P	1.29	1.06	1.00	0.93	1.00	1.28	1.12	1.12
367	S15-143	2700	2200	1000	200	R	114	97.0	501	1.43	775.3	P	2.04	1.47	1.22	0.98	0.99	1.22	1.17	1.17
												Minimum =			**0.49**	**0.64**	**0.57**	**0.75**	**0.73**	**0.76**
												Maximum =			**2.32**	**2.04**	**1.82**	**2.42**	**1.69**	**1.69**
												Average =			**1.26**	**1.14**	**1.04**	**1.31**	**1.21**	**1.20**
												COV=			**0.249**	**0.174**	**0.152**	**0.214**	**0.151**	**0.152**
												5th Percentile =			**0.75**	**0.80**	**0.76**	**0.90**	**0.91**	**0.89**

Notes:
Unit conversion: 1 mm = 0.03937 in; 1 kN = 0.2248 kip; 1 MPa = 145.038 psi.)
Column (3) – [#] corresponds to the number of each reference given in the main paper and in pages A25 to A28
Column (9) – Column shapes: S = Square; R = Rectangular; C = Circular
Column (15) – Observed Failure Mode: F = Flexural Failure; P = Punching Failure
Column (16) – ρ_{fs} is taken to be 0.007 for the proposed Simplified Method as shown by Eq. (12b)
Column (17) – ρ_{fs} = proposed limiting reinforcement ratio, calculated using Eq. (12a)

E.2 Property and analysis results of 148 SFRC slab specimens

Columns 2 to 14 Table E.2 show the original slab ID, material properties, observed failure mode and failure load V_{exp} of 148 slab data including the current 10 SFRC slabs. Columns 15 and 16 of Table E.2 show the failure mode predictions by the proposed simplified and standard methods, respectively. Columns (17) to (22) show the ratio of the failure load to the calculated punching shear strength V_{exp}/V_{calc} of each design method such as Narayanan and Darwish (1986), Shaaban and Gesund (1990), Higashiyama et al. (2011), CSCT+VEM (Maya et al., 2012), the proposed simplified general method and the proposed standard general method, respectively.

Notes for Table E.2:

- Failure mode (Column 14): P– Punching; FL – Flexure; FP – Flexure-Punching
- All 148 slabs in Table E.2 have square columns.
- Notation of Fibre types in Column 10 of Table E.2

  RO - round

  ST - straight

  CR- crimped

  CO- corrugated

  JA - Japanese

  PA - Paddle

  SH - Single hooked

  DH - double hooked

Table E.2- Property and analysis results of 148 SFRC slab specimens

No.	Slab ID	L_1 mm	c_x mm	d mm	f'_c MPa	f_y MPa	ρ %	Fibre type	Fibre length L_f	Fibre Aspect ratio	V_f (%)	V_{exp} kN	Failure Mode	ρ/ρ_{fs} Simplified Method	ρ/ρ_{fs} Standard Method	V_{exp}/V_{calc}					
																Narayanan & Darwish	Shaaban & Gesund	Higashiyama et al.	CSCT+VEM	Simplified General Method	Standard General Method
(1)	(2)	(3)	(4)	(5)	(6)	(7)	(8)	(9)	(10)	(11)	(12)	(13)	(14)	(15)	(16)	(17)	(18)	(19)	(20)	(21)	(22)
Swamy and Ali (1982)																					
1	S-1	1800	150	100	40.0	460	0.56	0	0.0	0	0.0	198.0	P	0.80	1.05	0.93	0.92	1.04	1.20	1.22	1.17
2	S-2	1800	150	100	41.3	460	0.56	CR	50.0	100	0.60	244.0	P	0.80	0.97	0.71	1.12	0.92	0.99	1.25	1.20
3	S-3	1800	150	100	41.3	460	0.56	CR	50.0	100	0.90	263.0	P	0.80	0.94	0.75	1.20	0.90	0.92	1.25	1.20
4	S-4	1800	150	100	41.3	460	0.56	CR	50.0	100	1.20	281.0	P	0.80	0.92	0.84	1.29	0.91	0.87	1.25	1.21
5	S-5	1800	150	100	41.3	460	0.56	CR	50.0	100	0.90	267.0	P	0.80	0.94	0.76	1.22	0.92	0.93	1.27	1.22
6	S-6	1800	150	100	41.3	460	0.56	CR	50.0	100	0.90	239.0	P	0.80	0.94	0.68	1.09	0.82	0.84	1.14	1.09
7	S-7	1800	150	100	40.0	460	0.85	0	0.0	0	0.0	222.0	P	1.21	1.55	0.99	1.03	1.02	1.12	1.14	1.14
8	S-8	1800	150	100	41.3	460	0.85	CR	50.0	100	0.90	256.0	P	1.21	1.32	0.71	1.17	0.76	0.83	1.04	1.04
9	S-9	1800	150	100	31.2	460	0.26	CR	50.0	100	0.90	179.0	FL	0.37	0.59	0.56	0.94	0.82	0.80	1.34	1.20
10	S-10	1800	150	100	35.5	460	0.31	CR	50.0	100	0.90	203.0	FL	0.44	0.64	0.61	1.00	0.85	0.84	1.35	1.24
11	S-11	1800	150	100	41.3	460	0.85	CR	50.0	100	0.90	262.0	P	1.21	1.32	0.73	1.20	0.78	0.85	1.06	1.06
12	S-12	1800	150	100	41.3	460	0.85	SH	50.0	100	0.90	249.0	P	1.21	1.03	0.73	1.14	0.70	0.73	0.84	0.84
13	S-13	1800	150	100	41.3	460	0.85	RO	50.0	83	0.90	237.0	P	1.21	1.55	0.69	1.08	0.81	0.91	1.09	1.09
14	S-16	1800	150	100	38.9	460	0.56	CR	50.0	100	0.90	213.0	FL	0.80	0.96	0.62	1.00	0.73	0.76	1.03	0.99
15	S-19	1800	150	100	40.0	460	0.26	0	0.0	0	0.0	131.0	FL	0.37	0.50	0.65	0.61	0.89	1.16	1.18	1.12
Narayanan and Darwish (1987)																					
16	S1	780	100	45	43.3	460	2.01	0	0.0	0	0.0	86.5	P	2.87	2.37	1.25	1.48	1.19	0.99	1.25	1.25
17	S2	780	100	45	52.1	460	2.01	CR	30.0	100	0.25	93.4	P	2.87	2.14	1.00	1.46	1.08	0.93	1.21	1.21
18	S3	780	100	45	44.7	460	2.01	CR	30.0	100	0.50	102.0	P	2.87	2.13	1.07	1.72	1.04	1.01	1.32	1.32
19	S4	780	100	45	46.0	460	2.01	CR	30.0	100	0.75	107.5	P	2.87	2.03	1.09	1.79	1.01	0.99	1.31	1.31
20	S5	780	100	45	53.0	460	2.01	CR	30.0	100	1.00	116.6	P	2.87	1.89	1.13	1.76	1.00	0.93	1.28	1.28
21	S6	780	100	45	53.0	460	2.01	CR	30.0	100	1.25	122.2	P	2.87	1.82	1.32	1.89	1.03	0.94	1.32	1.32
22	S7	780	100	45	47.0	460	1.79	CR	30.0	100	0.75	92.6	P	2.56	1.84	0.95	1.52	0.90	0.86	1.16	1.16
23	S8	780	100	45	45.3	460	2.24	CR	30.0	100	0.75	111.1	P	3.20	2.21	1.12	1.86	1.00	1.02	1.32	1.32
24	S9	780	100	45	43.5	460	2.46	CR	30.0	100	0.75	111.3	P	3.51	2.39	1.11	1.90	0.97	1.03	1.30	1.30
25	S10	780	100	45	47.6	460	2.69	CR	30.0	100	0.75	116.3	P	3.84	2.52	1.09	1.85	0.96	1.00	1.29	1.29
26	S11	780	100	45	29.8	460	2.01	CR	30.0	100	0.75	82.1	P	2.87	2.18	0.93	1.70	0.81	0.92	1.14	1.14

No.	Slab ID	L_1 mm	c_x mm	d mm	f'_c MPa	f_y MPa	ρ %	Fibre type	Fibre length L_f	Fibre Aspect ratio	V_f (%)	V_{exp} kN	Failure Mode	ρ/ρ$_{fs}$ Simplified Method	ρ/ρ$_{fs}$ Standard Method	V_{exp}/V_{calc}					
																Narayanan & Darwish	Shaaban & Gesund	Higashiyama et al.	CSCT+VEM	Simplified General Method	Standard General Method
(1)	(2)	(3)	(4)	(5)	(6)	(7)	(8)	(9)	(10)	(11)	(12)	(13)	(14)	(15)	(16)	(17)	(18)	(19)	(20)	(21)	(22)
27	S12	780	100	45	32.4	460	2.01	CR	30.0	100	0.75	84.9	P	2.87	2.16	0.95	1.68	0.82	0.92	1.15	1.15
Alexander and Simmonds (1992)																					
28	P1FO	2750	200	138	33.2	438	0.53	0	0.0	0	0.0	257.0	P	0.76	1.03	0.78	0.70	0.77	1.05	0.92	0.88
29	P38FO	2750	200	111	38.1	438	0.66	0	0.0	0	0.0	264.0	P	0.94	0.96	0.89	0.91	0.98	1.35	1.10	1.10
30	P1F31	2750	200	138	35.8	438	0.53	CO	50.0	100	0.39	324.0	P	0.75	0.92	0.62	0.85	0.72	0.94	1.01	0.97
31	P1F66	2750	200	138	35.0	438	0.53	CO	50.0	100	0.84	345.0	P	0.75	0.86	0.59	0.92	0.66	0.78	0.96	0.93
32	P38F34	2750	200	111	38.4	438	0.66	CO	50.0	100	0.43	308.0	P	0.94	0.93	0.69	1.06	0.87	1.11	1.13	1.13
33	P38F69	2750	200	111	38.5	438	0.66	CO	50.0	100	0.88	330.0	P	0.94	0.91	0.67	1.13	0.80	0.91	1.08	1.08
Theodorakopoulos and Swamy (1993)																					
34	FS-1	1800	150	100	30.9	460	0.52	0	0.0	0	0.0	173.5	P	0.74	1.10	0.98	0.92	1.01	1.17	1.20	1.15
35	FS-10	1800	200	100	31.9	460	0.52	0	0.0	0	0.0	191.4	P	0.74	0.88	0.95	0.83	0.95	1.11	1.10	1.07
36	FS-19	1800	150	100	30.2	460	0.35	0	0.0	0	0.0	136.5	P	0.50	0.76	0.81	0.73	0.92	1.12	1.16	1.08
37	FS-8	1800	100	100	32.1	460	0.52	0	0.0	0	0.0	150.3	P	0.74	1.42	0.93	0.98	1.03	1.18	1.29	1.23
38	FS-2	1800	150	100	29.8	460	0.52	CR	50.0	100	0.50	225.0	P	0.74	1.03	0.76	1.21	0.96	1.10	1.35	1.27
39	FS-3	1800	150	100	31.2	460	0.52	CR	50.0	100	1.00	247.4	P	0.74	0.96	0.76	1.30	0.88	0.94	1.28	1.20
40	FS-4	1800	150	100	32.7	460	0.52	CR	50.0	100	1.00	224.4	P	0.74	0.94	0.68	1.15	0.79	0.83	1.15	1.08
41	FS-5	1800	150	100	33.3	460	0.35	CR	50.0	100	1.00	198.1	P	0.50	0.71	0.61	1.01	0.79	0.78	1.23	1.13
42	FS-6	1800	150	100	31.2	460	0.35	CR	50.0	100	1.00	174.5	FL	0.50	0.72	0.54	0.92	0.71	0.70	1.10	1.00
43	FS-7	1800	150	100	32.1	460	0.35	CR	50.0	100	1.00	192.4	FL	0.50	0.71	0.59	1.00	0.78	0.77	1.21	1.10
44	FS-20	1800	150	100	32.4	460	0.35	CR	50.0	100	1.00	211.0	P	0.50	0.71	0.65	1.09	0.85	0.84	1.32	1.21
45	FS-9	1800	100	100	31.2	460	0.52	CR	50.0	100	1.00	216.6	P	0.74	1.26	0.75	1.43	0.92	1.00	1.40	1.30
46	FS-11	1800	200	100	30.0	460	0.52	CR	50.0	100	1.00	259.8	FL	0.74	0.78	0.72	1.16	0.80	0.85	1.13	1.12
47	FS-12	1800	150	100	31.6	460	0.52	JA	25.0	60	1.00	217.5	P	0.74	1.00	0.70	1.14	0.87	0.99	1.25	1.17
48	FS-13	1800	150	100	29.3	460	0.52	SH	50.0	100	1.00	235.5	P	0.74	0.72	0.79	1.28	0.81	0.81	0.99	1.00
49	FS-14	1800	150	100	30.6	460	0.52	PA	53.0	70	1.00	239.5	P	0.74	1.00	0.75	1.27	0.93	1.09	1.35	1.26
50	FS-15	1800	150	100	27.3	460	0.52	CR	38.0	90	1.00	238.0	P	0.74	1.01	0.75	1.34	0.90	1.02	1.31	1.21
51	FS-16	1800	150	100	24.4	460	0.52	PA	53.0	70	1.00	227.8	P	0.74	1.07	0.76	1.36	0.94	1.13	1.36	1.27
52	FS-17	1800	150	100	41.0	460	0.52	PA	53.0	70	1.00	268.4	FL	0.74	0.90	0.77	1.23	1.00	1.09	1.40	1.34
53	FS-18	1800	150	100	12.4	460	0.52	PA	53.0	70	1.00	166.0	P	0.74	1.26	0.62	1.39	0.81	1.08	1.18	1.10
Shaaban and Gesund (1994)																					
54	SFO-1	1600	64	70	33.4	420	1.40	0	0.0	0	0.0	90.0	P	2.00	3.05	1.00	1.24	0.93	0.84	1.13	1.13

No.	Slab ID	L_1 mm	c_x mm	d mm	f'_c MPa	f_y MPa	ρ %	Fibre type	Fibre length L_f	Fibre Aspect ratio	V_f (%)	V_{exp} kN	Failure Mode	ρ/ρ_{fs} Simplified Method	ρ/ρ_{fs} Standard Method	V_{exp}/V_{calc}					
																Narayanan & Darwish	Shaaban & Gesund	Higashiyama et al.	CSCT+VEM	Simplified General Method	Standard General Method
(1)	(2)	(3)	(4)	(5)	(6)	(7)	(8)	(9)	(10)	(11)	(12)	(13)	(14)	(15)	(16)	(17)	(18)	(19)	(20)	(21)	(22)
55	SFO-2	1600	64	70	39.1	420	1.40	0	0.0	0	0.0	112.5	P	2.00	2.90	1.15	1.43	1.12	0.98	1.34	1.34
56	SFO-3	1600	64	70	31.1	420	1.40	0	0.0	0	0.0	81.0	P	2.00	3.13	0.94	1.16	0.87	0.77	1.04	1.04
57	SFO-4	1600	64	70	31.7	420	1.40	0	0.0	0	0.0	94.5	P	2.00	3.10	1.08	1.33	1.00	0.90	1.20	1.20
58	SF2-1	1600	64	70	34.5	420	1.40	CO	25.0	35	0.61	94.5	P	2.00	2.87	0.80	1.28	0.82	0.83	1.11	1.11
59	SF2-2	1600	64	70	37.3	420	1.40	CO	25.0	35	0.61	112.5	P	2.00	2.80	0.92	1.47	0.96	0.95	1.29	1.29
60	SF2-3	1600	64	70	29.7	420	1.40	CO	25.0	35	0.61	72.0	P	2.00	3.00	0.65	1.05	0.66	0.67	0.89	0.89
61	SF2-4	1600	64	70	24.8	420	1.40	CO	25.0	35	0.61	85.5	P	2.00	3.13	0.82	1.36	0.85	0.86	1.11	1.11
62	SF3-1	1600	64	70	37.7	420	1.40	CO	25.0	35	0.95	108.0	P	2.00	2.72	0.82	1.40	0.86	0.88	1.20	1.20
63	SF4-1	1600	64	70	46.8	420	1.40	CO	25.0	35	1.19	135.0	P	2.00	2.49	0.91	1.57	1.03	0.99	1.38	1.38
64	SF4-2	1600	64	70	36.6	420	1.40	CO	25.0	35	1.19	117.0	P	2.00	2.69	0.87	1.54	0.89	0.95	1.28	1.28
65	SF6-1	1600	64	70	22.4	420	1.40	CO	25.0	35	1.86	99.0	P	2.00	2.85	0.78	1.66	0.79	0.96	1.18	1.18
66	SF6-2	1600	64	70	22.1	420	1.40	CO	25.0	35	1.96	103.5	P	2.00	2.83	0.81	1.75	0.81	1.00	1.23	1.23
Harajli et al. (1994)																					
67	A1	650	100	39	29.6	501	1.12	0	0.0	0	0.0	62.5	P	1.60	1.66	1.58	1.56	1.41	1.13	1.50	1.50
68	A2	650	100	39	30.0	501	1.12	SH	50.0	100	0.45	67.7	P	1.60	1.30	1.03	1.68	1.05	1.04	1.28	1.28
69	A3	650	100	39	31.4	501	1.12	SH	50.0	100	0.80	77.8	FP	1.60	1.12	1.15	1.88	1.04	1.06	1.25	1.25
70	A4	650	100	39	24.6	501	1.12	SH	30.0	60	1.00	68.8	FP	1.60	1.26	1.06	1.88	1.04	1.11	1.28	1.28
71	A5	650	100	39	20.0	501	1.12	SH	30.0	60	2.00	62.1	FP	1.60	1.01	1.23	1.88	0.84	0.96	0.94	0.94
72	B1	650	100	55	31.4	501	1.12	0	0.0	0	0.0	99.4	P	1.60	2.32	1.42	1.53	1.33	1.05	1.48	1.48
73	B2	650	100	55	31.4	501	1.12	SH	50.0	100	0.45	114.6	P	1.60	1.82	1.02	1.76	1.07	1.07	1.36	1.36
74	B3	650	100	55	31.8	501	1.12	SH	50.0	100	0.80	117.3	P	1.60	1.57	1.01	1.79	0.95	1.00	1.20	1.20
75	B4	650	100	55	29.1	501	1.12	SH	30.0	60	1.00	117.7	P	1.60	1.73	1.03	1.88	1.04	1.09	1.33	1.33
76	B5	650	100	55	29.2	501	1.12	SH	30.0	60	2.00	145.6	P	1.60	1.38	1.61	2.32	1.14	1.20	1.30	1.30
McHarg et al (2000)																					
77	NU	2300	225	118	30.0	434	1.25	0	0.0	0	0.0	306.0	P	1.79	1.81	0.98	1.01	0.86	0.89	0.94	0.94
78	NB	2300	225	118	30.0	434	2.00	0	0.0	0	0.0	349.0	P	2.86	2.59	0.97	1.16	0.84	0.87	0.92	0.92
79	FSU	2300	225	118	39.0	434	1.25	SH	30.0	60	0.50	422.0	FP	1.79	1.41	0.82	1.23	0.84	0.95	1.03	1.03
80	FSB	2300	225	118	39.0	434	2.00	SH	30.0	60	0.50	438.0	FP	2.86	2.10	0.79	1.27	0.74	0.87	0.93	0.93
Ozden et al. (2006)																					
81	NR1E0F0	1500	200	100	21.6	0	0.73	0	0.0	0	0.0	188.0	P	1.04	1.72	1.14	0.99	1.01	0.94	1.04	1.04
82	NR2E0F0	1500	200	100	20.0	0	1.09	0	0.0	0	0.0	202.	P	1.56	2.40	1.16	1.11	0.98	0.91	1.00	1.00

No.	Slab ID	L_1 mm	c_x mm	d mm	f'_c MPa	f_y MPa	ρ %	Fibre type	Fibre length L_f	Fibre Aspect ratio	V_f (%)	V_{exp} kN	Failure Mode	ρ/ρ_{fs} Simplified Method	ρ/ρ_{fs} Standard Method	V_{exp}/V_{calc}					
																Narayanan & Darwish	Shaaban & Gesund	Higashiyama et al.	CSCT+VEM	Simplified General Method	Standard General Method
(1)	(2)	(3)	(4)	(5)	(6)	(7)	(8)	(9)	(10)	(11)	(12)	(13)	(14)	(15)	(16)	(17)	(18)	(19)	(20)	(21)	(22)
83	HR1E0F0	1500	200	100	74.0	0	1.50	0	0.0	0	0.0	331.0	P	2.14	2.03	0.81	0.94	1.08	0.85	0.96	0.96
84	HR1E0F0r	1500	200	100	75.0	0	1.50	0	0.0	0	0.0	371.0	P	2.14	2.02	0.90	1.05	1.21	0.95	1.07	1.07
85	HR2E0F0	1500	200	100	63.7	0	2.25	0	0.0	0	0.0	405.0	P	3.21	3.06	1.01	1.24	1.16	0.95	1.07	1.07
86	HR2E0F0r	1500	200	100	74.7	0	2.25	0	0.0	0	0.0	489.0	P	3.21	2.90	1.10	1.39	1.40	1.08	1.23	1.23
87	NR1E0F1	1500	200	100	19.6	0	0.73	SH	30.0	55	1.00	266.0	P	1.04	1.21	0.83	1.47	0.89	1.01	1.07	1.07
88	NR2E0F1	1500	200	100	19.3	0	1.09	SH	30.0	55	1.00	245.0	P	1.56	1.66	0.74	1.37	0.72	0.87	0.90	0.90
89	HR1E0F1	1500	200	100	81.3	0	1.50	SH	30.0	55	1.00	576.0	P	2.14	1.58	1.10	1.57	1.29	1.07	1.34	1.34
90	HR2E0F1	1500	200	100	79.3	0	2.25	SH	30.0	55	1.00	691.0	P	3.21	2.31	1.27	1.90	1.35	1.20	1.44	1.44
De Hanai and Holanda (2008)																					
91	L1	1160	80	80	23.1	0	1.57	0	0.0	0	0.0	137.2	P	2.24	4.61	1.27	1.64	1.19	1.10	1.35	1.35
92	L2	1160	80	80	24.4	0	1.57	SH	30.0	55	1.00	139.6	P	2.24	3.31	0.74	1.62	0.74	0.95	1.03	1.03
93	L3	1160	80	80	28.1	0	1.57	SH	30.0	55	1.00	163.6	P	2.24	3.28	0.84	1.77	0.83	1.04	1.17	1.17
94	L4	1160	80	80	57.0	0	1.57	0	0.0	0	0.0	192.9	P	2.24	3.61	1.07	1.47	1.34	1.08	1.40	1.40
95	L5	1160	80	80	59.7	0	1.57	SH	30.0	55	1.00	215.1	P	2.24	2.81	0.89	1.60	1.02	0.98	1.26	1.26
96	L6	1160	80	80	52.4	0	1.57	SH	30.0	55	1.00	236.2	P	2.24	2.92	1.02	1.87	1.12	1.14	1.43	1.43
97	L7	1160	80	80	36.6	0	1.57	SH	50.0	48	1.00	182.9	P	2.24	3.26	0.89	1.74	0.90	1.11	1.25	1.25
98	L8	1160	80	80	46.1	0	1.57	SH	50.0	48	1.00	210.9	P	2.24	3.10	0.96	1.78	1.04	1.16	1.36	1.36
Cheng & Parra-Montesinos(2010)																					
99	S1	1520	152	127	47.7	471	0.83	0	0.0	0	0.0	433.0	P	1.19	1.81	1.17	1.30	1.38	1.24	1.49	1.49
100	S2	1520	152	127	47.7	471	0.56	0	0.0	0	0.0	379.0	P	0.80	1.25	1.07	1.14	1.37	1.28	1.55	1.49
101	S3	1520	152	127	25.4	455	0.83	SH	30.0	55	1.00	386.0	P	1.19	1.58	0.84	1.59	0.92	1.06	1.20	1.20
102	S4	1520	152	127	25.4	455	0.56	SH	30.0	55	1.00	389.0	P	0.80	1.13	0.87	1.60	1.06	1.15	1.41	1.33
103	S5	1520	152	127	59.3	471	0.83	SH	35.0	70	1.50	530.0	P	1.19	1.11	1.06	1.43	1.02	0.83	1.11	1.11
104	S6	1520	152	127	57.9	471	0.56	SH	35.0	70	1.50	444.0	P	0.80	0.80	0.90	1.21	0.97	0.73	1.08	1.08
105	S7	1520	152	127	31.0	449	0.83	SH	30.0	55	1.50	522.0	P	1.19	1.32	1.09	1.94	1.08	1.20	1.37	1.37
106	S8	1520	152	127	31.0	449	0.56	SH	30.0	55	1.50	472.0	P	0.80	0.94	1.00	1.76	1.11	1.14	1.43	1.37
107	S9	1520	152	127	46.1	449	0.83	SH	30.0	80	1.50	530.0	P	1.19	1.07	1.29	1.62	1.01	0.84	1.11	1.11
108	S10	1520	152	127	59.1	449	0.56	SH	30.0	80	1.50	503.0	FP	0.80	0.72	1.16	1.36	1.09	0.75	1.16	1.19
Higashiyama et al. (2011)																					
109	t100-0.67	1200	100	70	24.6	377	0.85	SH	30.0	48	0.67	137.5	FP	1.21	1.29	0.93	1.71	1.14	1.24	1.43	1.43
110	t140-0.67	1200	100	110	24.6	377	0.54	SH	30.0	48	0.67	210.2	P	0.77	1.22	0.73	1.35	1.00	1.03	1.35	1.27

No.	Slab ID	L_1 mm	c_x mm	d mm	f'_c MPa	f_y MPa	ρ %	Fibre type	Fibre length L_f	Fibre Aspect ratio	V_f (%)	V_{exp} kN	Failure Mode	ρ/ρ_{fs} Simplified Method	ρ/ρ_{fs} Standard Method	V_{exp}/V_{calc}					
																Narayanan & Darwish	Shaaban & Gesund	Higashiyama et al.	CSCT+VEM	Simplified General Method	Standard General Method
(1)	(2)	(3)	(4)	(5)	(6)	(7)	(8)	(9)	(10)	(11)	(12)	(13)	(14)	(15)	(16)	(17)	(18)	(19)	(20)	(21)	(22)
111	t100-0.67	1200	100	150	24.6	377	0.40	SH	30.0	48	0.67	297.6	P	0.57	1.13	0.63	1.18	0.93	0.95	1.37	1.20
112	t100-0.72	1200	100	65	42.4	377	0.91	SH	30.0	48	0.72	140.8	FP	1.30	1.09	0.84	1.48	1.11	1.12	1.36	1.36
113	t140-0.72	1200	100	105	42.4	377	0.57	SH	30.0	48	0.72	213.2	P	0.81	1.03	0.63	1.12	0.93	0.90	1.22	1.16
114	t100-0.72	1200	100	145	42.4	377	0.41	SH	30.0	48	0.72	290.7	P	0.59	0.94	0.52	0.92	0.83	0.79	1.19	1.07
115	t100-0.91	1200	100	65	21.6	377	0.91	SH	30.0	48	0.91	120.8	FP	1.30	1.30	0.84	1.78	1.05	1.19	1.33	1.33
116	t140-0.91	1200	100	105	21.6	377	0.57	SH	30.0	48	0.91	183.1	P	0.81	1.24	0.64	1.35	0.88	0.95	1.19	1.13
117	t100-0.91	1200	100	145	21.6	377	0.41	SH	30.0	48	0.91	231.2	P	0.59	1.14	0.49	1.03	0.73	0.76	1.07	0.94
118	t100-0.63	1200	100	70	27.8	377	0.85	SH	30.0	48	0.63	152.3	P	1.21	1.26	1.00	1.78	1.23	1.32	1.55	1.55
119	t100-0.94	1200	100	70	24.0	377	0.85	SH	30.0	48	0.94	147.9	P	1.21	1.47	0.73	1.86	1.13	1.23	1.44	1.44
120	t100-1.03	1200	100	70	24.0	377	0.85	SH	30.0	48	1.03	158.9	P	1.21	1.83	0.63	2.00	1.19	1.26	1.52	1.52
Nguyen-Minh et al.(2012)																					
121	A0	1050	200	105	21.7	492	0.66	0	0.0	0	0.0	284.0	P	0.94	1.83	1.63	1.40	1.46	1.12	1.54	1.52
122	A1	1050	200	105	22.3	492	0.66	SH	60.	80	0.38	330.0	P	0.94	1.45	1.07	1.60	1.20	1.13	1.44	1.42
123	A2	1050	200	105	23.4	492	0.66	SH	60.	80	0.58	345.0	P	0.94	1.30	1.00	1.64	1.11	1.09	1.36	1.34
124	A3	1050	200	105	25.3	492	0.66	SH	60.	80	0.77	397.0	P	0.94	1.18	1.08	1.81	1.16	1.15	1.41	1.39
125	B0	1350	200	105	21.7	492	0.75	0	0.0	0	0.0	275.0	P	1.07	1.80	1.54	1.36	1.36	1.14	1.41	1.41
126	B1	1350	200	105	22.3	492	0.75	SH	60.	80	0.38	328.0	P	1.07	1.42	1.05	1.59	1.14	1.17	1.36	1.36
127	B2	1350	200	105	23.4	492	0.75	SH	60.	80	0.58	337.0	P	1.07	1.28	0.97	1.60	1.04	1.10	1.27	1.27
128	B3	1350	200	105	25.3	492	0.75	SH	60.	80	0.77	345.0	P	1.07	1.16	0.93	1.57	0.96	1.03	1.17	1.17
129	C0	1650	200	105	21.7	492	0.70	0	0.0	0	0.0	264.0	P	1.00	1.58	1.50	1.30	1.33	1.21	1.39	1.39
130	C1	1650	200	105	22.3	492	0.70	SH	60.	80	0.38	307.0	P	1.00	1.25	0.99	1.49	1.09	1.17	1.30	1.30
131	C2	1650	200	105	23.4	492	0.70	SH	60.	80	0.58	310.0	P	1.00	1.13	0.90	1.47	0.98	1.08	1.18	1.18
132	C3	1650	200	105	25.3	492	0.70	SH	60.	80	0.77	326.0	P	1.00	1.02	0.89	1.49	0.93	1.02	1.13	1.13
Gouveia et al. (2014)																					
133	ND0 (-)	1650	200	103	35.9	523	1.00	0	0.0	0	0.0	289.2	P	1.43	1.94	1.18	1.14	1.04	1.13	1.18	1.18
134	ND1 0.5%	1650	200	103	33.8	523	1.00	SH	35.0	65	0.50	296.0	P	1.43	1.63	0.82	1.21	0.83	0.97	1.03	1.03
135	ND2 0.75%	1650	200	103	31.8	523	1.00	SH	35.0	65	0.75	369.3	P	1.43	1.52	0.98	1.55	0.97	1.14	1.22	1.22
136	ND3 0.75%	1650	200	103	46.2	523	1.00	SH	35.0	65	0.75	450.7	P	1.43	1.38	1.06	1.57	1.14	1.20	1.34	1.34
137	ND4 1.00%	1650	200	103	45.8	523	1.00	SH	35.0	65	1.00	456.0	P	1.43	1.29	1.07	1.60	1.08	1.13	1.28	1.28
138	ND5 1.25%	1650	200	103	44.5	523	1.00	SH	35.0	65	1.25	474.7	P	1.43	1.22	1.15	1.69	1.08	1.10	1.26	1.26
The author's current slab specimens																					

No.	Slab ID	L_1 mm	c_x mm	d mm	f'_c MPa	f_y MPa	ρ %	Fibre type	Fibre length L_f	Fibre Aspect ratio	V_f (%)	V_{exp} kN	Failure Mode	ρ/ρ$_{fs}$ Simplified Method	ρ/ρ$_{fs}$ Standard Method	V_{exp}/V_{calc}					
																Narayanan & Darwish	Shaaban & Gesund	Higashiyama et al.	CSCT+VEM	Simplified General Method	Standard General Method
(1)	(2)	(3)	(4)	(5)	(6)	(7)	(8)	(9)	(10)	(11)	(12)	(13)	(14)	(15)	(16)	(17)	(18)	(19)	(20)	(21)	(22)
139	F09-00	2200	200	117	80.0	585	0.90	0	0.0	0	0.0	382.4	P	1.29	1.59	0.70	0.85	1.18	1.05	1.03	1.03
140	F09-03	2200	200	117	89.0	585	0.90	DH	60.	65	0.30	461.4	P	1.29	1.26	0.67	0.97	1.19	1.05	1.01	1.01
141	F09-06	2200	200	117	87.0	585	0.90	DH	60.	65	0.60	556.4	P	1.29	1.10	0.79	1.18	1.26	1.11	1.05	1.05
142	F09-09	2200	200	117	90.0	585	0.90	DH	60.	65	0.90	678.4	FP	1.29	0.96	0.95	1.42	1.40	1.18	1.12	1.13
143	F09-12	2200	200	117	100.0	585	0.90	DH	60.	65	1.20	7314	FP	1.29	0.84	1.03	1.45	1.42	1.10	1.06	1.11
144	F14-00	2200	200	114	80.0	575	1.40	0	0.0	0	0.0	382.4	P	2.00	2.28	0.68	0.88	1.06	0.91	0.92	0.92
145	F14-03	2200	200	114	89.0	575	1.40	DH	60.	65	0.30	466.4	P	2.00	1.83	0.67	1.02	1.08	0.95	0.93	0.93
146	F14-06	2200	200	114	87.0	575	1.40	DH	60.	65	0.60	587.4	P	2.00	1.59	0.83	1.29	1.19	1.08	1.03	1.03
147	F14-09	2200	200	114	90.0	575	1.40	DH	60.	65	0.90	806.4	FP	2.00	1.39	1.13	1.75	1.50	1.33	1.25	1.25
148	F14-12	2200	200	114	100.0	575	1.40	DH	60.	65	1.20	977.4	FP	2.00	1.22	1.38	2.01	1.71	1.41	1.34	1.34
													Minimum =			0.49	0.61	0.66	0.67	0.84	0.84
													Maximum =			1.63	2.32	1.71	1.41	1.55	1.55
													Average =			0.92	1.38	1.00	1.01	1.22	1.19
													COV=			0.250	0.238	0.191	0.146	0.129	0.130
													5th Percentile =			0.61	0.91	0.73	0.77	0.94	0.93